iconst.org

iconst est'23

30 August - 01 September, 2023

6th International Conferences on Science and Technology

Budva, Montenegro

Engineering Science and Technology

Abstracts & Proceedings Book

iconst iconst iconst iconst iconst iconst iconst iconst iconst iconst iconst iconst iconst iconst iconst iconst

ICONST EST 2023

International Conferences on Science and Technology

Engineering Science and Technology

August 30 - September 1, 2023 in Budva, MONTENEGRO

ABSTRACTS
&
PROCEEDINGS BOOK

ICONST EST 2023

International Conferences on Science and Technology

Engineering Science and Technology

August 30 - September 1, 2023 in Budva, MONTENEGRO

Editors

Dr. Mustafa Karaboyacı
Dr. Abdullah Beram
Dr. Hamza Kandemir
Dr. Serkan Özdemir

Technical Editors

MSc. Tunahan Çınar
MSc. Şerafettin Atmaca
Ma. Fıratcan Çınar

Cover design & Layout

Dr. Okan Koç

Copyright © 2023

All rights reserved. The papers can be cited with appropriate references to the publication. Authors are responsible for the contents of their papers.

Published by

Association of Kutbilge Academicians, Isparta, Türkiye
E-Mail: info@kutbilge.org

Publication Date: 20/10/2023
ISBN: 978-625-98911-1-8

ICONST EST 2023

International Conferences on Science and Technology

Engineering Science and Technology

August 30 - September 1, 2023 in Budva, MONTENEGRO

Scientific Honorary Committee

Prof. Dr. Rade RATKOVIC, Fakultet za biznis i turizam Budva University, Montenegro
Prof. Dr. Mehmet SALTAN, Suleyman Demirel University, Türkiye
Prof. Dr. İlker Hüseyin ÇARIKÇI, Member of Council of Higher Education, Türkiye
Prof. Dr. Yılmaz ÇATAL, Isparta University of Applied Sciences, Türkiye
Prof. Dr. Vujadin VEŠOVIĆ, Faculty of Transport Communications and Logistics, Montenegro
Prof. Dr. Mentor ALİSHANİ, University of Prizren, Kosovo
Prof. Dr. Edmond HAJRİZİ, University for Business and Technology, Kosovo
Prof. Dr. Naime BRAJSHORİ, Kolegji Heimerer, Kosovo
Prof. Dr. Nermina HADŽİGRAHİĆ, University of Tuzla, Bosnıa and Herzegovına
Prof. Dr. Kseanela SOTİROFSK, University of Durres, Albanıa
Prof. Dr. Kürşad ÖZKAN, Isparta University of Applied Sciences, Türkiye

Organizing Committee

Dr. Mustafa Karaboyacı, Suleyman Demirel University, Türkiye
Dr. Hamza Kandemir, Isparta University of Applied Science, Türkiye
Dr. Serkan Özdemir, Isparta University of Applied Science, Türkiye
Dr. Abdullah Beram, Pamukkale University, Türkiye
Dr. Ergin Kala, University of Prizren, Kosovo
Dr. Joanna Machnik-Slomka, Silesian University of Technology, Poland
Dr. Elzbieta Pawlowska, Silesian University of Technology, Poland
Dr. Fatmir Mehmeti, Prizren University, Kosovo
Prof Dr. Indrit Bimi, Durres University, Albanıa
Dr. Viliem Kurtulaj, Qiriazi University, Albanıa
Ma. Dragana Zecevic, Fakultet za biznis i turizam Budva University, Montenegro

Technical Committee

MSc. Şerafettin Atmaca, Suleyman Demirel University, Türkiye
MSc. Tunahan Çınar, Düzce University, Türkiye
Ma. Fıratcan Çınar, Isparta University of Applied Sciences, Türkiye

ICONST EST 2023

International Conferences on Science and Technology

Engineering Science and Technology

August 30 - September 1, 2023 in Budva, MONTENEGRO

Scientific Committee

Dr. Alev Akpınar Borazan, Bilecik Seyh Edebali University, Turkey
Dr. Amer Kanan, Al-Quds University, Palestine
Dr. Andrea G. Capodaglio, University of Pavia, Italy
Dr. Aybeyan Selim, International Vision University, North Macedonia
Dr. Apostolos Kiritsakis, Alexander Tech. Educational Ins. of Thessaloniki, Greece
Dr. Ayodeji Olalekan Salau, Obafemi Awolowo University, Nigeria
Dr. Bülent Derviş, International Vision University, North Macedonia
Dr. Cristian Fosalau, Technical University of Iasi, Romania
Dr. Driton Vela, University of Business and Technology, Kosovo
Dr. Eda Mehmeti, University of Business and Technology, Kosovo
Dr. Elvida Pallaska, University of Business and Technology, Kosovo
Dr. Ermek A. Aubakirov, Al – Farabi Kazakh National University, Kazakhstan
Dr. Fecir Duran, Gazi University, Turkey
Dr. Gauss M. Cordeiro, Federal University of Pernambuco, Brazil
Dr. Gholamhossein Hamedani, Marquette University, USA
Dr. Gülcan Özkan, Süleyman Demirel University, Turkey
Dr. Hamid Doost Mohammadian,FHM University of Applied Sciences, Germany
Dr. Ines Bula, University of Business and Technology, Kosovo
Dr. Izabela Zimoch, Silesian Universum of Technology, Poland
Dr. Joanna Boguniewicz-Zabłocka, Opole University of Technology, Poland
Dr. Kari Heliövaara, University of Helsinki, Finland
Dr. Kłosok-Bazan Iwona, Opole University of Technology, Poland
Dr. Kubilay Akçaözoğlu, Niğde Ömer Halisdemir University, Turkey
Dr. Leyla Tavacıoğlu, Istanbul Technical University, Turkey
Dr. Lulzim Beqiri, University for Business and Technology, Kosovo
Dr. Mathew Ademola Jayeola, Obafemi Awolowo University, Nigeria
Dr. Mehmet Kılıç, Suleyman Demirel University, Turkey
Dr. Mehmet Kitiş, Suleyman Demirel University, Turkey
Dr. Merita Barani, University for Business and Technology, Kosovo
Dr. Meruyert Kaygusuz, Pamukkale University, Turkey
Dr. Mirosław Kwiatkowski, AGH- University of Science And Technology, Poland
Dr. Mohd Aswadi Bin Alias, Unıversıty Kuala Lumpur- Bmı, Malaysia
Dr. Muhamet Ahmeti, University of Business and Technology, Kosovo
Dr. Naushad Ali Mamode Khan, University of Mauritius, Mauritius
Dr. Nicholas Baldacchino, Malta College of Arts, Science & Technology, Malta
Dr. Nuray Benli Yıldız, Duzce University, Turkey
Dr. Rahmon Ariyo Badru, Obafemi Awolowo University, Nigeria
Dr. Ramazan Şenol, Suleyman Demirel University, Turkey
Dr. Salina Muhamad, Universiti Selangor, Malasıa
Dr. Sami Makolli, University of Business and Technology, Kosovo
Dr. Serhat Oğuzhan Kıvrak, Hitit University, Turkey
Dr. Shpend Dragusha, University of Business and Technology, Kosovo
Dr. Şule Sultan Uğur, Suleyman Demirel University, Turkey
Dr. Valmir Hoxha, University of Business and Technology, Kosovo
Dr. Vehebi Sofiu, University of Business and Technology, Kosovo
Dr. Vincenzo Naddeo, University of Salerno, Italy
Dr. Zhandos T. Mukayev, Shakarim State University of Semey, Kazakhstan

ICONST 2023

International Conferences on Science and Technology

Engineering Science and Technology

Life Science and Technology

Natural Science and Technology

August 30 - September 1, 2023 in Budva, MONTENEGRO

Dear Readers;

The sixth of ICONST organizations was held in Budva/Montenegro between August 30 - September 1, 2023 with the theme of '***science for sustainable technology***' again. In recent years, weather changes due to climate change have reached a perceptible level for everyone and have become a major concern. For this reason, scientific studies that transform technological progress into a sustainable one is seen as the only solution for humanity's salvation. Here we ask ourselves "which branch of science is responsible for sustainability?". Sustainability science is an interdisciplinary field of study that covers all basic sciences with social, economic, ecological dimensions. If we consider technology as the practical application of scientific knowledge, the task of scientists under these conditions is to design products that consume less energy, require less raw materials, and last longer.

ICONST organizations organize congresses on sustainability issues of three main fields of study at the same time in order to present different perspectives to scientists. This year, 136 papers from 22 different countries presented by scientists in **ICONST Organizations**.

89 papers from 14 countries presented in our **International Conference on Engineering Science and Technology** organized under ICONST organizations. Türkiye leads the way with 48.8% of the participants, followed by Poland with 17.9%, Kosovo with 8.3%, Algeria, Azerbaijan and Montenegro with %4.8, Hungary with 2.4, Italy, Iraq, North Macedonia, Netherland, Iran, Bangladesh and South Africa with 1.2%.

25 papers from 11 countries presented in our **International Conference on Life Science and Technology** organized under ICONST organizations. Türkiye leads the way with 40% ofthe participants, followed by North Macedonia with 13%, Kosovo and Poland with 8.7%,Sweden, Finland, United Kingdom, Czech Republic, Portugal, Iran and Slovakia with 4.3%.

Finally, 22 papers from 9 countries presented in our **International Conference on Natural Science and Technology** organized under ICONST organizations. Türkiye leads the way with 45.5% of the participants, followed by Kosovo, Russia, Poland and Azerbaijan with 9.1% and India, Ethiopia, Serbia and Albania with 4.5%.

As ICONST organizations, we will continue to organize organizations with the value you deserve in order to exchange ideas against the greatest threat facing humanity, to inspire each other and to contribute to science. See you at your future events.

ICONST Organizing Committee

ICONST EST 2023

International Conferences on Science and Technology

Enginnering Science and Technology

August 30 - September 1, 2023 in Budva, MONTENEGRO

Contents

Location Detection of Water and Sewer Pipelines Using IMU Sensor

Akif Demircali[1], Omer Boyaci*[2]

Abstract: Drinking water is one of our most valuable natural resources. Drinking water pipelines carry water between sources and destinations. Similarly, sewer and drainpipes carry wastewater and various liquids from customer to the processing plants. Inspection and maintenance of water and sewer pipelines are crucial to maintaining a firm water supply, protecting the supply, and preventing contamination and clearing blockages from leaky sewer pipes. Because pipes are often located underground and come in different sizes and configurations, inspection of pipelines, including leak detection and fluid quality monitoring, is difficult. As it is known, there is no detailed location data of all old drinking water and sewerage pipeline networks in local governments. In excavations to be made for maintenance, repair and renovation works, it is important to correctly determine positions of the relevant lines. In this study, an IMU sensor-based location algorithm has been developed for the location detection of drinking water and sewer pipeline networks. The developed algorithm uses the acceleration, gyroscope and magnetometer data recorded by the IMU sensor that is left to pipeline while there is liquid flow. In this way, movements such as rotation around itself can be observed, as well as the instantaneous progress of the left sensor in liquid in the x, y and z axes. The IMU sensor used is the MPU9250 on the 9-axis Razor IMU M0 development board developed by SparkFun. The corresponding development board allows data to be saved on the SD card and transmitted via various communication protocols. With the developed system, precise location determination is made and the integration of the obtained data on the map is carried out. In addition, since the data obtained in the developed system includes rotational movements of the sensor in the liquid, it also allows interpretation of unusual flows of the liquid and potential leaks.

Keywords: Pipeline, Sewer, Position Detection, IMU Sensor.

[1]**Address:** Pamukkale University, Faculty of Engineering, Denizli/Turkiye
[2]**Address:** Pamukkale University, Cardak Organized Industrial Zone Vocational School, Denizli/Turkiye

***Corresponding author**: omerboyaci@pau.edu.tr

3D Printers: The Future Role and Application Areas of Technology

Sertaç Salçini*[1]

Abstract: This paper aims to examine the future potential and broad application areas of 3D printer technology. 3D printers are an innovative technology that works on the principle of layer-by-layer construction of objects. This technology offers advantages such as optimizing production processes, providing design freedom, and enabling rapid prototype development. This paper will address the evolution of 3D printers and their future role. 3D printers are devices that construct objects layer by layer, utilizing various materials. This technology provides a range of advantages, including reducing production costs, facilitating customized production, and speeding up the prototyping process. This paper discusses the evolution of 3D printers and their potential future role. 3D printers create three-dimensional objects by layering different materials. Basic printing techniques such as Fused Deposition Modeling (FDM), Stereolithography (SLA), and Selective Laser Sintering (SLS) are elaborated upon in this section. The role of material selection and its impact on the design process are also examined. 3D printers offer advantages across a wide range of industries, from manufacturing to healthcare, education, and even space exploration. This section delves into the flexibility of design, customized production, and reduced waste production. It also highlights the improvements made in rapid prototyping processes. Despite its advantages, 3D printer technology faces challenges such as material quality, printing speed, cost factors, and difficulties in large-scale production. Various application-specific challenges are also addressed, considering different sectors. 3D printers have the potential to make significant impacts in various fields. Bioprinting could revolutionize the medical field by enabling the production of customized organs and tissues. In the construction sector, complex geometric structures can be efficiently built. Additionally, there is substantial potential in fields like space exploration, food production, and education. 3D printer technology holds the potential to transform industries in the future. By discussing the fundamental principles, current advantages, and future potential, this paper emphasizes the role of 3D printers in global innovation and production processes.

Keywords: 3D printing, additive manufacturing, future technology, application areas, ınnovation

[1]**Address:** University of Prizren Ukshin Hoti, Prizren, Kosovo

***Corresponding author**: sertacsalcini@gmail.com

Electricity Generation from Jerusalem Artichoke Waste by Leuconostoc mesenteroides in a Microbial Fuel Cell

Ömer Boyacı *[1], Büşra Onat [1], Zeynep Onat[1]

Abstract: As an alternative to fossil fuels, the search for renewable energy sources has become increasingly important in recent years. We should develop renewable energy sources and make them sustainable and use them. The applicability of the generated electricity to real-life processes is as important as generating electricity. From this point of view, it is aimed to make biochemical electricity production using food waste and microorganisms and how to make this electricity applicable. We determined the food waste and microorganism in our project by taking advantage of the outputs of our TUBITAK 2209-B "Symbiotic Water Kefir Production with Immune Boosting Jerusalem Artichoke Additive" study we did last year. We are considering using Jerusalem artichoke peels as food waste. The reason for this is that the best food source used by the microorganism we will use in the other project is yams and peels. The microorganism is Leuconostoc mesenteroides and according to the result we obtained from water kefir production, Leuconostoc mesenteroides is the probiotic bacterium that forms the basic flora that develops and adapts the most with the contribution of yams in the drink. At this point, it will be ensured that Leuconostoc mesenteroides can realize electricity production by using yams peels as substrate.Previous studies have utilized algae and Shewanella putrefaciens as microbial fuel cells. Electricity generation from disaccharides (usually D-cellobiose, D-maltose, glucose and acetate) and wastewater (such as whey, olive blackwater) as substrates has been studied. The substrate in this study, Jerusalem artichoke peels and the bacterial species Leuconostoc mesenteroides, have not been studied before and are thought to contribute to the literature if investigated. R&D studies will be carried out to determine the capacity of this probiotic bacterium (Leuconostoc mesenteroides) to generate electricity and how the electricity produced can be evaluated with the analyzes we aim to make.

Keywords: Biochemical electricity production, microbial fuel cells, probiotic bacterium

[1]**Address:** Pamukkale University, Engineering Faculty, Çardak Organized Industrial Zone Vocational School , Denizli, Turkiye

***Corresponding author**: omerboyaci@pau.edu.tr

Comparison of Two Sensorless Control Methods for PMSM based on High-Frequency Signal Injection

Fehmi Sevilmiş*[1]

Abstract: In recent years, there has been a growing interest in the development and implementation of sensorless control methods for permanent magnet synchronous motor (PMSM) in various fields, such as electric vehicles and industrial applications. Since there is no need for a mechanical sensor to obtain the rotor position, sensorless control methods bring many advantages such as low-cost, robutness, and reliability in PMSM control. For sensorless operation of PMSM at zero and low speeds, high-frequency (HF) signal injection methods are used to estimate the rotor position. Among these methods, HF rotating signal injection and HF pulsating signal injection techniques are broadly operated for sensorless control of PMSM. A HF rotating signal is injected into the stationary reference frame while a HF pulsating signal is injected into the estimated synchronous refence frame. This paper presents a comparison for the two HF signal injection methods. The principle of these techniques is analyzed first. Then, the two methods are compared with each other, and the obtained findings are summarized.

Keywords: high frequency rotating signal injection, high frequency pulsating signal injection, permanent magnet synchronous motor (PMSM), sensorless control.

[1]**Address:** Selçuk University, Faculty of Technology, Konya/Türkiye

***Corresponding author**: fehmisevilmis@selcuk.edu.tr

Energy Storage Types in Transportation Vehicles -A Review-

Özge Küçükkör[1], Ali Burak Göğebakan[2], Ömür Küçükkör[3], Serkan Özeçoğlu[2], Mine Sertsöz*[4]

Abstract: Today, transportation is responsible for, on average, 30% of total energy consumption. While the increase and development of transportation vehicles continues with the advancing technology, the efficient use of energy in parallel with this progress is one of the important research topics.
After these vehicles are supplied with energy in some way (renewable or non-renewable sources), how vehicles manage their energy consumption is a key point in energy efficiency, but it is not enough on its own. Because after the correct energy management, all components used in the vehicle must be efficient.
In this study, energy storage options, which are perhaps the most difficult to choose from all these components, were investigated. Because when choosing an energy storage method and type, not only its efficiency, but also its economic aspect and environmental effects should be considered.
There are many energy storage types. These are generally classified as chemical, thermal, electrical, and mechanical energy storages. They are also divided into many types within themselves. Thanks to this study, the advantages and disadvantages of storage options which was carried out according to the mode of transportation (road, airway, rail system and sea) were investigated and samplings from the world were presented. Thus, it will be a resource for vehicle designers and researchers.

Keywords: Energy Storage, Transportation Vehicles, Energy Efficiency, Environmental Impact.

[1]**Address:** Kapadokya University, Vocational School of Kapadokya, Nevşehir/Türkiye
[2]**Address:** Eskisehir Technical University, Railway Systems Department (Postgraduate), Eskisehir/Türkiye
[3]**Address:** Kapadokya University, Political Science and Public Administration (Postgraduate), Nevşehir, Turkiye
[4]**Address:** Eskisehir Technical University, Railway Systems Department, Eskisehir/Türkiye

***Corresponding author**: msertsoz@eskisehir.edu.tr

Influence of the Content of Recycled Artificial Leather Waste in Particleboards on Their Selected Properties

Katarzyna Bartoszuk[1], Grzegorz Kowaluk*[2]

Abstract: Upholstery leather, commonly known as artificial leather, is a fabric-plastic layered composite that looks like natural leather. Due to a broad range of advantages, artificial leather is commonly used as an upholstery material in the renovation and production of furniture or even car upholstery. The material is distinguished by its flexibility and perfect imitation of eco-leather. The aim of the research was to manage the artificial upholstery leather waste by adding previously disintegrated pieces of artificial leather with different content (5, 10, 25 and 50% by weight) to particleboards. The tests of selected mechanical properties (bending strength and modulus of elasticity, as well as screw withdrawal resistance) and physical properties (density profile, thickness swelling after water immersion) have been completed. The dimensional characterization of produced waste upholstery fabric particles has been also done. The mechanical properties of the boards deteriorated with the increase in the amount of artificial leather in tested particleboards. However, for most of the features of the tested board variants, the minimum requirements of European standards for furniture boards were met. It can be concluded, that depending on the further use of the board, there is the possibility of using recovered pieces of leatherette as a reasonable addition to wood fibres in the production of particleboards. Thus, it is possible to positively contribute to tackling climate change and to circular economy, due to the extension of carbon sequestration in recovered waste upholstery materials.

Keywords: recycling, particleboard, artificial leather, upholstery furniture, circular economy.

Acknowledgement: The presented study was completed within the activity of the Student Furniture Scientific Group (Koło Naukowe Meblarstwa).

[1]**Address:** Faculty of Wood Technology, Warsaw University of Life Sciences – SGGW, Warsaw, Poland
[2]**Address:** Department of Technology and Entrepreneurship in Wood Industry, Institute of Wood Sciences and Furniture, Warsaw University of Life Sciences – SGGW, Warsaw, Poland

***Corresponding author**: grzegorz_kowaluk@sggw.edu.pl

APF Based Control Algorithm for Voltage Regulation of Self Excited Induction Generator Using DSTATCOM

Ali Sait Özer[1], Hulusi Karaca*[2], Fehmi Sevilmiş[2]

Abstract: Distribution Static Compensator (DSTATCOM) systems are widely used for voltage regulation of self-excited induction generator (SEIG). DSTATCOM provides the reactive power that SEIG and the load need. The performance of DSTATCOM depends on its control algorithm. The main goal of the control algorithm is to generate switching signals for the voltage source inverter (VSI) in the structure of DSTATCOM. These signals are generated by using reference currents. The active and reactive components required to generate the reference currents are obtained from the SEIG individual phase voltages and 90-degree lagging-phase. For this, SOGI and EPLL based current synchronous detection (CSD) methods have been suggested in the literature. The filtering capabilities of these methods are satisfactory, but they are relatively complex. In this paper, all pass filter (APF) based CSD method is proposed. This method is a simple and effective method with less mathematical calculations. The suggested algorithm has been tested under linear and nonlinear load conditions. The obtained results clearly represent the effectiveness of the suggested APF based CSD control algorithm.

Keywords: Distribution static compensator (DSTATCOM), Self-excited induction generator (SEIG), Wind energy conversion systems (WECS), Current synchronous detection (CSD) method, All pass Filter (APF)

[1]**Address:** Konya Technical University, Department of Control and Automation Technology, Konya/Türkiye
[2]**Address:** Selçuk University, Department of Electrical and Electronics Engineering, Konya/Türkiye

***Corresponding author**: hkaraca@selcuk.edu.tr.

Performance Analysis of SRF and CSD Based Algorithms for Voltage Control of Self-Excited Induction Generator

Ali Sait Özer[1], Hulusi Karaca*[2]

Abstract: Self-excited induction generator (SEIG) can be a good option for remote areas without grid connectivity. However, it is known that SEIG requires reactive power for voltage stability during load changes. Distribution static compensator (DSTATCOM) is a suitable option to provide the required reactive power. Various control algorithms have been developed to control DSTATCOM. Synchronous reference Frame (SRF) based and current synchronous detection (CSD) based algorithms are commonly used methods in the literature. This article tests the performance of these two theories under balanced, unbalanced, and nonlinear load conditions. It has been demonstrated that the SRF based method is simpler and more effective than the CSD based method.

Keywords: Distributed static compensator (DSTATCOM), Self-excited induction generator (SEIG), Wind energy conversion systems (WECS), Current synchronous detection (CSD) method.

[1]**Address:** Konya Technical University, Department of Control and Automation Technology, Konya/Türkiye

[2]**Address:** Selçuk University, Department of Electrical and Electronics Engineering, Konya/Türkiye

***Corresponding author**: hkaraca@selcuk.edu.tr.

Development of Microsphere Releasing Hydrogel System for Local Delivery of Anti-cancer Agents After Tumor Removal

Neslihan Barer[1], Bugse Tunc[1], Bengi Yilmaz[2], Yuk Yin Ng[3], Ali Deniz Dalgic[1]*

Abstract: One of the treatment approaches for solid tumors is the removal of tumor with surgical operation and application of systemic chemotherapy alongside local radiotherapy. However, the fact that tumor and healthy tissue do not have a clear border, limits the surgeon's ability to remove all the tumor cells from the healthy tissue. For this reason, after the tumor is removed, some micro-tumor tissues and cells are left in the wound area. The remaining cancerous cells are known to cause reappearance of tumor and cancer to metastasize to other tissues of the body. Systemic chemotherapy and local radiation therapy is applied to eliminate the remaining cancerous cells to prevent reoccurrence of the cancer. However, systemic chemotherapy can lead to serious side effects since anti-cancer agent can distribute systemically and targeted drug dose may not be achieved at the operation site. Novel local drug delivery approaches are needed to be developed to overcome systemic toxicity of drugs and create an efficient anti-cancer treatment. In this study, a hydrogel was fabricated to have micro chambers on the surface which will carry and deliver anti-cancer drug loaded microspheres. Anti-cancer drug, doxorubicin, was encapsulated into microspheres and drug release was studied. Scanning electron microscopy was used to show successful encapsulation of microspheres into micro-chambers. Anti-cancer effect of the produced hydrogel/microsphere system was tested in vitro on both monolayer and spheroid models formed by breast cancer cell line (MCF-7) and the hydrogel was successfully reduced cancer cell viability. When the anti-cancer drug loaded microspheres were released from the hydrogel, polymer scaffold was able to support viability of healthy cells which was shown by testing the proliferation of mouse fibroblast cell line (L929) on the hydrogel. This hydrogel/microsphere system, which has the capacity to kill cancer cells, is expected to create an environment for normal tissue cells to proliferate over time for the healing of the scar tissue after the release of cancer drug.

Keywords: Microsphere, Hydrogel, Local drug delivery, Post-Operative Treatment, Doxorubicin.

[1]**Address:** Istanbul Bilgi University, Faculty of Engineering and Natural Sciences, Istanbul/Türkiye
[2]**Address:** University of Health Sciences, Institute of Hamidiye Health Sciences, Istanbul/Türkiye
[3]**Address:** University of Applied Sciences, Institute of Life Sciences Utrecht, Utrecht/Netherlands

***Corresponding author**: deniz.dalgic@bilgi.edu.tr

The Use of Chestnut Starch as a Binding Mass Filler in the Plywood Technology

Julia Dasiewicz[1], Grzegorz Kowaluk*[2]

Abstract: Fillers play a crucial role in the production of plywood glues, providing enhanced performance and stability to the end product. Plywood, being a composite material, requires fillers to improve its mechanical properties, adhesion, and overall quality. One common filler used in plywood glues is calcium carbonate. It acts as a bulking agent, increasing the volume and density of the adhesive mixture while reducing production costs. Calcium carbonate also enhances the glue's viscosity, ensuring proper bonding and uniform application during the plywood manufacturing process. Another widely used filler is rye or wheat flour, which consists of finely ground grains. The flour not only improves the adhesive's viscosity but also contributes to the overall strength and stability of the plywood. It helps to prevent warping and enhances dimensional stability, making the final product more durable. Additionally, other fillers like talc or clay minerals may be incorporated into the glues to improve their adhesive properties and increase moisture resistance. Chestnut starch is a type of vegetable flour made by grinding edible chestnuts into a powder. It has a different texture and properties than traditional wheat or rye flour. When used as a binder filler in plywood technology, it can be biodegradable and environment-friendly. In the study, there were produced five types of plywood with 0, 1, 5, 10, and 20 parts by weight chestnut flour and one reference. All samples were produced in laboratory conditions and the selected mechanical and physical properties of the produced boards were studied. The mechanical properties of the boards increased with the addition of chestnut flour. In some tests, the results even met the highest requirements of European standards for plywood. According to this finding, a well-chosen addition of rice flour could be positively considered in plywood production. Research is still being conducted to improve the performance of plywood bonded with chestnut starch.

Keywords: plywood, chestnut, starch, binder
Acknowledgment: The presented study was completed within the activity of the Student Furniture Scientific Group (Koło Naukowe Meblarstwa).

[1]**Address:** Faculty of Wood Technology, Warsaw University of Life Sciences – SGGW, Warsaw/Poland
[2]**Address:** Department of Technology and Entrepreneurship in Wood Industry, Institute of Wood Sciences and Furniture, Warsaw University of Life Sciences – SGGW, Warsaw/ Poland

***Corresponding author**: grzegorz_kowaluk@sggw.edu.pl

Preliminary Characterization of Functional Features of Biopolymer – Suberinic Acid Residue Blends

Aleksandra Jeżo[1], Grzegorz Kowaluk*[2]

Abstract: Polymer blends have gained significant attention in the field of materials science due to their unique properties and versatile applications. At the same time, more attention is paid to a circular economy, including the usage of biodegradable resources. While biopolymers have numerous advantages, there are also challenges associated with their production. However, ongoing research and technological advancements have widespread adoption of biopolymers in various industries, including wood engineering. Therefore, in light of previous research findings, this study aims to prepare and evaluate blends of biopolymers, specifically poly(lactide) (PLA), polycaprolactone (PCL), and modified starch, with the incorporation of up to 10% suberin acid residues (SAR). The previous research showed that suberin acid residues (SAR) remaining from the extraction of birch bark are a promising bioresource that fits into the idea of upcycling. The blends have been produced through extrusion to form granules. The characteristics of the resulting biopolymer blends were assessed using scanning electron microscopy (SEM), spectroscopic techniques such as infrared absorption spectroscopy (IR), and thermal analysis methods including differential scanning calorimetry (DSC), thermogravimetry (TGA), and thermomechanical analysis (TMA). This research aims to address the following questions: 1) What are the key characteristics of the biopolymer blends concerning their suitability for use in wood-based composite technology? 2) What potential applications can be explored for the produced blends in wood technology? Can the prepared blends serve as raw materials for composite production or as binders? Is it feasible to create films/coatings on wood and wood composites? This study will show new promising paths to follow in the next research.

Keywords: polymer blends, suberin acid residues, biopolymers, polymer wood coatings, usage of polymer blends in wood engineering

Acknowledgment:The presented study was partially completed within the activity of the Student Furniture Scientific Group (Koło Naukowe Meblarstwa) under the BarkBuild project. The BarkBuild project is funded under the ERA-NET Cofund ForestValue program through Vinnova (Sweden), Valsts izglītības attīstības aģentūra (Latvia), Ministry of Education, Science and Sport (JIA) (Slovenia), Academy of Finland, The Research Council of Norway, and the National Science Centre, Poland (contract no. 2021/03/Y/NZ9/00038).

The ForestValue program received funding from the Horizon 2020 Research and Innovation program of the European Union under grant agreement No. 773324.

[1]**Address:** Faculty of Wood Technology, Warsaw University of Life Sciences – SGGW, Warsaw, Poland; ORCID 0000-0002-9128-6934
[2]**Address:** Department of Technology and Entrepreneurship in Wood Industry, Institute of Wood Sciences and Furniture, Warsaw University of Life Sciences – SGGW, Warsaw, Poland; ORCID 0000-0003-1463-0540

***Corresponding author**: grzegorz_kowaluk@sggw.edu.pl

Waste Banana Peel Flour as a Filler in Plywood Binder

Matylda Wojciechowska[1], Grzegorz Kowaluk*[2]

Abstract: Waste banana peel flour has gained attention as a potential filler in plywood binders due to its abundance, low cost, and positive environmental impact. Banana peels, which are typically discarded as waste, can be processed into flour and incorporated into plywood binders, offering several advantages. Firstly, banana peel flour acts as a natural filler, increasing the volume and reducing the amount of more expensive fillers required in plywood production. This can lead to cost savings without compromising the overall quality of the plywood. Secondly, banana peels contain a significant amount of cellulose, which contributes to the strength and stability of the binder. The cellulose fibers present in the peel flour improve the adhesive's mechanical properties, enhancing the plywood's resistance to warping, bending, and cracking. Furthermore, banana peels are rich in phenolic compounds, such as tannins, which possess adhesive properties. These compounds can enhance the bonding strength between the veneer layers in plywood, resulting in improved overall structural integrity. Using waste banana peel flour as a filler in plywood binders also presents environmental benefits. By repurposing banana peels, which would otherwise end up in landfills, it reduces waste and promotes sustainability. The study aimed to investigate the influence of various contributions of banana peel flour in bonding mass on the properties of plywood produced with such an investigated binder. The following plywood features have been tested: modulus of rupture and modulus of elasticity, bonding quality (shear strength and in-wood damage) and density profile. The achieved results have been referred to as the control plywood produced with regular, industrially composed bonding mass. The structure of banana peel has been also characterized, as well. The results have shown, that waste banana peel flour can be a valuable replacement of commercially applied filler in plywood technology.

Keywords: plywood, binder, glue, filler, banana, peel, waste

Acknowledgment: The presented study was completed within the activity of the Student Furniture Scientific Group (Koło Naukowe Meblarstwa).

[1]**Address:** Faculty of Wood Technology, Warsaw University of Life Sciences – SGGW, Warsaw/Poland
[2]**Address:** Department of Technology and Entrepreneurship in Wood Industry, Institute of Wood Sciences and Furniture, Warsaw University of Life Sciences – SGGW, Warsaw/Poland

***Corresponding author**: grzegorz_kowaluk@sggw.edu.pl

Application of Artificial Intelligence Technologies in the Detection of Explosives

Saida Ahmadova*[1]

Abstract: Terrorist incidents in the world have once again proved that terrorism remains a global problem in the face of aviation security systems. Historically, as a result of the countermeasures taken in this direction, it was possible to weaken the wave of terrorism relatively, but this problem has not yet been fully resolved. The act of terrorism is carried out by means of terrorism. Terrorist tools consisting of dangerous items and substances are carried on board the plane or in the airport area on persons or in cargo, baggage and hand luggage carried in HG, bypassing inspection control. Therefore, the first of the countermeasures against a terrorist act is to detect the person who committed the terrorist act and the means of terrorism. Using artificial intelligence technologies in the detection of explosives is recognized as a current research area.

Keywords: Explosive substance, plastic explosive device, portable X-ray-television complex, non-metallic objects

[1]**Address:** National Aviation Academy, Transport technologies, Baku/Azerbaijan

***Corresponding author**: saidaahmedovabaku@gmail.com

Detection of financial flash crash anomalies in real time using observations of the signal and its statistical properties in a preset time window

Adam Galuszka*[1], Tomasz Dzida[2], Eryka Probierz[1], Karol Jedrasiak[2], Tomasz Wisniewski[2]

Abstract: As data collection tools continue to evolve, there are now solutions that enable their analysis through digital platforms. These platforms offer automated financial planning services, utilizing algorithms and requiring minimal human oversight. Such platforms gather financial information and future goals from clients, utilizing this data to offer consulting services and automate the investment of client funds, often leveraging data from various reports.
The integration of artificial intelligence (AI) in data analysis is becoming increasingly prevalent, with around 70% of companies planning to implement AI-based solutions in the next year, according to research. The rapid advancement of data-driven technologies and AI has created promising development prospects for organizations actively involved in these domains.
To summarize, the market gaps identified include the absence of AI-based tools to support the investment process, the lack of a tool to identify historical events similar to the current situation by distinguishing current data from archival records using proprietary models based on deep networks, and the need for improved detection of flash crashes in financial threats. While there have been some works on mini flash crash detection and specific historical flash analysis, comprehensive solutions are still lacking.
Within the project detection of flash anomalies based on observation of the signal under study within a preset (assumed) time window is proposed. The size of the time window (signal length) is adjusted dynamically depending on the nature of the signal.
Assumptions of the method:
- For a signal in a time window, the parameters of the normal distribution of this signal can be determined, i.e. confidence intervals for the mean value and standard deviation;
- The onset of an anomaly is considered to be the moment when the observed current value of the sy-signal exceeds a threshold value depending on the estimates of the mean value and standard deviation;
- Parameterization of the algorithm, i.e . calibration of the threshold value, depends on the reference data of the type of anomaly under study;
- Parameterization of the algorithm involves assuming different dependencies of the threshold value on normal distribution estimates and checking the best fit;
- Anomaly detection occurs in real time, i.e., the time to analyze the tested signal for the occurrence of an anomaly is significantly shorter (i.e., at least 10 times) than the size of the tested time window.
Acknowledgement
The work has been developed within grant No. POIR.01.01.01-00-0162/19 „GPW Data Platform as an innovative system using artificial intelligence techniques to support investment decisions on the capital market" and implemented by Warsaw Stock Exchange SA in 2023. The work of Adam Galuszka was partially supported by the SUT under BK grant - the subsidy for maintaining and developing the research potential in 2023.

Keywords: machine learning, anomaly detection, flash crash, signal analysis.

[1]**Address:** Silesian University of Technology, Faculty of Automatic Control, Electronics and Computer Sciences, Akademicka 16, Gliwice/Poland
[2]**Address:** Warsaw Stock Exchange, Ksiazeca 4, Warsaw/Poland

***Corresponding author**: adam.galuszka@polsl.pl

Influence of Sr doping on the microstructure, morphology and optical properties of ZnO thin films prepared by SILAR method

Mokrani Nourelhuoda[1,*], Ghettaf Temam Elhachemi[1], Ben Temam Hachemi[1], Barkat Hadjer[1]

Abstract: The present study focused on the properties of Sr-doped ZnO thin films using the successive ionic layer adsorption and reaction (SILAR) method.The X-ray diffraction results show that the ZnO and Sr-doping ZnO samples exhibit hexagonal wurtzite structure having preferential growth along the (100) plane.The maximum crystallite size of 54 nm was observed for Sr-doping ZnO 3 wt. % sample.The SEM analysis revealed that the samples exhibit agglomerated grains and the EDX spectrum of the Sr-doping ZnO(3 and 7wt. %) samples showed the presence of Zn, Sr, and O elements.The UV–vis transmittion spectrum of the Sr-doping ZnO 7 wt. % sample revealed that it has higher tansmittion in the UV region. Finaly, Sr-doping has a significant impact on the physical and chemical properties of SILAR-deposited ZnO films.

Keywords: Sr-ZnO, thin films, SILAR, XRD, UV-vis.

[1]**Address:** Physics Laboratory of Thin Layers and Applications, Biskra University, BP 145 RP, Biskra 07000, Algeria

***Corresponding author**: nourelhouda.mokrani@univ-biskra.dz

Build Your Own Defense: Prevention of Ransomware

Mahmut Tokmak*[1]

Abstract: Ransomware attacks have become a formidable menace in the digital environment, causing severe disruptions and economic losses for businesses and individuals alike. This study presents a thorough examination of the growing threat landscape of ransomware, elucidating its various attack vectors, techniques, and implications. Moreover, it outlines a multifaceted and proactive approach to prevent ransomware incidents, offering practical strategies and best practices for achieving cybersecurity resilience. The study begins by highlighting the escalating frequency and sophistication of ransomware attacks, underlining the urgent need for robust prevention measures. It explores the primary methods employed by threat actors to propagate ransomware, such as phishing emails, exploit kits, and malicious downloads, to raise awareness about the evolving attack vectors. One of the core aspects of ransomware prevention lies in employee education and awareness. This study emphasizes the significance of ongoing cybersecurity training to empower employees in recognizing and reporting potential threats. By fostering a security-first culture, organizations can significantly reduce the risk of successful ransomware infiltrations. To fortify defenses, the study advocates for stringent software management practices. Regular updates and patching of operating systems, applications, and security tools are crucial to mitigating vulnerabilities that ransomware can exploit. Additionally, it stresses the importance of employing sophisticated endpoint protection solutions that utilize artificial intelligence and behavioral analysis to detect and neutralize ransomware in real-time. Creating and maintaining secure data backups is another pivotal aspect of ransomware prevention. The study highlights the benefits of implementing a well-defined data backup strategy, encompassing both on-site and off-site solutions, to facilitate rapid recovery without capitulating to ransom demands. Furthermore, adopting a zero-trust security model and network segmentation can significantly limit the lateral movement of ransomware within an organization's infrastructure. By compartmentalizing critical assets, businesses can minimize the extent of potential damage in case of an intrusion. In conclusion, this study underscores the necessity of a holistic and proactive approach to prevent ransomware attacks. By combining employee education, vigilant software management, robust endpoint protection, comprehensive data backups, and stringent network segmentation, organizations can enhance their cybersecurity resilience against the persistent and ever-evolving ransomware threat. Implementing these strategies will enable businesses and individuals to defend their digital assets, safeguard sensitive data, and thwart ransomware actors effectively.

Keywords: Malware, Ransomware, Build Own Defense, Prevention of Ransomware

[1]**Address:** Burdur Mehmet Akif Ersoy University, Bucak Zeliha Tolunay School of Applied Technology and Management, Burdur/Türkiye

***Corresponding author**: mahmuttokmak@mehmetakif.edu.tr

Determination of Direct Tensile Strength by Non-Destructive Test

Mustafa Kanik*[1], Zülfü Gürocak[1]

Abstract: Depending on the type of stress affecting a material, it exhibits various strength characteristics such as compression, tensile, shear, bending, and torsional strength. Among these, uniaxial compression and tensile strengths hold significant importance in rock mechanics applications and serve as indispensable parameters in geotechnical designs. Engineering geological studies often focus on unconfined compressive strengths, assuming that the rock is under compaction conditions. However, numerous researchers have emphasized that the tensile strength also plays a crucial role in determining the strength of rock material or rock mass against failure. They have highlighted its significance during the design stage. Unlike uniaxial compressive strength, which has standardized testing methods, rock tensile strength is determined using different test methods. These methods can be categorized into two main classes: direct and indirect tensile tests. Direct tensile tests are conducted along the axis of the specimen using various test apparatus. However, these tests often present significant challenges in obtaining accurate and reliable results. On the other hand, indirect tensile tests offer an alternative approach and are preferred by designers due to their simplicity and ease of application. Among the indirect methods, the most commonly used one is the Brazilian test method. Designers often use the values obtained through indirect methods directly as the tensile strength of the rock material. Alternatively, they may calculate the direct tensile strength (DTS) of the rock using empirical equations proposed in relevant studies.As an alternative to direct and indirect methods used to determine the tensile strength of rock materials, there are studies that propose empirical equations to estimate the tensile strength of rock materials based on various mechanical properties. In these studies, independent variables such as uniaxial compressive strength, point load strength, direct shear strength, and sonic velocity (SV) have been used. In this study, two sample groups, andesite and marl, were subjected to testing to uncover the correlation between DTS and SV. The study utilized a total of 20 samples to analyze this relationship. The individual evaluations of the groups yielded correlation coefficient (r) values of 0.84 and 0.62, respectively. However, when all the samples were collectively analyzed, the r value significantly increased to 0.89 and a very strong positive correlation has been identified between these two parameters.

Keywords: Tensile strength, direct tensile test, sonic wave test, non-destructive test

[1]**Address:** Firat University, Faculty of Engineering, Department of Geological Engineering Elazığ,Türkiye

***Corresponding author**: mkanik@firat.edu.tr

LCA Comparison of Digestate Management

Sıdıka Tuğçe Dağlıoğlu*[1], Melike Güler[2]

Abstract: Digestate is a versatile material with abundant nutrients, organic matter, and moisture, making it highly suitable for various applications in agriculture, soil development, and energy production. The digestate is divided into a liquid and solid phase once it exits the reactor. While the liquid phase can be used in a variety of ways, including fertilizer and the production of algae, the solid phase can be used as compost or fertilizer. The LCA method suggests which scenario should be more environmentally beneficial in this aspect. This abstract investigates different techniques involving digestate utilization as an output, substitution for conventional products, and the application of allocation methods to equitably distribute environmental impacts and benefits. To determine the environmental advantages of digestate usage, critical impact categories like greenhouse gas emissions, energy consumption, and land use are analyzed. The primary objective of this study is to assess and compare the environmental consequences of techniques used to assess both the solid and liquid phases of digestate. To achieve this goal, a comparative analysis is conducted, comparing the effectiveness and environmental impact of the proposed acclimation method to existing approaches. By undertaking this comparative analysis, the study aims to contribute significantly to the advancement of knowledge on the environmental sustainability of digestate, thereby offering valuable insights for optimizing its management and fostering the transition towards a circular economy.This research underlines the significance of incorporating comparative analysis within the life cycle assessment (LCA) framework to identify the most environmentally friendly options for acclimating digestate. Through such analysis, the study advocates the adoption of more sustainable waste management strategies, enhancing the potential for sustainable development and reduced environmental impact.

Keywords: digestate, LCA, sustainability, waste management

[1]**Address:** Ege University, Centre for Environmental Studies , Izmir/Türkiye
[2]**Address:** Ege University, Faculty of Engineering, Izmir/Türkiye

***Corresponding author**: tugce.daglioglu@ege.edu.tr

Acknowledgments
The authors wish to thank TUBITAK under the grant no 121Y488for the financial support of this study.

Investigating Electromagnetic Radiation for Improved Drying Efficiency

Magdalena Zielinska*[1], Zhongli Pan[2], Ragab Gebreil[2]

Abstract: Hot air convective drying (HACD) is time-cunsuming and it may result in low quality of final product. Therefore, the aim of this study is to present a modern method of drying intensification using electromagnetic intensification. The use of microwaves (MW) or infrared raiation (IR) may contribute to reducing time or high product quality. Microwave volumetric heating (MVH) is a method of using microwaves to evenly heat the entire volume of material. During IR heating, the energy can be rapidly transmitted from the emitter to foodstuffs in the form of waves without heating the surrounding environment, leading to low heat losses and reduced damage to product quality. The intensification of heat and mass transfer processes due to microwave or infrared radiation induced heating effect was analyzed. Several innovative processing technologies based on MW or IR heating have been developed for processing high moisture fruits and vegetables covered with thick surface layer which is a barrier to heat and mass transfer processes. They have also been used to produce functional dried snacks from e.g. fermented beetroots. Different types of intermittent drying have been introduced, for example, intermittent microwave convective drying. The regular IR equipment used electricity as the energy source, while the catalytic infrared (CIR) device used natural gas or propane to generate heat energy by the oxidative reactions in the presence of oxygen under the action of a catalyst The drying kinetics, effective moisture diffusivity, drying time, changes in material temperature, specific energy consumption were evaluated under different conditions and optimal conditions were defined. The obtained results allow stating that MW and IR make the drying process more effective and enhance the drying efficiency of final products without significant deterioration of product quality and elevation of material temperature.The applications of new MW or IR based processing technologies should bring significant economic and environmental benefits to the food industry and society.

Keywords: microwaves, electric infrared radiation, catalytic infrared radiation, drying kinetics, drying efficiency.

Acknowledgements: This study was supported by the Development Program of the University of Warmia and Mazury in Olsztyn (Project no POWR.03.05.00-00-Z310/17) and the Polish National Science Center (grant No. 2020/37/B/NZ9/00687, title: The effect of ultrasound, microwaves, infrared radiation and reduced pressure on the dehydration and drying kinetics of beetroots and the University of Warmia and Mazury in Olsztyn (grant No. 16.610.001-110).

[1]**Address:** Department of Systems Engineering, University of Warmia and Mazury in Olsztyn, Olsztyn, Poland
[2]**Address:** Department of Biological and Agricultural Engineering, University of California, Davis, Davis, CA, USA

***Corresponding author**: m.zielinska@uwm.edu.pl

Laboratory-Type Silage Production, Data Acquisition and Control System Sensor Performance Tests; Module-A Example

Fulya Tan[1], Figan Dalmış[2], Ersen Okur[1], İ. Savaş Dalmış[*1]

Abstract: The primary objective of this study is to investigate the performance of sensors integrated into the laboratory-type silage production, data acquisition, and control system. The system, developed through the TUBITAK 1002 project, is a PLC-controlled and multi-sensor system designed to enable numerous studies aimed at improving silage quality.

The system consists of grinding, weighing, silo, data acquisition, and control units. It provides the capability to apply/change/simulate various parameters during the silage production process. The silo unit is composed of two modules, module-A (compression principle) and module-B (vacuum principle). This research focuses on measurements conducted with plexiglass silos (24.5 cm^3) in the module-A unit. Plexiglass silos were equipped with oxygen sensor (±0-100 %), carbon dioxide sensor (0-5000 ppm), temperature sensor (±0.53 °C, -10 – 80 °C), humidity sensor (0-100 %), pH sensor (2-12), and pressure sensor (± 1000 mbar).

The sensors were placed on specially designed silo covers. The research utilized second-crop silage corn material with a dry matter content (DM) of 32%. Four different compression forces were applied during the experiments. Time measurements during silage production (total, cycle, application, waiting times) were defined on the setup page of the main screen. Sensor measurements were recorded as one data per second by connecting them to the data recording unit using 4-20 mA analog sensors. Due to the abundance of data, average values were taken. The data were displayed and monitored on the HMI operator panel programmed with ENDA-V2.0 editor software and stored in Excel format. The measurements were carried out during the silage (aerobic) and post-silage (anaerobic) periods.

According to the research results, it was observed that the six tested sensors performed accurate readings. However, issues related to the oxygen and carbon dioxide sensors were encountered. Due to the difficulty in reading at points with very low oxygen content, it was decided to be supported by controlling with sensors of different types and specifications. During measurements conducted at the compression stage in module-A, the pressure values varied between 0.34-0.67 bar with increasing compression force. The temperature ranged from 16-33 °C, humidity from 60-100 %, pH from 5.8-5.6, O_2 level from 8.1-0 mmol L^{-1}, and CO_2 level from 0-40 mmol L^{-1}. The measured value ranges in silage varied depending on the duration of silage, and accurate measurements were obtained in the desired direction. Sensor placements were updated considering measurement accuracy.

Keywords: Sensor, silage, silage production, simulation.

[1]**Address:** Tekirdağ Namık Kemal University, Faculty of Agriculture, Tekirdağ/Türkiye
[2]**Address:** Tekirdağ Namık Kemal University, Vocational College of Technical Sciences, Tekirdağ/Türkiye
[3]**Address:** Tekirdağ Namık Kemal University, Çorlu Faculty of Engineering, Tekirdağ/Türkiye

***Corresponding author**: idalmis@nku.edu.tr

A Comparative Study on Effects of The Number of Hidden Layers in Classification of Induction Motor Rotor Faults with Deep Neural Network

Hayri Arabaci*[1]

Abstract: Induction motors are widely used in industry. The motors are of solid construction. However, in case of any failure, it causes the system to which it is connected to stop or operate inefficiently. For this reason, it is important to detect the faults of induction motors. In few decades, studies on fault detection have been carried out using many methods in the literature. Motor current is the most used motor parameter for fault detection. In the studies, the frequency spectrum of the motor current is generally used as a feature. Machine learning and especially artificial neural networks are used in fault classification. In recent years, deep learning approaches have started to be used in this field as well. The deep neural network (DNN) comes to the fore in deep learning approaches because it requires less processing capacity. One of the parameters affecting the accuracy of the results obtained with DNN is the number of hidden layers. For this reason, in this study, the effects of the number of hidden layers on classification accuracy in the detection of broken rotor bar faults were investigated. Three different motors for experimental work were operated at rated loads in four different conditions: one broken bar fault, 2 broken bars fault, and 3 broken bars fault. The motor current for each condition was sampled and saved. The frequency spectrum of the currents was obtained using the fast Fourier transform. These frequency spectrums are used as input data for the deep neural network. The network was trained and tested on nine different hidden layers. The obtained test results were compared based on both the detection errors of the healthy motors and the test errors. The test results obtained show that test errors increase in cases where the number of hidden layers is low or high, and it gives the best results when the number of hidden layers is three. The error rate of 0.92% in the optimum network structure showed that the DNN approach could be used for rotor fault detection.

Keywords: Deep neural network, fault classification, hidden layers, induction motor, rotor faults.

[1]**Address:** Selcuk University, Faculty of Technology, Konya/Türkiye

***Corresponding author**: hayriarabaci@selcuk.edu.tr

Understanding the Outlines of Blockchain Integrations for Supply Chain Management in Healthcare Industry

Murat Tahir Çaldağ*[1], Ebru Gökalp[2]

Abstract: Emerging technologies present opportunities to improve systems existing features and add innovative additions. Blockchain as an emerging technology is featured with decentralized structure, transparent way of working, improved traceability and integration of cryptography-based methods for extra security. Since the healthcare systems are required to be safe and fast as possible, blockchain integration is a viable choice. Supply chain management (SCM) of healthcare systems are concerned with the flow of information, product, service and finances throughout the stakeholders that are participating in the creation, distribution and utilization. The increased number of stakeholders on supply chains in healthcare industry arises security, privacy and transparency challenge that can be minimalized with blockchain solutions. The aim of this study is to identify the outlying factors of blockchain integrated SCM systems in healthcare industry and provide a framework for further analysis.

In order to identify the outlying factors a systematic literature review (SLR) is conducted. The results of the review presented fourteen factors that are determined as significant drivers for the subject. The factors identified are compatibility, complexity, perceived benefit, security & privacy, standardization, IT infrastructure, financial resources, human resources & competencies, organizational culture, stakeholder participation & collaboration, top management support, competitive pressure, government support and inter organizational trust.

The research model is established with the identified factors according to Technology-Organization-Environment (TOE) framework. The reasoning behind the selection of TOE framework is to provide a holistic and structural model that is well accepted in the domain. The This study provides insights and determines the outliers with a holistic framework on blockchain integrated supply chains in healthcare industry. Another contribution of this study is to raise awareness by presenting a comprehensive framework for business managers, customers and researchers on blockchain solutions in SCM systems.

Keywords: Blockchain Integration, Supply Chain Management, Healthcare Industry, TOE Framework.

[1]**Address:** Başkent University, Department of Technology and Knowledge Management, Ankara/Türkiye
[2]**Address:** Hacettepe University, Department of Computer Engineering, Ankara/Türkiye

***Corresponding author**: mtcaldag@baskent.edu.tr

Classification of TMJ Sounds by Using One Dimensional Convolutional Neural Networks

Uğur Taşkıran*[1]

Abstract: The Temporomandibular Joint (TMJ) is the joint which connect the jawbone to the skull which are located at each side of the skull. Temporomandibular Joint Disorder (TMD) is generally defined as any problem arising from improper TMJ movement. TMD symptoms generally appear as pain in the jawbone and muscles which controls the jaw movement. One of the diagnose method used by the physicians is to listen to sound produced by the joint during opening and closing of the jaw. In this research, previously collected TMJ sounds are used to diagnose the TMD by using one dimensional (1-D) convolutional neural networks (CNN), a subclass of deep learning algorithms. Results are, then, compared to the results of previously used two deep learning algorithms known as two dimensional CNN generally used for image processing and LSTM network generally used for time series analysis.

Keywords: Temporomandibular Joint Disorder, Sound Classification, Deep Learning, 1-D CNN

[1]**Address:** Selcuk University, Technology Faculty, Konya/Türkiye

***Corresponding author**: utaskiran@selcuk.edu.tr

Classification of Motor Imagery Tasks Using Imaginary Coherence

Fatih Ekrem Onat*[1], Ahmet Ademoğlu[2]

Abstract: Electroencephalogram (EEG) motor imagery signals are widely used for the implementation of brain-computer interfaces (BCI). Recently, functional connectivity measures have attracted attention as it can be used to capture statistical dependencies between EEG channels. However, functional connectivity during motor imagery tasks have not been fully explored. This study aims to use imaginary part of coherency, or imaginary coherence, as a functional connectivity metric for the classification of left-hand/right-hand motor imagery. To that end, multichannel EEG signals from 106 subjects were first decomposed into intrinsic mode functions (IMFs) using multivariate empirical mode decomposition, and imaginary coherence values were calculated between same level IMFs across different EEG channels as a function of time and frequency. Statistical descriptors such as mean, standard deviation and were calculated for resulting connectivity functions for each channel combination as features for model training. Train-test split, leave-one-subject-out, and inter-subject training schemes were used to train the models. With train-test split scheme, best accuracy was achieved with gradient boosting classifier (GBC) as 0.67. With inter-subject training, the average accuracy was obtained as 0.58±0.11 and maximum accuracy for a single subject as 0.95 with GBC. Finally, with leave-one-subject-out scheme, the average accuracy was 0.55±0.09 with maximum accuracy of 0.81 for a single subject using logistic regression model. Results show that while the performance of the models has variability across subjects, imaginary coherence can be used as a feature for distinguishing left-hand/right-hand motor imagery tasks.

Keywords: Motor imagery, Electroencephalogram, Empirical mode decomposition, Functional connectivity, Imaginary coherence

[1]**Address:** Bogazici University, Institute of Biomedical Engineering, Istanbul/Türkiye
Yildiz Technical Univertsity, Faculty of Electrical & Electronics, Istanbul/Türkiye
[2]**Address:** Bogazici University, Institute of Biomedical Engineering, Istanbul/Türkiye

***Corresponding author**: fatih.onat@boun.edu.tr

Evaluation of Gamma Attenuation Coefficient for Monoatomic and Composit Absorbers: Experimental Measurements and XCom data

Boukhalfa-Salma*[1], Khelifi-Rachid[1]

Abstract: Background: Radiation shielding materials are carefully chosen for radiation exposure safety, background decreasing in spectrometry measurement especially in the laboratory, decreasing particle intensity, and also to studying material attenuation proprieties, etc. Objective: In this work, we aim to: (a) evaluate the dependency or not of attenuation coefficient with several parameters including incident source beam energy, and the chemical characteristics for mono atomic and composite target i.e., density and effective atomic number, and (b) comparing the experimental values of the massique attenuation coefficient with the theoretical XCom data. Methods: The experimental values of the attenuation coefficient of five different types of samples were calculated for different gamma rays energies emitted from standard radioactive sources namely Europium-152, Cobalt-60, and Cesium-137, where the experimental setup was based on the transmission method. The employed spectrometer is a 3"×3" scintillator detector. Besides the empirical results, the XCom data is directly used to extract the theoretical values of the massique attenuation coefficient of the studied samples. Results: The obtained results were in good agreement with the theoretical XCom data. The use of monoatomic and composite material allows for several results: (a) high dependency on attenuationcoefficient with incident gamma energy, (b) the linear attenuation decrease for high-density values chemical composition, and sample density. Conclusion: In this study, a procedure for measurement of experimental combined with the theoretical XCom data is followed. The attenuation coefficient increase for low energy values; a high fraction of gammas are attenuated for high-density values. The obtained results will be valuable for the estimation of massique attenuation coefficient, density, and effective atomic number if the data are correlated as a mathematical mapping problem i.e., data extrapolation.

Keywords: Attenuation coefficient, XCom, gamma radiation, Transmission method,

[1]**Address:** Blida -1 University, Faculty of Sciences, Department of Physics, Laboratory of Theoretical Physics and Interaction of Radiations with Matter, Blida /Algeria

***Corresponding author**: boukhalfasalma@gmail.com

Adsorption Based Surfactant Removal - A Case Study in Industrial Wastewater Treatment

Iwona Klosok-Bazan[1], Joanna Boguniewicz-Zablocka[1], Andrea G. Capodaglio[2], Mustafa Karaboyacı[3]

Abstract: The summary text should be written in 10 punto in Times New Roman between 200-500 words with a single line spacing. There will be no Turkish abstract (Özet) in articles written only in English. It should not use Bold and italic spelling. The summary text should be written in 10 punto in Times New Roman between 200-500 words with a single line spacing. There will be no Turkish abstract (Özet) in articles written only in English. It should not use Bold and italic spelling. The summary text should be written in 10 punto in Times New Roman between 250-500 words with a single line spacing. There will be no Turkish abstract (Özet) in articles written only in English. It should not use Bold and italic spelling. The summary text should be written in 10 punto in Times New Roman between 200-500 words with a single line spacing. There will be no Turkish abstract (Özet) in articles written only in English. It should not use Bold and italic spelling. The summary text should be written in 10 punto in Times New Roman between 200-500 words with a single line spacing. There will be no Turkish abstract (Özet) in articles written only in English. It should not use Bold and italic spelling. The summary text should be written in 10 punto in Times New Roman between 250-500 words with a single line spacing. There will be no Turkish abstract (Özet) in articles written only in English. It should not use Bold and italic spelling.

Keywords: 10 punto, Times New Roman, not italic, between 4-6 words.

[1]**Address:** Department of Thermal Engineering and Industrial Facilities, Opole University of Technology, 45040 Opole, Poland.
[2]**Address:** Department of Civil Engineering & Architecture, University of Pavia, 27100 Pavia, Italy
[3]**Address:** Süleyman Demirel University, Engineering Faculty, Chemical Engineering Department, Isparta, Türkiye

***Corresponding author**: J.Boguniewicz-Zablocka@po.edu.pl

Combination of GRAVEL unfolding package and Geant4 simulation for radioactivity monitoring: Application to gamma spectrometry technic

Boukhalfa-Salma*[1], Khelifi-Rachid[1]

Abstract:
Methods: In this work, we consist to combine GRAVEL unfolding package and Geant4 as Monte Carlo code for spectra unfolding and detector response function respectively. Without passing via more literature details, the overlap problem is successfully applied for gamma spectrometry analysis. It consists to restore the incident spectrums counted via calibrated gamma-ray spectrometer. The employed spectrometer was a 3"×3" iodine sodium scintillator detector with an energy resolution equal to 7.18 % at 137-Cesium peak. To assume the convergence of the restored spectrum combined with the existing positive solution, the original spectrum T(E), a minimum value of χ^2 must be obtained by increasing the number of iteration. For this reason, and during the iteration procedure, the algorithm runs the logarithms of K values. Therefore, in each n+1 iteration previous solution is considered. It should be noted that the number of iterations is not arbitrary. In this work, 10.000 iterations were made.

Results: For proposal application for non-identical conditions, i,e., different gamma-ray peaks, the deconvoluted area is defined here by the real distribution of the coming signal to the instrument (detector) without the contributions of the other contributions e.g., background radiation, electronic noise escape peaks etc. After restoring the incident spectrum, the specific activities can easily be calculated where the restored area describes the real activity of the radionuclide without the contribution of other radionuclides.

Conclusion: The specific activities of natural radionuclides namely 238-Uranium, 232-Thorium, and 40-Potassium were determined via poor energy resolution gamma spectrometry technic. The combination of the GRAVEL unfolding algorithm and Geant4 code is powerful solution for poor resolution detector.

Keywords: Gamma Spectrometry, GRAVEL, Monte Carlo, Uranium, Potassium, Thorium.

[1]**Address:** Blida -1 University, Faculty of Sciences, Department of Physics, Laboratory of Theoretical Physics and Interaction of Radiations with Matter, Blida /Algeria

***Corresponding author**: boukhalfasalma@gmail.com

Integration of Renewable Energy Sources in the SMART

Vehebi Sofiu[1], Sami Gashi[1], Besa Veseli[1], Faton Maloku[1], Muhaxherin Sofiu[1]

Abstract: The demands of the global market for environmental protection have significantly increased the need for our country to follow the basic EU legislation for climate change, renewable energy and simplified regulation on the implementation of policies according to the European directives for generation of electricity. The challenge of this work is the adaptation of the current network with new generating capacities that come from alternative energy. The integration of the advanced network increases the adaptability of the modern network and the functionalization of effective generators with a reliable consumption system. Part of this work is the research of future visions related to the optimization of user power and planned control with the mix of generating energy sources in the distribution of network. The integration of the renewable energy network and the modernization of the SMART network is dedicated to being the bearer of the development and follow-up of technological steps to the constant threats to sustainable development. The objective of this work is the development of new economic frameworks that include services and the lowest costs for energy facilities related to the efficiency and effectiveness of technological users. Simulative modulation improves the reliability of the energy transition with a range of the best services, rather than focusing on the use of traditional fossil fuels.

Keywords: RES, distribution network, environment, strategies, innovation of technologies.

[1]**Address: U**BT- Higher Education Institution, Faculty of Engineer of Energy, Kalabria 65, 10000, Pristina, Kosovo

***Corresponding author**: sami.gashi@ubt-uni.net

Hygienic Surfaces and the Evolution of House Applications with Smart Materials: A Comprehensive Overview

Halit Coza*[1], Mahmed Sari Njjar[2]

Abstract: This paper explores two revolutionary trends reshaping interior design and construction: hygienic surfaces and smart materials integration in house applications. With a growing focus on health, cleanliness, and sustainability, these innovative approaches have the potential to redefine living spaces, creating safer, more efficient, and adaptable environments for occupants. The first part examines hygienic surfaces, engineered materials and coatings designed to resist dirt, grime, and microbial growth. They play a vital role in maintaining higher hygiene standards, especially in critical spaces like hospitals, clinics, and kitchens. Antimicrobial coatings containing silver ions or copper effectively inhibit bacteria and microorganisms, while non-porous tiles and laminates facilitate easy cleaning by preventing dirt adherence. Additionally, self-cleaning surfaces, employing photocatalysis or hydrophobic properties, ensure a more sterile environment by breaking down and repelling dirt and grime. The second part delves into smart materials integrated into house applications, capable of responding to external stimuli and adapting their properties accordingly. Smart windows, for example, adjust tint or transparency based on light conditions, regulating indoor temperature and reducing energy consumption. Self-healing materials extend the lifespan of household items by autonomously repairing minor damages or scratches. Shape memory alloys offer efficient space utilization and customization in adaptive furniture and structures. Smart lighting systems adjust brightness and color temperature based on occupants' preferences, enhancing comfort and well-being. The integration of sensing materials embedded with advanced sensors enables real-time monitoring of temperature, humidity, and occupancy, facilitating better indoor environment control and energy management. The confluence of hygienic surfaces and smart materials presents a transformative opportunity for the evolution of house applications. Combining these technologies enables homes to foster healthier living environments, reducing infection risks, and enhancing overall quality of life for residents. As technology continues to advance, further groundbreaking innovations are expected to redefine the way we design, build, and interact with our living spaces, offering unprecedented levels of safety, sustainability, and comfort.

Keywords: Hygienic Surfaces, Antimicrobial Coatings, Interior Design, Health, Indoor Environment

[1]**Address:** Pamukkale University, Faculty of Architecture and Design, Department of Architecture, Denizli, Türkiye.
[2]**Address:** Pamukkale University, Faculty of Technology, Department of Biomedical Engineering, Denizli, Türkiye.

***Corresponding author**: hcoza@pau.edu.tr

The Impact of Electric Vehicles on Environment, Energy Systems, and the Economy

Ahmad Al-Sarraj*[1], Fatih Yigit[2], Ahmet Kabul[2]

Abstract: Energy efficiency is becoming more important for many equipment and devices that are used to provide people with comfort as conventional energy resources are depleting and environmental harm from their use is growing. Utilizing domestic and renewable energy sources has replaced energy efficiency as the fundamental policy of nations. Electric vehicles are now widely used, and many nations with environmental concerns have boosted their incentives, which may have significant environmental, energy, and economic repercussions. Countries have set a variety of goals in their energy policies for a more habitable environment and a reduction in their reliance on foreign energy sources, and steps are being taken in this regard. Countries promote the usage of electric cars while attempting to limit the environmental harm caused by transportation. This study discusses the effects of electric vehicles on the environment, energy systems, the economy, and the employment market. The widespread usage of electric vehicles has the potential to have a positive influence on the environment by lowering greenhouse gas emissions and enhancing air quality. Analysis of the effects of EVs on energy systems includes consideration of topics including the rise in electricity demand, grid integration, and charging infrastructure. The effects on energy distribution and consumption are also covered. Regarding the economy, the spread of electric vehicles has the potential to open up new job opportunities in the automotive industry. In this framework, topics including home production, employment expansion, and industry restructuring are considered. Finally, it should be underlined that policies and incentives are crucial to the spread of EVs. There are suggestions for effective policy changes, infrastructural upgrades, and international cooperation tactics. This report is a crucial resource for comprehending the difficulties and possibilities that businesses may encounter when they make the switch to electric vehicles. Electric vehicles can help nations move closer to having a sustainable transportation system. However, further analysis is needed, as well as changes to policy.

Keywords:. Electric vehicles, energy efficiency, environmental impact, sustainability.

[1]**Address:** Ministry of higher education and scientific research, consultancy Department, Baghdad/IRAQ
[2]**Address:** Isparta University of Applied Science, Faculty of Technology, Isparta/Türkiye

***Corresponding author**: ahmed.emad846@gmail.com

Characteristics of Wood Particles Recovered from Post-Consumer Windows and Doors Joinery

Anita Wronka*[1], Grzegorz Kowaluk[1]

Abstract: Wooden doors and windows recycling plays a crucial role in promoting sustainability and reducing the environmental impact of the construction industry. Recycling these products allows for the efficient reuse of valuable wood resources, minimizing the need for fresh timber extraction and reducing waste, for example with the purpose of wood chips production for the particleboard industry. Using post-consumer wood from window and door joinery is often not fully utilized due to the variety of coatings and joints which are used on these materials. Due to the fact, that the coatings on the wood need to be stripped away before this wood can be recycled, it can be expensive. There are several volatile compounds which are contained in varnishes and oils that are released when such wood is burned. Based on the characterization, we can determine how varnish, paint, or veneer influence the geometry of particles after industrial cutting. In order to characterize the recycled wood raw material, tests such as sieve analysis and fractional composition of the particles, water absorption, as well as Total Volatile Organic Compounds (TVOC) emission will be carried out. Based on the results of this study, a decision can be made about how to reuse raw wood most effectively. In addition to the environmental benefits, wooden doors and windows recycling also offers economic advantages. Recycling creates job opportunities in the collection, processing, and manufacturing sectors. It contributes to a circular economy model, where materials are kept in use for as long as possible, reducing the need for resource extraction and supporting local industries.

Acknowledgement: The presented study was completed within the activity of the Student Furniture Scientific Group (Koło Naukowe Meblarstwa).

Keywords: recycling, upcycling, particleboard, post-consumer, window, circular economy

[1]**Address:** Department of Technology and Entrepreneurship in Wood Industry, Institute of Wood Sciences and Furniture, Warsaw University of Life Sciences – SGGW, Nowoursynowska St. 159, 02-776 Warsaw/Poland

***Corresponding author**: anita_wronka@sggw.edu.pl

Application of Post-Consumer Wood-Based Composites for Liquid Biofuels Purposes

Aneta Skręta[1], Jan Szadkowski*[2]

Abstract: The development of the economy involves an increasing demand for 'basic' raw materials such as metal ores, wood, fibre materials, etc., which have limited capacity or resources in the Earth's crust. Industrial development in the 20th and 21st centuries will be confronted with the need to switch to other raw materials (plastics) or to reuse a raw material after its useful life or waste material. The repeated use of biological raw material such as wood or its processing by-products is associated with a decrease in the mechanical parameters of the raw material used in industry, an increase in the mineral impurities content and hindered processing of the raw material after a certain time (micronisation of the structural components of the biomass occurs). Therefore, such biomass should be removed from the production process, e.g. in furniture factories or paper mills, and used in another industry. The aim of this study was to use post-consumer biomass in liquid biofuel (bioethanol) technology. For ethanol production, simple sugars are used, which are converted to ethanol and carbon dioxide in a biochemical process by yeasts or bacteria. In order to verify the efficiency of the process, the chemical composition of the post-consumer biomass will be characterized to determine the content of sugars, lignin, hemicelluloses and associated substances. Enzymatic hydrolysis of the biomass will be carried out to verify the potential of the post-consumer biomass as a feedstock for liquid biofuels.

Acknowledgment: This project was completed by the activity of the Chemical Wood Technology Student Scientific Group (Koło Chemiczne Technologów Drewna). The part of the presented study was completed thanks to the activity of the Student Furniture Scientific Group (Koło Naukowe Meblarstwa).

Keywords: bioethanol, woody biomass, post-consumer material, hydrolysis, chemical composition

[1]**Address:** Faculty of Wood Technology, Warsaw University of Life Sciences – SGGW, Warsaw, Poland
[2]**Address:** Department of Wood Science and Wood Protection, Institute of Wood Sciences and Furniture, Warsaw University of Life Sciences – SGGW, Warsaw, Poland; ORCID 0000-0002-3884-7392

***Corresponding author**: jan_szadkowski@sggw.edu.pl

Empowering Sustainable Urban Transformation in developing societies: Lessons from the "Smart City Kosova" Initiative

Shqiprim Ahmeti *[1], Besa Veseli [1]

Abstract: The "Smart City Kosova" initiative, a collaborative effort aiming to involve five international universities, seeks to drive sustainable urban development in Kosova's municipalities. By leveraging digital technology and interdisciplinary expertise, the project aims to create a National Strategy for Smart and Sustainable Urban Development, as well as Smart City Strategies for seven major municipalities in Kosova. These strategies encompass various dimensions of urban life, from sustainable living and efficient resource use to participatory governance and improved mobility. The initiative recognizes that Smart City development is complex and context-specific, necessitating customized solutions for each municipality. The project spans three distinct phases, involving data collection, stakeholder engagement, and the formulation of comprehensive strategies. These strategies address both technological and non-technological aspects, with action plans devised to achieve tangible outcomes. The impact of the initiative is broad, involving planning experts, young professional employment, international academic collaboration, and expert guidance. Ultimately, the goal is to transform these municipalities into interconnected smart cities, fostering holistic development, citizen well-being, and environmental sustainability. The project signifies a significant step toward addressing urbanization challenges and promoting a brighter, more interconnected urban future in Kosova. This conference paper tends to share a real-life experience of a long-term initiative for making cities of a society in transition smart, sustainable and climate neutral. The paper adopts a deductive method to explore the conceptual framework of smart cities and sustainable development. It analyzes various dimensions and domains of smart urbanization, considering the intricacies of contextual relevance. This analytical foundation is followed by an exploration of the cities and municipalities involved in the project, shedding light on their unique profiles and challenges. Additionally, the paper delves into specific suggestions and concrete projects proposed by the initiative's authors, illustrating the tangible outcomes of the project's meticulous planning and execution.

Keywords: Smart City Kosova, sustainable development, digital technology, interdisciplinary collaboration, Smart City Strategies, climate-neutral cities

[1]**Address:** Institution of Higher Education, UBT-College, Kosovo

***Corresponding author**: shqiprim.ahmeti@ubt-uni.net

Analysis of The Efficient Recover of Li And Cobalt Metals From The Spent LIB Based on A Case Study

Joanna Boguniewicz-Zabłocka [1,*], Mustafa Karaboyacı [2] and Domenico Guida [3]

Abstract: From the point of view of environmental protection, the recovery of major components or valuable resources and the preservation of natural resources through the recycling of used LIBs is very desirable and its importance will grow in the future. To achieve future e-waste management policy goals, efficient recycling systems based on metals recovery should be used more widely. In this work the review of the current status of recycling techniques and technologies concerning spent lithium-ion batteries (LIBs) is presented. The most common treatment processes include pyrometallurgy, hydrometallurgy, and biometallurgy. The single recycling processes were summarized and some examples of typical combined processes were described. The case study from Italy and Poland region shows that there is great potential for investors interested in recovering li and cobalt from spent lithium-ion batteries (LIBs).

Keywords: Lithium-ion battery recycling, environmental protection, resource recovery, sustainable e-waste management, metal recycling technologies

[1]**Address:** Department of Thermal Engineering and Industrial Facilities, Faculty of Mechanical Engineering, Opole University of Technology, Prószkowska 76 Street, 45-758 Opole, Poland
[2]**Address:** Süleyman Demirel University, Engineering Faculty, Chemical Engineering Department, Isparta, Turkiye
[3]**Address:** Departament of Industrial Enginering, University of Salerno, 84084 Fisciano, Italy

***Corresponding author**: j.boguniewicz-zablocka@po.edu.pl

Estimating health exposure to nitrates (V) from drinking water - a case study

Iwona Kłosok-Bazan*[1], Izabela Zimoch[2]

Abstract: Nitrates in water occur due to fertilization of fields in agriculture, due to leaking septic tanks, and in extreme cases due to dumping of waste with high concentrations of nitrates from factories or through municipal sewage. The presence of nitrates in water is harmful to human health. Studies conducted indicate the occurrence of a number of adverse symptoms in both animals and humans exposed to the consumption of water with elevated nitrate and nitrite content. Nitrates (V) are not toxic compounds. Their harmfulness is due to their oxidizing properties and ability to reduce to nitrate (III). They can cause oxidation of hemoglobin to methemoglobin (anemia), oxidation of vitamin A, the deficiency of which causes a number of dangerous disorders, impaired utilization of nutrients such as proteins and fats, and failure to absorb B vitamins. Nitrite poisoning is particularly dangerous for young children, mainly infants, as it can cause methemoglobinemia. Therefore, the WHO recommended nitrate (V) level is 50 mg/L. The article will present an estimation of health exposure to nitrate (V) delivered with water to consumers in a small distribution system exploiting Quaternary groundwater resources. The average daily production of water in 2017-2022, varied from 55 m^3 to 80 m^3. The analysis of the dynamics of changes in the multiplicity of nitrate concentrations in water for years 2018 – 2023, shows a clear upward trend. According to the ongoing water quality monitoring, nitrate concentrations of 45.6 mg/L were recorded in April 2018, and 48.3 mg/L in December 2019. Another test performed in March 2021, showed nitrate concentrations close to the maximum allowable value in drinking water, and was then 49.8 mg/L. In March 2022, more than 50% exceedance of the parametric value was recorded, the nitrate concentration was then 75.8 mg/L. The health risk of nitrates (V) included in tap water was assessed by comparing the acceptable daily intake of ADI (Acceptable Daily Intake) with the value of the estimated daily intake (EDI). Based on the results of conducted analyses, the following conclusions were drawn: the water in the analyzed system, despite the exceedance of parametric values, does not pose a potential health risk for adults - the calculated limiting safe concentration of nitrates in drinking water for adults is the level of 105 mg/L, for the adopted ADI value of 3 m /kg body weight per day and the weight of an adult of 70 kg. Taking into account the guidelines and recommendations of the WHO, which allows the temporary supply of water with a nitrate concentration of 100 mg/L, the water in the analyzed system can be used for the preparation of food for newborns and infants under 3 months of age. Nevertheless, information campaigns should be conducted among pregnant women and mothers of children under 3 years of age on the potential health risks of exposure to methemoglobinemia. This campaign should include a piece of information on the orders to use products with low nitrate and high antioxidant content in the diet. n the situation of nitrate concentrations in the water above 100 mg/L (result repeated, within two days) in this case, to ban on the use of water for children's consumption, should be implemented. And in the situation of the occurrence of contamination in the water at the level of the calculated limit the safe concentration of nitrates (V) in drinking water for adults above 105 mg /L for a period of 10 days - absolutely ban on drinking water must be obligatory.

Keywords: drinking water, nitrates (V), health exposure, risk assessment.

[1]**Address:** Opole University of Technology, Faculty of Mechanical Engineering, Department of Thermal Engineering and Industrial Facilities, Mikolajczyka 5, Opole 45-271, Poland
[2]**Address:** Silesian University of Technology; Faculty of Energy and Environmental Engineering; Institute of Water and Wastewater Engineering, Konarskiego 18, Gliwice 44-100, Poland

***Corresponding author**: i.klosok-bazan@po.edu.

Extended Reality as a Visual Tool for Architectural Fabrication and Inspection

Faruk Can Ünal

Abstract: This study explores the transformative role of extended reality as an innovative visual tool within the processes of architectural fabrication and inspection. By seamlessly merging virtual and physical environments, extended reality offers architects, designers, and engineers an unprecedented level of visualization, interaction, and quality control throughout the architectural lifecycle. This study presents the potential of extended reality in architectural fabrication and inspection through case studies, technological explorations, and critical analysis. The integration of extended reality in fabrication processes aids in streamlining workflows, reducing errors, and optimizing material usage, ultimately leading to more efficient and sustainable construction practices. It enables real-time overlay of digital information onto physical structures, facilitating on-site comparisons between digital models and actual construction progress for architectural inspection. This real-time alignment enhances error detection, expedites issue resolution, and ensures adherence to design specifications, thereby elevating the overall construction quality. This study highlights the convergence of digital visualization and tangible craftsmanship, and demonstrates how extended reality's immersive capabilities provide users with a comprehensive toolkit to push the boundaries of manufacturing, enhance collaboration and increase the precision and excellence of the product. The digital transformation of architecture has blurred the boundaries between the physical and virtual realms, and the integration of extended reality in architectural fabrication and inspection processes signifies a paradigmatic shift in the field.

Keywords: Extended reality, visual tool, architectural fabrication, architectural inspection.

Address: Yeditepe University, Faculty of Architecture, Department of Architecture, Istanbul/Türkiye

Corresponding author: farukcan.unal@yeditepe.edu.tr

An assessment of over-tourism risk in Safranbolu, Turkey

Büşra Nur Gündoğdu*[1], Sırma Turgut[2]

Abstract: While tourism can be seen as a way to integrate historical sites with contemporary life, it has become increasingly clear that this seemingly innocent activity has negative effects, especially when it comes to historical sites that have turned into popular tourist attractions. Overtourism is a global serious threat to the conservation of the underlying values and Outstanding Universal Values of heritage sites. This worry has grown, particularly in light of the growing number of visitors and the uncontrolled tourism development. Safranbolu as a World Heritage Site since 1994, has been a popular tourist destination for decades, thanks to its authentic architectural fabric and well-protected traditional Ottoman houses. As a matter of fact, the number of tourists visiting between 2000 and 2018 has increased almost 7 times and Safranbolu is confronting an enduring continuous trend of tourism growth. This study aims to evaluate the over-tourism risk in Safranbolu, Karabuk in the context of Butler's (1980) Tourism Area Life Cycle and Doxey's (1975) Irritation Index approaches. To do this, using qualitative and quantitative methods, the data obtained from secondary documents on tourism development, tourism statistics, and the results of the survey conducted with 250 participants in April 2019 are evaluated together. The findings demonstrate that tourism in Safranbolu is still in a development stage and residents have mixed feelings about how they are affected. This research highlighted that there is a potential of overtourism but that it has not yet turned into a significant issue.

Keywords: Over-Tourism, Heritage, Historical Sites, Residents, Doxey, Butler

[1]**Address:** Republic of Turkiye Ministry of Culture and Tourism, Istanbul/Türkiye
[2]**Address:** Yıldız Technical University, Faculty of Architecture, Department of Urban Planning, Istanbul/Türkiye

***Corresponding author**: nur.gundogdu@std.yildiz.edu.tr

The Enneagram and Conflict Resolution in the New Design of Universal Systems in the Era of Digital Nomadism

Özgü Hafızoğlu*[1]

Abstract: Every year and at every age humans move. From one idea to another, from one house to another, from one school to another, from one job to another, from one city to another, from one country to another, from one culture to another. No time is the Digital Nomad era more true than today. Covid 19 caused the biggest mass movement and made every country, family, culture and workplace rethink new parameters for how people live and work causing an explosion in digital nomadism that creates digital, physical and transitional conflicts all over the world individually or socially since World War II. Natural and artificial pressures like climate change and international crises are also huge emerging factors in the Digital Nomad era, as people move to adapt to the changing ecological environment. In this paper, first, the main theme of conflict resolution emerges from the above mentioned changing ecological environment. Secondly, divergent identities of four generations- Boomers, Gen X, Millennials and Gen Zers - and how these hard-wired systems of brains can affect, enhance, impair and change their adaptation in this new era to ignite a world demanding sustainable solutions that shifts to implement lasting changes through unity is discussed. Finally, the individual and social behavioral types in the pre/post-pandemic world are addressed through the Enneagram. As the era of the digital nomad is operating through cognitive, physical and emotional transitions, the design and management logic of this emerging world is appearing with conflicts like precise and fuzzy, interconnected and in real time, asynchronous and synchronous. These conflicts are being addressed through the Enneagram to ignite and unite humans and organizations. On a generational basis, Baby Boomers, GenX, Millennials and now Gen Zers are living different inputs to shape and reshape the world. They all have a different generational characteristic that can -be explained with Enneagram strategies. Given the monumental post-pandemic paradigm shift of Covid 19, generational identity is a proven design and management parameter that can help individuals and organizations identify strengths and weaknesses and become more efficient and productive as mankind is forced to adapt under stress to new demands on health care, financial, industrial construction and government systems. Given this paradigm shift through the Enneagram strategies, identifying individual, organizational and generational skills can show how to utilize divergence for a better future. The divergence within and between four generations will show three hard-wired syndromes (Flight, Freeze, Fight) compose the obstacles that can cause resistance to change, resistance to adapt and resistance to evolve. As a result the divergence can be woven together to reduce conflicts to figure out the most efficient solutions to global problems in the new emerging digital world.

Keywords: Unity, Conflict Resolution, Design Management, Generations, Enneagram, Digital Nomadism

[1]**Address:** Pamukkale Universitesi, Faculty of Architecture and Design, Denizli/Türkiye

***Corresponding author**: drozgutr@gmail.com

Prioritizing Port`s Development Direction by Analytic Heirarchy Process Method

Deda Đelović*[1]

Abstract: Ports are no longer the simple maritime services providers of the past. They are multimodal transport and logistics centres, focal points of leisure and tourism and hubs for sustainable industry and clean energy (ESPO, 2021). They have a huge potential for job creation and investment. The European Commission has estimated that by 2030 between 110 000 and 165 000 new jobs can be created in ports (European Commission, 2013). Pre-existing megatrends – generators of port development – are (UNCTAD, 2021): geopolitical, technological, and environmental. In the recent technology-in-maritime report by the American Bureau of Shipping (ABS) (ABS, 2022) future maritime technologies are organized into three major categories or trends: digitalisation (AI, digital twins, autonomous operations, …), applied research (new materials, green ecosystems, blue economies, …) and clean energy transition. As well, Deloitte Global Port Advisory, in their Study published on 2020, recognized following key development trends in the port sector in the time horizon to 2030: Space productivity; Port infrastructure; Changes in supply and demand; More technological solutions; More cyber risk; Less focus on physical infrastructure investments; Shift from big, bigger, biggest to green, greener, greenest; Sustainability; etc.
There are different important deadlines wich ports have to take into account when creating development strategies/plans. For example, in line with the upcoming new Alternative Fuels Infrastructure Regulation, 2030 will be the deadline for having shore side electricity infrastructure in place (ESPO, 2023). The transition to sustainable ports, digital nodes, and energy hubs requires radical system-led changes based on new knowledge and innovation. All previously mentioned require extensive innovation and transformational capabilities in ports (Lind, 2023). Realising a modal shift to more sustainable transport modes is one of the domains in which digitalisation can be an enabler, improving the integration of the freight transport system (European Environment Agency, 2022). Acting in accordance with new trends/demands have to be followed by huge investments. On the https://maritime-executive.com/ is available information that, for example, The Biden Administration in USA announced an additional $4 billion in funding for new programs that are designed to support the electrification of U.S. ports as well as to reduce emissions to air in the ports. If all mentioned is taken into consideration, it becomes clear how challenging is proper definition/selection of development priorities of a port. After a theoretical analysis of port development trends, in this paper is proposed an approach to selecting port development priorities based on Analytic Hierarchy Process (AHP) method. Object of the research is Port of Bar (Montenegro). Selection od development priorities is done having as the base following four criteria: level of revenues/profit, level of productivity, contribution to safety/security in the port, contribution to envirnmental protection in the port. AHP Hierarchy framework used was a three level model: “level 0” – goal; “level 1” – criterion; “level 2” – choice.

Keywords: Port Development Trends, Analytic Hierarchy Process.

[1]**Address:** Deda Đelović, Port of Bar, Obala 13.jula 2, 85 000 Bar, Montenegro.

***Corresponding author**: djelovic.deda@gmail.com

Incorporation of Different Anthocyanin Sources to SLA Resin at Different Solvent Compositions: An Optimization Study

Munevver Beyza Karabiyik[1], Kardelen Sena Kirdi[1], Sevil Cikrikci Erunsal*[1]

Abstract: In recent years, 3D printing (3DP) has gained so much attention in different fields, from biomedical to food applications. Since it enables us to fabricate complex geometries, manipulate surface area or formulate personalized dosages, different printing techniques might be used for personalized, efficient, and economical productions. One of the examples from the food side could be the fabrication of colorimetric indicators. Printing pH-sensitive indicators at varying dimensions and shapes is possible depending on your demand. Stereolithography (SLA) is one of the printing techniques based on photopolymerization reaction using laser light and liquid photosensitive resin. Although commercial SLA resins are already available in the markets, they do not show any sensing or other kind of properties. Under the light of these findings, this study aims to add a colorimetric response functionality to regular SLA resin during environmental changes. For this purpose, different kinds of anthocyanin (ACN) sources (black carrot powder, red beet powder, red cabbage juice) were added to SLA resin (clear color) at varying ACN: SLA resin ratios (20:80, 50:50, 80:20) to examine their color intense after printing. At this stage, they were printed only in single rectangular form (1x0.5x0.1 cm). Additionally, the ethanol: water ratio (20:80, 50:50, 80:20) was changed during sample preparation to check the solvent effect on the color. The results showed that the highest color intensity and stability were observed in the samples prepared by 2% (w/w) black carrot solution (50:50 ethanol: water mixture) combined with 50:50 ACN: SLA resin. This outcome is the starting point for designing anthocyanin-added SLA resin-based indicators. In this way, they could be used as a sensor in various food products to monitor food freshness. As a further step, they need to be investigated for pH sensitivity (changing their colors) at different conditions, because environmental pH differs during food spoilage, and printed samples might be indicative of such changes by giving a color response.

Keywords: SLA resin, 3D printing, anthocyanins, indicator, color

[1]**Address:** Konya Food and Agriculture University, Faculty of Engineering and Architecture, Konya/Türkiye

***Corresponding author**: sevil.cikrikci@gidatarim.edu.tr

Note: This study is funded by TUBITAK 2209-A as a student project.

Food Waste Management

Elvin Shaliyev*[1]

Abstract: Food engineering plays an important role in food production and processing. However, the food waste generated during these processes poses a major problem both environmentally and economically. This article addresses the importance of effectively managing food waste in the field of food engineering.

Sources of food waste vary from the consumer level to the production stage. This article examines the causes and formation processes of food waste in detail. It also addresses strategies to reduce food waste by designing and improving food production processes. Management of food waste is of great importance in terms of sustainability and environmental protection. This article discusses reducing the environmental impact of food waste through methods such as recycling, composting and energy production. It also addresses the impacts of reducing food waste on food safety and economic efficiency.

This study emphasizes the importance of food waste management in the field of food engineering and indicates the necessity of focusing on this issue in terms of environmental sustainability, economic efficiency and food safety. Food engineers play an important role in effectively managing food waste, and increasing work in this area could be a critical step for the future of the food industry.

Keywords: Food waste, sustainability, utilization, recycling

[1]**Address:** AQTA, Food Safety Agency of the Republic of Azerbaijan

***Corresponding author**: elvin.shaliyev@gmail.com

Analysis of Parameters of Treated Effluents from On-Site Sewage Treatment Plants

Monika Pawlita-Posmyk[1], Małgorzata Wzorek*[2]

Abstract: Domestic sewage treatment solutions such as septic tanks or on-site wastewater treatment plants are widely favoured by homeowners, especially in areas where conventional sewage system connections are not feasible. This is especially relevant to rural areas characterized by dispersed settlements, situated on hilly and mountainous terrains. The operation of on-site sewage treatment plant must ensure the preservation of the natural environment, and the parameters must adhere to the legal standards. To assess the environmental impact, a specific on-site sewage treatment plants were selected for evaluation. Over the course of one year, parameters in treated effluents, including total suspended solids, COD_{Cr}, and BOD_5, were closely monitored. The year-long monitoring process provided valuable insights into the plant's effectiveness in meeting environmental protection goals and complying with regulatory standards. The studies revealed that the tested on-site sewage treatment plants operated according to the manufacturer's specifications and met the requirements defined by the law. It can be concluded that despite testing several on-site sewage treatment devices, each of them operates differently. However, the most crucial aspect is that their operation is correct. The variations in the operation of domestic treatment plants stem from factors such as the quantity and quality of sewage directed to the treatment plant, as well as the adherence to proper usage rules by the system's users.

Keywords: on-site sewage treatment plant, treated effluents, environment, parameters

[1]**Address:** Opole University of Technology, Faculty of Mechanical Engineering, Opole/Poland
[2]**Address:** Opole University of Technology, Faculty of Mechanical Engineering, Opole/Poland

***Corresponding author**: m.wzorek@po.edu.pl

Latest Developments and Applications in The Field of Biotechnology

Kamila Sobkowiak[1*]

Abstract: In our rapidly developing technological world, the concept of biotechnology has an important place. Biotechnology can be defined as a branch of science that aims to manipulate the genes, cells and biological processes of organisms by bringing together life sciences and technology. This discipline enables revolutionary innovations in many fields such as agriculture, medicine, food industry, energy production and environmental protection.
The basis of biotechnology is to understand the structure and functioning of gene stone materials (DNA and RNA). Genetic science aims to discover the genes that determine the characteristics of organisms and to give new features to living things by manipulating the genes through this information.

For example, in the agricultural field, biotechnology aims to obtain more durable, productive and nutritious products by changing the genes of plants and animals. Thanks to biotechnology in the field of medicine, the diagnosis and treatment of many diseases have become more effective. mRNA vaccines during the COVID period can be given as an example of biotechnological development. Bioenergy is one of the most important contributions of biotechnology in the energy sector. Renewable energy resources such as biomass energy, biogas and biohydrogen are developed with biotechnology.

Despite all these positive aspects, advances in the field of biotechnology also raise ethical and social problems. Issues such as possible risks of genetic changes and confidentiality of genetic information are the subject of debate.

In this study, biotechnology studies on agriculture, medicine, food and environment were compiled and important benefits that will increase our ability to control the forces of nature were determined. However, the points where these powers should be used consciously and ethical rules should be taken into consideration are also stated.

Keywords: Biotechnology, food, agriculture, medicine, environment, ethics

[1]**Address:** Lodz University of Technology, Chemistry Faculty, Lodz/Poland
***Corresponding author**: camilla.river.50@gmail.com

Influence of Sr doping on the microstructure, morphology and optical properties of ZnO thin films prepared by SILAR method

Mokrani Nourelhuoda[1,*], Ghettaf Temam Elhachemi[1], Ben Temam Hachemi[1], Barkat Hadjer[1]

Abstract: The present study focused on the properties of Sr-doped ZnO thin films using the successive ionic layer adsorption and reaction (SILAR) method.The X-ray diffraction results show that the ZnO and Sr-doping ZnO samples exhibit hexagonal wurtzite structure having preferential growth along the (100) plane.The maximum crystallite size of 54 nm was observed for Sr-doping ZnO 3 wt. % sample.The SEM analysis revealed that the samples exhibit agglomerated grains and the EDX spectrum of the Sr-doping ZnO(3 and 7wt. %) samples showed the presence of Zn, Sr, and O elements.The UV–vis transmittion spectrum of the Sr-doping ZnO 7 wt. % sample revealed that it has higher tansmittion in the UV region. Finaly, Sr-doping has a significant impact on the physical and chemical properties of SILAR-deposited ZnO films.

Keywords: Sr-ZnO, thin films, SILAR, XRD, UV-vis..

[1]**Address:** Physics Laboratory of Thin Layers and Applications, Biskra University, BP 145 RP, Biskra 07000, Algeria

***Corresponding author**: nourelhouda.mokrani@univ-biskra.dz

Computer Science and Informatics: Journey from Past to Present and Future

Berkan Başa*[1]

Abstract: This paper presents a comprehensive review of the past, present and future of computer science and informatics. Computer science represents one of the most important technological advances in human history, and advances in this field have transformed and shaped the way we live on Earth. The foundations of computer science were built on mathematical logic and theories of computation. In the 19th and 20th centuries, computers started with mechanical devices and over time electronic computers were developed. During the Second World War, the first computers such as the ENIAC appeared. Then, with revolutionary advances in programming, personal computers and the software industry emerged. Today, computer science is in every aspect of our lives with technologies such as smartphones, laptops, cloud computing and data centers. The internet has revolutionized communication and information flow between people. Areas such as Big Data analytics, artificial intelligence and machine learning have had a huge impact on business, medicine, transportation and many other sectors. The future of computer science and computing looks very exciting. Technologies such as artificial intelligence, autonomous vehicles, the Internet of Things (IoT), quantum computing, etc. will cause major changes in the coming years. Artificial intelligence will enable the development of systems with human-like thinking abilities, while IoT will make our lives smarter and more efficient with increased communication between objects. Quantum computers, on the other hand, have great potential to solve problems of complexity that traditional computers cannot. In conclusion, the field of computer science and informatics is rapidly evolving and has a profound impact on our world. This journey from the past to the present will lead to even more exciting technologies and innovations in the future. Keeping abreast of changes in this field and understanding how to use these technologies is an important requirement for individuals and societies.

Keywords: Computer Science, History of Informatics, Technology Development, Artificial Intelligence, Data Analytics, Internet of Things, Future Technologies

[1]**Address:** Prizren University, Faculty of Computer Science, Prizren, Kosovo

***Corresponding author**: besaberkant@gmail.com

Effects of computer science and informatics on the education system

Akif Gaş*[1]

Abstract: In the era of digital transformation, computer science and informatics has become an important element in the field of education. Technological devices and the internet, which have become an integral part of students' daily lives, should be integrated into the educational process. Computer science and informatics help students understand and use these technologies effectively. Interactive educational tools make students more interested in the lessons. This contributes to making learning processes more effective. Computer science and informatics education provides students with important digital skills. These skills are of great importance not only in education but also in the business world of the future. Training educators in computer science and informatics contributes to the effective use of this field in classrooms. School administrators should also be informed about updating the technological infrastructure and using resources effectively. Distance education has become increasingly important, especially due to global events. Computer science and informatics help in the successful implementation of such educational methods. Students who master technology can compete in the workforce of the future. Computer science and informatics education prepares students for this and increases their ability to adapt to new technologies. As a result, computer science and informatics in education improves student achievement, makes teachers' and administrators' jobs easier, and helps build the skills needed for the future workforce. In the era of digital transformation, these fields should become a fundamental part of the education system.

Keywords: Educational Technologies, Computer Science Education, Informatics Education, Digital Skills, Student Achievement, Interactive Education, Future Workforce

[1]**Address:** Prizren University, Faculty of Computer Science, Prizren, Kosovo

***Corresponding author**: akifgas@hotmail.com

Human-Machine Collaboration Systems in Mechanical Engineering

Abbas Hasanov[*1]

Abstract: Mechanical engineering plays an important role in a wide range of areas, from industrial processes to product design. However, the automation of traditional machines and the interaction of people with machines are undergoing significant change with developing technology. This article discusses a new paradigm in mechanical engineering, highlighting the importance and application areas of human-machine collaboration systems.

The article begins by introducing the basic concepts and components of human-machine collaboration systems. These systems enable people to collaborate with machines to create more efficient and flexible production processes. Technologies such as collaborative robots, smart manufacturing cells, and unmanned aerial vehicles have great potential in industrial applications. The design and control of human-machine collaboration systems are of great importance in terms of safety, ergonomics and human factors. The article examines key components such as interfaces, control systems, and learning algorithms used to optimize the interaction of humans with machines. Mechanical engineers play an important role in this new paradigm. Integration of human-machine collaboration systems in design, production and process improvement helps create more competitive and flexible businesses.

In conclusion, this article encourages mechanical engineers to be interested in human-machine collaboration systems. These systems will play an important role in the future of the industry and offer great potential to increase productivity, reduce error rates and improve occupational safety.

Keywords: Mechanical, engineering, collaboration, learning, algorithms

[1]**Address:** Amelioration and Water Farm Open Joint Stock Company/Azerbaijan

***Corresponding author**: mirtelekom5281@gmail.com

Disaster Management Strategies

Faruk Bojaxhi*[1]

Abstract: Disaster management represents a very important interdisciplinary field that studies the effects of natural disasters on people's quality of life and environmental sustainability and develops strategies to reduce or manage these effects.

The study examines disaster management strategies used to increase the resilience of infrastructure, water resources, waste management and energy systems in regions where natural disasters are common. Disaster management and environmental engineering play a critical role in pre-disaster preparedness, response during disaster, and post-disaster recovery. The study also considers the impact of disasters on environmental factors such as environmental pollution, waste management and water supply. Evaluates the short and long-term effects of disasters on the environment and the reflections of these effects on environmental engineering practice.

Forests play an important role in mitigating the effects of natural disasters. Forest management aims to use and protect forests in a sustainable manner. Forests can increase ecosystem resilience by preserving biodiversity. This can speed up the natural recovery process after a disaster. Environmental and forest management plays a critical role in minimizing the effects of natural disasters and protecting natural resources. Bringing these two fields together is an important step towards the goal of building a safer and more sustainable world for future generations. This article reveals the relationship between the common working points of these two fields and sustainability.

Keywords: Natural disasters, forests, water, air, engineering strategies

[1]**Address:** University of Prizren, Forestry and Environment Faculty, Rruga e Shkronjave, nr.1, 20000 Prizren, Kosovo

***Corresponding author**: faruk.bojaxhi@uni-prizren.com

Biomass Efficiency in Production of Green Energy

Ylli Kortoçi*[1]

Abstract: Today's energy needs must be compatible with environmental protection and sustainability goals. Biomass energy stands out as an energy source that meets these needs and minimizes environmental impacts. Because biomass fuels are considered a part of the carbon cycle. Plants produce oxygen by taking carbon dioxide from the atmosphere during photosynthesis. Plant materials used in biomass energy production release this carbon back into the atmosphere when converted into energy. This makes the circulation of carbon sustainable.

Efficiency is critical for the effective use of biomass energy. Technological advances in recent years have made biomass conversion processes more effective. For example, anaerobic digestion techniques for biogas production and high-efficiency reactors developed for thermal conversion have increased biomass productivity. Biomass conversion processes can be carried out by thermal, biochemical and biological methods. The efficiency of these processes is increased and energy output is maximized. In particular, methods such as biomass gasification and pyrolysis have significantly increased biomass productivity.

Biomass energy production also plays an important role in waste management. Biomass resources such as agricultural waste and wood residues are evaluated correctly and create a solution in waste management. Additionally, afforestation projects for biomass energy production are critical to maintain the balance of ecosystems.

Biomass efficiency is an important step on the path to a sustainable future. Biomass efficiency and green energy play a critical role in reducing the environmental impact of fossil fuels and building a sustainable future. Thanks to technological advances and scientific research, biomass energy is becoming more effective and efficient day by day. In this study, energy production methods using efficient methods from forest industry waste in parallel with the developing technology are discussed.

Keywords: Biomass, green energy, sustainability, Efficiency

[1]**Address:** University "Ukshin Hoti" Prizren, Faculty of Life and Environmental Sciences, Rruga e Shkronjave, nr.1, 20000 Prizren, Kosovo

***Corresponding author**: ylli.kortoci@uni-prizren.com

Food Safety and Microbiology Management

Kamila Sobkowiak

Abstract: Food safety covers the measures taken to ensure that individuals living all over the world have access to healthy and safe foods. An integral part of this process is microbiology management. Microbiology is a critical discipline for improving food safety by studying the potential hazards that microorganisms (bacteria, viruses, fungi) can cause in foods.

Food safety is a comprehensive field that investigates how microorganisms, toxins and other contaminants that can harm the health of consumers can be controlled in food production and processing processes. The article discusses the challenges faced by food engineers in food safety and microbiology and the strategies they can use to overcome these challenges. Microbiological contamination poses a major threat to food safety. This article examines how the design and management of food processing processes, hygiene practices, microbiological testing methods and food safety management systems can be improved. With the rapidly growing world population, the demand for food production is also increasing. Therefore, microbiology management and food safety are increasingly important. With advancing technology and research, more effective food safety strategies will be developed and stronger foundations will be laid for future food production.

In conclusion, this study addresses the food industry's duty to protect consumer health and ensure the safety of food products by emphasizing the critical importance of food safety and microbiology management. In this study, the relationship between the correct management of microorganisms and safe production in the food industry is questioned. In this way, healthier food consumption and safe nutrition can be ensured for future generations.

Keywords: Microbiology, food, sustainable production, food safety

[1]**Address:** Lodz University of Technology, Chemistry Faculty, Lodz/Poland
***Corresponding author**: camilla.river.50@gmail.com

The Importance of Technology in Access to Clean Water: Sustainable and Universal Access to Water Resources

Elsever Şukurov[*1]

Abstract: Clean water is a basic requirement for human survival and healthy living, and technology is an important tool in meeting this requirement. Water treatment systems are a fundamental element to transform contaminated water into clean water. Advanced treatment technologies ensure that water is free of contaminants and made potable. Smart water distribution systems and monitoring technologies ensure efficient management of water resources and reduce water leakages. Technology for sustainable use of water resources helps us better understand the water cycle and effectively reuse water. Technology plays an important role in preparing for emergencies such as water crises or natural disasters. Ensuring the security of water supply and treatment equipment is critical. For people living in areas far from water sources, portable water purifiers increase access to clean water and reduce health problems. Ultimately, access to clean water is a fundamental right for people to survive and live healthy lives. Technology is an important tool for protecting, purifying and distributing water resources and plays a critical role in tackling the water crisis. Investing in technological innovation for sustainable and universal access to water resources is vital to preserve clean water resources for future generations.

Keywords: Clean Water, Water Treatment Technologies, Sustainable Water Resources, Water Crisis, Universal Access

[1]**Address:** Amelioration and Water Farm Open Joint Stock Company/Azerbaijan

***Corresponding author**: elik0009@hotmail.com

Truck and Van Trip Generation at Logistical Sites

Gürkan Günay*[1], Gökmen Ergün[2], Ilgın Gökaşar[3]

Abstract: It is known that freight transportation planning differs a lot from passenger transportation planning. Trip generation is the first step of transportation planning, and there are significant differences in passenger and freight trip generation mechanisms. In freight transportation, trip generation patterns of freight vehicles differ across various logistical site types. This study aims to develop freight trip generation models for trucks and vans in different logistical site types. In order to serve this goal, two specific objectives are pursued. First, to identify similarities and create homogeneous logistical site type groups based on freight trip generation patterns of vans and trucks using Analysis of Covariance (ANCOVA). Second, to develop specific regression models for freight trip generation patterns of these groups. It aims to understand whether a single regression model can examine a group. For this, the market segmentation method is used. However, this paper investigates freight trip generation of only one specific homogeneous logistical site type group, the one with the highest number of truck and van trips. The data used in this study is from Kocaeli Logistics Master Plan in Turkiye. The results indicate that homogeneous logistical site type groups can be created using ANCOVA. Further, according to the result of market segmentation analysis, these groups' trip generation behavior can be explained using a single regression equation.

Keywords: Freight trip generation, truck, van, ANCOVA, market segmentation.

[1]**Address:** Istanbul Bilgi University, Faculty of Engineering and Natural Sciences, Department of Civil Engineering, Kazim Karabekir Cd. No: 2/13, 34060 Eyupsultan/Istanbul/Turkiye
[2,3]**Address:** Bogazici University, Faculty of Engineering, Department of Civil Engineering, 34342, Bebek/Istanbul/Turkiye

***Corresponding author**: gurkan.gunay@bilgi.edu.tr

Chemical Waste Reduction and Recycling Strategies

Iwona Klosok-Bazan[*1], Joanna Boguniewicz-Zablocka[1], Mustafa Karaboyacı[2]

Abstract: The chemical industry produces large amounts of waste around the world, and managing this waste can have negative impacts on the environment. This article highlights the importance of chemical waste reduction and recycling strategies. Chemical waste management plays a critical role in achieving sustainability goals.

The study addresses strategies to reduce chemical waste through source reduction, recycling and reuse. Waste reduction involves changes to chemical processes and the design of products. This minimizes environmental impacts by reducing waste generation at the source. Recycling means reprocessing and gaining value from chemical waste. This strategy encourages recycling of waste into resources and reduces depletion of natural resources. The study provides information on the effectiveness and economic benefits of recycling processes. Chemical waste management is closely related to legal regulations, industry standards and environmental policies. Therefore, the study highlights the importance of compliance with appropriate regulations for chemical industry enterprises.

In conclusion, this study addresses the environmental and economic benefits of chemical waste reduction and recycling strategies. Chemical engineers can contribute to the development of environmentally friendly and sustainable production processes by adopting waste management strategies. Zero waste processes, which are the most effective method for reducing waste, are discussed in the study. In addition, theoretical and field information has been provided to help understand that these strategies are of critical importance in achieving long-term sustainability goals for businesses and societies.

Keywords: Chemical industry, waste management, zero emission, waste reduction

[1]**Address:** Department of Thermal Engineering and Industrial Facilities, Opole University of Technology, 45040 Opole, Poland
[2]**Address:** Süleyman Demirel University, Engineering Faculty, Chemical Engineering Department, Isparta, Turkiye

***Corresponding author**: i.klosok-bazan@po.edu.pl

Design and Optimization of Low Voltage Induction Motor for Standalone PV Systems by FEM

Mustafa Tumbek*[1], Enagnon Appolinaire Dantondji[2]

Abstract: Photovoltaic (PV) cells were in widespread production by the end of the 1950s, and by the end of the decade were primarily used to power satellites in orbit around the earth. In the following years, the development in the manufacturing and the increase in the efficiency of the PV modules helped to reduce the costs and give opportunities for many remote applications that require low power. The aim of the study is to improve the performance of the induction motor for off-grid PV systems, which are often used in remote locations where grid connection is not feasible. By optimizing the shape of the motor's slots, the researchers aim to increase the motor's torque and efficiency, thereby improving the overall performance of the PV system. The use of finite element method (FEM) allows a detailed analysis of the motor's electromagnetic properties, enabling the design to be fine-tuned for maximum performance. This approach is particularly important for off-grid PV systems, where efficiency and reliability are critical to providing consistent power to remote applications. Overall, this study highlights the ongoing efforts to improve the performance of off-grid PV systems, which play an important role in providing clean energy to off-grid locations. The study aims to contribute to the further development of renewable energy technologies by focusing on induction motor design.

Keywords: Shape Optimization, Induction Motor Design, Low Voltage Motor Design, PV systems.

[1]**Address:** Pamukkale University, Faculty of Engineering, Denizli/Turkiye
[2]**Address:** Paris-Saclay University, Faculty of Engineering and Systems Sciences, Paris / France

***Corresponding author**: mustafatumbek@pau.edu.tr

Sustainable innovation management in water and wastewater companies in Poland

Joanna Machnik-Słomka*[1], Elżbieta Pawłowska[2]

Abstract: Due to contemporary trends in the area of environmental protection, social and economic development, the issue of sustainable innovation management is becoming more and more popular among researchers and business managers. Activities in this area are particularly relevant to water and wastewater companies because of water, which, as a valuable and indispensable resource, plays a particular role in social, economic and environmental development. It is therefore necessary not only to manage its resources responsibly, but also to protect it from pollution. To ensure this, it is important to sustainably manage innovations, implement eco-innovations and measure their impact on the environment, society and the economy. The innovative activities of enterprises are important not only for improving the competitiveness of the economy, but also for reducing the negative impact on the environment and improving the quality of human life. The purpose of the article is to identify the role of innovation management in sustainable development in water and wastewater enterprises in Poland. In order to achieve the formulated objective, literature research, documentary research and the case study method of a purposefully selected company operating in the water and sewage sector in Poland were used. The example of the company under study shows its activity for sustainable management translating into environmental, social and economic effects.

Keywords: sustainable management, innovation management, eco-innovation, water and wastewater companies.

[1]**Address:** Silesian University of Technology, Faculty of Organization and Management, Zabrze/Poland
[2]**Address:** Silesian University of Technology, Faculty of Organization and Management, Zabrze/Poland

***Corresponding author**: Joanna.machnik-slomka@polsl.pl

1. INTRODUCTION

Sustainable innovation management is an important issue increasingly being addressed by both researchers and practitioners (Schiederig et al., 2012). Indeed, due to contemporary challenges, sustainability has become a fundamental element of enterprise innovation strategies (Berkhout, 2014). Enterprises are even forced to target sustainable innovation management using dynamic innovation capabilities. Dynamic innovation capabilities are necessary to effectively and efficiently implement innovations, including eco-innovations, or sustainable development innovations that affect social, economic and environmental development.

Innovation activities in the area of sustainable management are particularly important for water and wastewater companies. This is important because of the role these enterprises play in environmental, social and economic development. These enterprises should responsibly manage water resources and protect them from pollution, which is the basis for proper water management and the development of various ecosystems (GUS, 2022). Rational, efficient and sustainable water management ensuring access to water for the entire population is one of the fundamental tasks of any state. In this, a large role at the regional and local level is played precisely by water and wastewater companies, which are an important part of the ecosystem.
.
It may be helpful for these enterprises to sustainably managing innovation and targeting the creation and implementation of so called eco-innovations, which can help improve people's quality of life, the competitiveness of the economy, as well as reduce the negative impact on the environment.

Identifying the role of innovation management in the sustainable development of water and wastewater utilities in Poland is the purpose of the article.

2. MATERIAL AND METHOD

In order to realize the formulated objective, the research methodology was adapted, which included:

- theoretical-cognitive research,
- documentary research,
- qualitative research using a case study.

Theory-cognitive research focused on a literature review of the role and importance of sustainable innovation management in companies and related eco-innovation.

Qualitative research was carried out using the case study method of a water and sewerage company purposely selected for the study, operating Silesian province in Poland. The research included an interview with the management of the studied enterprise on the topic of sustainable innovation management.

The research was complemented by desk research focusing on strategic documents, reports on innovation management, implementation of innovations in water and sewage enterprises and documents of the studied water and sewage enterprise.

3.THE ESSENCE AND İMPORTANCE OF SUSTAİNABLE İNNOVATİON MANAGEMENT İN COMPANİES

Due to the growing importance of the concept of sustainability in the aspect of innovation management, some authors focus on the relationship between these constructs (e.g. Cillo et al., 2019). Many articles are devoted to this issue, but few authors focus on explaining the construct of sustainable innovation management. In attempting to define and understand sustainable innovation management, it is necessary to start from the definition of innovation management, where many authors refer to the basic functions of management. This approach is also taken in the Oslo Manual 2018. According to this Manual, innovation management is defined as „*all systematically carried out activities of planning, management and control of internal and external resources for innovation*" (Oslo Manual 2018, 2018). Sustainable innovation management can therefore refer to these functions with a direction towards sustainability. In sustainable innovation management, it is worth emphasizing the importance of proper management by companies of both internal and external relationships (Berkhout F., 2014). This is because it has a significant impact on the effective management of innovation processes, which increases the chances of success and competitiveness of these companies. With regard to managing sustainable innovation, Aagaard (Aagaard, 2018) points to three key elements: a way of managing and measuring that ensures a higher level of ethical, social and environmentally friendly approaches; targeting the results of innovation management processes towards sustainable innovation; and ensuring effective and efficient external cooperation within the innovation management process (Aagaard, 2018). Forming good relationships with different stakeholder groups is related to the concept of CSR, which plays an important role in the context of sustainable management (Klein, 2018). This concept emphasizes ethical behavior toward one's stakeholders (Usman, Amran, 2015). Such conduct increases the chances of success and raising competitive advantage (Wu, Dluhošová, Zmeškal, 2021; Xu, Wei, Lu, 2019). R.W. Griffin (2013) points out that CSR is an organization's responsibilities to strengthen and protect the community. The ISO 26000 definition of CSR emphasizes an organization's responsibility to take action toward the environment and society based on ethical behavior toward stakeholders to achieve sustainable development (ISO 26000, 2010).

Contemporary innovation management conditioned by a turbulent environment requires the effective use of dynamic innovation capabilities (Bessant, Philips, 2013). They are essential to the management of innovation processes in enterprises (Cheng, Chen, 2013). Dynamic capabilities relate to the capacity to integrate and reconfigure different capabilities in response to the rapid pace of change (Teece et al., 1997). Thus, in sustainable innovation management, it is important to use different capabilities to manage innovation processes. A high level of dynamic innovation capabilities related to eco-innovation research and internationalization, among others, is essential for sustainable innovation management in companies (Chakrabarty, Wang, 2012). In order to effectively implement innovation, companies should target the effective use of dynamic innovation capabilities.

This is because sustainable innovation management involves the creation and implementation of innovations, particularly sustainable innovations, or eco-innovations. Sustainable innovation can be understood as innovation that affects social, environmental and economic outcomes in the area of sustainable development (Boons, et al., 2013).

In the field of sustainable innovation management, eco-innovation plays an important role, which is of great importance for achieving the goals of the European Green Deal through better use of resources, reduction of negative environmental impact and positive social and economic impact (https://green-business.ec.europa.eu/eco-innovation_en.). Eco-

innovation also aims to support a closed-loop industrial transformation (https://green-business.ec.europa.eu/eco-innovation_en.).

The approach adopted in the article considers the relationship between the sustainable management of innovation, eco-innovation and the effects achieved (see Figure 1).

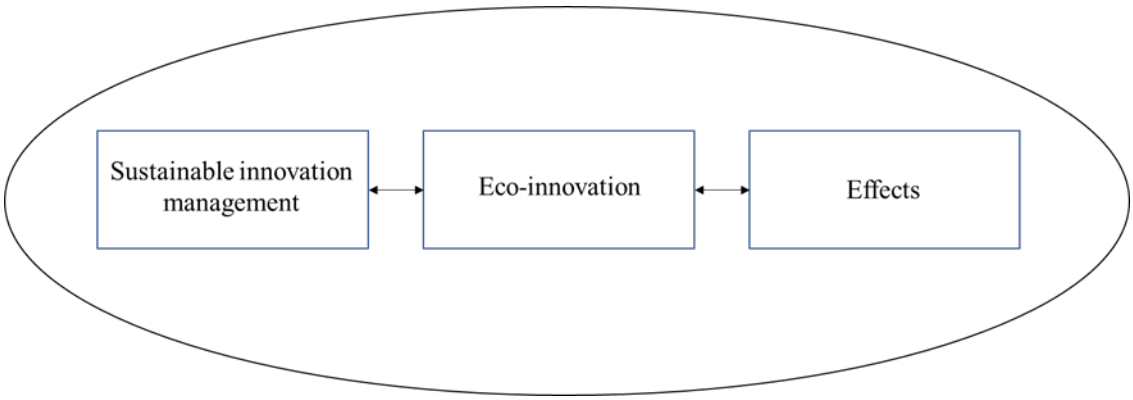

Figure 1. Relationship between sustainable innovation management, eco-innovation and impact

At the level of EU member states, the eco-innovation index is measured, which takes into account 12 indicators. Depending on the results obtained, individual countries are included in one of three groups: eco-innovation leaders group, average Eco-innovation performers group, eco-innovation catching-up group. The performance of individual countries according to the Eco-Innovation Index 2022 for 2021 is shown in Figure 2.

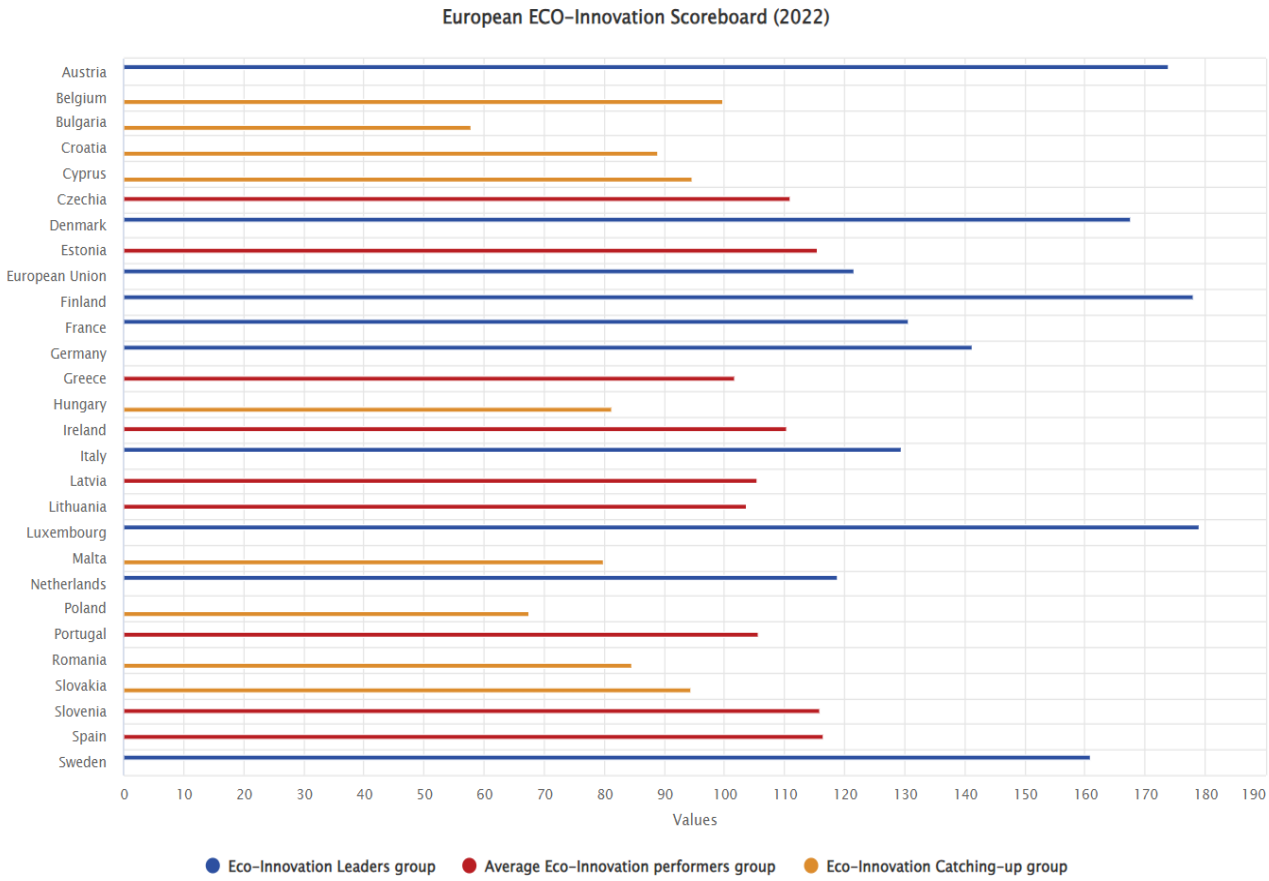

Figure 2. The Eco-Innovation Index 2022

Źródło:Eco-Innovation at the heart of European policies, European Commission,https://green-business.ec.europa.eu/eco-innovation_en (accessed 28 May 2023).

According to The Eco-Innovation Index 2022 collecting data from EU member states and beyond, countries with the highest Eco-innovation indexes include Luxembourg (179.02), Finland (178.01), Austria (173.86), Denmark (167.49), Sweden (160.95) (https://green-business.ec.europa.eu/eco-innovation_en.). The indicator for the European Union is 121.47. Poland, on the other hand, ranks below the EU average with an indicator of 67.37 (https://green-business.ec.europa.eu/eco-innovation_en.). As relatively strong points of Poland can be considered social behavior, water productivity, scientific publications, while as weak points especially those related to eco-innovation activities, the number of ISO 14001 certificates and patents related to eco-innovation (Jasińska, 2022).

4. OBJECTİVES AND EFFECTS OF SUSTAİNABLE İNNOVATİON MANAGEMENT İN WATER AND SEWAGE ENTERPRİSES İN POLAND - CASE STUDY

Sustainable innovation management for water and wastewater enterprises, given their role and mission to society, is particularly important. Surveys conducted in Poland on the innovative activities of enterprises show that in 2019-2021, among enterprises classified as manufacturing in the Sewage Collection and Treatment/Sewerage division, there were 27.8% of innovative enterprises, i.e. those that introduced at least one innovation in the period under consideration (GUS, 2022). On the other hand, in the section Water collection, treatment and supply, innovative enterprises accounted for 22.4% (Innovation activities of enterprises in the years 2019-2021, Statistical analyses, GUS, Warsaw, Szczecin 2022).

Sustainable innovation management, the implementation of eco-innovation in enterprises based on accepted standards, should contribute according to the formulated objectives to the achievement of sustainable development goals and translate into expected effects. According to the Oslo Manual 2018, effects that have an impact on society, the environment or the economy should result from the formulated goals in the area of innovation and be related, for example, to reducing the negative impact of activities on the environment, achieving benefits for the environment or society through improved safety and health (Oslo Manual 2018, 2018).

In order to identify the effects resulting from sustainable innovation management activities of the water and sewerage company purposely selected for the study in Poland, a qualitative research was conducted. As part of this research, management was interviewed and desk research was conducted. The analyzed enterprise is engaged in water and wastewater management at the local level in the Silesian Voivodeship. One of the company's priorities is an environmental policy focused on the protection of natural resources, monitoring of environmental impact, sustainable development. In this regard, the company is ISO 14001 certified, which is the standard in the area of environmental management. The company is also focused on improving the efficiency of energy use, developing an energy management system with ISO 50001 (Energy Management System) certification. The company is also certified as an integrated management system in accordance with ISO 9001.

Based on the qualitative research carried out, effects affecting sustainability resulting from the activities of the studied water and sewerage company operating in the Silesian province in Poland were identified. The identified effects in the social, environmental and economic areas are shown in Table 1.

Table 1. Identified effects in the social, environmental and economic areas

Area of effects	Effects
Social	- increase the environmental awareness of the company's employees - improved relations with stakeholders - improvement of working conditions - increase in pro-environmental behavior - improving environmental conditions of the local community - improvement of the company's image
Environmental	- lower energy consumption at various stages of the process water supply and wastewater treatment - better waste management - reduction in consumption of raw materials, resources - reduction of pollution
Economic	- cost reduction through greater energy savings - lower costs due to better management of resources, raw materials - savings resulting from more efficient waste management - savings in operating costs

Source: own study

The analyzed company, through the implementation of a modern pro-environmental policy, improvement of management standards, tries to reduce the negative impact on the environment in a systematic and continuous manner building lasting and positive relations with various groups of external stakeholders.

The company is also focused on implementing pro-environmental innovations, in particular to improve energy efficiency, water treatment processes.

5. DISCUSSION AND CONCLUSIONS

In view of the growing global pressure to protect the environment and offset negative environmental impacts, an increasingly conscious orientation of companies towards sustainable management has become evident over the past few years. This is increasingly associated with the creation of enterprise innovation strategies focused on the creation and implementation of eco-innovations for stakeholder value creation.

Sustainable innovation management for water and wastewater utilities due to their role and mission to society is particularly important. Today's challenges and global conditions are forcing companies to apply new methods and mechanisms for managing innovation focused on sustainability. This increasingly requires a holistic approach to innovation management that makes effective use of dynamic innovation capabilities.

The example of the analyzed water and sewage company located in Poland indicates that aspects of sustainable innovation management are important to the company. The company takes a number of measures focused on sustainable and responsible management. As the results of the research conducted at this company show, sustainable management translates into not only economic, but also environmental and social effects.

Given the limitations of research focusing on a single case study, further research directions could take into account the more cross-sectional nature of quantitative research.

Ethics Committee Approval
N/A

Peer-review
Externally peer-reviewed.

Author Contributions
Conceptualization: J.M.S, E.P.; Investigation: J.M.S, E.P.; Material and Methodology: J.M.S, E.P.; Supervision: J.M.S, E.P.; Visualization: J.M.S, E.P.; Writing-Original Draft: J.M.S, E.P.; Writing-review & Editing: J.M.S, E.P.; Other: All authors have read and agreed to the published version of manuscript.

Conflict of Interest
The authors have no conflicts of interest to declare.

Funding
The authors declared that this study has received no financial support.

REFERENCES

Aagaard, A. (2018). Managing Sustainable Innovation, in: Altenburger, R. (Eds.), Innovation Management and Corporate Social Responsibility. CSR, Sustainability, Ethics & Governance. Springer, Cham. https://doi.org/10.1007/978-3-319-93629-1_2.

Berkhout F. (2014). Sustainable innovation management, in: Dodgson M., Gann D.M., Phillips N. (Eds.), The Oxford Handbook of Innovation Management. Oxford University Press.

Bessant, J., Phillips, W. (2013). Innovation management and dynamic capability, in: Harland C., Nassimbeni G., Schneller E. (Eds.), The SAGE handbook of strategic supply management. London: Sage Publications Ltd., pp. 353-371.

Boons, F.; Montalvo, C.; Quist, J.; Wagner, M. (2013). Sustainable innovation, business models and economic performance: An overview. Journal of Cleaner Production. 45, pp. 1-8.

Chakrabarty S., Wang L. (2012). The Long-Term Sustenance of Sustainability Practices in MNCs: A Dynamic Capabilities Perspective of the Role of R&D and Internationalization, Journal of Business Ethics. 110, pp. 205–217. https://doi.org/10.1007/s10551-012-1422-3.

Cheng, C.C., Chen, J.S. (2013). Breakthrough innovation: the roles of dynamic innovation capabilities and open innovation activities. Journal of Business & Industrial Marketing. 28(5), pp. 444–454.

Cillo, V., Petruzzelli AM., Ardito, L., Del Giudice M. (2019). Understanding sustainable innovation: A systematic literature review. Corporate Social Responsibility and Environmental Management, John Wiley & Sons, 26(5); 26: 1012–1025.

Eco-Innovation at the heart of European policies, European Commission, https://green-business.ec.europa.eu/eco-innovation_en (accessed 28 May 2023).

Foss, N.J. Klein, P.G. (2018). Stakeholders and Corporate Social Responsibility: An Ownership Perspective. Sustainability, Stakeholder Governance, and Corporate Social Responsibility. Advances in Strategic Management, Vol. 38, Emerald Publishing Limited, pp. 17-35.

Griffin, R.W. (2013). Fundamentals of management, Cengage Learning. Inc., Florence, KY.

Innovation activities of enterprises in the years 2019–2021. (2022). Statistical analyses, GUS, Warszawa, Szczecin.

International Organizaton for Standardization, ISO 26000 Społeczna Odpowiedzialność. (2010). Switzerland.

Jasińska A. (2022). Eco-Innovation Country Profile 2022: Poland, Ecorys.

Oslo Manual 2018: Guidelines for Collecting, Reporting and Using Data on Innovation, 4th Edition, The Measurement of Scientific, Technological and Innovation Activities. (2018). OECD/Eurostat.

Oslo Manual 2018: Guidelines for Collecting, Reporting and Using Data on Innovation, 4th Edition, The Measurement of Scientific, Technological and Innovation Activities. (2018). OECD/Eurostat.

Schiederig, T., Tietze, F., Herstatt, C. (2012). Green innovation in technology and innovation management - an exploratory literature review. R&D Management, 42(2).

Teece, D.J., Pisano, G., Shuen, A. (1997). Dynamic capabilities and strategic management. Strategic Management Journal, 18(7).

Usman, A.B. and Amran, N.A.B. (2015). Corporate social responsibility practice and corporate financial performance: evidence from Nigeria companies. Social Responsibility Journal. Vol. 11 No. 4, pp. 749-763.

Wu X., Dluhošová D., Zmeškal Z. (2021). Corporate Social Responsibility and Profitability: The Moderating Role of Firm Type in Chinese Appliance Listed Companies. Energies, 14, 227. https://doi.org/10.3390/en14010227.

Wskaźniki zielonej gospodarki w Polsce 2022. (2022). GUS, Urząd Statystyczny w Białymstoku. Warszawa, Białystok.

Xu, J.; Wei, J.; Lu, L. (2019). Strategic stakeholder management, environmental corporate social responsibility engagement, and financial performance of stigmatized firms derived from Chinese special environmental policy. Business Strategy and the Environment, 28, 1027–1044. https://doi.org/10.1002/bse.2299.

Estimation of Direct Tensile Strength by a Non-Destructive Test

Mustafa Kanık*[1], Zülfü Gürocak[1]

Abstract: Depending on the type of stress affecting a material, it exhibits various strength characteristics such as compression, tensile, shear, bending, and torsional strength. Among these, uniaxial compression and tensile strengths hold significant importance in rock mechanics applications and serve as indispensable parameters in geotechnical designs. Engineering geological studies often focus on unconfined compressive strengths, assuming that the rock is under compaction conditions. However, numerous researchers have emphasized that the tensile strength also plays a crucial role in determining the strength of rock material or rock mass against failure. They have highlighted its significance during the design stage.
Unlike uniaxial compressive strength, which has standardized testing methods, rock tensile strength is determined using different test methods. These methods can be categorized into two main classes: direct and indirect tensile tests. Direct tensile tests are conducted along the axis of the specimen using various test apparatus. However, these tests often present significant challenges in obtaining accurate and reliable results. On the other hand, indirect tensile tests offer an alternative approach and are preferred by designers due to their simplicity and ease of application. Among the indirect methods, the most commonly used one is the Brazilian test method. Designers often use the values obtained through indirect methods directly as the tensile strength of the rock material. Alternatively, they may calculate the direct tensile strength (DTS) of the rock using empirical equations proposed in relevant studies.
As an alternative to direct and indirect methods used to determine the tensile strength of rock materials, there are studies that propose empirical equations to estimate the tensile strength of rock materials based on various mechanical properties. In these studies, independent variables such as uniaxial compressive strength, point load strength, direct shear strength, and sonic velocity (SV) have been used.
In this study, two sample groups, andesite and marl, were subjected to testing to uncover the correlation between DTS and SV. The study utilized a total of 20 samples to analyze this relationship. The individual evaluations of the groups yielded correlation coefficient (r) values of 0.84 and 0.62, respectively. However, when all the samples were collectively analyzed, the r value significantly increased to 0.89 and a very strong positive correlation has been identified between these two parameters.

Keywords: Tensile strength, direct tensile test, sonic wave test, non-destructive test

[1]**Address:** Firat University, Faculty of Engineering, Department of Geological Engineering Elazığ/Türkiye

***Corresponding author**: mkanik@firat.edu.tr

1. INTRODUCTION

Stresses that act on any selected cross-sectional area can be classified into four types: normal stresses (compression and tension), shear stress, torsional stress, and bending stress. The resistance that a material exhibits against these different types of stresses is defined as strength. Among these strength types, compressive and tensile strengths hold significant importance in rock mechanics applications and are considered indispensable parameters in geotechnical designs. Goodman (1989) states that engineering studies often focus on the unconfined compressive strength, assuming the rock is subjected to compression. However, he emphasizes that tensile strength is also a crucial parameter in determining the resistance of rock materials or rock masses against failure.

In engineering applications, the tensile strength has been emphasized to hold an equally important position as the compressive strength. Various researchers have highlighted this fact in their studies. For instance, Diederichs and Kaiser (1999) state that tensile strength is a critical controlling property in determining the critical span of underground openings. Similarly, Cai et al. (2001) and Pine et al. (2007) have shown through their research that tensile stresses can significantly influence slope stability. Zhang (2016) expressed the necessity of considering tensile strength in design for blasting due to its value is lower than the uniaxial compressive strength. Huang et al. (2020) conducted a study where they found that during tunnel excavation within a slope supported by diaphragm walls, deformation could induce tensile stresses in pre-stressed rock bolts. These tensile stresses can counteract the tensile stresses in the geological formation where rock bolts

are installed, highlighting the importance of tensile strength in stability. In conclusion, accurately determining the strength of rock materials under tensile conditions plays a vital role in ensuring safe and economically sound engineering designs.

Unlike uniaxial compressive strength, different test methods have been proposed to determine the tensile strength of rock. These methods can be divided into two main categories: direct and indirect tensile test methods. Direct methods involve applying tensile stress along a single axis using different testing apparatus. On the other hand, indirect tensile tests can be performed using various methods. There are five types of indirect tests used to determine the tensile strength of rock materials: three-point bending, four-point bending, disk bending, ring tension test, and Brazilian test. Among these, the Brazilian test method is the most commonly used. While the direct tensile method is the fundamental testing approach, it comes with significant challenges related to precise alignment and sample preparation, which can affect obtaining accurate and successful test results. Moreover, as the sample size increases, the presence of micro-cracks within the rock material can pose difficulties in directly pulling the rock sample during testing (Goodman, 1989). On the contrary, the test methods used for indirectly determining tensile strength are simpler and more easily applicable. Therefore, the relationships between direct and indirect tensile strengths have been investigated by different researchers, and attempts have been made to establish these relationships. Figure 1 compares data obtained from various indirect tensile tests with data from direct tensile methods. When examining Figure 1, it can be observed that the results closest to those of direct tensile methods are obtained from the hydraulic fracturing method. However, the hydraulic fracturing method is one of the in-situ testing methods, and determining the tensile strength using this method indirectly is much more challenging compared to the Brazilian method. While the Brazilian method is simple, its results do not represent the direct tensile strength (DTS) of the rock material. Results obtained from indirect methods tend to be higher than those obtained from direct methods (Klanphumeesri, 2010; Fuenkajorn and Klanphumeesri, 2011).

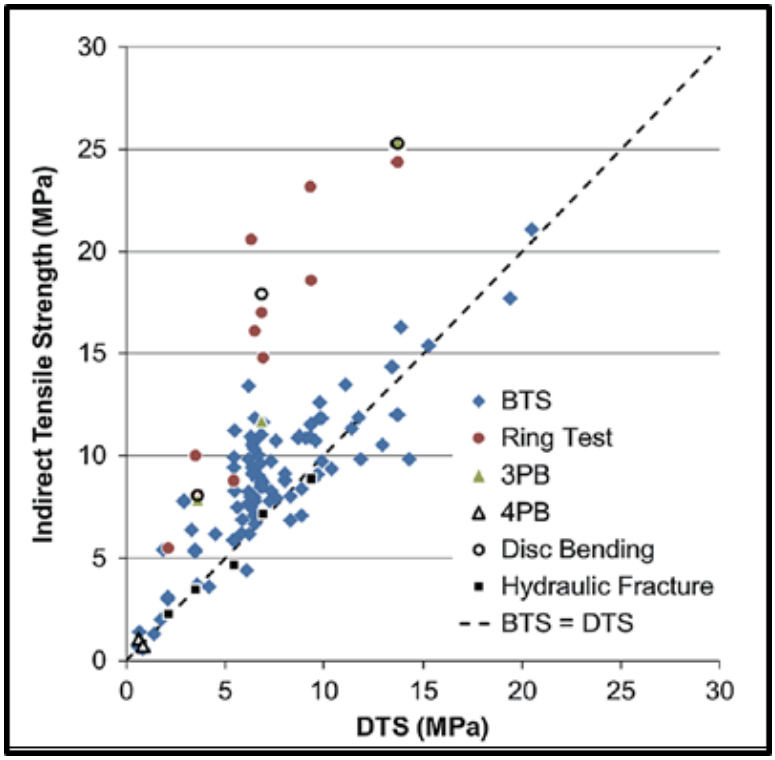

Figure 1. Comparison between DTS and various alternative indirect tensile testing methods (Perras, M.A. ve Diederichs 2014)

Furthermore, there are studies conducted by various researchers (Schrier, 1988; Sulukçu and Ulusay, 2001; Mishra and Basu, 2012; Jamshidi and Fereidooni, 2022) aimed at predicting the tensile strength of rock materials. In these studies, empirical equations were proposed, where Brazilian tensile strength, uniaxial compressive strength, and direct shear strength of the rock material were used as independent variables. These equations allow for the estimation of the tensile strength of rock materials. Apuani et al. (1997) and Khandelwal (2013) have also examined the relationships between Brazilian tensile strength and sonic velocity of rock materials. However, there is no existing study that investigates the relationships between the DTS of rock materials and their physical properties. In this study, experimental investigations were conducted to examine the relationships between DTS and SV in two different rock groups: andesite and marl. The

obtained results were statistically evaluated, and empirical equations that can be used to predict the DTS of rock materials were proposed.

2. MATERIAL AND METHOD

In this study, core samples of andesite and marl were selected from the storage area of the General Directorate of State Hydraulic Works (DSİ) 9th Regional Directorate. These core samples were cut to the appropriate dimensions for laboratory testing. A total of 20 core samples, 10 from each rock group, were used for direct tensile and sonic velocity tests in the Rock Mechanics Laboratory of the Department of Geological Engineering at Fırat University, following the methods recommended by the International Society for Rock Mechanics (ISRM) in 2007.

2.1. Sonic velocity (SV) test

The sonic velocity tests conducted to determine the SV values of the samples were performed using the Pundit Plus test apparatus, following the recommendations of ISRM (2007) (Fig. 2).SV are calculated from travel times measured and the distance, d, between transmitter and receiver by using the equation:

$$V_p = d * t_p^{-1} \quad (1)$$

where V_p is the velocity of the longitudinal wave, t_p is the time which the P-wave took to travel the distanced (ISRM, 2007). The results of the sonic velocity tests are provided in Table 1

Figure 2. Sonic wave velocity testing

2.2. Direct tensile test

In the determination of the DTS (Direct Tensile Strength) of rock materials, the methods recommended by ISRM (2007) and ASTM D2936 (2008a) are generally preferred as they show similarities with each other. In this study, the ISRM (2007) method was chosen due to its more general use. The specimens prepared for the direct tensile test can be seen in Figure 3.

The prepared specimens following the guidelines of ISRM (2007) for the direct tensile test were kept in an oven at 100°C for 24 hours before attaching the tensile grips. After removing the specimens from the oven, steel grips were attached to the specimens using Loctite EA340 epoxy adhesive. To prevent movement of the grips, the specimens and steel grips were wrapped with paper tape and placed in a vacuum-sealed environment for 5 days to allow the epoxy to fully cure and achieve sufficient tensile strength (Fig. 4).

Figure 3. The specimens used for the direct tensile strength test

Afterward, the tensile tests were conducted using a uniaxial press with the help of an apparatus. The apparatus used and a view of the failed samples can be seen in Figure 5. All the experimental results from the tests are provided in Table 1.

Figure 4. Curing phase of the specimens

Table 1. The statistical evaluation of the experimental results

Group	Sample No	Direct Tensile Strength				Sonik Wave Velocity			
		Max. (MPa)	Min. (MPa)	Average (MPa)	Standard Deviation	Max. (m/sec)	Min. (m/sec)	Average (m/sec)	Standard Deviation
Marl	10	4.87	1.98	3.394	0.863	3386	2655	2965	223.338
Andesite	10	7.21	4.07	6.001	1.050	3702	3275	3497	130.71
All	20	7.21	1.98	4.698	1.632	3702	2655	3231.4	325.642

According to Table 1, the highest DTS value of 7.21 MPa was obtained from the andesite group, while the lowest average DTS value of 1.98 MPa was obtained from the marl group. The highest SV value of 3702 m/sec was observed in the andesite group, and the lowest SV value of 2655 m/sec was recorded in the marl group.

Figure 5. The apparatus used for the direct tensile test, the grips utilized, and the failed samples.

3. REGRESSION ANALYSES

The most common statistical method used to determine relationships between two parameters is simple or multiple regression analysis. These analyses aim to identify cause-and-effect relationships between two or more variables and use this relationship to make predictions or estimations related to the subject.
In this analysis method, a mathematical model is used to explain the relationship between two or more variables, and this model is called the Regression Model. The simple regression model can be represented as $Y = \alpha + \beta X$, where:

Y: is the dependent (outcome) variable and is assumed to have some error.
X: is the independent (cause) variable and is assumed to be measured without error.
A: is the regression constant value and represents the value of Y when X is 0.
B: is the regression coefficient, indicating the amount of change in Y, in its own unit, corresponding to a 1-unit change in X.

In this study, simple regression analyses were performed to establish the relationships between DTS and SV. These analyses were conducted for each sample group separately and for all groups together to examine the relationships comprehensively.

3.1. Simple regression analysis for the marl group samples

In this group, the samples are sedimentary-origin marls, and upon evaluating the data from the experiments conducted on the cores of this group using a simple regression analysis (Fig.6), the correlation coefficient (r) was determined to be 0.62. This value indicates a strong positive correlation between DTS and SV in the marl group samples.

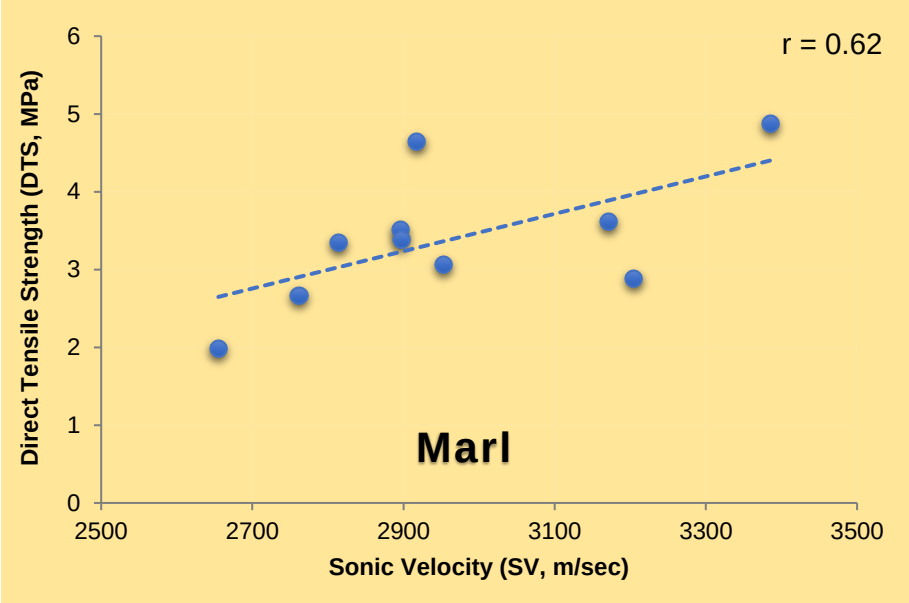

Figure 6. Data distribution graph for marl samples

3.2. Simple regression analysis for the andesite group samples

The samples in this group consist of volcanic-origin andesites. Upon evaluating the results of the experiments conducted on andesite cores using a simple regression analysis, a strong positive relationship with an r-value of 0.84 between DTS and SV of andesites has been determined (Fig. 7).

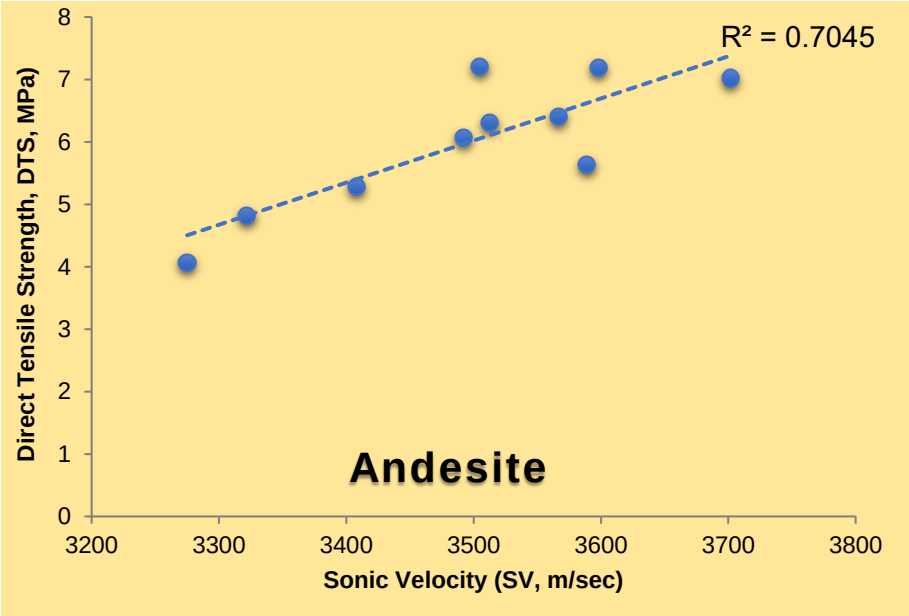

Figure 7. Data distribution graph for andesite samples

3.3. Overall evaluation

In this study, data for marl and andesite samples were evaluated together to explore the relationship between DTS and SV of the specimens. The data distribution graph for the regression analysis, where DTS is the dependent variable and SV is the independent variable, is provided in Figure 8. According to the results of the regression analysis, there is a very strong positive correlation between DTS and SV. The r-value is 0.89, and the equation describing the correlation is as follows;

$$DTS = 0.0045\ SV - 9.805 \quad (2)$$

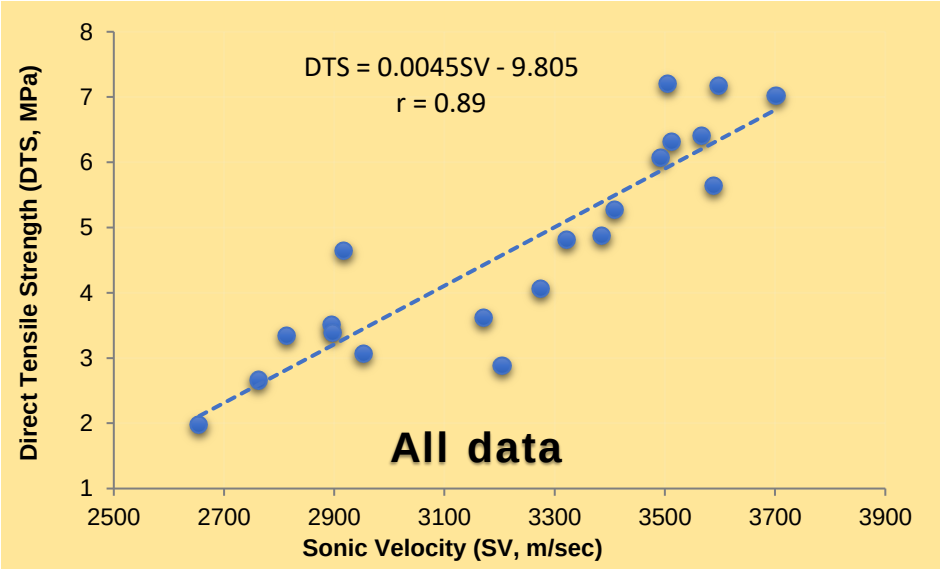

Figure 8. . Data distribution graph for both groups

4. DISCUSSION AND CONCLUSIONS

In the literature, there are numerous studies on determining the DTS of rock materials using indirect methods. The results of these studies indicate that the values obtained through indirect methods for the tensile strength are generally higher than the actual DTS values of the rock materials (Andreev, 1991a; Andreev, 1991b; Gorski and Conlon, 2007; Klanphumeesri, 2010; Fuenkajorn and Klanphumeesri, 2011; Perras and Diederichs, 2014; Jensen, 2016; Liao et al., 2019). Although there are contrasting views (Covielo et al., 2005; Li and Wong, 2012), the prevailing opinion is in line with the findings from the widely used indirect method, Brazilian test. To overcome this issue, it may be possible to explore the relationships between the rock's direct tensile strength and other physical and mechanical properties. Therefore, this study was conducted with the aim of addressing this significant gap in the literature, even if only to a limited extent.

In this study, the relationships between the DTS and SV values of rock materials were examined using the simple regression method. For this purpose, experimental studies were conducted on core samples of marl and andesite rocks, and the obtained results were statistically evaluated to determine the relationships between the DTS and SV of the rock materials. As a result of the regression analyses, an empirical equation was proposed, which can be used to predict the DTS of rock materials.

Similar studies in the literature (Apuani et al., 1997; Khandelwal, 2013) have investigated the relationships between tensile strength obtained from Brazilian tests and SV for rock materials. However, this study is the first to examine the relationship between DTS and SV for rock materials. The evaluation of the results obtained from the experimental studies through regression analyses indicates strong positive relationships, with an r-value of 0.62 for the marl group rocks and an r-value of 0.84 for the andesite rocks.

The combined evaluation of data from both rock groups yields an r-value of 0.89, indicating a very strong positive correlation between the DTS and SV through regression analysis. The empirical equation derived from this study for the determined correlation is highly effective and can be used by engineers to predict the DTS of rock materials. In future experimental studies conducted on different lithologies, with new data, it will be possible to establish more reliable empirical equations that represent this relationship even better.

Acknowledgements

All studied data presented in this study were obtained under a research project (122Y067) supported by TÜBITAK (The Scientific and Technological Research Council of Turkey).

Ethics Committee Approval
N/A

Peer-review
Externally peer-reviewed.

Author Contributions
Conceptualization: M.K.; Investigation: M.K., Z.G..; Material and Methodology: M.K., Z.G.; Supervision: M.K., Z.G.; Visualization: M.K.; Writing-Original Draft: M.K., Z.G.; Writing-review & Editing: M.K., Z.G.; Other: All authors have read and agreed to the published version of manuscript.

Conflict of Interest
The authors have no conflicts of interest to declare.

Funding
The authors declared that this study has received financial support under a research project (122Y067) supported by TÜBITAK (The Scientific and Technological Research Council of Turkey).

REFERENCES

Andreev, G. A. 1991a. “Review of the Brazilian test for rock tensile strength determination. Part I: calculation formula”, Min Sci Technol,13(3):445–456.

Apuani, T., King, M.S., Butenuth, C., De Freitas, M.H. 1997. Measurements of the relationship between sonic wave velocities and tensile strength in anisotropic rock. Geological Society, London, Special Publications, 122, 107-119

Andreev, G. A. 1991b. “Review of the Brazilian test for rock tensile strength determination. Part II: contact conditions” Min Sci Technol, 13(3):457–465.

Cai, M., Kaiser, P., Martin, C. 2001. “Quantification of rock mass damage in underground excavations from microseismic event monitoring”, Int J Rock Mech Min Sci., 38(8):1135–1145.

Coviello, A., Lagioia, R., Nova, R. “On the measurement of the tensile strength of soft rocks”, Rock Mech Rock Eng. 2005;38(4):251–273.

Diederichs, M. S., Kaiser, P. K. 1999. “Tensile strength and abutment relaxation as failure control mechanics in underground excavations”, Int J Rock Mech Min Sci, 36:69–96

Fuenkajorn, K., Klanphumeesri, S. 2011. “Laboratory determination of direct tensile strength and deformability of intact rocks”, Geotech Test J.”,34(1):1–6

Goodman RE. Introduction to Rock Mechanics. 2nd ed. New York: Wiley; 1989.

Gorski B, Conlon B, Ljunggren, B. 2007. Forsmark Site investigation—Determination of the direct and indirect tensile strength on cores from borehole KFM01D. SKB P-07-76,Svensk ämbränslehantering AB

Huang, F., Zhang, M., Wang, F., Ling, T.H., Yang X.L. 2020. “The failure mechanism of surrounding rock around an existing shield tunnel induced by an adjacent excavation”, Computers Geotechnics, 117.

Jamshidi, A., Fereidooni, D. 2022. “Evaluation of the block punch index test for predicting the strength of sandstones”, Scientific Quarterly Journal of Iranian Association of Engineering Geology, 15(1), 105-118.

Jensen, S. S. 2016. “Experimental Study of Direct Tensile Strength in Sedimentary Rocks”, Norwegian University of Science and Technology, master thesis, 111p

Khandelwal, M. 2013. Correlating P-wave Velocity with the Physico-Mechanical Properties of Different Rocks, Pure Appl. Geophys. 170, 507–514

Klanphumeesri, S. 2010. "Direct tension testing of rock specimens", Suranaree University of Technology , master thesis, 104p

Li, D. Y., Wong, L. 2012. "The Brazilian disc test for rock mechanics applications: review and new insights", Rock Mech Rock Eng., 46(2):269–287.

Liao, Z.Y., Zhu, J.B., Tang C.A. 2019. "Numerical investigation of rock tensile strength determined by direct tension, Brazilian and three-point bending tests", Int J Rock Mech Min Sci, 115, 21-32

Mishra, D.A., Basu, A. 2012. "Use of the block punch test to predict the compressive and tensile strengths of rocks", International Journal of Rock Mechanics & Mining Sciences, 51, 119-127.

Perras, M.A., Diederichs, M.S. 2014. "A Review of the Tensile Strength of Rock: Concepts and Testing", Geotech Geol Eng, 32, 525–546

Pine, R., Owen, D., Coggan, J. 2007. A new discrete fracture modelling approach for rock masses. Geotech. 2007;57(9):757–766.

Schrier van der J.S. 1988. "The block punch index test", Bulletin of Engineering Geology and the Environment, 38, 121-126.

Sulukcu, S., Ulusay, R. 2001. "Evaluation of the block punch index test with particular reference to the size effect, failure mechanism and its effectiveness in predicting rock strength", International Journal of Rock Mechanics and Mining Sciences, 38, 1091-1111

Ulusay, R., ve Hudson J. A. 2007. "The blue book—the complete ISRM suggested methods for rock characterisation, testing and monitoring 1974–2006". ISRM and Turkish National Group of ISRM, Ankara

Zhang, Z-X. 2016. "Free Surface and Swelling in Blasting. Rock Fracture and Blasting Theory and Applications", 239-254, https://doi.org/10.1016/B978-0-12-802688-5.00011-7

The Importance of Carbon Fibers: Research on Türkiye and The World

Tugay Üstün*[1], Sinan Can Altuntaş[1]

Abstract: Carbon fibers, one of the engineering materials, are one of the materials preferred by designers. Since these fibers have many forms, they also play an important role in the development of high-tech products. Since carbon fibers are the main element especially in fiber-reinforced composites, they allow the emergence of different shapes. This is the only reason why carbon fibers are in the form of fiber and weaving. Despite the fact that these materials have different forms, their great advantages compared to traditional materials pave the way for their use in products produced in daily life. However, the high production cost of carbon fibers hinders the development in this field, even if it is a little bit. Carbon fibers used in fields such as defense, aviation and space are turning into a strategic material from the point of view of countries. Countries want to make their own production of this product to meet their own needs, but they also import it. For this reason, research on carbon fibers is still ongoing. In this study, the interest of G-20 countries towards this material was investigated by using secondary data. In this direction, export and import figures were examined and country-based percentages of these figures were revealed. However, due to the fact that this product is a strategic product, historical data could not be obtained, only 2022 and later data were obtained, and it was revealed that some countries did not share this information. In addition, data for 2022 and 2023 for Türkiye have been reached and detailed analysis has been made on a country basis.

Keywords: Carbon fiber, imports, export, data.

[1]**Address:** Başkent University, Kahramankazan Vocational School, Ankara/Türkiye

***Corresponding author**: tugayustun@baskent.edu.tr

1. GİRİŞ

Sürekli gelişmeye devam etmekte olan teknolojiyle beraber mühendislik malzemeleri önem kazanmaktadır. Bu mühendislik malzemelerinden bir de kompozitlerdir ve kendi içerisinde de çeşitli sınıflara ayrılmaktadır. Üstün özelliklerinden dolayı endüstriyel ve ticari olarak birçok uygulama alanına sahip olan elyaf takviyeli kompozitler bu sınıfın en önemli malzemeleri olarak karşımıza çıkmaktadır (Agarwal vd., 2017). Metal malzemeler ile kıyaslandığında birçok uygulama alanın olmasının temel sebebinde düşük yoğunlukları bundan dolayı ağırlık kazanımı, yüksek dayanım sergilemeleri olarak gösterilebilir (Mallick, 2007; Wang vd., 2011). Bu malzemelerle elektronik kartlar, robotik kollar gibi elektronik, rüzgâr tribünleri gibi enerji, dişliler, rulmanlar gibi makine, havacılık ve savunma gibi birçok sektörde ürün üretilmektedir (Gay, 2014).

Elyaf takviyeli kompozit malzemelerin temel bileşenlerinden biri olan elyaflar kompozite güç ve sağlamlık katmaktadırlar (Ünlü, 2023). Elyaflar kendi içinde doğal ve sentetik olarak iki sınıfa ayrılırken, sentetik elyaflardan biri olan karbon elyaflar birçok araştırmacının ilgisini çekmektedir. Aslında karbon elyafların keşfedilmesi çok eski dönemlere dayanmaktadır. Thomas Edison elektrik lambaların geliştirilmesinde pamuk ipliğini karbonize ederek karbon elyafı elde etmiş ve bunu kullanmıştır (Edison, 1879). Bu süreçte yapılan çalışmalara rağmen tungsten tellerin icadı ile karbon elyaf kullanımı son bulmuştur. Dupont firması tarafından geliştirilen poliakrilonitril (PAN)' den elde edilen elyaflar ile birlikte karbon elyafın temeli oluşturulmuştur (Houtz, 1950). İlerleyen süreçlerde Amerika ve İngiltere başta olmak üzere birçok ülke havacılık ve uzay alanındaki çalışmaların artmasıyla karbon elyaf üretimi ve üretilen karbon elyafların geliştirilmesi konularındaki araştırmalar hızlanmıştır (Koçoğlu, 2023). Günümüzde geliştirilen karbon elyaflar ile birlikte yüksek dayanım, korozyon direnci, yanmazlık, elektriksel iletkenlik, biyolojik uyumluluk, düşük genleşme gibi avantajlardan bahsedile bilinirken, gevrek kırılma, yöne bağlı özellikler ve üretim maliyeti gibi olumsuzlukları da vardır (Bajpai, 2021). Bu malzemelerin avantaj ve dezavantajlarından bahsetmemize karşın diğer malzemeler ile kıyaslandığında önemli artıları vardır. Dayanım açısından bakıldığında çeliklerden 7 kat, alüminyumdan 15 kat daha iyi iken yoğunluk açısından bakıldığında ise çeliklerden 4 kat daha hafiftir (Bajpai, 2021). Genel olarak, karbon elyaflar diğer malzemelerle karşılaştırıldığında üstün dayanım ve iletkenlik özelliklerine sahiptir.

Üretim açısından incelendiğinde diğer geleneksel malzemelere göre birtakım zorlukları bulunan karbon elyafların üretim maliyetleri diğer malzemelere göre daha yüksektir. Karbon elyaf üretiminde bir öncül malzeme kullanılmakla beraber, bu malzemeden üretilen liflerin karbonizasyonu ile gerçekleştirilir. Karbon elyafın genel olarak üretim aşamaları; lif yapma, stabilizasyon, karbonizasyon, yüzey iyileştirme ve kaplama olarak sıralanabilir (Mazumdar, 2001). Karbon elyafın üretim aşmaları aynı olup kullanılan öncül malzemeler değişmektedir. PAN öncülünde karbon elyaf üretimi, günümüzde en çok tercih edilen bir yöntem olup Poliakrilonitril (PAN) hammaddesinden yapılmaktadır. Ticari karbon elyaf üretiminin %90 PAN öncül malzemesi ile gerçekleştirilmektedir (Ünlü, 2023). Diğer bir öncül malzeme olan zift ile karbon elyaf üretimini 1960'larda ticarileştirilmiştir. Zift, petrol veya kömür katranından üretilir ve PAN bazlı elyaflarla kıyaslandığında elektriksel ve termal özellikleri daha gelişmiştir (Bajpai, 2021). Zift öncülü kullanılarak üretilen karbon elyafların, PAN'a ile üretilen karbon elyaflara kıyasla daha ucuz ve daha yüksek oryantasyona sahip olması da bir diğer avantajları arasında gösterilebilir (Morgan, 2005).

Bu çalışmanın amacı stratejik mühendislik malzemelerinden bir olan karbon elyafların, ikincil verilerden elde edilerek sektörel değerlendirmesi yapılmaktadır. Hem Dünya'da hem de Türkiye'de çeşitli sektörlerde kullanılan karbon elyaf ve karbon elyaftan mensucat ürünlerinin ithalat ve ihracat rakamları da ülkeler bazında kıyaslaması yapılmıştır.

2. MATERYAL VE METOT

Karbon elyaflar ülkelerin üretimini yapmak ve geliştirmek istediği stratejik bir malzeme olmasından dolayı sürekli araştırılması yapılmakta olan güncel bir konudur. İthalat ve ihracatta yer alan bu ürün çeşitli şekillerde ticarete konu olmaktadır. Dünyada ve Türkiye'de ticarete konu olan ürünlerden olan karbon elyaf ve karbon elyaftan üretilen mensucat (TDK: dokuma ürünü olan şeyler, dokuma) emtialarının Gümrük Tarife İstatistik Pozisyon (GTİP) numaraları sırası ile 681511000000 (681511) ve 681512000000 (681512) şeklindedir. Bahsi geçen GTİP kodu terimi ise; T.C. Ticaret Bakanlığı tarafından Türk Gümrük Tarife Cetvelinde kullanılan 12 rakamlı kod olarak belirtilmektedir. Bu kodun ilk 6 rakamı Dünya Gümrük Örgütü'ne üye tüm ülkelerce kullanılan Armonize Sistem (HS: Harmonized System) Nomanklatürü kodunu, 7-8'inci rakamları Avrupa Birliği ülkeleri tarafından kullanılan Kombine Nomanklatür (Combined Nomenclature-CN) kodunu, 9-10'uncu rakamları farklı vergi uygulamalarımız nedeniyle açılan pozisyonları gösteren kodlarını, 11-12 inci rakamlar ise istatistik kodlarını göstermek için kullanılmaktadır (T.C. Ticaret Bakanlığı, 2023). 681511 ve 681512 olarak belirlenen ve seçilen GTİP kodları 2022 HS revizyonunda oluşturulmuş ve sisteme dâhil edilmiştir. 2022 yılına kadar 681511 GTİP kodlu ürün olan Karbon Elyaf ve 681512 GTİP kodlu ürün olan Karbon Elyaftan Mensucat 681599 GTİP kodlu ürün altında ve kapsamında Dünyada ve Türkiye'de uluslararası ticarete (ithalata ve ihracata) konu olmuştur. 2022 yılında HS revizyonu olan GTİP kodları Resim.1'de gösterilmektedir.

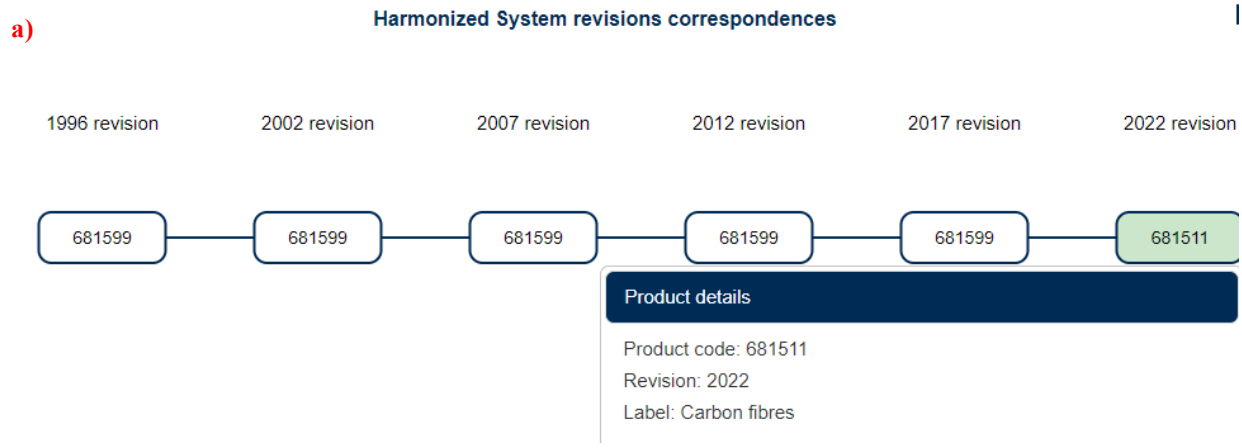

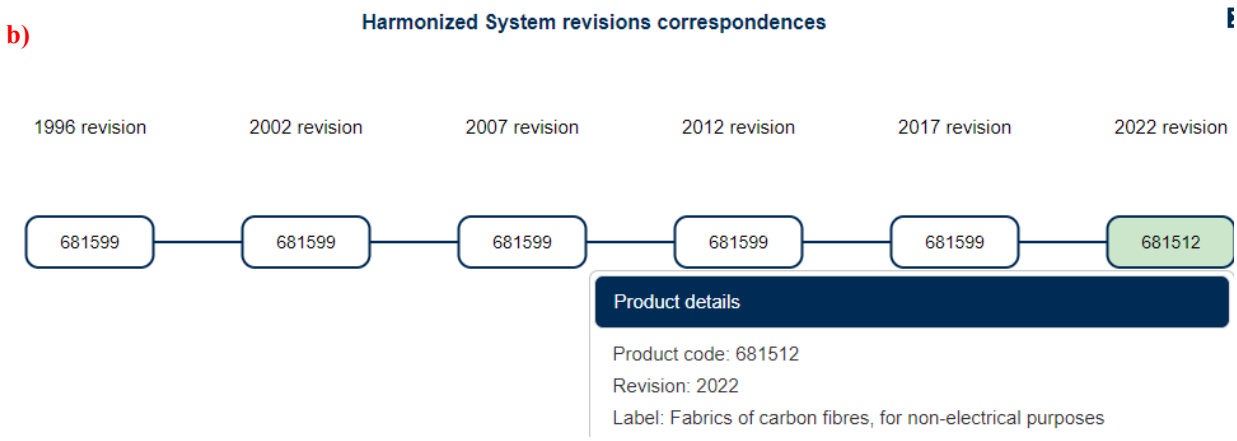

Şekil 1.- 2022 Yılı a)681511 ve b) 681512 HS Kodları Revizyonu (Trademap, 2023)

Uluslararası Ticaret Odası tarafından kurgulanmış ve yürütülmekte olan Trademap.org internet sitesi, 220 ülkenin ve bölgenin harmonize sistemde kayıtlı bulunan 5300 ürününü içerek şekilde tasarlanmıştır. Trademap.org internet sitesi sisteme dahil olan ülkelerin ilgili resmi istatistik kurumlarının veri tabanlarından ilgili ürünlerin ihracat ve ithalat rakamlarını çeşitli ölçütler (aylık, 3 aylık, 6 aylık, yıllık, kg/ton/lt, para birimi vb.) doğrultunda kendi bünyesine aktarmaktadır. İnternet sitesini kullanan araştırmacılar, ülkelerin ilgili ürünlerdeki dünya payına, yeni pazarlara, rekabetçi pazarlara, ihracatçı-ithalatçı detaylarına tablolar, grafikler ve haritalar şeklinde ulaşabilmektedir. Kısaca; Trademap.org sitesi uluslararası ticaretin ve iş olanaklarının geliştirilebilmesi için kullanılan istatistiki bilgiler sağlayan veri tabanı niteliğinde bir sistemdir.

681599 GTİP kodlu ürün olan ‘’Taştan ve Minerallerden Diğer Eşya’’ başlıklı ürün tanımı içerisinde birçok mineral, madde ve ürün olması dolayısı ile bu ürünlerin Dünyadaki ve Türkiye’deki ticari verilerine doğru şekilde ulaşılsa bile ilgili ürünler olan Karbon Elyaf ve Karbon Elyaftan Mensucat, ilgili verilerden 2022 yılına kadar elde edilememiştir. Bu duruma istinaden Karbon Elyaf ve Karbon Elyaftan Mensucat ürünleri ile ilgili 2022 HS revizyonu ile birlikte 2022 ve 2023/1. ay verileri bu çalışmada ele alınarak tablolarda kullanılmıştır

3. BULGULAR

Karbon Elyaf ve Karbon Elyaftan Mensucat ile ilgili bilgiler karşılaştırılması yapılırken öncelikle Türkiye’ye ait veriler yer almıştır. Tablo 1 ve Tablo 2’de Türkiye’nin ihracat verileri bulunmaktadır. 681511 GTİP kodlu karbon elyaf ürününün 2022 yılında Türkiye’den Dünyaya ihracat rakamı 4 milyon 636 bin Amerikan doları şeklinde gerçekleşmiştir. Aynı GTİP kodlu ürünün Türkiye’den Dünyaya 2023 yılı Ocak ayı ihracat verisi ise; 508 bin Amerikan doları şeklinde bilgi yer almaktadır (Trademap, 2023).

Tablo 1. 681511 GTİP Kodlu Karbon Elyaf Ürününün Türkiye’den Dünyaya İhracat Verileri (2022-2023M01) (Trademap, 2023)

Ürün Kodu	Ürün Tanımı	Türkiye’nin Dünyaya İhracatı (2022’deki Değer (milyon $))
681511000000	Karbon Fiber	4,636

Tablo.2’den anlaşılabileceği üzere 681512 GTİP kodlu karbon elyaftan mensucat ürününün 2022 yılında Türkiye’den Dünyaya ihracat rakamı 7 milyon 110 bin Amerikan doları şeklinde gerçekleşmiştir. Aynı GTİP kodlu ürünün Türkiye’den Dünyaya 2023 yılı Ocak ayı ihracat verisi ise; 1 milyon 517 bin Amerikan doları şeklinde trademap.org sitesinden elde edilmiştir. Her iki karbon elyaf ürün birlikte ele alındığı takdirde Türkiye 2022 yılında yaklaşık 11 milyon 800 bin Amerikan doları ihracat gerçekleştirmiştir.

Tablo 2. 681512 GTİP Numaralı Karbon Elyaftan Mensucat Ürününün Türkiye'den Dünyaya İhracat Verileri (2022-2023M01) (Trademap, 2023)

Ürün Kodu	Ürün Tanımı	Türkiye'nin Dünyaya İhracatı (2022'deki Değer (milyon $))
681512000000	Karbon Elyaftan Üretilen Mensucat	7,110

Benzer şekilde Türkiye'nin bu ürünler için ithalat rakamları trademap sitesinden alınmış olup ülke bazlı ihracat ve ithalat verileri incelenmiştir. 681511 GTİP kodlu karbon elyaf ürününde 2022 yılında Türkiye'nin Dünyadan yapmış olduğu ithalat rakamı 47 milyon 922 bin Amerikan doları şeklinde gerçekleşmiştir. Aynı GTİP kodlu ürünün Türkiye'nin Dünyadan 2023 yılı Ocak ayı ithalat verisi ise; 4 milyon 196 bin Amerikan doları şeklinde Trademap.org sitesinden elde edilmiştir.

Tablo 3. 681511 GTİP Numaralı Karbon Elyaf Ürününde Türkiye'nin Dünyadan İthalat Verileri (2022-2023M01) (Trademap, 2023)

Ürün Kodu	Ürün Tanımı	Türkiye'nin Dünyaya İthalatı (2022'deki Değer (milyon $))
681511000000	Karbon Fiber	47,922

Tablo 4. 681512 GTİP Numaralı Karbon Elyaftan Mensucat Ürününde Türkiye'nin Dünyadan İthalat Verileri (2022-2023M01) (Trademap, 2023)

Ürün Kodu	Ürün Tanımı	Türkiye'nin Dünyaya İthalatı (2022'deki Değer (milyon $))
681512000000	Karbon Elyaftan Üretilen Mensucat	17,050

Tablo.4'ten anlaşılabileceği üzere 681512 GTİP kodlu karbon elyaftan mensucat ürününde 2022 yılında Türkiye'nin Dünyadan yapmış olduğu ithalat rakamı 17 milyon 50 bin Amerikan doları şeklinde gerçekleşmiştir. Aynı GTİP kodlu ürünün Türkiye'nin Dünyadan 2023 yılı Ocak ayı ithalat verisi ise; 1 milyon 149 bin Amerikan doları şeklinde trademap.org sitesinden elde edilmiştir.

Ülke bazlı olarak ele alınan bu ürünler G-20'ye (Dünyanın gelişmiş ve gelişmekte olan ülkelerini bir araya getiren platform) dâhil olan ülkeler açısından da incelenmiştir. G-20'ye dâhil olan ülkelerde 2022 yılına ait 681511 GTİP kodlu ürünlerin ülke bazlı ithalat ve ihracat verileri Tablo 5'te paylaşılmıştır.

Tablo.5- 681511 Kodlu GTİP Ürünlerinin G-20'deki Ticari Verileri (2022) (1.000 Amerikan doları) (Trademap, 2023)

GTİP: 681511000000 – Karbon Elyaf		
G-20 Ülkeleri	**İthalat ($)**	**İhracat($)**
Almanya	334,005	212,142
ABD	224,586	451,910
Arjantin	*Bilgi Yok	*Bilgi Yok
Avustralya	4,133	525
Birleşik Krallık	148,266	147,490
Brezilya	2,629	46
Çin	218,027	35,384
Endonezya	7,579	0
Fransa	159,718	204,259
Güney Afrika	1,692	2,026
Güney Kore	70,475	170,408
Hindistan	*Bilgi Yok	*Bilgi Yok
İtalya	188,752	38,312
Japonya	52,574	435,227
Kanada	23,475	8,567
Meksika	*Bilgi Yok	*Bilgi Yok
Rusya	*Bilgi Yok	*Bilgi Yok
Suudi Arabistan	*Bilgi Yok	*Bilgi Yok
Avrupa Birliği-27 (Almanya, Fransa, İtalya Hariç)	405,727	448,121
Türkiye	47,922	4,636
Toplam:	1.889,560	2.159,053

(*) Trademap.org sitesinde bazı ülkelerin ilgili ürünlerde ithalat ve ihracat verileri paylaşılmadığından dolayı veri bilgisine ulaşılamamış olup ticari verilere eklenmemiştir.

G-20 ülkelerinin ihracat ve ithalat yüzdeleri ise Şekil 2'de verilmiştir. 2022 yılında 681511 GTİP kodlu üründe G-20 ülkeleri arasında ülkesel bazda en fazla ihracat; ABD, Japonya, Almanya şeklinde sıralanmıştır. En fazla ithalat ise; Almanya, ABD, Çin şeklinde meydana gelmiştir. İlgili sektörde toplam 1 milyar 889 milyon Amerikan doları şeklinde ithalat, 2 milyar 159 milyon Amerikan doları ihracat meydana gelmiştir.

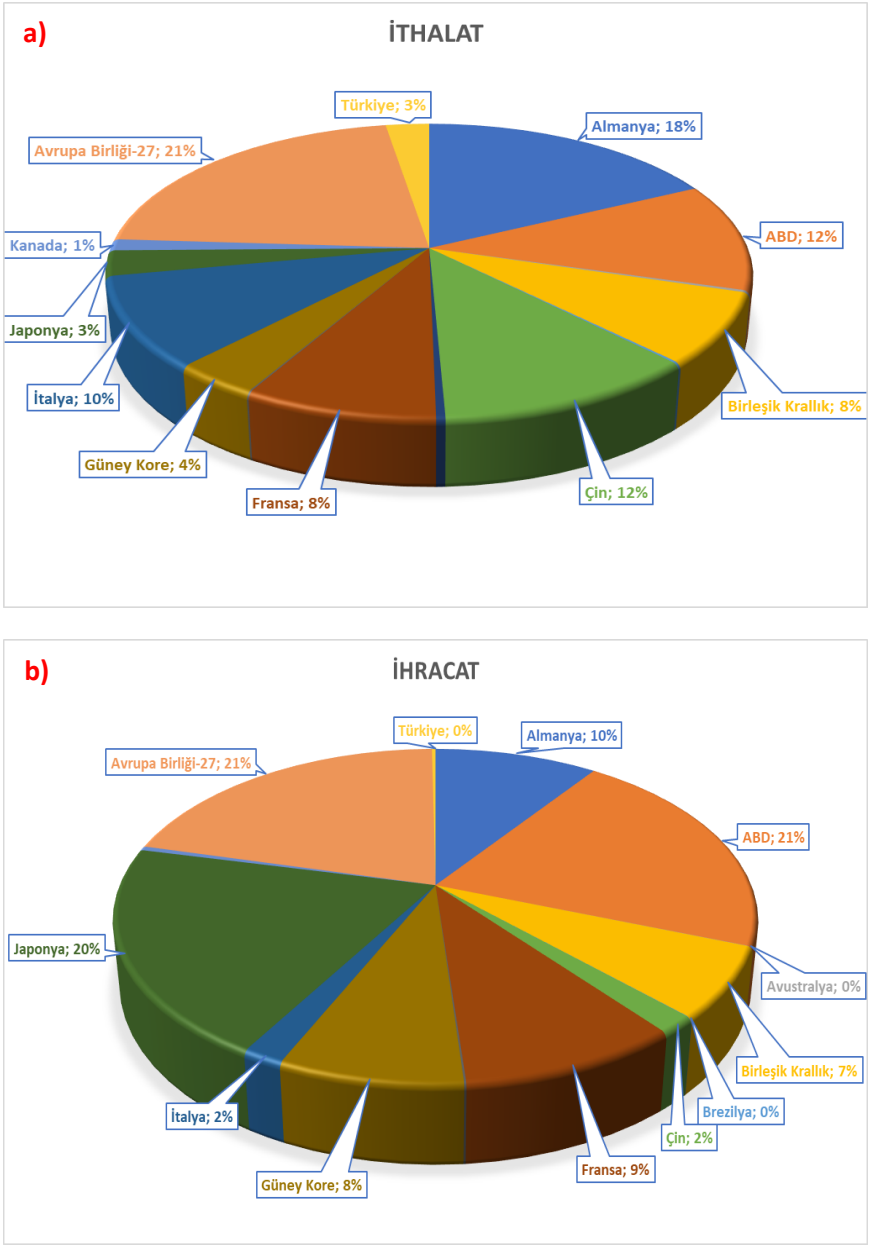

Şekil 2. 681511 GTİP kodlu üründe G-20 ülkelerin a)İthalat yüzdeleri b)İhracat yüzdeleri

G-20'ye dâhil olan ülkelerde 2022 yılına ait 681512 GTİP kodlu ürünlerin ülke bazlı ithalat ve ihracat verileri Tablo 6'da paylaşılmıştır. Ayrıca G-20 ülkelerinin ihracat ve ithalat yüzdeleri ise Şekil 3'te verilmiştir. 2022 yılında 681512 GTİP kodlu üründe G-20 ülkeleri arasında ülkesel bazda en fazla ihracat; Almanya, Japonya, ABD şeklinde sıralanmıştır. En fazla ithalat ise; İtalya, Birleşik Krallık, Çin şeklinde meydana gelmiştir. İlgili sektörde toplam 554 milyon Amerikan doları şeklinde ithalat, 825 milyon Amerikan doları ihracat meydana gelmiştir.

Tablo 6. 681512 Kodlu GTİP Ürünlerinin G-20'deki Ticari Verileri (2022) (1.000 Amerikan doları) (Trademap, 2023)

GTİP: 681512000000 – Karbon Elyaftan Mensucat		
G-20 Ülkeleri	**İthalat ($)**	**İhracat($)**
Almanya	36,676	181,012
ABD	42,599	116,409
Arjantin	*Bilgi Yok	*Bilgi Yok
Avustralya	10,105	59
Birleşik Krallık	75,701	112,243
Brezilya	13,454	37
Çin	63,683	28,902
Endonezya	464	Bilgi Yok
Fransa	38,042	107,192
Güney Afrika	3,893	225
Güney Kore	3,170	3,388
Hindistan	*Bilgi Yok	*Bilgi Yok
İtalya	82,174	51,537
Japonya	29,315	151,158
Kanada	1,650	1,156
Meksika	*Bilgi Yok	*Bilgi Yok
Rusya	*Bilgi Yok	*Bilgi Yok
Suudi Arabistan	*Bilgi Yok	*Bilgi Yok
Avrupa Birliği-27 (Almanya, Fransa, İtalya Hariç)	136,330	65,357
Türkiye	17,050	7,110
Toplam:	554,306	825,785

(*) Trademap.org sitesinde bazı ülkelerin ilgili ürünlerde ithalat ve ihracat verileri paylaşılmadığından dolayı veri bilgisine ulaşılamamış olup ticari verilere eklenmemiştir.

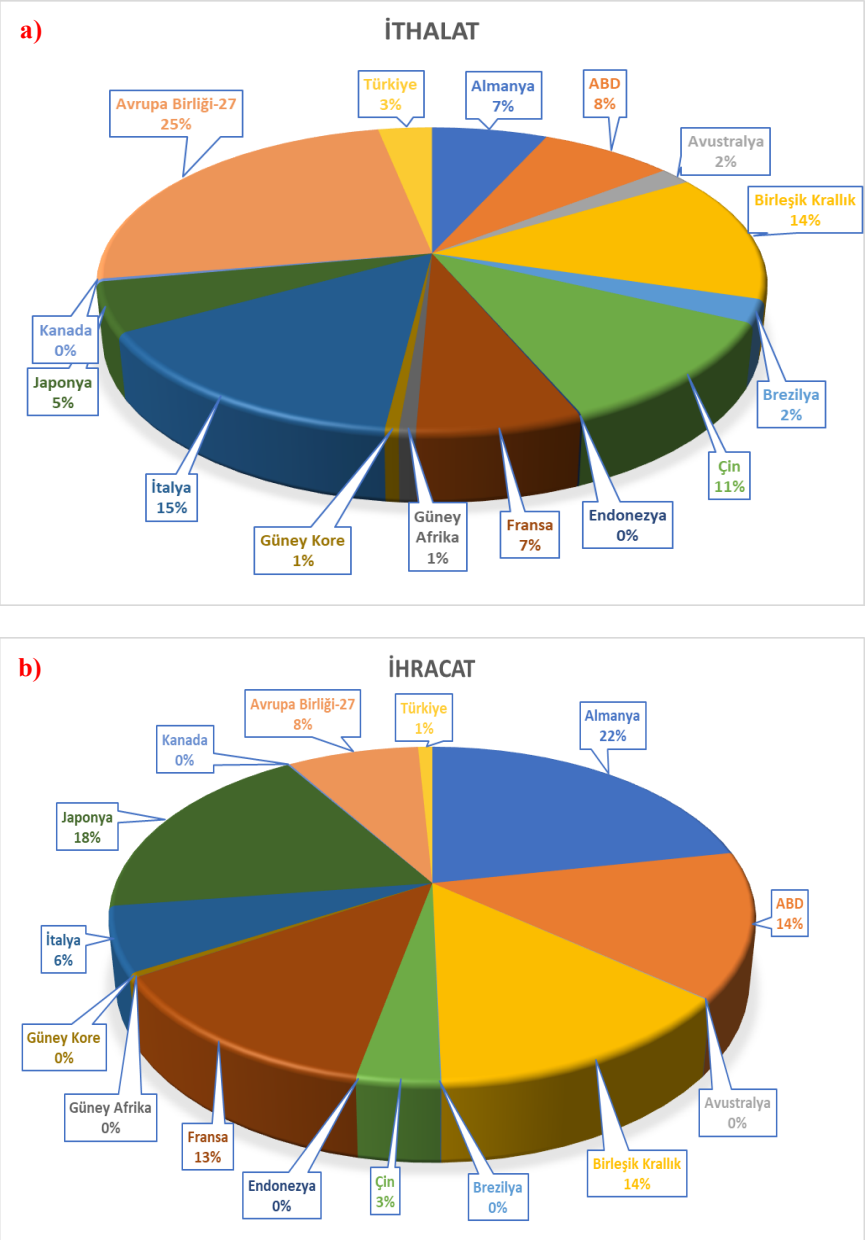

Şekil 3. 681512 GTİP kodlu üründe G-20 ülkelerin a)İthalat yüzdeleri b)İhracat yüzdeleri

4. TARTIŞMA VE SONUÇLAR

Mühendislik malzemelerinden biri olan karbon elyafların ticarete konu olan ihracat ve ithalat anlamında G-20 ülkeleri açısından incelemesi yapılmıştır. Ticarete konu olan ürünlerden olan karbon elyaf ve karbon elyaftan üretilen mensucat emtialarının GTİP numaraları vasıtasıyla 2022 yılına ait ikincil verilerden faydalanarak Türkiye ve G-20 ülkeleri bazlı bakılmıştır. Her iki GTİP numarasına bakıldığında en fazla ihracat; ABD, Japonya, Almanya; En fazla ithalat ise, Almanya, ABD, Çin şeklinde sıralanmaktadır. Türkiye bazında bireysel olarak bakıldığında ise her iki GTİP numarası 2022 yılına ait verilerinde yaklaşık 11 milyon 800 bin Amerikan doları ihracat gerçekleştirirken, 65 milyon Amerikan doları da ithalat yapmıştır.

KAYNAKLAR

Agarwal, B. D., & Broutman, L. J. (1990). Analysis and performance of fiber composites Second edition. John Wiley & Sons.

Bajpai, P. (2021). Applications of carbon fiber/carbon fiber-reinforced plastic/recycled carbon fiber-reinforced polymers. Carbon Fiber (Second Edition), 139-155.

Edison, T. A. (1879). Electric lamp. Patent US, 223898.

Gay, D. (2022). Composite materials: design and applications. CRC press.

Houtz, R. C. (1950). " Orlon" Acrylic Fiber: Chemistry and Properties. Textile Research Journal, 20(11), 786-801.

HS Kodları, (2022). https://www.trademap.org/Index.aspx (Erişim 5 Haziran 2023).

Koçoğlu, H. (2023) Atık Karbon Elyaf Yeniden Kullanımı İçin Polimer Matrisli Hibrit Kompozit Malzeme Geliştirilmesi. Gebze Teknik Üniversitesi Fen Bilimleri Enstitüsü.

Mallick, P. K. (2007). Fiber-reinforced composites: materials, manufacturing, and design. CRC press.

Mazumdar, S. (2001). Composites manufacturing: materials, product, and process engineering. CrC press.

Morgan, P. (2005). Carbon fibers and their composites. CRC press.

Türkiye Cumhuriyeti Ticaret Bakanlığı, (2022). https://ticaret.gov.tr/gumruk-islemleri/sikca-sorulan-sorular/ticari/tarife (Erişim 5 Haziran 2023).

Ünlü, S. (2023). Polimer matrisli elyaf takviyeli kompozit malzeme imalatı ve balistik özelliklerin incelenmesi. Sakarya Üniversitesi Fen Bilimleri Enstitüsü.

Wang, R. M., Zheng, S. R., & Zheng, Y. P. G. (2011). Polymer matrix composites and technology. Elsevier.

Visualization of beetle brain with analog artificial intelligence

Zoltán Attila Godó[1*]

Abstract: The closest possible analogy of artificial neural networks to the living nervous system can bring us closer to understanding the independent reactions induced by connectomics. We can assume that a similar data flow takes place in the living nervous system, but the visibility of which has not yet been resolved. The 4-dimensional visualization of AI analog signals with colors, developed by us, provides insight into the learning process of the neural network. The learning of the AI is caused by pleasant or unpleasant signals from the sensors of a beetle robot. So stroking or hitting the robot triggers the reorganization of the weights of the AI node. The output of the neural network controls the movement of the robot beetle. We managed not only to implement the visualization, but also to create an effective didactic tool for teaching AI to programming major university's students.

Keywords: connenctomy, visualiser, neural network, beetle brain, artificial intelligence

[1] University of Debrecen, Faculty of Informatics, Department of Information Technology, Debrecen, Hungary
* Corresponding author: zoltan.godo@inf.unideb.hu

1. Introduction

The more we know about the functioning of the living nervous system, the more new questions arise. We know exactly the connection between the nerve cells of some simpler organisms. This is connectomics. The nematode Caenorhabditis Elegans (C. Elegans), for example, is such a reference organism whose anatomy is well mapped. (White et al. 1986).

During a very exciting research, Timothy Busbice (Timothy B. 2014) created a program that can be started three hundred and two times where each program inherits the attributes one of each of the worms 302 neurons and uses interprocess communications to connect the programs together in a manner similar to that of synaptic communication. Wrapping the entire connectome into a framework whereby sensory input can be derived from robotic sensors and directed to connectome sensory neurons, which in turn activates interneurons, which activate motor neurons, and muscle output can be accumulated to activate robotic motors, the simulated connectome and connectome framework allows for a biological simulation and study of the entire connectome from sensory input to muscular output.

The experiments discussed in his paper show that the connectome alone is enough to give rise to experimental behaviors shown in the biological organism. This, in part, answers the age-old question of whether the connectome alone can have value in determining animal phenotypes.
The connectomics of more complicated organisms has only recently been processed at the level of the fruit fly (*Drosophila melanogaster*) . This is already the result of enormous research work. The brain of the fruit fly contains 127,978 neurons (Dorkenwald S. 2023). How so many neurons can perform such a complex function as flying (Takemura S. et al. 2023) is still an area of intense research today.

The closer analogy of artificial neural networks with the living nervous system can bring us closer to understanding the independent reactions induced by connectomics. However,

modeling the analog characteristics of the living nervous system results in an unprocessable amount of information. Therefore, visualizing the process of learning and rebuilding AI helps the human brain see the previously invisible processes inside the neural network (Boyle J. 2012). The closest possible analogy assumes that a similar data flow takes place in the living nervous system, but the visibility of which has not yet been resolved.

2. Objectives

- Novel, 4-dimensional visualization of neural network AI
- Visualization of analog signals with colors
- Visualization of the reorganization and learning mechanism of AI
- Output control of a beetle robot
- Realization of AI through the signals of the beetle robot's sensory organs (sensors) and visualization
- Creating an AI learning process with reflexes

2. Material ve Method

The neural network visualization software was created under the Linux operating system in the C++ programming language. The beetle is directly controlled by an arduino uno microcontroller. The movement is done by Adafruit 2201 servo motors. The distance is detected by the Iduino ST1099 Ultrasonic sensor. The mechanical receptors are replaced by the Joy-it SEN-VIB01 vibration sensor. The communication between the PC and arduino with Xbee chip.

3. Artificial Intelligence (AI) imitating the beetle brain

The beetle's "brain" is a neural network program developed by us. The software is capable of generating a three-dimensional neural network of any size. The number of nodes of the neural network is given in the program argument. Thus, it starts with the allocation of memory of the required size. Each node is stored in an array data structure. Weights, i.e. connections between nodes, are stored in a separate, dynamic data structure. Thus, the number of connections between nodes is arbitrary. During the operation of the neural network, the number of connections can change without limitation. So, during the learning process, new connections can be created, which shows analogous characteristics to the plasticity of the living nervous system. In addition, redundant, i.e. unused, connections can be built up, which is similar to the apoptosis of living systems. With the characteristics of the dynamic structure of the neural network, we tried to achieve the best similarity of the characteristics of the living nervous system.
Nodes represent individual neurons. The weights between the nodes are the axons and dendrites. Since the communication of nerve cells in synapses is one-way, the weights of the neural network are also limited to one-way traffic. In the living nervous system, the synapses of axons release neurotransmitters across the presynaptic membrane. It diffuses across the synaptic cleft and binds to receptors on the postsynaptic membrane. Here, it causes a local potentiation, which triggers the further stimulation of the targeted nerve cell. That is, information passes from one nerve cell to another, in one direction. Even so, the one-way weights between the nodes of the neural network function as synapses.

3. Visualization of how AI works

One of the great innovations of the project is the visualization of neural processes. Since neural processes are extremely fast and moreover represent analog values, our idea is visualization with colors. It is true that neurons work digitally. That is, there is a resting potential. This is an average voltage difference of 90 mV measured on both sides of the nerve cell membrane. When an information signal passes through the membrane of the nerve cell, a series of local potential changes passes through it. At these points, the resting potential changes to a so-called action potential, the average value of which is +30 mV. The cell has no choice, no way back. That is, if an action potential is triggered, the "all or nothing law" comes into effect. So when the process starts, it changes completely into an action potential and then back into a resting potential. This is welcome for us bioinformaticians, since the cell works roughly with discrete values. In other words, we can distinguish between a binary resting potential of 0 and an action potential of 1 value.

However, the information is carried by the frequency, which is basically an analog signal. And the frequency is not only affected by the information content. But it is influenced by many analogous processes. In other words, if there is a signal with a certain frequency, it is not certain that the same frequency will reach the central nervous system. A number of things influence this. The channels of the nerve cell membrane, the ions, the capacity of the sodium-potassium ion pump responsible for recovery, the condition of the synapses, the amount of neurotransmitters, their release, their rate of elimination, etc... We also think differently when we are hungry, dehydrated, didn't get enough sleep or drank alcohol, etc. In other words, we influenced the quality of neural information processes.

In the neural network, this can be modeled in many different ways. There are many theories about this. They are all different, try to model the processes of the living nervous system as best as possible. The more or the more typical physiological features are described with the models, the greater the analogy with the functioning of the living nervous system.

Our AI model system also searches for optimal solutions. Therefore, the weights between the nodes transmit an analog signal. These can be summed up and the nodes only transmit signals above the threshold value.

We solved the visualization of many and fast analog signals with colors. Thus, during the operation of AI, we practically see the communication between neurons and its weight, that is, the strength of the analog signal, which is analogous to the signal frequency of the communication between neurons. It's like looking into the brain and seeing the thoughts. It's a stunning sight.

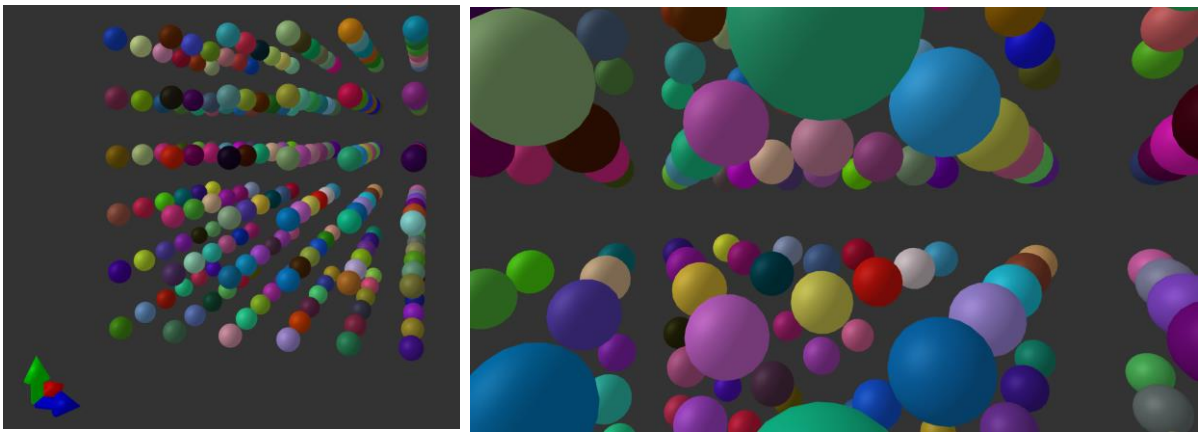

Figure 1. The colors of the analog signals running in the neural network

The visualization is performed by an independent software called "visualiser". It is separate software because we have ensured the universality and free development of the system. The program is extremely close to hardware, made in the c++ programming language based on linux and uses the OpenGL library. A file created in virtual memory is used for communication. The file contains exactly three times as many bytes as the number of nodes in the neural network. One node is described by three RGB bytes. The nodes can record True Color color values, that is, in principle, they can display 16.7 million analog values. The program reads the file at a very high speed and if there is a change in it, it is displayed immediately. Thus, we can create the AI neural network in any programming language.

We can operate it, store it, save it. But the visualization is solved by an independent program running in parallel. This makes the system very efficient and fast.

3. Its role in AI education

It has proven to be a particularly effective tool in university education. University students can start their project work in the field of AI immediately and do not have to worry about complicated visualization. As soon as a network has been declared and the data has appeared in the array, the contents of the memory section can be paged out one by one into the file by writing a block. And the "visualizer" displays it immediately. The memory state of the three, or more precisely, four-dimensional arrays along with changes over time can be monitored in real time, and the processes can be visualized. Thus, they quickly gain a sense of success in AI programming and immediately see the results and continuous operation of their program. The visualizer provides extremely advanced visualization. The three-dimensional neural network object can be rotated as desired using the mouse. Furthermore, we can zoom in and get into its interior, as if we ourselves were tiny signs in a living brain. Meanwhile, signals are constantly rushing around us, from node to node. Informative for researchers and a fascinating sight for students. In this way, we also utilize its didactic significance.

4. Learning AI

We did not upload the known connectomics of a living species into our neural network, but a fictitious initial connection system. Then we started teaching AI. We also tried to implement

learning in a model as close to life as possible. That's why we created the body of the beetle. This is still under development, but we are currently building a robot beetle controlled by arduino microcontrollers and powered by servo motors. The outputs of the AI, which controls the muscles in the living nervous system, here the equivalent of the muscles are the motors. So the outputs move the beetle robot. The AI's inputs are the beetle's senses. In this case, a phototransistor, which is an analogue of the eye, an ultrasonic distance sensor and some vibration sensors, which represent the beetle's mechano-receptors.

Figure 1. Robot beetle

During the teaching process, reflexes can be built up with pleasant and unpleasant stimuli. Pleasant reinforcement is, for example, stroking (weak vibration). Unpleasant reinforcement is, for example, hitting the beetle (strong vibration on the vibration sensors) or, for example, bright light on the phototransistors. So teaching AI is teaching a robot beetle. By stroking or beating with a stick. The independent movement resulting from the connector is confirmed or extinguished. This affects the AI system and relationships are built or broken because of it. Thus, AI is taught with a completely novel input. On the one hand, the system is much closer to living systems than previous learning mechanisms. On the other hand, the "visualiser" immediately shows the changes in the brain (AI) when the beetle is poked. That is, the rushing cavalcade of colors shows the analog signals running on nodes and weights. As we vexation the beetle, the operation and restructuring of the AI neuron network changes, which is immediately visible. This is a highly effective teaching and learning reinforcement for University students as well.

5. Further developments

We will supplement our system with a neural network built from real hardware. We are currently developing a real neural network built from 6x6x6 nodes. Here, the nodes are represented by STM32 microcontrollers and the weights are represented by the analog and digital data lines between them. Learning is provided by the use or inactivation of data lines, by logically creating arbitrarily long data paths between nodes that are far from each other. We connect the hardware neural network with the software neural network. Thus, a neural network and the real neuron network will jointly form the AI.

4. Discussion and Conclusions

We managed to create a visualization that can show the internal data flow of an analog neural network created in any programming language. We can track data traffic in real time, which is indicated by TrueColor colors. During the learning process, connections are built, rebuilt or destroyed in the neural network. The change of AI can therefore be visualized in real time. During our current development, we modeled the brain of a fictitious beetle, which is similar to the connectomics of already known living nervous systems. So far, the nervous system of Caenorhabditis Elegans (C. Elegans) consisting of 302 neurons has been fully modeled. The fruit fly's nervous system contains too many neurons in comparison. Our AI system controls a robot imitating a beetle with its output. The beetle's sensors correspond to living senses. Vibration, distance and light sensors are input signals given to AI. We achieve the training of our system by vexating the beetle robot. That is, we caress or hit, which sends pleasant or unpleasant, i.e. strong or weak, vibration signals to the neural network. As a result, the neural network is rebuilt, which our visualization system makes immediately visible. The novel learning model is extremely spectacular and shows a closer analogy with living systems. The spectacular visualization and the visibility of the inner workings of AI have a great didactic value in the University Education of programming students. The closest possible analogy to living systems, such as connecting AI with a hardware neural network and teaching AI with reflexes, helps to build more natural artificial systems. We need to understand what phenomena in living systems are caused by connectomics alone and what carries the higher organization above e, the entity of living beings.

References

Boyle J H, Berri Sand Cohen N (2012) Gait modulation in C. elegans: an integrated neuromechanical model. Front. Comput. Neurosci. 6:10. doi: 10.3389/fncom.2012.00010

Dorkenwald S, Matsliah A, Sterling AR, Schlegel P, Yu SC, McKellar CE, et al. (2023). Neuronal wiring diagram of an adult brain. bioRxiv 10.1101/2023.06.27.546656.

Raphael Norman-Tenazas, Erik C. Johnson, William R. Gray Roncal (2019). Training a neural model using the C. elegans connectome to perform exploration tasks. Society for Neuroscience 2019. URL: https://www.jhuapl.edu/isc/publication/35

Takemura S. et al. (2023). The Connectome of the Male Drosophila Ventral Nerve Cord, bioRxiv. doi: https://doi.org/10.1101/2023.06.05.543757 Timothy Busbice (2014). Extending the C. Elegans Connectome to Robotics - SOLID 2014 conference. URL: https://goo.gl/pxavvY

White, JG, Southgate, E., Thomson, JN, and Brenner, S. (1986). The structure of the nervous system of the nematode Caenorhabditiselegans. Philos. Trans. R. Soc. Lond. B 314, 1–340.doi:10.1098/ rstb.1986. 0056

Biometric Personal Classification by EMG Signals Using The AlexNet Method

Bekir Bilgin[1], Mehmet İsmail Gürsoy*[2], Ahmet Alkan[3]

Abstract: Person classification systems are technologies developed to recognize individuals based on their physical or behavioral characteristics. These systems use features such as a person's fingerprint, face, iris structure, vein pattern and speech. These features may be insufficient to protect personal data in terms of risks arising from information leakage, theft, fraud or personal faults. For higher security, electrical signal-based bioelectric systems that include both biometric and behavioral features are needed. Bioelectrical signal measurements such as EEG and EMG allow for the obtaining of unique bioelectrical signatures that reflect the unique physiological characteristics of each individual. EMG signals include both conscious hand and wrist movements and the physiological characteristics of the person. These EMG signals are unique to each individual and can be identified using these features. In this study, it is aimed at identifying the person with the deep learning algorithm by determining the features in the EMG signals. In this study, the Gesture Recognition and Biometrics ElectroMyogram (GrabMyo) dataset from the open-access PhysioNet database was used. A person recognition model was developed using the signals obtained from the fist movements of the hands of 10 different people with a 28-channel EMG device. The data were recorded with the EMG device for 5 seconds at a sampling frequency of 2048 Hz. Each person repeated the fist movement of the hand seven times. In this study, the Continuous Wavelet Transform (CWT) method was used to obtain the feature vector. The data obtained from each channel was divided into 500 ms (1024 samples) windows and 10 scalogram images (227 x 227) were obtained. A total of 280 scalogram images were obtained from 28 channels, and a total of 1960 scalogram images were obtained from one person since each person repeated the first movement seven times. The created scalogram images were classified using the AlexNET algorithm, one of the deep learning methods. In the model developed in the classification process, 80% of the dataset was used for training and 20% for testing. As a result of classification, 93.11% accuracy was found. The obtained results show that the proposed method can recognize people with high accuracy. It is thought that it can be widely used in financial instruments, military fields, telephones, and communication application areas that require a very high level of security.

Keywords: EMG, Personal Classification, Continuous Wavelet Transform, AlexNet.

[1]**Address:** Kahramanmaraş Sütcü İmam University, Electrical Electronics Engineering Department, Kahramanmaraş/Türkiye

[2]**Address:** Adiyaman University, Electrical and Energy Department, Adiyaman/Türkiye

[3]**Address:** Kahramanmaraş Sütcü İmam University, Electrical Electronics Engineering Department, Kahramanmaraş/Türkiye

***Corresponding author**: mgursoy@adiyaman.edu.tr

1. GİRİŞ

Elektromiyografi (EMG), kasların elektriksel aktivitesini ölçmek için kullanılan bir testtir. Kaslar kasıldığında, kas lifleri elektriksel sinyaller üretir. EMG, bu sinyalleri ölçerek kasların ne kadar iyi çalıştığı ve sinirlerin kaslara sinyal gönderip gönderemediği hakkında bilgi verebilir(Phinyomark, Limsakul, and Phukpattaranont 2011; Shin, Jung, and Kim 2017). "Elektro" kaslar ve "miyografi" ise kasların aktivitesini ölçme anlamına gelir. EMG, vücuttaki kasların kasılmaları sırasında ürettikleri elektriksel sinyalleri kaydederek çalışır. Kaslar, sinirler tarafından kontrol edilir ve sinirler kaslara beyinden gelen elektriksel sinyalleri ileterek onları hareket ettirir. EMG, elektrot adı verilen küçük metal elektrotlar kullanılarak bu kaslardan elde edilen elektriksel sinyalleri kaydeder. Elektrotlar, cilt yüzeyine yerleştirilir ve kaslardan gelen elektriksel aktiviteyi algılar.Başta Periferik nöropati, Kas distrofisi, Miyoklonus, Titreme, Amyotrofik lateral skleroz (ALS), Polimiyozit, Romatoid artrit, Kas yaralanmaları olmak üzere birçok hastalık için kullanılmaktadır. EMG, bir nörolog veya fizik tedavi uzmanı tarafından yapılmaktadır(Shioji et al. 2017; Taşar 2022; Venugopalan et al. 2015).

Kişi tanıma sistemleri, bir kişinin kimliğini doğrulamak, tanımak veya sınıflandırmak için kullanılan teknolojilerdir. Bu sistemler, bir kişinin benzersiz fiziksel veya davranışsal özelliklerini kullanarak tanıma işlemini gerçekleştirir. Kişileri tanımak için kullanılan farklı kişi tanıma sistemleri türleri bulunmaktadır. Biyometrik Tanıma Sistemleri, kişilerin

benzersiz fiziksel veya davranışsal özelliklerini kullanarak kimlik doğrulama veya tanıma işlemidir(Fan et al. 2022; Lu et al. 2020). Parmak izi tanıma, yüz tanıma, iris tanıma, retina taraması, parmak damarı, el geometrisi, ses tanıma ve yürüme biyometrisi gibi farklı biyometrik özellikler kullanılarak kişiler tanınır.

Yüz Tanıma Sistemleri, Yüz tanıma sistemleri, kişilerin yüzlerini kullanarak kimlik doğrulama veya tanıma işlemini gerçekleştiren bir biyometrik tanıma türüdür. Yüz tanıma, yüzün benzersiz özelliklerini ve yapılarını kullanarak kişileri sınıflandırır veya eşleştirir. Parmak İzi Tanıma Sistemleri, Parmak izi tanıma, kişilerin parmak izlerini kullanarak kimlik doğrulama veya tanıma yapar. Parmak izleri, parmakların dış yüzeyindeki benzersiz desenler sayesinde her kişi için farklıdır. Sesi Tanıma Sistemleri: Ses tanıma sistemleri, kişilerin sesini kullanarak kimlik doğrulama veya tanıma işlemleri gerçekleştirir. Kişilerin konuşma tarzları, ses tonları ve diğer ses özellikleri kullanılarak kişiler tanınır. Retina Tarama Sistemleri: Retina tarama, gözün retina tabakasındaki benzersiz damar desenlerini kullanarak kişi tanımada kullanılan bir biyometrik tanıma türüdür. Parmak Damarı Tanıma Sistemleri, Parmak damarı tanıma, parmakların iç yüzeyindeki damar desenlerini kullanarak kimlik doğrulama veya tanıma yapar. El Geometrisi Tanıma Sistemleri, El geometrisi, elin genel şekli ve parmakların uzunlukları gibi özelliklerini kullanarak kişileri sınıflandırır(Gui et al. 2019; Kim and Pan 2017; Lu et al. 2020).

Kişi tanıma sistemleri, güvenlik, erişim kontrolü, dolandırıcılık önleme, kişi tanıma ve diğer uygulamalarda kullanılır. Ancak, bu sistemlerin etik ve gizlilik konuları göz önünde bulundurularak uygulanması önemlidir. Kişisel verilerin güvenliğinin sağlanması ve kötü amaçlı kullanımın önlenmesi için uygun önlemler alınmalıdır.

2. MATERAL VE METOT

Bu çalışmada, CWT yöntemi ile EMG sinyallerindeki özellik vektörü elde edlmiştir. Bu özellik vektörlerinin 227 x 227 boyutunda her bir kişiye ait 10 tane scalogram görüntüleri bulunmuştur. Oluşturulan scalogram görüntüleri, derin öğrenme yöntemlerinden AlexNET algortiması kullanılarak sınıflandırma işlemi yapılmıştır.

2.1. Veriseti

Bu çalışmada açık erişimli PhysioNet veritabanından Gesture Recognition and Biometrics electroMyogram (GrabMyo) veriseti kullanılmıştır(Pradhan, He, and Jiang 2022).10 farklı kişiden elin yumruk haraketlerinden 28 kanallı (16 kanal kol, 12 kanal bilek) EMG cihazı ile elde edilen sinyalleri kullanarak kişi tanıma modeli geliştirilmiştir (Şekil.1). EMG cihazı ile veriler 2048 Hz örnekleme frekansı ile 5 saniye süresince kaydedilmiştir (Şekil 3). Her kişi elin yumruk hareketini 7 defa tekrar etmiştir.

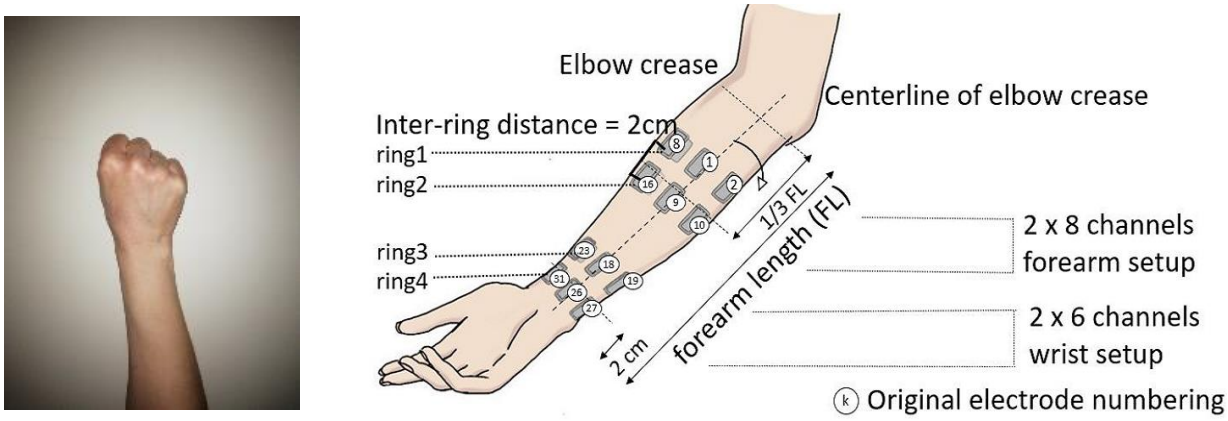

a b

Şekil.1 (a) Elin yumruk hareketi, (b) EMG ölçüm bölgeleri

Her kanaldan elde edilen veriler 500 ms (1024 örnek) pencerelere ayrılarak 10 tane 227 x 227 boyutunda scalogram görüntüsü elde edildi. 28 kanaldan toplam 280 scalogram görüntüsü ve her kişi yumruk hareketini 7 defa tekrar ettiğinden bir kişiden toplam 1960 scalogram görüntüsü elde edildi. Oluşturulan scalogram görüntüleri Derin öğrenme yöntemlerinden AlexNET algoritması ile sınıflandırma işlemi yapıldı. Sınıflandırma işleminde Geliştirilen modelde verisetinin %80 eğitim için, %20 test için kullanıldı. Sınıflandırma sonucunda % 93.11 doğruluk bulunmuştur. Elde edilen sonuçlar, önerilen yöntemin yüksek doğrulukta kişi tanıyabildiğini göstermektedir. Çok yüksek seviyede güvenlik

gerektiren finansal araçlarda, askeri alanlarda, telefon ve iletişim uygulama alanlarında yaygın olarak kullanılabileceği düşünülmektedir.

2.2 Continuous Wavelet Transform (CWT)

Continuous Wavelet Transform (CWT), bir sinyal veya zaman serisi verisini farklı ölçeklerde analiz etmek için kullanılan bir zaman-frekans analiz yöntemidir. CWT, zaman ve frekans bilgisini aynı anda elde edebilme yeteneği sayesinde bazı diğer zaman-frekans dönüşümlerine göre avantajlıdır. CWT'nin temel amacı, sinyaldeki zamanla değişen frekans bileşenlerini belirlemektir. Sinyaldeki farklı frekans bileşenlerinin zaman içindeki varlığını ve şiddetini açığa çıkarmak, birçok farklı uygulama için önemlidir. CWT, özellikle durağan olmayan ve zaman içinde değişen sinyallerin analizinde faydalıdır(Lu et al. 2019a, 2020).

Matematiksel olarak, CWT, sinyali bir analiz işlevi olan dalgacıkla (wavelet) süzerek elde eder. Dalgacık, belirli bir özellik ve ölçekte bir tür şablon işlevi olarak düşünülebilir. Bu işlem, sinyalin farklı zaman noktalarında dalgacıkla çapraz korelasyonunu hesaplayarak gerçekleştirilir. Bu çapraz korelasyon işlemi, zaman-frekans uzayında dağılım elde etmek için sinyalin farklı zaman noktalarında dalgacıkla örtüşme düzeyini ölçer(Lu et al. 2019b).

$$CWT(a,b) = \int_{-\infty}^{\infty} x(t) \frac{1}{\sqrt{a}} \psi\left(\frac{t-b}{a}\right) dt \quad (1)$$

Burada x(t) giriş sinyali, ψ(t) wavelet fonksiyonu, a kaydırma parametresi (zaman) ve b ölçek parametresi (frekans) temsil etmektedir.
CWT, sinyallerin ve veri setlerinin zamanla değişen özelliklerini belirlemek, gürültüleri gidermek, sıkıştırma ve veri sıkıştırma, ses ve görüntü işleme, biyomedikal sinyallerin analizi ve diğer çeşitli uygulamalarda kullanılır. CWT, çeşitli dalgacık türleri ve parametrelerle uygulanabilir ve analiz edilen sinyalin özelliklerine uygun olarak uyarlanabilir. CWT'nin uygulamaları, bilgi işlem, mühendislik, tıp, finans ve daha birçok disiplinde geniş bir yelpazede bulunmaktadır(Güneş and Akkaya 2023).

CWT, bir sinyali veya zaman serisini farklı ölçeklerde analiz etmek için kullanılan bir zaman-frekans dönüşüm yöntemidir. Bu dönüşüm, sinyali bir analiz işlevi olan dalgacık (wavelet) ile süzerek gerçekleştirilir(Lu et al. 2020).

2.3. AlexNET

AlexNet, 2012 yılında Alex Krizhevsky, Ilya Sutskever ve Geoffrey Hinton tarafından geliştirilen bir evrişimli sinir ağı (CNN) mimarisidir(Krizhevsky, Sutskever, and Hinton 2017). Bu mimari, ImageNet Large Scale Visual Recognition Challenge (ILSVRC) yarışmasında büyük bir başarı elde ederek derin öğrenmenin popüler hale gelmesine önemli katkıda bulunmuştur(Doğan and Türkoğlu 2018).

AlexNet, görüntü sınıflandırma görevlerini gerçekleştiren bir derin öğrenme modelidir. Temel olarak bir evrişimli sinir ağıdır ve verileri konvolüsyon, aktivasyon fonksiyonları, havuzlama (pooling) ve tam bağlantı katmanları kullanarak sınıflandırır. AlexNet, önceki dönemlerdeki geleneksel sınıflandırma yöntemlerine kıyasla daha derin ve daha geniş bir mimari kullanarak o dönem için oldukça büyük ve başarılı bir model olmuştur(Toğaçar, Ergen, and Özyurt 2020).

AlexNet'in temel özellikleri şunlardır:

Evrişim Katmanları: Evrişim katmanları, veriler üzerinde öğrenilebilir filtrelerin uygulanarak özellik haritalarının elde edilmesini sağlar. Bu katmanlar, görüntüdeki önemli özellikleri algılamak için kullanılır.

Aktivasyon Fonksiyonları: AlexNet, evrişim katmanlarının ardından ReLU (Rectified Linear Unit) aktivasyon fonksiyonunu kullanır. ReLU, doğrusal olmayan bir aktivasyon fonksiyonudur ve ağın non-lineer özelliklerini öğrenmesine yardımcı olur.

Havuzlama Katmanları: Havuzlama katmanları, boyut azaltma ve invariyans (değişmezlik) sağlamak için kullanılır. AlexNet, maksimum havuzlama (max-pooling) kullanarak boyut azaltma işlemi yapar.

Tam Bağlantı Katmanları: Son evrişim katmanlarının ardından tam bağlantı (fully-connected) katmanlar kullanılır. Bu katmanlar, sınıflandırma için özellikleri birleştirir ve son çıktıları elde eder(Krizhevsky et al. 2017).

AlexNet, ImageNet veri kümesinde 1000 farklı nesne sınıfını tanımak için eğitilmiştir ve o dönemdeki diğer yöntemlere göre büyük bir performans artışı sağlamıştır(Krizhevsky et al. 2017). Ayrıca, AlexNet, derin öğrenmenin popülerliğini artırmış ve günümüzde kullanılan birçok derin öğrenme modelinin temelini oluşturmuştur (Şekil.2).

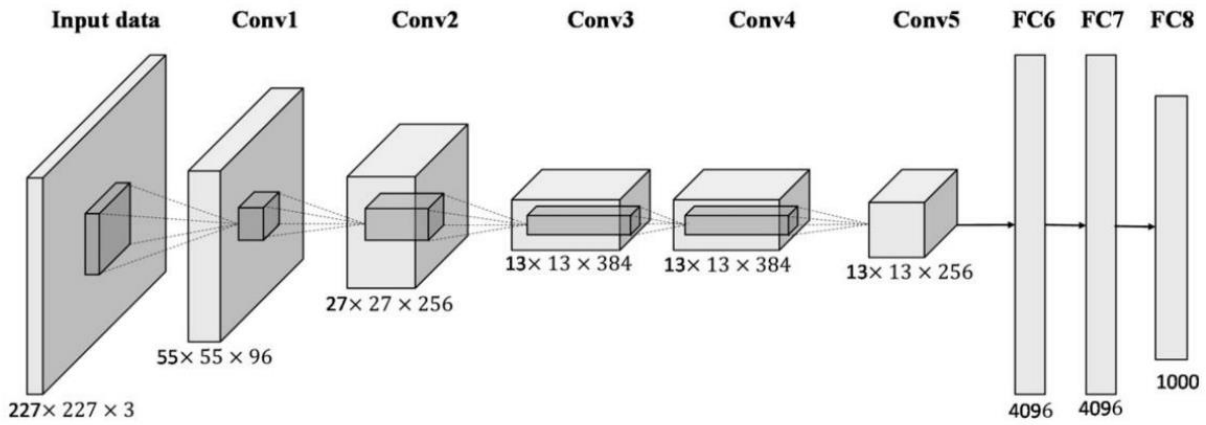

Şekil 2. AlexNet derin öğrenme mimarisi(Doğan and Türkoğlu 2018).

3. BULGULAR

Bu çalışmada geliştirilen model MATLAB programı ile geliştirilmiştir. Windows 11 işletim sistemi ile IntelCore i7 2.2 GHz işlemci ve 32 GB RAM özelliklerine sahip bilgisayar kullanılmıştır.

Açık erişimli PhysioNet veri tabanından Gesture Recognition and Biometrics ElectroMyogram (GrabMyo) veri seti kullanıldı. Yumruk hareket örüntüsü için 10 sınıflı kişi tanıma problemi oluşturuldu. Kullanılan 28 kanallı EMG cihazı ile 10 farklı kişinin ellerinin yumruk hareketlerinden elde edilen sinyaller Şekil.3'de gösterilmektedir.

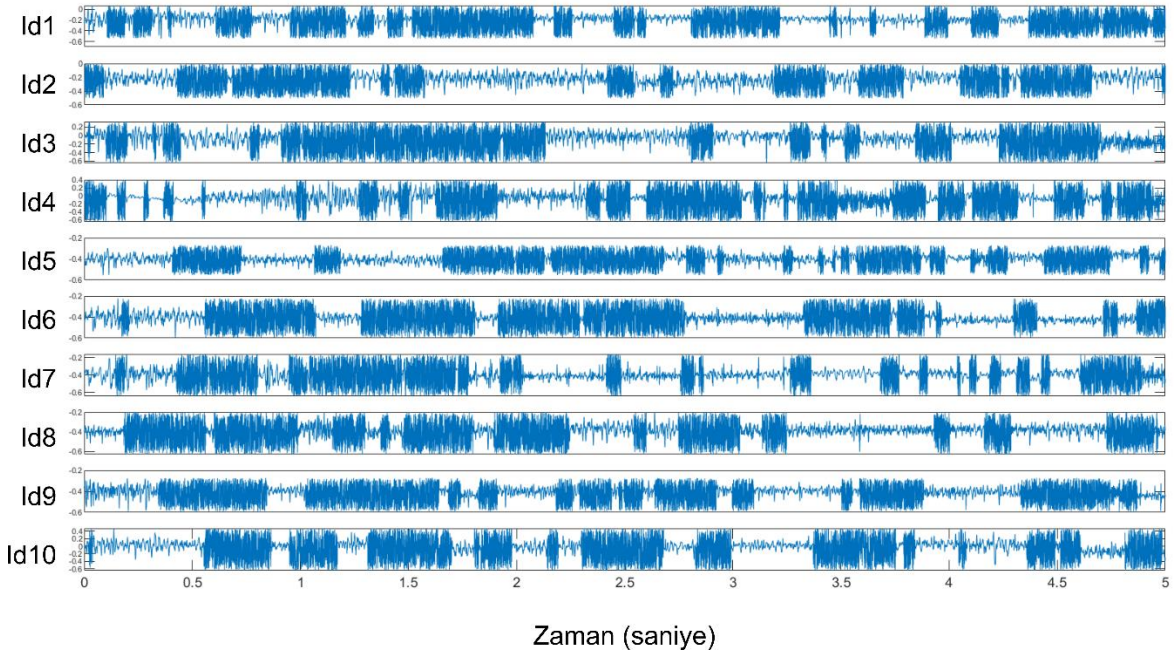

Şekil 3. 10 kişiye ait EMG sinyalleri

Her bir gönüllüden elde edilen 5 saniye uzunluğundaki sinyaller 250 ms'lik (512 örnek) pencerelere ayrıldı. Her bir penceredeki veriler CWT yöntemi ile analiz edilerek 227 x 227 boyutunda skalogram görüntüleri oluşturuldu (Şekil 4).

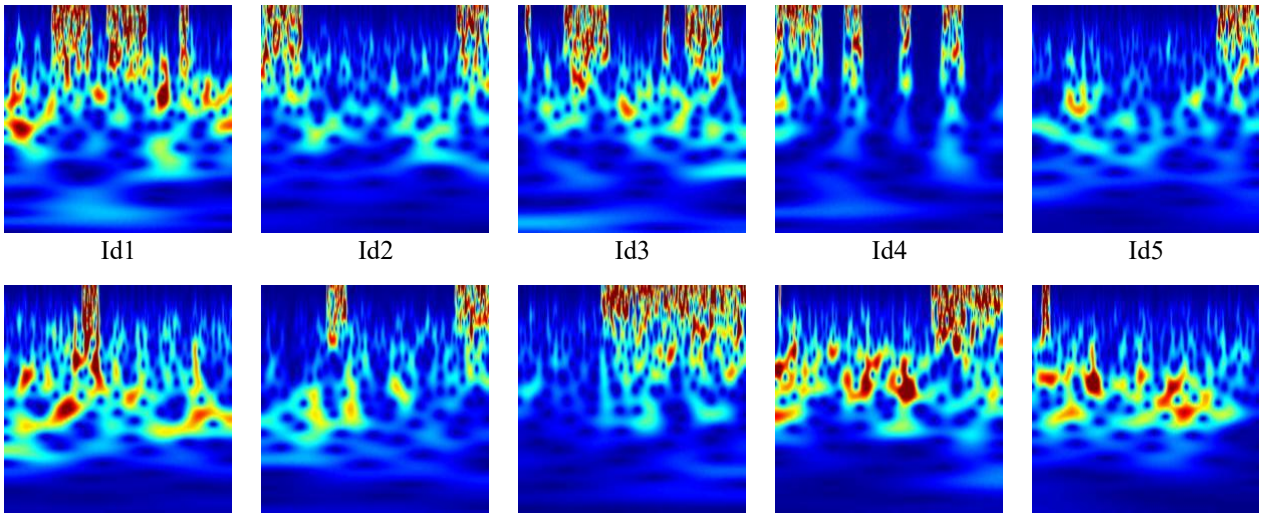

Şekil.4 Bilek hareketlerinin skalogram görüntüleri

CWT yöntemi ile oluşturulan skalogram görüntüleri Derin öğrenme yöntemlerinden AlexNET algortiması ile sınıflandırma işlemi yapılmıştır. Veri setinin %80 eğitim ve kalan %20 kısmı test işlemi için ayrılmıştır. AlexNET algoritmasında eğitim fonksiyonu için 'adam' fonsiyonu kullanıldı. Toplam 10 epoc ile eğitim işlemi tamamlandı. Sınıflandırma işlemi sonucunda %93,11 doğruluk oranı ile sonuçlar elde edildi. Sınıflandırma işlemi sonucunda elde edilen karışıklık matrisi (confusion matrix) Şekil.5 de gösterilmektedir.

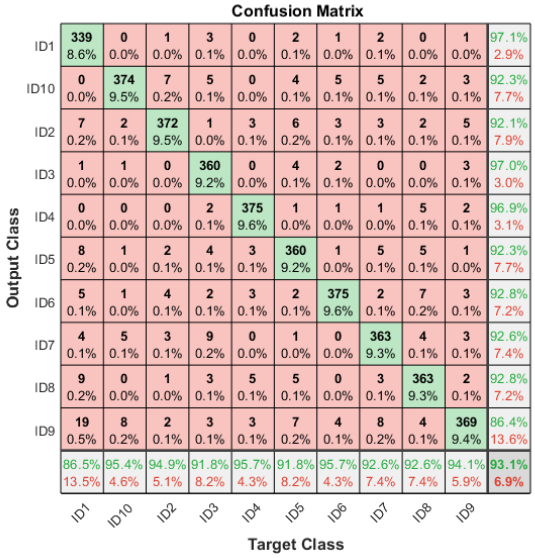

4. TARTIŞMA

Bu çalışmada, elin yumruk hareketi sırasında kaydedilen EMG sinyallerini kullanarak kişi tanıma için öğrenme tabanlı bir yaklaşım geliştirilmiştir. Önerilen modelde, yumruk hareketi sırasında kolda oluşan EMG sinyallerinin kişi tanıma problemlerinde yüksek doğrulukta sonuçlar elde ettiği gösterilmiştir. CWT yöntemi ile elde edilen özellik vektörü derin öğrenme algoritmalarından AlexNET yöntemi ile %93,11 sınıflandırma başarısı sağlamıştır. Bu sonuçlar doğrusal olmayan EMG sinyallerinin fizyolojik ve davranışsal biyometrik kişi tanıma probleminin başarısını göstermektedir.
Kişinin davranışsal yumruk hareketi ile kol ve bilek kaslarında meydana gelen fizyolojik EMG elektriksel sinyallerin başkaları tarafından kopyalanamaz olması, yüksek güvenlik gerektiren durumlarda çok yüksek güvenlik sağlayacağı düşünülmektedir.

Etik Kurul Onayı
N/A

Çıkar Çatışması
Yazarların beyan edecekleri çıkar çatışmaları yoktur.

Finansal Destek
Yazarlar bu çalışmanın herhangi bir maddi destek almadığını beyan etmişlerdir.

KAYNAKLAR

Doğan, Ferdi, and İbrahim Türkoğlu. 2018. "Derin Öğrenme Algoritmalarının Yaprak Sınıflandırma Başarımlarının Karşılaştırılması The Comparison Of Leaf Classification Performance Of Deep Learning Algorithms." *Molecular Plant-Microbe Interactions* 22(2):213–19.

Fan, Jiahao, Xinyu Jiang, Xiangyu Liu, Xian Zhao, Xinming Ye, Chenyun Dai, Metin Akay, and Wei Chen. 2022. "Cancelable HD-SEMG Biometric Identification via Deep Feature Learning." *IEEE Journal of Biomedical and Health Informatics* 26(4):1782–93. doi: 10.1109/JBHI.2021.3115784.

Gui, Qiong, Maria V. Ruiz-Blondet, Sarah Laszlo, and Zhanpeng Jin. 2019. "A Survey on Brain Biometrics." *ACM Computing Surveys* 51(6). doi: 10.1145/3230632.

Güneş, Harun, and Abdullah Erhan Akkaya. 2023. "Using Wavelet Analysis and Deep Learning for EMG-Based Hand Movement Signal Classification." *Sakarya University Journal of Science* 27(1):214–25. doi: 10.16984/saufenbilder.1176459.

Kim, Jin Su, and Sung Bum Pan. 2017. "A Study on EMG-Based Biometrics." *Journal of Internet Services and Information Security (JISIS)* 7(2):19–31. doi: http://dx.doi.org/10.22667/JISIS.2017.05.31.019.

Krizhevsky, Alex, Ilya Sutskever, and Geoffrey E. Hinton. 2017. "ImageNet Classification with Deep Convolutional Neural Networks." *Communications of the ACM* 60(6):84–90. doi: 10.1145/3065386.

Lu, Lijing, Jingna Mao, Wuqi Wang, Guangxin Ding, and Zhiwei Zhang. 2019a. "An EMG-Based Personal Identification Method Using Continuous Wavelet Transform and Convolutional Neural Networks." Pp. 5–8 in *BioCAS 2019 - Biomedical Circuits and Systems Conference, Proceedings*. IEEE.

Lu, Lijing, Jingna Mao, Wuqi Wang, Guangxin Ding, and Zhiwei Zhang. 2019b. "An EMG-Based Personal Identification Method Using Continuous Wavelet Transform and Convolutional Neural Networks." *BioCAS 2019 - Biomedical Circuits and Systems Conference, Proceedings* 31–34. doi: 10.1109/BIOCAS.2019.8919230.

Lu, Lijing, Jingna Mao, Wuqi Wang, Guangxin Ding, and Zhiwei Zhang. 2020. "A Study of Personal Recognition Method Based on EMG Signal." *IEEE Transactions on Biomedical Circuits and Systems* 14(4):681–91. doi: 10.1109/TBCAS.2020.3005148.

Phinyomark, A., C. Limsakul, and P. Phukpattaranont. 2011. "Application of Wavelet Analysis in EMG Feature Extraction for Pattern Classification." *Measurement Science Review* 11(2):45–52. doi: 10.2478/v10048-011-0009-y.

Pradhan, Ashirbad, Jiayuan He, and Ning Jiang. 2022. "Multi-Day Dataset of Forearm and Wrist Electromyogram for Hand Gesture Recognition and Biometrics." *Scientific Data* 9(1):1–10. doi: 10.1038/s41597-022-01836-y.

Shin, Siho, Jaehyo Jung, and Youn Tae Kim. 2017. "A Study of an EMG-Based Authentication Algorithm Using an Artificial Neural Network." *Proceedings of IEEE Sensors* 2017-Decem:1–3. doi: 10.1109/ICSENS.2017.8234158.

Shioji, Ryohei, Shin-ichi Ito, Momoyo Ito, and Minoru Fukumi. 2017. "Personal Authentication Based on Wrist EMG Analysis by a Convolutional Neural Network." Pp. 12–18 in *5th IIAE International Conference on Intelligent Systems and Image Processing*.

Taşar, Beyda. 2022. "Deep-BBiIdNet: Behavioral Biometric Identification Method Using Forearm Electromyography Signal." *Arabian Journal for Science and Engineering*. doi: 10.1007/s13369-022-06909-z.

Toğaçar, Mesut, Burhan Ergen, and Fatih Özyurt. 2020. "Evrişimsel Sinir Ağı Modellerinde Özellik Seçim Yöntemlerini Kullanarak Çiçek Görüntülerinin Sınıflandırılması." *Fırat Üniversitesi Mühendislik Bilimleri Dergisi* 32(1):47–56. doi: 10.35234/fumbd.573630.

Venugopalan, Shreyas, Felix Juefei-Xu, Benjamin Cowley, and Marios Savvides. 2015. "Electromyograph and Keystroke Dynamics for Spoof-Resistant Biometric Authentication." *IEEE Computer Society Conference on Computer Vision and Pattern Recognition Workshops* 2015-Octob:109–18. doi: 10.1109/CVPRW.2015.7301326.

Design and analysis of geothermal energy-driven combined plant for the production of power, freshwater and heating.

Fatih Yılmaz[*1]

Abstract: Geothermal energy is gaining importance day by day because it is an energy source that is least affected by environmental impacts among renewable energy sources. In this work, a comprehensive thermodynamic examination of a geothermal energy-assisted combined system for clean water, power, and heating generation purposes is presented. This study mainly consists of a flash-Binary power plant. As a subsystem, the secondary system consists of an organic Rankine cycle and a reverse osmosis unit (RO) for clean water production. In addition, a comparison of the efficiency with different refrigerants is carried out. The irreversibility occurring in the systems are determined and the parameters affecting the system performance change are analysed by parametric analyses. According to the analysis results, it has a net power generation capacity of 1807 kW. In addition, the total hot water production capacity is determined as 4195 kW. Moreover, the energy performance of the whole system is calculated as 18.06% and the exergy performance as 25.60%.
Keywords: Energy, exergy, geothermal, power, freshwater

[1]**Address:** Department of Mechatronics Engineering, Faculty of Technology, Isparta University of Applied Sciences, Isparta Turkiye

***Corresponding author**: fatiyilmaz7@gmail.com

1. INTRODUCTION

Energy usage is one of the key indicators showing countries' development level and societies' living standards. Population growth, urbanization, industrialization, and technological development straight enlargement energy consumption. This increase has led to environmental problems in parallel. Currently, about 80% of electricity is still generated from fossil fuels (Kaushik et al. 2011). Therefore, the use and production of energy is one of the most important environmental issues and one of the most important ways to overcome environmental problems is renewable energy sources. Renewable energy sources are depicted that solar, biomass, hydraulic, wind, and geothermal sources. Among these energy sources, geothermal energy is contained as thermal energy in the earth's interior. The source of this heat is linked to the internal structure of our planet and the physical processes that occur there (Barbier, 2002). Moreover, among these resources, electricity generation from geothermal energy has a significant potential for Turkey. It can be applied for purposes such as electricity, heating, and cooling, as well as being the oldest renewable energy source. Today, the most mutual technique is the low-temperature Flash-Binary power generation system (Yilmaz, 2018).

The use of the geothermal energy in the diverse combined systems for beneficial products also affects the method to be switching a clean and sustainable future. Herein, the geothermal energy-powered combined plant come to the fore. In the open literature, there are several papers about geothermally driven integrated plants. Kanoglu et al. (2010) investigated a geothermally driven plant with a PEM unit for the generation of hydrogen. They investigated the performance of the model including energy and exergy performance methods. The exergy efficiency of their plant (Case 1) is determined as 28.5%. The author (Yilmaz 2022) proposed a geothermal-driven multigeneration plant for the production of beneficial products. The paper is investigating a thermodynamic and environmental assessment. Total energy and exergy efficiency are determined as 52.01% and 29.45%, respectively. Furthermore, in 2023, Vaccari et al. (2023) examined a geothermal plant in terms of environmental performance for different configurations. Also, Huang et al. (2023) developed a single flash geothermal power plant that includes transcritical CO_2. They computed that the total plant's exergetic efficiency is figured as 32.46%. Continue, Güler et al. (2023) designed and developed a geothermal energy-driven power plant that advanced exergoeconomic analysis method. They found the cost per CO_2 emission of the system as 0.049 $/kWh.

As shown in the short literature investigation of the above-mentioned, the different design of geothermal energy-based power plant has gained more and more importance day by day for acquiring more power and more efficiency. The proposed paper investigates the thermodynamic performance analysis of the flash-Binary geothermal plant for producing power, heating, and fresh water. To generate these valuable outputs, a system is designed and then the overall system is examined with energetic and exergetic efficiencies methods.

2. MATERIAL AND METHOD

In this developed study, a geothermal energy-supported system was designed and then a comprehensive thermodynamic analysis was carried out. The system definition and analysis method will be mentioned in the subsections.

2.1. System description

The developed geothermal energy-based cycle, which is exemplified in Figure 1, is proposed and analyzed. The system is made up of the main four sub-cycles which are a geothermal cycle, ORC, RO, and domestic water preparation.

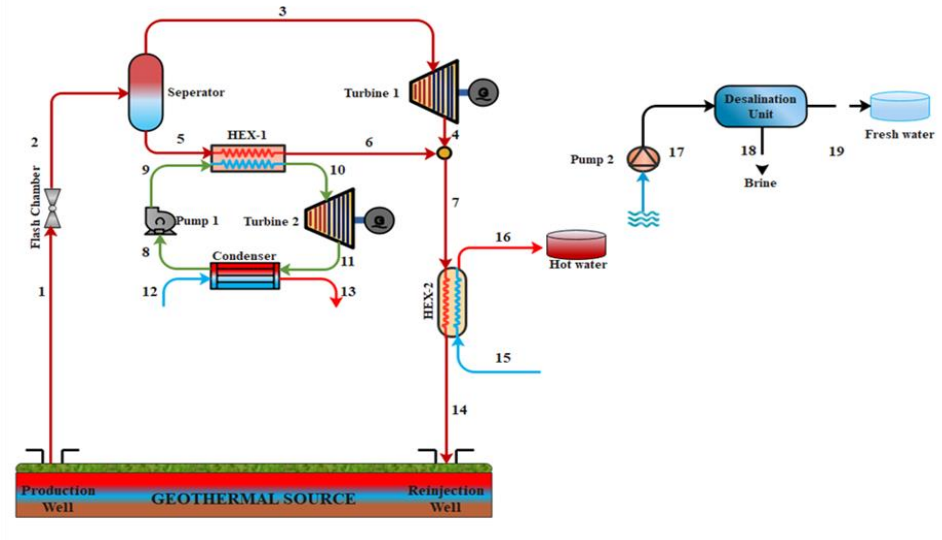

Figure 1 Representation plan of the developed system

Briefly, geothermal energy from underground enters the flash chamber and comes to the separator as a steam-water mixture. Then, in the separator, the saturated steam (point 3) and the saturated liquid separate at (point 5) and go to the subsystems. Steam expands in Turbine 1 and electricity generation occurs. The geothermal source at point 5 provides the necessary thermal energy for the R134a fluid ORC system and the ORC system operates. In the hot water preparation unit, it is possible to produce hot water between 40-60 °C for domestic applications. Finally, clean is obtained with the RO unit. The whole system continues to work simultaneously

2.2. Thermodynamic performance analysis

In this developed study, a detailed thermodynamic performance investigation is conducted and analyzed using the energy and exergy efficiencies methods. Generally, a thermodynamic analysis employed general four balance equations, which are mass, energy, entropy, and finally exergy. These thermodynamic balance formulations can be depicted below (Cengel and Boles, 2015; Bejan et al., 1995; Dincer, 2020);

$$\sum \dot{m}_i = \sum \dot{m}_e \tag{1}$$

$$\sum \dot{m}_i h_i + \sum \dot{Q}_i + \sum \dot{W}_i = \sum \dot{m}_e h_e + \sum \dot{Q}_e + \sum \dot{W}_e \tag{2}$$

$$\sum \dot{m}_i s_i \sum \left(\frac{\dot{Q}}{T}\right) + \dot{S}_{gen} = \sum \dot{m}_e s_e \tag{3}$$

$$\sum \dot{m}_i ex_i + \dot{Ex}_i^{\dot{Q}} + \dot{Ex}_i^{\dot{W}} = \sum \dot{m}_e ex_e + \dot{Ex}_e^{\dot{Q}} + \dot{Ex}_e^{\dot{W}} + \dot{Ex}_D \tag{4}$$

In these formulations, the subscripts i and e define the inputs and outputs of the system components. Then, the terms h, s, $\dot{Q}$ and $\dot{W}$ represent specific enthalpy, specific entropy, heat transfer, and work, respectively. The terms $\dot{E}x^{Q}$, $\dot{E}x^{W}$ and ex in Equation 4 are work heat and specific exergies and can be formulated as follows;

$$\dot{E}x^{Q} = (1 - \frac{T_0}{T_k})Q \quad (5)$$

$$\dot{E}x^{W} = W \quad (6)$$

The specific exergy can be written as below after disregarding the potential and kinetic energy terms;

$$ex = (h - h_0) - T_0(s - s_0) + ex_{ch} \quad (7)$$

herein, the ex_{ch} terms define the chemical exergy. To sum up, the thermodynamic efficiencies can be modeled as;

$$\eta_{sys} = \frac{\dot{W}_{net} + \dot{Q}_{hot\ water} + \dot{m}_{fw} h_{fw}}{\dot{m}_1 h_1 - \dot{m}_{14} h_{14}} \quad (8)$$

$$\psi_{sys} = \frac{\dot{W}_{net} + \dot{E}x^{\dot{Q}}_{hot\ water} + \dot{m}_{fw} ex_{fw}}{\dot{m}_1 ex_1 - \dot{m}_{14} ex_{14}} \quad (9)$$

3. RESULTS AND DISCUSSION

To perform the thermal performance examination of this paper, the Engineering Equation Solver (EES) program is employed and also some acceptance is presented in Table 1. Moreover, this study is modeled as steady-state flow condition, kinetic and potential energy changes are ignored, pumps and turbines have isentropic efficiency, and the heat loss between plant's apparatuses and the environment is neglected. In light of Table 1 assumption and inputs values, the analysis base case results are tabulated in Table 2. Based on herein values, the system net power production load is 1.8 MW and the freshwater generation rate is 1.664 kg/s, respectively. Also, total system energy and exergy efficiencies are determined as 18.06% and 25.60%.

Table 1. The design parameters and input variables for the developed system

Parameters	Value	Unit
P_1	900	℃
T_1	150	kPa
$\dot{m}_{geo}$	100	kg/s
rp_{FC}	3.5	-
$\eta_{is,T1}$	88	%
$\eta_{is,P1}$	82	%
Working fluid	R134a	-
ε_{HEX}	80	%
T_{17}	30	℃
P_{17}	101.325	kPa
Sea water salinity rate	42000	ppm
Freshwater salinity rate	0	ppm
Brine salinity rate	70000	ppm
Pinch point temperature	10	℃
T_0	10	℃
P_0	101.325	kPa

Table 2. Thermodynamic analysis results of the developed geothermal power plant

Parameters	Value
$\dot{W}_{T1}$	604 kW
$\dot{W}_{T2}$	1257 kW
$\dot{W}_{net}$	1807 kW
$\dot{m}_{fw}$	1.664 kg/s
$\dot{Q}_{heating\ load}$	4195 kW
η_{SG}	5.171 %
η_{sys}	18.06 %
ψ_{SG}	23.65 %
ψ_{sys}	25.60 %

After the given case study results, there are some parametric studies are also conducted and presented here. Figure 2 illustrates the impact of geothermal temperature on the net power rate. It is noted that the net power rate rises with the geothermal temperature. Looking at another perspective, Figure 3 presents the variation in the heating and freshwater rate versus geothermal source temperature. Finally, the effect of the geothermal source temperature on the plant efficiency is also given in Figure 4. To sum up, the geothermal temperature on the plant products and performance has a positive effect, which increases both system performance and generated products.

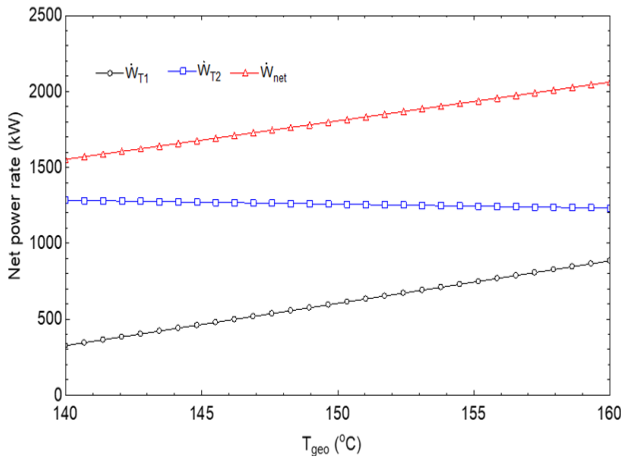

Figure 2. Variation of net power rate with a different geothermal source temperature

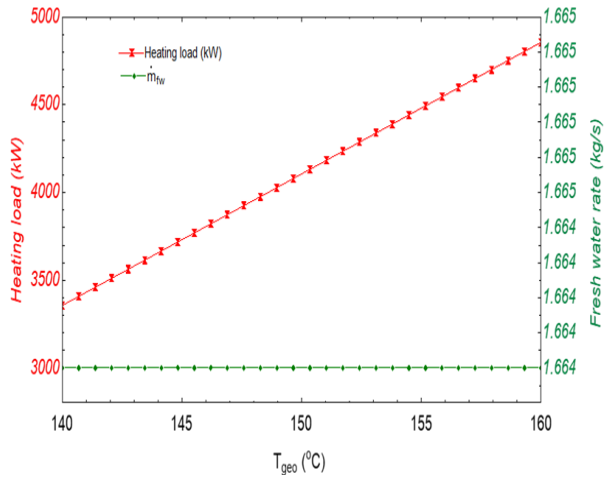

Figure 3. Variation of heating load and freshwater rate with a different geothermal source temperature

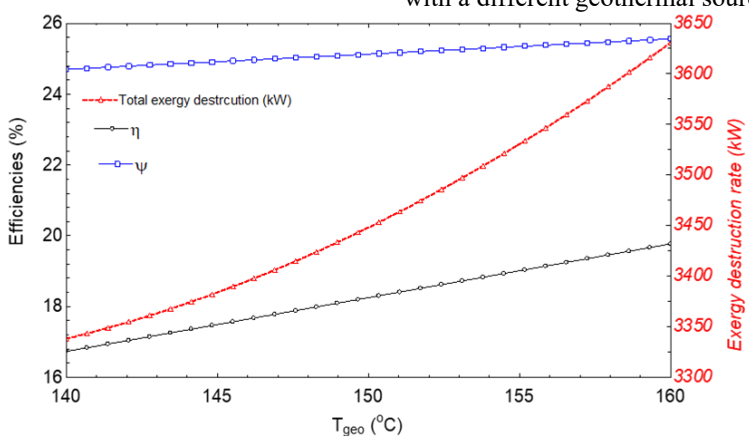

Figure 4. Variation of efficiencies and irreversibility rate with a different geothermal source temperature

Another important factor is the geothermal source capacity which is the mass flow rate. Increasing the geothermal capacity from 80 kg/s to 120 kg/s leads to an increase in the generated heat and freshwater capacities (as shown in Figure 5) and also increases the system performance (Figure 6). As indicated in Figure 5, the heating load is increased

linearly however the fresh water is not increased linearly. the plant's energetic and exergetic efficiencies are directly goes up with the capacity increase as indicated in Figure 6.

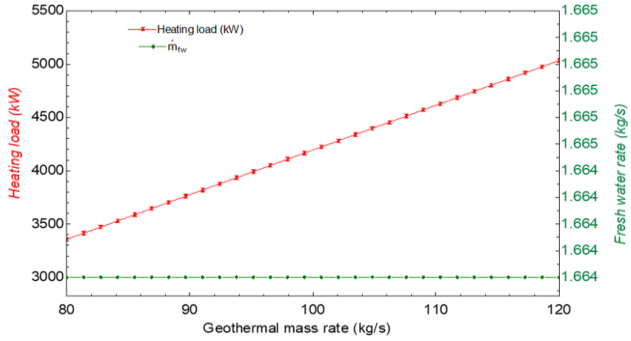

Figure 5. The effect of geothermal capacity on heating and fresh water rate

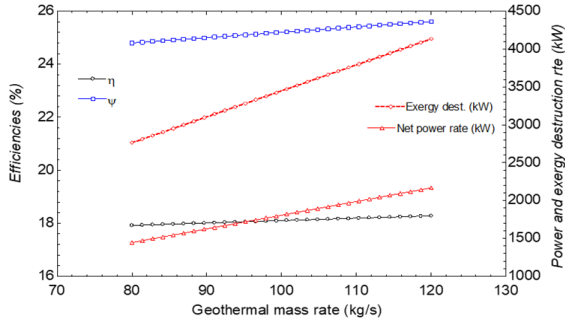

Figure 6. The influence of geothermal capacity on efficiencies and products of the overall system

Figure 7 and Figure 8 examine the effects of the increase in steam quality going to the separator on the system. According to Figure 7, since the increase in steam quality is directly related to the mass flow to the subsystems, the amount of power produced increases in Turbine 1 and decreases in Turbine 2. But as a result, net production increases. Figure 8 presents the total system efficiency and exergy destruction variation according to steam quality. As a result of the increase in system efficiency, the total exergy destruction decreases.

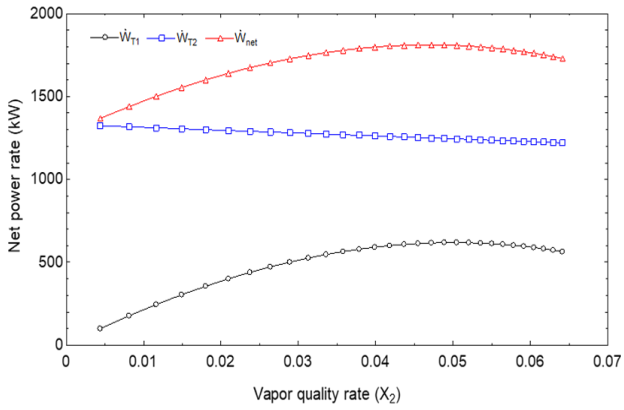

Figure 7. Net power rates varying against vapor quality ratio

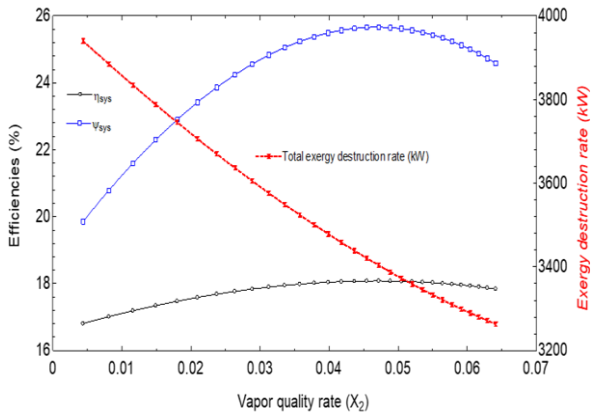

Figure 8. Overall system efficiencies and irreversibility rate varying against vapor quality ratio

Finally, the system performances of the power-only single generation (SG) and trigeneration system (electricity, clean water, and heating) are compared and revealed in Figure 9. As seen in the figure, the whole system is more efficient than single systems. Therefore, it is possible to achieve higher efficiency by designing geothermal energy systems with low efficiencies for multiple generation purposes.

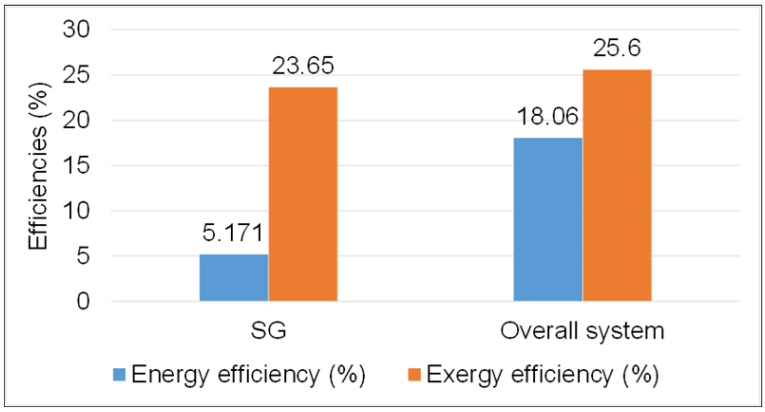

Figure 9. Performance comparation of SG and total plant

4. CONCLUSION

In this designed study, a thermodynamic performance investigation of the geothermal energy-supported integrated system for power, heating, and clean water production is carried out. To determine the system performance, parametric studies are carried out by applying both energy and exergy efficiency methods. Some important results that emerged as a result of the examination findings can be written as;

- The net power production is calculated as 1807 kW. In addition, the net domestic hot water production capacity was determined as 4195 kW.
- The clean water production capacity of this system is 1.664 kg/s.
- The energetic and exergetic efficiencies for the total model are figured as 18.06% and 25.60%.
- It has been determined that both the increase in geothermal temperature and the rise in geothermal capacity have a positive impact on the plant's performance.
- The increase in steam quality also increases the system's performance.

REFERENCES

Barbier, E. (2002). Geothermal energy technology and current status: an overview. *Renewable and sustainable energy reviews*, *6*(1-2), 3-65.

Bejan A, George T, Moran MJ. Thermal design and optimization. Wiley; 1995.

Cengel YA, Boles MA. Thermodynamics: an engineering approach. 8th ed. Mc. New York: McGraw-Hil;2015; 2015.

Dincer I. Thermodynamics: A Smart Approach. USA: John Wiley & Sons Ltd; 2020.

Güler, O. V., Gürbüz, E. Y., Georgiev, A. G., & Keçebaş, A. (2023). Advanced Exergoeconomic Assessment of CO2 Emissions, Geo-Fluid and Electricity in Dual Loop Geothermal Power Plant. *Energies*, *16*(8), 3466.

Huang, J., Abed, A. M., Eldin, S. M., Aryanfar, Y., & García Alcaraz, J. L. (2023). Exergy analyses and optimization of a single flash geothermal power plant combined with a trans-critical CO2 cycle using genetic algorithm and Nelder–Mead simplex method. *Geothermal Energy*, *11*(1), 1-20.

Kanoglu, M., Bolatturk, A., & Yilmaz, C. (2010). Thermodynamic analysis of models used in hydrogen production by geothermal energy. *International journal of hydrogen energy*, *35*(16), 8783-8791.

Kaushik, S. C., Reddy, V. S., & Tyagi, S. K. (2011). Energy and exergy analyses of thermal power plants: A review. *Renewable and Sustainable energy reviews*, *15*(4), 1857-1872.

Vaccari, Marco, et al. "Rigorous simulation of geothermal power plants to evaluate environmental performance of alternative configurations." *Renewable Energy* 207 (2023): 471-483.

Yilmaz, C. (2018). Thermoeconomic cost analysis and comparison of methodologies for Dora II binary geothermal power plant. *Geothermics*, *75*, 48-57.

Yilmaz, F. (2022). Development and modeling of the geothermal energy based multigeneration plant for beneficial outputs: Thermo-economic and environmental analysis approach. *Renewable Energy*, *189*, 1074-1085.

The Preservation Proposal for Zion Orphanage of Zincidere

Büşra Uzaslan*[1], Gonca Büyükmıhçı[2]

Abstract: Historical buildings are documents that help us understand the architectural features, social and economic status, culture, and values of the society in which they were built and help us establish a connection between the past and the present. To ensure physical and cultural continuity, it is important to understand and evaluate the values of cultural heritage.
The documentation of cultural heritages constitutes the beginning of the conservation activities. The documentation studies include the recording of the current station of the heritage and demonstrate the original values and the periods and stages that the building has undergone. Documentation of cultural heritages constitutes a source for archive studies and important for the accessibility of heritages and for the management and supervision of activities that will affect cultural heritage in the future with information.
This study includes documentation studies; surveys, restitution, and restoration decisions of Darüleytam of Zincidere. The building located in Zincidere town of Kayseri, including its architectural structure, physical condition, materials, and construction techniques. The building is one of the darüleytams established in many cities of Anatolia, especially in Istanbul, to shelter orphaned children and to provide them with a profession to bring them into society with the rapid increase in the number of orphans in a very short time after the Balkan Wars and World War I. The building was one of the 3 darüleytams in Kayseri. The study aims to transfer the building to the future, to participate in modern life, and to set an example for similar studies.

Keywords: Conservation, Darüleytam, Orphanege, Zincidere.

[1]**Address:** Erciyes University, Faculty of Architecture, Kayseri/Türkiye
[2]**Address:** ErciyesUniversity, Faculty of Architecture, Kayseri/Türkiye

***Corresponding author**: buscaglibulanik@gmail.com

1. ZİNCİDERE DARÜLEYTAMI

Yapı Kayseri İli, Talas İlçesi, Zincidere Mahallesi, Yurt Sokakta yer almaktadır. Yapının kitabesi bulunmamaktadır. Özbek, Erciyes gazetesinin 17 Aralık 1912 tarihli 26.sayısında, okulda düzenlenen mezuniyet ve diploma töreninin anlatıldığı yazının içeriğinden, yapının İsviçreli Miss Griber tarafından yetimhane olarak yaptırıldığı bilgisini aktarmaktadır (Özbek, 2011). Miss Griber ismiyle bahsedilen kişinin Maria Gerber olduğu anlaşılmaktadır. Miss Maria Gerber, Türkiye'de bulunduğu dönemdeki anılarını kaleme aldığı kitabında, Kayseri yakınlarında yer alan Zincidere'deki Zion yetim evi yapılarının inşaatına 1904 yılında başlandığını ve 2 yıl içinde tamamlandığını söylemektedir (Gerber,1917). Yetimhane olarak inşa edilen yapı, Eski Eserler ve Müzeler Genel Müdürlüğü'nün 23.05.2003 tarih ve 3317 envanter numaralı kararı ile tescillenmiştir.

Figure 1. Zincidere yetimhane yapısı 1924 sonrası (Ali Peker Arşivi).

Yetimhane geniş bir arazi içinde inşa edilmiş olup inşa edildiği arazinin etrafı ihata duvarı ile çevrelenmiştir. Arazinin kuzeyinde günümüze gelememiş çamaşırhane yapısı ve bir dönem cezaevi olarak kullanılan yatakhane binası, bu binanın kuzeyinde günümüze gelebilmiş olan tescilli bir hamam, yurdun kuzeybatısında muhdes su deposu ve güneydoğusunda tek katlı müştemilat yer almaktadır. Yapının içinde yer aldığı arazide, güney cephenin açıldığı avlunun kuzeybatı duvarında yuvarlak kemerli bir çeşme, avlunun güneyinden üç basamak ile çıkış sağlanan taş döşemeli bir merasim alanı ve merasim alanının kuzeyinde büstü günümüze gelememiş olan büst kaidesi, merasim alanının güneyinde sekizgen planlı havuz ve havuzun da güneyinde ağaçlandırılmış geniş bir alan bulunmaktadır (Figure 2).

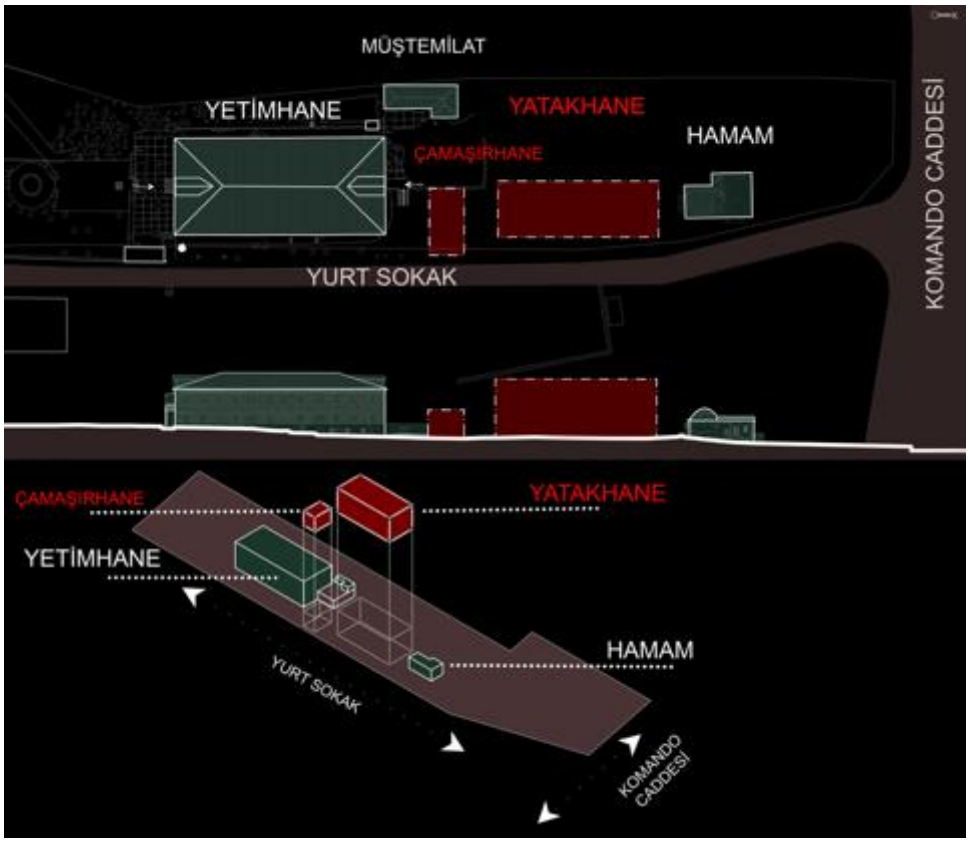

Figure 2. Vaziyet Planı, arazi içindeki mevcut ve zamanla yıkılan yapılar (Uzaslan 2022).

2. BELGELEME ÇALIŞMALARI

Yapının belgeleme çalışmaları, yapıya zarar vermeden, hassas ve doğru şekilde tespiti için lazer tarama yöntemi ile gerçekleştirilmiştir. Yapının ölçümünde kullanılan lazer tarayıcı, 360º yatay X 270º düşey olmak üzere, geniş açı ile tarama ve fotoğrafla belgelemenin yanı sıra, tanımlanan kısmi alan ve yüzeylere odaklanarak bu bölgelerin detaylı ve hassas taranması ve fotoğraflanması özelliklerine de sahiptir. Mekanlar arasındaki bağlantının kurulması için, cihaza bütünleşmiş pusula, altimetre, eğim ölçer özellikleri ile birlikte A4 boyutlu 'siyah-beyaz' referans kağıtları ve 12 adet referans küreleri (Sphere) kullanılmıştır.

Figure 3. Pointcab programından alınan data görünümü (Çağ Restorasyon, 2021).

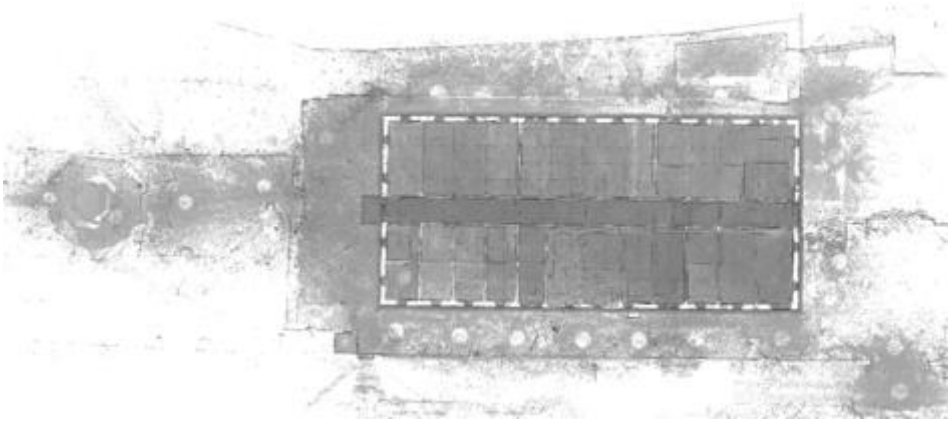

Figure 4. PointCab'den alınan istasyonların data görünümü (Çağ Restorasyon, 2021).

Yapının elemanları, taş duvar ve döşeme kaplamaları vb. yerlerde şerit metre ile ayrıntılı ölçüler alınarak detay çizimleri sahada elle yapılmıştır. Alınan detay ölçüleri lazer tarayıcı verileri ile birlikte değerlendirilmiştir. Yapının tüm bölümlerinin ayrıntılı ve eksiksiz belgelenmesi için yapıyı farklı açılardan gören birçok değişik noktadan fotoğraf çekimleri yapılmış, yapı bileşenleri hem genel hem de detaylı olmak üzere belgelenmiştir. Bu çekimlerden elde edilen fotoğraflar hem yapının cephe ve plan düzlemindeki taş elemanlar, derzleri ile süsleme vb. yapı bileşenlerinin belgelenmesinde lazer tarayıcı verileri ile birlikte kullanılarak değerlendirilmiştir. Lazer tarama sonucunda nokta bulutları ve elde edilen diğer datalar plan ve cephe çizimlerinde kullanılmıştır (Figure 3 ve 4).

2.1. Plan özellikleri

Zemin kat mekanlarının iki girişi bulunmaktadır. Bunlardan biri güney cephenin ortasında diğeri kuzey cephenin ortasında yer almaktadır. İki giriş birbiri ile aynı düzende kurgulanmıştır. Zemin kat mekanları kuzey-güney yönünde konumlanan koridorun iki yanında sıralanmaktadır. Zemin kat 14 mekandan oluşmaktadır. Üst kata çıkış günümüzde bu koridordan sağlanmaktadır (Figure 6).

Figure 5. Zemin Kat Koridoru, birinci katta kapatılmış merdiven (Uzaslan, 2021).

Bodrum kat yerleşim alanı, yetimhanenin inşa edildiği arazinin doğu-batı ve kuzey- güney doğrultusundaki kot farkından dolayı kuzeydoğu köşesinde kısmi olarak oluşturulmuştur (Figure 6). Bodrum kat 6 mekandan oluşmaktadır. Mekanların duvarları kesme ve moloz taş üzeri sıva, döşemeler beton şap, üst örtüler ise betonarmedir. Bodrum kata, bahçede doğu yönünde yer alan iki farklı kapı ile ulaşılmaktadır.

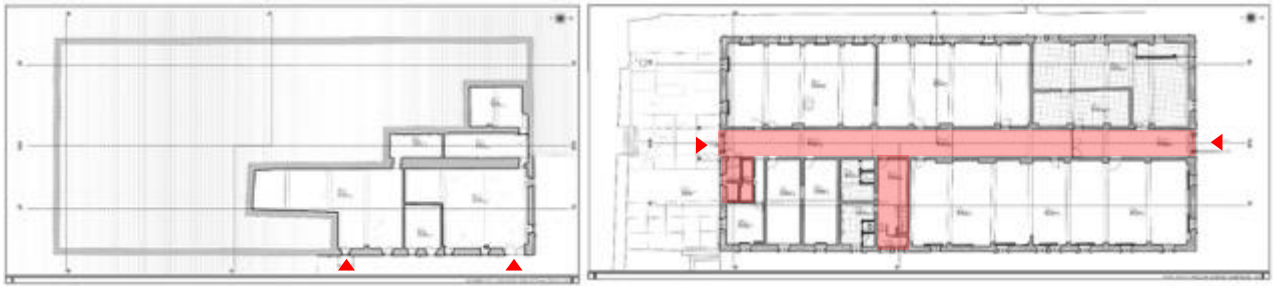

Figure 6. Bodrum kat ve zemin kat planı, rölöve çizimi (Uzaslan, 2021).

Birinci kat kotuna ulaşım iki merdiven ile sağlanabilmektedir. Merdivenlerden zemin kat rölöve planında yer alan Z-11 numaralı odanın doğusunda yer alan, sonradan üst kattan kapatılan merdiven kullanılamamaktadır (Figure 6). Birinci kat koridorun iki yanında konumlanan 12 mekandan oluşmaktadır. Birinci katta güney yönünde konumlanan balkon, ferforje korkuluk ile sınırlandırılmıştır (Figure 7). Balkonun döşemesi muhdes mozaik, üst örtüsü ise ahşap sundurma çatıdır.

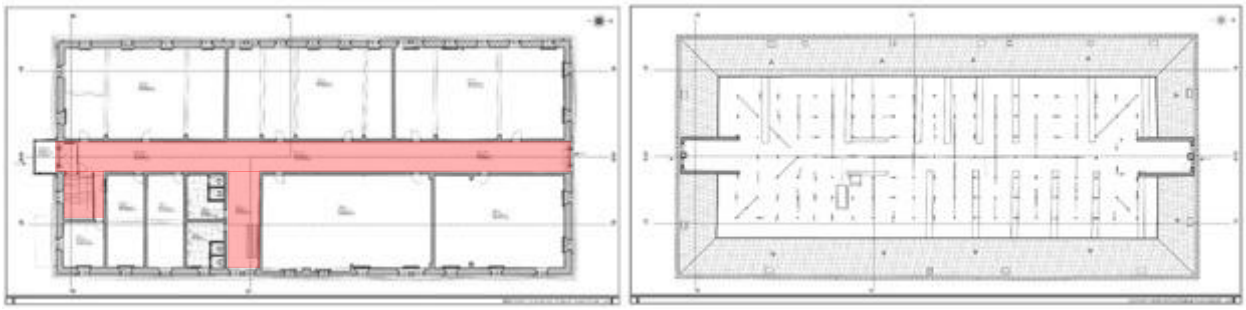

Figure 7. Birinci kat ve çatı katı planı rölöve çizimi (Uzaslan, 2021).

Yetimhanenin çatı katına çıkış birinci katta yer alan 1-05 numaralı mekanın güneybatısındaki demir merdiven ile sağlanmaktadır (Figure 7). Çatı katının döşemesi betonarme olup birinci katın betonarme kirişleri 30 cm kadar çatı katının döşemesinden taşırılmıştır. Çatı katının üst örtüsü ahşap strüktür ile taşınan kırma çatı ile oluşturulmuştur. Çatı katının kuzey ve güney ucunda üçgen alınlıklı cihannümalar yer almaktadır (Figure 7 ve 8).

Figure 8. Çatı Katı kuzey yöndeki cihannüma ve çatı katı bağlantısı (Uzaslan, 2021).

2.2. Cephe özellikleri

Yapının cepheleri, ortası kabartılmış kırmızı renkli andezit malzemeden, yığma tekniğinde inşa edilmiştir. Doğu cephe, bodrum kat mekanlarının girişini barındıran cephedir. Bu girişler muhdes demir doğrama kapılar ile kapatılmıştır. Cephenin bodrum kat girişlerinin bulunduğu kısım ve su basman seviyesi muhdes çimento esaslı harç ile sıvanmıştır. Cephenin zemin kat mekanlarının yer aldığı seviyede, aynı yatay aksta 14 adet pencere boşluğu açılmıştır (Figure 9). Pencere boşlukları dikdörtgen formlu, basık kemerli, taş söveli olup ahşap doğramalı bir kanadı açılır olmak üzere çift kanatlı pencere ile içten kapatılmıştır. Pencere boşlukları dıştan demir parmaklıklar ile örtülmüştür. Cephenin üst katı, zemin kattan, cephe boyunca yatay taş silme kuşağı ile vurgulanarak ayrılmıştır. Cephenin birinci katına da alt kattaki gibi aynı yatay aksta ve formda 14 adet pencere açılmış olup bu pencereler zemin kattaki gibi demir parmaklık ile kapatılmamıştır.

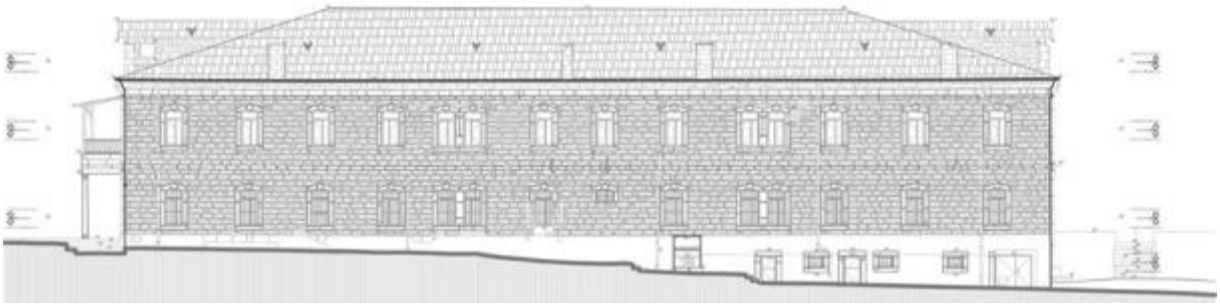

Figure 9. Doğu cephe rölöve çizimi (Uzaslan, 2021).

Yapının batı cephesi, zemin kat mekanlarının yer aldığı seviyede, aynı yatay aksta, 12 adet pencere boşluğu açılmıştır (Figure 10). Pencere boşlukları dikdörtgen formlu, basık kemerli, taş söveli olup ahşap doğramalı bir kanadı açılır olmak üzere çift kanatlı pencere ile içten kapatılmıştır. Pencere boşlukları dıştan demir parmaklıklar ile örtülmüştür. Cephenin üst katı, zemin kattan, cephe boyunca yatay taş silme kuşağı ile vurgulanarak ayrılmıştır. Cephenin birinci katına da alt kattaki gibi aynı yatay aksta ve formda, 16 adet pencere açılmış olup bu pencereler zemin kattaki gibi demir parmaklık ile kapatılmamıştır. Üst katın tavan seviyesi, cepheden dışa taşırılmış, bir adet taş silme kuşağı ile vurgulanmıştır. Cephenin saçak seviyesinde de iki kademeli silme kuşağı yer almaktadır.

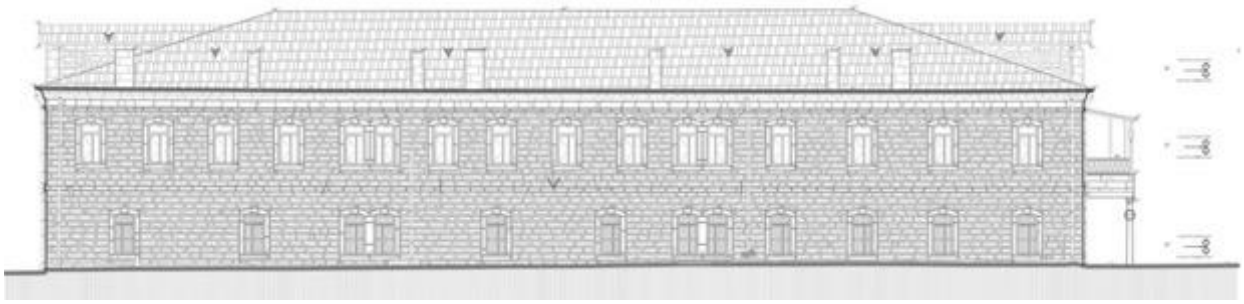

Figure 10. Batı cephe rölöve çizimi (Uzaslan, 2021).

Yapının kuzey cephesi, yapının iki girişinden birini barındırmakta olup, yapının konumlandırıldığı geniş araziye açılmaktadır. Yapının doğu ve batısındaki kot farkından dolayı cephenin doğusunda, bodrum katının da cephesi algılanırken, batısında kot yükseldiği için sadece zemin kat mekanının cephesi algılanmaktadır (Figure 11). Kapı açıklığının bulunduğu bölüm, cephedeki kırmızı renkli andezit taşlarından farklı olarak gri renkli taşlar ile oluşturularak vurgulanmıştır. Kapı açıklığı yuvarlak kemerli olup açıklık iki yandan birer adet dar formlu, yuvarlak kemerli pencere açıklığı ile sınırlandırılmıştır. Kapı açıklığı çift kanatlı demir doğrama kapı ile örtülmüştür. Kapı açıklığının üst bölümünün iki yanındaki boşluklar, açıklık ile aynı hizaya denk gelen üst kat balkon girişi ve güney cephedeki balkon ve revaklı bölüm göz önüne alındığında; bu bölümde bulunması gereken balkon ve girişin önündeki revak kısmınının günümüze gelemediği anlaşılmaktadır. Zemin kat giriş kapısının iki yanında ikişer adet aynı yatay aksta dört adet pencere yer almaktadır. Pencere boşlukları dikdörtgen formlu, basık kemerli, taş söveli olup ahşap doğramalı bir kanadı açılır olmak üzere çift kanatlı pencere ile kapatılmıştır. Pencere boşlukları dıştan demir parmaklıklar ile örtülmüştür. Cephenin üst katı, zemin kattan, cephe boyunca yatay taş silme kuşağı ile vurgulanarak ayrılmıştır. Üst katın ortasındaki, alt kattaki giriş kapısı ile aynı dikey aksta, dikdörtgen formlu kapı açıklığı yer almaktadır. Kapı açıklığı çift kanatlı demir doğramalı kapı ile kapatılmıştır. Kapı, iki yandan dar formlu, yuvarlak kemerli, birer adet pencere açıklığı ile sınırlandırılmıştır. Kapının açıldığı balkon, alt katta bulunması gereken revak bölümü gibi günümüze gelememiştir.

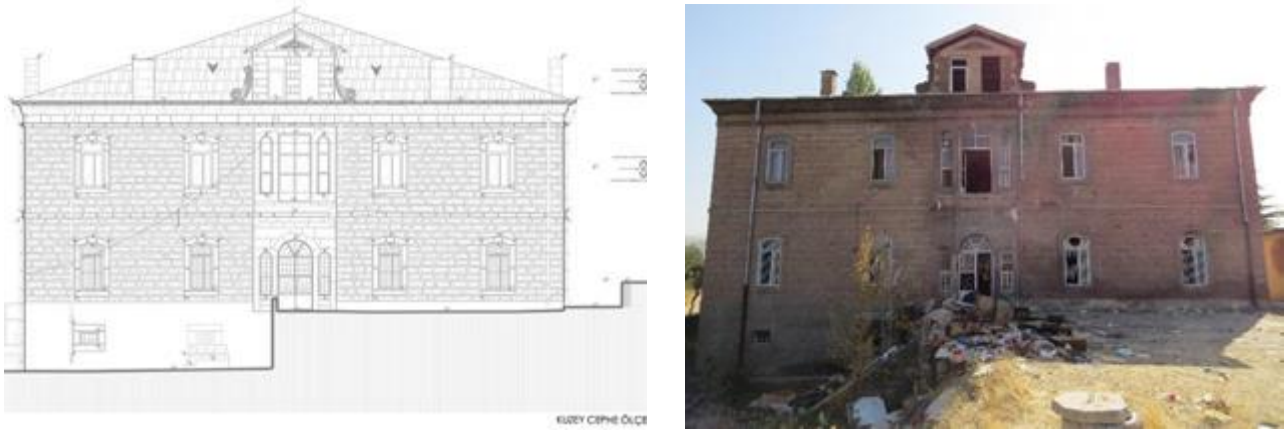

Figure 11. Kuzey Cephe Rölöve Çizimi ve Fotoğrafı (Uzaslan,2021).

Kuzey ve güney cephelerde, girişler ile aynı dikey aksta, çatıdan taşırılmış cihannüma yer almaktadır. Cihannümanın kuzey cephesine iki adet dikdörtgen formlu pencere boşluğu açılmış, pencerelerin doğramaları günümüze gelememiştir. Cihannüma iki yandan birer adet yekpare volüt ile sınırlandırılmıştır. Cihannümanın üçgen alınlığının yüzeyinde üçgen formlu taş süsleme panosu yer almaktadır (Figure 11).

Figure 12. Güney Cephe Rölöve Çizimi ve Fotoğrafı (Uzaslan, 2021).

Yapının güney cephesi, sal taşı döşemeli bahçeye açılmaktadır. Cephenin zemin kat seviyesinin ortasında yapının iki giriş kapısından biri konumlandırılmıştır (Figure 12). Kapıya ulaşım iki adet sütun ile oluşturulmuş revak bölümünden sağlanmaktadır. Revak bölümü ahşap ve cam bölmelerle ile kapatılmıştır. Kapı açıklığı yuvarlak kemerli olup açıklık iki yandan birer adet dar formlu, yuvarlak kemerli pencere açıklığı ile sınırlandırılmıştır. Kapı açıklığı çift kanatlı demir doğrama kapı ile örtülmüştür. Cephenin üst katı, zemin kattan, cephe boyunca yatay taş silme kuşağı ile vurgulanarak ayrılmıştır. Üst katın ortasındaki, alt kattaki giriş kapısı ile aynı dikey aksta, dikdörtgen formlu kapı açıklığı yer almaktadır. Kapı açıklığı çift kanatlı demir doğramalı kapı ile kapatılmıştır. Kapı, iki yandan dar formlu, yuvarlak kemerli, birer adet pencere açıklığı ile sınırlandırılmıştır. Kapının açıldığı balkon, üç yönden "S" formlu ferforje ile çevrelenmiş olup üstten ahşap sundurmalı çatı örtülmüştür (Figure 12).

Figure 13. Z-03 ve Z-05 numaralı iç mekanlar (Uzaslan, 2021).

2.3. Analitik Rölöve Çalışmaları

Yapıda malzeme kullanımı

Yapının beden duvarlarında kırmızı tonlu bosajlı andezit taş malzeme, bölme duvarlarında kesme taş malzeme, avlu döşemesinde sal taşı, bodrum kat mekanlarında moloz taş malzeme kullanılmıştır. İç mekanda, taşıyıcı olarak betonarme kolon, kiriş ve döşeme sistemleri yer almaktadır (Figure 13). Döşeme malzemesi, zemin kat koridorunda özgün taş döşemenin bir kısmı görülmekle birlikte diğer mekanların döşeme kaplamalarında muhdes mozaik malzeme ve beton şap kullanılmıştır. Duvarlarda yer alan taş yastıklar, özgünde ahşap tavan ve hezenleri işaret etmektedir (Figure 15).

Figure 14. Malzeme Analizi, Kesit ve Cephe Çizim Örnekleri, Lejant (Uzaslan, 2021).

Ahşap malzeme, yapının mekan giriş kapılarında, pencere sövelerinde ve çatı katında görülmektedir. Yapının ana giriş ve bodrum kat giriş kapılarında, pencere korkuluklarında muhdes demir malzeme kullanılmıştır. Islak hacim mekanlarında, döşeme ve duvarlarda fayans kaplama ve pvc malzemeden üretilmiş kapılar yer almaktadır.

Figure 15. Özgün ve muhdes yapı elemanları (Uzaslan,2021).

Yapısal Bozulmalar

Yapıdaki bozulmalar, malzeme sorunları, yapısal sorunlar ve muhdes olarak üç başlık altında incelenmiştir. Malzeme sorunları başlığı altında rutubetlenme, yosunlanma, bitkilenme görülen beden duvarları, dış etkenler sebebiyle çürüyen, ahşap elemanlar, korozyona uğrayan metal elemanlar ve çeşitli malzeme kayıpları belirlenmiş ve belgelenmiştir (Figure 16). İç mekan duvarlarında, sıva dökülmeleri, neme bağlı kararma ve kirlenmeler gözlemlenmektedir.

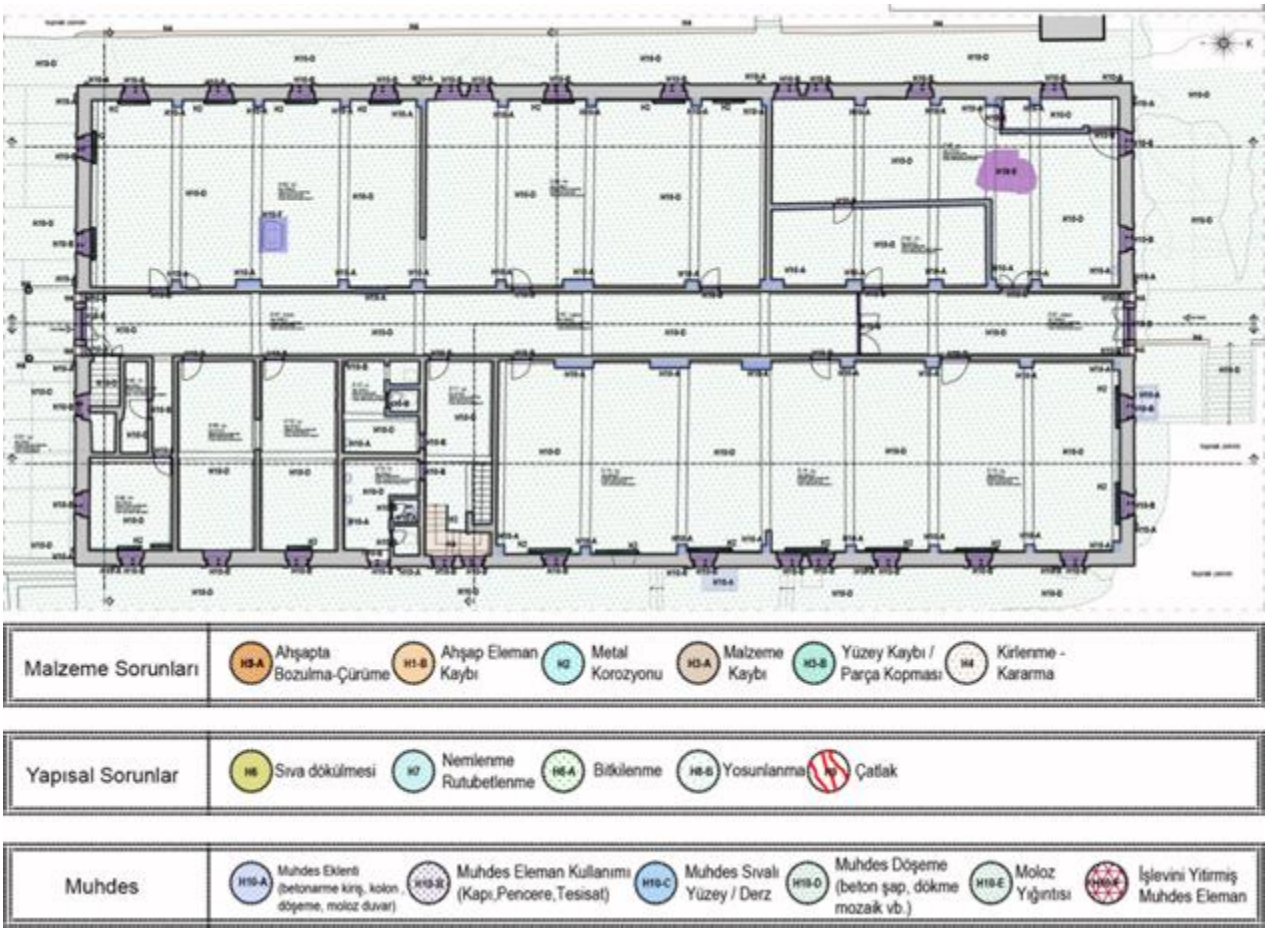

Figure 16. Hasar Analizi, Lejant ve Plan çizim örneği (Uzaslan, 2021).

Yapısal sorunlar başlığında ilk olarak, yapının cephelerinde görülen sıva dökülmesi, çatlaklar incelenmiştir. Cephede muhdes tesisat elemanlarının montajı sırasında, kesme taş yüzeyler zarar görmüştür. Yapısal problemlere sebep olan suyun yapıdan uzaklaştırılamaması, taş yüzeylerde nemlenme, bitkilenme ve yosunlanmalar, sıvalı kısımlarda sıva dökülmelerine sebep olmuştur. Muhdes eklentiler kapı, pencere doğramaları, iç mekanlarda döşemeler, muhdes beton şap ve duvarlarda çimento esaslı sıvalar, tesisat eklentileri olarak incelenmiştir.

Figure 17. Hasar Analizi, Lejant, Plan, Cephe Çizim Örnekleri (Uzaslan,2021).

2. RESTİTÜSYON ÇALIŞMALARI

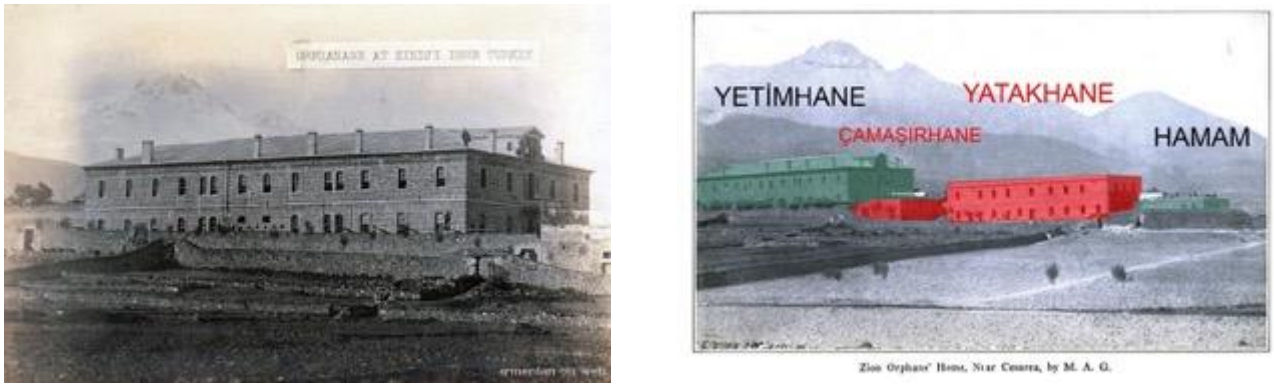

Figure 18. Zincidere yetimhanesi tarihi bilinmeyen fotoğraf ve Gerber'in kitabında yer alan foto altlık olarak kullanılarak kaldırılan yapılar ve 2021 yılındaki mevcut yapıların işlendiği görsel (Url 1 ve Gerber, 1917).

Restitüsyon çalışması için öncelikle yapının kendisi incelenerek, yapıdaki izler ve malzemelerin detaylı değerlendirilmesi yapılmıştır. Yapı ile ilgili eski fotoğraf ve belgelerin elde edilmesi için Başbakanlık Osmanlı Arşivi, Kayseri Kültür Varlıklarını Koruma Bölge Kurulu arşivi, kişisel fotoğraf arşivleri ve kaynak yayınlar araştırılmıştır.

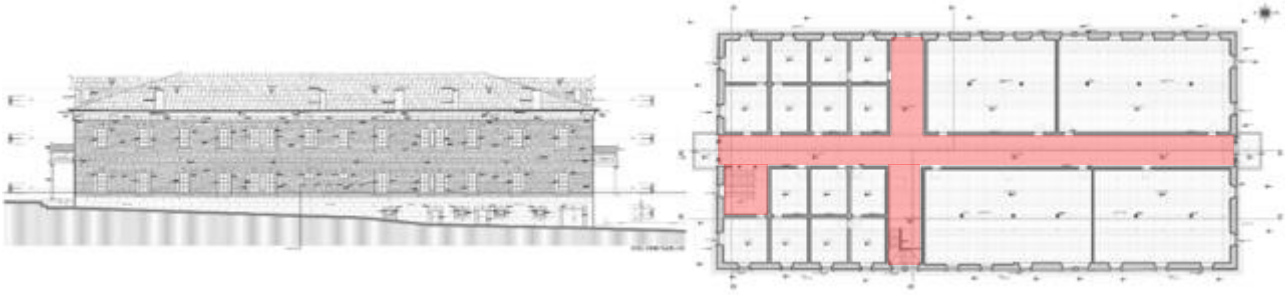

Figure 19. Restitüsyon, Doğu cephesi ve Birinci Kat Planı (Çağ Restorasyon 2021).

Başbakanlık Osmanlı arşivinde yer alan vaziyet planı, güney ve doğu cephesi çizimleri ile kat planlarının yer aldığı belge (BOA,1910) ile yapının güncel durumu kıyaslandığında farklılıklar olduğu görülmektedir. Arşiv çizimlerinde cephelerde yer alan açıklık sayılarının farklı olduğu ve yapıdaki izlerden bu açıklıklardan doğu cephesinde yer alan havalandırma pencerelerinin sonradan kapatıldığı anlaşılmaktadır (Figure 21).

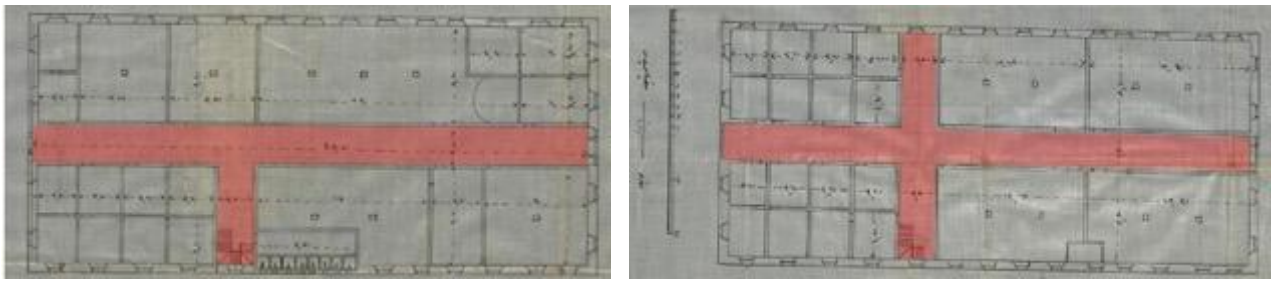

Figure 20. Başbakanlık Osmanlı Arşivi – 3759.281887.003 numaralı belgede yer alan, yapının zemin kat ve birinci kat çizimleri (BOA, Babıali Evrak Odası Evrakı-BEO, 3759.281887.003, H.22.05.1328- M.30.05.1910).

Planlar incelendiğinde zemin katta fonksiyon değişikliği sebebiyle mekanlarda değişiklikler yapıldığı ve arşiv çizimlerinde yer almayan yapının güneydoğusunda yer alan merdivenin ise ölçüleri, kullanılan malzemeler değerlendirildiğinde özgün olduğu düşünülmektedir. Yapının döşemelerinin betonarme döşeme ile değiştirildiği, özgün döşemelerin ahşap olduğu duvarlarda görülen hezen kirişler için taş yastık izleri ile desteklenmektedir. Birinci katta, arşiv çizimleri ile yapının güncel durumunda, balkonlar ve güneydoğusunda yer alan merdiven dışında farklılık bulunmamaktadır (Figure 20).

Figure 21. Başbakanlık Osmanlı Arşivi – 3759.281887.003 numaralı belgede yer alan, yapının cephe çizimleri (BOA, Babıali Evrak Odası Evrakı-BEO, 3759.281887.003, H.22.05.1328- M.30.05.1910).

Yapının çatısı arşivdeki çizimler ile farklılık gösterse de eski fotoğraflardan günümüzdeki gibi olduğu görülmektedir (Figure 18). Çatı arşivde yer alan çizimlerde beşik çatı ve kalkan duvarının üzerinde kapı ve yanlarında pencereler yer alacak şekilde görülürken, günümüzde kırma çatı ve kalkan duvarlar yerine de cihannümalar yer almaktadır. Elde edilen çizimler, eski fotoğraflar ve aynı dönemdeki benzer yapılar ile yapının güncel durumu karşılaştırılarak restitüsyon paftaları hazırlanmıştır.

4. RESTORASYON ÖNERİSİ

Yapının restorasyonunda yapının özgün niteliklerinin ortaya çıkarılması, özgün biçimlerin korunması hedeflenmiştir. Yapıya en az müdahale yapılması temel ilkesi ışığında; özgün elemanlara yapılan olumsuz müdahalelerin yapıya zarar vermeden uzaklaştırılması ve özgün niteliklerin iyileştirilerek korunması adına müdahale kararları geliştirilmiştir. Yapının özgün işlevin sürdürülmesi çağdaş koruma anlayışı gereği ve kent belleği, aidiyet hissi, yapısal ve mekansal müdahalelerin en aza indirgemesiyle sürdürülebilirlik avantajları sebebiyle önerilmektedir.

Figure 22. Restorasyon, Zemin Kat Planı (Çağ Restorasyon 2021).

Mekansal kararlar: Günümüzde kullanılmayan yapı geçirdiği dönemler boyunca farklı kurumlar tarafından eğitim yapısı olarak kullanılmış, aynı parseli paylaştığı cezaevine ek atölye olarak kullanıldığı dönemde de özgün işlevini dolaylı olarak sürdürmüştür. Bu durum yapının mekansal olarak büyük ölçüde korunmasına sebep olmuştur. Restitüsyon çalışmaları ve yapıdaki izler ışığında mekan organizasyonu düzenlenerek, özgün yapıda yer aldığı düşünülen yeni bölücü duvarlar eklenmiştir.
Yapısal kararlar: Yapı strüktürel açıdan genel olarak sağlam olmakla birlikte, özgün olmayan betonarme döşemelerin tekniğine göre uygulanmadığı ve taşıyıcı özelliğini yitirdiği görülmektedir. Çatı döşemesinin askıya alınarak yapıdan uzaklaştırılması önerilirken, statik raporlar ışığında birinci kat döşemelerinin sökümünün yapıya verebileceği zarar göz önünde bulundurularak, muhdes mozaik kaplamanın kaldırılarak yükünün azaltılmasına karar verilmiştir.

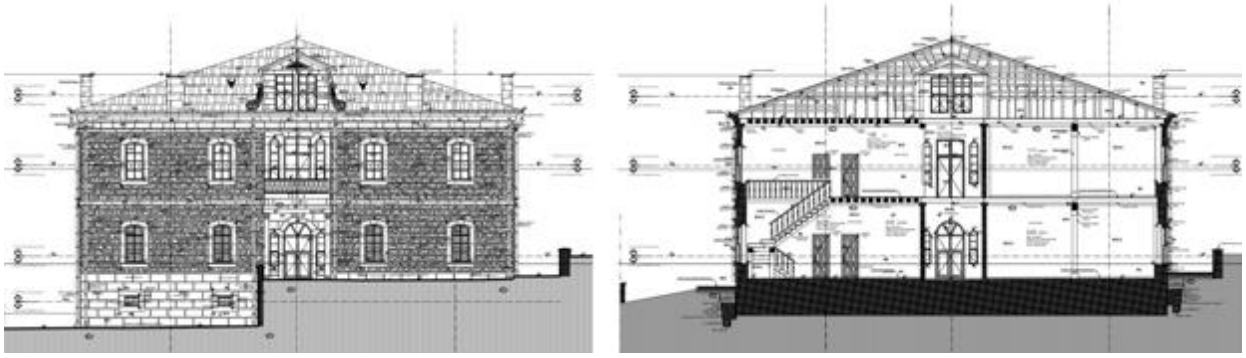

Figure 23. Restorasyon, Kuzey Cephe ve Kesit Çizimleri (Çağ Restprasyon 2021).

Yapının çatısında yağmur sularının uzaklaştırılmasındaki problemler yapının özgün elemanlarına zarar vermektedir. Çatı askıya alınarak muhdes betonarme döşemenin sökümü, ahşap döşeme ile değiştirilmesi sonrası nem sebebiyle çürüme ve bozulmaların görüldüğü çatı elemanlarının yenilenmesi esnasında doğru çatı eğimleri ve kaplama malzemeleri ile bu sorun çözülmelidir.
Yapının zemin kotunda görülen nem sorunları için, beden duvarlarından temel kotuna kadar yapıya zarar vermeden kazı yapılarak, kötü durumda olan taşların yenilenmesi, yalıtım, doğru drenaj uygulanarak, yapının su alması engellenmesi kararı alınmıştır.

Figure 24. Müdahale Analizi Kesit Çizimleri (Çağ Restorasyon 2021).

Malzeme Kararları: Yapıda görülen nem sorunları, beden duvarlarında, ahşap ve metal elemanlarda tuzlanma, kirlenme, paslanma problemlerine sebep olmaktadır. İlk olarak çimento esaslı muhdes sıvalar raspa edilmeli, nemin uzaklaştırıldığı beden duvarlarında gerekli yerlerde çatlaklara statik raporda da belirtildiği gibi hidrolik kireç enjeksiyonu yapılarak, kireç esaslı sıva uygulaması yapılmalıdır. Hasar görmüş ya da tamamen kaybolmuş yapı elemanları uygun malzeme ve boyutta tamamlanmalıdır. Boşalmış ve bozulmuş derzlerde hidrolik kireç derz uygulaması yapılması ve dış etkilere bağlı olarak çürüyen ve kaybolan ahşap elemanların yenilenerek, kullanılabilecek durumda olanların gerekli bakımları yapıldıktan sonra tekrar kullanılması önerilmektedir. Yapıda korozyona uğrayan metal elemanlar, mekanik yöntemlerle temizlenerek, kullanılamayacak durumda olanlar için yeni metal malzemeler kullanılmalıdır.

4. SONUÇ

Zincidere Darüleytam yapısının özgün malzemelerinin korunmasına azami özen gösterilerek, çağdaş ihtiyaçlara cevap verecek bir eğitim yapısı öngörülmüştür. Tarihi yapı, anlamsal, mekansal, yapısal ve estetik özellikleri ile Zincidere köyü için önemli olduğu kadar kent tarihi ve ülkemiz için de önemli bir dönemi işaret etmektedir.
Yapının yapısal ve mekansal bütünlüğü bozulmadan teknik ve teknolojik sistemlerle güncellenerek toplum yaşamına katılması ve bu süreç yönetilirken tasarım ve donanımlarının güncel konfor ihtiyaçlarını karşılaması, gelişen dönüşen bir sürece dahil edilmesi, korumanın sürekliliği için vazgeçilmezdir.

Teşekkür
It should be written as short as possible and expressing the contribution made without giving the number.

Etik Kurul Onayı
N/A

Akran Değerlendirmesi
Externally peer-reviewed.

Yazar Katkıları
Conceptualization: H.S.; Investigation: H.S.; Material and Methodology: H.S., S.Ö.; Supervision: H.S., E.T.E.; Visualization: S.Ö.; Writing-Original Draft: H.S., D.A.; Writing-review & Editing: D.A., S.Ö.; Other: All authors have read and agreed to the published version of manuscript.

Çıkar Çatışması
The authors have no conflicts of interest to declare.

Finansal Destek
The authors declared that this study has received no financial support.

KAYNAKLAR

Peker, A. Kişisel fotoğraf arşivi.

BOA, Babıali Evrak Odası Evrakı-BEO, 3759.281887.003, H.22.05.1328- M.30.05.1910).

Gerber, M.A. (1917). Passed Experiences, Present Conditions, Hope for the Future. Ramsey-Burns Printing:Pasadena Cal.

Özbek, Y. (2011). Kayseri'de Tarihi Okul Yapıları, Laçin Yayınları: Kayseri.

Url-1: https://team-aow.discuforum.info/t17825-Kayseri-Talas-Zincidere-Ermeni-Rum-Protestan-cemaatleri-kilise-yetimhane-ve-tehcir.htm (Son Erişim Tarihi: 15 Aralık 2022).

Çizimler: Restitüsyon, Restorasyon çizimleri ve Müdahale Analizi çizimleri Çağ Restorasyon,2021.

Assessment of Cargo Hold Wastage Due to Corrosion in General Cargo Ships: Nonlinear approach

Špiro Ivošević [1*], Nataša Kovač[2]

Abstract: Corrosion can cause local damage to the structure and can also initiate huge damage that can cause partial or complete loss of the ship, loss of human life or environmental pollution. That is why numerous inspections are carried out by the Port State, Flag State and Classification Societies to identify potential hazards in a preventive manner. This is supported by mandatory maintenance activities carried out by the Ship Management Company following the International Safety Management Code. Damage to the structure depends on many factors specific to the type of ship, environmental factors, transported cargo and manipulative equipment, as well as other important influential factors. To reveal the degree of damage to the cargo holds of dry cargo ships, in this article, we investigate the impact of corrosion on the cargo holds expressed through the amount of replaced steel. Namely, each cargo holds of these ships included the longitudinal and transverse bulkheads and the tank top plating. By measuring the thickness of steel plates, systematizing measurement data and identifying corroded surfaces that need to be replaced, in this research, we analyze the cumulative amount of replaced steel. A group of 10 ships carrying different general cargoes was considered and were measured in the period from 15 to 27 years of vessel age. The considered data show that the Normal function satisfactorily describes the considered data after 15 years of exploitation. By applying regression analysis, data were obtained that describe with a high degree of precision the increase in the amount of replaced steel over time.

Keywords: corrosion, general cargo ships, cargo holds, normal distribution

[1] University of Montenegro, Maritime Faculty, Kotor, Montenegro
[2] University of Donja Gorica, Faculty of Applied Sciences, Mathematical Department, Podgorica, Montenegro

* Corresponding author: spiroi@ucg.ac.me

1. Introduction

Numerous studies in the marine industry confirm that tankers, bulk carriers, general and dry cargo ships have the highest probability of casualties. Collision, loss of control, hull failure, contact, grounding, fire or explosion are some of the most frequently registered causes that led to numerous accidents. Accidents can lead to the loss of human life, material damage or environmental pollution.

The probability of critical casualties increases with the vessel's age and approximately 85% of losses due to structural failure are attributed to ships over the age of 15 years (Holmes and Pippenger 1996). Inadequacy maintenance may have significant safety and business implications. Bright and Bell (1996) reported that 23% of the failures refer to mechanical and structural components.

To keep vessels safe and secure for navigation and operations the International Maritime Organization introduced the International Safety Management Code. This Code pays special attention to the maintenance of ships. Maintenance costs increase proportionally with the age of vessels. Considering total annual technical costs, it can be assumed that approximately 25% of the ship's total operating costs (i.e. crew, technical, management and others), while maintenance reaches up to 60% of those charges, are estimated (Poggi et al. 2022).

To prevent the harmful consequences that can occur as a result of ship accidents, ship owners, ship management companies, Flag states and Classification Societies have taken numerous measures and activities regarding the reduction of accidents. Inspections are carried out on all types of ships, regardless of their age. However, there are numerous guidelines, mostly by Port State Control that focus on certain types of ships, Flag States, previous vessels' condition, age of ships and other issues connecting to the previous status of ships.

While the surface protection is effective, no corrosion on metal surfaces needs to be replaced. Usually, steel replacements during the first 10 years of exploitation are related to wastage caused by cracks or structural damage. When the surface coating brakes the corrosion process starts and develops over the time of operation. Metal surfaces appear that need to be replaced when extensive corrosion can occur. This usually happens after 10 to 15 years of exploitation. Research on the effect of corrosion on maritime steel structures can be carried out in real seawater environment conditions (Pastorčić et al. 2023) or in simulated conditions (Gudić et al. 2022). Certainly, the most significant are those studies that take into account extensive databases on the wear and tear of structural elements in different ships (Wang et al 2021).

Corrosion can be found in different forms as general, pitting, microbacterial, local, growing, or other. Most investigated corrosion forms are general and pitting corrosion (Paik et al. 1998, Paik 2003, Paik 2004, Momcilovic et al. 2023). Wastage of metals due to corrosion may be reported as weight loss expressed in grams or kilograms. In some previous research wastage of corrosion well considered in mm or percentage of deminution of as build thickness (Paik et al. 1998, Paik 2003, Paik 2004, Soares and Garbatov 1999., Yamamoto and Ikegami, 1998., Ivošević et al., 2019, Ivošević et al., 2021, Ivošević et al., 2022).

Corrosion prevention and control are crucial to maintaining the structural integrity and safety of vessels. Regular preventive maintenance, protective coatings, and corrosion-resistant materials are commonly used to address and mitigate corrosion issues. Corrosion can affect various parts of a cargo vessel, but some of the most commonly corroded areas include: ballast tanks, hatch covers, cargo holds, bulkheads, tank top plating, deck structure and pipes and piping systems.

Corrosion in the cargo holds of any cargo vessel can have significant negative effects on the vessel's structural integrity and cargo safety. Numerous research identifies some of the key influences of corrosion: increasing the risk of structural failure, cargo contamination, reduce vessel lifespan and increase maintenance cost. Due to specific types of cargo, or cargo operation in Cargo Holds, deterioration in the cargo hold can result from factors like corrosion, wear and tear, moisture, improper maintenance, or exposure to harsh conditions. Regular visual inspections, proper ventilation, regular maintenance, appropriate cargo handling, etc., can ensure the safety and integrity of the transported cargo and the vessel itself.

Damage caused by corrosion requires additional inspections and ultrasonic thickness measurements regarding the assessment of further exploitation of structural areas. Damaged surfaces need to be replaced, which greatly affects maintenance costs. Often these costs can reach values that influence the ships to be scraped earlier. That is why it is very important to properly maintain the vessels using appropriate maintenance methods, which can include preventive and corrective activities that will ensure the desired exploitation of the vessel.

As it is prescribed in Classification Rules, corrosion intensity is measured in mm or percentage of wear concerning the as build thickness value of specific structural members (plate, bracket, stiffener). The rules of the Classification Societies define the degree of acceptability and in this way, the surfaces for replacement are identified by measurements. Corroded areas are usually treated as amounts of replaced steel expressed in kg of steel or tons of replaced steel.

The decrease in metal weight and the increase in corrosion rate increase with time and according to previous research, there are different linear and nonlinear models of corrosion. A linear model is developed by (Southwell et al. 1979, Soares and Garbatov 1999), while non-linear models are presented by (Yamamoto and Ikegami, 1998; Paik et. al., 1998; Paik, 2003; Paik, 2004; Melchers, 1999; Melcher, 2003) and papers by other researchers.

All models developed so far are based on exposure time while some more advanced models take into account other parameters such as salinity, pH, seawater temperature and flow rate, the content of oxygen dissolved, sulfur pollution, and fouling (Melchers, 1999).

The most common structural damage due to corrosion occurs in ballast tanks and cargo holds. In this paper, based on measurement data on structural damage of cargo holds in general cargo ships, we consider how the amount of steel changes during exploitation.

The paper is structured through 4 chapters. The second chapter presents a related methodology, discusses the relevant database of General Cargo ships and presents the used methods. The third chapter presents research results, while the fourth chapter presents conclusion remarks.

2. Methodology

To assess the condition of the structure, the classification rules require a visual inspection of the structure and then a thickness measurement. With vessels age, the scope and intensity of measurements increase, according to the rules of Classification Societies. Measurements of structural elements include three states of measurement, namely acceptable measurements, substantial corrosion and excessive corrosion. Steal plate areas or lengths of structural elements or plate pieces with excessive values must be replaced before further exploitation of the vessel. In this sense, metal surface area, lengths or pieces of corroded metal structure are identified, which are expressed in kg, or more often in tons of replaced steel. In this way, the quantities of steel that need to be replaced in certain areas are identified, as well as the time necessary for the realization of these works. Due to specific commercial requirements, it is very important to take into account the scope of the replacement, location, contact surfaces, repair location, etc., to optimize and reduce the total maintenance costs as much as possible.

Based on huge measurements carried out on ten different general cargo ships, including complete reports on thickness measurements, an insight into excessive corrosion was made. In

this way, the areas that needed to be replaced were identified, and thus the amount of steel to be replaced, expressed in tons. Following the above, the data on the total amount of steel during the period of exploitation are presented below. Conducted research includes information during special surveys that provide information on replaced steel quantities after 15, 20, 25 and 27 years.

Based on the data evaluated in this research, several statistical methods were implemented in order to develop non-linear corrosion models.

2.1. Database

The database considered in this research includes ten ageing general cargo ships. According to the available data, the vessel transported steel coins, iron profiles, stone, and other types of general cargo. The trade route was missing and didn't consider as well as environmental condition parameters. The age of the ships was between 15 and 27 years and they were measured in the period from 2005 to 2015. Measurements were made during the regular Special Survey, considering specific requirements by the Classification Society. Some vessels were observed once, twice or three times, as shown in Table 1.

Table 1. Estimated quantity of replaced steal in Cargo Holds in tons

Ships/ Time (years)	Ves. 1 (tons)	Ves. 2 (tons)	Ves. 3 (tons)	Ves. 4 (tons)	Ves. 5 (tons)	Ves. 6 (tons)	Ves. 7 (tons)	Ves. 8 (tons)	Ves. 9 (tons)	Ves. 10 (tons)
15		65	65	65	10					10
20		615	485	520	500	3	12	20	65	95
25	3					4	38	265	910	405
27	6					10	135		102	

Descriptive statistics of input empirical data are shown in Table 2, based on data grouped by year. We observe a very large variability when comparing the data for years, which is to be expected considering the relatively small database and the limited amount of available information. In addition, for data related to 20-year-old ships, it is noticeable that the mean is almost identical to the standard deviation, which significantly complicates the modelling of these data.

Table 2. Descriptive statistics of input data

Variable	Mean	StDev	Minimum	Q1	Median	Q3	Maximum
15 years	20.00	8.94	10.00	10.00	20.00	30.00	35.00
20 years	89.1	88.5	1.0	5.0	45.0	163.8	240.0
25 years	101.6	163.4	1.0	3.5	32.5	112.5	610.0
27 years	21.08	32.84	0.00	0.50	4.00	36.25	100.00

Figure 1 shows a Box plot of the input data. The diagram shows outliers for 25 years (these are the blue dots). The existence of these outliers points to the fact that we have some very large extremes in the considered empirical data. However, we did not exclude them from consideration, for the data to remain credible, because we believe that there was no error in the measurements, but rather extreme conditions (influence of corrosion, exploitation conditions and other influential factors) occurred which was necessary to replace those large amounts of steel.

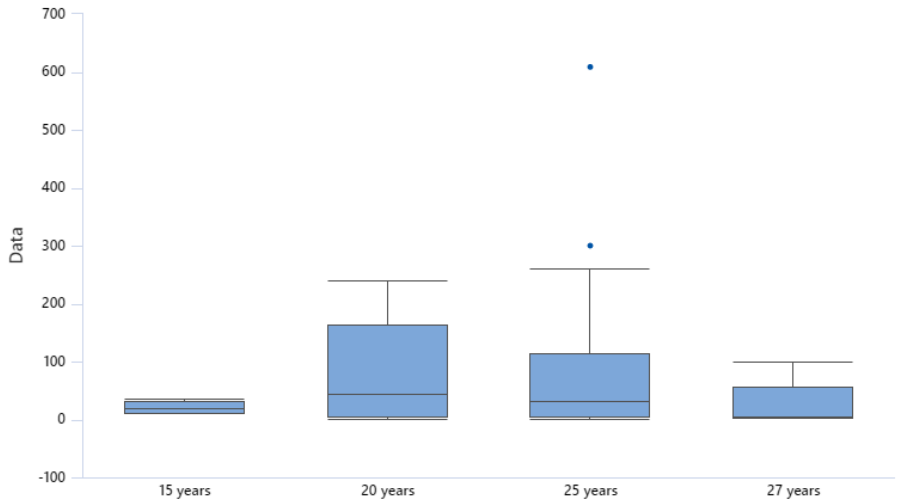

Figure 1. Estimated quantity of replaced steal in Cargo Holds in tons

Table 3 shows the 95% confidence intervals for the mean and standard deviation. Furthermore, with 95% certainty, we can claim that the mean value for 15 years will be between 13,991 tons and 26,009 tons, while the standard deviation of the empirical data will be in the interval 6,2495 and 15,697. We observe a very wide confidence interval for the mean at 25 years, and a very large variability of the data, considering that the confidence interval for standard deviation is wide and has large values of the lower and upper limits of the interval.

Table 3. Descriptive statistics of input data

Group	Mean	95% CI	StDev	95% CI
15 years	20	(13.991, 26.009)	8.9443	(6.2495, 15.697)
20 years	89.077	(53.349, 124.80)	88.455	(69.372, 122.10)
25 years	101.56	(14.488, 188.64)	163.41	(120.71, 252.91)
27 years	28.111	(0.8195, 55.403)	35.505	(23.982, 68.020)

2.2. Methods

In this research, several standard scientific research methods were applied. The thickness measurement procedure was carried out using digital ultrasound devices that measure the thickness of the metal over the protective coating. These measurements obtained the initial values of the reduction in the steel thickness of structural elements of the cargo holds due to corrosion. Then special software programs were used for data processing following the rules of the classification societies. Based on clearly defined acceptance criteria, established by classification societies, the surfaces of the steel structure for replacement were identified. Considering the significant number of influencing parameters regarding the replacement of corroded surfaces (class requirements, minimum catting surfaces, the influence of contacted areas, structural designs, etc.), it is very difficult to determine precise and accurate amounts of steel replaced solely due to corrosion. This is precisely why the amount of replaced steel was estimated, which included exclusively the surface damage due to corrosion and not due to mechanical and other damages, as well as different structural requirements. Statistical data analyses were conducted on the input data obtained in this way about the estimated amount of steel to be replaced in cargo holds of general cargo ships.

Our approach to data analysis encompassed a suite of classical statistical techniques. By utilizing descriptive analysis, box plots, and trend line visualizations, we were able to comprehensively analyze the dataset, unveil underlying patterns, and provide a robust foundation for further analysis.

In our analytical process, we executed an Anderson-Darling normality check, a method widely employed to assess the normal distribution of data. This involved calculating AD squared values and corresponding p-values for each dataset under scrutiny. Additionally, generated normal probability plots revealed that data are not following Normal distribution except in the case of 15 years.

Given the intricate and complex nature of the data patterns, our initial approach involved harnessing regression analysis. To capture the nuanced relationships within the data, we opted for both exponential and polynomial models. These modelling techniques are particularly adept at accommodating non-linear trends and variations that extend beyond the scope of linear models.

3. Results

Based on the Anderson Darling test, corresponding p-values, and observing probability plots of resulting data, it was possible to conclude that empirical databases have complex structures. Having that in mind, modelling with nonlinear functions was carried out on the empirical dataset considering that the data do not follow the Normal distribution, except for 15 years. That conclusion led us to the decision to model these data with other curve shapes. We investigated the regression analysis shown in Figures 2 a, b, c, and d. In each graph, we see the function that best describes the data and the R^2 value that shows how well the function follows the data. Values that are close to 1 show a higher degree of accuracy and reliability of the expressed function. As all the displayed values are always very close to 1, it means that our approximations are good on each graph. On the x-axis is the number of measurements, and on the y-axis is the amount of replaced steel. The red line is our prediction when the formula shown on the graph is taken into account.

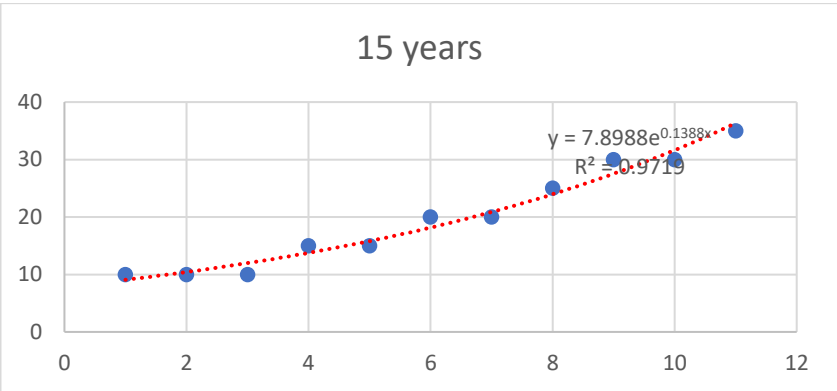

a)

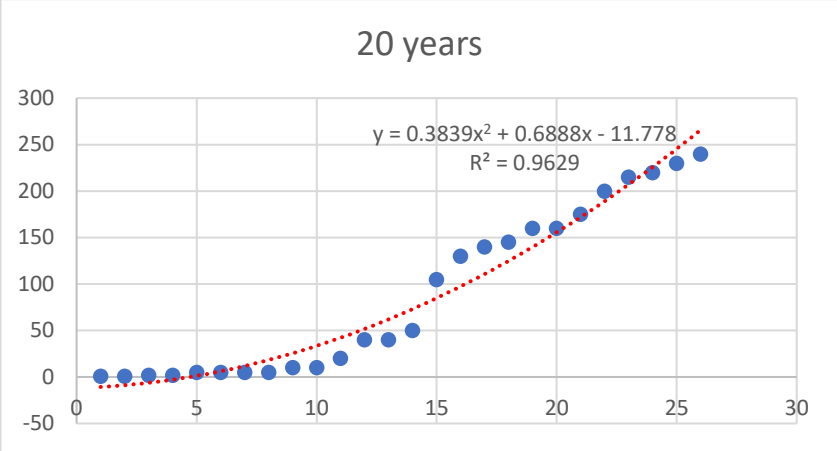

b)

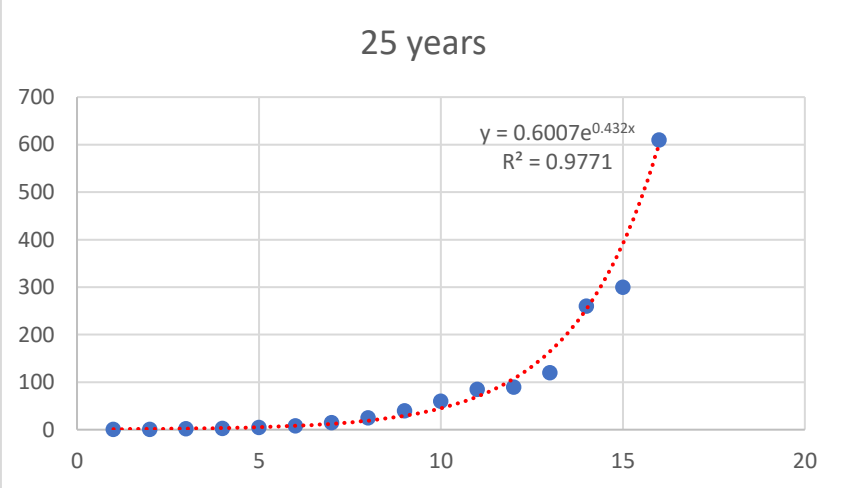

c)

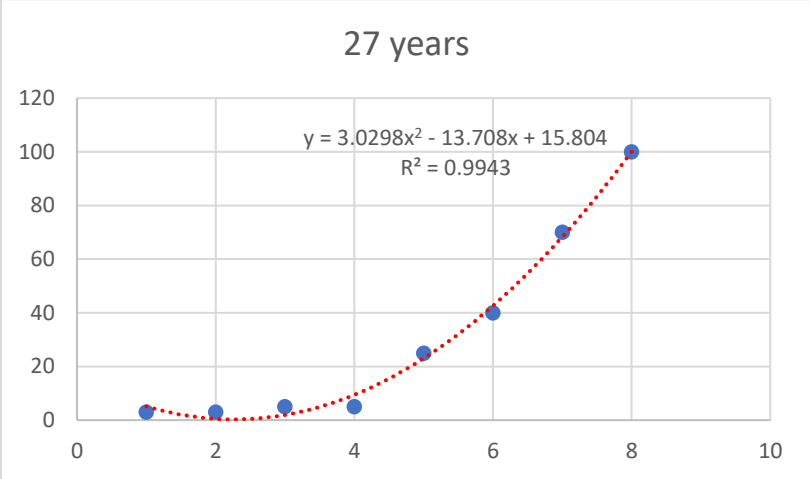

d)

Figure 2. Modelling with non-linear functions for 15 (a), 20 (b), 25 (c), and 27 (d) years

4. Conclusions

In this paper, the authors have dealt with the development of regression models that will adequately describe the quantity of steel to be replaced in the cargo holds of ten dry cargo ships. Empirical data on the amount of replaced steel after 15 years follows a normal distribution, which is not the case for the other considered time periods.

Using the regression analyses, all four presented functions follow the proposed non-linear functions with a high degree of accuracy, greater than 95%, which gives us the right that they will also follow standard statistical distributions well. In the continuation of these studies, we could make an assessment of how the data behaves in accordance with the well-known probabilistic distributions. Also, it is possible to consider the total amount of replaced steel by individual structural areas of the cargo holds.

Acknowledgements

This research work has been supported by the approved Thickness Measurement Company - INVAR-Ivošević Company. Some more information about the Company can be found at URL: http://www.invar.me/index.html. Namely, the data collected and systematized during the last twenty-five years by the Company operators and experts have been included in the presented probabilistic analysis of the corrosion effects on the analyzed group of aged bulk carriers. Last decades the INVAR-Ivošević Company completed ultrasonic thickness measurement reports for vessels under the recognized classification societies such as LR, BV, DNV, GL, RINA, ABS, and ClassNK. Currently, more than four hundred vessels, are being inspected by the Company.

References

Holmes, J.M., Pippenger, D.T. (1996). Human elements in bulk carrier inspections and repair. *Ship Structure Symposium '96*; Nov 18–20; Arlington (VA)

Bright, C.K., Bell, S.P. (1996). Improving human factors in marine maintenance. *Ship Structure Symposium '96*; Nov 18–20; Arlington (VA)

Poggi, L., Gaggero, T., Gaiotti, M., Ravina, E. & Rizzo, C.M. (2022) Robotic inspection of ships: inherent challenges and assessment of their effectiveness, *Ships and Offshore Structures,* 17:4, 742-756, DOI: 10.1080/17445302.2020.1866378

Momčilović, N., Ilić, N., Kalajdžić, M., Ivošević, Š., Petrović, A. (2023) Pitting and uniform corrosion effects on ultimate strength of a bulk carrier, Procedia Structural Integrity (48) 12–18.

Paik, J. K., Kim, S. K., & Lee, S. K. (1998). Probabilistic corrosion rate estimation model for longitudinal strength members of bulk carriers. Ocean Engineering, 25(10), 837-860.

Paik, J. K. (2003). A time-dependent corrosion wastage model for bulk carrier structures. Int J Marit Eng R Just Naval Arch, 145(2), 61-87.

Paik, J. K. (2004). Corrosion analysis of seawater ballast tank structures. International Journal of Maritime Engineering, 146(A1), 1-12.

Ivošević, Š., Meštrović, R., Kovač, N. (2019). Probabilistic estimates of corrosion rate of fuel tank structures of aging bulk carriers, International Journal of Naval Architect and Ocean Engineering, 11(1), 165-177.

Ivošević, Š., Kovač, N., Momčilović, N., Vukelić, G. (2021). Analysis of corrosion depth percentage on the inner bottom plates of aging bulk carriers with an aim to optimize corrosion margin, Shipbuilding: Theory and Practice of Naval Arhitecture, Vol.72 No.3, http://dx.doi.org/10.21278/brod72306

Ivošević, Š., Kovač, N., Momčilović, N., Vukelić, G. (2022). Evaluation of the Corrosion Depth of Double Bottom Longitudinal Girder on Aging Bulk Carriers. Journal of Marine Science and Engineering, 10, 1425. https://doi.org/10.3390/jmse10101425

Pastorcic, D., Vukelic, G., Ivosevic, S. (2023) Welded steel in marine environment – Experimental and numerical study of mechanical properties degradation, Materials Today Communications, Volume 34, 105280, ISSN 2352-4928, https://doi.org/10.1016/j.mtcomm.2022.105280.

Melchers, R. E. (1999). Corrosion uncertainty modelling for steel structures. Journal of Constructional Steel Research, 52(1), 3-19.

Melchers, R. E. (2003). Probabilistic model for marine corrosion of steel for structural reliability assessment. Journal of Structural Engineering, 129(11), 1484-1493.

Gudic, S., Nagode, A., Šimic, K., Vrsalovic, L., Jozic, S. 2022. Corrosion Behavior of Different Types of Stainless Steel in PBS Solution. Sustainability 14, 8935. https://doi.org/10.3390/su14148935

Southwell, C.R., Bultman, J.D., H.J. CW. (1979). Estimating of service life of steel in seawater, In: Schumacher M., editor. Seawater corrosion handbook, 374-387.

Yamamoto, N., & Ikegami, K. (1998). A study on the degradation of coating and corrosion of ship's hull based on the probabilistic approach.

Soares, C.G., Garbatov, Y. (1999). Reliability of maintained, corrosion protected plates subjected to non–linear corrosion and compressive loads. Marine Structure 12, 425–445.

Wang, Z., Sobey, A.J., Wang, Y. (2021) Corrosion prediction for bulk carrier via data fusion of survey and experimental measurements, Materials & Design, Volume 208, 109910, ISSN 0264-1275.

Comparison of The Mechanical Properties of Cellulose Paper Reinforced Hybrid Composites

Servet Tulum*[1], Tuncer Demirel[1]

Abstract: Since hybrid composites are a more stable material type, their use is starting to become widespread today compared to traditional composites. Although hybrid composites are used in the aerospace and defense industries, different mechanical properties can be obtained with different arrays of fibers in layered composites. Due to this situation, researches on the subject are increasing. Carbon fiber and glass fibers are the most preferred fiber types in fiber reinforced composites. If these two fibers are hybridized, they enter their negative sides against each other. In addition to the different arrays of fibers, there are also methods such as surface treatments and matrix reinforcement to increase the strength and reduce the delamination between layers in laminated composites. Matrix reinforcement is made using different methods such as nanoparticles, nanofiber mats and films. In addition to these methods, environmentally friendly materials have become one of the preferred elements, especially to increase matrix reinforcement. Cellulose fibers are one of the environmentally friendly materials due to their low density, low cost and recyclability. Cellulose fibers are a great natural resource as they are derived from plants such as kenaf, hemp, flax and bamboo. By using cellulose paper obtained from cellulose fibers between layers in layered composites, these cellulose fibers take the loads on the matrix. The aim of this study is to investigate the effect of cellulose paper between layers. In this direction, hybrid composites with glass/carbon fiber layer and carbon/glass fiber layer were produced and cellulose paper was added between these layers and their mechanical properties were examined.

Keywords: Carbon fiber, cellulose paper, glass fiber, hybrid composite, tensile test.

[1]**Address:** Başkent University, Kahramankazan Vocational School, Ankara/Türkiye

***Corresponding author**: stulum@baskent.edu.tr

1. GİRİŞ

Kompozit malzemeler günümüzde her alanda kullanılan malzeme türü olarak karşımıza çıkmaktadır. Buna bağlı olarak kompozit malzemeler de kendi içinde çeşitlenmeye başlamıştır. Hibrit kompozit, takviye elemanının birden fazla olması durumundaki kompozit malzemeler için kullanılmaktadır (Demir, 2017). Bu tür kompozitler daha stabil mekanik özellikler sunarken, aynı zamanda tokluğun artmasına olanak sağlamaktadır. Hibrit kompozit tasarımında fiberlerin hibritlenmesi bir yöntem olup, her bir fiberin sahip olduğu dezavantajları ortadan kaldırmaya yaramaktadır (Swolfs vd., 2014). Fiber hibritlenmesinde genellikle düşük uzamalı ve yüksek uzamalı fiberler bir arada kullanılır. Bu şekilde önce düşük uzamalı fiber hasara uğrarken, yüksek uzamalı fiber büyük bir uzamada kopma değerine ulaşabilir (Demir, 2017).

Hibrit özelliği ilk olarak; Hayashi (1972) tarafından karbon/cam fiber tabakalı kompozitte kopma uzamasının sadece karbon fiberden oluşan kompozite göre daha yüksek olduğu gözlenmiştir. Sentetik fiberlerin hibritleşmesi sertlik, dayanım, nem dayanımı ve korozyonu önleyici özellikler katar (Kumar, 2012). Sentetik fiberler düşük maliyet, düşük yoğunluk, yüksek sertlik ve dayanım sunarlar. Bundan dolayı taşıtlarda metal alaşımlar yerine sentetik fiberlerin kullanımı ile %30'a kadar ağırlık ve %20'ye kadar maliyetten tasarruf edilebilir (Erkendirici, 2023; Karacor, 2022). Matrisin aynı olup da fiber kombinasyonlarının farklı olarak kullanıldığı hibrit kompozitlerden en çok bilineni cam/karbon fiber takviyeli kompozitlerdir (Taş, 2018). Cam/Karbon fiber takviyeli kompozitin en çok tercih edilmesinde, yüksek modül ve düşük uzama fiber yapılar (karbon fiber) yüksek yapısal bütünlük ve yük yükleme sağlarken, düşük modül ve yüksek uzama fiber yapılar (E-camı) düşük yapısal bütünlük ve yüksek uzama ile darbe tokluğu sağlar (Erkendirici, 2023). Bu yapılar sonucunda mekanik özellikleri bakımında yüksek sonuçlar sağlanırken zayıf yönler ise minimum düzeye indirilir. Cam/karbon fiber tabakalı kompozitlerde fiber tabakaların yerlerinin değişmesi sonucunda mekanik özellikleri önemli ölçüde değişmektedir. Örneğin, cam fiberler dış tabakalarda ve karbon fiberler iç tabakalarda olacak şekilde bir tabakalanma sırası ile cam fiber iç tabakalarda, karbon fiber dış tabakalarda olacak şekilde bir tabakalanma sırasına göre daha yüksek çekme dayanımı ve kopma uzamasına sahip olduğu belirlenmiştir (Pandya vd., 2011). Ayrıca Zhang vd. (2012) tarafından yapılan çalışmada kompoziti oluşturan fiberlerin %50'si karbon fiber ve %50'si cam fiber oranında olacak şekilde üretimi yapıldığında çekme dayanımının tabakayı oluşturan fiberlerin sırasına bağlı olmadığı fakat eğilme

dayanımının karbon fiberlerinin en dış tabakada olduğu hibrit kompozit yapılarında en iyi sonuçlar elde edildiği görülmüştür. Karbon fiberin hibrit kompozitlerde bu kadar çok kullanılmasında düşük yoğunluk ve yüksek dayanımları nedeniyle havacılık ve uzay sanayisi olmak üzere birçok alanda mühendislik malzemesi olarak tercih edilmektedir. Karbon fiberler ani ve gevrek bir biçimde hasara uğramaları sonucunda tasarımda yüksek emniyet katsayıları kullanılmasını gerektirdiğinden diğer elyaf türleri ile hibritlenmektedir. Literatürde karbon fiberlerin, başta cam fiber (Dong ve Davies, 2015; Dong vd., 2015; Yu vd., 2015) olmak üzere, Kevlar (Zweben, 1977; White vd., 2003; Kim vd., 2011; Woo, 2016), bazalt (Dorigato ve Pegoretti, 2013; Ferrante vd., 2015), nylon 12 (Hine vd., 2014) gibi sentetik fiberlerle, kenaf (Sapiai vd., 2014), kenevir (Fong vd., 2012) gibi doğal fiberler ve metalik fiberlerle (Hannemann vd., 2016, 2017) hibritlendiği görülmektedir. Bu şekilde karbon fiberlerin dezavantajları ortadan kaldırılmaya çalışılmaktadır.

Hibrit kompozitlerde mekanik özellikleri daha da geliştirmek için yüzey işlemleri (Nega vd., 2022), fiber oryantasyonları (Seyed Yaghoubi vd., 2012) ve matris takviyesi (Zhang vd., 2014) gibi çeşitli yöntemler de mevcuttur. Kompozit malzemelerin kullanım yerlerinden kaynaklı olarak fiber oryantasyonunda değişimler yapılamamaktadır. Bu durumda en çok tercih edilen yöntemler matris takviyesidir (Zarei vd., 2017). Matris takviyesi olarak nanoparçacıklar (Nega vd., 2022), nanofiber matlar (Saghafi vd., 2014) ve filmler (Dhaliwal ve Newaz, 2016) tercih edilmektedir. Son yıllarda çevre dostu malzemeler daha çok tercih edilmeye başlanmıştır (Gholampour ve Ozbakkaloglu, 2020). Düşük yoğunluklu, düşük maliyetli ve geri dönüştürülebilir olması sebebiyle selüloz lifleri kompozitlerde kullanılmaya başlanılmıştır (Alamri ve Low, 2012). Kompozit malzemelerin mekanik ve fiziksel özellikleri üzerindeki etkisini incelemek için kenaf, kenevir, keten, bambu ve ahşap gibi çeşitli selüloz lifleri üzerinde çeşitli araştırmalar yapılmıştır. Selüloz lif içeren tabakalar kompozitlerde matris takviyesi olarak son yıllarda kullanılmaya başlanmıştır (Alamri ve Low, 2012).

Bu çalışmada kağıt takviyeli hibrit kompozitlerin üretimi yapılmış ve kağıt takviyesinin dayanım üzerindeki etkisi araştırılmıştır. Kağıt takviyesinin tabakalar arası kırılmada etkin bir rol oynadığı gözlenmiştir. Simetrik bir kompozit yapı elde edebilmek için en dışta cam fiber içeren hibrit kompozitler ile en dışta karbon fiber içeren iki ayrı hibrit kompozit üretilmiştir. Çekme durumunda oluşacak hibrit etkisi de gözlemlenmiştir.

2. MATERYAL VE METOT

Hibrit kompozit üretimi için gerekli olan kumaşlar Dost Kimya firmasında temin edilmiştir. 200 g/m2 ’lik nominal ağırlığa sahip düz örgü cam kumaşların elyaf çapları yaklaşık 9 µm’dir ve örgüdeki her elyaf demeti 3000 elyaftan oluşmaktadır. Yüksek mukavemetli karbon kumaşlar da 200 g/m2 ’lik nominal ağırlığa sahip düz örgü şeklinde olup elyaf çapları 7 µm’dir ve elyaf demeti 3000 elyaftan oluşmaktadır. İnfüzyon ve laminasyon özelliğine sahip olan Epoksi reçine sistemi Hexion firması tarafından üretilmiş olup düşük viskoziteli MGS L160 diglisidil eter bisfenol A (DGEBA) epoksi ve sertleştirici olarak aynı firmaya ait MGS L260 amin sertleştirici tercih edilmiştir. Kumaş tabakalar arasında kullanılacak olan selüloz kağıt ise 80 g/m2 olup Ve-Ge firmasından alınmıştır.

2.1. Hibrit kompozitlerin üretimi

Hibrit kompozit malzemelerin üretimi için cam, karbon kumaşlar ve selüloz kağıtlar belirlenen ölçülerde kesildi. Vakum Destekli Reçine Transfer Kalıplama (VARTM) üretimi uygulanacağından dolayı aynı boyutlarda ayırma kumaşı ve dağıtıcı file kesildi. Bu üretim yönteminin seçilmesindeki temel etken üretim prosesinin kolay ve çok ekipman gerektirmemesidir (Asim vd., 2017). Vakum naylonu ise belirtilen boyutlardan daha büyük olacak şekilde kesildi (Şekil 1).

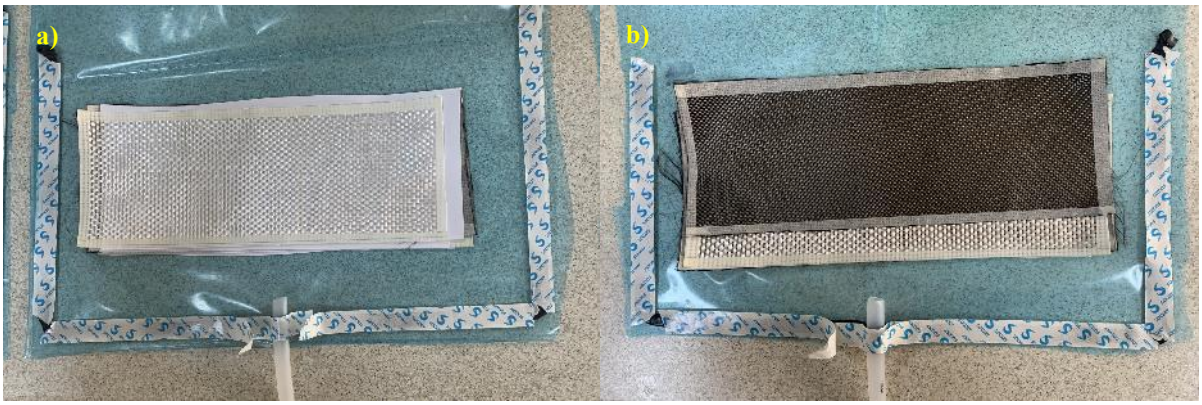

Şekil 1. Kompozit üretim öncesi hazırlık aşamaları a) En dışta cam kumaşların b) En dışta karbon kumaşların bulunduğu numuneler

Hibrit kompoziti oluşturacak kumaşlar 6 kat olacak şekilde düzenlenmiştir. Kumaşların sıralamasında iki farklı dizilim uygulanmıştır. Bu iki farklı dizilim için hibrit kompozitin en dış tabakasında cam kumaşlar (Şekil 2a) ve yine en dış tabakada karbon kumaşlar (Şekil 3a) olacak şekilde dizilim yapılmıştır. Ayrıca her iki tür dizilimde kağıt takviyesi olacak şekilde her kumaş tabakası arasına selüloz kağıt yerleştirilmiştir (Şekil 2b ve 3b).

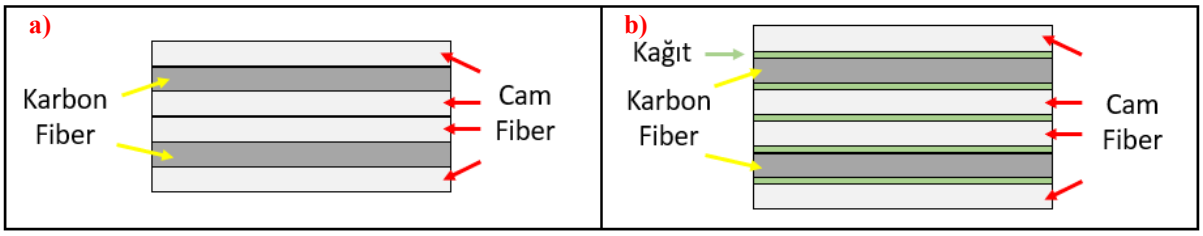

Şekil 2. Kompozitte cam kumaşların en dış tabakada olduğu yerleşim düzeni a) Kağıt takviyesiz b) Kağıt takviyeli

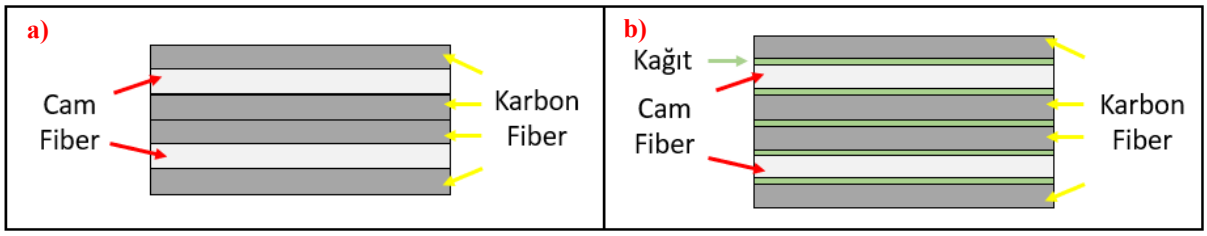

Şekil 3. Kompozitte karbon kumaşların en dış tabakada olduğu yerleşim düzeni a) Kağıt takviyesiz b) Kağıt takviyeli

Kumaşların üzerine sırasıyla ayırma kumaşı ve dağıtıcı file serildi. Sistemde vakum ortamı sağlayabilmek için etrafına sızdırmazlık bandı çekildi ve vakum naylonu ile kapatıldı. Daha sonra sisteme vakum pompası bağlanarak, Şekil 4'te gösterildiği gibi, sisteme vakum altında epoksi verildi ve içerideki hava ve fazla epoksi diğer taraftan tahliye edildi. Kompozit malzeme 80 ºC'de 4 saat olacak şekilde kürlendi. Kompozit levhalar yüksek hızlı dairesel testere ile kesilerek çekme testi numunesi boyutlarına getirildi.

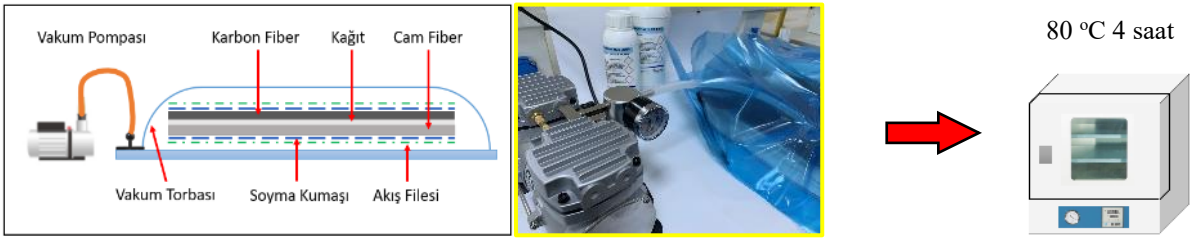

Şekil 4. Hibrit kompozitin üretim aşamalarının şematik gösterimi

2.2. Mekanik test

Kompozit malzemelerin çekme testleri Instron 8801 test cihazında ASTM D3039 standardına göre numune boyutları 250 mm × 25 mm × 3 mm boyutlarında olacak şekilde 2 mm/dk çene ilerleme hızında ve beş tekrarlı oda sıcaklığında yapılmıştır. Üniversal test cihazının çeneleri arasına bağlanarak çekme kuvveti uygulanan bir numuneye ait fotoğraf Şekil 5'te gösterilmiştir.

Şekil 5. Çekme testi sırasındaki görüntü

3. BULGULAR

Üretimi yapılan kompozitler çekme testine tabi tutularak kompozitin çekme dayanımı bulunmuştur. Ayrıca her tabaka arasına yerleştirilen kağıdın kompozitin dayanımına olan etkisine bakılmıştır. En dış tabakada cam kumaştan oluşan kağıt takviyeli ve kağıt takviyesiz hibrit kompozite ait gerilme-birim şekil değişimi grafiği şekil 6'da verilmiştir.

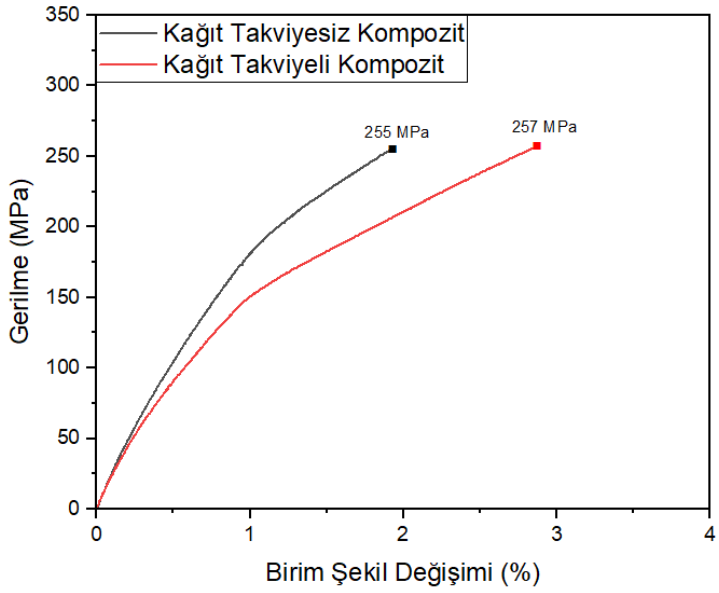

Şekil 6. En dış tabakada cam kumaşın bulunduğu hibrit kompozite ait çekme testi sonuçları

Cam kumaş tabakanın en dışta yer aldığı hibrit kompozit kağıt takviyesiz olduğu durumda 255 MPa'lık bir çekme dayanımı meydana gelirken kağıt takviyeli olduğu zaman 257 MPa' lık bir sonuç ortaya çıkmıştır. Kağıt takviyesi ile birlikte çekme dayanımında önemli bir artış gözükmezken şekil değişiminde artışa sebep olmuştur. Çekme testi sonucunda oluşan kırılma yüzeyinden alınan mikroskop görüntüleri şekil 7 ve 8'de verilmiştir. Kağıt takviyesiz kompozitten alınan görüntülerde (Şekil 7) cam fiberlerde, fiber kırılması ve sıyrılmasının yaygın olduğu belirlenmiştir. Karbon kumaş tabaka ile cam kumaş tabaka arasında ise delaminasyonların yaygın olduğu görülmektedir

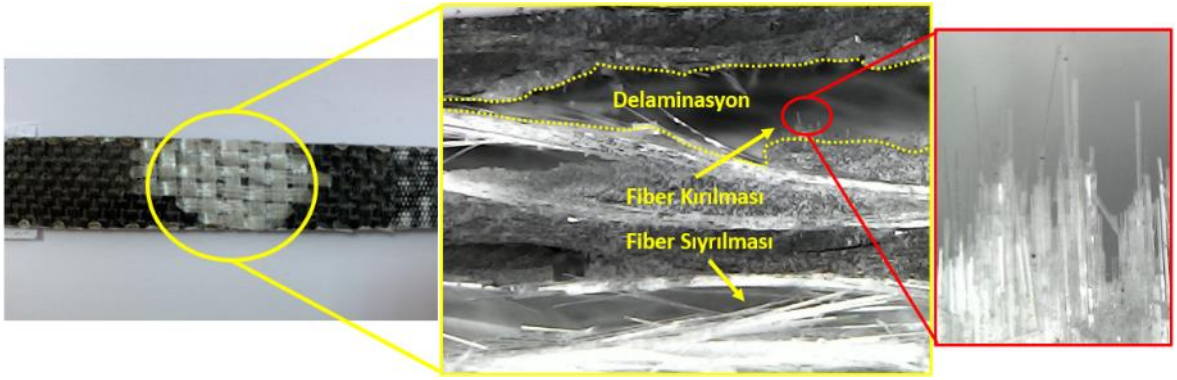

Şekil 7. En dış tabakada cam kumaşın bulunduğu kağıt takviyesiz hibrit kompozitin mikroskop görüntüleri

Kağıt takviyesi olan kompozitten alınan mikroskop görüntülerinde ise benzer hasar türleri mevcut olup kağıt tabakasının kumaş yüzeylerine yapışmasından dolayı selüloz liflerin sıyrılmasını görmekteyiz. Yine cam tabakaları arasında delaminasyonun olduğu ve delaminasyonun olduğu bölgede kağıt tabakasının olmasından dolayı kohezyon hasarı vardır.

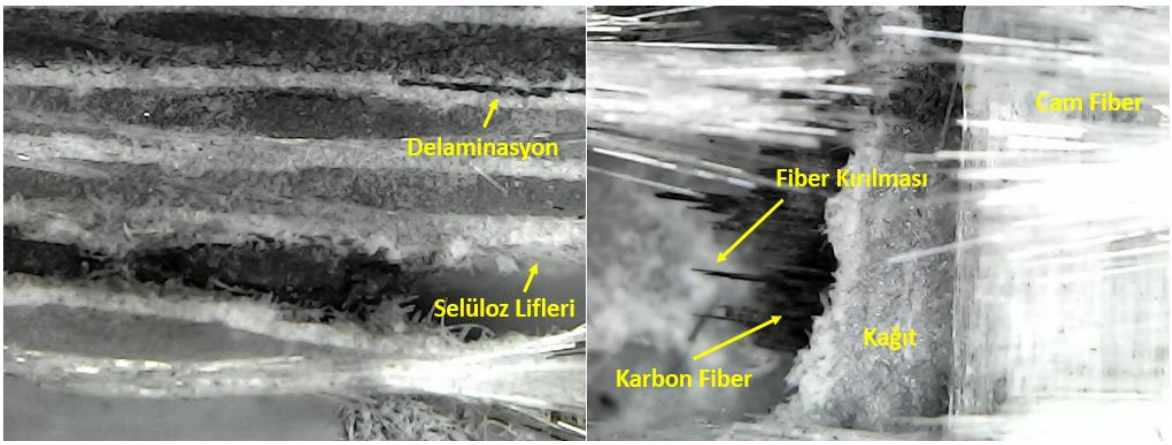

Şekil 8. En dış tabakada cam kumaşın bulunduğu kağıt takviyeli hibrit kompozitin mikroskop görüntüleri

Diğer dizilim türüne sahip (en dış tabaka karbon kumaş) kağıt takviyeli ve kağıt takviyesiz hibrit kompozitin gerilme-birim şekil değişimi grafiği de şekil 9'da verilmiştir. Çekme testi sonuçları incelendiğinde kağıt takviyesi kompozitte 302 MPa ve kağıt takviyeli kompozitte ise 272 MPa'lık çekme dayanımı çıkmıştır. Karbon fiber ağırlıklı bir kompozitte kağıt takviye edildiğinde dayanımda %10 azalma meydana gelmiştir. Cam fiber ağırlıklı kompozitle kıyaslandığı takdirde ise daha yüksek dayanım sergilemektedir Bunu da karbon fiberden kaynaklı olmaktadır. Aydın vd., (2018) tarafından yapılan çalışmada da cam ve karbon fiberler kullanarak hibrit kompozit yapının üretimi yapıldığı ve bu yapının mekanik ve dinamik özelliklerini incelemişlerdir. Test sonuçlarına göre sadece karbon yapının dinamik ve mekanik özellikler bakımından en iyi sonucu verdiği gözlemlenmişlerdir.

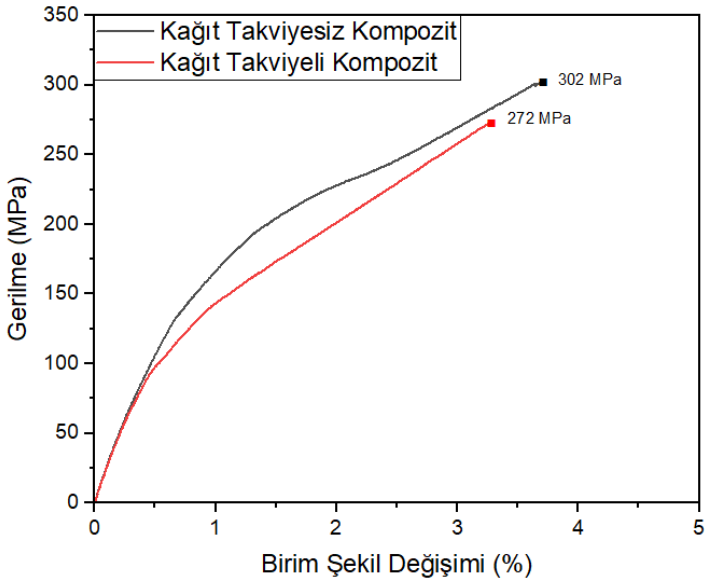

Şekil 9. En dış tabakada karbon kumaşın bulunduğu hibrit kompozite ait çekme testi sonuçları

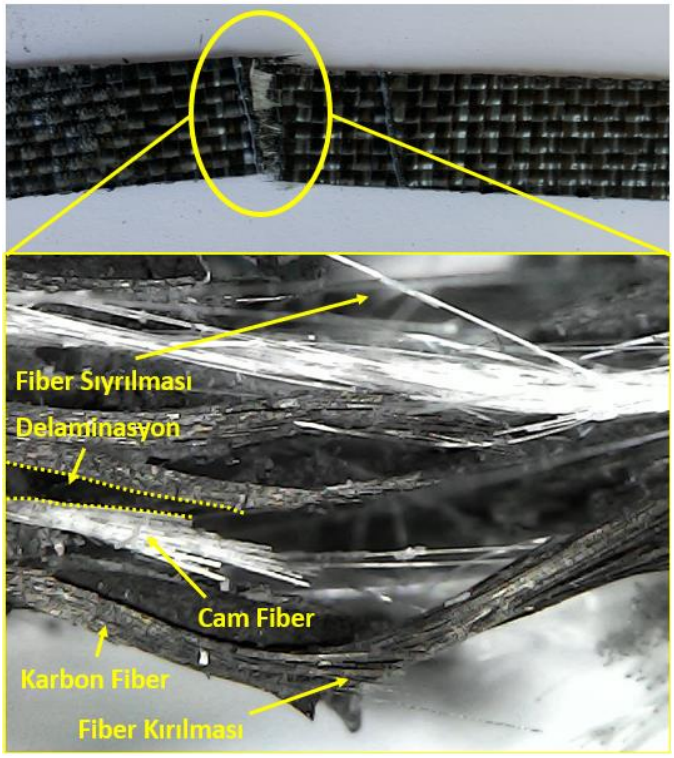

Şekil 10. En dış tabakada karbon kumaşın bulunduğu kağıt takviyesiz hibrit kompozitin mikroskop görüntüleri

Mikroskop görüntüleri incelendiği takdirde kağıt takviyesiz numunede (Şekil 10) çekme testinden kaynaklı olarak yaygın olarak fiber kırılmaları ve sıyrılmaları mevcuttur. Yine karbon fiber tabaka ile cam fiber tabaka arasında delaminasyonların yaygın olduğu görülmektedir. Kağıt takviyeli kompozitte ise selüloz kağıt tabakasından kaynaklı olarak karbon tabakalar arasında kohezyon hasarının oluştuğu belirlenmiştir.

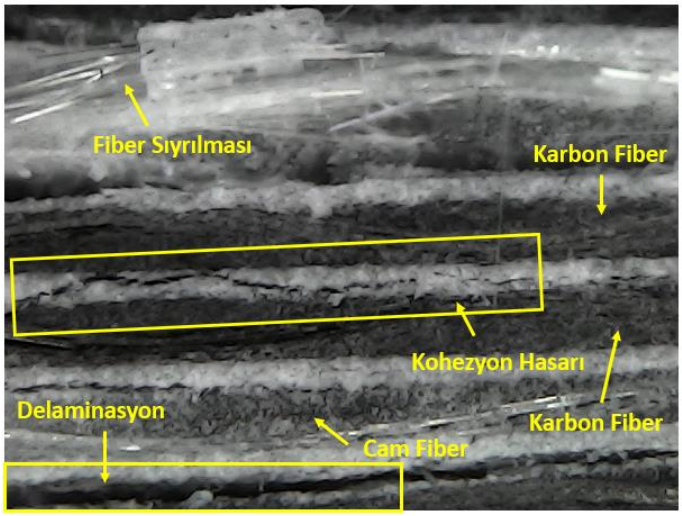

Şekil 11. En dış tabakada karbon kumaşın bulunduğu kağıt takviyeli hibrit kompozitin mikroskop görüntüleri

4. TARTIŞMA VE SONUÇLAR

Kağıt takviyesinin hibrit kompozit yapıların dayanımı üzerinde etkisi araştırılmıştır. Bu doğrultuda karbon ve cam kumaşlar kullanılarak kompozitler VARTM yöntemi ile üretilmiştir. Bu kompozitler hazırlanırken en dış tabakada cam fiberler olduğu ve diğer bir grup olarak da en dışta karbon fiberlerin olduğu bir dizilim tercih edilmiş. Tabaka sayısı bakımından %67'si karbon fiberden oluşan hibrit kompozit ile %67'si cam fiberden oluşan hibrit kompozitin çekme dayanımı sırasıyla 302 ve 255 MPa'dır. Ayrıca bu iki tür için de kağıt takviyesi yapılmış ve her grup kendi içerisinde çekme testi sonuçları incelenmiştir. Cam fiber ağırlıklı hibrit kompozitte kağıt takviyesi sonucunda birim şekil değişiminde artış olurken dayanımda da çok az bir artış olmuştur. Fakat karbon fiber ağırlık hibrit kompozitte ise kağıt takviyesi çekme dayanımında düşüşe sebep olmaktadır. Kağıt takviyesinde çekme dayanımının düşmesinin sebebi karbon fiberin elastik modülünün çok yüksek olmasından kaynaklı olduğu şeklinde yorumlanabilir.

KAYNAKLAR

Alamri, H., & Low, I. M. (2012). Microstructural, mechanical, and thermal characteristics of recycled cellulose fiber-halloysite-epoxy hybrid nanocomposites. Polymer Composites, 33(4), 589-600.

Asim, M., Jawaid, M., Saba, N., Nasir, M., & Sultan, M. T. H. (2017). Processing of hybrid polymer composites—a review. Hybrid polymer composite materials, 1-22.

Aydın, M. R., Acar, V., Yapıcı, F., Yıldız, K., Topcu, M. V., & Gündoğdu, Ö. (2018). Inter-ply Hibrit Kompozit Yapılarda Elyaf Diziliş Sıralamasının Mekanik ve Dinamik Özelliklere Etkisi . Journal of the Institute of Science and Technology , 8 (3) , 255- 263 . DOI: 10.21597/jist.458649

Demir, O. (2017). Karbon Nanotüp Katkılı Cam-Karbon Fiber/Epoksi Hibrit Nanokompozitlerin Mekanik Özellikleri ve Düşük hızlı Darbe Davranışları. Selçuk Üniversitesi Fen Bilimleri Enstitüsü.

Dhaliwal, G. S., & Newaz, G. M. (2016). Effect of layer structure on dynamic response and failure characteristics of carbon fiber reinforced aluminum laminates (CARALL). Journal of Dynamic Behavior of Materials, 2, 399-409.

Dong, C., & Davies, I. J. (2015). Flexural strength of bidirectional hybrid epoxy composites reinforced by E glass and T700S carbon fibres. Composites Part B: Engineering, 72, 65-71.

Dong, C., Kalantari, M., & Davies, I. J. (2015). Robustness for unidirectional carbon/glass fibre reinforced hybrid epoxy composites under flexural loading. Composite Structures, 128, 354-362.

Dorigato, A., & Pegoretti, A. (2014). Flexural and impact behaviour of carbon/basalt fibers hybrid laminates. Journal of Composite Materials, 48(9), 1121-1130.

Erkendirci, Y. H. (2023). Cam karbon kumaş ve polipropilen takviyeli hibrit kompozitlerin mekanik özelliklerinin araştırılması ve analizi. Marmara Üniversitesi Fen Bilimleri Enstitüsü.

Ferrante, L., Tirillò, J., Sarasini, F., Touchard, F., Ecault, R., Urriza, M. V., ... & Mellier, D. (2015). Behaviour of woven hybrid basalt-carbon/epoxy composites subjected to laser shock wave testing: Preliminary results. Composites Part B: Engineering, 78, 162-173.

Fong, K. Y., Mariatti, M., & Takagi, H. (2012). Effect of Matrix and Staking Sequence of Recycled Jute/Carbon Fiber Hybrid Laminated Composites. Journal of Polymer Materials, 29(4).

Gholampour, A., & Ozbakkaloglu, T. (2020). A review of natural fiber composites: Properties, modification and processing techniques, characterization, applications. Journal of Materials Science, 55(3), 829-892.

Hannemann, B., Backe, S., Schmeer, S., Balle, F., & Breuer, U. P. (2016). Metal fiber incorporation in carbon fiber reinforced polymers (CFRP) for improved electrical conductivity: Steigerung der elektrischen Leitfähigkeit von kohlenstofffaserverstärkten Kunststoffen (CFK) durch Integration von Metallfasern. Materialwissenschaft und Werkstofftechnik, 47(11), 1015-1023.

Hannemann, B., Backe, S., Schmeer, S., Balle, F., Breuer, U. P., & Schuster, J. (2017). Hybridisation of CFRP by the use of continuous metal fibres (MCFRP) for damage tolerant and electrically conductive lightweight structures. Composite structures, 172, 374-382.

Hayashi, T. (1972). On the improvement of mechanical properties of composites by hybrid composition. In Proc. 8th Intl. Reinforced Plastics Conf. (pp. 149-152).

Hine, P. J., Bonner, M., Ward, I. M., Swolfs, Y., Verpoest, I., & Mierzwa, A. (2014). Hybrid carbon fibre/nylon 12 single polymer composites. Composites Part A: Applied Science and Manufacturing, 65, 19-26.

Karaçor, B., & Özcanlı, M. (2022). The effect of use of different types of matrix material on mechanical characteristics in jute/carbon fiber reinforced hybrid composites. Niğde Ömer Halisdemir Üniversitesi Mühendislik Bilimleri Dergisi, 11(2), 439-448.

Kim, S. C., Kim, J. S., & Yoon, H. J. (2011). Experimental and numerical investigations of mode I delamination behaviors of woven fabric composites with carbon, Kevlar and their hybrid fibers. International Journal of Precision Engineering and Manufacturing, 12, 321-329.

Kumar, A. P., Jeyalal, L. P., & Kumar, D. B. (2012). Hybridization of polymer composites. Int J Adv Mater Sci, 3, 173-182.

Nega, B. F., Pierce, R. S., Yi, X., & Liu, X. (2022). Characterization of Mechanical and Damping Properties of Carbon/Jute Fibre Hybrid SMC Composites. Applied Composite Materials, 29(4), 1637-1651.

Pandya, K. S., Veerraju, C., & Naik, N. K. (2011). Hybrid composites made of carbon and glass woven fabrics under quasi-static loading. Materials & Design, 32(7), 4094-4099.

Saghafi, H., Zucchelli, A., Palazzetti, R., & Minak, G. (2014). The effect of interleaved composite nanofibrous mats on delamination behavior of polymeric composite materials. Composite Structures, 109, 41-47.

Sapiai, N., Jumahat, A., & Hakim, R. N. (2014). Tensile and compressive properties of hybrid carbon fiber/kenaf polymer composite. Adv. Environ. Biol, 8(8), 2655-2661.

Seyed Yaghoubi, A., Liu, Y., & Liaw, B. (2012). Stacking sequence and geometrical effects on low-velocity impact behaviors of GLARE 5 (3/2) fiber–metal laminates. Journal of thermoplastic composite materials, 25(2), 223-247.

Swolfs, Y., Gorbatikh, L., & Verpoest, I. (2014). Fibre hybridisation in polymer composites: A review. Composites Part A: Applied Science and Manufacturing, 67, 181-200.

Taş, H., & Soykök, İ. F. (2018). Tabakalı Hibrit Kompozit Profillerin Doğal Frekanslarının Sonlu Elemanlar Metodu ile Belirlenmesi. Dokuz Eylül Üniversitesi Mühendislik Fakültesi Fen ve Mühendislik Dergisi, 20(60), 1045-1056.

White, D. M., Taylor, E. A., & Clegg, R. A. (2003). Numerical simulation and experimental charcterisation of direct hypervelocity impact on a spacecraft hybrid carbon fibre/kevlar composite structure. International journal of impact engineering, 29(1-10), 779-790.

Woo, S. C., & Kim, T. W. (2016). High strain-rate failure in carbon/Kevlar hybrid woven composites via a novel SHPB-AE coupled test. Composites Part B: Engineering, 97, 317-328.

Yu, H., Longana, M. L., Jalalvand, M., Wisnom, M. R., & Potter, K. D. (2015). Pseudo-ductility in intermingled carbon/glass hybrid composites with highly aligned discontinuous fibres. Composites Part A: Applied Science and Manufacturing, 73, 35-44.

Zarei, H., Brugo, T., Belcari, J., Bisadi, H., Minak, G., & Zucchelli, A. (2017). Low velocity impact damage assessment of GLARE fiber-metal laminates interleaved by Nylon 6, 6 nanofiber mats. Composite Structures, 167, 123-131.

Zhang, H., Gn, S. W., An, J., Xiang, Y., & Yang, J. L. (2014). Impact behaviour of GLAREs with MWCNT modified epoxy resins. Experimental Mechanics, 54, 83-93.

Zhang, J., Chaisombat, K., He, S., & Wang, C. H. (2012). Hybrid composite laminates reinforced with glass/carbon woven fabrics for lightweight load bearing structures. Materials & Design (1980-2015), 36, 75-80.

Zweben, C. (1977). Tensile strength of hybrid composites. Journal of materials science, 12, 1325-1337.

Nonlinear Seismic Analysis Of A 24 Stories Reinforced Concrete Building

İsra Yilmaz*[1], Muhammet Karaton [2]

Abstract: Two destructive earthquakes in the Kahramanmaraş province of Turkey hit with an epicenter of Pazarcık and Elbistan on February 6, 2023. The magnitudes and depths of the earthquakes were recorded as h=8.6 km for Mw=7.7 and h=7 km for Mw=7.6, respectively. The earthquakes affected a wide region covering 11 provinces and more than 50 thousand citizens lost their lives. Absolute maximum acceleration value of the earthquake acceleration records were determined that bigger than predicted design earthquake acceleration values in some regions of the Turkey Earthquake Hazard Map (TEHM). For this reason, damages above the calculated damage were observed in the structures. In this study, a 24-story reinforced concrete building with frame and shear walls is selected. Nonlinear time history analyses of the building are obtained under two earthquake acceleration records. Damage cases are compared for two analyses results. The first earthquake records used in the analyses are data from station 4614 recorded in Pazarcık (Kahramanmaraş) during the Pazarcık earthquake. The second earthquake records are artificially generated by using the design acceleration spectrum graph in the Turkish Building Earthquake Code (TBEC).

Keywords: Reinforced concrete building, Pazarcık Earthquake, Artificially generated earthquake records and nonlinear time history analyses.

[1]**Address:** Bilecik Seyh Edebali University, Faculty of Engineering, Bilecik/Türkey
[2]**Address:** Fırat University, Faculty of Engineering, Elazığ/Türkey
***Corresponding author**: isra.yilmaz@bilecik.edu.tr

1. GİRİŞ

Deprem, Türkiye'nin bulunduğu konumundan dolayı günümüze kadar yaşadığı en fazla can ve mal kaybına neden olan afet türüdür. Türkiye, Alp-Himalaya deprem kuşağında ve büyük depremler üretebilen Kuzey Anadolu Fay Zonu (KAFZ), Doğu Anadolu Fayı Zonu (DAFZ) ve Ege Dalma-Batma Fay Zonu üzerinde yer almaktadır (Yön, 2021). Ülkemizde depremlerin meydana gelmesi Afrika-Arabistan levhalarının kuzey-kuzeydoğuya doğru hareket etmeleri ile Avrasya levhası arasında bulunan Anadolu levhasının sıkışması ile ilgilidir. Arabistan levhası kuzeye doğru itilirken, Avrasya levhasının altına doğru dalma hareketine zorlanmaktadır. Şekil 1' de gösterildiği gibi Arabistan levhası ile Avrasya levhası arasında kalan Doğu Anadolu levhası sıkışmakta ve batıya doğru Ege dalma-batma bölgesine hareket etmektedir. Böylece KAF ile DAF' ı içeren Anadolu levhasındaki sıkışma günümüze kadar oluşan depremlerin ana nedenini oluşturmaktadır (Atabey, 2000).

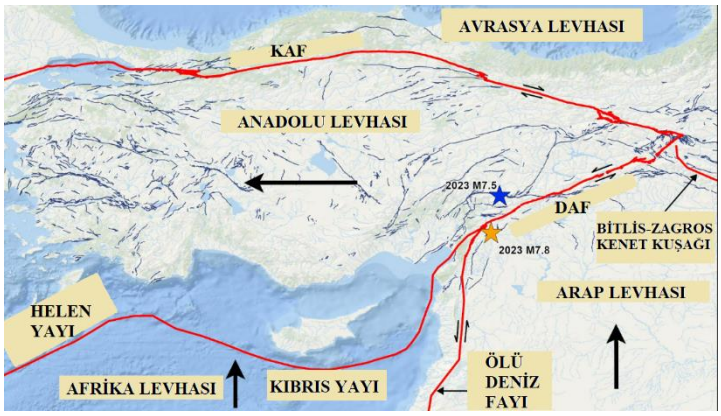

Şekil 1. Levha hareketleri ve Anadolu levhasının batıya hareketi (USGS, 2023)

1900' den günümüze kadar büyüklüğü Mw 6 ve üzerinde olan birçok depremin yaşandığı (Anadolu Ajansı, 2023) ülkemizde, 06 Şubat 2023' te önce Pazarcık (Kahramanmaraş) merkezli Mw 7.7 büyüklüğünde 8.6 km derinliğinde ilk deprem aynı gün Elbistan (Kahramanmaraş) merkezli Mw 7.6 büyüklüğünde yerin 7 km derininde ikinci deprem

meydana gelmiş ve büyük bir yıkım yaşanmıştır. Kısa bir zaman içinde gerçekleşen iki çok şiddetli deprem, 11 ili içeren çok geniş bir bölgeyi etkileyerek çok sayıda can ve mal kaybına yol açmıştır (AFAD, 2023). Ana depremlerden sonra meydana gelen şiddetli artçı depremler de hasarlı binaların hasar düzeyini artırmıştır. 27 Şubat 2023' te, kaydedilen bazı istasyonların ivme kayıtlarına ait tepki spektrumlarının geometrik ortalaması ile %5 sönüm oranı ve ZC zemin sınıfı için DD-1 (Deprem Yer Hareketi Düzeyi-1) yatay elastik tasarım ivme spektrumu karşılaştırılmıştır. Belirli periyotlarda (0.25 s, 0.5 s, 1.0 s ve 2.0 s) tepki spektrumlarının geometrik ortalamasının yatay elastik tasarım ivme spektrumunun üzerinde kaldığı tespit edilmiştir. Bu durum en çok Hatay' da görülmüştür (İTÜ, 2023). DD2 (Deprem Yer Hareketi Düzeyi-2) tasarım depreminin üzerinde spektral ivme değerlerinin kaydedilmesinin yanı sıra Türkiye Bina Deprem Yönetmeliği (TBDY, 2018)' nde DD1 depremi için olması beklenen spektral ivme değerlerinin de aşıldığı periyot aralıkları oluşmuştur (Avşar vd., 2023). Depremin etkisi sonucunda birçok farklı hasarın oluştuğu belirtilmiştir (Akgül ve Etli, 2023). Binaların göçmesine sebep olan etkenlerden biri de rezonans ile birlikte binaların doğal titreşim periyotlarının, depremin hakim periyodu ile çakışması sonucu binaların davranışlarındaki beklenmedik artışlardır. Yüksek periyotlardaki büyütmeler yüksek binaları ve düşük periyotlardaki büyütmeler ise yüksek olmayan binaları etkilemektedir (Perk ve Özer, 2019). Ayrıca yapısal düzensizliklerden kaynaklı hasarlar da meydana gelmiş olup taşıyıcı sistemi rijitlik bakımından düzenli olmadığı için burulma davranışı sonucunda göçmelerin yaşandığı durumlar da görülmüştür (TMMOB İMO, 2023). Bu bakımdan binaların taşıyıcı sisteminde perde kullanımı önem arz etmektedir. Bina yüksekliğine bağlı olarak yüksek binaların taşıyıcı sistemleri çerçeveli, perdeli ve perdeli-çerçeveli olarak farklı şekillerde tasarlanabilmektedir (Zeybek, 2022).

Bu çalışmada, 24 katlı betonarme perdeli-çerçeveli binanın TBDY (2018)' ye göre doğrusal olmayan sismik analizi yapılmıştır. Bina planının her iki doğrultusunda Kahramanmaraş ilinin 4614 kodlu istasyonunda kaydedilen 6 Şubat 2023 Kahramanmaraş-Pazarcık (gerçek) deprem ivme kaydı ve zemin sınıfı ZD için aynı istasyon konumu dikkate alınarak TBDY (2018)' de belirtilen yatay tasarım ivme spektrumuyla uyumlu üretilen yapay deprem ivme kaydı kullanılmıştır. Doğrusal olmayan davranış kuvvete dayalı fiber eleman yöntemi ile hesaba katılmıştır. Analiz sonucunda yapısal elemanlarda meydana gelen hasarlar incelenmiştir.

2. MATERYAL VE METOT

Deprem etkisinde bina tasarımı için TBDY (2018)' de, Dayanıma (Kuvvete) Göre Tasarım (DGT) ve Şekil Değiştirmeye Göre Değerlendirme ve Tasarım (ŞDGDT) olmak üzere iki yaklaşım mevcuttur. Doğrusal davranışı esas alan DGT' de doğrusal hesap yöntemleri olan eşdeğer deprem yükü yöntemi ve modal hesap yöntemleri (mod birleştirme yöntemi ve mod toplama yöntemi) kullanılmaktadır. Deprem yüklemesinin itme yöntemleri ve zaman tanım alanında doğrusal olmayan hesap yöntemlerinden biri kullanılarak yapıldığı ŞDGDT' ise deprem sebebiyle taşıyıcı elemanlarda meydana gelen hasar hesaba katılmaktadır. Binaların taşıyıcı sistemleri, etkiyen yükler için doğrusal davranış dikkate alınarak tasarlanırlar ancak deprem etkisi altında doğrusal davranışa göre yapılan hesaplar gerçekçi sonuçlar vermeyebilir. Doğrusal olmayan hesap yöntemleri, doğrusal hesap yöntemlerine göre malzemelerin davranışını ve geometri değişimini daha kesin hesapladığı için daha gerçekçi sonuçlar vermektedir (Aksoylu, 2020).

2.1. Fiber eleman yöntemi

Binalarda doğrusal olmayan davranış için yığılı ve yayılı plastik davranış modeli kullanılmaktadır. Yayılı plastik davranış modeli olan fiber eleman yönteminde, kuvvet (esneklik) ve yer değiştirme (deplasman) esaslı olmak üzere iki yaklaşım mevcuttur. Bu yöntemde, Şekil 2' de görüldüğü gibi integrasyon noktalarındaki kesitler kendi içinde fiber (kesit hücresi/lif) elemanlara bölünmektedir. Betonarme kesitin içinde, beton ve çelik fiber elemanların doğrusal olmayan davranışları birlikte dikkate alınmaktadır (Taucer vd., 1991). Bu çalışmada, kuvvete dayalı fiber eleman yöntemi kullanılmış olup elemanın integrasyon noktalarındaki kesitlerinde ortaya çıkan iç kuvvetler dikkate alınarak her bir elemanın doğrusal olmayan çözümleri elde edilmektedir. Aynı zamanda, her bir kesitte yer alan beton fiberler için Mander, Priestly ve Park modeli ve donatı fiberleri için ise Menegotto-Pinto modeli kullanılmıştır (Mander vd., 1988; Menegotto ve Pinto, 1973).

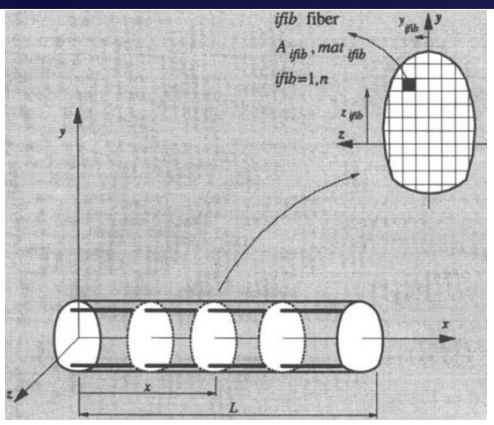

Şekil 2. Eleman ve fiber (hücre) elemanlara bölünen kesit (Taucer vd., 1991)

2.1.1. Mander, Priestly ve Park beton modeli

Popovics (1973) tarafından betonun tek eksenli çekme ve basınç davranışını modelleyen bir eğri önerilmiştir. İlerleyen dönemlerde Mander vd. (1988) bu modeli sargılı ve sargısız betonlar için Şekil 3' teki gerilme-şekil modelini geliştirmişlerdir.

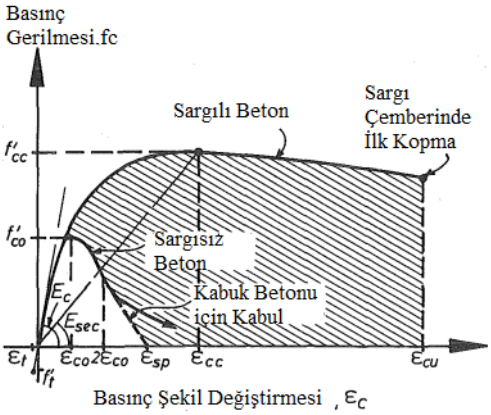

Şekil 3. Sargılı ve sargısız betonun tek eksenli yükleme için gerilme-şekil değiştirme modeli (Mander vd., 1988)

2.1.2. Menegotto-Pinto modeli

Donatı çeliğinin doğrusal olmayan gerilme şekil değiştirme davranışında Bauschinger etkisini dikkate alan model önerilmiştir (Menegotto ve Pinto, 1973). Bu model daha sonra izotropik şekil değiştirme pekleşmesini içerecek şekilde değiştirilmiştir (Filippou vd., 1983). Şekil 4'te verilen Menegotto-Pinto modeline ait eşitlik Denklem (1)'de verilmiştir.

$$\sigma^* = b.\varepsilon^* + \frac{(1-b).\varepsilon^*}{\left(1+\varepsilon^{*R}\right)^{1/R}} \quad (1)$$

Bu denklemle E_0 eğimli asimptottan-(a) çizgisi E_1 eğimli asimptota-(b) çizgisi kavisli geçiş tanımlanmaktadır. Denklem 2' de σ_0 ve ε_0 iki asimptotunun birleştiği B noktasındaki, σ_r ve ε_r yükün son kez boşaltıldığı ve tekrar yüklendiği A noktasındaki gerilme ve şekil değiştirmedir. b, E_1 ve E_0 eğimleri arasındaki oranı (şekil değiştirme sertleşme oranı) ve R ise geçiş eğrisinin şeklini etkileyen Bauschinger etkisini ifade etmektedir.

$$\varepsilon^* = \frac{\varepsilon-\varepsilon_r}{\varepsilon_o-\varepsilon_r}; \qquad \sigma^* = \frac{\sigma-\sigma_r}{\sigma_o-\sigma_r} \quad (2)$$

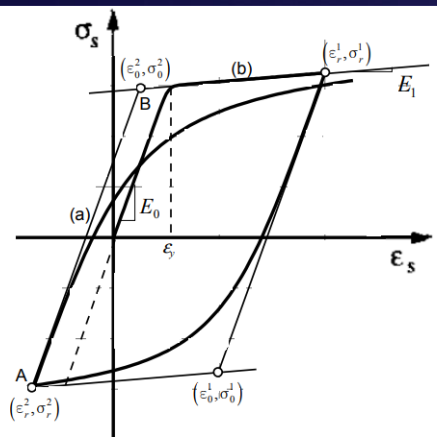

Şekil 4. Menegotto-Pinto çelik modeli (Menegotto ve Pinto, 1973)

2.2. Betonarme elemanlarda hasar sınırları ve hasar bölgeleri

TBDY (2018)' de sünek eleman kesitlerinde, elastik ötesi davranışın sırasıyla sınırlı miktarda, kesit dayanımın güvenli olarak sağlanabileceği düzeyde olduğu ve ileri düzeyde olduğu Sınırlı Hasar (SH), Kontrollü Hasar (KH) ve Göçme Öncesi (GÖ) hasar durumu ve sınır değerleri tanımlanmıştır. Kritik kesitlerinin hasarının bulunduğu bölgeye göre elemanların hasar durumu belirlenmektedir. Şekil 5' te SH' ye ulaşmayan elemanlar SH bölgesinde, SH ile KH arasında kalan elemanlar BH bölgesinde, KH ile GÖ arasında kalan elemanlar İH bölgesinde, GÖ' yü geçen elemanlar ise göçme bölgesinde (GB) yer almaktadırlar.

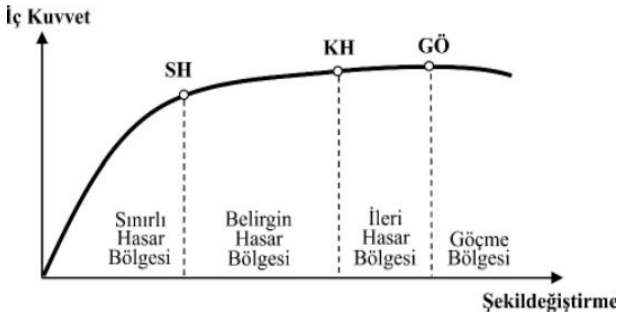

Şekil 5. Kesit hasar bölgeleri (TBDY, 2018)

Yayılı plastik davranış modeline göre şekil değiştirme hasar sınırları betonarme dikdörtgen kesitli elemanlar için GÖ sınır değerleri Denklem (3) ve Denklem (4) kullanılarak hesaplanmaktadır.

$$\sum_{C}^{(GÖ)} = 0.0035 + 0.04\sqrt{w_{we}} \leq 0.018 \quad (3)$$

$$w_{we} = \alpha_{se}\rho_{sh,min}\frac{f_{ywe}}{f_{ce}} \quad (4)$$

Bu denklemlerde, w_{we}, α_{se} ve $\rho_{sh,min}$ sırasıyla etkin sargı donatısına ait mekanik donatı oranını, sargı donatısı etkinlik katsayısını ve dikdörtgen kesitlerde iki yatay doğrultuda hacimsel enine donatı oranının küçük olanını göstermektedir. f_{ywe} ve f_{ce} ise enine donatının ortalama akma dayanımını ve betonun ortalama basınç dayanımı olarak tanımlanmaktadır. KH ve SH sınır değerleri ise Denklem (5) ve Denklem (6) ile hesaplanmaktadır.

$$\varepsilon_{C}^{(KH)} = 0.75\varepsilon_{C}^{(GÖ)} \quad (5)$$

$$\varepsilon_{C}^{(SH)} = 0.0025 \quad (6)$$

3. BULGULAR

Bu çalışmada, 24 katlı ve 5 katlı betonarme perdeli-çerçeveli binaların TBDY (2018)' ye göre doğrusal olmayan sismik analizleri yapılmıştır. Deprem yükü olarak Kahramanmaraş ilinin 4614 kodlu istasyonunda kaydedilen 6 Şubat 2023 Kahramanmaraş-Pazarcık (gerçek) deprem ivme kaydı ve zemin sınıfı ZD için aynı istasyon konumu dikkate alınarak TBDY (2018)' deki yatay ivme spektrum eğrisiyle uyumlu üretilen yapay deprem ivme kaydı kullanılmıştır. Her iki deprem ivme kaydı binanın iki yatay doğrusuna aynı anda uygulanmıştır. Sayısal modellerde kat döşemeleri rijit diyafram olarak kabul edilerek ölü ve hareketli yükler kirişlere yayılı yük olarak uygulanmıştır. Temel ortamı ise rijit olarak kabul edilmiştir. Kat yükseklikleri 3.5 m seçilmiştir. Binalarda çerçeve sistemle birlikte kullanılan perdeler, binaların dış kenar ortalarında yer almaktadır. Binaların planı ve sonlu eleman modeli Şekil 6' da görülmektedir. 24

katlı binanın sonlu eleman modelinde 500 adet düğüm noktası, 96 adet perde, 192 adet kolon ve 480 adet kiriş eleman; 5 katlı binada ise 120 adet düğüm noktası, 20 adet perde, 40 adet kolon ve 100 adet kiriş eleman kullanılmıştır. Kuvvete dayalı fiber eleman yönteminde, taşıyıcı elemanlar 150 adet fiber elemana (kesit/lif hücresi) ayrılmış olup taşıyıcı elemanların donatıları Şekil 7' de verilmiştir. Her bir integrasyon noktasında bir kesit dikkate alınarak elemanların doğrusal olmayan davranışları modellenmiştir. Kesitlerdeki sargılı bölgelerin sargılama etki katsayıları Tablo 1' de verilmiştir. Betonun tek eksenli basınç dayanımı ve donatının akma dayanımı sırasıyla 25 MPa ve 420 MPa olarak seçilmiştir. Betonun tek eksenli çekme dayanımı (f_{ct}) ile elastisite modülü (E_c) ACI-318 (1995)' e göre Denklem (7) ve Denklem (8) ile 2.782 MPa ve 23500 MPa olarak hesaplanmıştır.

$$f_{ct} = 0.5563\sqrt{f_{cc}} \quad \text{(MPa)} \tag{7}$$

$$E_c = 4700\sqrt{f_{cc}} \quad \text{(MPa)} \tag{8}$$

Donatının elastisite modülü ise 200000 MPa olarak dikkate alınmıştır.

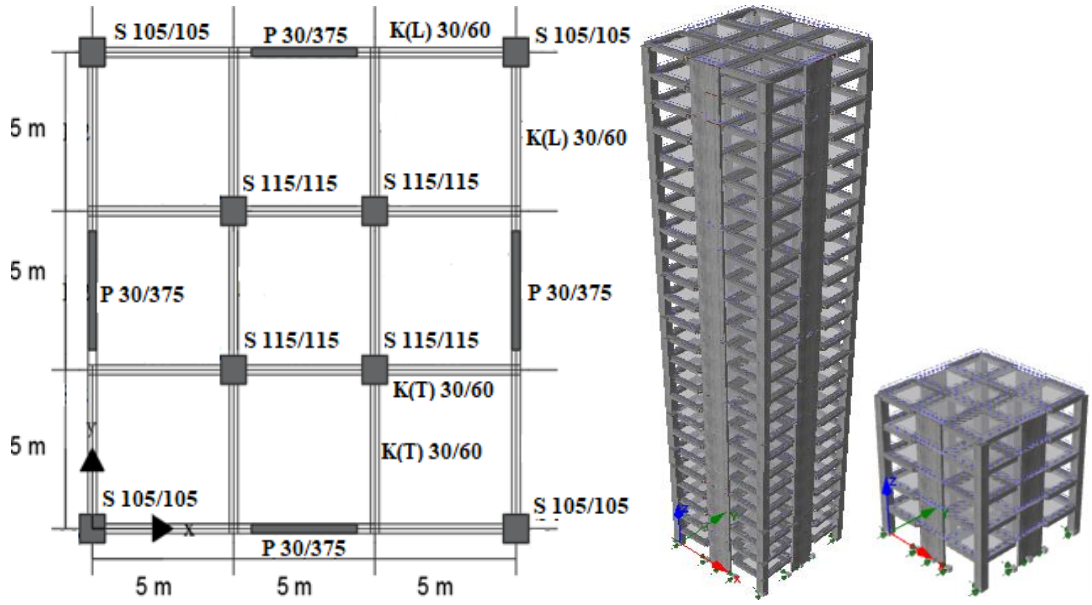

a) b)

Şekil 6. 24 ve 5 katlı binanın a) planları b) sırasıyla sonlu eleman modeli (Yılmaz, 2022)

Binaların modal analizleri 21 mod için yapılmış olup ilk modların elde edilen etkin modal kütle oranları ve periyotları Tablo 2' de verilmiştir. İlk modun periyotları kullanılarak binalardaki viskoz sönümler hesaplanmış olup sönüm oranları %5 olarak hesaba dahil edilmiştir. Nümerik analizler için SeismoStruct (2022) programı kullanılmış olup binaların doğrusal olmayan davranışları için kuvvete dayalı fiber eleman yöntemi kullanılmıştır. Sismik analizler için HHT-α integrasyon metodu kullanılmış olup integrasyon zaman adımı 0.01 s' dir. Çözümlerde, gerçek deprem ivme kaydı olarak Kahramanmaraş-Pazarcık depreminin (105s) Şekil 8 ve 9' da gösterilen Doğu-Batı (DB) ve Kuzey-Güney (KG) bileşenleri seçilmiştir. Aynı zamanda, kaydın alındığı koordinatlar dikkate alınarak DD2 ve ZD zemin sınıfı için TBDY (2018)' deki yatay elastik tasarım ivme spektrumuyla uyumlu yapay ivme kaydı üretilmiştir (Şekil 10). Bu spektrum eğrisine ait S_{DS} ve S_{D1} değerleri sırasıyla 1.182 ve 0.593 olarak belirlenmiştir. Söz konusu bu ivme kayıtları 24 katlı ve 5 katlı betonarme binalara enine ve boyuna doğrultularda etki ettirilmiştir.

Tablo 1. Sargılama etki katsayıları (Karaton ve Yılmaz, 2022)

Eleman	Sargılama Etki Katsayısı
P (30/375)	1.238
S (105/105)	1.414
S (115/115)	1.393
K (30/60)	1.021

Tablo 2. Binaların modal analizi

Bina	Etkin Modal Kütle Oranı (U_x, %)	Periyot (T_1, s)

24 katlı	37.2	1.94
5 katlı	37.6	0.26

Tablo 3. Betonarme kesitteki hasar sınır değerleri (Karaton ve Yılmaz, 2022)

Eleman	SH	KH	GÖ
P (30/375)	0.0025	0.0066	0.0088
S (105/105)	0.0025	0.0120	0.0160
S (115/115)	0.0025	0.0115	0.0154
K (30/60)	0.0025	0.0080	0.0107

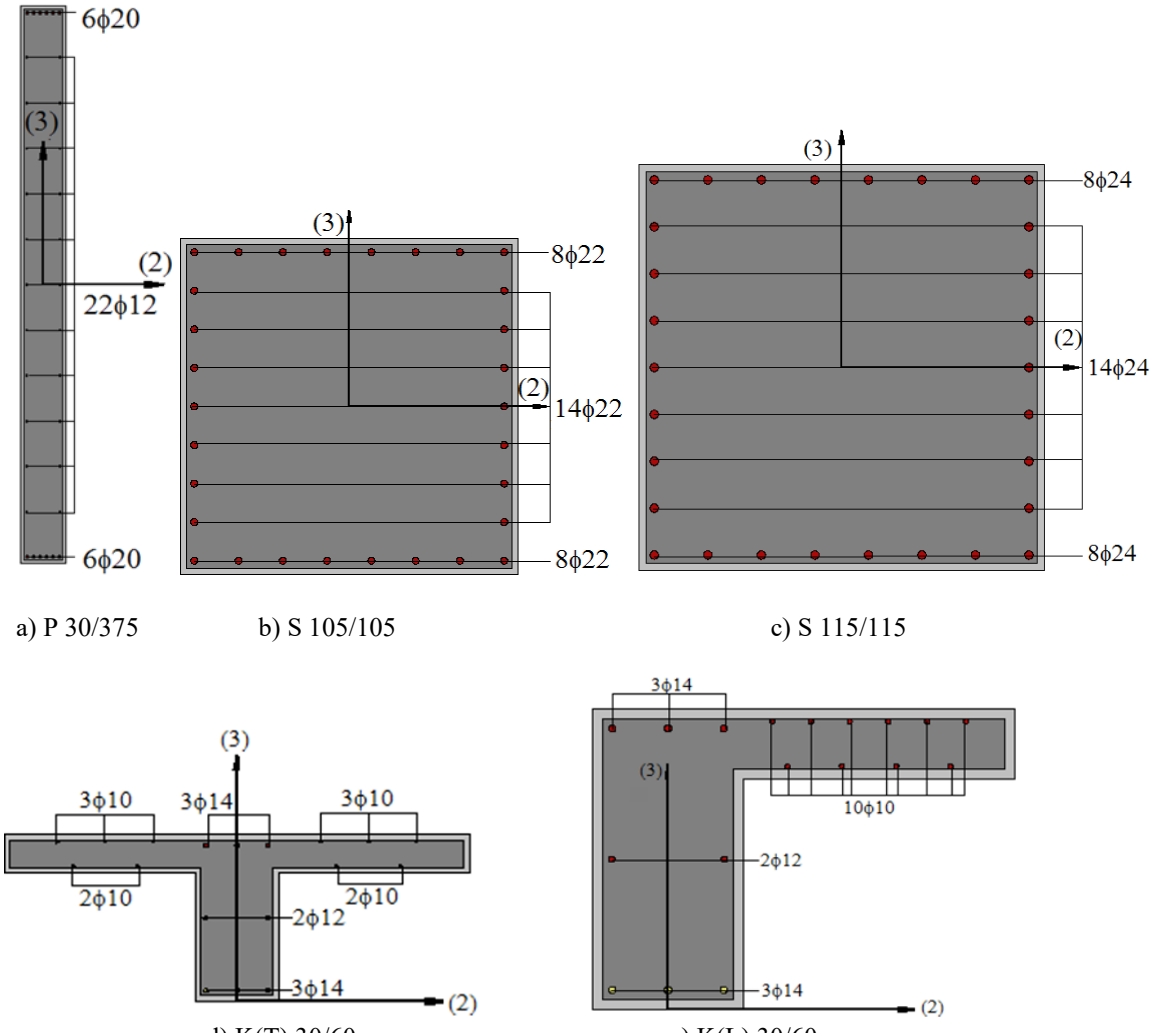

a) P 30/375 b) S 105/105 c) S 115/115

d) K(T) 30/60 e) K(L) 30/60

Şekil 7. Binaların taşıyıcı elemanları (Yılmaz, 2022)

Betonarme elemanlardaki hasar sınır değerleri Tablo 3' te görülmekte olup nümerik analizlerde elde edilen hasarlar söz konusu Tablo' ya göre belirlenmektedir. Bu amaçla BH, İH ve GB sırasıyla sarı, mavi ve siyah renkler ile ifade edilmiştir. Nümerik analizlerden elde edilen hasarlar Şekil 11 ve 12' de görülmektedir. 24 katlı binaya 4614 kodlu istasyonda kaydedilen (gerçek) deprem ivme kaydı uygulandığı durumda, zemin katta 1 adet perde ve binada toplam 100 adet kiriş elemanda BH tespit edilmiştir. Yapay ivme kaydı uygulandığında zemin katta 4 adet perde ve toplamda 125 adet kiriş elemanda BH ortaya çıkmıştır. Her iki çözüm için kolon elemanlarda herhangi bir hasar görülmemiştir. Aynı zamanda, 5 katlı binaya Gerçek ve yapay deprem ivme kaydı uygulanması durumunda da kolonlarda hasar oluşmamıştır. Gerçek deprem ivme kaydı için, zemin katta 4 adet perde elemanda ve birinci katta 1 adet perde elemanda BH görülmüştür. Binada, 37 adet kiriş elemanın BH, 7 adet kiriş elemanın İH aldığı ve 7 adet kirişin ise GB' de olduğu gözlenmiştir. Yapay deprem ivme kaydı uygulanması halinde ise kiriş eleman hasarı görülmeyip sadece 2 adet perde elemanda BH meydana gelmiştir.

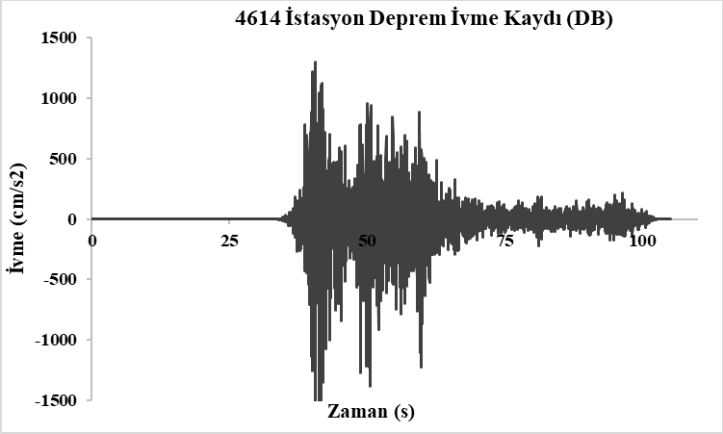

Şekil 8. Gerçek deprem ivme kaydı (DB)

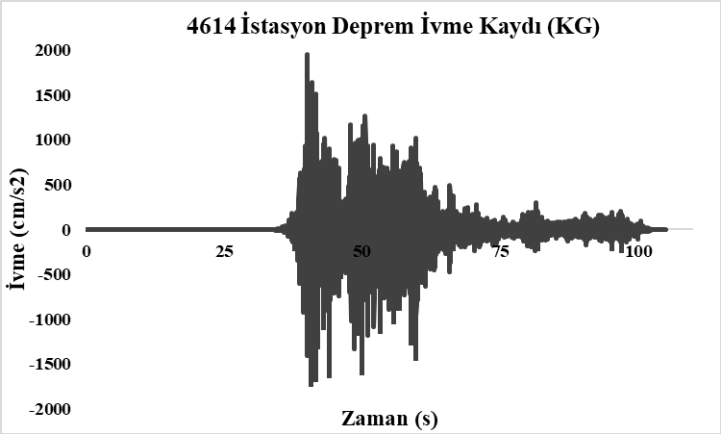

Şekil 9. Gerçek deprem ivme kaydı (KG)

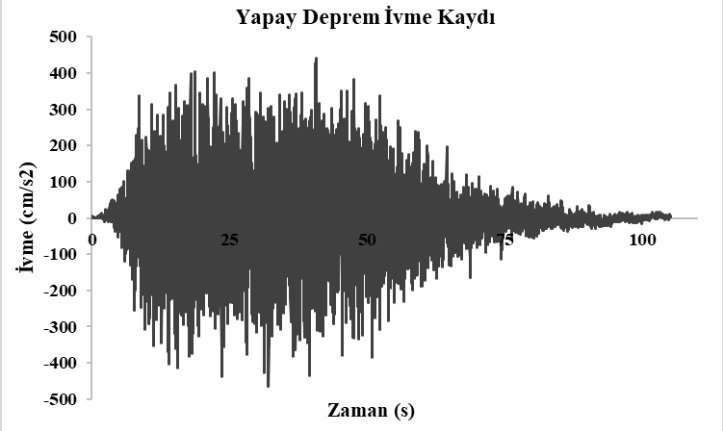

Şekil 10. Yapay deprem ivme kaydı

a) b)

Şekil 11. 24 katlı binada a) yapay b) gerçek deprem ivme kaydı uygulandığında oluşan hasarlar

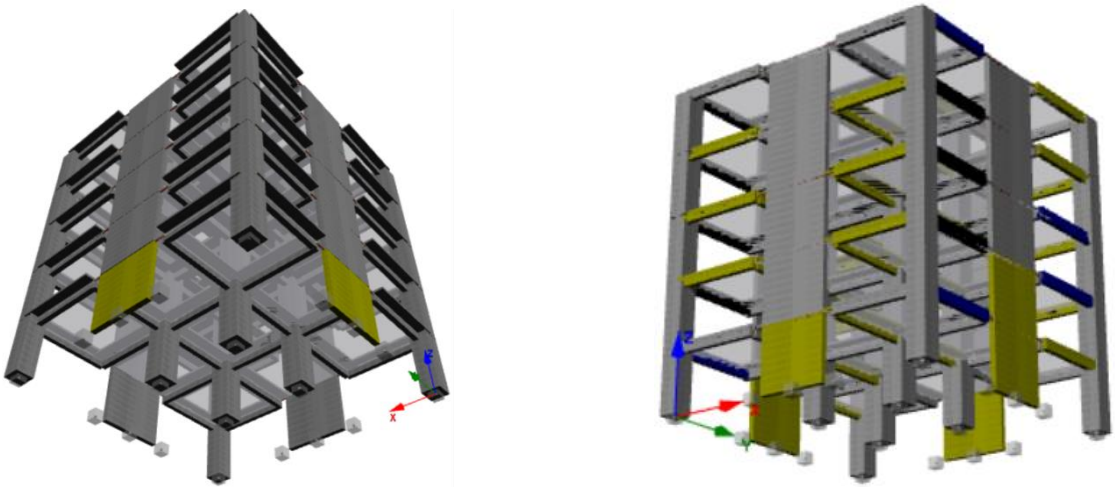

a) b)

Şekil 12. 5 katlı binada a) yapay b) gerçek deprem ivme kaydı uygulandığında oluşan hasarlar

4. TARTIŞMA VE SONUÇLAR

Bu çalışmanın amacı, 6 Şubat 2023' te Türkiye-Kahramanmaraş' ta meydana gelen Pazarcık depreminin gerçek deprem ivme kaydı ve Türkiye Bina Deprem Yönetmeliği 2018' de belirtilen tasarım ivme spektrumu ile uyumlu yapay deprem ivme kaydı kullanıldığında 24 ve 5 katlı betonarme binaların doğrusal olmayan davranışlarına olan etkilerini incelemektir. Gerçek deprem ivme kaydı 4614 istasyonunda kaydedilen ivme verileri olup yapay deprem ivme kaydı ise ZD zemin sınıfında Deprem Yer Hareketi Düzeyi-2 için üretilmiştir. Doğrusal olmayan davranış kuvvete dayalı fiber eleman yöntemi ile hesaba katılmıştır. Sismik analizler için HHT-α integrasyon metodu kullanılmış olup integrasyon zaman adımı 0.01 s seçilmiştir.

Yapay deprem ivme kaydı altında 24 katlı betonarme binanın doğrusal olmayan analizleri sonucunda, BH bölgesine geçen perde ve kiriş eleman oranları sırasıyla %4.2 ve %26.0 olarak elde edilmiştir. Gerçek deprem ivme kaydı uygulandığında ise perde ve kiriş elemanların sırasıyla %1.0 ve %20.8' inin BH bölgesine geçtiği görülmüştür. Her iki ivme kaydının kullanılması durumunda kolon elemanlarda hasarlar görülmemiştir. Böylece, gerçek deprem ivme kaydı

kullanılması durumunda yapay deprem ivme kaydı kullanılması durumuna göre daha az sayıda perde ve kiriş eleman hasarlarının görüldüğü belirlenmiştir. Ayrıca aynı plana sahip 5 katlı betonarme bina için yapılan çözümler sonucunda; gerçek deprem kaydı uygulandığında perde ve kiriş elemanların sırasıyla %25.0' i ve %37.0' si BH bölgesine geçmiştir. İlave olarak, kirişlerin %7.0' si İH bölgesine ve %7.0' si GB' ye geçmiştir. Yapay deprem ivme kaydı kullanılması durumunda ise kirişlerde hasar meydana gelmezken perdelerde %10.0 BH bölgesine geçen elemanlar görülmüştür. 5 katlı bina için her iki yükleme durumunda kolonlarda herhangi bir hasar oluşmamıştır. Böylece, gerçek deprem ivme kaydı kullanılması durumu yapay deprem ivme kaydı kullanılması durumuna göre daha fazla sayıda perde ve kiriş elemanın hasar görmesine neden olmuştur. Her iki binanın hasar durumları karşılaştırıldığında deprem yüklemesinden faklı etkilendikleri görülmüştür. Bu durumda, 5 katlı binanın periyodunun 25 katlı binanın periyoduna göre daha kısa olmasından dolayı 5 katlı binada ivme etkisinin daha fazla görüldüğü sonucuna ulaşılmıştır.

Çıkar Çatışması
Yazarların beyan edecekleri herhangi bir çıkar çatışması bulunmamaktadır.

Finansal Destek
Yazarlar bu çalışmanın herhangi bir finansal destek almadığını beyan etmişlerdir.

KAYNAKLAR

ACI 318, (1995). Building code requirements for structural concrete (ACI 318-95) and commentary (ACI318R-95), American Concrete Institute Committee 318, Farmington Hills, MI, USA.

AFAD, (2023). 06 Şubat 2023 Pazarcık-Elbistan (Kahramanmaraş) Mw: 7.7 – Mw: 7.6 Depremleri Raporu Ankara:AFAD Deprem dairesi başkanlığı.

AFAD-TADAS, (2023). https://tadas.afad.gov.tr/map (erişim 23 Temmuz 2023).

Akgül, M., Etli, S. (2023). 06 Şubat 2023 Kahramanmaraş (Pazarcık, Elbistan) depremleri sonrası betonarme binalarda gözlenen hasar durumları. International conference on scientific and innovative studies, 1(1), 309–318. https://doi.org/10.59287/icsis.618.

Aksoylu, T. (2020). 40 Katlı Asimetrik Betonarme Bir Binanın Deprem Performansının Zaman Tanım Alanında Doğrusal Olmayan Hesap Yöntemi ile Belirlenmesi, Yüksek Lisans Tezi, İstanbul Teknik Üniversitesi, Fen Bilimleri Enstitüsü.

Anadolu Ajansı, (2023). Türkiye ve Çevresi 123 Yılda 6 ve Üzeri Büyüklüğündeki 231 Depremle Sarsıldı. https://www.aa.com.tr/tr/asrin-felaketi/turkiye-ve-cevresi-123-yilda-6-ve-uzeri-buyuklugundeki-231-depremle-sarsildi/2836124 (erişim 20 Temmuz 2023).

Atabey, E., (2000). Deprem. https://www.mta.gov.tr/v3.0/sayfalar/bilgi-merkezi/deprem/pdf/deprem.pdf (erişim 20 Temmuz 2023)

Avşar, Ö., Bozer, A., Tunaboyu, O., Sülev, E., Demirtaş, Y. (2023). Mw 7.7-7.6 Şubat 2023 Kahramanmaraş Depremlerinde 2000 Sonrası Yapılmış Betonarme Binalar ile Bölgedeki Karayolu Köprülerinin Sismik Performansı: Hatay Saha Gözlemleri Teknik Raporu Hatay: ESTÜ.

Filippou, F. C., Popov, E. P., & Bertero, V. V. (1983). Modeling of R/C joints under cyclic excitations. Journal of Structural Engineering, 109(11), 2666-2684.

İTÜ. (2023). 6 Şubat 2023 04.17 Mw 7.8 Kahramanmaraş (Pazarcık, Türkoğlu), Hatay (Kırıkhan) ve 13.24 Mw 7.7 Kahramanmaraş (Elbistan/Nurhak-Çardak) Depremleri Nihai Rapor

Karaton, M., Yılmaz, İ. (2022). Betonarme binaların fiber eleman yöntemiyle burulma davranışının incelenmesi. Dokuz Eylül Üniversitesi Fen ve Mühendislik Dergisi. 24(72), 773-785. https://doi.org/10.21205/deufmd.2022247208.

Mander, J. B., Priestly, M. J. N. ve Park, R. (1988). Theoretical Stress-Strain Model for Confined Concrete. Journal of the Structural Engineering, ASCE, 114(8).

Menegotto, M., & Pinto, P. E. (1973). Method of analysis for cyclically loaded R.C. plane frames including changes in geometry and non-elastic behaviour of elements under combined normal force and bending. In IABSE Symposium on Resistance and Ultimate Deformability of Structures Acted on by Well Defined Repeated Loads (pp. 15–22). Lisbon.

Perk, Ş., Özer, Ç. (2019). İvme-Ölçer İstasyonları Altındaki Zemin Özelliklerinin Deprem Kaydı Kullanılarak İncelenmesi: Hatay Örneği, Türkiye. Turkish Journal of Earthquake Research. 1(2), 167-179. https://doi.org/10.46464/tdad.652332.

Popovics, S. (1973). A numerical approach to the complete stress-strain curves for concrete. Cement and Conor. Res., 3(5), 583-599.

Seismosoft. (2022). SeismoArtif 2022–Çerçeveli yapıların statik ve dinamik doğrusal olmayan analizi için bir bilgisayar programı.

Seismosoft. (2022). SeismoStruct 2022–Çerçeveli yapıların statik ve dinamik doğrusal olmayan analizi için bir bilgisayar programı.

Taucer, F. F., Spacone, E., Filippou, F. C. (1991). A fiber beam-column element for seismic response analysis of reinforced concrete structures (Report No. UCB/EERC-91/17), Berkeley, USA: Earthquake Engineering Research Center College of Engineering.

TBDY (2018). Türkiye Bina Deprem Yönetmeliği, Afet ve Acil Durum Yönetimi Başkanlığı, Ankara.

TMMOB İMO. (2023). 6 Şubat 2023 Kahramanmaraş Pazarcık ve Elbistan depremleri ön değerlendirme raporu Erişim adresi: https://www.imo.org.tr/Eklenti/8175,imo-deprem-raporu-2pdf.pdf?0

USGS, (2023). https://www.usgs.gov/media/images/tectonic-map-turkey-region (erişim 20 Temmuz 2023).

Yılmaz, İ. (2022). Fiber Eleman Yöntemi Kullanılarak Betonarme Yapıların Doğrusal Olmayan Sismik Analizi ile Burulma Davranışının İncelenmesi, Yüksek Lisans Tezi, Fırat Üniversitesi, Fen Bilimleri Enstitüsü.

Yön, B. (2021). Identification of failure mechanisms in existing unreinforced masonry buildings in rural areas after April 4, 2019 earthquake in Turkey. Journal of building engineering. 43. https://doi.org/10.1016/j.jobe.2021.102586

Zeybek, K. F. (2022). Deprem Etkisi Altındaki Yüksek Binaların 2018 Türk Deprem Yönetmeliğine Göre İncelenmesi, Yüksek Lisans Tezi, Kütahya Dumlupınar Üniversitesi, Fen Bilimleri Enstitüsü.

Seismic Performance Evaluation of Different Structural Systems

Fidan Guzel*[1], Yunus Dere[2]

Abstract: Seismic performance of building structures are associated with the structural systems. The structural systems are the load-carrying elements transferring the vertical and lateral loads to the foundation systems in the buildings as well as delivering seismic energy dissipation. In this study, the three main structural systems and their main characteristics under earthquake events are briefly reviewed and explicitly demonstrated through response spectrum analyses. Mainly, the frame system, shear wall system and dual system (consisting of frames and shear walls) are explained. In addition, 8 storey building models with different structural systems are modelled and analysed through response spectrum analyses. The results of the analyses support the typical behaviours of the frame, shear wall and dual systems. That is, the building model having frame system experiences greater lateral displacement at the lower floor levels. On the contrary, the building model owning shear wall system displaces less at the lower levels and it displaces increasingly more towards the top storey level. When the dual system is adapted, shear walls and frames limit the lateral movement at the lower and higher storey levels, respectively. Therefore, designing building structures with the involvement of both shear walls and frames shows better capacity of controlling the lateral displacement. Therefore, the dual system is always recommended in the building design, in particular, when designing mid-rise and high-rise building structures.

Keywords: Earthquake load, design response spectra, lateral displacement, structural systems.

[1]**Address:** Igdir University, Faculty of Engineering, Igdir/Türkiye
[2]**Address:** Necmettin Erbakan University, Faculty of Engineering, Konya/Türkiye

***Corresponding author**: xyfidanozdemir@hotmail.com

1. INTRODUCTION

The rise of the immigrations from suburban areas to major cities leads to the increase of building densities that causes the limits in construction sites. In order to use these limited areas in big cities high-rise buildings are becoming increasingly popular. With the increase in the height of the structural buildings, the rigidity of the structures and the lateral forces (i.e. earthquake and wind loads) plays very crucial roles in their designs. This becomes particularly important in regions which are positioned close to the tectonic plates between which major earthquake events takes place. Turkey, United States, Italy, Iran and Japan are some of well-known places of remarkable earthquake event occurrences.

Turkey, in particular interest, sits on top of Anatolian and Eurasian plates neighbouring with the Arabian plates at the south-east sides. Because of the Arabian plate motion towards northwards, the Anatolian plate is forced to the westwards (Bulut et al., 2012; Yavasoglu et al., 2012). These movements have been created several earthquake events along the North Anatolian and East Anatolian Fault Zones, stretching within Turkey through the east-west and east-southwest directions with 1600km and 500 km in length, respectively (Figure 1). Some of the most memorable earthquake events occurred in these fault zones are; the 2011 Van earthquake with 7.1 magnitude, the 1999 Izmit earthquake with 7.6 magnitude, the 1992 Erzincan earthquake with 6.7 magnitude and the 1939 Erzincan earthquake with 7.8 magnitude. Due to these earthquakes, considerable number of masonry and reinforced concrete buildings are severely damaged or totally collapsed as they were build not in accord with the code in place or the code design rules were not comprehend enough. This clearly indicate that when a building can stand safely under static loads, it will not mean that its dynamic performance can be sufficient enough in terms of life safety and collapse matters. Hence, with these experiences of earthquakes and their effects, consideration of seismic performance design of buildings becomes extremely vital (Guzel and Guzel, 2022).

In order to deliver the load carrying and resistance to the gravitational and lateral forces, as well as dissipating the seismic forces different structural systems have been implemented. For low-rise and mid-rise buildings, a frame structural system, consisting of columns and beams, can sufficiently carry gravitational loads when designed in compliance with the seismic design codes (e.g., Turkish Building Earthquake Code, TBEC 2018, ASCE 7 and Eurocode 8, EC8). However, when lateral forces of wind and earthquake are involved, the columns may endure the second-order moments as a consequence of lateral displacements. This will become even apparent with the rise of the building height. Therefore, the shear walls

having higher flexural rigidity than the columns are suggested in order to limit the lateral displacements causing the second-order moments.

Frame, shear wall and Dual (frame + shear wall) structural systems have been implementing for many years. In addition, their design is being guided comprehensively in the seismic design codes. In this short work, general structural characteristics of these three systems are explained. Moreover, three buildings modelled in ETABS with frame, shear wall and dual systems are analysed using response spectrum analysis method. Subsequently, the results are discussed comparatively. Lastly, the outcomes from this study are presented.

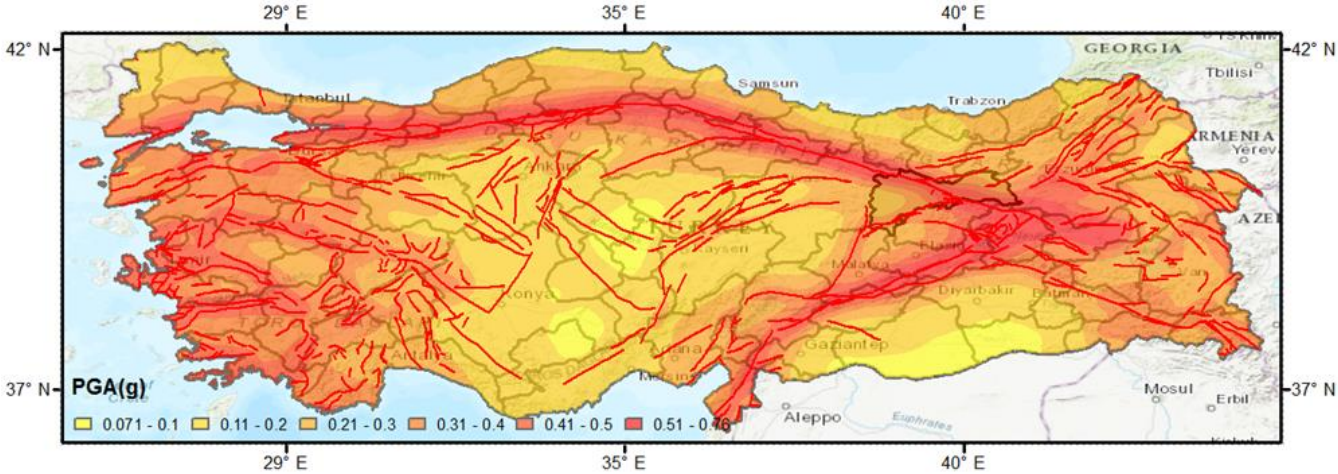

Figure 1. Seismic intensity level over the country of Turkey along with the fault lines.

2. FRAME SYSTEM

Frame system is formed with the joints of columns, beams and plates. In general, columns and beams are the main structural elements of the system but parts of the plates can also perform with the beam elements. It is mostly designed to withstand the vertical loads. The frame system can be used in buildings with height not greater than 25 m when it is designed in compliance with the seismic design codes and implemented rigorously (Kasap et al., 2015). In Turkey, this system are in popular use in low-rise buildings as it is more economic than the shear wall system.

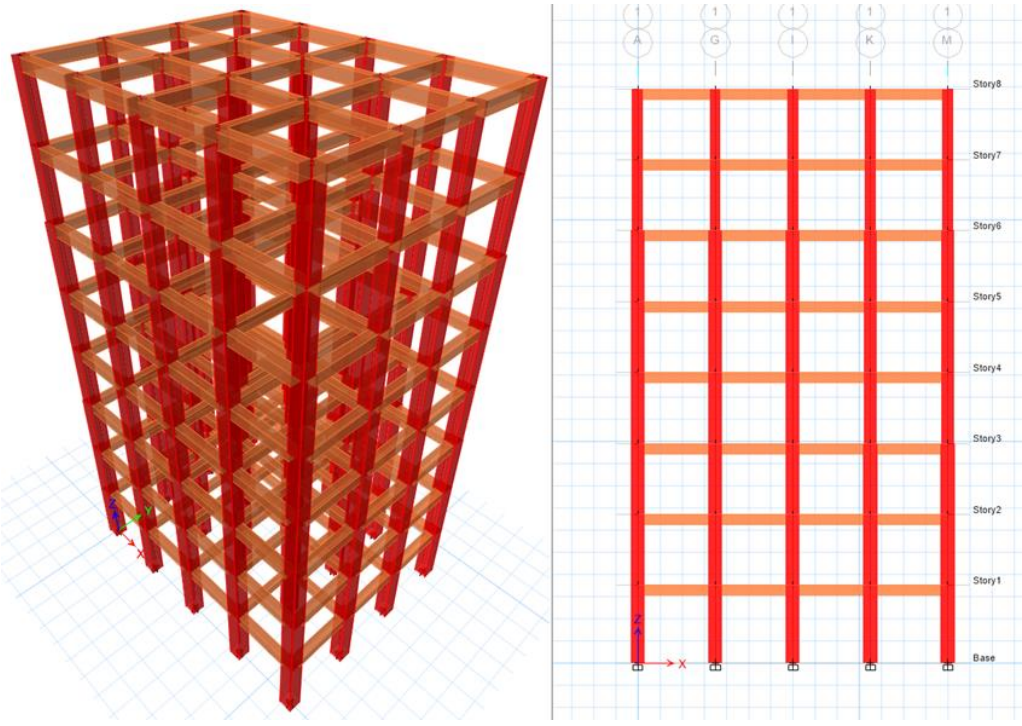

Figure 2. A sample building model consisting of a frame system used in this study.

Beams should be joint to columns at least in two directions to create a frame system. Moreover, this allows to obtain enough rigidity such that second-order moment and buckling effects are limited. In the frame systems, columns and beams are designed as load-carrying elements transferring the vertical and lateral loads to the foundations and they are joint as rigid, creating space system. When earthquake forces implemented in the one horizontal direction, the buckling effect in the other horizontal direction is thought to be minimal and negligible but may move laterally.

The columns sections can be altered with the increase of the building height but the eccentricity should be kept in minimum, (or should be avoided if possible) in order to prevent additional moments. The general three dimensional and side view of a frame system structural model used in this study can be seen in Figure 2. Physical dimensions and reinforcement rebars of the building model is given in Table 1.

Table 1. Physical properties of the frame system structural model used in this study.

System	Floor level	Column			
		size	reinf		Explanations
Frame system	1-6	60×60	22Φ20		Corner columns
		50×50	20Φ20		The remaining columns
	7-8	50×50	20Φ20		corner columns
		40×40	16Φ20		remaining columns
		Beam			
	Floor level	size	Top reinf	Bot reinf	Explanations
	1-6	30×50	4Φ20	4Φ20	All column to column connections
	7-8	30×40	4Φ20	4Φ20	All column to column connections

3. SHEAR WALL SYSTEM

The vertical load carrying elements having the height, at least six times of its width in plan are called shear wall (TBEC, 2018). One structural system can purely be formed by the shear walls or designed with the frames. The shear walls can able to carry and transfer the loads coming from plates and beams to the foundations, they can also resist the lateral loads of wind and earthquakes. Additionally, due to their higher level of rigidity, they limits the lateral displacements.

In general, the shear wall systems are more capable of limiting the lateral displacements and keeping the damage level at low level than the frame systems. Under earthquake excitations, in order to retain the buildings in function (after the event) and avoid the damage to the non-structural elements (which is essential in life-line buildings like, hospital, nuclear power plant, school, etc.) seismic-code complaint shear walls should be involved (Gul, 2006). Although the shear wall system cannot exhibit as such high level of ductility as the frame system, the system can still be able to show satisfactory ductility when it is designed with detailed modern seismic code designs (Taranath, 2009).

In Figure 3, the shear wall system 8 storey building model used in this study is demonstrated. While the two U-shape shear walls are modelled around the centre of the model, L-shape shear walls are positioned at the four corners. Two additional shear walls in the x direction and one additional shear wall in the y direction with 2 m length are designed. The thickness of all the aforementioned shear walls is assigned as 20 cm.

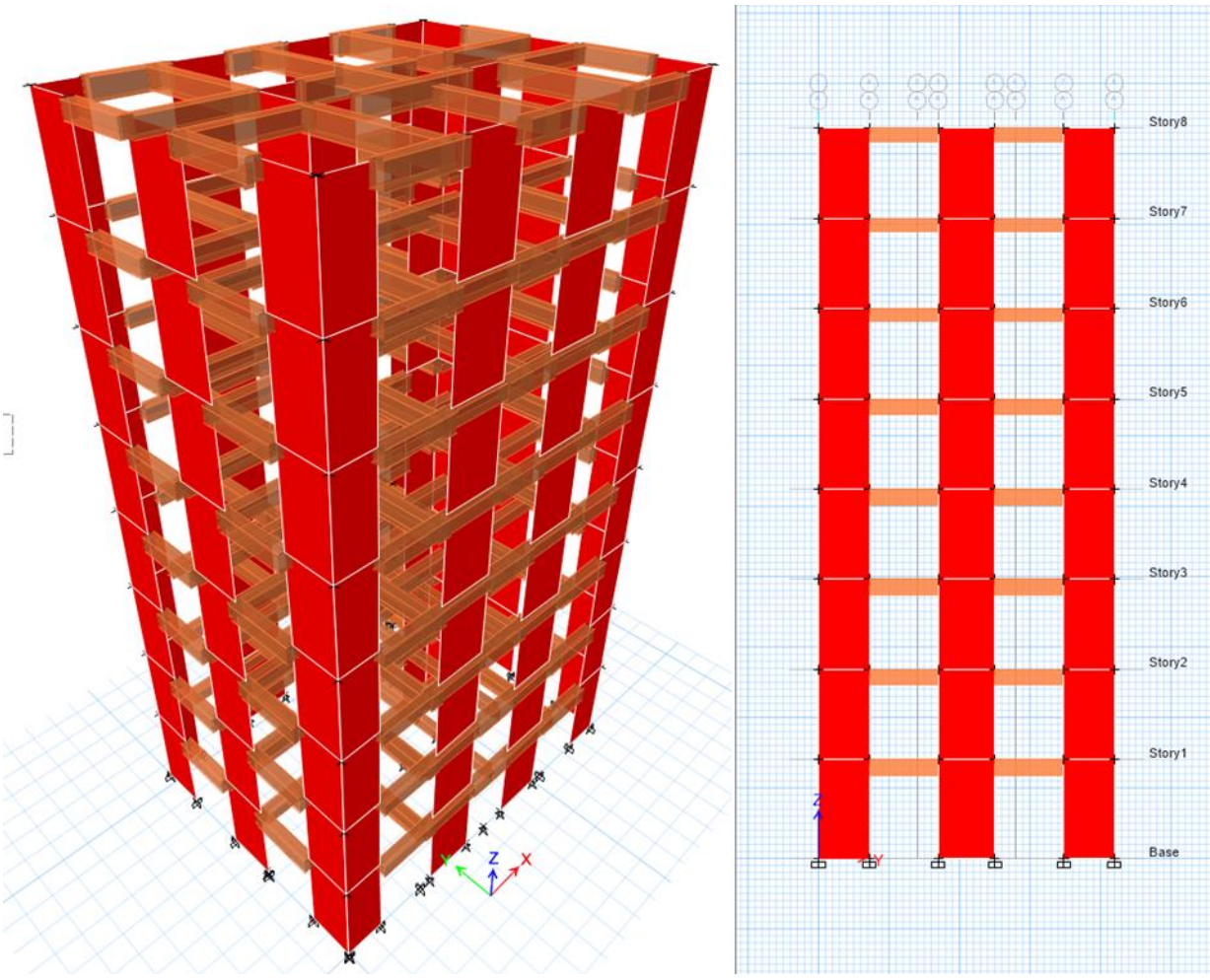

Figure 3. A sample building model consisting of a shear wall system used in this study

4. DUAL SYSTEM (FRAME + SHEAR WALL)

Dual systems are designed with the involvements of shear wall and frames. In multi-storey buildings, in order to decrease the relative floor deformations and limit the second-order moments, it is critical that the shear walls take major parts of the lateral forces (TBEC, 2018). In Turkey, frame structural systems are most widely preferred. However, contribution of the shear walls to the overall rigidity and resistance as well as to the relative movement necessitate the use of such structural elements, in particular in sites having high level of seismicity (Kaya and Özbay, 2019).

As the behaviours of frame and shear wall are different under lateral forces, the shear walls act like bending resisting beam, the frames behave as though shear beams. When both systems are adapted in one single building design, there is an interaction taking place between bending and shear resistance behaviours. The shear walls experience the maximum displacement at the top floor of the building, while this occurs at the lower floors. Hence, in dual systems, the shear walls take the most of the lateral forces at the lower floors, while the frames limits the displacements at the higher floors (Aka et al., 2001). For low rise buildings, the frame systems are more economic and more ductile than the shear wall systems (Doğangün, 2016). However, it should always be kept in mind that shear wall systems have greater level of seismic energy dissipation than the frame systems.

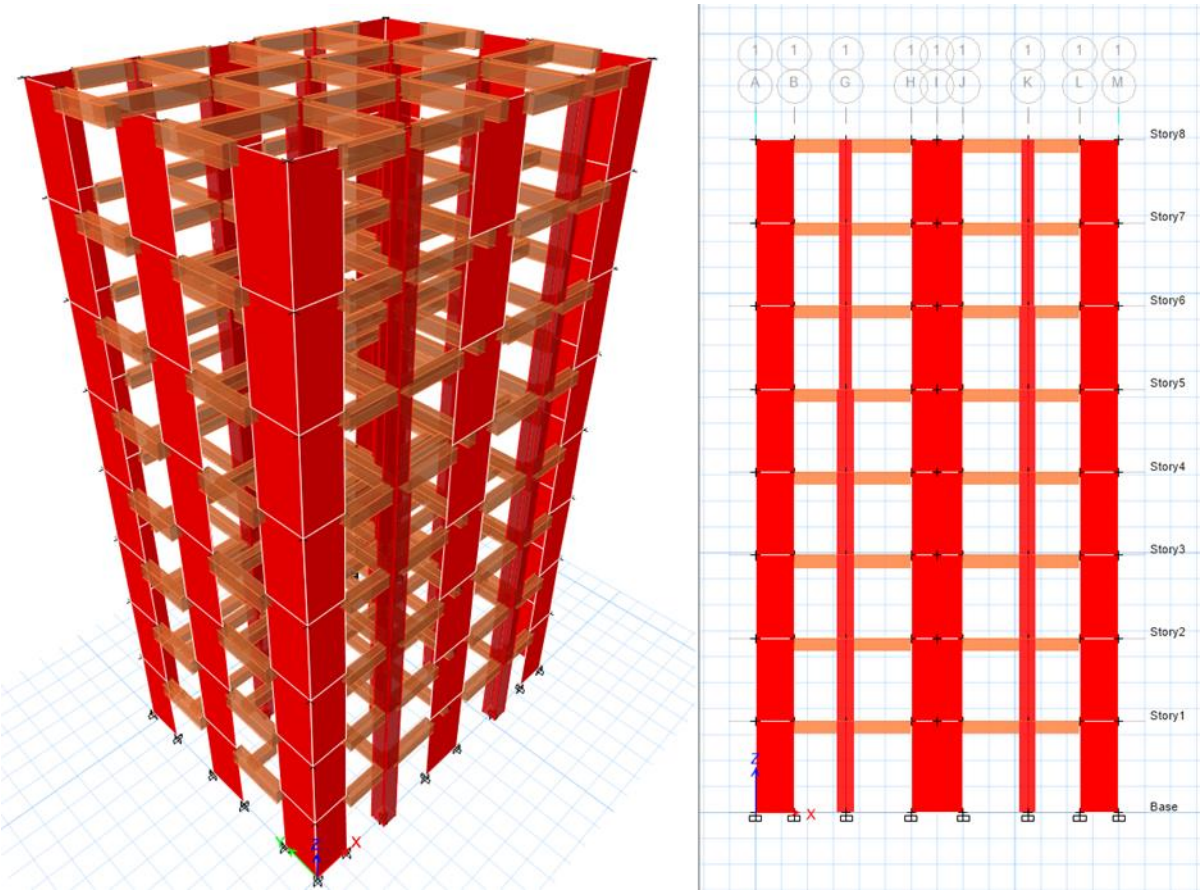

Figure 4. A sample building model consisting of a dual system (frame + shear wall) used in this study.

Table 2. Physical properties of the dual system structural model used in this study.

System	Floor level	Column		
		size	reinf	Explanations
Dual system	1-5	60×60	22Φ20	Columns connected to shear walls
		50×50	20Φ20	The remaining columns

	6-8	50×50	20Φ20		Outer columns
		40×40	16Φ20		Inner columns
		Beam			
	Floor level	**size**	**Top reinf**	**Bot reinf**	**Explanations**
	1-8	40×60	4Φ20	4Φ20	Column to shear wall and shear wall to shear wall connections
	1-8	30×50	4Φ20	4Φ20	Column to column connections

5. DESCRIPTION OF THE BUILDING MODEL ANALYSES

Three-dimensional and side views of the frame, shear wall and dual system structural models are presented in previous sections (Figures 2, 3 and 4). Moreover, the physical properties of the models are given in Tables 2 and 3. For all the three building models, 2 kN/m^2 live loads and 7.7 kN/m^2 dead loads are assigned. Compressive strength of concrete and yield strength of rebar is equivalent to 30 MPa and 420 MPa, respectively. The models are residential buildings, therefore the importance factor is taken as 1. All the structural elements (i.e. columns, beams, shear walls, slabs) are designed in accord with TBEC guidance. The shear walls and slabs thicknesses through all floors of the three building models are equal to 20 cm and 18 cm, respectively. The building models are modelled and analysed in ETABS platform (Computers and Structures, 2018). First three modes periods of the frame, shear wall and dual system building models are 0.696 s-0.67 s-0.58 s, 0.53 s-0.39 s-0.30 s and 0.58 s-0.56 s-0.36 s, respectively.

For the design response spectrum analyses, a site in Erzincan province is chosen. The latitude and longitude of the location is 39.72^0 and 39.46^0, respectively. The site has a reference peak ground acceleration (PGA_{rock}) of 0.549g (AFAD) with 475 years of return period. The site is designated with site class of D according to the TBEC soil classification scheme. The design response spectrum curve for this specific site is given in Figure 5.

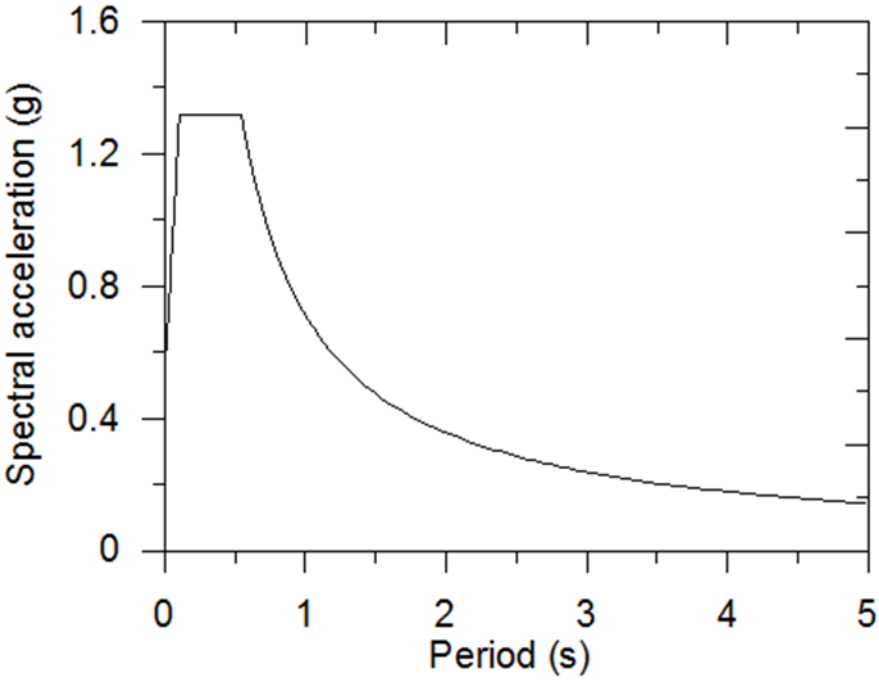

Figure 5. The design response spectrum curve for the specific site in Erzincan province.

6. RESULTS

The results from response spectrum analyses of the frame, shear wall and dual systems building models are interpreted, firstly, in terms of displacement and normalized displacement by the building height. Later, the lateral forces are compared for these three different structural models.

The displacements over the building height represented in Figure 6a demonstrates that the frame system building model is experienced the greatest level of displacements at all storey levels. The model displaces about 2.75 mm at the first floor, while this value equals to 26.30 mm at the top storey. However, the displacement increment is decreasing by the increase of storey level. In other words, there is a decreasing exponential displacement trend with the building height is observed. In contrast, the shear wall system structural model exhibits the least displacement values and follows almost linear increase with the increase of building height. The shear wall system building model displays lateral movement of 1.31 mm and 21. 85 mm at the first and top of the storey levels, accordingly. The building model with the dual system shows displacements that fits between the performances of the frame and shear wall system building models. This can also be observed from Figure 6b including the normalized displacement values over the building height.

These results directly reflects the differences in the performances of structural building models formed by discrete structural systems. Because, the frame system building model tends to deform more at the lower storey levels, while the shear wall system building model has relatively lower displacement at the lower storey levels but becoming greater with the height. Therefore, when the building model is designed by the dual system, part of the structural elements (the shear walls) limits the displacements at the lower storey levels. In addition, the other part of the structural elements (frames) controls the lateral movement of the building model at the higher storey levels, as can be depicted in Figures 6a-b.

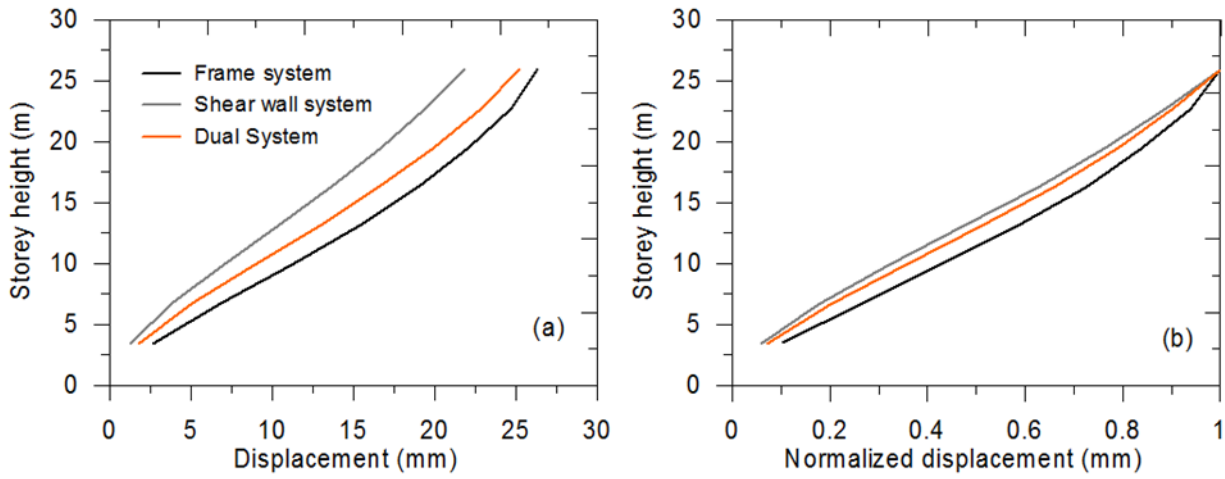

Figure 6. The results from response spectrum analyses of the building models in terms of; (a) storey displacements and (b) normalized storey displacements.

Shear forces from the response spectrum analyses are represented in Figure 7 for the building models with different structural models. From top storey to the third storey level, all three structural models illustrate almost same shear forces. Moreover, the overall shear forces acted on these building models (i.e. at the ground level) are similar, too. For instance, the shear force for the frame system building model is 2628 kN, when it is 2550 kN and 2624 kN for the shear wall and dual system buildding models, respectively.

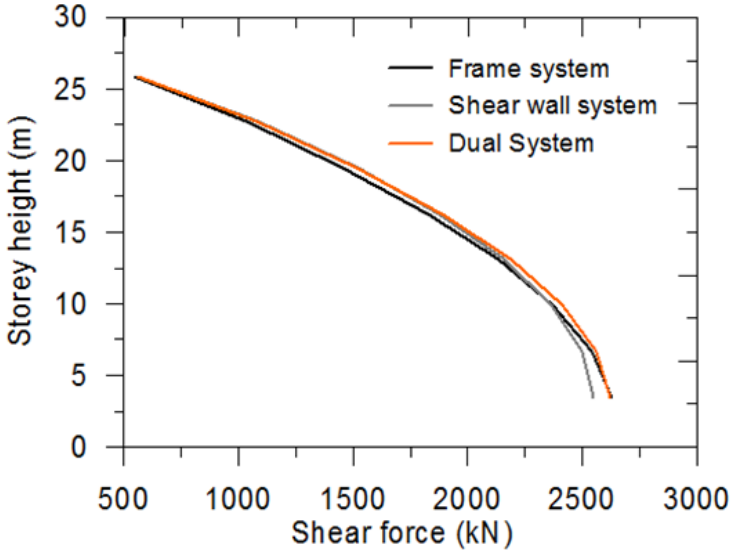

Figure 7. Shear forces from response spectrum analyses acted on building models.

7. CONCLUSIONS

This study focuses on the main seismic performance behaviour of three different structural systems. These are the frame, shear wall and dual (frame + shear wall) systems. For this, it includes explaining the main features of these three structural systems. It also covers the modelling and analyses of three 8 storey building models with varied structural models. A site from the Erzincan province is chosen. The PGA level of 0.549g with 475 years of return period is considered. The major highlights of the work are:

- The frame system building model tends to deform laterally more than the other two system building models at the lower storey levels.
- However, the lateral movement of the shear wall system building model increasing with the increase of the building height.
- The dual system building model involves the characteristics of both frame and shear wall systems, hence able to control the lateral movement of the building model over the building height.

Ethics Committee Approval
N/A

Author Contributions / Yazar Katkıları
Conceptualization: F.G.; Investigation: F.G.; Material and Methodology: F.G., Y.D.; Supervision: Y.D.; Visualization: F.G.; Writing-Original Draft: F.G.; Writing-review & Editing: Y.D.; Other: All authors have read and agreed to the published version of manuscript.

Conflict of Interest
The authors have no conflicts of interest to declare.

Funding
The authors declared that this study has received no financial support.

REFERENCES

Aka, İ., Keskinel, F., Çılı, F., & Çelik, O.C., 2001. Betonarme. İstanbul: Birsen Yayınevi.

American Society of Civil Engineers, 2017, June. Minimum design loads and associated criteria for buildings and other structures. American Society of Civil Engineers.

Bulut, F., Bohnhoff, M., Eken, T., Janssen, C., Kılıç, T. and Dresen, G., 2012. The East Anatolian Fault Zone: Seismotectonic setting and spatiotemporal characteristics of seismicity based on precise earthquake locations. Journal of Geophysical Research: Solid Earth, 117(B7). http://doi.org/10.1029/2011JB008966.

CEN (2005). Eurocode 8: Design of structures for earthquake resistance–Part 1: General rules, seismic actions and rules for buildings. CEN Brussels.

Doğangün, A. (2016). Betonarme Yapıların Hesap ve Tasarımı, İstanbul, Birsen Yayınevi.

Kaya G., ÖZBAY, A.E.Ö. (2019). Perde Ve Çerçeveli Betonarme Yapılarda Perde Konumunun Planda Düzenlenmesi Ve Yapısal Davranışa Etkisi. Mühendislik Bilimleri ve Tasarım Dergisi. 7(1), 7-17. https://doi.org/10.21923/jesd.429880.

Gül, B.S. (2006). Perde-çerçeve Sistemlerin Dinamik Analizi. Doctoral dissertation, Fen Bilimleri Enstitüsü, Istanbul Teknik Universitesi.

Guzel, Y., Guzel, F. 2022. Influence Of Input Motion Scaling Methods On Decoupled SSI Dynamıc Analysis. Eskişehir Osmangazi Üniversitesi Mühendislik ve Mimarlık Fakültesi Dergisi. 30(1), 130-140. https://doi.org/10.31796/ogummf.1004457.

Disaster and Emergency Management Presidency, AFAD (2013-present) AFAD Deprem katalogu; Ministry of Interior Ankara, https://deprem.afad.gov.tr/ddakatalogu (accesses 23 May 2023).

Kasap, H., Necati, M.E.R.T., Sevim, E., Şeber, B. (2015). Perdeli-Çerçeveli Taşıyıcı Sistemli Binalarda Taşıyıcı Sistem Seçiminin Yapı Davranışı Üzerindeki Etkisinin İncelenmesi. Academic Platform Journal of Engineering and Science. 3(1), 48-55. http://doi.org/10.5505/apjes.2015.68442.

ÖZSOY, A.E., ÖZGEN, K. (2005). Perdelerdeki Boşlukların Yatay Ötelenmeye Etkisi. Deprem Sempozyumu. Kocaeli, Mart.

Taranath, B.S. (2009). Reinforced concrete design of tall buildings. CRC press.

Turkish Building Earthquake Code (2018). Türkiye Bina Deprem Yonetmeligi, Deprem Etkisi Altında Binaların Tasarımı icin Esaslar. Ankara.

Yavaşoğlu, H., Tarı, E., Tüysüz, O., Çakır, Z., Ergintav, S. (2011). Determining and modeling tectonic movements along the central part of the North Anatolian Fault (Turkey) using geodetic measurements. Journal of Geodynamics. 51(5), 339-343. http://doi.org/10.1016/j.jog.2010.07.003.

Computers & structures (2018). ETABS: Extended three-dimensional analysis of building systems. Version 9.0, Berkeley.

Studies of motion and the creation of movement-inspired architectural spatial forms

Ferenc Sebestény*[1]

Abstract: The intense connection of experience with creative application has been an effective way to improve architectural attitude and abstract vision. In the teaching methodology of the author of this paper, motion is the main means of learning and experiencing space one moment, and an inspiration for space creation in the next. The use of movement-based spatial experiments in architectural education is intended to develop the individual experience-based sense of interior space, which in turn forms the base for abstraction in the design process. The examination, recording and geometric analysis of different types, complexity and dynamics of motion may effectively lead to the inception of new types of free and abstract forms. A spatial form can be a result not only of following functional needs, structural and technological logic, or traditional geometry, but also of other influences and creative realizations, for instance, through the abstract conversion of the motion's own internal mechanisms. Once one realizes that the original (inspirational) material's own compositional properties (its proportions, rhythm, dynamics, internal energy) can be "deciphered" through perception and analysis, and "translated" into our architectural toolkit, the goal - the conception of movement-inspired free architectural forms at the end of the analytical and creative process - has already been achieved.

Keywords: space and motion, spatial perception, modelling, spatial experimenting, architecture education

[1]**Address:** Budapest University of Technology and Economics, Faculty of Architecture, Hungary

***Corresponding author**: sebesteny.ferenc@epk.bme.hu

1. INTRODUCTION

The first description of space through movement and the observation of the world in motion is often linked to the Futurist trends of the 20th century. Umberto Boccioni in his 1912 book 'Futurist Painting Sculpture (Plastic Dynamism)' argued that Futurists launched an attack on the notion of stillness and static formality in favour of movement and dynamism, and they introduced a new interpretation of space, juxtaposing interior and exterior. Rudolf von Laban, the renowned dance theorist who, among others, studied and described the spatial relations of movement and developed the concept of 'Motion Space' stated: "Movement is, so to speak, living architecture - living in the sense of changing emplacements as well as changing cohesion. This architecture is created by human movements and is made up of pathways tracing shapes in space, and these we may call 'trace-forms'". The examination of space in the context of movement - alongside the extensive progress in natural sciences (primarily nuclear physics), philosophy and technology - launched a new approach from the beginning of the 20th century, as a result of which our understanding of architectural space also fundamentally transformed.

2. MATERIAL AND METHOD

In 2001, the author of this paper introduced the theoretical and experimental study of the relations between Space and Motion in the frame of an eponymous course at the Department of Graphics, Form & Design at the Faculty of Architecture of the Budapest University of Technology and Economics. The course, which has been in offered for over two decades, focuses on a new topic every semester, thus securing its relevancy, strengthening the experimental approach and the diverse use of tools and technologies. Traditional graphics is used as well as photography, video and digital tools, traditional models and virtual spaces generated with state-of-the-art software. Stepping beyond the conventional academic framework, students of the course frequently work together with creative workshops of visual and fine arts, theaters, and progressive contemporary artists.

3. RESULTS

The methodology developed and introduced in university architecture education - the theoretical and practical examination of the interrelations between space and movement, as well as the application of the findings through

creative exercises – has been found to improve the skills of architecture students in space and structural formation and to make certain spatial theoretical considerations more understandable and interactive. It also helps creative decision-making considerations become more conscious in the complex process of architectural design.

4. DISCUSSION AND CONCLUSIONS

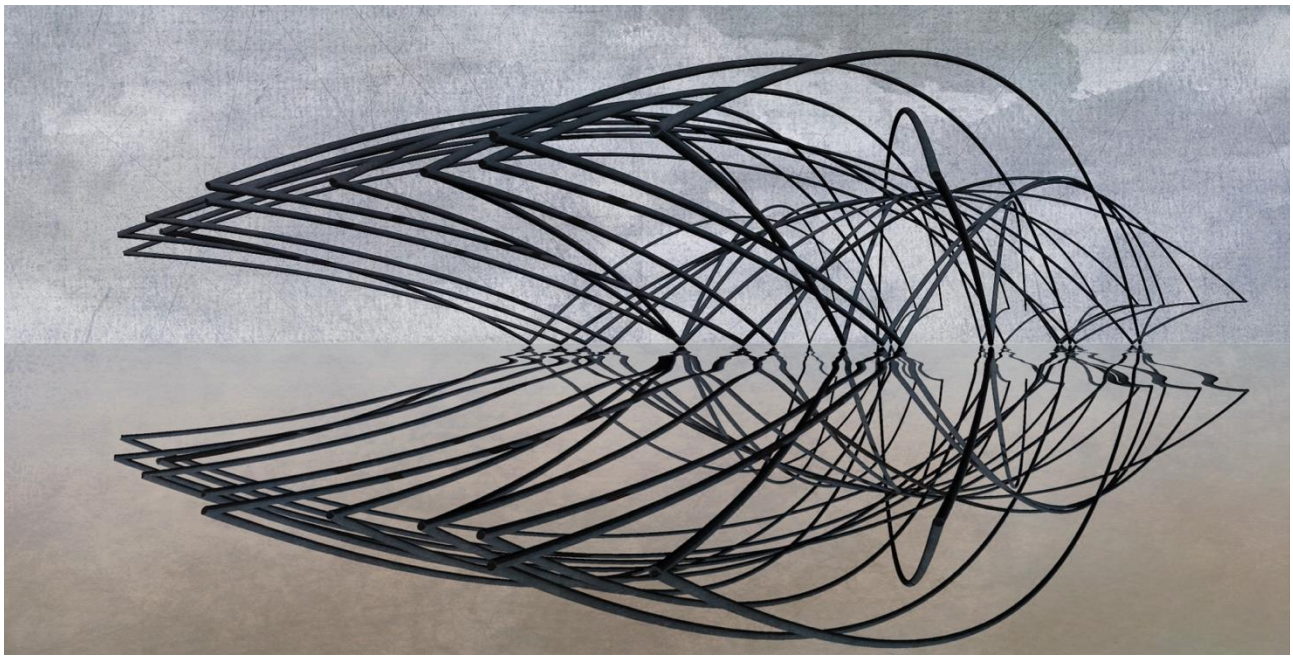

Figure 1. Zoltán Csakurda and Lidia Kékesi, Dynamic and kinetic space (Space and Motion, university course)

Movement can be captured in space as long as its existence can be perceived with our senses. (Moholy-Nagy, L., 1947). The first type of experiments presented in this paper are attempts to capture and represent the temporal process of movement. The aim was to find graphic techniques that provide the opportunity to capture the dynamics abstracted from the forms, and to display them spatially according to some known or arbitrary system of rules. Depending on the level of abstraction, students used a variety of approaches, from simplified human figures depicted in motion to abstract, disembodied momentum-arcs. Therefore, among the presented works one finds dynamic "gesture drawings" that trace and capture the curve and speed of rotations and limb movements, but also linear, sheet music-like representations of movement beats which focus on the rhythm, emphasis, and temporality of the motion.
It is interesting to observe the parallel between the centuries-old methods of dance recording, the modern kinetographic notation systems of the 20th century, and the students' own experiments (Fügedi, J. (1993). This similarity in form and thought is quite natural. The forms of visual representation of the essential parameters of movement inherently identify with visual elements learned from perceived stimuli. These motion images, energies, invisible force lines occupied the attention of artists associated with the Futurist trend in the beginning of the 20th century, as well. In their 1922 manifesto on "The Dynamic-Constructive System of Forces", László Moholy-Nagy and Alfréd Kemény contemplated: „Carrying further the unit of construction, a dynamic constructive system of force is attained whereby man, heretofore merely receptive in his observation of works of art, experiences a heightening of his own faculties, and becomes himself an active partner to the forces unfolding themselves. The first projects looking toward the dynamic-constructive system of forces can be only experimental demonstration devices for the testing of connections between man, material, forces, and space. Next comes the utilization of the experimental results for the creation of freely moving (free from mechanical and technical movement) works of art" (Moholy-Nagy, L., 1947). There were various other experiments in the era in attempt to visualize motion.

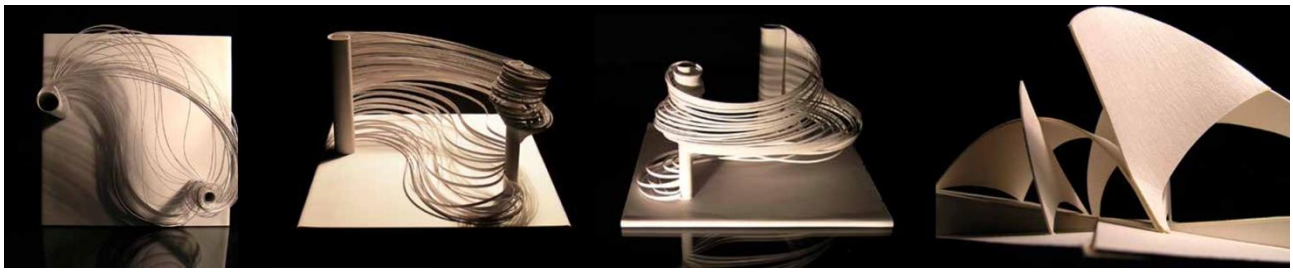

Figure 2. Zoltán Maczelka, Capoeira (Space and Motion, university course)

Archipenko made mobile 'sculpto-peintures' (sculpture-paintings), Brancusi placed his sculptures on rotating stands to bring the parameter of time into the creation, the sculptures of Joost Schmidt represent the space-time perspective of distortion, but also Giacometti and Alexander Calder harnessed in their kinetic sculptures the potential in reflecting the experience of motion. Thomas Eakins (who in 1884 created the famous stroboscopic action photo 'Man Pole Vaulting'), and later Harold Edgerton, Herbert Matter and Moholy-Nagy all implemented photographic methods which provided the opportunity to display the time factor (and therefore movement) in various - but essentially analogous - ways.
„These interpretations of vision in motion denote not only an artistic achievement but also an important practical step in visual perception as well as in the skill of rendering. (...) Photomontage, superimpositions, diagrams, explosion, phantom, x-ray, cut-away techniques, stroboscopic motion projections and other combinations may enlarge the scope [of this new method of visualization] tremendously. (...) These speed photographs are of more recent date, but they are astonishingly similar to futuristic paintings. In fact, they are their exact repetitions: e.g., (…) 'Nude Descending the Stairway', 1912, by Marcel Duchamp. They all show the same juxtaposition of frozen movement."

Figure 3. Lilla Szücs, Kinetic space (Space and Motion, university course)

Long exposure photos are able to present a movement in its entirety, but due to the continuous exposure to light (as opposed to stroboscopic shots), the moving parts of the body (or object) become blurred. Most of all, these images resemble billowing smoke, and their character primarily enables a 'sculptural' capture of the curvature and space of the movement. In the motion capture experiments - in addition to these traditional photographic techniques - students can take the advantage of the possibilities offered by video and computer technology. Images taken with high-speed or very small endoscopic cameras can reveal never-before-seen details and angles of certain movements. In another group of experiments students considered movement as a source of inspiration, recorded its form, dynamics, and interpreted and visualized - in an abstract way (in drawing, model, film, etc.) - the space the movement described (cut out) in time. This type of exercise has two important purposes. Through free associations and creative thinking, the abstract reinterpretation of the connections uncovers the forms, tools, and techniques with which these internal compositional principles and energies can be reinterpreted in architecture. In this recreation students seek to "invent" and develop their own tools and set of rules, which in turn will become one of the criteria and conditions for the authenticity of the creative process. Capturing motion is an exceptionally difficult task. There are various artworks known to have captured in a single moment the characteristic visual image, internal dynamics, rhythm, and tension of a movement. Here, time, the duration of a given sequence of movements, takes place in the mind of the creative artist, who compresses and condenses it, until finally - stretched into a single moment - it can be presented. Time is therefore merely virtually present, or more precisely, it is in a bound state, only to be released and run in the mind of the observer. However, when the continuous flow of a dance movement needs to be recorded (without the use of a camera), the presence and passage of real time creates extreme difficulties. The problem, primarily, is not that during the time it takes to draw - to outline the main gestures - the view changes, but that it is the change, time itself, we want to capture. The usual view, according to which one could capture the final result of the events created and interpreted internally, however, is very different

from this. An essentially difference, in which one realizes that in order to depict the movement in its temporal process, and not as an image recollected from the past, one has to create the way and form of expression for himself.

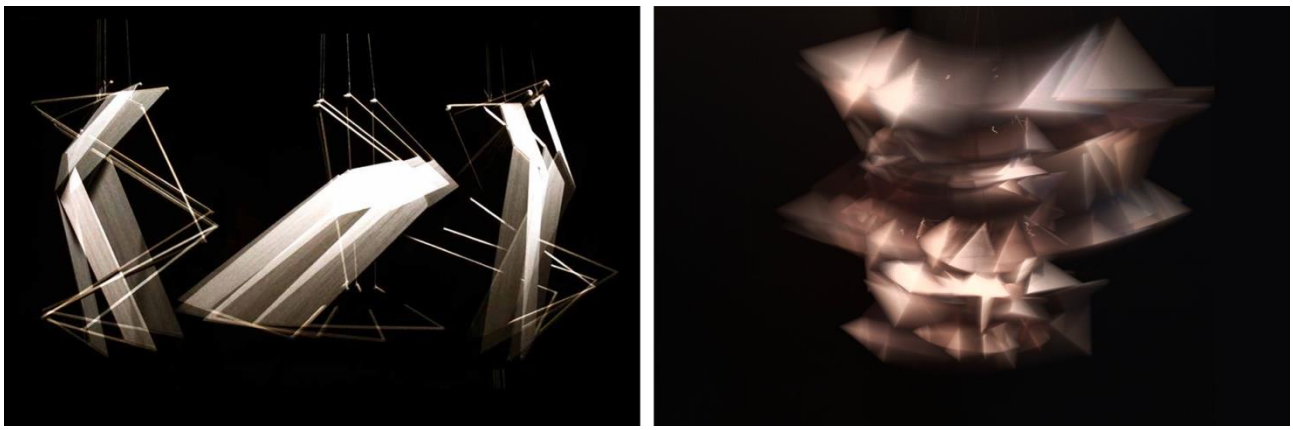

Figure 4. Anna Rátkai and Lidia Kékesi, Mobilion (Space and Motion, university course)

The spatial structure "Mobilion", designed specifically to move in space, is also meant to deepen the understanding of the relationship between motion and space, as it is supposed to exert its spatial and aesthetic effect during a pre-programmed movement. The design process thus begins with the vision of the future spatial movement, which is then verified and adjusted during various intermediate experiments, and it concludes with the construction of the structure. The task is complex, since the object and the envisioned movement mutually affect each other; the structure's centre of gravity, stability, and aerodynamic properties all influence its subsequent behaviour. In addition to the obvious forms of actions - like swinging, rotation, uniform rectilinear motion, or free fall - more complicated forms of movements or even complex motion sequences are also welcome. The task includes the creative invention and aesthetic shaping of these structures and their movement. The kinetic objects are then set in motion and their movement is recorded with photo and video cameras using special techniques. The final documentation of the project is a series of photos compiled in a poster.

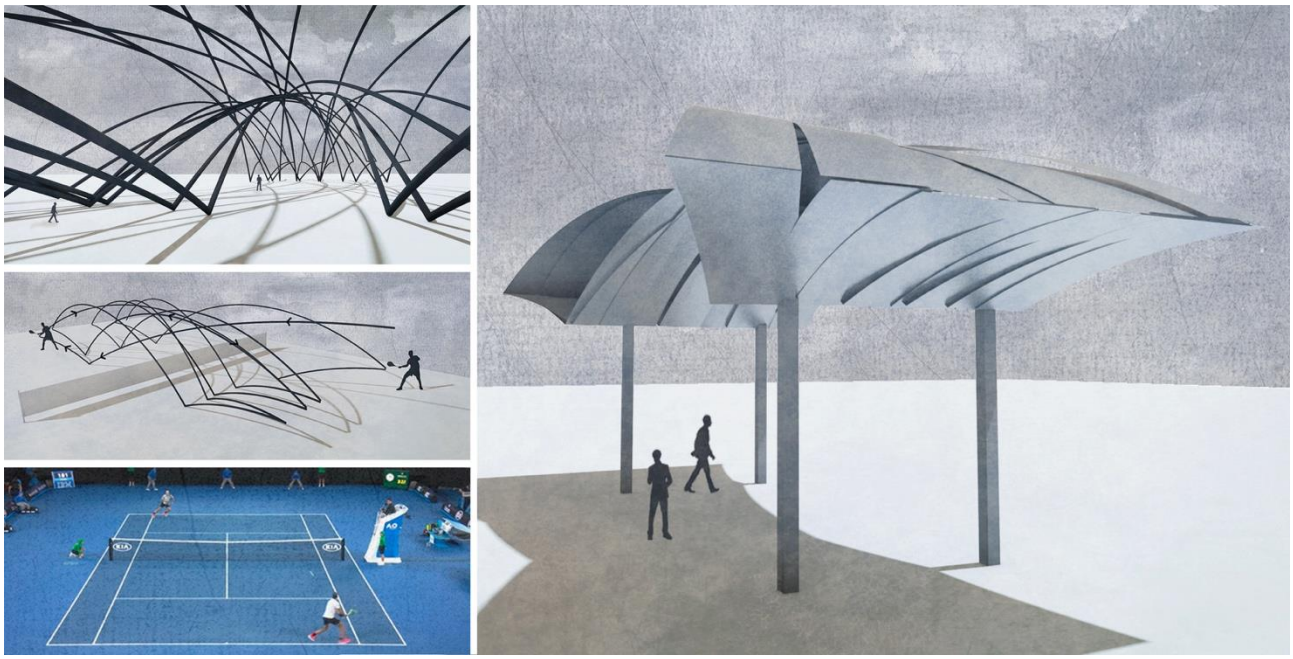

Figure 5. Zoltán Csakurda and Lidia Kékesi, Dynamic and kinetic space (Space and Motion, university course)

A special aspect of the relationship between space and time can be grasped in relation to movement-generated space. The tension between the contemporaneity of movement, its confinement to the moment, and the striving for eternity in architecture can be resolved in the common creative environment, in the forming space, which, due to the way it was created, carries both essences at the same time. Space constructed in this way looks for its balance on the sharp border between the "here and now" and timelessness and is able to articulate its independently valid philosophy.

Acknowledgements
Special thanks to the students at the Budapest University of Technology and Economics that took part in this research, namely Zoltán Csakurda, Lidia Kékesi, Zoltán Maczelka, Anna Rátkai, Lilla Szücs.

Ethics Committee Approval
N/A

Peer-review
Externally peer-reviewed.

Conflict of Interest
The authors have no conflicts of interest to declare.

Funding
The authors declared that this study has received no financial support.

REFERENCES

Boccioni, U. (1912). Pittura scultura futuriste, Milano, Edizioni Futuriste di „Poesia”

Moholy-Nagy L. (1947). Vision in Motion, Chicago, Paul Theobald Company

Fügedi J. (1993). Tá clejegyző rendszerek 3. Tá cművészet 18, 5-6, 47-49.

Evaluation of Critical Success Factors for Digital Education with Hesitant Fuzzy Linguistic MCDM Approach

Esin Mukul*[1], Gülçin Büyüközkan[1], Merve Güler[1]

Abstract: Digital education is an approach to learning that aims to optimize the use of digital technology, open-source material, individualized data, and connection. It strives to raise creative and inventive persons by ensuring that individuals have better living circumstances and possibilities within the context of life's sustainability. This educational approach helps the student to develop himself according to the changes in society; encourages students to develop their ability to apply new technologies. At this point, determining the factors for the success of digital education has critical importance in increasing the quality of education. In this context, the study aims to propose the Critical Success Factors (CSFs) for digital education and evaluate these factors with Hesitant Fuzzy Linguistic (HFL) method. Given the complexity and uncertainty of this multi-criteria decision-making (MCDM) situation, the HFL approach is used. This approach is used to provide experts more flexibility by employing comparative linguistic terms and to create an evaluation environment that is more similar to human thinking. In this study, the CSFs are identified with the literature review and experts' opinions. Then, the HFL Analytic Hierarchy Process (AHP) method is applied for the evaluation of CSFs of digital education. This method is practical, adaptive to varied fuzzy environments, versatile, dependable, and resilient. Finally, an application demonstrating the potential of the proposed approach is offered.

Keywords: AHP, critical success factors, digital education, hesitant fuzzy linguistic term sets, MCDM.

[1]**Address:** Galatasaray University, Faculty of Engineering and Technology, Industrial Engineering Department, Istanbul/Türkiye

***Corresponding author**: emukul@gsu.edu.tr

1. INTRODUCTION

Digital education is an approach to learning that aims to optimize the use of individualized data, digital technology, connection, and open-source material. It strives to raise creative and inventive persons by ensuring that individuals have better living circumstances and possibilities within the context of life's sustainability. This educational approach helps the student to develop himself according to the changes in society; encourages students to develop their ability to apply new technologies (Ibanez et al., 2023).

Fisk (2017) mentioned the existence of nine trends in the digital education concept. These trends are as follows:

- Learning may occur at any time and in any location.
- Students are more exposed to project-based learning.
- Learning is personalized for individual learners.
- Students become more involved in collaborative practices as their field experience increases, such as consulting projects and projects that adopt a collaborative approach.
- Students are exposed to applications that will reveal their abilities in interpreting the numbers they obtained by analyzing the data. Some basic skills that seem so important today (mathematical literacy, memorizing formulas or dates, etc.) are becoming irrelevant.
- Students have the opportunity to determine how they want to learn.
- Students are evaluated individually and traditional assessment platforms become inadequate.
- Students' ideas and changing needs should be taken into account in designing and updating the curriculum. There is a need for more customizable and adaptable curricula.
- With the teachers taking a guiding role for the students in this process, the students are freer in individual learning.

In light of these trends, the efficiency of digital education systems and the quality of their output are among the most important issues to be examined. Digital education, which has become important with the pandemic period and is

accessible, fast, flexible, egalitarian, low initial-operating cost, and customizable, should be considered as an alternative, supplement, or supporter of face-to-face education.

At this point, determining the factors for the success of digital education has critical importance in increasing the quality of education. In this context, this study aims to propose the Critical Success Factors (CSFs) for digital education and evaluate these factors with Hesitant Fuzzy Linguistic (HFL) Multi-Criteria Decision Making (MCDM) approach.

The structure of the evaluation of CSFs for digital education is multifaceted, multi-actor, multi-disciplinary, dynamic, comprehensive, and complicated. As a result, this evaluation problem is treated as an MCDM problem in this study (Hwang and Yoon, 1981). Considering the complex and uncertain nature of this MCDM problem, the HFL approach (Rodriguez et al., 2012) is employed. This approach is used to provide experts more flexibility by employing comparative linguistic terms and to create an evaluation environment that is more similar to human thinking. The CSFs in this study are determined using a literature review and expert views. Then, the HFL Analytic Hierarchy Process (AHP) method (Zhu and Xu, 2014) is applied for the evaluation of CSFs of digital education. This method is practical, applicable to many fuzzy situations, versatile, dependable, and resilient.

This proposed approach is applied for the digital education system in Turkey to show the effectiveness of the proposed approach. The contributions of this paper are proposing a new and conceptual evaluation model including CSFs for digital education, presenting an analytic method such as the HFL AHP method in this area, and providing an application for the evaluation of CSFs for digital education.

The following is how this paper is organized. The conceptual foundation of the subject is discussed briefly in the next section. The study's technical basis is then supplied. The proposed CSFs for digital education are shown in the fourth section, and the application is shown in the fifth section. Finally, the final part brings the paper to a conclusion.

2. CONCEPTUAL BACKGROUND

CSFs are those elements that are crucial to the performance of any organization, as defined by the Massachusetts Institute of Technology study team (Rockart, 1979). The term CSFs was coined in response to a question regarding why some organizations appear to be more successful than others.

CSFs are initially utilized in project management research. In general, it is frequently employed in a variety of situations such as organizational management, operational management, and supply chain management, among others. CSFs should be few and controllable (Freund, 1988). When the research is examined, it is seen that e-learning is examined separately from the perspectives of technology, pedagogical, organization, student, and instructor, depending on the fields of expertise of researchers. In this context, it is possible to say that there are not many studies that see e-learning projects and their stakeholders as a whole and evaluate the factors that are effective in the success of the project and that are related to each other.

There are research in the literature on success factors for digital education. A comprehensive literature review is carried out in this field. Table 1 lists the studies discovered as a consequence of the literature review.

Table 1. Studies on CSFs for digital education

Year	Author	Aim of the Study	Location
2023	Ibanez et al.	to identify key success factors for effective online teaching	Paraguay
2023	König et al.	to determine CSFs for digital education	-
2021	Kanojia et al.	to uncover the CSFs of knowledge transfer from universities to industry	India
2021	Moya & Camacho	to develop a taxonomy for categorizing the elements influencing mobile learning acceptance	Catalonia
2021	Milic & Simeunovic	to identify the e-learning CSFs with the students' perceptions	Bosnia and Herzegovina
2019	Blieck et al.	to validate the quality of online learning	-
2019	De Paepe et al.	to present Dutch L2 learning in adult education	Germany
2018	Barclay et al.	to investigate CSFs in online learning environments	Caribbean
2017	Fabito	to find out the CSFs of e-learning in universities	Philippines
2016	Alrasheedi et al.	to identify the factors affecting mobile learning	-

2015	Alrasheedi et al.	to analyze studies on CSFs for success of mobile learning	-
2013	Cortés & Barberà	to discover success criteria in online learning based on student perspective	Mexico
2011	Sharma et al.	to outline the CSFs for e-learning at HP University	India
2006	Papanikolaou & Mavromoustakos	to determine CSFs for mobile learning applications	-
2001	Volery	to determine CSFs for online education	Australia

It is possible to say that the studies in Table 1 belong to the last 20 years. Most of the studies are in the field of higher education. Studies have been applied in many different places such as Paraguay, Germany, Bosnia and Herzegovina, India, Catalonia, Mexico, Australia etc.

In this study, the CSFs of the digital education system in higher education will be determined and these factors will be evaluated. This evaluation will be supported by an analytical method and this gap in the literature will be filled.

3. TECHNICAL BACKGROUND

3.1. Hesitant fuzzy linguistic approach

Uncertain situations frequently present significant decision-making issues in the real world. Linguistic knowledge may be useful in managing ambiguity in this setting. Torra introduced hesitant fuzzy sets in 2010. Rodriguez et al. (2011) presented the Hesitant Fuzzy Linguistic Term Set (HFLTS). HFLTS is favored to address experts' hesitancy while expressing their ideas on the MCDM challenge. In HFLTS, experts may express themselves using language such as "at least," "between," and "at most," giving them versatility. As a result of using comparison linguistic terms in the HFLTS, a more human-like evaluation environment is created (Rodriguez et al., 2012).

The superior (H_{s+}) and inferior (H_{s-}) bounds are explained as (Torra, 2010; Rodriguez et al., 2011):

$$H_{s+} = max(s_i) = s_j \text{ , } si \in H_S \text{ et } s_i \leq s_j \forall_i \quad (1)$$

$$H_{s-} = min(s_i) = s_j \text{ , } s_i \in H_S \text{ et } s_i \leq s_j \forall_i \quad (2)$$

Liu and Rodriguez (2014) provide the envelope for HFLTS, $env(H_S)$, which is a linguistic interval with superior and inferior bounds:

$$env(H_S) = [H_s^-, H_s^+], H_s^- \leq H_s^+ \quad (3)$$

3.2. Hesitant fuzzy linguistic AHP method

The AHP model developed by Saaty (1990) is the most often utilized in the MCDM field. It is a strong and simple MCDM tool that prioritizes a variety of criteria. When there is ambiguity in the decision-making process, HFL AHP is frequently used. Multiple alternative values reflect a tentative judgment (Zhu and Xu, 2014). The AHP approach is widely used in MCDM literature due to its simple structure and ability to solve complex choice problems. The HFL AHP approach was used to calculate the criterion weights in this article. The HFL AHP stages are outlined next (Büyüközkan et al., 2018):

Step 1. The criteria are assessed using pairwise comparison matrices. The language expressions are then transformed to HFLTS. Table 2 depicts the linguistic scale employed in HFL AHP.

Step 2. The fuzzy envelope, which produces a trapezoidal fuzzy number, is created using the OWA operator (Liu and Rodriguez, 2014).

$A = \{a_1, a_2,..., a_n\}$ denotes a collection of components that will be aggregated. It is worth mentioning that it differs from the collection of alternatives. The OWA operator F is characterized as follows (Liu and Rodriguez, 2014):

$$F(a_1, a_2,..., a_n) = wb^T = \sum_{i=1}^{n} w_i b_i, \quad (4)$$

where $w = (w_1, w_2,..., w_n)^T$ signifies the weights vector, with $w_i \in [0, 1]$ and $\sum_{i=1}^{n} w_i = 1$ and b signify the related ordered values vector, and $b_i \in b$ is the ith greatest value in A.

Table 2. Linguistic expressions for HFL AHP (Onar et al., 2016)

Linguistic expression	Fuzzy numbers
Absolutely Low Importance (ALI)	(0.11,0.11,0.14)
Very Low Importance (VLI)	(0.11,0.14,0.2)
Essentially Low Importance (ESLI)	(0.14,0.2,0.33)
Weakly Low Importance (WLI)	(0.2,0.33,1)
Equally Low Importance (ELI)	(0.33,1,1)
Exactly Equal (EE)	(1,1,1)
Equally High Importance (EHI)	(1,1,3)
Weakly High Importance (WHI)	(1,3,5)
Essentially High Importance (ESHI)	(3,5,7)
Very High Importance (VHI)	(5,7,9)
Absolutely High Importance (AHI)	(7,9,9)

Step 3. In the pairwise comparison matrix ($\widetilde{C}$), reciprocal values are calculated as:

$$\widetilde{c_{ij}} = \left(\frac{1}{c_{iju}}, \frac{1}{c_{ijm2}}, \frac{1}{c_{ijm1}}, \frac{1}{c_{ijl}}\right) \tag{5}$$

Step 4. Each pairwise comparison matrix's consistency is checked. These matrices are de-fuzzified to ensure consistency (Camci et al,2018). Considering TFN $A = (l, m_1, m_2, u)$, it is converted to a crisp number with:

$$\boldsymbol{\mu_d} = \frac{l+m_1+m_2+u}{6} \tag{6}$$

These equations are used to calculate the consistency ratio (CR):

$$CI = \frac{\lambda_{max}-n}{n-1} \tag{7}$$

$$CR = \frac{CI}{RI} \tag{8}$$

where CI refers to the consistency index, λ_{max} is the largest eigenvector of the matrix, n is the number of criteria, and RI is the random index. Experts have to reconsider the pairwise comparison matrices if they are not consistent.

Step 5. The fuzzy geometric mean ($\tilde{r}_i$) of $\tilde{C}$ is calculated as:

$$\tilde{r}_i = (\tilde{c}_{i1} \otimes \tilde{c}_{i2} \ldots \otimes \tilde{c}_{in})^{1/n} \tag{9}$$

Step 6. The fuzzy weight ($\widetilde{w}_i^{CR}$) of every main criterion is computed as:

$$\widetilde{w}_i^{CR} = \tilde{r}_i \otimes (\tilde{r}_1 \otimes \tilde{r}_2 \ldots \otimes \tilde{r}_n)^{-1} \tag{10}$$

Step 7. Fuzzy global weights of the sub-criteria's are calculated as:

$$\widetilde{w}_{ij}^{G} = \widetilde{w}_i^{CR} \times \widetilde{w}_j^{CR} \tag{11}$$

where $\widetilde{w}_{ij}^{G}$ signify sub-criteria global weight.

Step 8. Trapezoidal fuzzy numbers $\widetilde{w}_{ij}^{G}$ are defuzzified and normalized as:

$$w_{ij}^{G} = \frac{\alpha+2\beta+2\gamma+\delta}{6} \tag{12}$$

$$w_{ij}^{N} = \frac{w_{ij}^{G}}{\sum_i \sum_j w_{ij}^{G}} \tag{13}$$

Steps 1-6 are performed for both the main and sub-criteria, and steps 7-8 are used to calculate the weights of the sub-criteria.

4. PROPOSED CRITICAL SUCCESS FACTORS' FOR DIGITAL EDUCATION

As a result of the literature review and expert opinions, the CSFs for digital education (Volery, 2001; Sharma et al., 2011; Alrasheedi et al., 2015; Fabito, 2017; Barclay et al., 2018; Blieck et al., 2019; Moya and Camacho, 2021; Kanojia et al., 2021; König et al., 2023) are structured as in Table 3.

Table 3. CSFs for digital education

Critical Succes Factors	
Technological Factors (F1)	screen design and aesthetics (F11)
	Internet quality (F12)
	ease of access (F13)
	system interactivity and system response (F14)
	privacy and reliability of system (F15)
Human Factors (instructors) (F2)	previous computer experience (F21)
	continuous digital awareness (F22)
	pedagogical digital competence (F23)
	timely response (F24)
	encourage students interaction (F25)
Human Factors (students) (F3)	technical competency (F31)
	perception of content and system (F32)
	students' mindset about online learning (F33)
	self-efficiency (F34)
	student involvement and participation (F35)
Organizational Factors (institution) (F4)	technical support (F41)
	technical equipment availability (F42)
	program flexibility (F43)
	course/instruction authorization (F44)
	digital strategy roadmap (F45)
Resources Factors (courses) (F5)	course quality and sufficiency (F51)
	course flexibility (F52)
	curriculum management and assessment (F53)
	integration of e-learning into curriculum (F54)
	offering more ICT-related courses (F55)

5. APPLICATION

Determining the CSFs is an important step to take to increase the quality of digital education and provide an efficient education environment for students. In this study, the CSFs given in Table 3 were determined as a result of expert opinions and a literature review. There are five main factors and twenty-five sub-factors. An application for the evaluation of CSFs for digital education is realized to show the potential of the proposed approach. Three experts evaluate this proposed model. All experts have appropriate knowledge and expertise in the field of digital education. The experts' weights are regarded as equal.

To begin, experts evaluate the main CSFs using the linguistic scale shown in Table 2. Table 4 shows the evaluation of the main criteria. The language expressions in Table 4 are transformed into fuzzy numbers using (4). The weights of each main CSF are then calculated using (5)-(10). Table 5 shows the relative weights of the main CSFs.

Table 4. Pairwise comparison matrix of the main CSFs

	F1	**F2**	**F3**	**F4**	**F5**
F1	EE	Between EHI and WHI	Between EHI and WHI	Between ESHI and AHI	Between WHI and ESHI
F2		EE	Between ELI and EHI	Between WHI and ESHI	Between EHI and WHI
F3			EE	Between EHI and WHI	Between WHI and ESHI
F4				EE	Between ESLI and ELI
F5					EE

Table 5. Relative weights of the main CSFs

	F1	F2	F3	F4	F5	Relative Weights
F1	(1,1,1,1)	(1,1,3,5)	(1,1,3,5)	(3,6.78,7.22,9)	(1,3,5,7)	(0.106,0.232,0.682,1.478)
F2	(0.2,0.33,1,1)	(1,1,1,1)	(0.33,1,1,3)	(1,3,5,7)	(1,1,3,5)	(0.050,0.127,0.369,0.860)
F3	(0.2,0.33,1,1)	(0.33,1,1,3)	(1,1,1,1)	(1,1,3,5)	(1,3,5,7)	(0.050,0.127,0.369,0.860)
F4	(0.11,0.14,0.15,0.33)	(0.14,0.2,0.33,1)	(0.2,0.33,1,1)	(1,1,1,1)	(0.14,0.32,0.34,1)	(0.01,0.040,0.095,0.272)
F5	(0.14,0.2,0.33,1)	(0.2,0.33,1,1)	(0.14,0.2,0.33,1)	(1,3,3,7)	(1,1,1,1)	(0.028,0.067,0.172,0.500)

Each sub-CSF's assessment matrices are generated using the linguistic scale supplied in Table 2 to determine the weights of sub-CSFs. The first CSF (F1) assessment matrix is shown in Table 6. Table 6 shows how the various sub-CSF assessment matrices are organized.

Table 6. Pairwise comparison matrix of the first CSF (F1)

	F11	F12	F13	F14	F15
F11	EE	Between ESLI and ELI	Between VLI and ESLI	Between ESLI and ELI	Between ALI and VLI
F12		EE	Between ELI and EHI	Between ELI and EHI	Between ESLI and ELI
F13			EE	Between EHI and WHI	Between ESLI and ELI
F14				EE	Between VLI and ESLI
F15					EE

The language expressions in Table 6 are translated into fuzzy numbers using (4). The weights of each sub-CSF are determined using (5)-(10). The values are then normalized with (13) after being defuzzified using (12). Table 7 contains the final findings. The CR is computed for the evaluation matrices with (6)-(8). The results showed that experts' evaluations are consistent.

Table 7. Weights of CSFs

Sub-Criteria	Global Weights				Defuzzified Weights	Normalized Weights
F11	0,002	0,009	0,035	0,253	0,057	0,016
F12	0,004	0,032	0,111	0,999	0,215	0,061
F13	0,006	0,035	0,163	1,164	0,261	0,074
F14	0,003	0,022	0,099	0,643	0,148	0,042
F15	0,015	0,101	0,391	2,289	0,548	0,156
F21	0,002	0,023	0,105	0,884	0,190	0,054
F22	0,003	0,034	0,140	1,158	0,252	0,072
F23	0,003	0,029	0,147	1,220	0,262	0,075
F24	0,001	0,007	0,038	0,325	0,069	0,020
F25	0,001	0,007	0,035	0,406	0,082	0,023
F31	0,005	0,037	0,233	1,324	0,311	0,089
F32	0,001	0,009	0,043	0,441	0,091	0,026
F33	0,001	0,006	0,026	0,227	0,049	0,014
F34	0,004	0,028	0,168	0,959	0,226	0,064
F35	0,001	0,011	0,053	0,522	0,108	0,031
F41	0,000	0,003	0,011	0,122	0,025	0,007
F42	0,000	0,003	0,011	0,110	0,023	0,007
F43	0,002	0,008	0,045	0,360	0,078	0,022
F44	0,001	0,008	0,030	0,265	0,057	0,016
F45	0,001	0,007	0,030	0,236	0,052	0,015
F51	0,003	0,019	0,077	0,645	0,140	0,040
F52	0,002	0,016	0,058	0,553	0,117	0,033
F53	0,002	0,013	0,058	0,444	0,098	0,028
F54	0,001	0,003	0,011	0,124	0,025	0,007
F55	0,001	0,003	0,011	0,124	0,025	0,007

The most appropriate CSF is found as "privacy and reliability of system (F15)", the second important one is "technical competency (F31)", and the third-ranked CSF is "pedagogical digital competence (F23)".

6. CONCLUSIONS

The aim of this study was evaluating CSFs for digital education with a HFL MCDM approach. HFL AHP-method is used for the determination of the weights of CSFs. The contributions of this paper were proposing a new and conceptual evaluation model including CSFs for digital education, presenting an analytic method such as the HFL AHP method in this area, and providing an application for the evaluation of CSFs for digital education.

At the end of the application, the most important CSF is found as "privacy and reliability of system (F15)". Instructors and students need a special place where they can study online. For this reason, the first feature that the digital education approach should have in order for education to be sustainable is that the system is confidential and reliable.

For future research, the evaluation problem can be solved by the HFL Analytic Network Process (ANP) method, considering the connections between the CSFs. Other extensions of fuzzy sets (for example, elicit information, pythagorean fuzzy sets, spherical fuzzy sets) may be added into the framework.

Acknowledgements
This work has been supported by the Scientific Research Projects Commission of Galatasaray University under grant number FOA-2021-1059 and FOA-2023-1181.

Ethics Committee Approval
N/A

Peer-review
Externally peer-reviewed.

Author Contributions
Conceptualization: E.M., G.B., M.G.; Investigation: E.M., G.B., M.G.; Material and Methodology: E.M., G.B., M.G.; Supervision: G.B.; Visualization: E.M., G.B., M.G.; Writing-Original Draft: E.M.; Writing-review & Editing: E.M., G.B., M.G. ; Other: All authors have read and agreed to the published version of manuscript.

Conflict of Interest
The authors have no conflicts of interest to declare.

Funding
The authors declared that this study has received no financial support.

REFERENCES

Alrasheedi, M., Capretz, L. F., & Raza, A. (2015). A systematic review of the critical factors for success of mobile learning in higher education (university students' perspective). Journal of Educational Computing Research, 52(2), 257.

Alrasheedi, M., Capretz, L. F., & Raza, A. (2016). Management's perspective on critical success factors affecting mobile learning in higher education institutions—An empirical study. Journal of Educational Computing Research, 54(2), 253-274.

Barclay, C., Donalds, C., & Osei-Bryson, K. M. (2018). Investigating critical success factors in online learning environments in higher education systems in the Caribbean. Information Technology for Development, 24(3), 582-611.

Blieck, Y., Ooghe, I., Zhu, C., Depryck, K., Struyven, K., Pynoo, B., & Van Laer, H. (2019). Consensus among stakeholders about success factors and indicators for quality of online and blended learning in adult education: a Delphi study. Studies in Continuing Education, 41(1), 36-60.

Büyüközkan, G., Karabulut, Y., & Mukul, E. (2018). A novel renewable energy selection model for United Nations' sustainable development goals. Energy, 165, 290-302.

Cortés, A., & Barberà, E. (2013). STUDENTS'PERCEPTIONS TOWARDS ONLINE LEARNING SUCCESS FACTORS. In EDULEARN13 Proceedings (pp. 5654-5660). IATED.

De Paepe, L., Zhu, C., & Depryck, K. (2019). Development and implementation of online Dutch L2 courses in adult education: educators' and providers' perceptions of constraints and critical success factors. Innovation in language learning and teaching, 13(3), 277-291.

Fabito, B. S. (2017, September). Exploring critical success factors of mobile learning as perceived by students of the college of computer studies–National University. In 2017 International Conference on Soft Computing, Intelligent System and Information Technology (ICSIIT) (pp. 220-226). IEEE.

Fisk, P. (2017). Education 4.0… the future of learning will be dramatically different, in school and throughout life.

Freund, Y. P. (1988). Critical success factors. Planning Review.

Hwang, C. L., Yoon, K., (1981). Methods for multiple attribute decision making. Multiple attribute decision making: methods and applications a state-of-the-art survey, 58-191.

Ibanez, A., Krogt, A. V. D., & Neubert, M. (2023). Impact and success factors of online education methods at university level in times of COVID-19: a case study of Paraguay. International Journal of Technology Enhanced Learning, 15(1), 58-73.

Kanojia, M., Shukla, B., Wali, A., & Joshi, M. (2021). Critical success factors for leveraging technology transfer from higher education institutions to industry: Indian context. International Journal of Innovation and Technology Management, 18(04), 2150018.

König, C. M., Karrenbauer, C., & Breitner, M. H. (2023). Critical success factors and challenges for individual digital study assistants in higher education: A mixed methods analysis. Education and Information Technologies, 28(4), 4475.

Liu, H., & Rodríguez, R. M. (2014). A fuzzy envelope for hesitant fuzzy linguistic term set and its application to multicriteria decision making. Information Sciences, 258, 220-238.

Milic, S., & Simeunovic, V. (2021). Exploring e-learning critical success factors in digitally underdeveloped countries during the first wave of the COVID-19. Interactive Learning Environments, 1-13.

Moya, S., & Camacho, M. (2021). Identifying the key success factors for the adoption of mobile learning. Education and Information Technologies, 1-29.

Onar, S. Ç., Büyüközkan, G., Öztayşi, B., & Kahraman, C. (2016). A new hesitant fuzzy QFD approach: an application to computer workstation selection. Applied Soft Computing, 46, 1-16.

Papanikolaou, K., & Mavromoustakos, S. (2006, February). Critical Success Factors for the Development of Mobile Learning Applications. In EuroIMSA (pp. 19-24).

Rockart, J. F. (1979). Chief executives define their own data needs. Harvard business review, 57(2), 81-93.

Rodriguez, R. M., Martinez, L., & Herrera, F. (2011). Hesitant fuzzy linguistic term sets for decision making. IEEE Transactions on fuzzy systems, 20(1), 109-119.

Saaty, T. L. (1990). How to make a decision: the analytic hierarchy process. European journal of operational research, 48(1), 9-26.

Sharma, K., Pandit, P., & Pandit, P. (2011). Critical success factors in crafting strategic architecture for e-learning at HP University. International Journal of Educational Management.

Torra, V. (2010). Hesitant fuzzy sets. International journal of intelligent systems, 25(6), 529-539.

Volery, T. (2001). Online education: An exploratory study into success factors. Journal of educational computing research, 24(1), 77-92.

Zhu, B., & Xu, Z. (2014). Analytic hierarchy process-hesitant group decision making. European Journal of Operational Research, 239(3), 794-801.

The Influence of Strontium on Eutectic Modification in Al-Si Alloys

Biljana Zlaticanin*[1], Sandra Kovačević[2]

Abstract: Eutectic Al-Si alloys widely applied in automotive engines, because of their good mechanical properties. In order to improve mechanical properties, strontium is added to Al-Si alloy to transform the eutectic silicon. The modification treatment of Al-Si alloys by adding of Sr has been known for about a century. Yet, the mechanisms behind the strong element assisted eutectic refinement is still not fully understood. The appropriate concentration of Sr is sufficient for well-modified of the eutectic silicon.

Keywords: Al-Si alloys, microstructure, properties

[1]**Address:** University of Montenegro, Faculty of Metallurgy and Technology, Cetinjski put bb, 81000 Podgorica, Montenegro
[2]**Address:** Central School of Chemical Technology Spasoje Raspopović, 81000 Podgorica, Montenegro

***Corresponding author**: biljana@ucg.ac.me

1. INTRODUCTION

Al-Si alloys are the most widely used aluminum casting alloys owing to their superior castability, light weight, low thermal expansion coefficient, excellent thermal conductivity, high wear resistance and good corrosion resistance (Liu et al., 2015). In hypoeutectic Al-Si alloy, the Si content varies from 5 to 12 wt.%. There are very few data on the size of unmodified Al-Si eutectic grains. The irregular shape of the eutectic/liquid interface makes accurate measurement of the Al-Si eutectic grain size difficult. Modification of Al-Si castings is standard practice.The growth characteristics of eutectic Si in unmodified and Sr -modified Al-10.7wt%Si alloys were investigated. The eutectic Si of the alloy is present as a thick needle. It is of great importance to improve the mechanical properties of Al-Si alloys by modification. Modification have been widely used because they are simple to operate and inexpensive to perform.

2. MATERIAL AND METHOD

Two alloys of composition Al-10.7wt%Si (unmodified) and Al-10.7wt%Si-0.02wt%Sr (Sr-modified) were made. The alloys were melted in an induction furnace at 720°C. The method of Sr addition is through master alloy Al-10wt%Sr. The modifying effect exerted by Sr is most pronounced if all Sr is brought into liquid solution. After the alloying step, degassing was performed for 30 minutes. The melt was poured on a temperature at 720°C into the molds. Metallographic samples were sectioned horizontally and were mounted and polished. An optical microscope was used to analyze the microstructures.

Chemical composition of the Al-Si alloys used in this study is shown in Table 1. These compositions were chosen because of their eutectic volume fractions. In the Al-10.7wt%Si (unmodified) and Al-10.7wt%Si-0.02wt%Sr, the formation of the Al-Si eutectic is the major solidification reaction because it has a large eutectic volume fraction.

Table 1. Chemical composition of the investigated alloys (in wt%)

TYPE OF SAMPLE	%Fe	%Si	%Ti	%Cu	%Zn	%V	%Cr	%Mn	%Mg	%Sr
Al-10.7wt%Si	0.25	10.74	0,001	0.004	0.043	0.004	0.002	0.002	0.000	0.016
Al-10.7wt%Si-0.02wt%Sr	0.24	10.66	0.001	0.005	0.035	0.005	0.006	0.002	0.000	0.017

Properties of the Al-10.7wt%Si (unmodified) and Al-10.7wt%Si-0.02wt%Sr alloys have been investigated. Hardness has been measured by use of the Brinell method.

3. RESULTS

Figure 1 shows the as-cast microstructure of an Al-10.7wt%Si unmodified near-eutectic alloy. Figures 2 and 3 shows image taken with the Sr-modified sample Al-10.7wt%Si. At low magnification we can see the dendritic nature of the fine solidification structure. At high magnification this is not observed, instead we see the fine eutectic and randomly oriented α -Al grains. Further in the image sequence Si-needles are seen to form. Small additions of Sr modify the silicon phase. The result is a increase in mechanical properties.

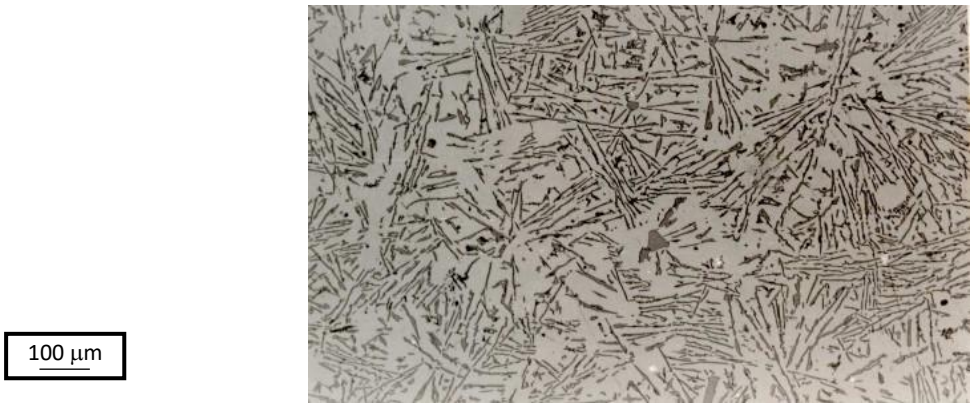

Figure 1. Microstructure of Al-10.7wt%Si (unmodified) alloy

Figure 2. Microstructure of Al-10.7wt%Si-0.02wt%Sr alloy

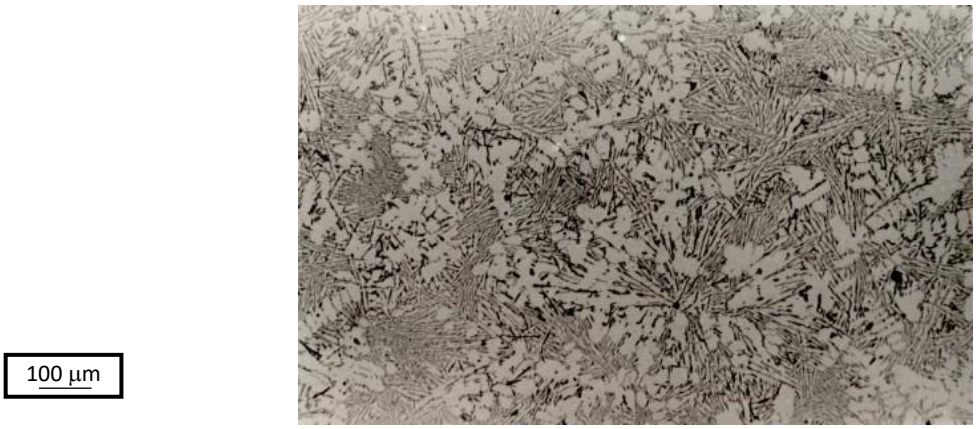

Figure 3. Microstructure of Al-10.7wt%Si-0.02wt%Sr alloy

We have also examined the properties of these materials: hardness measurement. The hardness of the modified alloy is higher than the hardness of the alloy without any modification treatment (Table 2).

Table 2. Hardness of the investigated alloys

TYPE OF SAMPLE	$HB_{average}$
Al-10.7wt%Si	39.8
Al-10.7wt%Si-0.02wt%Sr	50.9

4. DISCUSSION AND CONCLUSIONS

Al-Si alloys have considerable commercial importance as casting alloys. Al-Si based alloys are the most widely used Al based foundry alloys due to their excellent combination of mechanical properties and castability (Chen and Xu, 2016). Near-eutectic alloys generally containing eutectic modifiers, are also widely used. The Al-Si binary phase diagram is the basis for understanding the microstructure of these alloys. Our experiments were designed to investigate the effects of strontium on the eutectic silicon for Al-Si alloys. Solidification is a process of nucleation and growth. In Al-10.7wt%Si (unmodified) and Al-10.7wt%Si-0.02wt%Sr alloys the first phase to be nucleated is α - Al. According to the Al-Si phase diagram α phase has a low silicon content, max 1.65%. The Si content determines the conditions for growth. The formation of the Al-Si eutectic is the major solidification reaction in the Al-10.7wt%Si alloy, constituting approximately two-thirds of the volume. Strontium is added to Al-Si alloy to transform the eutectic silicon from faceted acicular flakes to a fine fibrous structure (Hegde and Prabhu, 2008).

For hypoeutectic Al-Si based alloys, the modification of eutectic Si have a significant impact on the mechanical properties. The results of this investigation show that the strontium modified alloy Al-10wt%Si-0.02wt%Sr had porosity level lower than Al-10.7wt%Si (unmodified).

REFERENCES

Liu, X., Zhang, Y., Beausir, B., Liu, F., Esling, C., Yu, F. (2015). Twin-controlled growth of eutectic Si in unmodified and Sr modified Al-12.7%Si alloys investigated by SEM/EBSD. Acta Materialia. 97, 338-347.

Chen, R., Xu, Q. (2016). Modeling of aluminum-silicon irregular eutectic growth by cellular automaton model. Research and Development. 13, 114-122.

Hegde, S., Prabhu, K.N. (2008). Modification of eutectic silicon in Al–Si alloys. J. Mater. Sci. 43, 3009-3027.

iconst est
6th International Conferences on Science and Technology
30 August - 01 September 2023, in Budva, Montenegro
Engineering Science and Technology

Structure and Simulation of Single Phase Seven Level Inverter

Abdullatif Emlik *[1], Ali Bekir Yıldız [2]

Abstract: In this article, a one-phase seven-level inverter structure will be examined and this inverter will be simulated in computer environment by using Matlab Simulink program. Sinus triangle pulse width modulation will be used for the control circuit of the inverter, and in order to generate the trigger signal in this control structure, three peak value reference values, namely DC component, will be added and rectified, and will be realized after comparing the sinus signals with the same frequency with a carrier triangle signal. By keeping the amplitude of the said carrier triangle signal constant and its frequency being much higher than the reference rectified sine signals, the output voltage of the inverter is provided to resemble a pure sine wave, and the output current is provided to appear as almost pure sine with the load containing the coil. Of course, because the inverter structure has seven levels, sine triangle pulse width modulation is made here. In higher order inverter topologies, the output voltage and current can be approximated to a pure sine form without harmonic, even without applying sine-triangle pulse width modulation. However, in such a case, the cost will increase because too many semiconductors and voltage sources will be used. However, in the inverter topology realized in this study, seven levels were obtained by using only six mosfets. In addition, the voltage source is used as three equal-level voltage sources by using 3 series-connected capacitors to the voltage source. These 3 different comparison signals, which are used for the inverter output voltage to be seven-level, will enable the switches to turn on and off, respectively, in the inverter structure, and with the pulse width modulation, the total harmonic distortion will be reduced by approaching the pure sinus form of the output voltage form. This inverter structure and everything described has been tested only in the computer environment by means of the Matlab Simulink program, and the realized circuit structure can be run correctly.

Keywords: Seven Level İnverter, Pulse Width Modulation, Total Harmonic Distortion

[1]**Address:** Kocaeli University, Graduate School of Natural and Applied Sciences, Department of Electrical Engineering, Kocaeli, Türkiye
[2]**Address:** Kocaeli University, Faculty of Engineering, Department of Electrical Engineering, Kocaeli, Türkiye
***Corresponding author**: latifemlik@gmail.com

1. INTRODUCTION

Today, multilevel inverters are used in almost every industrial application and have many different types. They are preferred because their output voltages are very close to sine. Their total harmonic distortion is also low. The higher the number of levels, the higher the level of decay. However, the higher the level, the higher the voltage source and the number of semiconductors used. This will make the inverter structure very complex and increase the cost. For this reason, inverter design should be done in accordance with the needs. When looking at the types of multilevel inverters, they are diode clamped inverters, capacitor clamped inverters, H bridge inverters. In this article, a bidirectional six-switch h-bridge inverter structure is constructed in a modified structure using a new sine-triangle pulse width modulation.

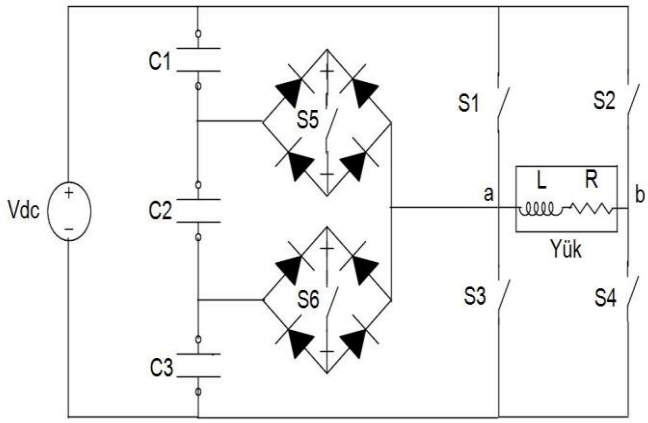

Figure 1. Phase Seven Level Inverter Circuit

2. PROPOSED MULTI-LEVEL INVERTER TOPOLOGY

As can be seen in Figure 1, a different h bridge inverter structure is applied in this study. It consists of a combination of bidirectional switches and the traditionally used h bridge inverter. Capacitors C1, C2 and C3 are used, dividing the input voltage into three equal sources. In this wide bridge inverter structure, a multilevel inverter is obtained by using more power switches and power diodes. By properly switching the power switches, respectively, Vdc, 2Vdc/3, Vdc/3, 0V, -Vdc/3, -2Vdc/3 and –Vdc voltages will be given to the output of the circuit. So my output voltage will become seven level. Thus, we can divide the proposed inverter operating principle into 7 parts. Figure 2 represents these 7 different operating states between (a) and (g) and these situations are explained below.

i. The maximum output voltage, Vdc, is given on the load when the S1 and S4 switches are active and all other switches are disabled, and thus the voltage appearing on the load becomes the Vdc voltage, as can be seen in Figure 2 (a).

ii. With the bidirectional switch S5 and S4 switches active and all other switches disabled, a voltage of 2Vdc/3 is applied to the load and thus the voltage appearing on the load is 2Vdc/ It has 3 voltages.

iii. When the bidirectional switch S6 and S4 switches are active and all other switches are deactivated, Vdc/3 voltage is applied to the load and thus the voltage appearing on the load is Vdc/V by following the current path shown in Figure 2(c). It has 3 voltages.

iv. In this structure, which is used to get zero output voltage, there are two ways to make the voltage on the load zero. The first case is when switches S3 and S4 are only active. All other switches should be disabled. The second situation is when only the S1 and S2 switches are active. All other switches should be disabled in this case. Any of these two principles will make the output voltage zero. However, it would be useful to use them in order for the switches to age equally or to complete their life in the same way. Thus, the voltage appearing on the load becomes 0V by following the current path seen in Figure 2(d).

v. With the bidirectional switch S5 and S2 switches activated and all other switches deactivated, -Vdc/3 voltage is applied to the load, so that the voltage appearing on the load follows the current path shown in Figure 2(e) - Vdc/3 voltage becomes.

vi. When the S6 switch and S2 switches are active and all other switches are disabled, a voltage of -2Vdc/3 is applied to the load and thus the voltage appearing on the load follows the current path shown in Figure 2(f) - There will be a voltage of 2Vdc/3.

vii. The maximum negative output voltage, -Vdc, is given on the load with the S2 and S3 switches activated and all other switches disabled, and thus the voltage appearing on the load becomes -Vdc as it can be seen in Figure 2 (g)..

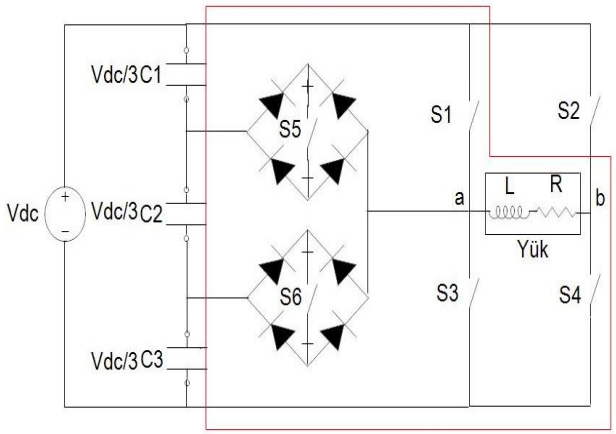

(a)

Figure 2. Required switching combinations to generate output voltage (a) Vab=Vdc

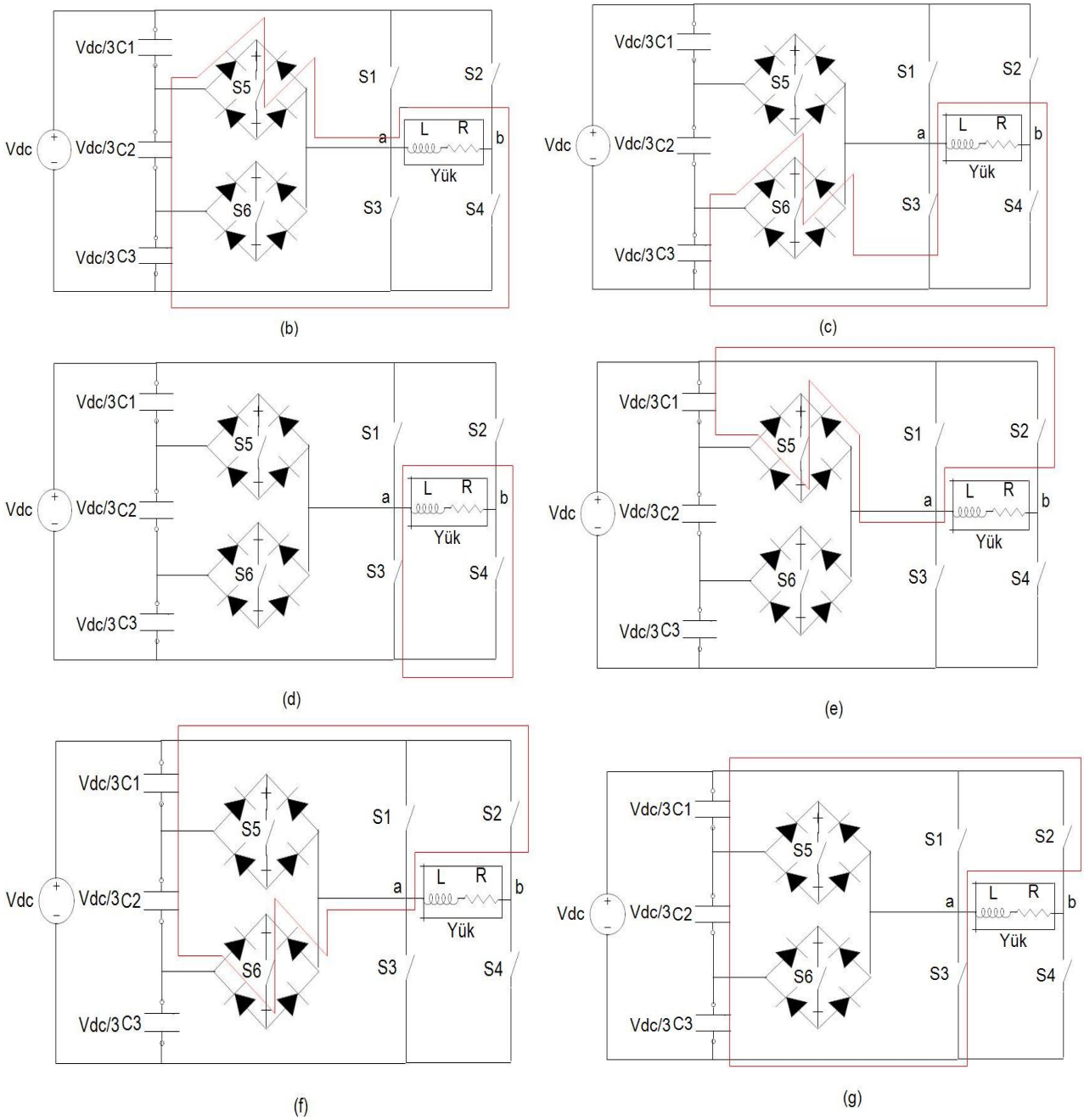

(b) (c) (d) (e) (f) (g)

Figure 2. (Continued) Required switching combinations to generate output voltage (b) Vab=2Vdc/3, (c) Vab=Vdc/3, (d) Vab=0V, (e) Vab=-Vdc/3, (f) Vab=-2Vdc/3, (g) Vab=-Vdc

Table 1. Output voltage table according to whether the switches are active or not (1-0) is presented below.

Voutput	S1	S2	S3	S4	S5	S6
Vdc	1	0	0	1	0	0
2Vdc/3	0	0	0	1	1	0
Vdc/3	0	0	0	1	0	1
0V	0	0	1	1	0	0
-Vdc/3	0	1	0	0	1	0
-2Vdc/3	0	1	0	0	0	1
-Vdc	0	1	1	0	0	0

3. SINUS TRIANGLE IMPACT WIDTH MODULATION

In this article, a new structure was developed for sine-triangle pulse width modulation. Three reference signals were generated. These reference signals, named Vref1, Vref2 and Vref3, were compared with a carrier/triangle signal to enable or disable the power switches. The frequencies of the signals created as a reference are equal and in phase with each other. Differently from the Vref1 signal, the Vref2 and Vref3 signals have DC components, and thus the peak value of the Vref2 signal is reduced by 1 unit compared to Vref1. Likewise, the Vref3 signal was obtained by decreasing the peak value by 2 units compared to Vref1. It is used to create 0V level when carrier/triangle signal for positive alternans is greater than Vref1 signal. Therefore, S3 and S4 switches are activated in this interval. In cases where the carrier/triangle signal is smaller than the Vref1 signal and larger than the Vref2 signal, the Vdc/3 level is generated. Therefore, switches S6 and S4 are activated in this interval. A voltage of 2Vdc/3 is generated when the carrier/triangle signal is smaller than the Vref2 signal and at the same time greater than the Vref3 signal. Therefore, switches S5 and S4 are activated in this interval. In cases where the carrier/triangle signal is smaller than the Vref 3 signal, the Vdc voltage is generated. Therefore, switches S1 and S4 are activated in this interval. It is used to create 0V level when carrier/triangle signal for negative alternans is greater than Vref1 signal. Therefore, S1 and S2 switches are activated in this interval. In cases where the carrier/triangle signal is smaller than the Vref1 signal and larger than the Vref2 signal, the -Vdc/3 level is created. Therefore, at this interval, switches S2 and S5 are activated. A voltage of -2Vdc/3 is generated when the carrier/triangle signal is smaller than the Vref2 signal and at the same time greater than the Vref3 signal. Therefore, switches S2 and S6 are activated in this interval. In cases where the carrier/triangle signal is smaller than the Vref 3 signal, -Vdc voltage is generated. Therefore, S2 and S3 switches are activated in this interval. Thus, the output voltage becomes seven-level. This switching structure is shown in Figure 3. As you can see, switches S1, S3, S5 and S6 operate at the speed of the carrier/triangle signal. But the frequency of switches S2 and S4 is equal to the fundamental frequency.

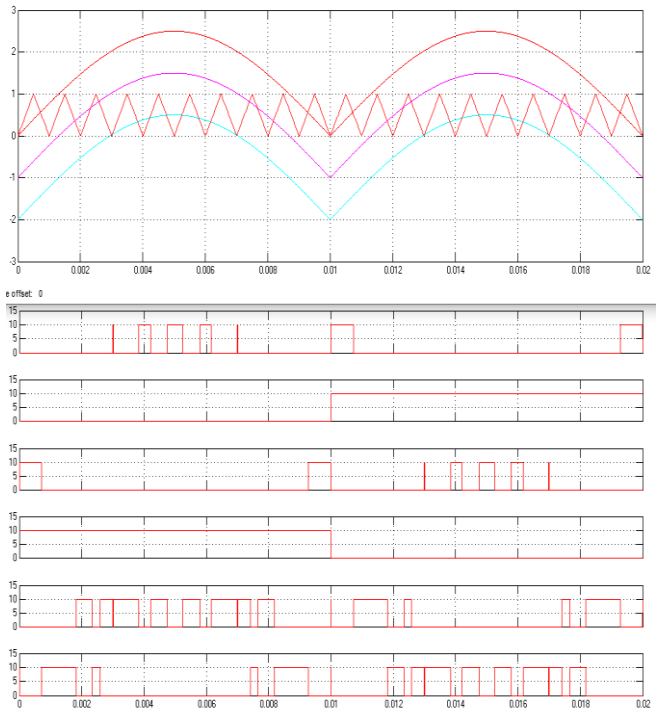

Figure 3. Switching structure for one-phase seven-level inverter

4. SIMULATION RESULTS

The inverter circuit realized in this article is simulated in computer environment by using Matlab/Simulink program.

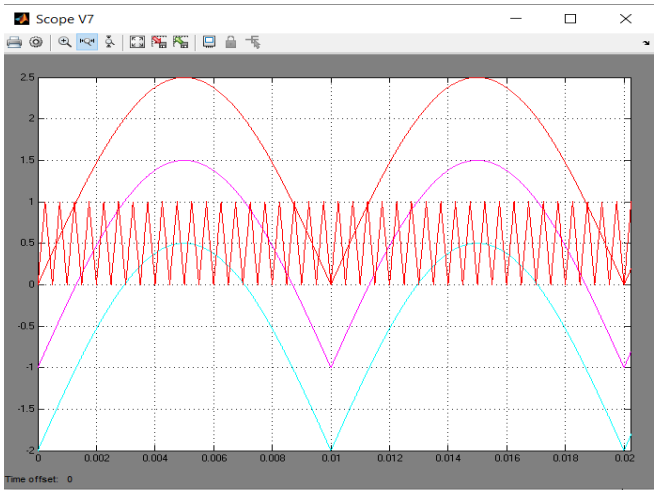

Figure 4. Reference signals used to generate PWM switching signals

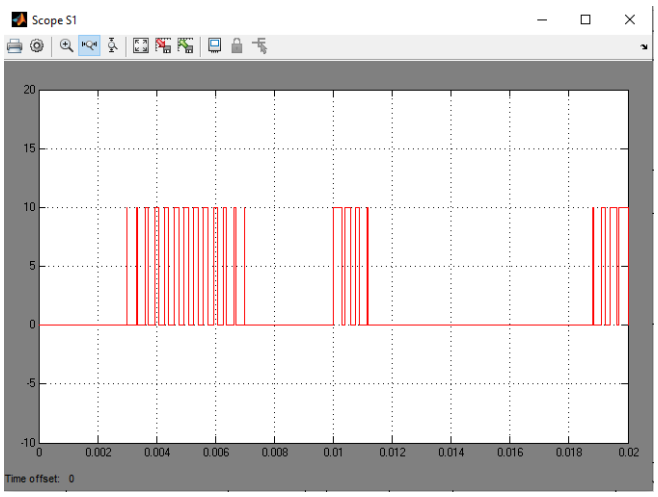

Figure 5. PWM signal for switch S1

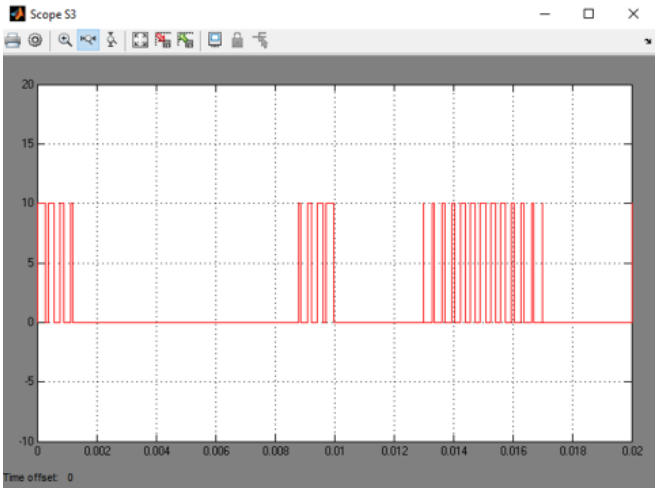

Figure 6. PWM signal for switch S3

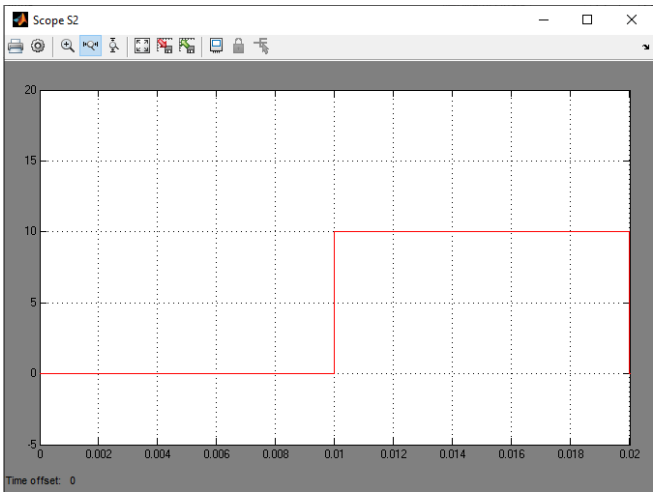

Figure 7. PWM signal for switch S2

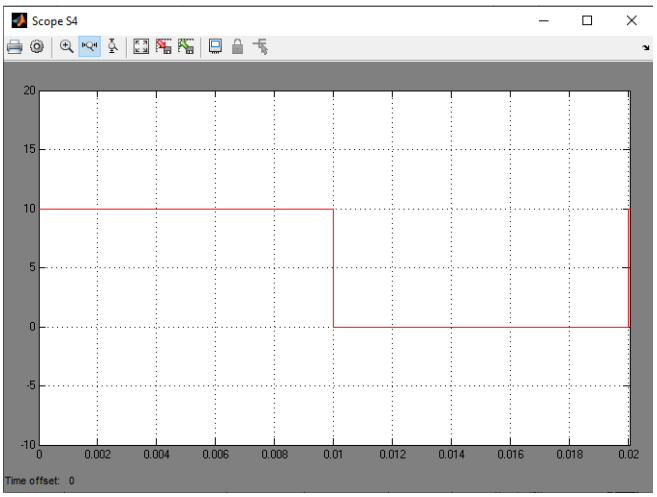

Figure 8. PWM signal for switch S4

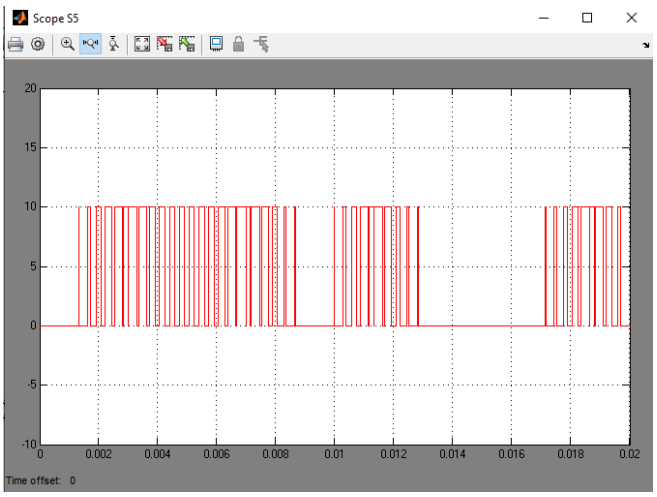

Figure 9. PWM signal for switch S5

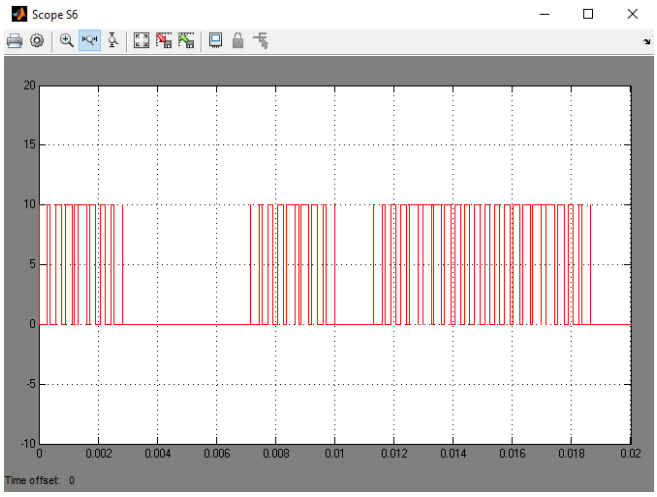

Figure 10. PWM signal for switch S6

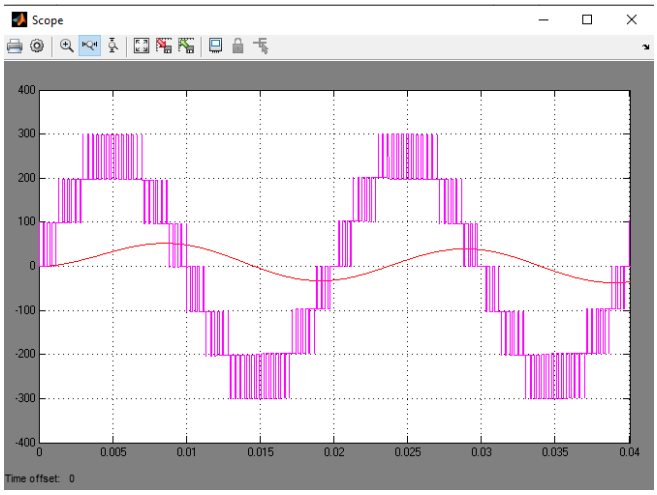

Figure 11. PWM inverter output voltage and current

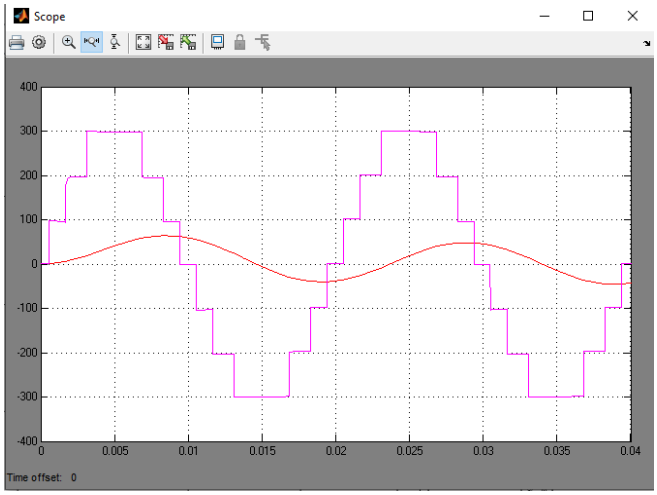

Figure 12. Inverter output voltage and current at full load without PWM

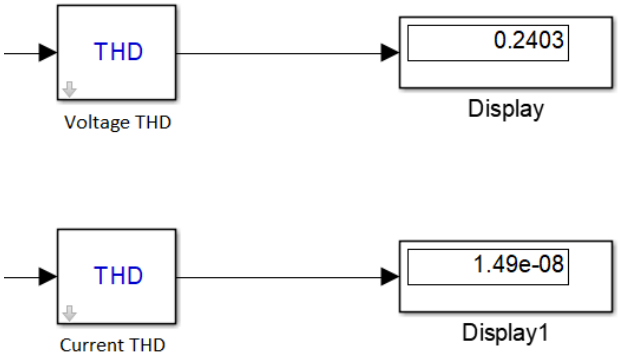

Figure 13. Total harmonic distortion values for output voltage and current

5. CONCLUSIONS

Multilevel inverters are similar to pure sine in output voltage and thus have low total harmonic distortion. In this article, a new different pulse width modulation algorithm is implemented and three reference signals and a carrier/triangle signal are compared, enabling switches to switch on and off, thus obtaining a seven-level inverter. This inverter model has been realized in computer environment by means of Matlab/Simulink program and it has run successfully.

REFERENCES

[1] Çolak I, Kabalcı E, Bayındır R. "Review of multilevel voltage source inverter topologies and control schemes". Energy Conversion and Management, 52, 1114-1128, 2011.
[2] Sabarad J, Kulkarni GH. "Comparative analysis of SVPWM and SPWM techniques for multilevel inverter". International Conference on Power and Advanced Control Engineering, Bangalore, India, 12-14 August 2015.
[3] Babaei E, Hosseini SH. "New cascaded multilevel inverter topology with minimum number of switches". Energy Conversion and Management, 50(11), 2761-2767, 2009.
[4} Sezen S, Özdemir E. "Modeling, simulation and control of three phase three level multilevel ınverter for grid connected PV system". SOLAR TR2 Solar Electricity Conference and Exhibition, Antalya, Turkey,7-9 November 2012.
[5] Ray, R., Shadh, M.A. and Reza, S., 2019. Cascaded HBridge multilevel inverter using SVPWM modulation. 1st International Conference on Advances in Science, Engineering and Robotics Technology (ICASERT 2019).
[6] Islam, N.J., Sarker, S., Merazul Islam N.M. and Reza, S., 2019. Implementation of finite control set model predictive control on 7-level flying capacitor multilevel inverter using space vector. 1st International Conference on Advances in Science, Engineering and Robotics Technology (ICASERT 2019).
[7] T. Lipo and D. Holmes, Pulse Width Modulation for Power Converters (Principles and Practice). Hoboken, NJ: Wiley, 2003.
[8] Kushare, B.E., A.A. Ghatol, and M.S. Aphale. Survey of Interharmonics in Indian Power System Network. in Power Engineering Conference, 2007. IPEC 2007. International. 2007.
[9] Sirisukprasert, S. (1999). Optimited Harmonic Stepped Waveform For Multilevel İnverter, Master Thesis, Blacksburg Virginia.
[10] Çamur S., Arifoğlu B., Beşer E. Kandemir and Beşer E., "Design and Application of a Novel Structure and Topology for Single-Phase FiveLevel Inverter", Wseas Transactions on Electronics, 2006.

Assessment of The Seismic Hazard For Adıyaman With Deterministic Analysis Due To Probable Earthquake In The Akçadağ Segment (Malatya Fault)

Seyhan Okuyan Akcan*[1], Senem Tekin[2], Fatih Tekir[3], Mehmet Fatih Boybey[4], Oğuzhan Çetindemir[5]

Abstract: On February 6, 2023, at 04.17 and 13.24 hours local time in Turkey, two earthquakes with an instrumental magnitude (Mw) of 7.8 and 7.6 with epicenters in Pazarcık (Kahramanmaraş) and Elbistan (Kahramanmaraş) occurred 9 hours apart. It was felt in Southeastern Anatolia, Eastern Anatolia, Mediterranean, and Central Anatolia regions. It caused great destruction, damage, and many casualties in Adıyaman and neighboring provinces. This study aims to determine the probable seismic hazard around Adıyaman due to a scenario earthquake in the Akçadag segment (Malatya fault). According to Wells and Coppersmith (1994), an earthquake with a magnitude of Mw 7.3 is expected in the Akçadağ segment, which cause damage in Malatya and the surrounding provinces. The probable earthquake is analyzed with scenario-based seismic hazard analysis by using the earthquake information such as magnitude, lon, lat, dip, and rake angle and Chiou and Youngs 2014 attenuation relationship, by taking into account the ground conditions in the region. The impact of the earthquake on Adıyaman province was analyzed deterministically using OpenQuake, an open-source seismic hazard and risk analysis software. Probable earthquake intensity (PGA, MMI) distribution around Adıyaman for the expected ground motion level is obtained and evaluated. The computational results from this study can help provide a reference for seismic hazard assessment around any region under any probable earthquake scenario.

Keywords: Earthquakes, Southeastern Anatolia, Akçadag Segment (Malatya fault, Seismic Hazard Assessment

[1]**Address:** Civil Engineering Department, Boğaziçi University, İstanbul, Türkiye
[2]**Address:** Mining and Mineral Extraction Department, Adıyaman University, Adıyaman, Türkiye
[3]**Address:** Adıyaman Municipality, Directorate of Zoning and Urbanization, Adıyaman, Türkiye
[4]**Address:** Adıyaman Municipality, Directorate of Reconstruction and Urbanization, Adıyaman, Türkiye
[5]**Address:** Civil Engineering Department, Gebze Technical University, Kocaeli, Türkiye

***Corresponding author**: seyhan.okuyan@boun.edu.tr

1. INTRODUCTION

Turkey is a country located in a region with high earthquake risk and at the intersection of active fault lines. Earthquake is one of the natural disasters that cause the most loss of life and property in Turkey.
The Eastern Anatolia Region has been adversely affected many times by earthquakes on the Eastern Anatolia Fault Line, which was formed as a result of the collision of the Anatolian Plate and the Arabian Plate. Earthquakes in the Eastern Anatolia Region have caused great damage and death. 1939 Erzincan Earthquake, 1976 Çaldıran Earthquake, 1999 Van Earthquake and February 6, 2023 earthquakes are some of the major earthquakes that occurred in the Eastern Anatolia Region. These earthquakes caused thousands of deaths and injuries. Earthquakes in the Eastern Anatolia Region are some of the biggest natural disasters in Turkey. The earthquake risk of the region is high and efforts are being made to reduce this risk.

Adıyaman province is located in a seismically active region. The DAF zone is a 4-25 km wide deformation belt starting from Karlıova (Bingöl) in Eastern Anatolia and extending towards Antakya along a length of approximately 580 km. Within the provincial borders, there are Pazarcık, Erkenek, Pütürge segments of the Eastern Anatolia Fault segment, Gerger and Narince segments of the Southeastern Anatolia Thrust, Besni Fault, Bozava Fault and certain segments of Sürgü Faults. Many earthquakes with magnitudes ranging from 6.7 to 7.8 have occurred in these segments along the DAF and caused severe damage. Earthquake hazard analyses are of great importance in terms of determining the earthquake risk and predicting the possible effects of earthquakes that may occur in the future. In this context, an earthquake hazard analysis was performed for Adıyaman province according to the scenario of an earthquake of Mw 7.3 on the Akçadağ segment of the Malatya Fault, which is located around the borders of Adıyaman province and will remain within the impact area in case of an earthquake (Figure 1). With this study, it is thought that earthquake hazard analysis will provide basic data for disaster management and emergency preparedness in the Disaster Management and Emergency Preparedness phase for Adıyaman province.

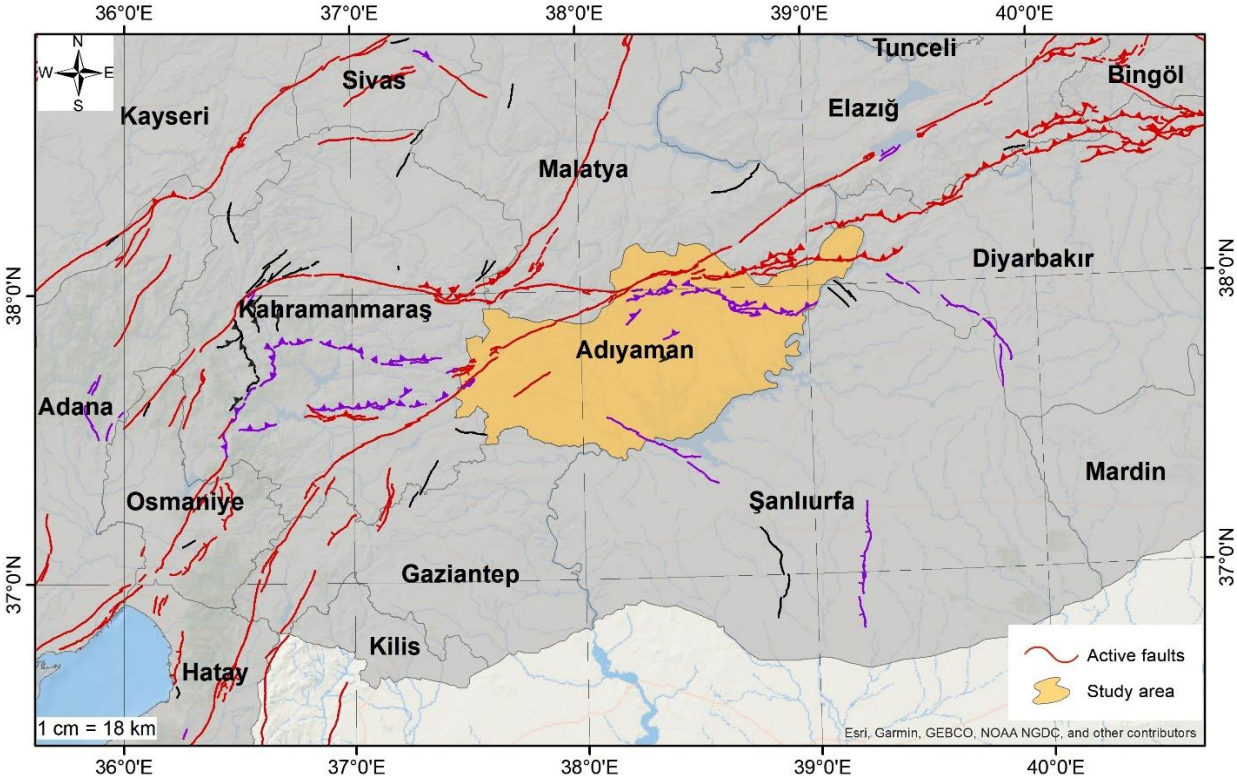

Figure 1. Study area.

2. Seismicity of Adıyaman Province

Adıyaman province is located in the Southeastern Anatolia Region of Turkey and is one of the provinces with high earthquake risk. There are many faults around Adıyaman, especially the Eastern Anatolia Fault Zone, which have the potential to produce earthquakes of 6 or more. In particular, Adıyaman province, located in the Southeastern Anatolia region, has a high risk of seismicity with approximately 420 km of active fault lines passing through the province, especially the DAF and part of the GAB.

According to historical earthquake records, the 20 earthquakes with the most destructive effects are 1822 Antakya Earthquake, 1866 Göynük-Karlıova, 1872 Lake Amik Earthquake, 1874 and 1875 Tortum-Hazar Lake Earthquakes, 1893 Malatya Earthquake, 1457 Erzincan-Erzurum, 1046 Diyarbakır-Elazığ and 242 Osmaniye earthquakes. According to the earthquake records of the instrumental period (1900-present), 917 earthquakes with magnitude 4 and above occurred (Figure 2b). The largest earthquake with a magnitude of 6.9 occurred on August 19, 1966 in Varto district of Muş, which is located on the DAF. 2394 people lost their lives in this earthquake. The last major earthquake on the DAF occurred on January 24, 2020 with a magnitude of 6.8 centered in Elazığ. This earthquake was felt in many provinces in Turkey such as Batman, Bingöl, Çorum, Diyarbakır, Gaziantep, Hatay, Mardin, Osmaniye, Elazığ, Malatya, Kahramanmaraş and Adıyaman. According to the instrumental earthquake records, there are many earthquakes that have had a destructive effect in Adıyaman since 1900. On March 2, 1955, an earthquake with a magnitude of 6.8 occurred in Adıyaman. This earthquake caused serious damage to buildings and infrastructure in the city. On January 24, 1987, an earthquake with a magnitude of 6.1 occurred in Samsat district of Adıyaman. In this earthquake, 62 people lost their lives and hundreds were injured. Throughout the history, the epicenter of which was Adıyaman, there were the 1964 Mw=6.0 Sincik-Adıyaman earthquake and Kızılöz - Samsat-Adıyaman (Mw=5.5) earthquake on March 02, 2017. Finally, the February 6, 2023 earthquakes, which caused major destruction in 11 provinces of Turkey, caused the collapse or heavy damage to approximately 1500 buildings in Adıyaman province. On February 6, 2023, at 04.17 and 13.24 hours local time in Turkey, earthquakes with the epicenters in Pazarcık (Kahramanmaraş) and Elbistan (Kahramanmaraş) with an instrumental magnitude (Mw) of 7.7 and 7.6 occurred. The earthquakes were felt mainly in the provinces of Hatay, Kahramanmaraş, Adıyaman, Malatya, Adana, Şanlıurfa and in the Southeastern Anatolia, Eastern Anatolia, Mediterranean and Central Anatolia regions. The earthquake at 04:17 occurred on the Pazarcık and Amonos segments of the Eastern Anatolia Fault zone. The earthquake at 13:24 occurred on the Çardak fault starting in the southern part of Elbistan. Approximately 5000 earthquakes occurred in the region until 24:00 on July 15, 2023. According to the Shear Wave Velocity Vs(30) map of Adıyaman province, it is seen in Figure 2c that especially the Central and Besni districts have weak ground properties.

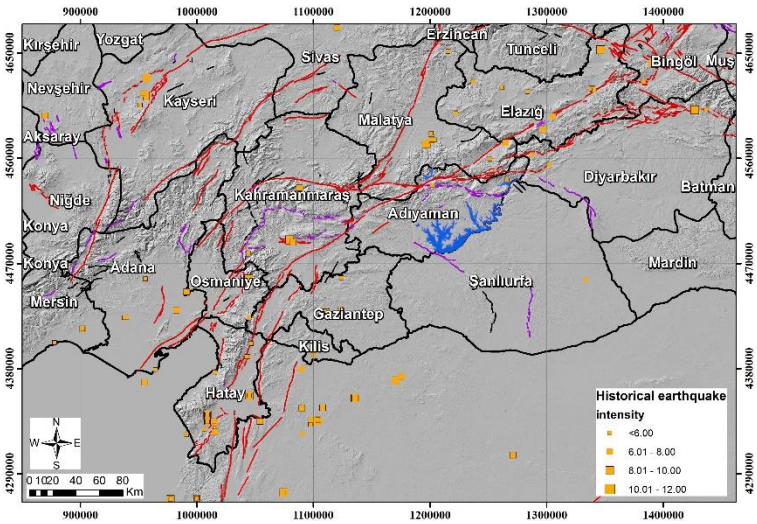

(a)

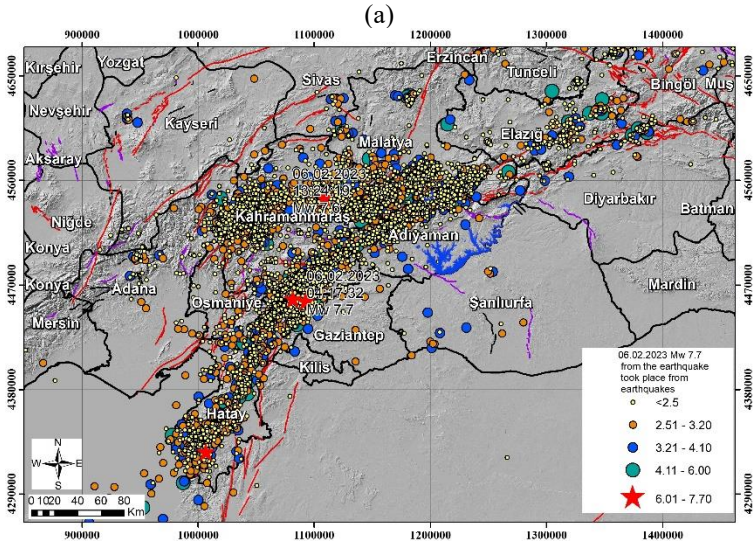

(b)

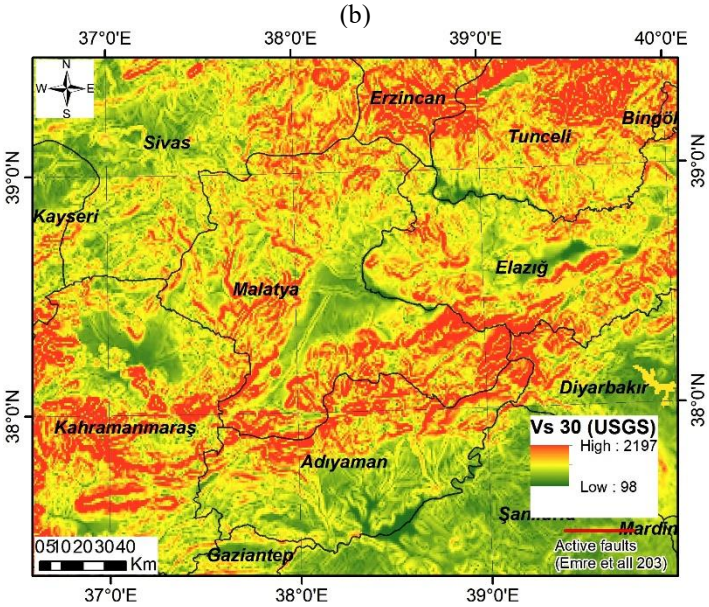

(c)

Figure 2. The earthquakes in and around the province of Adıyaman historical (a), and instrumental earthquake records (b), Vs 30 map (c).

An earthquake with a magnitude of Mw 6.8 occurred in the Sivrice district of Elazığ province at 20:55 on January 24, 2020, at a depth of 8.06 km and lasted for 20.4 seconds around Adıyaman. As seen in the MMI intensity distribution, this earthquake had a magnitude of 7 in Adıyaman (Figure 3a). According to the USGS PGA-MMI relationship, the PGA level of this earthquake in Adıyaman ranges between 0.1-0.3g. On 06.02.2023, two earthquakes of magnitude Mw 7.7 and Mw 7.6 occurred at 04:17 and 13:24, respectively, with epicenters in Pazarcık (Kahramanmaraş) and Elbistan (Kahramanmaraş). The magnitude 7.7 earthquake occurred at a depth of 8.6 km, while the magnitude 7.6 earthquake occurred at a depth of 7 km. These earthquakes also had a devastating impact on the neighboring provinces. The MMI intensity distribution map of the earthquake for Adıyaman province is shown in Fig. Especially in the city center of Adıyaman, the intensity was observed to be between 9-11 on the MMI scale. As a result of the 8 scenario analysis of the second earthquake, Mw7.6 Elbistan earthquake, it was observed that the MMI intensity distribution in Adıyaman region was between 9-10 (Figure 3b).

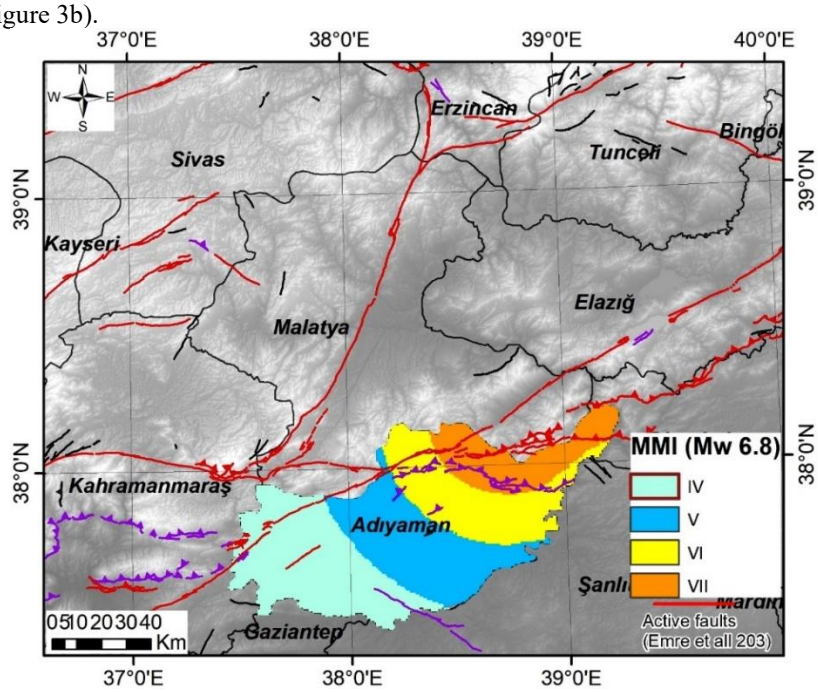

(a)

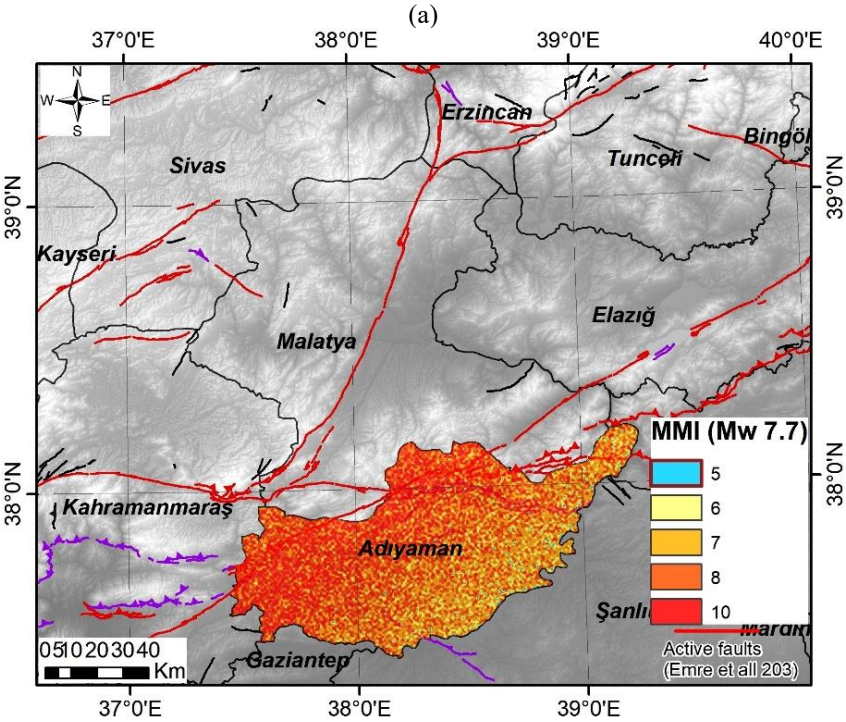

(b)

Figure 1 Elazığ earthquake- Adıyaman province MMI- intensity map (a), Kahramanmaraş-Pazarcık Mw 7.7 earthquake scenario analysis –Adıyaman province MMI distribution map (b).

3. Malatya Fault Tectonics

Malatya Fault consists of 3 segments; Kemaliye segment, Akçadağ segment and Arguvan segment (Emre et al., 2013). This fault line, also referred to as the Malatya - Ovacik fault zone in the literature, constitutes one of the important tectonic structures corresponding to the internal deformation of the Anatolian block during the neotectonic period (Sancar et al., 2017). The fault that forms the eastern boundary of the Malatya plain is a left-trending fault line in the northeast direction. The total length of the fault zone is 176.35 km, of which Akçadağ segment is 74.33 km, Arguvan segment is 40 km and Kemaliye segment is 65.3 km (Figure 5). Each segment has the potential to produce earthquakes of 7 and above.

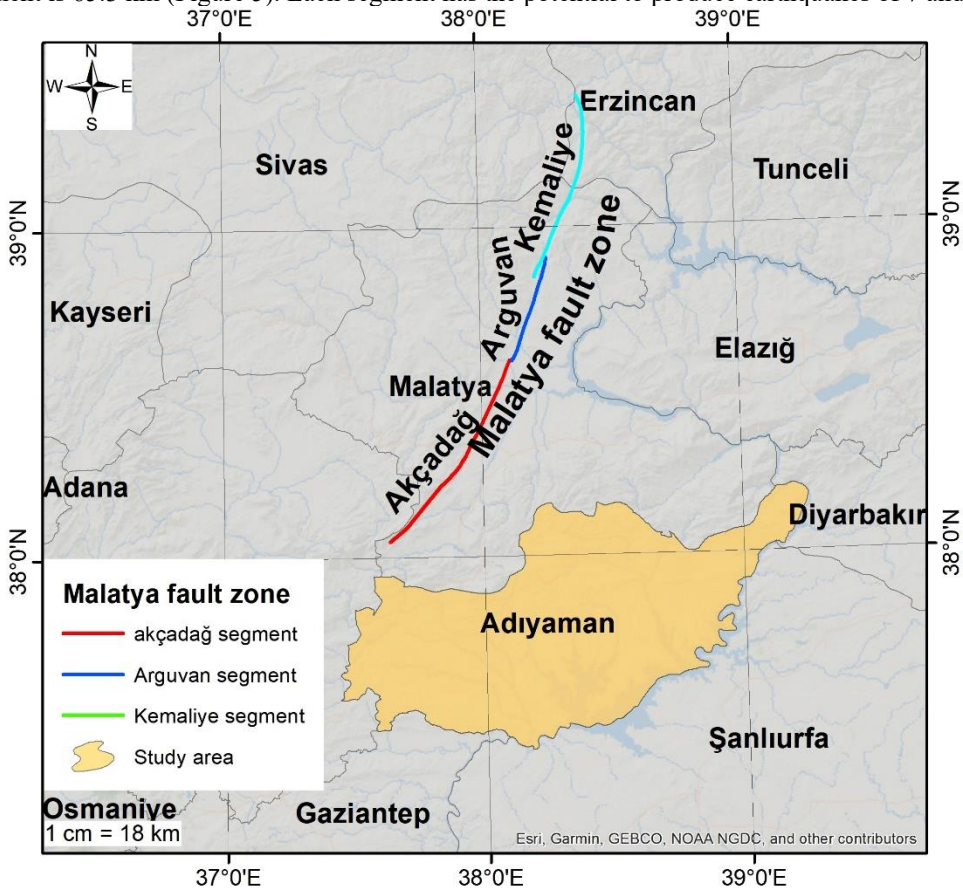

Figure 5. Malatya fault zone and segments (Emre et all 2013).

2. Seismic Hazard Analysis

Within the scope of pre-disaster risk management, disaster scenarios created to determine the existing seismic hazard and to estimate the possible impacts/damages can provide information on the rates and effects of physical, social and economic losses that may occur after the disaster. Determination of earthquake risk requires first determining the possible earthquake hazard in the region. Gürbüz et al. (2000) and Erdik et al.(2004) define earthquake hazard as the probability of occurrence of the largest ground motion caused by an earthquake of a magnitude that may cause damage and loss of life at a certain place and time. There are uncertainties in the location, magnitude and timing of expected earthquakes. Earthquake hazard analyses are pioneering in the design of structures and planning of new settlement areas. Earthquake hazard is realized by probabilistic and deterministic methods. Probabilistic seismic hazard analysis considers the probability that ground motion that may cause damage may occur at a specific location and at a specific time, taking into account uncertainties about the magnitude, location and time of occurrence of the earthquake. In deterministic seismic hazard analyses, the level of ground motion generated by the largest earthquake that may occur in the region is determined by scenario earthquakes. In order to create earthquake scenarios using the deterministic method, the existing live fault lines and the maximum earthquake magnitudes that these fault lines can produce are determined. Probabilistic earthquake scenarios enable the determination of the probable earthquake hazard in the target region. In scenario-based earthquake hazard analysis, possible seismic sources that will affect the region are identified, the closest distance between the source and the study area is calculated, and the possible seismic hazard in the region is calculated by using ground motion prediction equations suitable for the seismic activity of the region (Figure 6). For the scenario, the effect of earthquake

magnitude, earthquake source and ground information on the risk is analyzed. The results obtained from the scenario analysis will enable us to see the disaster response and recovery capacity of the region.

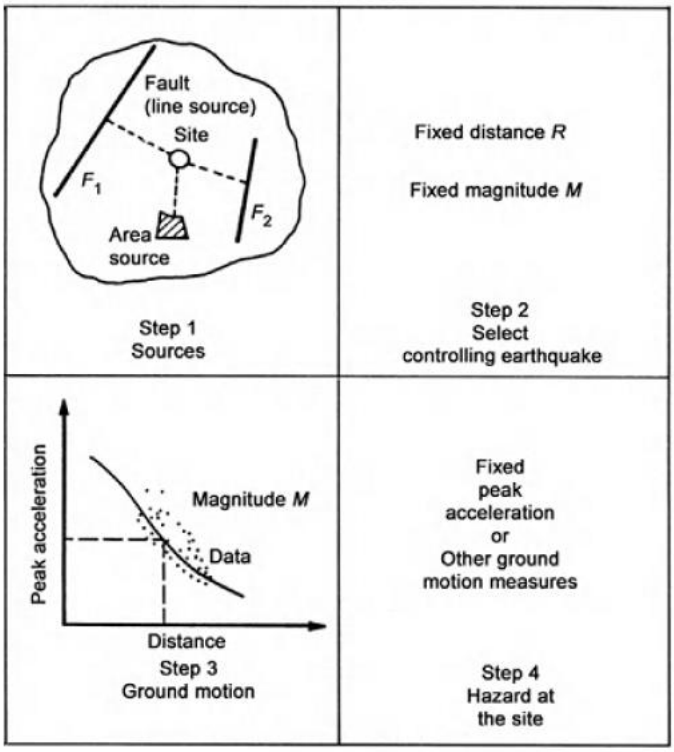

Figure 6. Sceanrio seismic hazard analysis steps (Marmureanu et al.(1993)).

Within the scope of the study, an earthquake scenario was created to predict the damage that may occur as a result of a possible earthquake in the Akçadağ segment located in Malatya province with scenario-based modeling using the OPENQUAKE simulation program (Pagani et al.,2014). The results of the analysis are important in terms of estimating the losses that may occur after a possible earthquake.

Malatya province is located in the 1st-degree earthquake zone according to the earthquake zones map of Turkey. The DAF (Eastern Anatolian Fault), which has caused past and future earthquakes in and around Malatya, extends along the Hazar-Sincik, Çelikhan-Gölbaşı and Sürgü Faults. Since the earthquake magnitude, one of the uncertainties of the earthquake is assumed to be the worst-case scenario, the magnitude of the earthquake is assumed to be Mw 7.3 in this study. The impact of this earthquake on Adıyaman province was determined by earthquake hazard analysis.The OpenQuake Engine open-source software written in the Python programming lan-guage software provides calculation and assessment of seismic hazard, risk and decision-making tools via the data, methods and standards that are being developed by GEM (Global Earthquake Model) and its collaborators (Pagani et al.,2014).

The scenario analysis of a possible Mw 7.3 earthquake on the Akçadağ segment of the Malatya Fault was defined in the OpenQuake platform. The fault and the possible earthquake epicenter are shown in Figure 7. In the scenario earthquake hazard analysis, Chiou and Youngs (2014) ground motion prediction equation, which is generally used for Turkey, was used. The PGA distribution in Adıyaman province as a result of the earthquake scenario is shown in Figure 7. Figure 8 shows the MMI distribution. The expected PGA level in the north of Adıyaman reaches 0.4g. As seen in the MMI distribution, the MMI reaches 7 in the north of Adıyaman. According to the USGS MMI-PGA table (Chock et al.,2006), the PGA value corresponding to MMI 7 corresponds to approximately 0.35g.

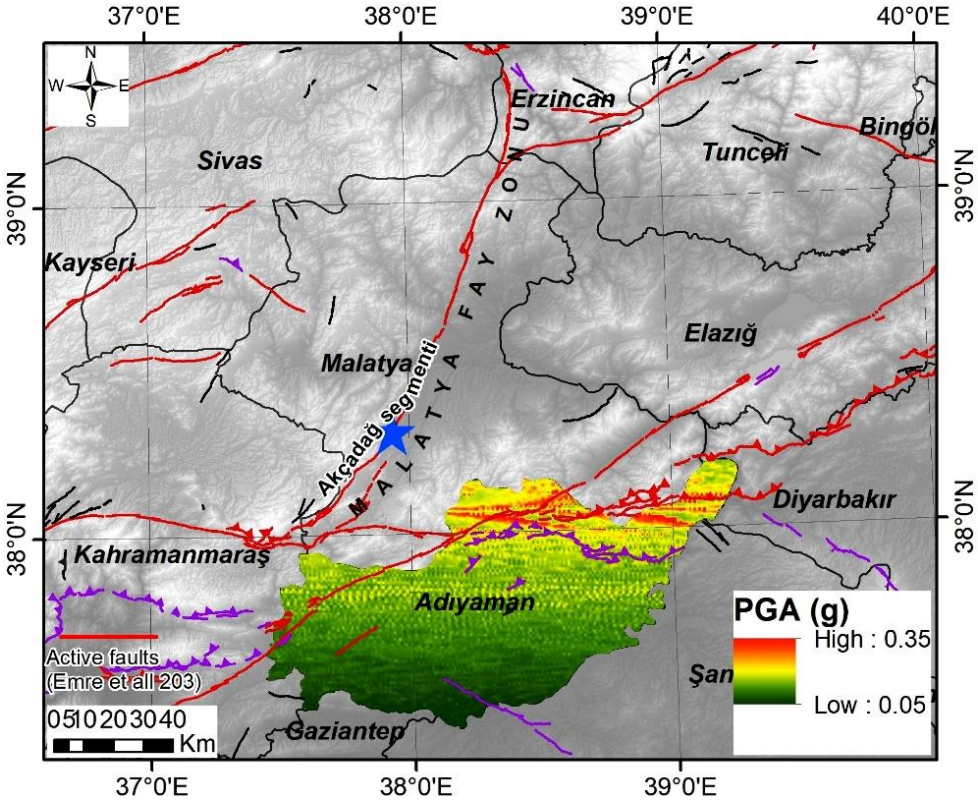

Figure 7. Scenario seismic hazard analysis-PGA distribution map.

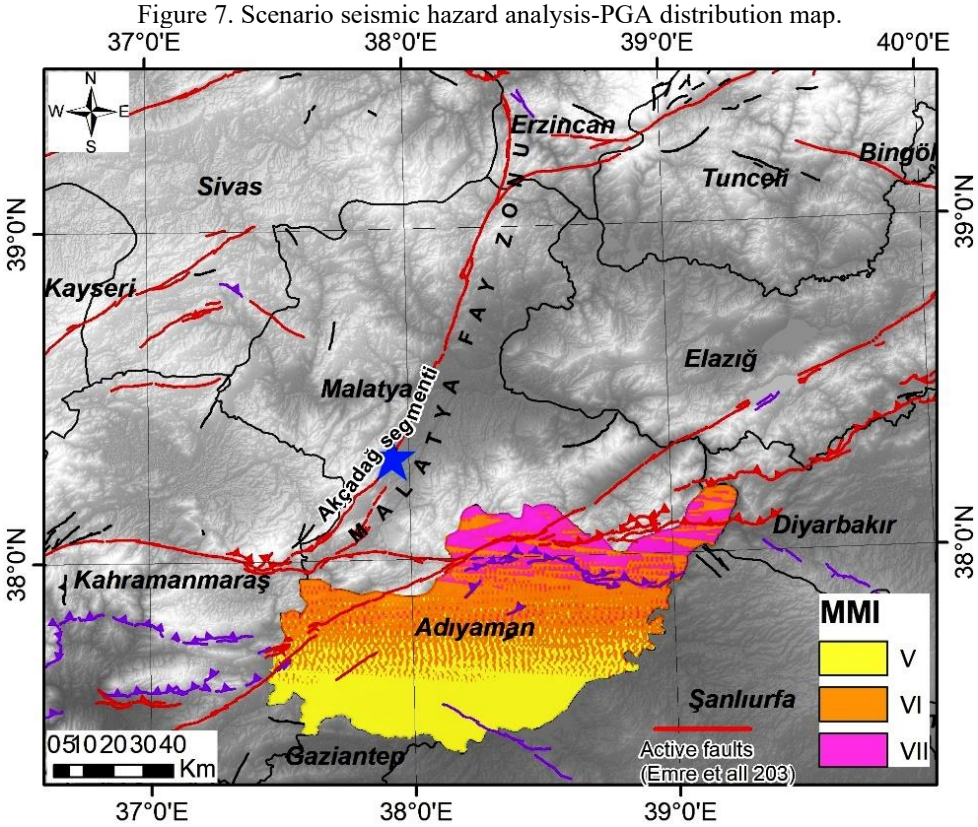

Figure 8. Scenario seismic hazard analysis-MMI distribution map

3.Conclusion

Adıyaman and its surroundings are one of the regions with high earthquake hazard. Therefore, it is important to be aware of the earthquake risk and to take measures to prevent the destructive effects of earthquakes. At the same time, informing

and educating the public about earthquake awareness and disaster management can help minimize post-earthquake damages. Especially in construction processes, earthquake hazard should be taken into consideration and buildings should be built in accordance with earthquake regulations. Thus, the possible effects of earthquakes can be minimized and a safe living space can be created. In the event of a 7.3 magnitude earthquake on the Akçadağ segment, one of the sub-segments of the Malatya fault, which is one of the important seismic gaps in the region, it is seen that the earthquake hazard continues throughout the province according to the maximum ground acceleration and intensity distribution analyzes for Adıyaman. As a result, it is thought that the results obtained from this study will form an important basis for risk assessments to be made in the region.

Author Contributions

The authors carried out joint studies at every stage of the manuscript. All authors have read and agreed to the published version of manuscript.

REFERENCES

Chiou, B. S. J., & Youngs, R. R. (2014). Update of the Chiou and Youngs NGA model for the average horizontal component of peak ground motion and response spectra. Earthquake Spectra, 30(3), 1117-1153.

Chock, G., Robertson, I., Nicholson, P., Brandes, H., Medley, E., Okubo, P., ... & Holmes, W. (2006). Compilation of observations of the October 15, 2006, Kiholo Bay (Mw 6.7) and Mahukona (Mw 6.0) earthquakes, Hawaii. Earthquake Engineering Research Institute, 31, 1-53.

Emre, Ö., Duman, T.Y., Özalp, S., Elmacı, H., Olgun, Ş. and Şaroğlu, Ş., 2013. Active fault map of Turkey.

Erdik, M., Demircioglu, M., Sesetyan, K., Durukal, E., & Siyahi, B. (2004). Earthquake hazard in Marmara region, Turkey. Soil Dynamics and Earthquake Engineering, 24(8), 605-631.

Gurbuz C, Aktar M, Eyidogan H, Cisternas A, Haessler H, Barka A, Ergin M, Turkelli N, Polat O, Ucer B, Kuleli S, Baris S, Kaypak B, Bekler T, Zor E, Bicmen F, Yoruk A. The seismotetonis of the Marmara region (Turkey): results from a microseismic experiment. Tectonophysics 2000;316:1–17.

Marmureanu, G., Cioflan, C. O., Marmureanu, A., Ionescu, C., & Manea, E. F. (1993). Bridging the Gap Between Nonlinear Seismology as Reality and Earthquake Engineering. Perspectives on European Earthquake Engineering and Seismology, 218, 409.

Pagani, M., Monelli, D., Weatherill, G., Danciu, L., Crowley, H., Silva, V., ... & Vigano, D. (2014). OpenQuake engine: An open hazard (and risk) software for the global earthquake model. Seismological Research Letters, 85(3), 692-702.

Sançar, T., Zabcı, C., Karabacak, V., Yazici, M., Akyuz, H. S., (2019). Geometry and Paleoseismology of the Malatya Fault (Malatya-Ovacık Fault Zone), Eastern Turkey: Implications for intraplate deformation of the Anatolian Scholle. Journal of Seismology. 23. 319-340. 10.1007/s10950-018-9808-z.

Development and analysis of a solar PV/T and wind-based system for power and freshwater generation; a comprehensive thermodynamic assessment

Fatih Yılmaz[*1]

Abstract: One of the important ways to struggle with global warming and environmental challenges is the effective use of renewable energy resources. In this context, solar energy is almost the basis of renewable energy sources. It is also noted that humanity is required clean and drinkable water as well as a clean energy source. That is the clean water scarcity is been in many counties around the world. Therefore, this study examines the design and analysis of a solar and wind-powered model for clean electricity and water generation. This work comprises of a solar photovoltaic thermal (PV/T) subsystem, wind turbines, an Organic Rankine cycle with the R32 refrigerant, and a reverse osmosis (RO) desalination unit. The thermodynamic performance investigation is conducted by applying the energy and exergy efficiency methods. Also, to define the system performance change versus some different factors, a parametric study is done. Based on analysis results, total energy generation and fresh water capacity are computed as 341.7 kW and 2.08 kg/s. The energetic and exergetic efficiency of the developed study is determined as 37.60 % and 39.75%.

Keywords: Energy, exergy, solar, PV/T, thermal, wind

[1]**Address:** Department of Mechatronics Engineering, Faculty of Technology, Isparta University of Applied Sciences, Isparta Türkiye

***Corresponding author**: fatiyilmaz7@gmail.com

1. INTRODUCTION

Energy demand is increasing day by day due to many factors such as population growth, industrial development, and industrialization. It is a fact that fossil fuels are still preferred to meet this increasing demand. In this case, as a result of the use of carbon-based fuels, global warming and acid rain, etc., which are expressed as environmental problems, arise (Venkatesh et al., 2022). For the future of the globe, these environmental problems must be elaborate and destroyed, and at this point, renewable energy sources are coming to the fore, because renewable energies have many advantages, for example, there is no emission and independence from other countries. Among these resources is an plentiful primary energy source that can be used in cost-effective and reliable ways for thermodynamic cycles in solar energy plants, as well as for electrical power generation for heating or cooling purposes (Herrando et al., 2023). Moreover, Solar and wind energy can be an appreciated source of sustainable energy with insignificant environmental challenges (Hossain et al., 2022).

Another important aspect is that concerns about worldwide water accessibility and effects have been stated in recent years using the worrying terms “global water crisis” and “water scarcity” (Dhakal et al., 2022). Parallel to global warming, people's access to clean water is getting harder day by day and water shortages are emerging. For this reason, especially for today and for the future, using renewable energy technologies and manned needs such as clean water is one of the most fundamental issues that need to be solved. For this motive, numerous academic trainings and projects have been carried out in these fields in the literature in recent years and active studies are continuing. In 2023, for zero-emission hydrogen generation, Zaik and Werle (2023) proposed a solar and wind energy system for electrolysis. They used a proton exchange membrane to generate clean hydrogen. They determined that PEM is generate an average 158.1 cc/min of hydrogen with efficiency 69.87%. Bamisile et al. (2023) illustrate an analysis of the solar-wind-geothermal assisted multigeneration system for cleaner products. Their proposed system’s energetic and exergetic efficiencies are 48.61% and 88.31%, respectively. Sherwani (2022) examines the assessment of the solar energy-based ORC-refrigeration cycle. For more details, some recent studies are presented here (Hassan et al., 2022; Mousavi et al., 2022; Abu-Rayash and Dincer 2023; Ata et al., 2023; Wu et al., 2023).

This study deals with the clean and sustainable power and freshwater generation employed by solar and wind energy sources. Also, the thermodynamic performance analysis is conducted with energy and exergetic efficiency methods. Moreover, the system is investigating the efficiency aspects and also the irreversibility rate.

2. SYSTEM DEFINITION AND ANALYSIS

The suggested plant is presented in Figure 1 which is the layout of the developed cycle, for power and freshwater generation. The system consists of a series of PV/T collectors for generating both power and heat, a series of wind turbines that generate power, an ORC plant for power, and finally RO technology for freshwater generation.

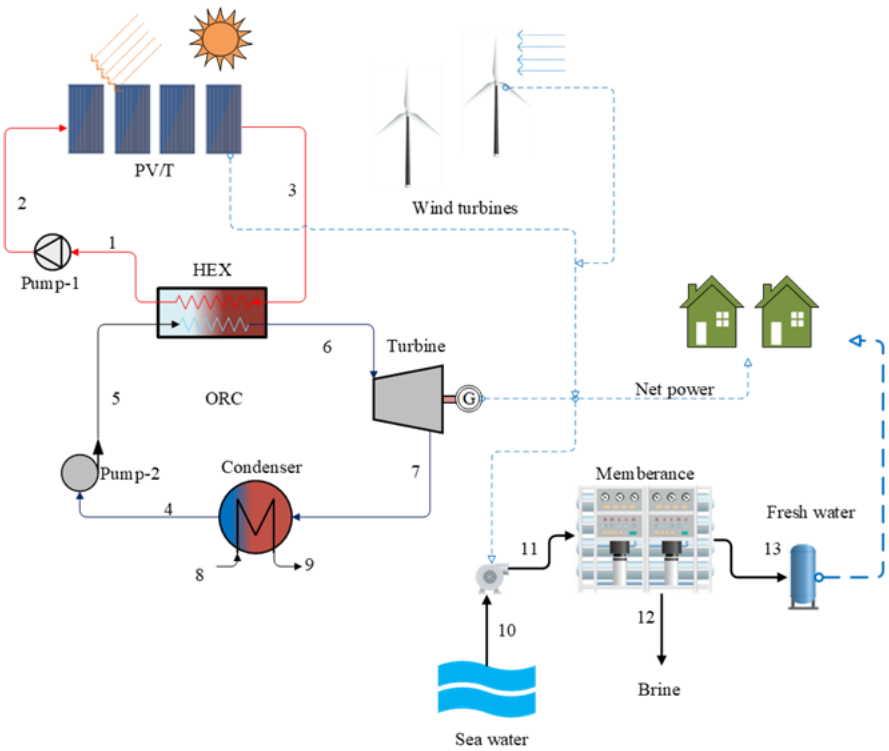

Figure 1. A schematic flow chart of the proposed system

The power is generated by PV/T and ORC units and the freshwater is also produced by the RO unit. The required electrical power of the RO unit is met with the ORC system. Here, a hybrid model for solar and wind has been designed and analyzed. Before performing the thermodynamic analysis, some assumptions made for the system can be listed below;

- The system works in steady-state conditions.
- Turbines and pumps have isentropic efficiency
- Solar flux is constant 600 W/m^2
- The working fluid of the ORC is selected R32.
- Sea water inlet temperature is assumed 30 ℃.
- Dead state temperature and pressure are taken into 25 ℃ and 101.325 kPa.

This study has been extensively investigated from a thermodynamic perspective and a series of examines have been carried out. Moreover, the system design and assumed constraints are presented in Table 1.

Table 1. System design and inputs boundaries

Parameters	Unit	Value
PV/T subsystem		
Solar radiation	W/m^2	600
PV reference temperature	℃	25
Optic efficiency of PVT	%	90
PV reference temperature coefficient	1/K	0.0045
Number of PV	-	20
Wind speed	m/s	3.5
Working fluid	-	Therminol_72
ORC		
Working fluid	-	R32
Pump inlet pressure	kPa	1697
Pump pressure ratio	-	3
Pump inlet temperature	℃	Saturated liquid at P4 pressure
Pinch point temperature	℃	8
Turbine isentropic efficiency	%	88
Reverse osmosis		
T_{sea}	℃	30
P_{sea}	kPa	101.325
Sea water inlet mass rate	kg/s	5.2
Sea water salinity rate	ppm	42000
Bine salinity rate	ppm	70000

For thermodynamic calculations, the equilibrium equations-mass, energy, entropy, and exergy- as below are handled separately and applied to each component (Cengel and Boles, 2015; Bejan et al., 1995; Dincer, 2020);

$$\sum \dot{m}_{in} = \sum \dot{m}_{out} \tag{1}$$

$$\sum \dot{m}_{in}\, h_{in} + \sum \dot{Q}_{in} + \sum \dot{W}_{in} = \sum \dot{m}_{out}\, h_{out} + \sum \dot{Q}_{out} + \sum \dot{W}_{out} \tag{2}$$

$$\sum \dot{m}_{in}\, s_{in} \sum \left(\frac{\dot{Q}}{T}\right) + \dot{S}_{gen} = \sum \dot{m}_{out}\, s_{out} \tag{3}$$

$$\sum \dot{m}_{in}\, ex_{in} + \dot{Ex}_{in}^{\dot{Q}} + \dot{Ex}_{in}^{\dot{W}} = \sum \dot{m}_{out}\, ex_{out} + \dot{Ex}_{out}^{\dot{Q}} + \dot{Ex}_{out}^{\dot{W}} + \dot{Ex}_{D} \tag{4}$$

In these equations, the sub terms of "in" and "out" describe the inlet and outlet flow of the state. Also, $\dot{m}$ is mass flow rate, $\dot{Q}$ is heat transfer rate and $\dot{W}$ is work rate. After that ex is define the specific exergy flow. The generated power from the solar and wind turbine can be formulated as;

$$\dot{W}_{PVT} = G \times A_{PVT} \times \eta_{PVT} \times n_{PVT} \tag{5}$$

where G is the solar flux rate, A_{PVT} is the area of PVT unit, η_{PVT} is the efficiency of the PTV and n_{PVT} is the number PVT units.

$$\dot{W}_{wt} = 1/2 \times \rho_{air} \times C_p \times n_{wt} \times A \times V^3 \tag{6}$$

here C_p is the Betz limit, n_{wt} is the number of wind turbines, A is the swept area and V is the wind speed. To sum up, the energetic and exergetic efficiency of the total plant can be modeled as;

$$\eta_{total} = \frac{\dot{W}_{net} + \dot{m}_{fw} h_{fw}}{\dot{Q}_{solar} + \dot{W}_{wt,ava}} \tag{7}$$

$$\psi_{total} = \frac{\dot{W}_{net} + \dot{m}_{fw} ex_{fw}}{\dot{Ex}_{Q,solar} - \dot{W}_{wt,ava}} \tag{8}$$

3. RESULTS AND DISCUSSION

With the above declared in Table 1 assumptions and system parameters, the thermodynamic analysis is conducted and the main findings are offered in Table 2. The power production rate of the PV/T and wind turbine are 5.037 kW and 315.8 kW, respectively. Also, the freshwater production size is determined as 2.08 kg/s. As finally, the total energetic and exergetic efficiency of the developed schema is 37.60% and 39.75%, respectively.

Table 2. Analysis results of the developed plant

Parameters	Unit	Value
PVT power rate	kW	5.037
PVT thermal energy rate	kW	81.38
Wind turbine power rate	kW	315.8
Net power rate	kW	341.7
Freshwater generation rate	kg/s	2.08
Efficiencies		
η_{ORC}	%	23.44
ψ_{ORC}	%	51.37
$\eta_{overall}$	%	37.60
$\psi_{overall}$	%	39.75

After the main results, parametric analysis was performed to examine the effects of system parameters. Figure 2 and Figure 3 examine the variation of net power generation and thermal losses in a PV/T system versus solar radiation value. According to Figure 2, a rise of 200 W/m2 in solar radiation increases the net electricity production from 338 kW to 344 kW. However, it is seen in Figure 3 that the losses in the PV/T system increase in response to this increase.

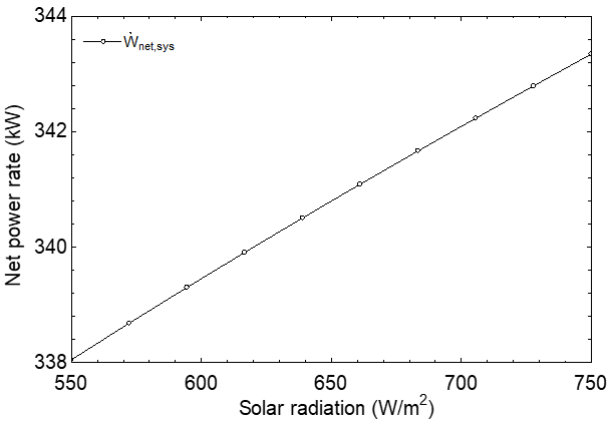

Figure 2. The effect of solar flux on net power production rate

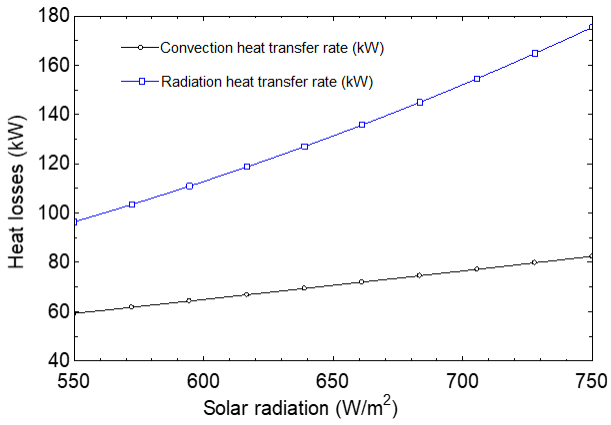

Figure 3. Impact of solar flux on the heat losses

The increase in work and thermal energy from the PV/T module relative to the increase in solar radiation is presented in Figure 4. The increase in radiation increases the useful products obtained from the PV/T module. Then, the negative effect of the increase in solar irradiance on the performance of the whole system is seen in Figure 5. Both the energy and exergy performance of the whole system increases negatively as a result of the losses in the PV/T. The reason for this efficiency drop can be expressed as the thermal losses pictured above (Figure 3).

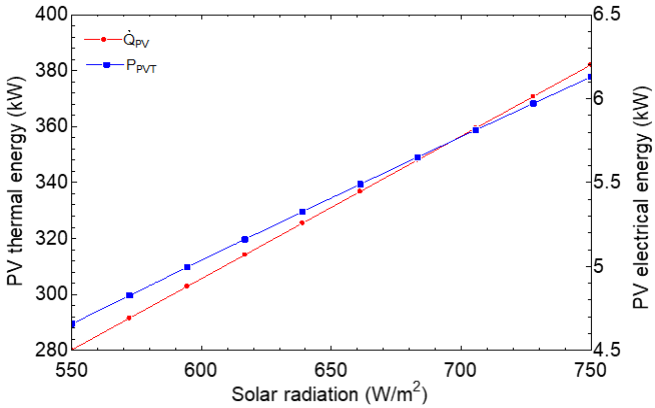

Figure 4. Effect of the solar radiation on the PV/T thermal and power rate

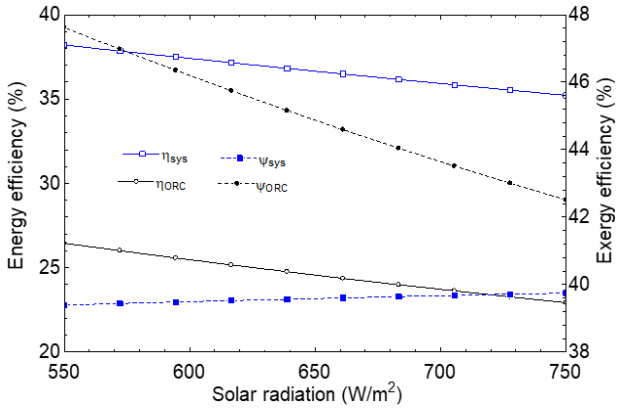

Figure 5. Influence of solar flux on the developed system's performance

Another important parameter is wind speed variation. Figure 6 shows the goes up in the net power and wind turbine capacity produced by the increase in wind speed from 2 m/s to 12 m/s. Parallel to this increase, Figure 7 shows a linear increase in the designed system performance with increasing wind speed. Up to a certain speed limit, the increase in wind speed rises the net work obtained from the model and also the system's performance.

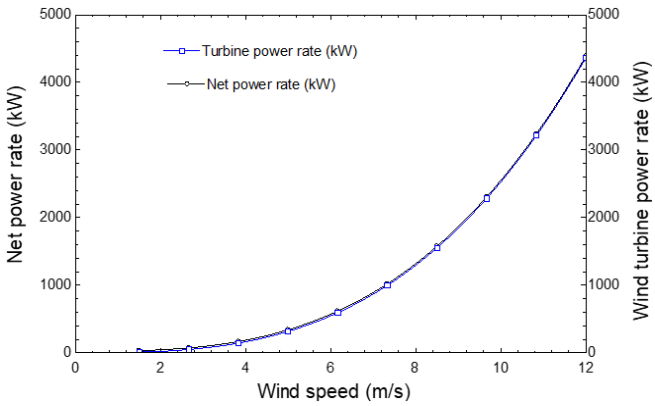

Figure 6. Variations of net power and wind turbine power rate vs wind speed

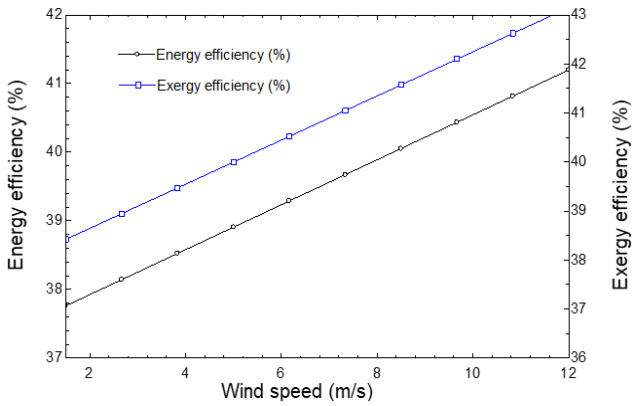

Figure 7. Variations of the system's performance vs wind speed

Figure 8 examines the impact of the HX pinch point temperature on the developed system's efficiency. When the HX pinch point temperature increases from 2 °C to 22 °C, the developed system's performance that is energy and exergy efficiencies are decreases. It is noted that the high difference the temperature of pinch point is means of increasing the irreversibility rate of HX and then decreasing the plant's performance.

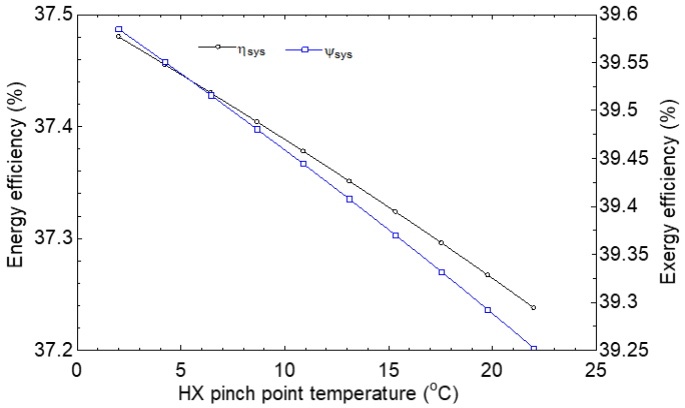

Figure 8. Variations of the developed system's performance with HX pinch point temperature

4. CONCLUSION

In this developed study, a solar and wind energy supported a hybrid model is designed and proposed for production of clean power and potable water. This system entails of a solar PV/T unit, an ORC, wind turbines and RO unit. Comprehensive thermodynamic performance analysis is also conducted to determine the system's performance in light of the energy and exergy efficiency methods. Moreover, the exergy destroyed analysis performed to define the system irreversibility. According to analyses results, the main conclusions can be drawn as below;

- The generated power and fresh water rate are determined as 341.7 kW and 2.08 kg/s, respectively.
- The power and thermal energy generation capacities of the PV/T system are 5.037 kW and 91.83 kW, respectively.
- Energy and exergy efficiencies are computed as 23.44% and 51.37%, for the ORC subsystem
- Energy and exergy efficiency of the total system are to be 37.60% and 39.75%, respectively.

REFERENCE

Abu-Rayash, A., & Dincer, I. (2023). Development and assessment of an integrated wind-solar based energy system for sustainable communities. *Energy Conversion and Management*, *277*, 116680.

Ata, S., Köse, Ö., Tutumlu, H., Yağlı, H., Koç, Y., & Koç, A. (2023). Which power cycle is the best fit for parabolic trough solar collectors? A comparative and comprehensive case study for six sub-configurations of the three main cycles. *Energy Conversion and Management*, *291*, 117338.

Bamisile, O., Cai, D., Adedeji, M., Dagbasi, M., Li, J., Hu, Y., & Huang, Q. (2023). Thermo-enviro-exergoeconomic analysis and multi-objective optimization of a novel geothermal-solar-wind micro-multi-energy system for cleaner energy production. *Process Safety and Environmental Protection*, *170*, 157-175.

Bejan A, George T, Moran MJ. Thermal design and optimization. Wiley; 1995.

Cengel YA, Boles MA. Thermodynamics: an engineering approach. 8th ed. Mc. New York: McGraw-Hil;2015; 2015. Dhakal, N., Salinas-Rodriguez, S. G., Hamdani, J., Abushaban, A., Sawalha, H., Schippers, J. C., & Kennedy, M. D. (2022).

Is desalination a solution to freshwater scarcity in developing countries?. *Membranes*, *12*(4), 381.

Dincer I. Thermodynamics: A Smart Approach. USA: John Wiley & Sons Ltd; 2020.

Hassan, A. A., Elwardany, A. E., Ookawara, S., Sekiguchi, H., & Hassan, H. (2022). Energy, exergy, economic and environmental (4E) assessment of hybrid solar system powering adsorption-parallel/series ORC multigeneration system. *Process Safety and Environmental Protection*, *164*, 761-780.

Herrando, M., Wang, K., Huang, G., Otanicar, T., Mousa, O. B., Agathokleous, R. A., ... & Markides, C. N. (2023). A review of solar hybrid photovoltaic-thermal (PV-T) collectors and systems. *Progress in Energy and Combustion Science*, *97*, 101072.

Hossain, F., Karim, M. R., & Bhuiyan, A. A. (2022). A review on recent advancements of the usage of nano fluid in hybrid photovoltaic/thermal (PV/T) solar systems. *Renewable Energy*, *188*, 114-131.

Mousavi, S. A., Mehrpooya, M., & Delpisheh, M. (2022). Development and life cycle assessment of a novel solar-based cogeneration configuration comprised of diffusion-absorption refrigeration and organic Rankine cycle in remote areas. *Process Safety and Environmental Protection*, *159*, 1019-1038.

Sherwani, A. F. (2022). Analysis of solar energy driven organic Rankine cycle-vapor compression refrigeration system. *Thermal Science and Engineering Progress*, *35*, 101477.

Venkatesh, T., Manikandan, S., Selvam, C., & Harish, S. (2022). Performance enhancement of hybrid solar PV/T system with graphene based nanofluids. *International Communications in Heat and Mass Transfer*, *130*, 105794.

Wu, J., Li, R., Xiang, Y., Wang, S., Wang, L., & Li, Q. (2023). Quantitative sustainability assessment and sensitivity analysis for a solar-driven combined heating and power system integrated with organic Rankine cycle and ground source heat pump. *Applied Thermal Engineering*, *220*, 119722.

Zaik, K., & Werle, S. (2023). Solar and wind energy in Poland as power sources for electrolysis process-A review of studies and experimental methodology. *International Journal of Hydrogen Energy*, *48*(31), 11628-11639.

Classification of mechanical faults in electric motors based on power spectral density of vibration signal

Yunus Emre Acar[1*]

Abstract: Unplanned shutdowns caused by mechanical and electrical failures of electric motors are among the most significant and preventable losses in manufacturing facilities. In the past few decades, the subject of preventive and predictive maintenance has attracted the intense interest of many researchers. Several studies have demonstrated that vibration, sound, temperature, and some electrical quantities of electric motors contain information about the current and potential faults. Extracting the best distinguishing feature by various methods is one of the significant issues in the field. This study focuses on the vibration signals corresponding to healthy operation and five distinct fault conditions in electric motors, like imbalance, misalignments, and bearing malfunctions. The effectiveness of measurements taken from 3-axis accelerometers placed in two different positions has been examined to classify these six cases. The power spectral densities of the vibration signals have been extracted to input for commonly employed machine learning algorithms. The performances of the machine learning methods have been presented comparatively. According to the results, one vibration signal recorded from the radial axis is adequate to distinguish the subjected mechanical faults with accuracies over %98.

Keywords: Electric motor, classification, machine learning, power spectral density, predictive maintenance, vibration.

Address: Selcuk University, Faculty of Technology, Konya/Türkiye
Corresponding author: yacar@selcuk.edu.tr

1. INTRODUCTION

Electric motors are among the most crucial components of today's industry. Owing to converting electrical energy into mechanical energy places electric motors at the heart of mobility in industry and at the core of mass production. An average of 70% of the energy consumption of electrical motors in production plants indicates their pivotal role (Saidur, 2010). Given their critical position, preventing failures in electric motors is one of the primary challenges in the industry. Companies must define their most suitable maintenance strategy for this purpose. In the literature, maintenance activities are categorized into three main titles: corrective, preventive, and predictive maintenance.

Corrective maintenance refers to repairing or replacing faulty equipment after a failure has occurred. This approach can be preferred when the repair or replacement is quickly completable, the failure does not significantly impact overall system operations, and the time required to address the malfunction isn't overly lengthy.

In contrast, preventive maintenance represents actions taken to prevent or delay a failure. It's crucial that breakdowns do not coincide with critical periods, especially when production is intensive. Based on the statistically determined usable life of the equipment, maintenance or replacement should be conducted before any failure occurs. However, the excess personnel in facilities, spare parts inventory, and early replacement or maintenance makes the approach inefficient.

Lastly, predictive maintenance enables personalized maintenance for equipment by continuously or periodically monitoring them using various sensors. It provides detection before a failure occurs or reaches a critical level and offers insights into the progression of the malfunction. When compared to preventive maintenance, many studies have highlighted the superiority of predictive maintenance because it does not require keeping excess personnel and spare parts on standby and prevents overly premature action taking. (Popescu et al., 2022; Ran et al., 2019; Vafaei et al., 2019). Selçuk has illustrated the preeminence of predictive maintenance over preventive maintenance using a critical example (Selcuk, 2017). She attracts attention to the failure time of previously tested identical bearings spanning a wide range, from 15 to 300 hours. As can be inferred from the example, a maintenance activity planned based on an average lifespan calculated statistically will not prevent failures for all bearings. When considering the shortest endurance time, maintenance would have to be performed much earlier than the lifespan for some.

For predictive maintenance activities of electric motors, two distinct approaches emerge: current-based and vibration-based. While current-based methods stand out for not requiring direct mounting on the electric motor and being

facilitated by inexpensive current sensors, vibration-based ones offer early diagnosis opportunities, especially for vibrations caused by mechanical failures. The techniques used in both methods are very analogous and with the base of time-frequency transformation.

The frequency content of the recorded signals is extracted using spectral methods such as Fast Fourier Transform (FFT) (Borghesani et al., 2013), Short-Time Fourier Transform (STFT) (Yu, 2019), wavelet-based methods (Al-Badour et al., 2011) autoregressive moving average (ARMA) (Chukwuekwe et al., 2016), and Power Spectral Density (PSD) (Yi et al., 2022).

The extracted frequency information is provided to classifiers directly or through additional feature extraction approaches. As the first step of predictive maintenance, failure classification is realized at the stage of the classifier output. Later on, predicting the progression of the malfunction and preparing a maintenance plan based on the progression and system priorities culminate the whole process.

In this study, the focus has been on the classification of failures, which is the initial phase of predictive maintenance. Section 2 explains the data and method used for the mentioned purpose. The results are discussed comparatively in Section 3. Finally, Section 4 concludes the study.

2. MATERIAL AND METHOD

Fault types in electrical machines are fundamentally divided into mechanical and electrical. Principal electrical faults include short circuits, open circuits, and ground faults in windings. Additionally, rotor bars can experience wear, cracks, and breaks. On the other hand, wear and deformations in bearings, misalignments, and eccentricity are common mechanical faults.

An electrical machine fault dataset (Riberio, 2016) containing data for one healthy and five different mechanical fault classes is subjected in this paper. The dataset includes vibration signals obtained by two three-axis accelerometers for the faults of horizontal misalignment, vertical misalignment, bearing malfunctions for two locations, imbalance errors, and a normally operating case (Marins et al., 2018). Healthy working data class involves vibration signals for 49 speeds between 737 rpm and 3686 rpm. The vibration data for 44 revolutions create 333 imbalance data classes for imbalance states originating with seven independent weights ranging from 6g-35g. The number of data for horizontal and vertical misalignments created by sliding the motor shaft is respectively 197 and 301. Data for bearing faults are recorded in two different classes based on the position where the faulty bearing is placed. Vibration signals for bearing faults are recorded with consciously created imbalances to make them practically detectable. There are 558 data for the underhang position, where the bearing is between the motor and the rotor, and 513 data for the overhang position, where the rotor is in the middle. A visual of the experimental setup is shown in Figure 1.

The six vibration signals recorded axially, radially, and tangentially for two positions were evaluated separately. Each vibration signal, sampled at a 50 KHz sampling rate and recorded as 5 seconds, was divided into 1-second sections. Each of these one-second vibration signals has been considered a separate signal, thus increasing the dataset size fivefold. The number of data for each class in the reorganized dataset is given in Table 1.

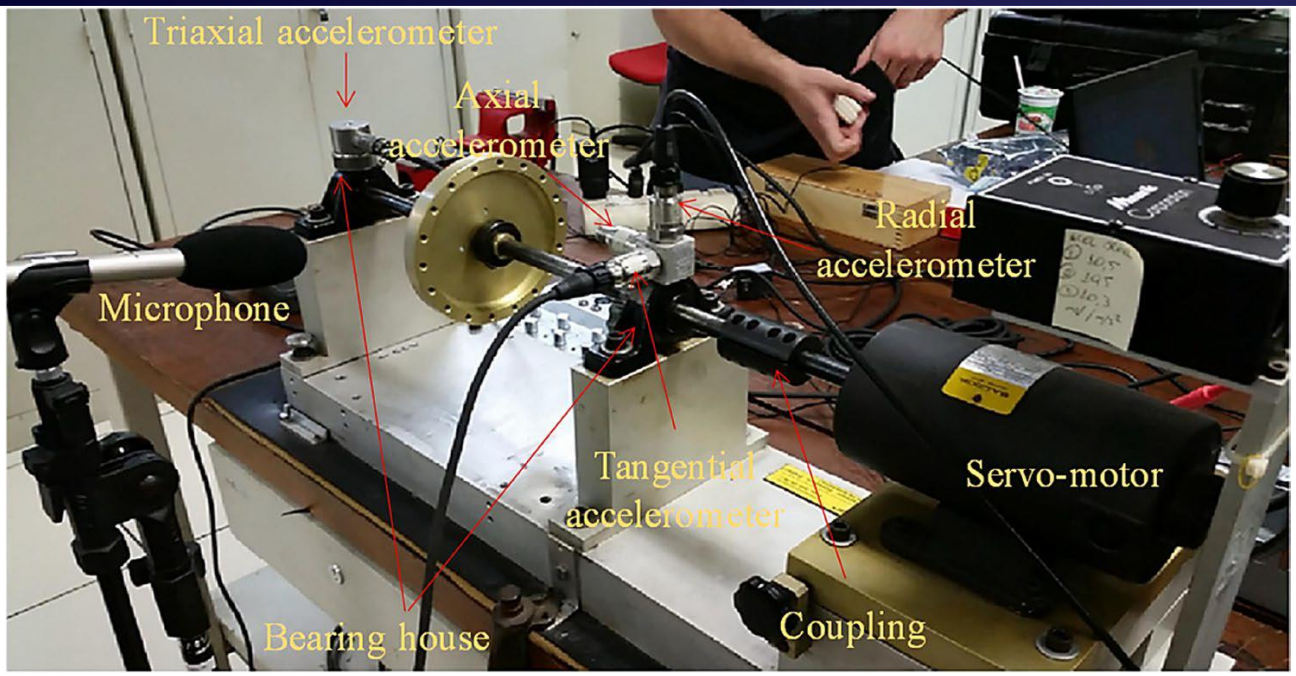

Figure 1. SpectraQuest Experimental Testbench System (Marins et al., 2018)

Table 1 Amount of data per each class

Class	Number of data
Horizontal misalignment	197x5=985
Imbalance	333x5=1665
Normal	49x5=245
Overhang	513x5=2565
Underhang	558x5=2790
Vertical misalignment	301x5=1505
Total	9755

2.1. Power Spectral Density (PSD)

The power spectral density (PSD) is a mathematical measure that depicts how the power of a signal is distributed across the frequency spectrum. It is widely used in analyzing the vibration characteristics of systems (Jin et al., 2023), noise analysis (Nielsen et al., 2023), optical applications (Dwik et al., 2023), and many other applications (Massara et al., 2023; Mitishita et al., 2023).

Estimation methods for power spectral density are divided into two categories such as parametric and non-parametric approaches. Parametric approaches like AR, MA, and ARMA assume that it is possible to model the system with a certain number of parameters. Estimating PSD becomes more challenging as the data size increases, and the accuracy of the estimation is proportional to the accuracy of the parametric model formed. On the other hand, non-parametric approaches like the periodogram provide a more general estimate with their flexible structures. As there's no need for any parametric model, non-parametric techniques are often preferred for systems that are difficult to model. Because it is difficult to model the electric motors linearly, the PSD was estimated using the Welch method, one of the non-parametric approaches. The Welch approach can essentially be summarized in 3 stages. Firstly, the signal is divided into K segments of length M with a certain overlap ratio, and these segments are multiplied by a window function $w(n)$. Given a window jump size of R, the weighted segments $x_m(n)$ are calculated as shown in Equation 1.

$$x_m(n) \cong w(n)x(n+mR), n = 0,1,2,\dots,M-1, m = 0,1,2,\dots,K-1 \quad (1)$$

Subsequently, the periodogram is calculated using the square of the absolute value of the N-length Fourier transform of these segments. The periodograms for each segment are computed as shown in Equation 2.

$$P_{x_m,M(w_k)} \cong \frac{1}{M}\left|\sum_{n=0}^{N-1} x_m(n)e^{\frac{-j2\pi nk}{N}}\right|^2 \tag{2}$$

Finally, by taking the average of the periodograms of all the segments, the variance is reduced and the PSD estimation is completed. The PSD calculated using the Welch method is determined as shown in Equation 3.

$$\hat{S}_x^W(w_k) \cong P_{x_m,M(w_k)} = \sum_{m=0}^{K-1} P_{x_m,M(w_k)} \tag{3}$$

3. RESULTS AND DISCUSSION

As previously mentioned, three-axis accelerometers placed in two different positions on the experimental setup are used to classify the normal state and five fault classes. Axial, radial, and tangential measurements from each location have been separately fed to the classifier to observe which accelerometer, position, and measurement axis would yield better results. Sample results obtained using the SVM method with a linear kernel are presented in Table 2.

Table 2 The classification accuracies of each class by different location and measurement direction using linear SVM

Class	**Accuracy (%)**					
	Accelometer on location 1 (underhang)			**Accelometer on location 1 (overhang)**		
	Axial	**Radial**	**Tangential**	**Axial**	**Radial**	**Tangential**
Horizontal misalignment	93.50	100	94.62	70.46	39.39	41.52
Imbalance	92.97	97.12	99.22	95.98	86.19	86.49
Normal	58.37	83.27	71.02	60.82	17.14	17.96
Bearing fault (Overhang)	76.18	99.92	85.81	97.82	95.48	95.21
Bearing fault (Underhang)	95.34	95.84	95.84	96.17	73.37	74.01
Vertical misalignment	95.68	99.47	97.61	95.68	67.51	66.18

Table 2 shows that all classifiers struggled to detect the normal operating condition. Additionally, upon examining Table 2, it is evident that vibration measurements taken solely in the radial direction from the accelerometer on location 1 are sufficient to successfully identify the specified fault conditions using the PSD estimation with the Welch method. To compare the performance of popular machine learning algorithms, the PSD of measurements only in the radial direction has been input into Decision Tree (DT), SVM, Linear Discriminant (LD), and K-nearest neighborhood (KNN) methods. While Table 3 is tabulating the performance of these methods, the confusion matrices are presented in Figure 2.

Table 3 The accuracies and training time for DT, SVM, LD, and KNN

Method	**Parameters**	**Accuracy (%)**	**Training time (s)**
DT	max. # of splits: 100 split criterion: Gini diversity index	98.4	22.26
SVM	kernel function: linear box constraint level: 1 multiclass meth.: one vs one	97.8	38.85
LD	preset: Linear discriminant covariance structure: full	71.5	16.86
KNN	# of neighbors: 1 distance metric: Euclidean distance weight: equal	99.9	1081.1

Table 3 indicates that DT is the best among all providing accuracies over %95 in terms of training time. It is possible to reach a shorter training time by readjusting the parameters, but the accuracy decreases with the increasing training speed. With a competitive training time, the accuracy of the SVM is slightly lower than DT. Although it is possible to increase the accuracy of SVM to around %99 by using a quadratic kernel, the training time increases dramatically up to 222.49 seconds which limits the practical usage. LD is the fastest one with the lower accuracy. As shown in Figure 2,

LD has no correct classification for class-3, the normally operating state, possibly because of the lower amount of class data. KNN is the best one considering the accuracy, but it requires a very long training time compared to others.

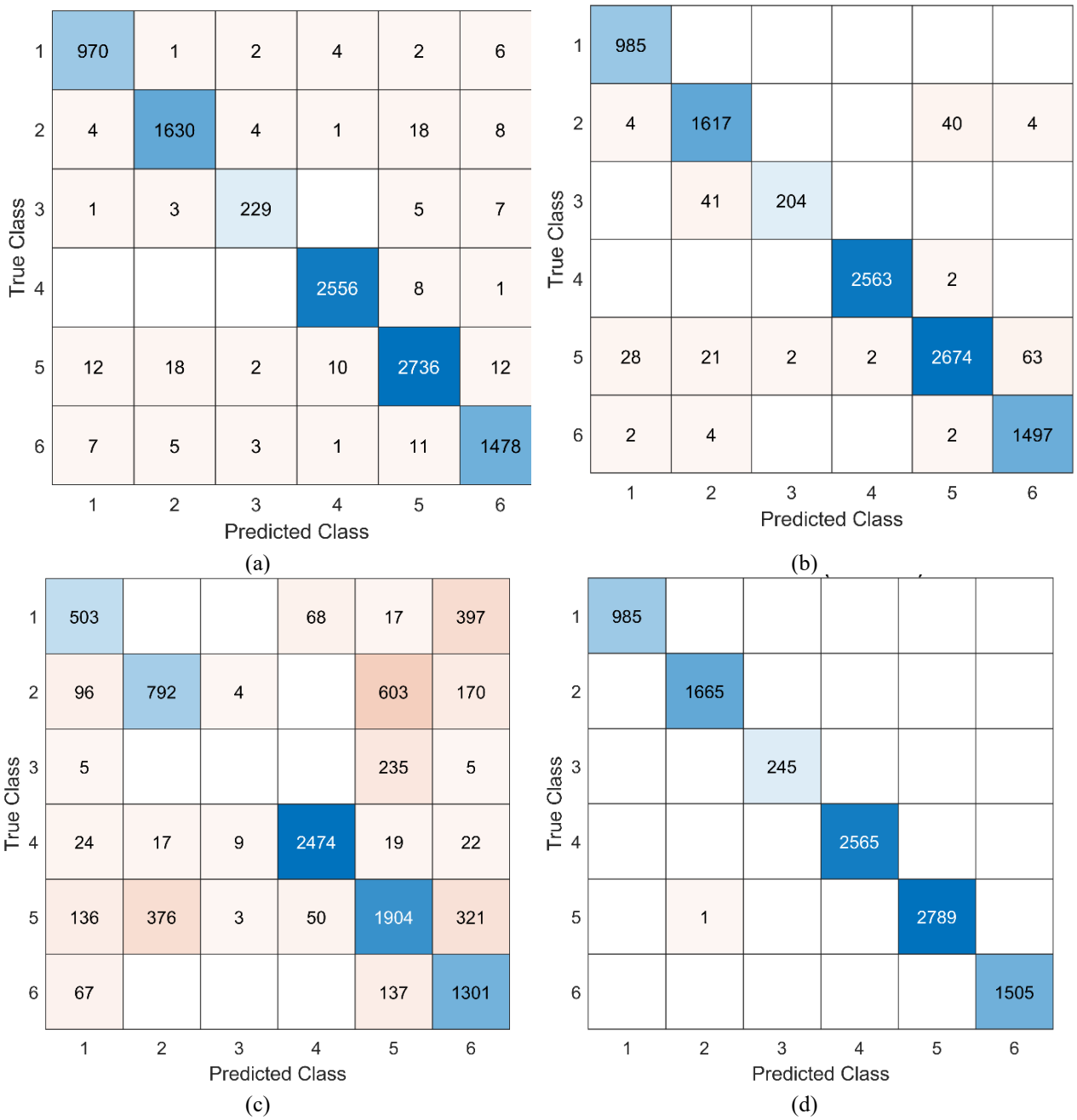

Figure 2 The confusion matrices obtained by using (a) DT, (b) SVM, (c) LD, and (d) KNN with the radial measurements

4. CONCLUSIONS

Fault classification in electric motors, one of the most critical equipment of today's industry, is the subject of this study. Healthy operation and a total of five malfunctions like imbalance, misalignments, and bearing failures have been studied. It has been investigated which of the six vibration data obtained from the accelerometers in two different positions from the axial, radial, and tangential directions is more successful in classifying the faults. The PSD of the vibration signals has been extracted by the Welch method. It has been seen that the data recorded only on the radial axis from the underhang position is sufficient alone to classify the faults. The performances of the popular machine learning methods have been compared in terms of accuracy and learning time with the input of PSD on radial axis data. It is concluded that the DT method is the most successful when the learning time and accuracy are considered. In applications where longer learning time is not a problem, the performance of the KNN method, which correctly classifies almost all failures, is quite remarkable.

Ethics Committee Approval / Etik Kurul Onayı
N/A

Peer-review / Akran Değerlendirmesi
Externally peer-reviewed.

Conflict of Interest
The author has no conflicts of interest to declare.

Funding
The author declared that this study has received no financial support.

REFERENCES

Al-Badour, F., Sunar, M., & Cheded, L. (2011). Vibration analysis of rotating machinery using time–frequency analysis and wavelet techniques. *Mechanical Systems and Signal Processing*, *25*(6), 2083-2101.

Borghesani, P., Pennacchi, P., Randall, R., Sawalhi, N., & Ricci, R. (2013). Application of cepstrum pre-whitening for the diagnosis of bearing faults under variable speed conditions. *Mechanical Systems and Signal Processing*, *36*(2), 370-384.

Chukwuekwe, D. O., Glesnes, T., & Schjølberg, P. (2016). Condition Monitoring for Predictive Maintenance–Towards Systems Prognosis within the Industrial Internet of Things.

Dwik, S., Sasikala, G., & Natarajan, S. (2023). Design and Simulation of a Reconfigurable Multifunctional Optical Sensor. *Optical Memory and Neural Networks*, *32*(2), 147-157.

Jin, X., Wang, J., He, X., Yan, Z., Xu, L., Wei, C., & Yin, G. (2023). Improving vibration performance of electric vehicles based on in-wheel motor-active suspension system via robust finite frequency control. *IEEE Transactions on Intelligent Transportation Systems*, *24*(2), 1631-1643.

Marins, M. A., Ribeiro, F. M., Netto, S. L., & Da Silva, E. A. (2018). Improved similarity-based modeling for the classification of rotating-machine failures. *Journal of the Franklin Institute*, *355*(4), 1913-1930.

Massara, E., Villaescusa-Navarro, F., Hahn, C., Abidi, M. M., Eickenberg, M., Ho, S., Lemos, P., Dizgah, A. M., & Régaldo-Saint Blancard, B. (2023). Cosmological information in the marked power spectrum of the galaxy field. *The Astrophysical Journal*, *951*(1), 70.

Mitishita, R. S., Elfring, G. J., & Frigaard, I. A. (2023). Statistics and spectral analysis of turbulent duct flows with flexible and rigid polymer solutions. *Journal of Non-Newtonian Fluid Mechanics*, *311*, 104952.

Nielsen, J. K., Christensen, M. G., & Boldt, J. B. (2023). An Analysis of Traditional Noise Power Spectral Density Estimators based on the Gaussian Stochastic Volatility Model. *IEEE/ACM Transactions on Audio, Speech, and Language Processing*.

Popescu, T. D., Aiordachioaie, D., & Culea-Florescu, A. (2022). Basic tools for vibration analysis with applications to predictive maintenance of rotating machines: an overview. *The International Journal of Advanced Manufacturing Technology*, 1-17.

Ran, Y., Zhou, X., Lin, P., Wen, Y., & Deng, R. (2019). A survey of predictive maintenance: Systems, purposes and approaches. arXiv 2019. *arXiv preprint arXiv:1912.07383*.

Riberio, F. M. L. (2016). *MAFAULDA - Machinery Fault Database.* . http://www02.smt.ufrj.br/~offshore/mfs/page_01.html

Saidur, R. (2010). A review on electrical motors energy use and energy savings. *Renewable and sustainable energy reviews*, *14*(3), 877-898.

Selcuk, S. (2017). Predictive maintenance, its implementation and latest trends. *Proceedings of the Institution of Mechanical Engineers, Part B: Journal of Engineering Manufacture*, *231*(9), 1670-1679.

Vafaei, N., Ribeiro, R. A., & Camarinha-Matos, L. M. (2019). Fuzzy early warning systems for condition based maintenance. *Computers & Industrial Engineering*, *128*, 736-746.

Yi, C., Wang, H., Zhou, Q., Hu, Q., Zhou, P., & Lin, J. (2022). An Adaptive Harmonic Product Spectrum for Rotating Machinery Fault Diagnosis. *IEEE Transactions on Instrumentation and Measurement*, *72*, 1-12.

Yu, G. (2019). A concentrated time–frequency analysis tool for bearing fault diagnosis. *IEEE Transactions on Instrumentation and Measurement*, *69*(2), 371-381.

Use of Green Synthesis Carbon Dots Derived from Pumpkin Waste in Food Packaging

Cemhan Doğan*[1], Nurcan Doğan[1]

Abstract: Food packaging plays a critical role in preserving the quality and safety of food products. However, the widespread use of synthetic packaging materials has raised concerns about their environmental impact. In this study, we propose a sustainable and innovative approach to develop food packaging materials using green synthesized carbon dots derived from pumpkin waste. The synthesis of carbon dots was carried out using a hydrothermal reactor, which provided an eco-friendly and cost-effective method. Pumpkin waste, a readily available agricultural byproduct, was utilized as the carbon source for the synthesis. To integrate the carbon dots into food packaging materials, sodium alginate, a natural biopolymer derived from seaweed, was used as the film-forming matrix. The incorporation of carbon dots into the sodium alginate film resulted in the development of multifunctional packaging materials with enhanced properties. The synthesized carbon dot-integrated sodium alginate films were evaluated for their antioxidant and antimicrobial activities. The films demonstrated significant antioxidant potential, as determined by their ability to scavenge free radicals using DPPH (2,2-diphenyl-1-picrylhydrazyl) assays. The presence of carbon dots in the films contributed to their antioxidant activity, which can help mitigate oxidative degradation of packaged food products. Furthermore, the carbon dot-integrated films exhibited remarkable antimicrobial properties against two common foodborne pathogens, *E. coli* and *S. aureus*. The films effectively inhibited the growth of these bacteria, indicating their potential for extending the shelf life of perishable food items and reducing the risk of foodborne illnesses. The utilization of pumpkin waste for green synthesis and the integration of carbon dots into sodium alginate films present a sustainable and eco-friendly approach to food packaging. The multifunctional properties of the resulting films, including antioxidant and antimicrobial activities, offer promising avenues for enhancing the quality and safety of packaged food products. This study highlights the potential of green synthesized carbon dots derived from pumpkin waste as a valuable resource for the development of sustainable food packaging materials, contributing to the reduction of environmental impact in the food industry.

Keywords: green synthesis, carbon dots, pumpkin waste, food packaging, antioxidant activity, antimicrobial activity.

[1]**Address:** Yozgat Bozok University, Bogazliyan Vocational School, Department of Food Technology, Yozgat/Türkiye

***Corresponding author**: cemhan.dogan@yobu.edu.tr

1. INTRODUCTION

The surge in demand for processed and packaged foods is experiencing an unprecedented rise due to the swiftly evolving global human lifestyle. In response, the food industry is tirelessly working to satisfy the growing consumer appetite for food that is both secure and conveniently accessible. The current market is inundated with an array of processed food options spanning from minimally processed items to fully heated products. While significant strides have been made in the preservation and packaging of pre-cooked and heated foods, the preservation methods for minimally processed foods, such as fresh fruits and thinly sliced raw meat, still face significant challenges. Notably, among these items, minimally processed meat products stand out as a staple, prone to rapid deterioration throughout storage and distribution, necessitating specialized preservation techniques and packaging solutions (Asgher vd., 2020).

Carbon dots (CDs), a novel addition to the realm of carbon nanomaterials, exhibit exceptional chemical and photochemical stability. Distinctively resembling semiconductor quantum dots (QDs), CDs have garnered attention as a promising contender within the domain of carbon nanomaterials. The allure of CDs emanates from their robust attributes, including remarkable fluorescence, strong photoluminescence (PL), hydrophilicity, favorable biocompatibility, and minimal toxicity. These qualities substantiate their potency, particularly in the sphere of biological applications, positioning them as a viable substitute for conventional QDs, often with comparable or superior

performance (Li vd., 2021). Recent years have witnessed CDs unleash their substantial potential across an array of domains. These encompass photocatalysis, solar energy harnessing, light-emitting diodes, antibacterial and antioxidant activities, chemical sensing, as well as bioimaging. Remarkably, CDs have ventured into the realm of sustainable food packaging polymers, where they serve as environmentally sound, secure, and non-toxic fillers. When integrated into packaging materials, CDs confer noteworthy antioxidant and antimicrobial attributes, thereby augmenting the longevity of packaged foods. Moreover, research has documented the synthesis of CDs from sustainable sources, expressly for application in food packaging (Ezati vd., 2022). Furthermore, CDs eclipse alternative functional additives in the realm of food packaging. Notably derived from agricultural byproducts, they offer economic advantages over chemically synthesized nanomaterials like metal oxides, which frequently find employment in food packaging contexts. Adding to their appeal, CDs, owing to their natural origins, boast high levels of biocompatibility and a lack of toxicity—attributes that often pose significant concerns with artificially manufactured nanomaterials (Moradi vd., 2023).

Pumpkin waste, an abundant byproduct of food processing and consumption, has garnered increasing attention as a valuable and sustainable resource in various applications. The efficient utilization of pumpkin waste presents a multifaceted solution, addressing both environmental concerns and the quest for novel bioresources. Typically arising from pumpkin carving, culinary preparation, and industrial processing, this waste stream encompasses peels, seeds, and fibrous matter. In recent years, researchers have explored innovative avenues to harness the untapped potential of pumpkin waste, transforming it into a resource-rich matrix for applications such as biofuel production, value-added food products, natural pigments, and bioactive compounds. By converting this underutilized waste into functional materials, an opportunity arises not only to mitigate environmental burdens but also to tap into a source of bioactive compounds that could contribute to various industries, aligning with the principles of a circular economy (Norfezah vd., 2011). The utilization of pumpkin waste as a precursor for the synthesis of CDs holds substantial promise in the realm of nanotechnology and materials science. Pumpkin waste, an abundant agricultural byproduct, offers a sustainable and environmentally friendly source for the production of CDs. These CDs, characterized by their intriguing optical and chemical properties, have emerged as a novel class of nanomaterials with a wide range of applications. The inherent carbon-rich composition of pumpkin waste can provides a foundation for the creation of CDs through cost-effective and eco-friendly synthesis routes. These CDs can exhibit exceptional fluorescence, biocompatibility, and low toxicity, making them suitable candidates for food packaging. By tapping into pumpkin waste as a resource for CD synthesis, researchers not only address waste management challenges but also contribute to the development of innovative, sustainable materials with diverse technological implications.

The primary aim of this study was to explore the potential of integrating carbon dots (CDs) into food packaging materials by employing sodium alginate, a natural biopolymer derived from seaweed, as the film-forming matrix. The objective was to create multifunctional packaging materials with improved properties by incorporating CDs into the sodium alginate films. The synthesized CD-integrated sodium alginate films were subjected to evaluation for their antioxidant and antimicrobial activities. The investigation sought to assess the films' ability to scavenge free radicals using DPPH (2,2-diphenyl-1-picrylhydrazyl) and ABTS (2,2'-azino-bis(3-ethylbenzothiazoline-6-sulfonic acid)) assays, indicative of their antioxidant potential. Additionally, the study aimed to determine the antimicrobial efficacy of the CD-integrated films against E. coli and S. aureus, common foodborne pathogens. Through this approach, the study aimed to contribute to the creation of sustainable and environmentally friendly food packaging solutions, offering enhanced preservation and safety of packaged food products while minimizing the environmental impact of the food industry

2. MATERIAL AND METHOD

2.1. Material

Pumpkins were sourced from local farmers in Boğazlıyan, Yozgat, Turkey. The strains of Escherichia coli ATCC 35218 and Staphylococcus aureus ATCC 29213 were acquired from the culture collection at Bogazliyan Vocational High School, Turkey. Pathogenic microorganisms were consistently stored at +4°C and subjected to periodic subculturing. The chemicals and microbial media utilized for the analyses were procured from Merck Sigma Aldrich (Darmstadt, Germany), unless otherwise specified.

2.1. CDs synthesis

Pumpkin waste-based CDs was synthesized method following the hydrothermal procedure outlined by Ezati vd., (2022). For this purpose, 20 g of pumpkin waste was mixed with 60 mL of distilled water, and the mixture was placed in a Teflon-lined stainless steel reactor (250 mL). The reactor was kept in an oven at 200 °C for 6 hours. After removal from the oven, the reactor was allowed to cool down to 25 °C, followed by centrifugation at 10,000 rpm for 20 minutes. The collected supernatant was filtered through a micro-membrane filter with a pore size of 0.22 µm (Whatman

International Ltd., Maidstone, England). The filtrate was subsequently lyophilized to obtain a powdered form. The obtained CDs were stored at 4°C until their use in film production.

2.2. Film production

Film solutions were prepared by mechanically stirring sodium alginate (10 g/L, W/V film solution), and glycerol (5 g/L) in a water bath (~60 °C) at a speed of 500 rpm for 2 hours to dissolve them in 350 mL of water. Different concentrations of CDs (SA-5CDs:5 g/L, SA-10CDs: 10 g/L, and SA-15CDs: 15 g/L, W/V film solution) were added to the solution, along with $CaCl_2$ (1.5 g/L) to reinforce the films. After an additional 15 minutes of mixing at 35 °C, the total solution volume was adjusted to 400 mL using distilled water. To remove air bubbles, the solutions were centrifuged at 1500 G for 3 minutes and then poured onto plexiglass plates (260 mm x 260 mm). The films were separated from the mold after approximately 24 hours of drying at 60 ± 2 °C in an oven and used for analyses.

2.3. In-vitro antioxidant activity

The assessment of antioxidant activity (AA) was conducted employing the 2,2-diphenyl-1-picrylhydrazyl (DPPH) method, a widely recognized approach for gauging antioxidant potential. In this experimental phase, a precise combination of 0.1 mL of the extracted substance and 3.9 mL of a methanolic DPPH solution (at a concentration of 25 mg/L) was meticulously prepared. The resulting mixture was allowed to incubate undisturbed in a darkened environment at room temperature for a duration of 30 minutes. Following the incubation period, the absorbance of the concoction was meticulously gauged at a wavelength of 515 nm. The quantification of antioxidant activity was subsequently conducted using the computational formula outlined below (Başyiğit vd., 2020).

AADPPH (%) = (Absorbance_control - Absorbance_sample) / Absorbance_control * 100

2.4. In-vitro antimicrobial activity

The antimicrobial activities of the samples were assessed against the foodborne pathogens, Gram-negative bacteria E. coli, and Gram-positive bacteria S. aureus. Initially, pathogen stock cultures were regenerated. For this purpose, cultures were inoculated into 5 mL of Mueller Hinton Broth (MHB) and incubated at 35°C overnight. After incubation, the cultures were diluted using optical density (OD_{600}) measurements until reaching a concentration of 10^8 CFU/mL. The antimicrobial activity was determined using the disk diffusion method, as follows:

A volume of 100 µL of the diluted bacterial cell suspension was injected into Mueller Hinton Agar (MHA), and the agar surface was inoculated in a spreading method by rotating the sterile loop in a clockwise direction for three complete turns with small intervals. The inoculated medium was left for 5 minutes to allow liquid absorption, and subsequently, sterilized (via UV exposure) films with a diameter of 6 mm were placed onto the agar surface. The Petri dishes were then incubated at 35°C for 24 hours. Following incubation, the zones formed around the disks were measured using a caliper. This approach allowed the assessment of the inhibitory effects of the samples against the bacterial growth by measuring the diameter of the inhibition zones (Doğan vd., 2022).

2.5. Statistical analysis

The statistical evaluation was performed using the IBM-SPSS 22.0 software package (SPSS Inc., Chicago, IL, USA). The results were subjected to analysis through one-way analysis of variance (ANOVA) and subsequently presented as mean ± standard deviation. Moreover, significant disparities ($P \leq 0.05$) among the means were identified using Tukey's multiple comparison test.

3. RESULTS AND DISCUSSION

3.1. In-vitro antioxidant activity

The DPPH assay, a widely recognized method for assessing radical scavenging ability, was employed to measure the films' efficacy in neutralizing free radicals, thus illuminating their potential as robust antioxidants (Gómez-Estaca vd., 2014). In contrast to the control film, which exhibited a modest antioxidant activity of 14.62%, the introduction of CDs into the film formulation heralded a significant upsurge in antioxidant potential. Notably, the SA-5CDs film displayed a substantial enhancement in antioxidant activity, registering a commendable 52.84%. This preliminary outcome underscores the favorable impact of even lower concentrations of CDs in augmenting the antioxidant capacity of the films. However, the most striking strides in antioxidant potential emerged with escalating CD concentrations. The SA-10CDs film stood out with an impressive antioxidant activity of 92.47%, while the pinnacle was reached with the SA-

15CDs film, showcasing a remarkable 95.13% antioxidant activity (Table 1). The dose-dependent amplification of antioxidant activity potentially arises from the inherent characteristics of CDs, such as their diverse surface chemistry and capacity to trap free radicals, which were further accentuated at higher concentrations.

These findings align harmoniously with prior research (Ezati vd., 2022; Li vd., 2021; Moradi vd., 2023), establishing carbon dots as potent candidates for exhibiting substantial antioxidant properties. The augmented antioxidant activity observed in our study is likely attributed to a synergistic interplay between CDs and the sodium alginate matrix. While CDs contribute to radical scavenging, the sodium alginate not only provides a stable structure but also potentially amplifies the overall antioxidant effect of the resulting film. The ascending trajectory of antioxidant activity with increasing CD concentrations not only underscores the potential of pumpkin waste-derived CDs but also accentuates their viability as efficient antioxidants for application in food packaging. This becomes especially pertinent in the context of extending the shelf life of packaged foods and bolstering food quality by mitigating oxidative deterioration. In summation, the successful integration of pumpkin waste-derived carbon dots into sodium alginate films engendered a marked augmentation in antioxidant activity. The discernible correlation between CD concentrations and heightened antioxidant potential substantiates the promise of CDs as effective antioxidants within food packaging materials. This study not only showcases the merit of harnessing CDs from pumpkin waste but also offers a sustainable and effective avenue for enhancing the antioxidant prowess of food packaging films. This promising endeavor opens doors to environmentally-conscious packaging solutions, thus contributing to both food preservation and environmental sustainability (Lindh vd., 2016).

Table 1. Antioxidant and antimicrobial activity of films

	Antioxidant Activitiy	Antimicrobial activity	
	DPPH (%)	*E.coli* (mm)	*S. aureus* (mm)
Control	14.62±0.59[c]	n.d	n.d
SA-5CDs	52.84±1.03[b]	3.84±0.16[c]	4.63±0.67[c]
SA-10CDs	92.47±1.24[a]	6.41±0.61[b]	7.42±0.62[b]
SA-15CDs	95.13±1.32[a]	8.93±0.52[a]	9.19±0.33[a]

3.2. In-vitro antimicrobial activity

The antimicrobial activity of the films, as assessed through the disk diffusion test against *E. coli* and *S. aureus*, offered insights into the potential of pumpkin waste-derived CDs-integrated sodium alginate films as effective antimicrobial agents. For *E. coli*, the control film exhibited a non-detectable zone of inhibition, indicating minimal inhibition of bacterial growth. In contrast, films containing CDs displayed increasingly prominent zones of inhibition as CD concentrations rose. The SA-5CDs film demonstrated a zone of inhibition measuring 3.84 mm, followed by a noticeable augmentation in the SA-10CDs film with a 6.41 mm zone of inhibition. The most substantial inhibition was witnessed with the SA-15CDs film, which showcased an impressive 8.93 mm zone of inhibition against E. coli. Similarly, in the case of S. aureus, the control film displayed no detectable zone of inhibition, indicative of limited antimicrobial effect. The introduction of CDs into the film matrix led to enhanced antimicrobial activity. The SA-5CDs film exhibited a 4.63 mm zone of inhibition, which further expanded in the SA-10CDs film with a notable 7.42 mm zone of inhibition. The pinnacle of antimicrobial inhibition was achieved with the SA-15CDs film, recording a substantial 9.19 mm zone of inhibition against S. aureus. These results underscore the potential of CDs in significantly augmenting the antimicrobial activity of sodium alginate films. The escalating trend of increasing CD concentrations correlating with larger zones of inhibition suggests a clear dose-dependent effect. The antimicrobial efficacy observed can be attributed to the CDs' inherent properties, which may disrupt the bacterial cell membrane, thus inhibiting growth.

The results revealed a notable discrepancy in the antimicrobial activity exhibited by the films against *S. aureus* compared to *E. coli*. The films demonstrated a consistently larger zone of inhibition against S. aureus as compared to E. coli. This distinct variation in antimicrobial efficacy between the two bacterial species could be attributed to several underlying factors. One contributing factor is the intrinsic structural and physiological differences between S. aureus and *E. coli*. *S. aureus*, a Gram-positive bacterium, possesses a relatively thick peptidoglycan layer in its cell wall, rendering it more susceptible to disruption by antimicrobial agents (Eaton vd., 2008). In contrast, E. coli, a Gram-negative bacterium, features an outer membrane that serves as an additional barrier, often providing greater resistance to antimicrobial substances (Tenover, 2006). Moreover, the diverse mechanisms of action of antimicrobial agents can result in varying degrees of efficacy against different bacterial species (Tenover, 2006). The CDs integrated into the films may exhibit interactions with specific components of S. aureus that render it more susceptible to inhibition (Ghirardello vd., 2021). Conversely, the intricate cell wall structure of *E. coli* might present some resistance against the CDs' antimicrobial effects. Another influencing factor could be the distinct metabolic and growth characteristics of *S. aureus* and *E. coli*. The differential response might stem from variations in growth rates, cellular metabolism, and

susceptibility to external stressors. These factors collectively contribute to the differing antimicrobial outcomes observed (Zaharia vd., 2013). Furthermore, bacterial species may exhibit varying levels of sensitivity to specific antimicrobial agents due to inherent genetic differences and adaptations. *S. aureus* and *E. coli* might possess dissimilar genetic makeup, resulting in diverse susceptibility profiles to the CDs' antimicrobial actions. The nuanced response highlights the need for comprehensive investigations into the antimicrobial efficacy of innovative materials, enabling a more targeted and effective approach to food safety and preservation through advanced packaging solutions.
These findings align with previous studies that have reported the antimicrobial potential of carbon dots derived from various sources (Azhdari & Moradi, 2022; Ezati vd., 2022; Moradi vd., 2023). The enhanced antimicrobial activity observed in this study is a testament to the synergistic effect between CDs and the sodium alginate matrix, where CDs contribute to antimicrobial activity while sodium alginate provides a stable film structure. In conclusion, the integration of pumpkin waste-derived carbon dots into sodium alginate films led to a considerable enhancement in antimicrobial activity. The increasing zone of inhibition with higher CD concentrations highlights the potential of CDs as effective antimicrobial agents within food packaging materials. This study accentuates the value of utilizing CDs from pumpkin waste to bolster the antimicrobial capacity of food packaging films, offering a sustainable approach to enhancing food safety and quality through innovative packaging solutions.

4. CONCLUSIONS

The present study illuminates the promising potential of pumpkin waste-derived carbon dot (CD)-integrated sodium alginate films as multifunctional materials with enhanced antioxidant and antimicrobial properties. The incorporation of CDs into the film matrix yielded remarkable improvements in both antioxidant activity and antimicrobial efficacy. This innovative approach showcases the sustainable utilization of agricultural waste for the development of functional packaging solutions, aligning with the principles of a circular economy. The significant enhancement in antioxidant activity observed with increasing CD concentrations underscores the viability of CDs as efficient scavengers of free radicals. This holds profound implications for prolonging the shelf life of packaged foods by mitigating oxidative degradation. Additionally, the escalating antimicrobial efficacy against Staphylococcus aureus and Escherichia coli underscores the potential of CDs to reinforce the antimicrobial capacity of sodium alginate films. The dose-dependent responses highlight the versatility of CDs in curbing bacterial growth, offering a valuable tool for enhancing food safety and quality. The differential responses of S. aureus and E. coli to the films' antimicrobial activity elucidate the intricate interplay between bacterial species, structural characteristics, and susceptibility to antimicrobial agents. This insight underscores the need for tailored approaches to antimicrobial applications, reflecting the complex nature of microbial interactions. The successful integration of pumpkin waste-derived CDs into sodium alginate films signifies a remarkable stride towards sustainable and functional food packaging. By repurposing agricultural waste into valuable resources, this study exemplifies the potential of green technologies to address environmental challenges while simultaneously contributing to advanced packaging solutions that extend beyond conventional preservation. In conclusion, the synergistic combination of pumpkin waste-derived CDs and sodium alginate films presents an innovative pathway towards enhancing food safety, extending shelf life, and promoting sustainable practices within the food packaging industry. This research paves the way for further exploration of novel materials derived from agricultural waste, driving the evolution of packaging technologies that align with both consumer demands and environmental stewardship.

Ethics Committee Approval
N/A

Peer-review
Externally peer-reviewed.

Author Contributions
Conceptualization: C.D, N.D.; Investigation: C.D, N.D.; Material and Methodology: C.D, N.D.; Supervision: C.D, N.D.; Visualization: C.D, N.D.; Writing-Original Draft: C.D, N.D.; Writing-review & Editing: C.D, N.D.; Other: All authors have read and agreed to the published version of manuscript.

Conflict of Interest
The authors have no conflicts of interest to declare.

Funding
The authors declared that this study has received no financial support.

REFERENCES

Asgher, M., Qamar, S. A., Bilal, M., & Iqbal, H. M. N. (2020). Bio-based active food packaging materials: Sustainable alternative to conventional petrochemical-based packaging materials. *Food Research International*, *137*, 109625. https://doi.org/10.1016/j.foodres.2020.109625

Azhdari, S., & Moradi, M. (2022). Application of antimicrobial coating based on carboxymethyl cellulose and natamycin in active packaging of cheese. *International Journal of Biological Macromolecules*, *209*, 2042-2049. https://doi.org/10.1016/j.ijbiomac.2022.04.185

Başyiğit, B., Alaşalvar, H., Doğan, N., Doğan, C., Berktaş, S., & Çam, M. (2020). Wild mustard (Sinapis arvensis) parts: Compositional analysis, antioxidant capacity and determination of individual phenolic fractions by LC–ESI–MS/MS. *Journal of Food Measurement and Characterization*, *14*(3), 1671-1681. https://doi.org/10.1007/s11694-020-00415-2

Doğan, N., Doğan, C., Eticha, A. K., Gungor, M., & Akgul, Y. (2022). Centrifugally spun micro-nanofibers based on lemon peel oil/gelatin as novel edible active food packaging: Fabrication, characterization, and application to prevent foodborne pathogens E. coli and S. aureus in cheese. *Food Control*, *139*, 109081. https://doi.org/10.1016/j.foodcont.2022.109081

Eaton, P., Fernandes, J. C., Pereira, E., Pintado, M. E., & Xavier Malcata, F. (2008). Atomic force microscopy study of the antibacterial effects of chitosans on Escherichia coli and Staphylococcus aureus. *Ultramicroscopy*, *108*(10), 1128-1134. https://doi.org/10.1016/j.ultramic.2008.04.015

Ezati, P., Rhim, J.-W., Molaei, R., Priyadarshi, R., Roy, S., Min, S., Kim, Y. H., Lee, S.-G., & Han, S. (2022). Preparation and characterization of B, S, and N-doped glucose carbon dots: Antibacterial, antifungal, and antioxidant activity. *Sustainable Materials and Technologies*, *32*, e00397. https://doi.org/10.1016/j.susmat.2022.e00397

Ghirardello, M., Ramos-Soriano, J., & Galan, M. C. (2021). Carbon Dots as an Emergent Class of Antimicrobial Agents. *Nanomaterials*, *11*(8), Article 8. https://doi.org/10.3390/nano11081877

Gómez-Estaca, J., López-de-Dicastillo, C., Hernández-Muñoz, P., Catalá, R., & Gavara, R. (2014). Advances in antioxidant active food packaging. *Trends in Food Science & Technology*, *35*(1), 42-51. https://doi.org/10.1016/j.tifs.2013.10.008

Li, S., Li, L., Tu, H., Zhang, H., Silvester, D. S., Banks, C. E., Zou, G., Hou, H., & Ji, X. (2021). The development of carbon dots: From the perspective of materials chemistry. *Materials Today*, *51*, 188-207. https://doi.org/10.1016/j.mattod.2021.07.028

Lindh, H., Olsson, A., & Williams, H. (2016). Consumer Perceptions of Food Packaging: Contributing to or Counteracting Environmentally Sustainable Development? *Packaging Technology and Science*, *29*(1), 3-23. https://doi.org/10.1002/pts.2184

Moradi, M., Molaei, R., Kousheh, S. A., T. Guimarães, J., & McClements, D. J. (2023). Carbon dots synthesized from microorganisms and food by-products: Active and smart food packaging applications. *Critical Reviews in Food Science and Nutrition*, *63*(14), 1943-1959. https://doi.org/10.1080/10408398.2021.2015283

Norfezah, M. N., Hardacre, A., & Brennan, C. S. (2011). Comparison of waste pumpkin material and its potential use in extruded snack foods. *Food Science and Technology International*, *17*(4), 367-373. https://doi.org/10.1177/1082013210382484

Tenover, F. C. (2006). Mechanisms of Antimicrobial Resistance in Bacteria. *The American Journal of Medicine*, *119*(6, Supplement 1), S3-S10. https://doi.org/10.1016/j.amjmed.2006.03.011

Zaharia, D. C., Muntean, A. A., Popa, M. G., Steriade, A. T., Balint, O., Micut, R., Iftene, C., Tofolean, I., Popa, V. T., Baicus, C., Bogdan, M. A., & Popa, M. I. (2013). Comparative analysis of Staphylococcus aureus and Escherichia coli microcalorimetric growth. *BMC Microbiology*, *13*(1), 171. https://doi.org/10.1186/1471-2180-13-171

The Investigation of Performance Analyses of a Stirling Engine with Bell-Crank Drive Mechanism

Derviş Erol

Abstract: Today, efforts to develop power generation systems that can use renewable energy sources continue to solve the environmental problems created by fossil-based fuels. The working principles of Stirling engines date back to ancient years. These engines have been known for over two centuries and are continuing to develop studies. Stirling engines can generate mechanical or electrical power using any heat source that can provide sufficiently high temperatures. The thermal efficiency, harmful exhaust emission values, noise, and vibration levels of these engines are quite good compared to internal combustion engines. In this study, thermodynamic and kinematic analysis of a beta-type Stirling engine with bell-crank drive mechanism were conducted. The volume and pressure changes depending on the crank angle of the engine with the bell-crank drive mechanism were calculated using the isothermal analysis method. In this study, the fundamental parameters related to engine performance such as working fluid mass, charge pressure, heater, and coolant temperature; the effects on the amount of net power are examined in detail. The simulation and optimization analysis of the bell-crank drive mechanism for the beta-type Stirling engine were made using the MSC Adams program. Part drawings and assemblies of the models used in the MSC Adams program were created in the SolidWorks program.

Keywords: Stirling engines, Bell-crank, Thermodynamic analysis, Kinematic analysis, Isothermal analysis

Address: Kırıkkale University, Department of Automotive Technology, Yahşihan, Kırıkkale/Türkiye

Corresponding author: derol40@gmail.com

1. INTRODUCTION

Stirling engines are an external combustion power generation system that can use all kinds of heat energy [1-2]. Today, these engines are used commercially for electric power generation in spacecraft of NASA and combi systems at houses. In addition, there are different application areas where it is used for electrical energy generation from solar energy and as a water pump [3]. Different drive mechanisms are used to convert heat energy into mechanical energy in Stirling engines [4]. Different drive mechanisms such as bell-crank, slider-crank, wobble yoke, rhombic drive, swash plate, scotch yoke, and ross yoke are used in kinematic Stirling engines [5]. The drive mechanisms differ according to engine type and power. Different drive mechanisms can be developed by engine designers to ensure higher engine power and efficiency are obtained from this type of engine.

The bell-crank drive mechanism is known to be the first drive mechanism used in Stirling engines [6-7]. The bell-crank drive mechanism is a simple part used to change the direction of movement. The inlet and outlet direction of the movement can be approximately 90° different. The bell-crank mechanism can be used for different purposes besides converting linear motion to circular motion in many mechanical systems [8-9]. It has been reported in the literature that the bell-crank mechanism provides better performance results for single-cylinder small engines [10-11]. This mechanism is not preferred very often in large-size engines due to negative conditions such as the weight of the mechanism and balance [12]. In this drive mechanism, it is seen as a disadvantage that the lateral friction forces occurring between the displacer piston rod and the power piston are higher than in other mechanisms [13]. In Figure 1, the 3D design pictures of the Stirling engine with bell-crank drive mechanism developed for this study, created in the SolidWorks program are shown.

In this study, it is aimed to investigate of design and thermodynamic analyses of a Stirling engine with bell-crank drive mechanism. It is planned to manufacture the Stirling engine by evaluating the results obtained according to the design and analysis results. Power and torque values of the Stirling engine with bell-crank drive mechanism will be experimentally determined by using a dynamometer in the next stages of manufacturing. Due to the wide usage area of

Stirling engines, it is foreseen that bringing a local original design to the industry will contribute significantly to our country's economy.

2. MATERIAL AND METHOD

More efficient design and testing of mechanical systems is a challenging process for engineers. In particular, the inability to fully examine the interaction of finite elements and rigid body dynamics analyses with each other during designs may cause the systems to have very different behavior after production. Therefore, the complexity of the events that occur in the real-life operating conditions of Stirling engines directs researchers to theoretical analysis.

Kinematics examines only the movements of objects without considering their masses and the forces acting on them. The kinematic analysis method is used to determine the properties of parameters such as position, displacement, velocity, and acceleration of machine parts [14-15]. MSC Adams (Automatic Dynamic Analysis of Mechanical System) software; is one of the most widely used dynamic and kinematic analysis software in the world. MSC Adams program; is advanced software used to analysis the parameters such as force, velocity, position, acceleration, and moment of a system designed in a computer environment in real-life operating conditions. With these features, the MSC Adams program has better features than other CAD programs. MSC Adams program, the design quality of the systems increases, while the design and prototype costs are significantly reduced [16-17]. In this study, kinematic analyses of a Stirling engine with bell-crank drive mechanism were made using the MSC Adams program. Part drawings and assemblies of the models used in the MSC Adams program were created in the SolidWorks program, a CAD program.

Many methods (Isothermal, Schmidt, and nodal analysis, etc.) are used in the literature in thermodynamic analysis, which is the basis for the design of Stirling engines. In this study, the isothermal analysis method is preferred. With the Isothermal analysis method developed by Gustav Schmidt in 1871, the performance parameters of the existing system such as pressure, volume, and power can be determined theoretically before the production of engine prototypes [18-19]. All heat losses in the Stirling engine are neglected in this analysis. Therefore, in the analysis, the temperatures of the gas masses in the expansion volume, compression volume, and regenerator are taken as equal to the wall temperatures of these parts. The equations used to determine the net work and pressure changes obtained from Stirling engines are given in below. Pressure and volume changes are taken into account in net work of engine calculations [3, 19].

$$M = \left[(m_c + m_k + m_r + m_h + m_e) \right] \tag{2.1}$$

$$m = \left[(pV)/(RT) \right] \tag{2.2}$$

$$M = \left[(p((V_c/T_k) + (V_k/T_k) + (V_r/T_r) + (V_h/T_h) + (V_e/T_h))/R) \right] \tag{2.3}$$

$$T_r = \left[(T_h - T_k)/\ln(T_h/T_k) \right] \tag{2.4}$$

$$p = \left[MR\left(\frac{V_c}{T_k} + \frac{V_k}{T_k} + \frac{V_r \ln(T_h/T_k)}{(T_h - T_k)} + \frac{V_h}{T_h} + \frac{V_e}{T_h} \right)^{-1} \right] \tag{2.5}$$

$$W = \left\lfloor \sum_{i=1}^{i=k} P_i (V_i - V_{i-1}) \right\rfloor \tag{2.6}$$

$$W = \left[(W_c + W_e) \right] \tag{2.7}$$

$$\eta = \left[(W \ / Q_e) \right] \tag{2.8}$$

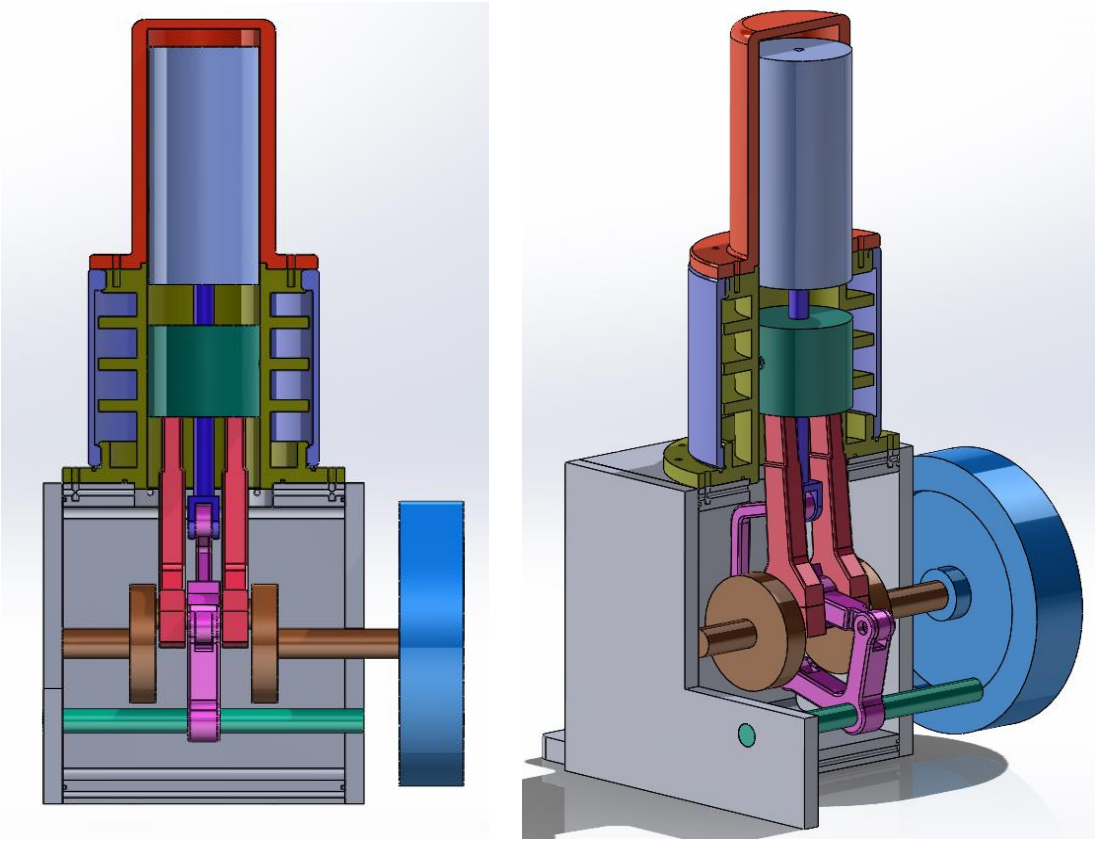

Figure 1. Schematic drawings in the SolidWorks environment of Stirling engine with bell-crank drive mechanism

3. RESULTS AND DISCUSSION

Position changes of the power and displacer pistons obtained with the MSC Adams program depending on the crankshaft angle of the Stirling engine with bell-crank drive mechanism are given in Figure 2. The volume changes obtained with the MSC Adams program depending on the crankshaft angle of the Stirling engine with bell-crank drive mechanism are given in Figure 3. When Figure 2. and Figure 3. graphics are examined, it can be seen that the designed bell-crank drive mechanism works flawlessly. When Figure 3 is examined, although the power piston and the displacer piston have the same stroke the compression volume and expansion volume values are different from each other. This is because when the crankshaft angle is around 225°, the power piston is at the top dead center and at the end of the compression stroke. After this point, while the displacer piston continues to move toward the top dead center, the power piston is due to the movement toward the bottom dead center. Therefore, the compression volume is different from the swept volume. Expansion volume and swept volume values are approximately equal to each other. Figure 4. shows comparison of the P-V diagrams for the expansion chamber and compression chamber.

Comparison of P-V diagrams at different heater temperatures, depending on volume change of Stirling engine with bell-crank drive mechanism is given in Figure 5. The mass of the working fluid was kept constant during this analysis. Cyclic work values of this engine with bell-crank drive mechanism in one cycle time were determined as 11.73 J, 12.85 J, 13.81 J, 14.65 J, and 15.38 J, respectively. The cyclic work values are thus obtained from Eq. (2). Comparison of P-V diagrams at different charge pressures, depending on volume change of Stirling engine with bell-crank drive mechanism is given in Figure 6. The mass of the working fluid varies at a certain rate as the amount of charge pressure increases. The heater temperature was kept constant at 1000 K. Under these conditions, cyclic work values of this engine with bell-crank drive mechanism were obtained as 12.85 J, 25.70 J, 38.55 J, 51.40 J and 64.25 J, respectively. When the graphic and results are examined, it is determined that the net cyclic work amount performed increases in direct proportion to the charge pressure.

The linear reciprocating motion of the pistons between the bottom dead center and the top dead center in the cylinder is converted into circular motion via the drive mechanism. The faster this movement of the pistons in the cylinder, the higher the engine speed. In fact, although the velocity of a point on the crankshaft and flywheel is constant at constant engine speed, the velocity and direction of the piston are constantly changing. Piston velocities are a frequently used quantity as a comparison value between engines [20-21]. The velocity changes of the power piston and displacer piston obtained with the MSC Adams program depending on the 600 and 900 rpm engine speeds of the Stirling engine with bell-crank drive mechanism are given in Figure 7. and Figure 8. When the graphics are examined, it is seen that when the pistons go up to the top dead center at 600 rpm, they reach a speed of nearly 1.9 m/s, and the power piston and the displacer pistons move at different speeds when descending towards the bottom dead center. It is seen that the displacer piston reaches a velocity of approximately 2.3 m/s as it descends toward the lower dead point. At 900 rpm engine speed, the pistons reach a speed of approximately 2.8 m/s as they move towards the top dead center, and the power piston reaches a speed of 2.8 m/s and the displacer piston reaches a speed of 3.5 m/s when descending towards the bottom dead center. As seen in Figure 7 and Figure 8, the engine is in 1 second; it performs 10 cycles for 600 rpm engine speed and 15 cycles for 900 rpm engine speed.

In this section, the work topic should be stated in the previous work on the subject, the purpose of working with the relevant references supported. The entire article will be written in Times New Roman in 10 pt with a single line spacing. In this section, the work topic should be stated in the previous work on the subject, the purpose of working with the relevant references supported. The entire article will be written in Times New Roman in 10 pt with a single line spacing.

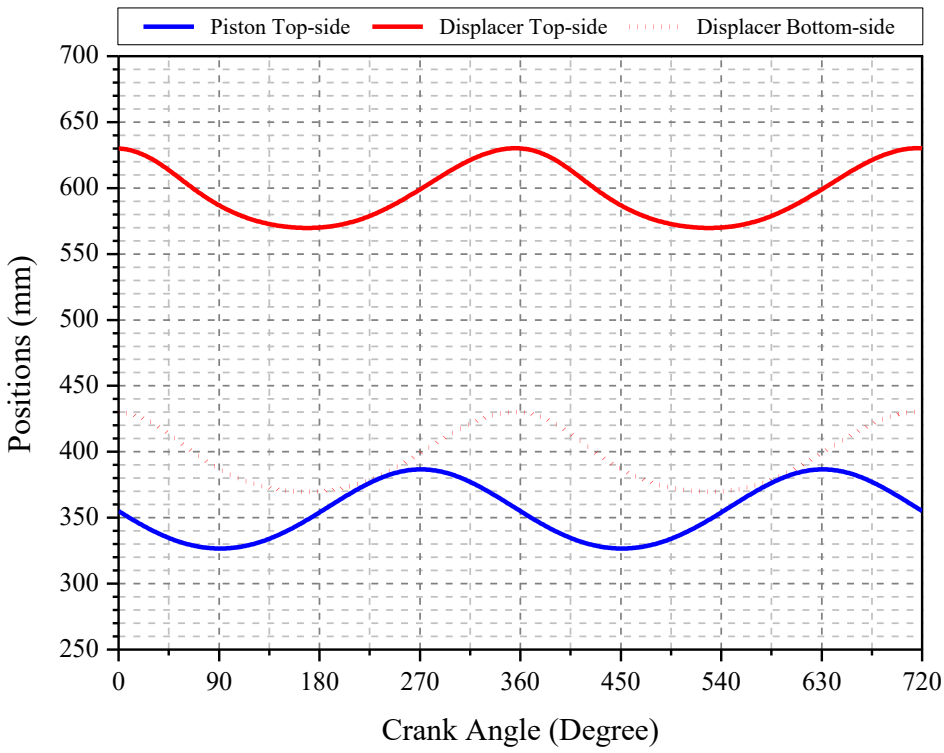

Figure 2. The variations of piston and displacer positions according to crank angle

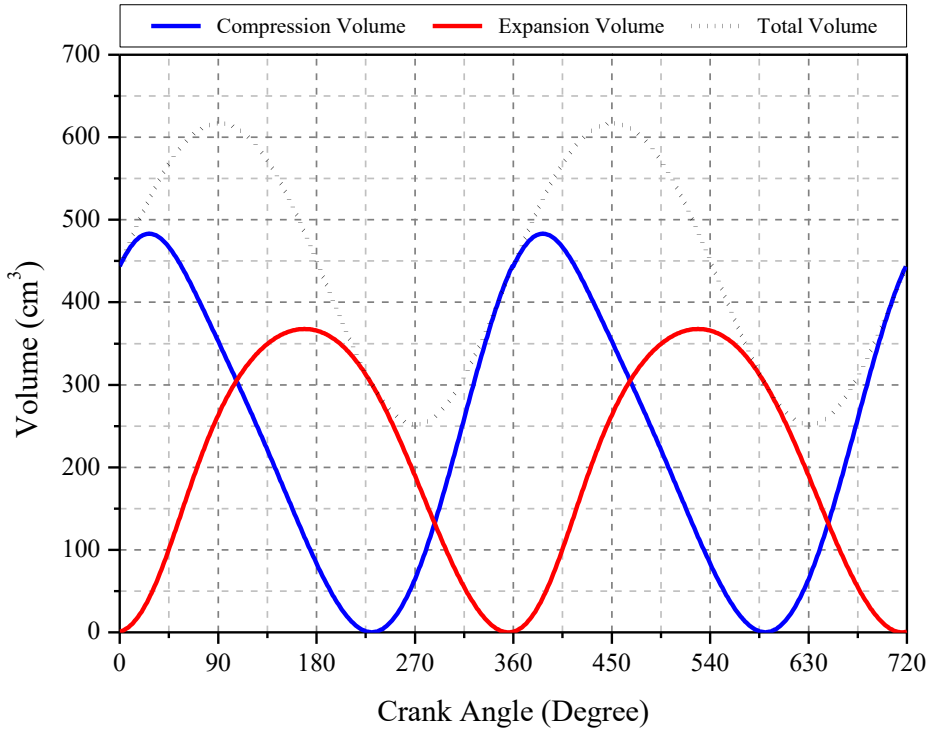

Figure 3. The variations of volume according to crank angle

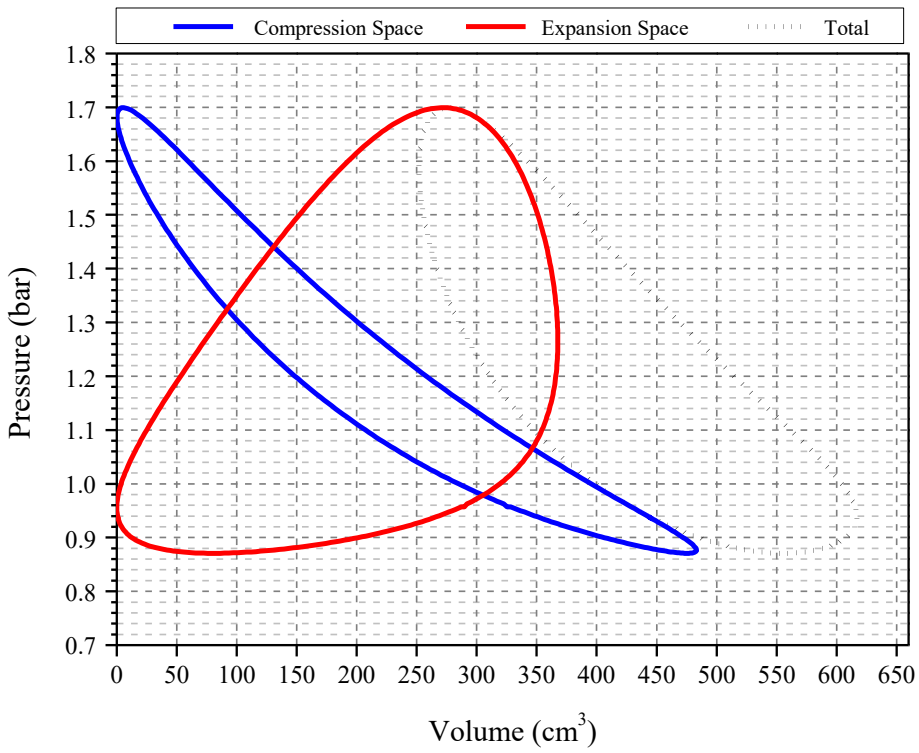

Figure 4. Comparison of expansion and compression chambers P-V diagrams

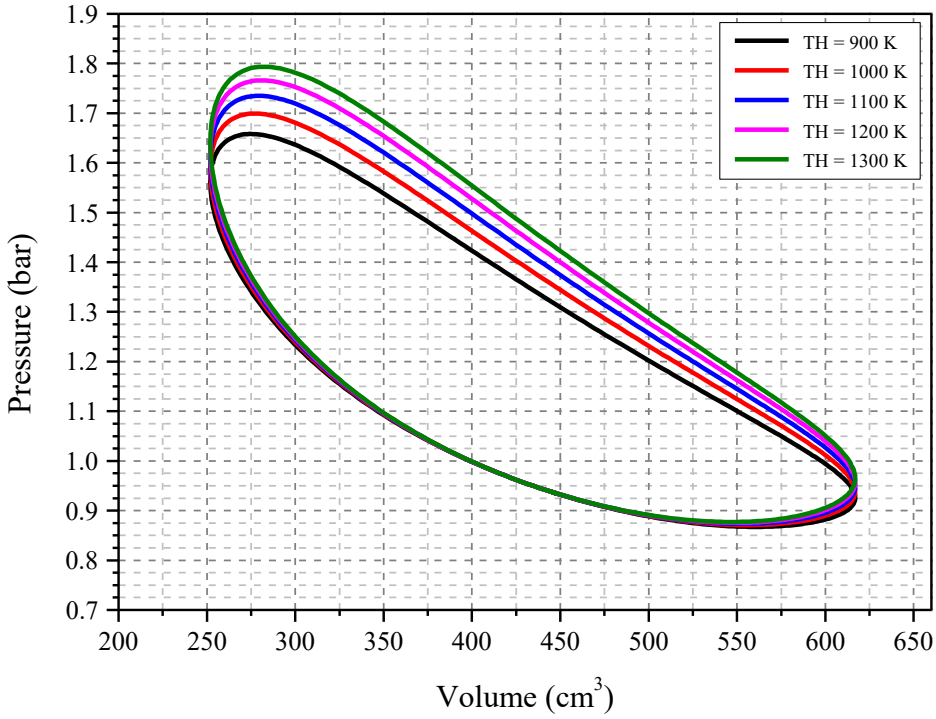

Figure 5. Comparison of P-V diagrams for different heater temperatures

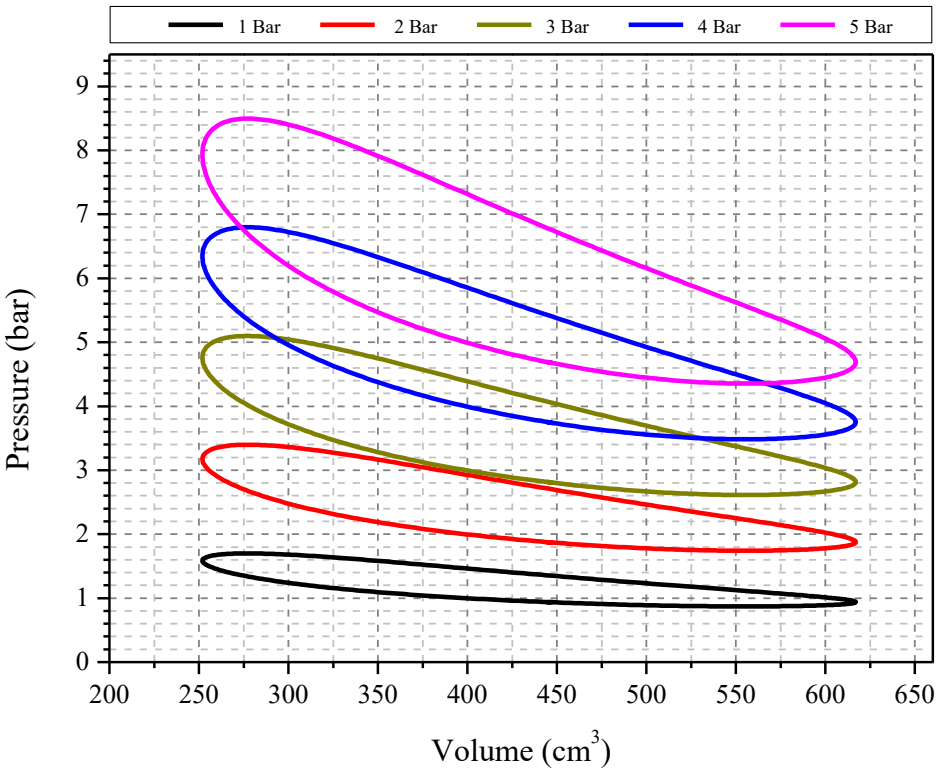

Figure 6. Comparison of P-V diagrams for different charge pressures

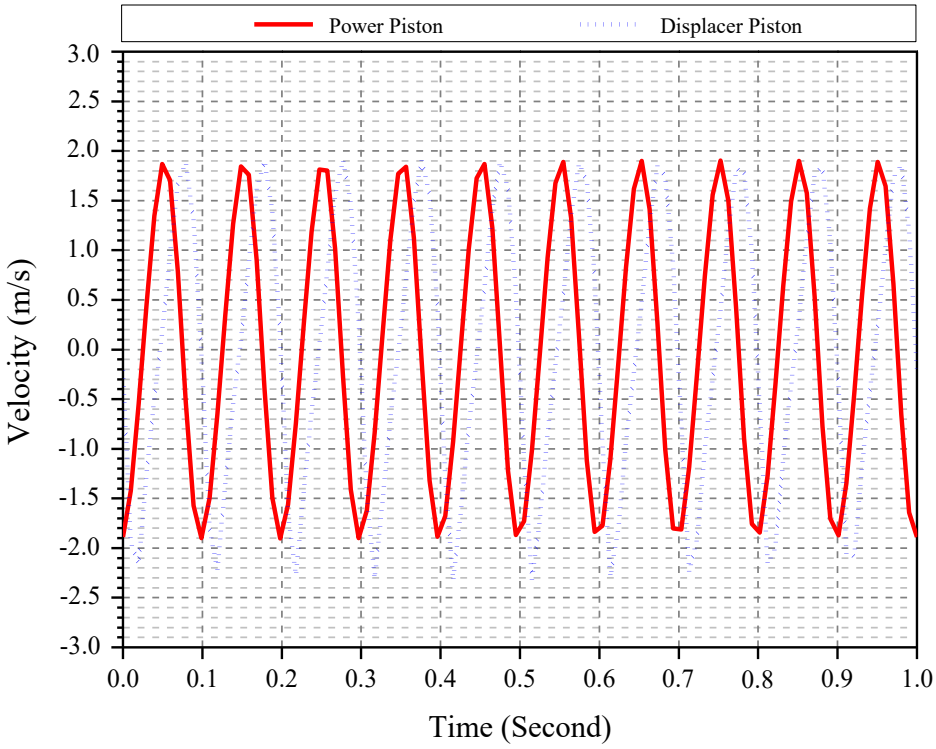

Figure 7. The variations of piston velocities according to time (600 rpm)

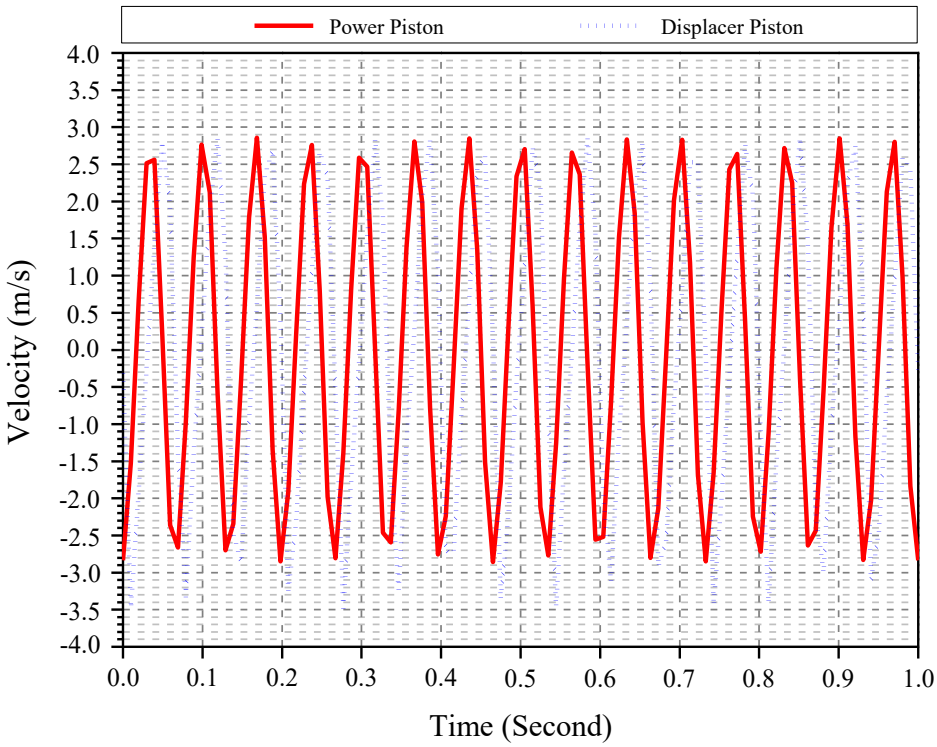

Figure 8. The variation of piston velocities according to time (900 rpm)

4. CONCLUSIONS

In this study, thermodynamic and kinematic analysis of a beta-type Stirling engine with bell-crank drive mechanism were examined. The fundamental parameters related to engine performance such as working fluid mass, charge pressure, heater and coolant temperature; the effects on the amount of net power are investigated. The pressure and volume changes of a beta type Stirling engine with bell-crank drive mechanism were determined using the MSC Adams program. In addition, velocity changes of the power and the displacer pistons were calculated at the 600 and 900 rpm engine speeds. It has been observed that the highest piston velocity values occurred at 900 rpm engine speed. It was determined that the velocities of the power and displacer pistons are nearly equal when they are moving toward the top dead center. The both pistons' velocities of moving towards the bottom dead center are different from each other.

Acknowledgements
This study was supported within the scope of project number 2023/058 by the Scientific Research Projects Coordination Unit of Kırıkkale University. I would like to thank the Scientific Research Projects Coordination Unit of Kırıkkale University for their support.

Ethics Committee Approval
N/A

Conflict of Interest
The author declares that they have no known competing financial interests or personal relationships that could have appeared to influence the work reported in this paper.

REFERENCES

[1] Erol, D., Yaman, H., Doğan, B. A review development of rhombic drive mechanism used in the Stirling engines. ***Renewable and Sustainable Energy Reviews,*** 2017;78:1044-1067.

[2] Meijer, R. J., The Philips Stirling thermal engine, analysis of the rhombic drive mechanism and efficiency measurements. Thesis, Technical University, Delft, 1960.

[3] Erol, D. and Çalışkan, S. The examination of performance characteristics of a beta-type Stirling engine with a rhombic mechanism: the influence of various working fluids and displacer piston materials. ***International Journal of Energy Research,*** 2021;45(9):13726-13747.

[4] Hargreaves, C.M. The Philips Stirling engine, Elsevier, New York, 1991.

[5] Finkelstein, T., and Organ, A. J. Air engines the history science and reality of the perfect engine. New York: The American Society of Mechanical Engineers; 2004.

[6] Stirling, R. Improvements for diminishing the consumption of fuel and in particular, an engine capable of being applied to the moving of machinery on a principle entirely new. British Patent No: 4081, 1816.

[7] Walker, G., Stirling engines. United States by Oxford University Press., 1980.

[8] Delyova, I., Hroncova, D., Frankovsky, P., Dzurisova, E., and Rakay, F. Kinematic analysis of crank rocker mechanism using MSC Adams/View. ***Applied Mechanics and Materials,*** 2014;611:90-97.

[9] Doane, J. Machine analysis with computer applications for mechanical engineers. John Wiley and Sons, 2015.

[10] Karabulut, H., Aksoy, F., and Öztürk, E. Thermodynamic analysis of a β type Stirling engine with a displacer driving mechanism by means of a lever. ***Renewable Energy,*** 2009;34(1):202-208.

[11] Karabulut, H., Çınar, C., Öztürk, E., and Yücesu, H. S. Torque and power characteristics of a helium charged Stirling engine with a lever controlled displacer driving mechanism. ***Renewable Energy,*** 2010;35(1):138-143.

[12] Erol, D., and Çalışkan, S. Comparative study on the performance of different drive mechanisms used in a beta type Stirling engine through thermodynamic analysis. ***International Journal of Automotive Engineering and Technologies,*** 2019;8(2):44-60.

[13] Weenen, F. L. V., (1947). The Construction of the Philips air engine. ***Philips Technical Review***, 1947;9(5):125-134.

[14] Martin, G. H. *Kinematics and dynamics of machines*. Waveland Press, Inc, United State of America, 2002.

[15] Waldron, K. J., Kinzel, G. L., and Agrawal, S. K. *Kinematics, dynamics, and design of machinery*. John Wiley & Sons, 2016.

[16] Orlandea, N.V. Multibody systems history of Adams. ***Journal of Computational and Nonlinear Dynamics,*** 2016;11(6):060301.

[17] Shabana, A. A. An important chapter in the history of multibody system dynamics. ***Journal of Computational and Nonlinear Dynamics,*** 2016;11(6):060303.

[18] Schmidt, G. Theorie der Lehmann'schen Calorischen Maschine (Theory of Lehmann's caloric machine). Zeitschrift des Vereins deutscher Ingenieure. 1871;15.

[19] Urieli, I., and Berchowitz, D.M. Stirling cycle engine analysis. Adam Hilger Ltd, Bristol; 1984.

[20] Taylor, C. F. The internal combustion engine in theory and practice. Massachusetts Institute of Technology, London, England, 1998.

[21] Ferrari, G., Onorati, A., and D'Errico, G. Internal combustion engines Societa Editrice Esculapio, 2014.

Prioritization of Cybersecurity Strategies: A Hesitant Fuzzy Linguistic MCDM Approach

Merve Güler*[1], Gülçin Büyüközkan[2], Esin Mukul[3]

Abstract: Cybersecurity threats have become a significant challenge for any important digital infrastructure, and numerous cyber-attacks have also become a major concern for society. Cybersecurity is an approach of guarding against digital attacks on systems, networks, and programs. Institutions aim to create effective cybersecurity procedures, create in-house awareness, train their employees on this issue, and strengthen their cybersecurity infrastructure. A strategic approach is required for institutions to effectively implement cybersecurity measures. This study aims to address security challenges and present a cybersecurity strategy prioritization model that would guide institutions in their cybersecurity operations. Hesitant Fuzzy Linguistic Term Sets (HFLTS) technique is used to represent Decision Makers' (DMs') opinions by addressing the problem of expressing concepts through crisp numbers, and ambiguity. The HFL AHP (Analytic Hierarchy Process) approach is used to compute the weights of the assessment criteria, while the HFL VIKOR (VIseKriterijumsaOptimizacija I KompromisnoResenje) method is used to prioritize the alternatives. The HFL AHP method was chosen because it is flexible, intuitive, practical and considers consistency. The HFL VIKOR method was chosen because it is a method that provides a consensus-based solution. To demonstrate the effectiveness of the proposed research methodology, a case study is provided. Finally, the results are presented along with suggestions for further research.

Keywords: AHP, Cybersecurity, Hesitant Fuzzy Linguistic Term Sets, MCDM, VIKOR.

[1,2,3]**Address:** Galatasaray University, Faculty of Engineering and Technology, İstanbul/Türkiye

***Corresponding author**: mguler@gsu.edu.tr

1. INTRODUCTION

Recently, cyber-attacks and security breaches of technological systems have been increasing rapidly. In most of the studies, it has been emphasized that the new generation technologies are an attack element and that the systems used have become targets. Cyber-attacks are actions that aim to steal, change or even destroy sensitive information by taking advantage of security vulnerabilities and generally aiming to gain financial gain. The target of these attacks may be the critical infrastructures of countries (energy, communication, health, finance, dams, pipelines, etc.). Therefore, cyber-attacks cause material and moral damage to many organizations around the world. For this reason, it is inevitable for institutions to attach importance to cybersecurity.

Cybersecurity is the set of measures taken against cyber-attacks. Organizations needs to prioritize their strategies to effectively establish cybersecurity procedures, create internal awareness, train their employees, strengthen their cybersecurity infrastructure and ultimately increase their cyber resilience (Erdoğan et al., 2020). The aim of the cybersecurity strategy is to increase the security of the systems and infrastructures that individuals and institutions use in their business and services. As a matter of fact, in this study, it is aimed to address the security issues of institutions and to propose a cybersecurity strategy prioritization model that will guide institutions in their cybersecurity practices.

The cybersecurity strategy prioritization problem should be considered from various dimensions. Therefore, due to the nature of the problem, there are many factors and uncertainties to consider. In this study, Hesitant Fuzzy Linguistic (HFL) Multi-Criteria Decision Making (MCDM) approach is applied. To overcome hesitation in decision-makers' (DMs) decisions, Hesitant Fuzzy Linguistic Term Sets (HFLTS) technique proposed by Rodríguez et al. (2011) is used. In the first part of the study; the weights of the factors in the cybersecurity model are found by the HFL AHP (Analytical Hierarchy Process) method. HFL AHP method is chosen because it is flexible, intuitive, practical and considers consistency. In the second part of the study; cybersecurity strategy alternatives are ranked with the HFL VIKOR (VIseKriterijumsaOptimizacija I KompromisnoResenje) method. HFL VIKOR method is chosen because it is a method that provides a consensus-based solution. In addition, VIKOR provides maximum group benefit for the majority of experts and minimum personal regret for dissenters. The evaluation model presented in the study is determined by reviewing the literature, examining industry reports and taking the opinions of experts. Then, a case study of the proposed approach is carried out and the results of the study are given.

In recent years, the studies about cybersecurity strategies has grown intensely, while some of the previous studies have examined the subject with various MCDM methods (Ganin et al., 2020; Kumar et al., 2020; Torbacki, 2021). Torbacki (2021) proposed a cybersecurity structure with Decision Making Trial and Evaluation Laboratory (DEMATEL), Analytic Network Process (ANP), and Preference Ranking Organization Method for Enrichment Evaluation II (PROMETHEE II) methods for sustainable manufacturing. Ganin et al. (2020) presented a model for cybersecurity risk assessment with Multi-Criteria Decision Analysis (MCDA) technique. Kumar et al. (2020) utilized fuzzy AHP-Technique for Order Preference by Similarity to an Ideal Solution (TOPSIS) approaches for evaluating cybersecurity systems of health information systems. As a result, the primary contribution of this paper is the first use of the HFL AHP and HFL VIKOR methods in prioritizing cybersecurity strategies.

The remainder of this paper is organized as follows. The research methodology is described in the second section. A presentation of the case study is included in the third section. The final section includes a summary of the findings and potential research areas for future research.

2. RESEARCH METHODOLOGY

The proposed HFL AHP-HFL VIKOR methodology includes 3 steps as seen in Figure 1.

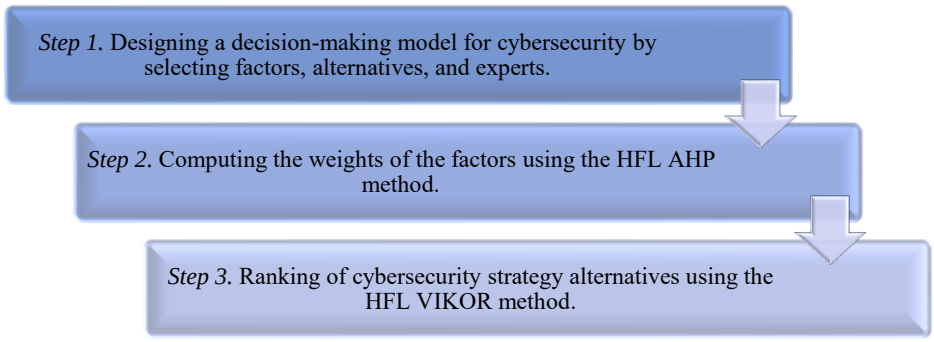

Figure 1. The main steps of the proposed research methodology

The HFLTS technique which was proposed by Rodríguez et al. (2011), was created using a collection of HFLTS. Please see (Rodríguez et al., 2011, 2013) for further details on the HFLTS technique. The next section explains the steps of the HFL AHP and HFL VIKOR approaches.

2.1. HFL AHP Method

Step 1. The experts evaluated the criteria by using the linguistic term set provided in Table 1.

Table 1. The linguistic term set used in HFL AHP method (Kulak & Kahraman, 2005)

Linguistic terms	Fuzzy Numbers
Just equal	(1,1,1)
Equally important	(1/2,1,3/2)
Weakly more important	(1,3/2,2)
Strongly more important	(3/2,2,5/2)
Very strongly more important	(2,5/2,3)
Absolutely more important	(5/2,3,7/2)

Step 2. The linguistic terms are translated into HFLTS, and pairwise comparison matrices are constructed.
Step 3. A matrix for pairwise comparison $(\tilde{C})$ is found. The reciprocal values are obtained (Büyüközkan & Güler, 2020):

$$\tilde{c}_{ij} = \left(\frac{1}{c_{iju}}, \frac{1}{c_{ijm2}}, \frac{1}{c_{ijm1}}, \frac{1}{c_{ijl}}\right) \quad (1)$$

Step 4. The fuzzy geometric mean $(\tilde{r}_i)$ of matrix $(\tilde{C})$ is calculated as follows:

$$\tilde{r}_i = (\tilde{c}_{i1} \otimes \tilde{c}_{i2} \ldots \otimes \tilde{c}_{in})^{1/n} \quad (2)$$

Step 5. The fuzzy weight ($\tilde{w}_i^{CR}$) of every main criteria is calculated:

$$\tilde{w}_i^{CR} = \tilde{r}_i \otimes (\tilde{r}_1 \otimes \tilde{r}_2 \ldots \otimes \tilde{r}_n)^{-1} \quad (3)$$

Step 6. The fuzzy global weights of sub-criteria are computed:

$$\tilde{w}_{ij}^{G} = \tilde{w}_i^{CR} \times \tilde{w}_j^{CR} \quad (4)$$

where $\tilde{w}_{ij}^{G}$ is the global weight of sub-criteria.
Step 7. The trapezoidal fuzzy numbers $\tilde{w}_{ij}^{G}$ using are defuzzified and they are normalized:

$$w_{ij}^{G} = \frac{\alpha+2\beta+2\gamma+\delta}{6} \quad (5)$$

$$w_{ij}^{N} = \frac{w_{ij}^{G}}{\sum_i \sum_j w_{ij}^{G}} \quad (6)$$

2.2. HFL VIKOR Method

Step 1. The experts evaluated the criteria by using the linguistic term set provided in Table 2.

Table 2. The linguistic term set used in HFL VIKOR method (Chou et al., 2008)

Linguistic terms	Fuzzy Numbers
Very bad	(0,0,3)
Bad	(0,3,3,5)
Medium	(2,5,5,8)
Good	(5,7,7,10)
Very good	(7,10,10,10)

Step 2. The linguistic terms are translated into HFLTS.

Step 3. The elements of the $\widetilde{R_{ij}}$ are computed as (Büyüközkan & Güler, 2021):

$$\widetilde{r_{ij}} = \left(\frac{xij1}{xij4^+}, \frac{xij2}{xij4^+}, \frac{xij3}{xij4^+}, \frac{xij4}{xij4^+}\right), C_j \in B \quad (7)$$

$$\widetilde{r_{ij}} = \left(\frac{xij1}{xij1^-}, \frac{xij2}{xij1^-}, \frac{xij3}{xij1^-}, \frac{xij4}{xij1^-}\right), C_j \in C \quad (8)$$

where $xij4^+ = \max_i\{\widetilde{X_{ij}}\}, C_j \in B$ and $xij1^- = \min_i\{\widetilde{X_{ij}}\}, C_j \in C$.

Step 4. The normalized matrix R_{ij} with crisp numbers is computed as:

$$\text{Defuzz}(Xij) = \int \frac{\mu(x).\,x\mathrm{d}x}{\mu(x).\,\mathrm{d}x} = \frac{\int_{x_{ij1}}^{x_{ij2}} \left(\frac{x-x_{ij1}}{x_{ij2}-x_{ij1}}\right).\,x\mathrm{d}x + \int_{x_{ij2}}^{x_{ij3}} x\mathrm{d}x + \int_{x_{ij3}}^{x_{ij4}} \left(\frac{x_{ij4}-x}{x_{ij4}-x_{ij3}}\right).\,x\mathrm{d}x}{\int_{x_{ij1}}^{x_{ij2}} \left(\frac{x-x_{ij1}}{x_{ij2}-x_{ij1}}\right)\mathrm{d}x + \int_{x_{ij2}}^{x_{ij3}} \mathrm{d}x + \int_{x_{ij3}}^{x_{ij4}} \left(\frac{x_{ij4}-x}{x_{ij4}-x_{ij3}}\right)\mathrm{d}x} = \frac{-x_{ij1}x_{ij2}+x_{ij3}x_{ij4}+\frac{1}{3}(x_{ij4}-x_{ij3})^2-\frac{1}{3}(x_{ij2}-x_{ij1})^2}{-x_{ij1}-x_{ij2}+x_{ij3}+x_{ij4}} \quad (9)$$

Step 5. The weighted normalized matrix's elements are calculated as:

$$v_{ij} = r_{ij}.w_j \quad (10)$$

Step 6. The ideal f_j^* and f_j^- values $(j=1,2,\ldots,n)$ are determined. If the jth function is related with benefit factors, then:

$$f_j^* = \max f_{ij} \ , \quad f_j = \min f_{ij} \tag{11}$$

If the jth function is related with cost factors, then:

$$f_j^* = \min f_{ij} \ , \quad f_j = \max f_{ij} \tag{12}$$

Step 7. The S_i , R_i, and Q_i, values $i=1,2,...,I$, are computed as:

$$S_i = \sum_{j=1}^{n} w_j \frac{(f_j^* - f_{ij})}{(f_j^* - f_j^-)} \tag{13}$$

$$R_i = \max \left[wj \frac{(f_j^* - f_{ij})}{(f_j^* - f_j^-)} \right] \tag{14}$$

$$Q_i = \theta \frac{(S_i - S^*)}{(S^- - S^*)} + (1-\theta) \frac{(R_i - R^*)}{(R^- - R^*)} \tag{15}$$

$$S^* = \min S_i, \qquad S^- = \max S_i \tag{16}$$

$$R^* = \min R_i, \qquad R^- = \max R_i \tag{17}$$

3. CASE STUDY

Cyber-attacks are actions that aim to steal, change or even destroy sensitive information by taking advantage of security vulnerabilities and generally aiming to gain financial gain. The target of these attacks may be the critical infrastructures of countries (energy, communication, health, finance, etc.). Cyber-attacks cause material and moral damage to many organizations around the world. It is inevitable for institutions to attach importance to cyber security. As stated in the "National Cyber Security Strategy and Action Plan (2020-2023)" report, Turkey needs to establish a good cyber security strategy to increase the cyber resilience of institutions (T.C. Ulaştırma ve Altyapı Bakanlığı, 2023).

This study proposes a model for prioritizing cybersecurity strategies that was developed after evaluating academic articles, industry reports, and expert opinions (Deloitte, 2022; Karabacak et al., 2016; PWC, 2018; Tu et al., 2018; Yeoh et al., 2022; Zammani et al., 2019). Figure 2 provides an illustration of this model. The cybersecurity alternatives are determined based on reports. These alternatives are (T.C. Ulaştırma ve Altyapı Bakanlığı, 2023):

1. Protecting Critical Infrastructures and Increasing Strength (A1)
2. Developing National Capacity (A2)
3. Organic Cyber Security Network (A3)
4. Security of Next Generation Technologies (A4)
5. Fighting Cybercrime (A5)
6. Development and Support of Domestic and National Technologies (A6)
7. Integration of Cyber Security into National Security (A7)
8. Developing International Cooperation (A8)

HFL AHP method is used in the first phase to compute the factors' weights. Table 3 displays the evaluations made by the DMs. The HFL AHP method's stages are applied with Eqs. (1)-(6). Table 4 illustrates the final factor weights.

Table 3. The evaluation about factors

	F1	F2	F3	F4	F5
F1	Just equal	At least weakly more important	At most weakly more important	-	-
F2	-	Just equal	-	-	-
F3	-	At least weakly more important	Just equal	-	-
F4	At most equally important	At least strongly more important	At least weakly more important	Just equal	At most equally important
F5	At most equally important	At least strongly more important	At least weakly more important	-	Just equal

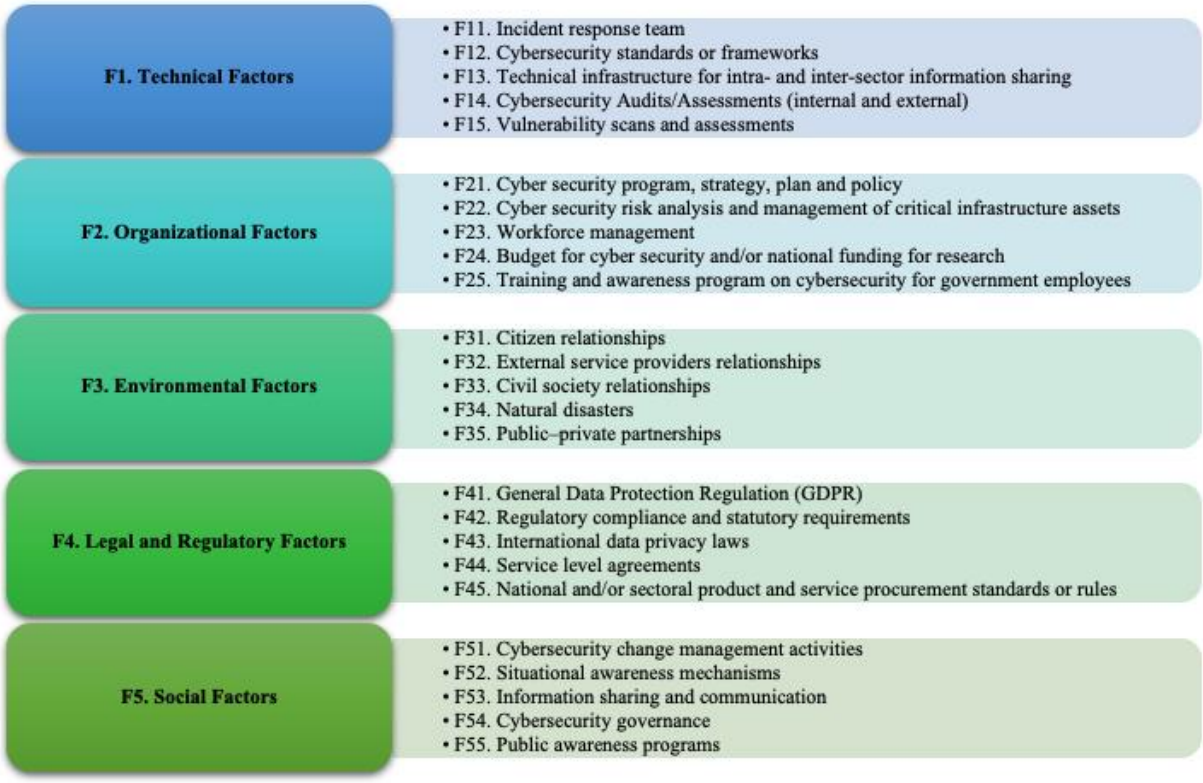

Figure 2. The factors in the proposed model (Deloitte, 2022; Karabacak et al., 2016; PWC, 2018; Tu et al., 2018; Yeoh et al., 2022; Zammani et al., 2019)

Table 4. The weights of the factors

Main Factors	Weights	Sub-Factors	Local Weights	Weights	Ranking
F1	0.180	F11	0.210	0.041	12
		F12	0.040	0.008	24
		F13	0.120	0.023	19
		F14	0.377	0.074	3
		F15	0.376	0.073	2
F2	0.055	F21	0.205	0.040	13
		F22	0.037	0.007	25
		F23	0.217	0.042	11
		F24	0.302	0.059	5
		F25	0.239	0.047	10
F3	0.123	F31	0.178	0.035	16
		F32	0.044	0.009	23
		F33	0.188	0.037	14
		F34	0.297	0.058	6
		F35	0.294	0.057	7
F4	0.307	F41	0.415	0.081	1
		F42	0.269	0.052	8
		F43	0.068	0.013	22
		F44	0.141	0.028	18
		F45	0.106	0.021	20
F5	0.335	F51	0.187	0.036	15
		F52	0.072	0.014	21
		F53	0.148	0.029	17
		F54	0.254	0.050	9
		F55	0.339	0.066	4

The most impotent criterion is found as "F41. General Data Protection Regulation (GDPR)", the second important one is "F15. Vulnerability scans and assessments" and the third-ranked criterion is "F14. Cybersecurity Audits/Assessments".

In the second step, the alternatives are assessed by using HFL VIKOR method. First, experts evaluated the alternatives regarding factors by using the linguistic scale given in Table 2. Table 5 shows the evaluations made by the DMs. Then, by using Eqs. (7)-(17), the steps of the HFL VIKOR technique are applied. Table 6 displays the ranking lists.

Table 5. The assessment about alternatives

	F11	F12	F13	F14	F15
A1	At least very good	At least very good	At least very good	Between good and medium	Vg
A2	At most bad	Between bad and very bad	Between bad and very bad	At most bad	Between bad and very bad
A3	Between good and medium	Between medium and good	At most medium	At most bad	Between medium and good
A4	Between good and medium	At least very good	At least very good	Between good and medium	At least very good
A5	At least very good	At most medium	At most medium	Between good and medium	At least very good
A6	At least very good	At least very good	At least vg	Between good and medium	At least very good
A7	Between medium and good	At most medium	At most medium	Between bad and very bad	Between bad and very bad
A8	At most bad	Between good and medium	Between bad and very bad	At most bad	Between bad and very bad

Table 6. The result of HFL VIKOR method

	Q_i (v=0.5)	Ranking	S_i	Ranking	R_i	Ranking
A1	0.949	6	39.123	6	3.052	8
A2	0.914	5	39.100	5	3.052	8
A3	0.250	3	38.992	3	3.010	3
A4	1.000	8	39.157	8	3.052	8
A5	0.137	2	38.917	2	3.010	3
A6	0.872	4	39.072	4	3.052	8
A7	0.000	1	38.827	1	3.010	3
A8	0.967	7	39.135	7	3.052	8

C1. Acceptable advantage:
The condition $Q(a'')-Q(a') \geq DQ$ (**) is not satisfied ($0.137 \ngeq 0.143$)
Where $DQ = 1/(8-1) = 0.143$
C2. Acceptable stability in decision making:
Alternative a' should also be the best ranked according to S and/or R values. A7 is the best alternative according to both Q and S values, this condition is met.
If condition $C1$ is unsatisfactory, alternatives $a', a'', \ldots, a(M)$ and $a(M)$ are determined by the relation (**) for maximum M. Therefore, A7, A5 and A3 alternatives are included in the compromise solution.

4. DISCUSSION AND CONCLUSIONS

Rapid digitalization in advanced economies during COVID-19 has led to new cyber vulnerabilities (McLennan & Group, 2022). In particular, elements such as communication, banking services, public activities, defense systems, military systems and network systems have become the main target (Kurtul & Zeyveli, 2022). As a result of rising threats and actual attacks, critical infrastructure cyber resilience has become a key necessity of national security (Karabacak et al., 2016).

The aim of this study was addressing the security issues of institutions and to propose a cybersecurity strategy prioritization model that will guide institutions in their cybersecurity practices. HFL AHP-HFL VIKOR methodology is used for the first time in this field. At the end of the application, the most important factor is found as "F41. General Data Protection Regulation (GDPR)", and the first ranked alternative is determined as A7; which is "Integration of Cyber Security into National Security". Cybersecurity is an integral part of national security. In our high-level national

security policies, it is aimed to protect our country from hybrid threats, including cyber elements, and to increase deterrence (T.C. Ulaştırma ve Altyapı Bakanlığı, 2023).

For future studies, the interaction between the factors can be taken into account and the HFL ANP method can be applied. Group decision making approach can be used. Furthermore, it is possible to improve work with advanced decision making techniques.

Acknowledgements
This work has been supported by the Scientific Research Projects Commission of Galatasaray University under grant number FOA-2021-1059 and FOA-2023-1181.

Ethics Committee Approval
N/A

Peer-review
Externally peer-reviewed.

Author Contributions
Conceptualization: M.G., G.B., E.M.; Investigation: M.G., G.B., E.M.; Material and Methodology: G.B., M.G., E.M.; Supervision: G.B.; Visualization: M.G., G.B., E.M.; Writing-Original Draft: M.G.; Writing-review & Editing: M.G., G.B., E.M.; Other: All authors have read and agreed to the published version of manuscript.

Conflict of Interest
The authors have no conflicts of interest to declare.

Funding
This work has been supported by the Scientific Research Projects Commission of Galatasaray University.

REFERENCES

Büyüközkan, G., & Güler, M. (2020). Analysis of companies' digital maturity by hesitant fuzzy linguistic MCDM methods. Journal of Intelligent and Fuzzy Systems, 38(1), 1119–1132. https://doi.org/10.3233/JIFS-179473

Büyüközkan, G., & Güler, M. (2021). A combined hesitant fuzzy MCDM approach for supply chain analytics tool evaluation. Applied Soft Computing, 112, 107812.

Chou, S. Y., Chang, Y. H., & Shen, C. Y. (2008). A fuzzy simple additive weighting system under group decision-making for facility location selection with objective/subjective attributes. European Journal of Operational Research, 189(1), 132–145. https://doi.org/10.1016/j.ejor.2007.05.006

Deloitte. (2022). Cybersecurity Strategy. In Reimagining OT cybersecurity strategy.

Erdoğan, M., Karaşan, A., Kaya, İ., Budak, A., & Çolak, M. (2020). A fuzzy based MCDM methodology for risk evaluation of cyber security technologies. Advances in Intelligent Systems and Computing, 1029, 1042–1049. https://doi.org/10.1007/978-3-030-23756-1_123

Ganin, A. A., Quach, P., Panwar, M., Collier, Z. A., Keisler, J. M., Marchese, D., & Linkov, I. (2020). Multicriteria Decision Framework for Cybersecurity Risk Assessment and Management. Risk Analysis, 40(1), 183–199. https://doi.org/10.1111/RISA.12891

Karabacak, B., Yildirim, S. O., & Baykal, N. (2016). A vulnerability-driven cyber security maturity model for measuring national critical infrastructure protection preparedness. International Journal of Critical Infrastructure Protection, 15, 47–59. https://doi.org/10.1016/j.ijcip.2016.10.001

Kulak, O., & Kahraman, C. (2005). Fuzzy multi-attribute selection among transportation companies using axiomatic design and analytic hierarchy process. Information Sciences, 170(2–4), 191–210.

Kumar, R., Pandey, A. K., Baz, A., Alhakami, H., Alhakami, W., Agrawal, A., & Khan, R. A. (2020). Fuzzy-based symmetrical multi-criteria decision-making procedure for evaluating the impact of harmful factors of healthcare information security. Symmetry, 12(4). https://doi.org/10.3390/SYM12040664

Kurtul, A., & Zeyvelİ, M. F. (n.d.). Siber Güvenlik Raporu.

McLennan, M., & Group, S. (2022). The Global Risks Report 2022. https://www.weforum.org/reports/global-risks-report-2022

PWC. (2018). Cyber Risk-Having better conversations on cyber. PwC. www.pwc.com/sg/risk-assurance

Rodríguez, R. M., Martinez, L., & Herrera, F. (2011). Hesitant fuzzy linguistic term sets for decision making. IEEE Transactions on Fuzzy Systems, 20(1), 109–119.

Rodríguez, R. M., Martínez, L., & Herrera, F. (2013). A group decision making model dealing with comparative linguistic expressions based on hesitant fuzzy linguistic term sets. Information Sciences, 241, 28–42.

T.C. Ulaştırma ve Altyapı Bakanlığı. (n.d.). Ulusal Siber Güvenlik Stratejisi ve Eylem Planı 2020-2023.

Torbacki, W. (2021). A hybrid mcdm model combining danp and promethee ii methods for the assessment of cybersecurity in industry 4.0. Sustainability (Switzerland), 13(16). https://doi.org/10.3390/su13168833

Tu, C. Z., Yuan, Y., Archer, N., & Connelly, C. E. (2018). Strategic value alignment for information security management: a critical success factor analysis. Information and Computer Security, 26(2), 150–170. https://doi.org/10.1108/ICS-06-2017-0042

Yeoh, W., Wang, S., Popovič, A., & Chowdhury, N. H. (2022). A systematic synthesis of critical success factors for cybersecurity. Computers and Security, 118. https://doi.org/10.1016/j.cose.2022.102724

Zammani, M., Razali, R., & Singh, D. (2019). Factors contributing to the success of information security management implementation. International Journal of Advanced Computer Science and Applications, 10(11), 384–391. https://doi.org/10.14569/IJACSA.2019.0101153

Analysis and Comparison of Commonly Used Three Level Inverter Topologies

Berkay Sabuncu[1], Ali Bekir Yıldız[1]

Abstract: With the widespread use of renewable energy systems, the design and features of the power equipment used in these systems are gaining importance day by day. In systems involving solar and wind energy, we come across inverters that work synchronously with the grid for energy transfer to the electricity grid.
In inverter topologies, it is expected that the values that are critical for the network and important in terms of converter quality parameters such as harmonic distortion values, power factor and efficiency parameters are kept high, or the quality standards are complied with. Therefore, many different techniques and topologies are applied to correct for efficiency and other operating values.
The reason for the use of topologies at high power values is that there are rooms of the level numbers and different switching techniques in the inverters. In particular, the size of the level dimensions and the output harmonic values and the limitation of the filter limits used accordingly, together with lower switching and reduction losses, multilevel inverters provide many advantages both in terms of cost and performance.
In this study, diode clamped and active clamped T-type structures in the three-level topology, which is frequently used as a multi-level inverter, are considered and their efficiency and performance values are compared.

Keywords: Multi level Inverter, Three Level T Type Inverter, Three Level Diode Clamped Inverter, Vector Control, Total Harmonic Distortion.

[1]**Address:** Kocaeli University, Department of Electrical Engineering, Kocaeli/Turkiye

***Corresponding author**: berkaysabuncu016@gmail.com

1. GİRİŞ

Günümüzde yeni enerji kaynakları üzerinde araştırmalar yapılmakta olup elimizde var olan enerji kaynaklarını, ekonomik şekilde kalitesini artırarak kullanıcıya ulaştırılması yönünde çalışmalar yapılmaktadır. Enerji ihtiyacının arttığı günümüzde yenilenebilir enerji sistemleri üzerine oldukça yoğun yatırımlar yapılmaktadır. Bu alanda rüzgar ve güneş enerjisi sistemlerine yapılan yatırımlar ve projeler ciddi önem teşkil etmektedir.

Yenilenebilir enerji sistemleri incelendiğinde, sistemlerin normal şartlarda sürekli güç transferi yapması yönündeki yetersizlikleri nedeniyle enerji depolama sistemleri ve bunların şebekeye entegrasyonunu sağlayacak güç elektroniği ekipmanlarının tasarlanması, gerekli sürekliliğin sağlaması açısından önemlidir. Depolama haricinde yenilenebilir enerji kaynağından elde edilen gücün elektrik şebekesine aktarılabilmesi için de enerjinin uygun forma getirilmesi gerekmektedir. Bu amaçla şebeke ile uygun formda çalışan ve standartlarda gerekli parametrelere uyan eviricilerin tasarlanması önemlidir.

1.1 Eviricilerin Sınıflandırılması

Eviriciler yapılarına göre incelendiğinde akım kaynaklı, empedans kaynaklı ve gerilim kaynaklı olarak ayrılmaktadırlar. Akım kaynaklı eviriciler genel olarak girişinde DC akım kaynağı sağlayan dönüştürücülerin kullanılmasıyla karşımıza çıkmaktadır. Empedans kaynaklı eviriciler girişinde bir empedans grubunun bağlanması ile girişleri kontrol edilmektedir. Uygulamalar genel olarak incelendiğinde gerilim kaynaklı eviricilerin yaygın olarak kullanıldığı görülmektedir. Gerilim kaynaklı eviriciler, DC girişlerinde kondansatör grubunun eklenmesiyle gerekli olan DC gerilimi karşılarlar.

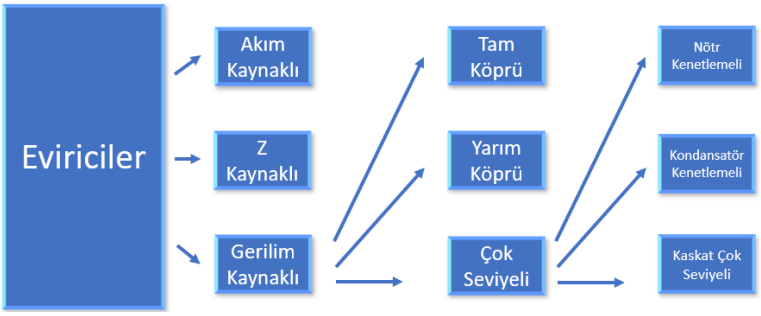

Şekil 1.1.1 Yapılarına Göre Evirici Türleri

Çok Seviyeli Eviriciler

Çok seviyeli eviriciler, nötr noktası kenetlemeli, kondansatör kenetlemeli ve kaskat bağlı olmak üzere farklı tip topolojilerle geliştirilebilir. Çok seviyeli eviriciler özellikle yüksek verim ve yüksek güç transferi gerektiren uygulamalarda tercih edilmektedir. Diğer bilinen iki seviyeli topolojilere kıyasla gerilim seviyelerini daha yüksek adımlarda oluşturarak çıkış geriliminin kalitesini arttırmakta ve kullanılacak filtre elemanlarının da boyutlandırılmasında yarar sağlamaktadırlar.

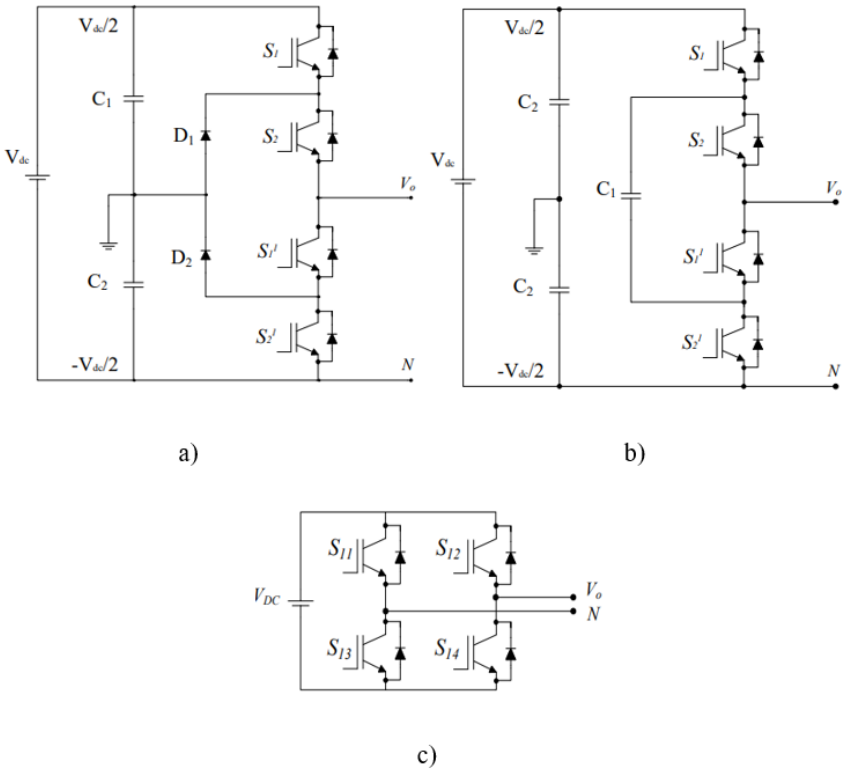

Şekil 1.1.2. a) Diyot Kenetlemeli Çok Seviyeli Evirici,, b) Kondansatör Kenetlemeli Çok Seviyeli Evirici, c) Kaskat Köprü Çok Seviyeli Evirici

Şekil 1.1.2' deki nötr noktası kenetlemeli eviriciler incelendiğinde giriş gerilimleri kondansatör gruplarıyla ikiye bölündüğü görülür. Anahtarların devreye girmesiyle +Vdc/2, -Vdc/2 ve 0 olmak üzere faz ve nötr uçlarında üç farklı gerilim düzeyi oluşturulur.

1.2 Üç Seviyeli Üç Fazlı Nötr Kenetlemeli Eviriciler

Şekil 1.2.1' de üç seviyeli üç fazlı diyot kenetlemeli evirici topolojisi gösterilmiştir. Devrede görüldüğü üzere her bir faz dört yarıiletken ve iki adet diyot üzerinden kontrol edilmektedir. Evirici bloğuna uygulanacak DC gerilim kondansatörler ile bölünerek orta noktası nötr ucu olarak alınmıştır.

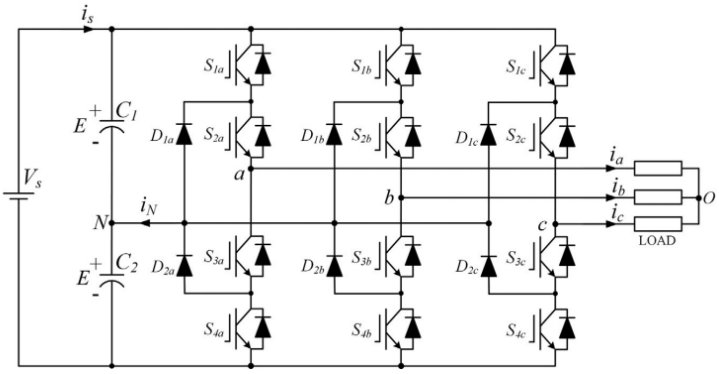

Şekil 1.2.1 Üç Seviyeli Üç Fazlı Diyot Kenetlemeli Evirici

Topoloji incelendiğinde yüksek gerilim uygulamalarında kondansatör gerilimlerini pasif olarak dengelemek için kullanılan kenetleme diyotları hem maliyet açısından hem de kontrol tekniğinin getirdiği bazı dezavantajlardan dolayı diyot kenetlemeli çok seviyeli eviricilerin kullanım alanlarını belli oranda sınırlamaktadır. Bu nedenle diyot kenetlemeli çok seviyeli evirici topolojileri beş seviye üzeri kullanımlarda tercih edilmemektedir. Anahtarlama metodu, temel frekansta kare dalga olarak uygulanabileceği gibi vektör kontrolü gibi gelişmiş darbe genişlik modülasyonlarını içeren metotlar da bu topolojide uygulanabilir.

T tipi kenetlemeli evirici topolojisi incelendiğinde diyot kenetlemeli yapıdan farklı olarak fazların nötr bağlantı noktaları yön olarak ters bağlı anahtarlar ile bağlıdır. Bu nedenle kondansatörlerdeki gerilim dengesizlikleri de aktif kenetleme yardımıyla ciddi anlamda önlenebilir.

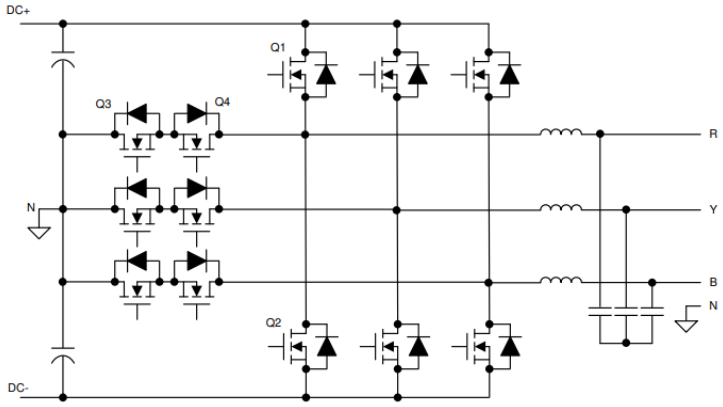

Şekil 1.2.2 Üç Seviyeli Üç Fazlı T Tipi Kenetlemeli Evirici

Topoloji incelendiğinde yüksek gerilim uygulamalarında kondansatör gerilimlerini aktif olarak dengelemek için kullanılan Q3 ve Q4 anahtarları hem maliyet açısından hem de kontrol tekniğinin getirdiği bazı avantajlardan dolayı T tipi kenetlemeli üç seviyeli evirici yüksek güç ve yüksek verim gerektiren uygulamalarda oldukça yaygın olarak tercih edilmektedir. Anahtarlama metodu, temel frekansta kare dalga olarak uygulanabileceği gibi vektör kontrolü gibi gelişmiş darbe genişlik modülasyonlarını içeren metotlar da bu topolojide uygulanabilir.

1.3 Üç Seviyeli Üç Fazlı Eviricilerde Kontrol

Üç seviyeli üç fazlı eviricilerde uzay-vektör kontrol yöntemi iki seviyeli klasik üç fazlı eviricide kullanılan metotların biraz daha geliştirilmesiyle sağlanmış olur. Diyot kenetlemeli üç seviyeli evirici ve T tipi nötr kenetlemeli eviricilerin vektör kontrol uygulamasında, clark ve park dönümümleri uygulanıp refereans gerilimi ve bu gerilimin θ açısı hesaplanır. Üç fazlı üç seviyeli eviricilerde ve diyot kenetlemeli 3 seviyeli eviricilerde gerekli çıkış gerilimleri oluşturulması için 27 farklı anahtarlama senaryosu gerçekleşmektedir. Oluşacak olan bu 27 alt devre 19 vektör ile tanımlanıp karşılık olarak aldığı değerler Şekil 1.3.1' deki tabloda belirtilmiştir.

$\overline{V_0}$	[PPP], [OOO], [NNN]	*Sıfır Vektörü*	0
$\overline{V_1}$	[ONN], [POO]	*Kısa Vektör*	$Vdc/3$
$\overline{V_2}$	[OON], [PPO]		
$\overline{V_3}$	[NON], [OPO]		
$\overline{V_4}$	[NOO], [OPP]		
$\overline{V_5}$	[NNO], [OOP]		
$\overline{V_6}$	[ONO], [POP]		
$\overline{V_7}$	[PON]	*Orta Vektör*	$Vdc*\left(\frac{\sqrt{3}}{3}\right)$
$\overline{V_8}$	[OPN]		
$\overline{V_9}$	[NPO]		
$\overline{V_{10}}$	[NOP]		
$\overline{V_{11}}$	[ONP]		
$\overline{V_{12}}$	[PNO]		
$\overline{V_{13}}$	[PNN]	*Uzun Vektör*	$Vdc*\left(\frac{2}{3}\right)$
$\overline{V_{14}}$	[PPN]		
$\overline{V_{15}}$	[NPN]		
$\overline{V_{16}}$	[NPP]		
$\overline{V_{17}}$	[NNP]		
$\overline{V_{18}}$	[PNP]		

Şekil 1.3.1 Üç Fazlı Üç Seviyeli Eviricinin Vektör Kontrol Değerleri

Tablodaki vektörlerin sayıları ve değerleri göz önünde bulundurulduğunda, üç fazlı üç seviyeli eviriciler için vektör diyagramı Şekil 1.3.2'daki gibi tanımlanmaktadır.

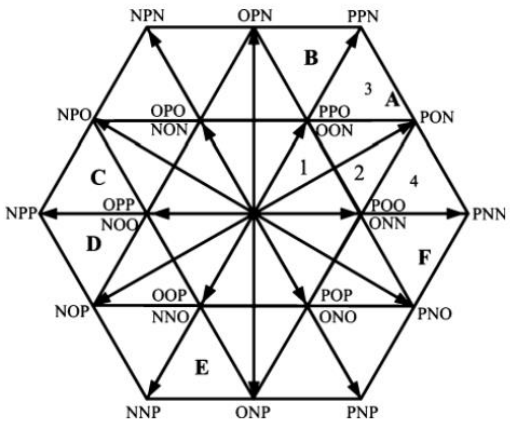

Şekil 1.3.2 Üç Fazlı Üç Seviyeli Eviricinin Vektör Kontrol Diyagramı

Vektör kontrol uygulamasında kontrol sinyallerinin üretilmesi için gerekli birtakım işlemler sırasıyla;

- Referans Gerilim Vektörünün Genliğinin ve Açısının Hesaplanması
- Vektör Diyagramında Sektör Belirleme
- Sektör Üzerinde Bölge Belirleme
- Konum Sürelerinin Belirlenmesi
- Darbe Sinyallerinin Belirlenmesi

olup, gerekli sinyaller oluşturulur. Referenas vektörünün genliği ve açısı;

$$V_a = V_m.\sin\omega t \tag{1.3.1}$$

$$V_b = V_m.\sin(\omega t - \frac{2\pi}{3}) \tag{1.3.2}$$

$$V_c = V_m.\sin(\omega t + \frac{2\pi}{3}) \tag{1.3.3}$$

$$\begin{bmatrix} V_d \\ V_q \end{bmatrix} = \frac{2}{3}\, x \begin{bmatrix} 1 & -1/2 & -1/2 \\ 0 & \sqrt{3}/2 & -\sqrt{3}/2 \end{bmatrix} x \begin{bmatrix} V_a \\ V_b \\ V_c \end{bmatrix} \tag{1.3.4}$$

$$V_{ref} = V_d + i.V_q = \frac{2}{3} * (V_a + a.V_b + a^2.V_c) \tag{1.3.5}$$

$$|V_{ref}| = \sqrt{{V_d}^2 + {V_q}^2} \tag{1.3.6}$$

$$\theta = tan^{-1}\left(\frac{V_q}{V_d}\right) \tag{1.3.7}$$

olacak şekilde hesaplanır. Belirlenen açı değeri ile referans vektörünün konumu;

Eğer θ açısı 0°≤ θ< 60° ise referans vektörü A sektöründedir.

Eğer θ açısı 60°≤ θ< 120° ise referans vektörü B sektöründedir.

Eğer θ açısı 120°≤ θ< 180° ise referans vektörü C sektöründedir.

Eğer θ açısı 180°≤ θ< 240° ise referans vektörü D sektöründedir.

Eğer θ açısı 240°≤ θ< 300° ise referans vektörü E sektöründedir.

Eğer θ açısı 300°≤ θ< 360° ise referans vektörü F sektöründedir.

durumları kontrol edilerek belirlenir.

Referans vektörünün belirlenmiş sektörün hangi bölgesinde olduğunu belirlemek için;

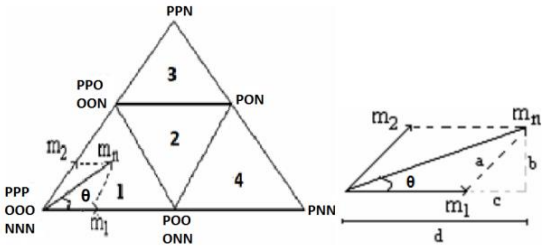

Şekil 1.3.3 A Sektöründe Belirtilmiş Referans Vektörü ve Sektör Üzerindeki Bölgeler

$$a = m_2 = \frac{b}{\sin\left(\frac{\pi}{3}\right)} = \frac{2.b}{\sqrt{3}} = \frac{2}{\sqrt{3}}.m_n.sin\theta \tag{1.3.8}$$

$$m_1 = m_n cos\theta - \left(\frac{2}{\sqrt{3}}.m_n.sin\theta\right).\cos\left(\frac{\pi}{3}\right) \tag{1.3.9}$$

$$m_1 = m_n.\left(cos\theta - \frac{sin\theta}{\sqrt{3}}\right) \tag{1.3.10}$$

Eğer m_2 ve $m_1 + m_2 < 0{,}5$ ise referans vektörü 1. bölgededir.

Eğer $m_1 > 0{,}5$ ise referans vektörü 4. bölgededir.

Eğer $m_2 > 0{,}5$ ise referans vektörü 3. bölgededir.

Eğer $m_1 ve\ m_2 > 0{,}5$ ve $m_1 + m_2 > 0{,}5$ ise referans vektörü 2. bölgededir.

Sektör ve bölge belirlemelerinin yapılmasının ardından konumu belirlenmiş referans vektörünün konum süreleri Ta, Tb ve Tc süreleri;

$$V_{ref}.T_s = V_1.T_a + V_8.T_b + V_2.T_c \tag{1.3.10}$$

$$T_s = T_a + T_b + T_c \tag{1.3.11}$$

$$T_a = T_s - 2Ksin(\theta) \tag{1.3.12}$$

$$T_b = 2Ksin\left(\frac{\pi}{3} + \theta\right) - T_s \tag{1.3.13}$$

$$T_c = T_s - 2Ksin(\frac{\pi}{3} - \theta) \tag{1.3.14}$$

$$K = \left(\frac{4\sqrt{3}}{3}\right)(m_a.T_s) \tag{1.3.15}$$

$$m_a = \left(\sqrt{3}\frac{V_{ref}}{V_{dc}}\right) \quad 0 \leq m_a \leq 1 \qquad m_a: modülasyon\ indeksi \tag{1.3.16}$$

olarak belirlenir.

Sonuç olarak uygulanan bu matematiksel algoritma sonucu A sektörü üzerindeki bölgelerde oluşturulan anahtarlama işaretleri Şekil 1.3.4’ teki gibidir.

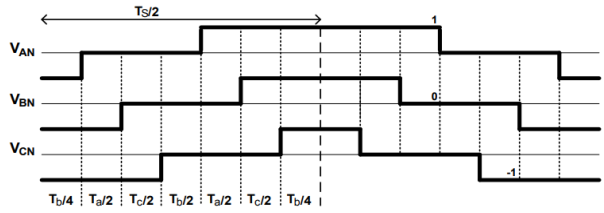

a) Sektör A, Bölge 1

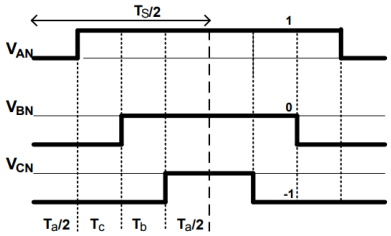

b) Sektör A, Bölge 4

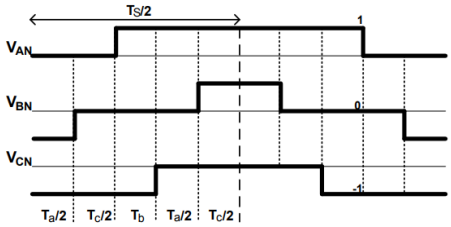

b) Sektör A, Bölge 2

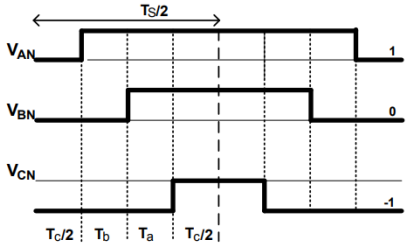

d) Sektör A, Bölge 3

Şekil 1.3.4 Sektör A Referans Vektörünün Bölgelere Göre Anahtarlama Durumu

2. MATERYAL VE METOT

Bu çalışmada üç seviyeli eviricilerin en sık kullanılan iki topolojisi olan diyot kenetlemeli ve T tipi kenetlemeli evirici topolojileri, vektör kontrol metoduyla ele alınmıştır. Ele alınan sistemler Mathlab/Simulink ortamında simüle edilerek sonuçları ayrı ayrı incelenmiştir. Giriş bölümünde ele alınan üç seviyeli eviriciler için vektör kontrol metodu, bu simülasyonda uygulanmıştır. Ele alınan iki evirici modelinin Simulink üzerindeki modellenmesi Şekil 2.1 ve Şekil 2.2' de gösterilmiştir.

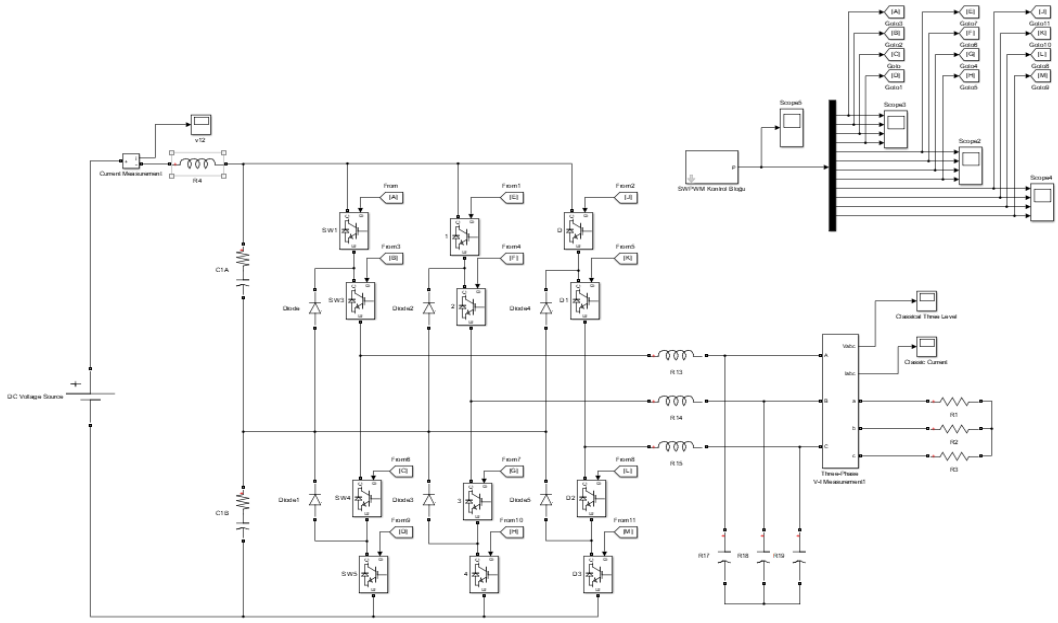

Şekil 2.1 Diyot Kenetlemeli Evirici Simulink Modellemesi

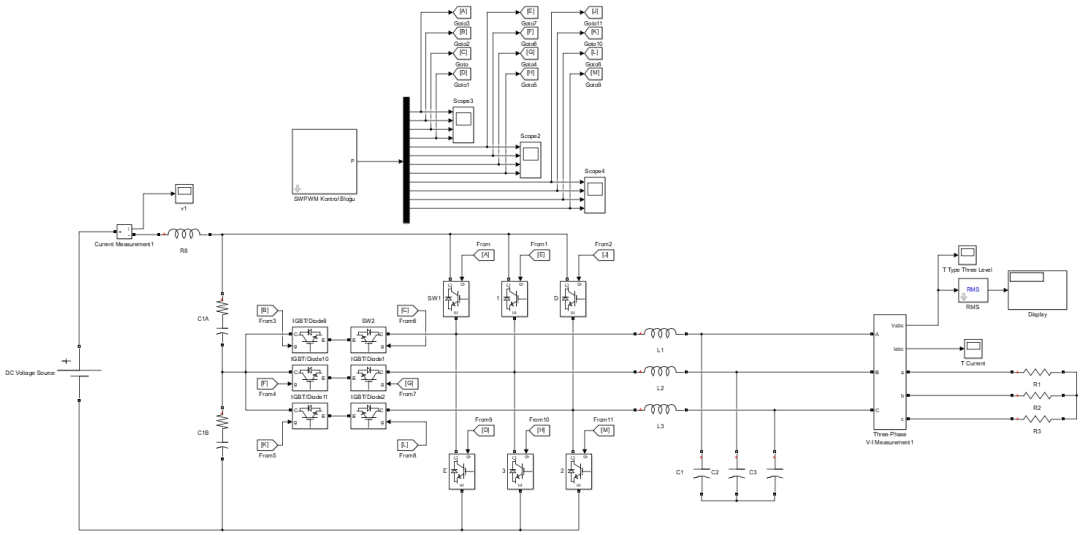

Şekil 2.2 T-Tipi Evirici Simulink Modellemesi

Sistemlerde üretilen anahtarlama işaretleri ortak olup vektör kontrol tabanlıdır. Giriş bölümünde belirtilen adımların uygulanmasıyla Şekil 2.3' de belirtilen kontrol bloğu oluşturulmuştur.

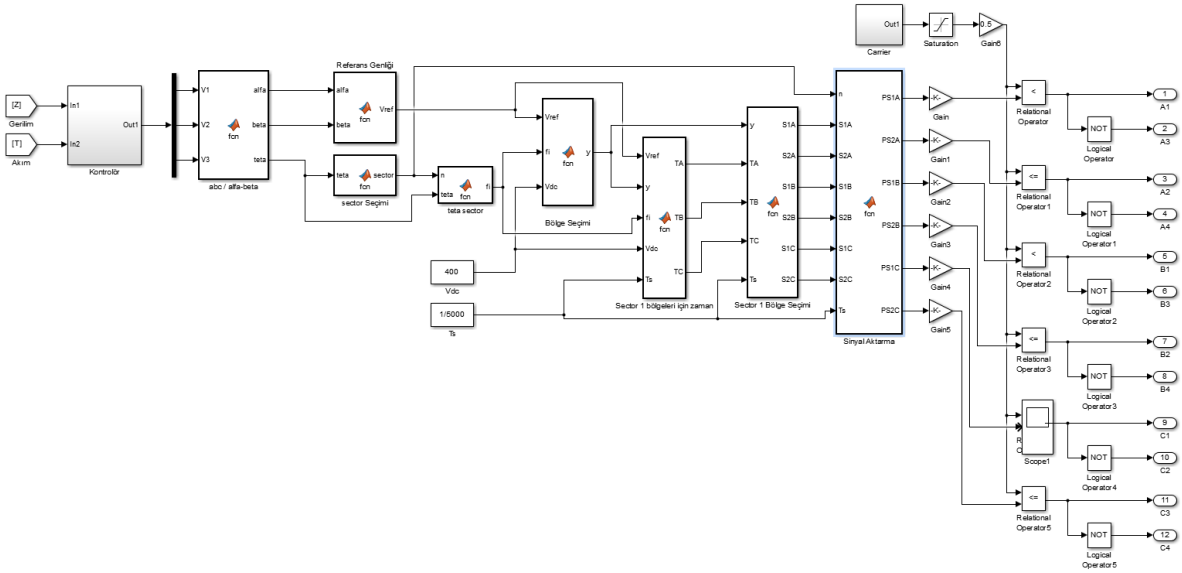

Şekil 2.3 Üç Seviyeli Evirici için Vektör Kontrol Bloğu ve Sinyal Çıkışları

Eviricilerin çıkış filtreleri uygulanmayıp, kontrol bloğunun çalıştırılmasıyla çıkışta elde edilen faz-faz gerilim dalga şekilleri Şekil 2.4'teki gibidir.

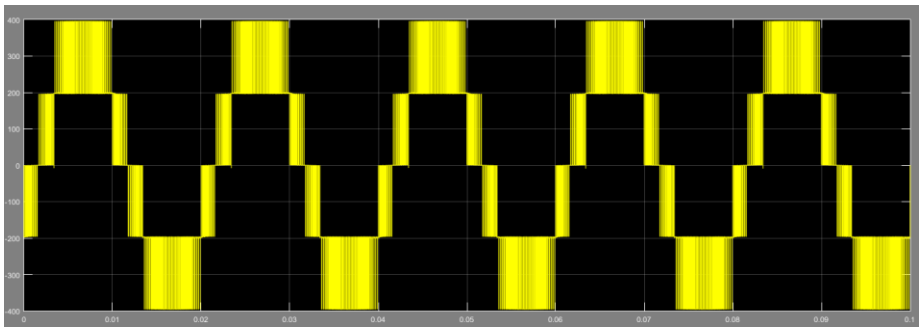

Şekil 2.4 Kontrol Bloğunun Oluşturduğu Evirici Çıkışı Faz-Faz Gerilimi

Çıkışın saf sinüs formunda uygulanması için evirici simülasyonunda LC filtre boyutlandırılması yapılmıştır. LC filtre boyutlandırılması yapılırken evirici çıkış akımı dalgalılığı referans alınarak boyutlandırılma yapılmıştır. L değerinin saptanması için endüktans uç denklemi kullanılarak akım dalgalılığına bağlı formül elde edilmiştir.

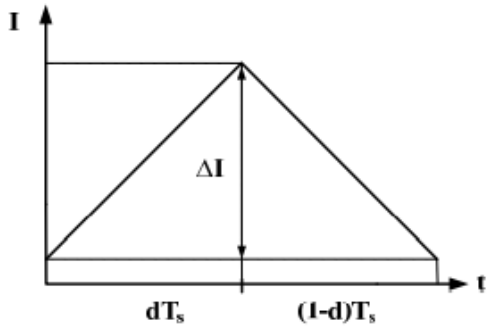

Şekil 2.5 Evirici Çıkış Akımı Dalgalılığı

$$V_L = L_f\left(\frac{\Delta I}{\Delta T}\right) \tag{2.1}$$

Anahtarlama durumuna bağlı olarak endüktör üzerinde denklem (2.2) ve denklem (2.3) ifadelerinde belirtilen gerilim değerleri oluşmaktadır.

$$L_f\left(\frac{\Delta I}{dT_s}\right) = \frac{V_{DA}}{2} \tag{2.2}$$

$$L_f\left(\frac{\Delta I}{(1-d)T_s}\right) = 0 \tag{2.3}$$

Bu iki denklemin ortak çözümüne bağlı olarak akım dalgalanmasına bağlı endüktans ifadesi denklem (2.4)'teki gibidir. Burada fs anahtarlama frekansı, V_{DA} DC bara gerilimi ve d anahtarlama doluluk oranıdır.

$$\Delta I = \left(\frac{V_{DA}}{2L_f f_s}\right) d(1-d) \tag{2.4}$$

Denklem (2.4) ve Şekil 2.5 dikkate alınıp d değerinin 0.5 olması durumunda akım dalgalılık ifadesinin maksimum değere ulaşacağı düşünüldüğünde maksimum akım dalgalılığı ifadesi denklem (2.5)'teki gibi olmaktadır. Denklem (2.5)' te VDA, DC bara gerilimi, fs, anahtarlama frekansı ve Lf ise hesaplanacak endüktans değeridir.

$$\Delta I = \left(\frac{V_{DA}}{8L_f f_s}\right) \tag{2.5}$$

Belirlenecek akım dalgalılığına bağlı olarak endüktans değeri hesaplanabilir. C değerinin belirlenmesinde LC filtre bloğunun anahtarlama frekansında filtreleme yapmasını sağlamak için belirlenen L değeri kullanılarak denklem (2.6) üzerinden C değeri hesaplanır.

$$f_r = \left(\frac{1}{2\pi\sqrt{LC}}\right) \tag{2.6}$$

3. BULGULAR

3.1 Üç Fazlı Üç Seviyeli T Tipi ve Diyot Kenetlemeli Evirici Simülasyonları

Şekil 2.1 ve Şekil 2.2' de gösterilmekte olan evirici simülasyonlarında her iki topolojide de 25kW'lık rezistif yük bağlanıp sırasıyla 3mH ve 2uF değerlerinde L ve C filtre elemanları kullanılmıştır. 650V DC giriş gerilimi uygulanmakta olup, evirici çıkışında 380V AC faz-faz gerilimi elde edilmektedir. Kullanılan bu değerler ile simülasyon yapıldığında Şekil 3.1' de gösterilmekte olan çıkış akım harmonik bozunum değerleri görülmektedir.

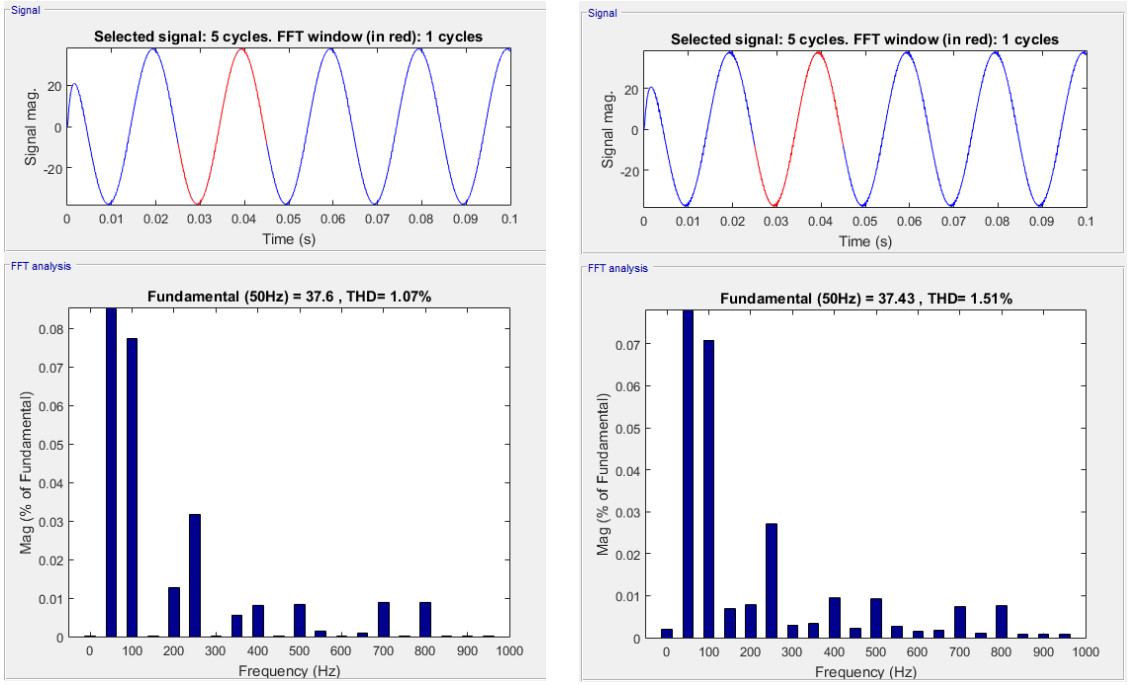

a) Diyot Kenetlemeli Evirici b) T Tipi Kenetlemeli Evirici

Şekil 3.1 Evirici Çıkış Gerilimi Harmonik Bozunum Değerleri

Simülasyon sonuçları 650V DC giriş gerilimi için akım değerleri bakımından incelendiğinde Şekil 3.2 ve Şekil 3.3'deki sonuçlar elde edilmektedir.

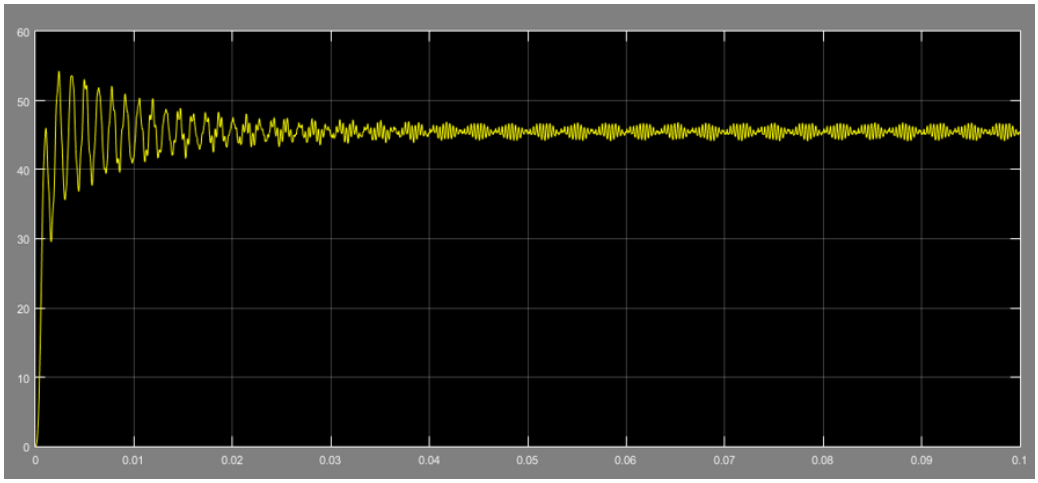

Şekil 3.2 Diyot Kenetlemeli Eviricide Giriş Akımı Formu ve Yaklaşık Değeri (45,6A)

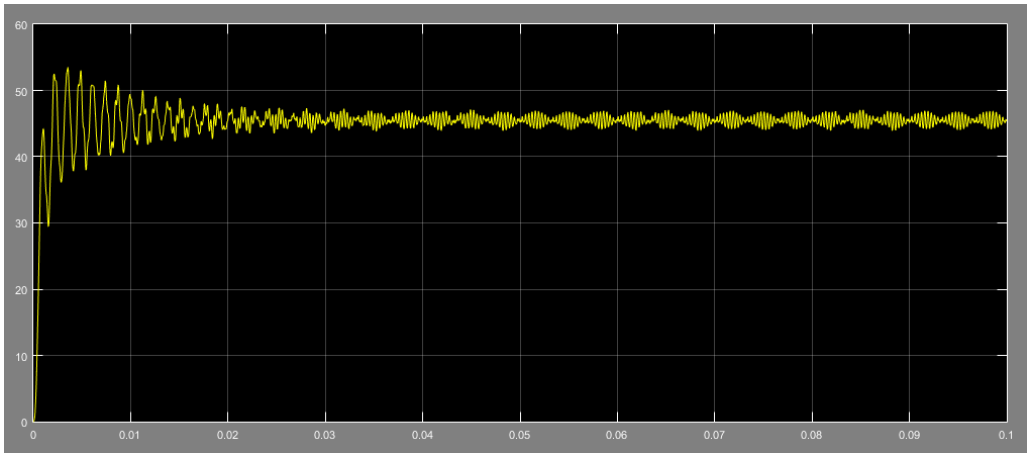

Şekil 3.3 T Tipi Kenetlemeli Eviricide Giriş Akımı Formu ve Yaklaşık Değeri (44,9A)

4.TARTIŞMA VE SONUÇLAR

Bu çalışmada, evirici uygulamalarında sıkça kullanılan üç seviyeli topolojilerden T tipi kenetlemeli evirici ve diyot kenetlemeli evirici yapıları ele alınmıştır. Üç seviyeye uyarlanmış vektör kontrol algoritması ve matematiksel modellemesi incelenmiştir.
Vektör kontrolünün üç seviyeli topolojilerde kullanılmasıyla modülasyon aralığı, skaler kontrol yöntemlerine göre daha fazla genişlik kazanıp özellikle motor kontrol uygulamalarında moment kontrolü daha efektif bir şekilde yapılabilmektedir. Bununla birlikte kontrol, tekbir referans vektörü üzerinden yapıldığından kontrol değişkenleri azaltılıp sistemin donanımsal gerçeklemesi daha işlevsel hale getirilebilir.
Vektör kontrolü uygulamasının 3 seviyeli T tipi evirici ve diyot kenetlemeli evirici yapılarına uygulanmasıyla elde edilen verim ve harmonik bozunum değerleri simülasyon ortamında analiz edilmiştir. Sonuçlara bakıldığında çıkış akım harmonik bozunumu bakımından diyot kenetlemeli evirici, 25kW' lık uygulamada yaklaşık %0,5 değerinde T tipi kenetlemeli eviriciye göre avantajlı haldedir. Fakat topolojilerin verimleri kıyaslandığında T tipi vericinin aktif kenetleme avantajı nedeniyle DC girişten diyot kenetlemeli yapıya göre daha az akım çektiği görülmüştür.
Evirici uygulamalarının topoloji seçimlerinde, verim ve harmonik bozunum değerlerinin sistem açısından önemi iyice araştırıldıktan sonra uygun topolojilerin kullanılması gerekmektedir.

KAYNAKLAR

Bilhan A., "Bölge ve Sektör Tespitinde Yapay Sinir Ağları Kullanan Uzay Vektör Darbe Genişlik Modülasyon Kontrollü Kaskat Bağlı Üç Seviyeli Evirci Tasarmı", Fırat Üniversitesi Fen Bilimleri Enstitüsü, Doktora Tezi, 2012.

Canver M., "Design And Implemention Of A Three Phase Grid Connected Sic Solar Inverter", Middle East Technical University, Yüksek Lisans Tezi, 2018.

Das, S., Narayanan, G., 2012. Novel switching sequences for a space-vector-modulated three-level inverter, Industrial Electronics, IEEE Transactions, 59(3). 1477 - 1487.

I. Colak, E. Kabalci, R. Bayindir, Review of multilevel voltage source inverter topologies and control schemes, Energ. Conver. Manage. 52 (2011) 1114–1128.

J.W. Kolar, High efficiency drive system with 3-level T-type inverter, in: Proceedings of the fourteenth European Conference on Power Electronics and Applications, EPE11, Birmingham, United Kingdom, 2011, pp. 1–10. September 30–October 1.

Kabalcı E., "Çok Seviyeli İnvertörler İçin Yeni Bir SDGM Tekniğinin Geliştirilmesi", Gazi Üniversitesi Fen Bilimleri Enstitüsü, Doktora Tezi, 2010.

Köseoğlu C. E., "Yenilenebilir Enerji Sistemleri için Çok Seviyeli Bir Eviricinin Gerçekleştirilmesi", İstanbul Teknik Üniversitesi Fen Bilimleri Enstitüsü, Yüksek Lisans Tezi, 2014.

The Effect of Titanium Contents on the Structure and Properties of the Al-Si Alloys

Biljana Zlaticanin*[1], Sandra Kovačević[2]

Abstract: Al-0.35wt%Si and Al-2.3wt%Si alloys were modified with Al-Ti5-B1master alloy. The effect of the added Al-Ti5-B1 on the microstructure and mechanical properties of the Al-Si alloys were investigated using an optical microscope and a hardness measurement. The results show that the size of the primary Si decreased with the titanium addition. It is of great importance to improve the mechanical properties of the Al-Si alloys by refining the primary Si. The mechanical properties of the alloy were improved after modification.

Keywords: Al-Si alloys, microstructure, properties

[1]**Address:** University of Montenegro, Faculty of Metallurgy and Technology, Cetinjski put bb, 81000 Podgorica, Montenegro
[2]**Address:** Central School of Chemical Technology Spasoje Raspopović, 81000 Podgorica, Montenegro

***Corresponding author**: biljana@ucg.ac.me

1. INTRODUCTION

Grain refinement is achieved in aluminium alloys by inoculating the molten metal with small amounts of titanium and boron. The refined grain size depends on the Ti content, Ti/B ratio and the matrix alloy composition. Although the exact grain refining mechanism is still being debated, the high melting point intermetallic phases $TiAl_3$ and TiB_2 present in these master alloys are thought to have an important role to play.

Grain refinement in Al-Si casting alloys improves the mass feeding characteristics during solidification, resulting in reduced shrinkage porosity and the promotion of smaller and improved porosity dispersion. Also, a fine grain size creates a more uniform distribution of secondary intermetallic phases in addition to pores which form from the evolution of dissolved gas in the melt (Agarwal, 2016).

2. MATERIAL AND METHOD

Experimental work can be divided in two phases. The first phase comprises melting and casting of six alloys of composition Al-0.35wt%Si and Al-2.3wt%Si. The solidification structure was modified by the addition of the Al-Ti5-B1 master alloy to give alloys containing: 0.01%Ti, 0.1%Ti, 0.2% titanium. The alloys were melted in an induction furnace at 800ºC. After the alloying step, degassing was performed for 30 minutes. The second phase includes characterization of cast samples with optical microscope.

Chemical composition of the Al-Si alloys used in this study is shown in Table 1. Properties of the materials have been investigated, eg.: hardness has been measured by use of the Brinell method.

Table 1. Chemical composition of the investigated alloys (in wt%)

TYPE OF SAMPLE		%Fe	%Si	%Ti	%Cu	%Zn	%V	%Cr	%Mn	%Mg	%Sr
Al-0.35wt%Si	0.01%Ti	0.20	0.35	0.009	0.003	0.049	0.002	0.000	0.002	0.000	0.00
	0.1%Ti	0.19	0.34	0.121	0.003	0.047	0.002	0.000	0.002	0.000	0.00
	0.2%Ti	0.19	0.36	0.248	0.003	0.048	0.002	0.000	0.002	0.000	0.00
Al-2.3wt%Si	0.01%Ti	0.21	2.31	0.007	0.004	0.035	0.004	0.000	0.002	0.000	0.00
	0.1%Ti	0.18	2.29	0.104	0.004	0.038	0.004	0.000	0.002	0.000	0.00
	0.2%Ti	0.19	2.28	0.240	0.004	0.040	0.004	0.002	0.002	0.000	0.00

3. RESULTS

Figure 1 shows the as-cast microstructure of an Al-2.3wt%Si unmodified alloy. Figures 2, 3 and 4 shows images taken with the Ti-modified samples of Al-2.3wt%Si.

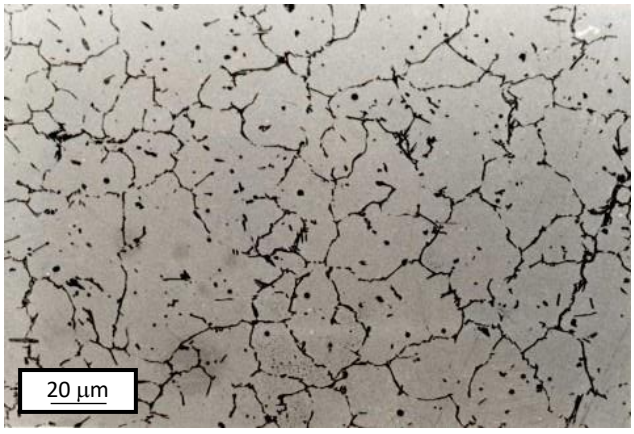

Figure 1. Microstructure of Al-2.3wt%Si (unmodified) alloy

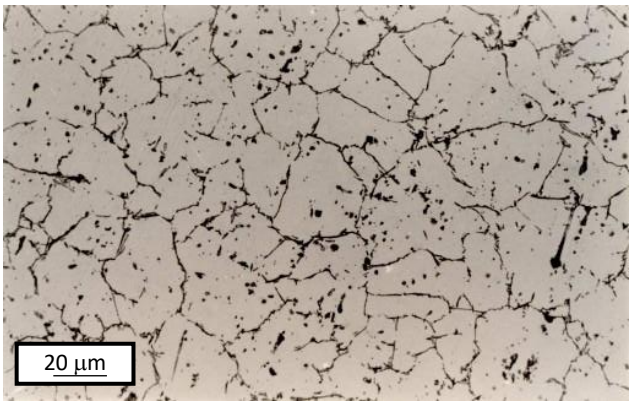

Figure 2. Microstructure of Al-2.3wt%Si-0.01wt%Ti alloy

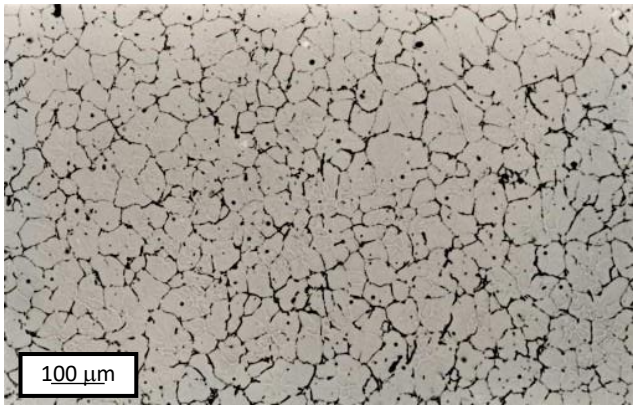

Figure 3. Microstructure of Al-2.3wt%Si-0.1wt%Ti alloy

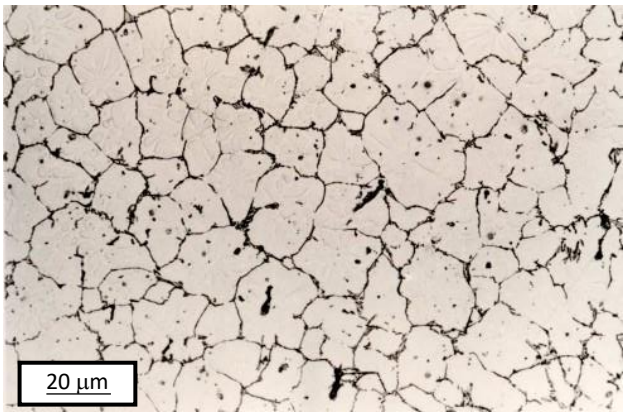

Figure 4. Microstructure of Al-2.3wt%Si-0.2wt%Ti alloy

We have also examined the properties of these materials: hardness measurement. The hardness of the modified alloy is higher than the hardness of the alloy without any modification treatment (Table 2).

Table 2. Hardness of the investigated alloys

TYPE OF SAMPLE		$HB_{average}$
Al-0.35wt%Si	0.01%Ti	31.1
	0.1%Ti	31.9
	0.2%Ti	32.8
Al-2.3wt%Si	0.01%Ti	34.6
	0.1%Ti	37.6
	0.2%Ti	39.8

4. DISCUSSION AND CONCLUSIONS

Grain refinement of castings is way to control the microstructure. Grain refinement of aluminum alloys has been used commercially and it has been a main feature in the control of quality products manufactured from aluminum alloys. Grain refinement of Al-Si casting alloys is commonly assessed by the presence of Ti and B in the melt. The binary Al-Si phase diagram is based on the study by Murray and McAlister (1984). The eutectic reaction occurs at 12.6wt.% Si and 577ºC. Additions of certain elements to aluminum alloys melts can provide nuclei for grain growth. Titanium has a nucleating effect and is the most commonly used grain refiner. The addition of boron together with titanium produces finer grains. Experimentation on Al-Si alloys has show the importance of boron in Al-Ti5-B1 master alloy. Ratio Ti/B is important. Various theories have emerged from this practice and the exact mechanism of grain size reduction is still in dispute. The mechanical properties of the Al-Si alloys were improved after modification (Chen and Xu, 2016). It is also important to appreciate that the effects of grain refinement in aluminum castings can be further enhanced when varying other production parameters such as pouring temperature, cooling rate, silicon morphology and heat treatments.

REFERENCES

Agarwal, S. (2016). Grain refinment in Al-Si alloys. International Journal of Recent Advances in Engineering and Technology. 5, 133-138.

Murray, J.L., McAlister, A.J. (1984). The Al-Si (Aluminum-Silicon) system. Bull. Alloy Phase Diagrams. 5, 74-84.

Chen, R., Xu, Q. (2016). Modeling of aluminum-silicon irregular eutectic growth by cellular automaton model. Research and Development. 13, 114-122.

Determination of the optimum operational conditions for leaching of Mg and Fe from chromium ore processing tailings by different acid solutions

Hüseyin Yazıcı*[1]

Abstract: The present study aimed to determine the optimum operational conditions for leaching of magnesium (Mg) and iron (Fe) from chromium ore processing tailings, which was rich in terms of Mg, Fe, and Si content, by different acid solutions. For this purpose, different leaching reactants including nitric (HNO_3), sulphuric (H_2SO_4) and ortho-phosphoric (H_3PO_4) acid solutions were used to investigate the effect of varying acid concentrations (0.5-4.0 molar, M), reaction times (15-120 min.), material dosages (5-35 g/L), and temperatures (20-80 °C) on the leaching efficiency. To determine the leaching performance of the acid solutions under the investigated operational conditions, residual concentrations of Mg and Fe as well as nickel (Ni), aluminum (Al), chromium (Cr), and silicon (Si) were measured in the obtained leachates by inductively coupled plasma-optical emission spectrometry (ICP-OES). Experimental results showed that the optimum concentration of HNO_3, H_2SO_4, and H_3PO_4 was found to be 0.5, 1.0 and 0.5 M, respectively. An acid concentration higher than the given optimum values did not cause any remarkable increase in the leaching efficiency of Mg and Fe. Similarly, an increase in the material dosage up to 35 g/L did not cause any decrease the leaching efficiency of Mg and Fe. However, the leaching efficiency of Mg and Fe as well as Al, Ni and Cr significantly increased with the increasing reaction time and temperature. The optimum values for the reaction time and temperature were found to be 90 min and 80 °C for each of the acid solutions used. Under the optimized conditions, the leaching efficiencies using HNO_3 and H_3PO_4 were maximized at value of 52.2 and 53.0% for Mg and 64.8 and 69.4% for Fe, respectively, while over 90% of the initial Mg and Fe content of the material (9030 and 1820 mg/L, respectively) could be leached with H_2SO_4. At the same time, the highest leaching efficiency for Al, Ni, Cr, and Si was determined to be 16.5% with H_2SO_4, 88.0% with H_2SO_4, 1.87% with H_3PO_4, and 4.42% with HNO_3, respectively.

Keywords: Tailings, leaching, magnesium, iron, acid solution.

[1]**Address:** Isparta University of Applied Sciences, Vocational School of Aksu Mehmet Süreyya Demiraslan, Department of Environmental Protection Technologies, 32510, Isparta/Türkiye

***Corresponding author**: huseyinyazici@isparta.edu.tr

1. INTRODUCTION

Expansion of industrial applications with the improved technologies and rapid increase in the generation of waste materials together with the ever-growing global population has created a motivation for research and development activities on waste recycling issues (Erüst et al., 2023). Among the wastes, metal finishing industry waste, medical waste, spent petroleum catalysts, fly ash, battery wastes, and electronic scraps have been shown some of the largest industrially-generated wastes (Krishnan et al., 2021). Beside these wastes, mining wastes pose a huge threat to the environment (Álvarez et al., 2022) since a huge amount of waste material is created due to the long-term mining and metallurgical activities (Šajn et al., 2022). It is estimated that the worldwide production of solid waste from the primary production of mineral and metallic raw materials is over 100 billion tons per year (de Palacios and Rodríguez, 2022).

Mining wastes refers to a broad group of waste materials that are originated from extracting the ground and processing the mineral sources to varying stages during the ore-processing and enrichment phases (BRGM, 2001). These materials have low or no economic value since they are considered as unusable mineralized materials and hence are stored or discarded rather than processed (Hitch et al., 2010). Usually, mining wastes are in the form of fine suspended materials (1-600 µm), including dissolved metals and reagents, chemicals, and inorganic and organic additives (Araujo et al., 2022). Typically, these wastes are classified as waste rocks, processing waste and tailings (Bellenfant et al., 2013; Carmo et al., 2020), which can be present in the form of solid, liquid, and gaseous depending on the physical form of residues (Araujo et al., 2022).

Disposal options of mining wastes include underground backfilling, submarine tailing disposal, regeneration of ground vegetation, producing glass or fertilizer, and utilization as construction materials for roads, dams and wall bricks (Lu and Cai, 2012). Because transportation of the waste to another site is not economically viable, mining wastes are

commonly deposited in large man-made embankments, referred to as tailings dams, near mining production site (Araujo et al., 2022). However, if these wastes are not managed properly, significant pollutions can occur both through air pathways (dust and gas emissions) and water leaching (acid mine drainage) (Lèbre and Corder, 2015). Furthermore, failure to manage can result in high-cost requiring catastrophic consequences. Up to now, several environmental problems as well as multiple human risks have been originated due to the failures in tailings dam storage (Álvarez et al., 2022). Recent events, such as the Los Frailes tailings dam failure in Spain (1998) and the Brumadinho tailings dam failure in Brazil (2019), have resulted in heightening attention of the industry and society to the catastrophic impacts of mining wastes (Tayebi-Khorami et al., 2019). Although tailings pose several environment risks as stated above, some extractive mining wastes still contain valuable and/or critical metals (Álvarez et al., 2022). However, the composition of mining waste remains largely unknown since mining companies generally do not monitor the waste they generate. This prevents opportunities for extracting further material from it or even reducing its generation, which add value for a better disposal option of the waste. However, an alternative waste management oriented towards resource recovery could potentially mitigate environmental impacts (Lèbre and Corder, 2015). At this point, an evaluation of waste materials for the recovery of their metal values together with stabilization of toxic elements present in them by proper waste management strategies for environmental safety has been considered as the driving force for research and development activities (Erüst et al., 2023). Nevertheless, the drive for most mining operations is to reduce the costs associated with the development of processes and procedures that have to be put in place to make sure that the tailings discharged meet the required environmental standards (Ndlovu et al., 2017).

Reprocessing of tailings ensures benefits on the transforming a linear economy into a circular economy and, therefore, reducing the dependence on reserve extraction (Šajn et al., 2022). Therefore, related to the circular economy strategy, some of these wastes have been considered as secondary source of raw materials in recent years (Álvarez et al., 2022). Various metal recovery processes involve physical, chemical, and thermal characteristics of waste streams and target metals for separation and extraction (Krishnan et al., 2021). It is well known that hydrometallurgy is one of the most efficient technologies to recover valuable metals from low-grade ores and wastes (Álvarez et al., 2022). Atmospheric acid leaching refers to hydrometallurgical processes that utilize non-pressurized, stirred reactor applications with temperatures <100 ˚C (URL-1, 2018). Typical steps involved in this process are leaching, concentration/purification, and recovery (Krishnan et al., 2021). Using this process, several research efforts have been put into recovering heavy metals and rare earth elements from different wastes such as printed circuit boards (Oliveira et al., 2009; Jha et al., 2010), electrical and electronic equipment (Marra et al., 2019) and fly ashes from municipal solid waste incineration (Weibel et al., 2021).

As one of the mined metals, chromium and its compounds find their widespread applications in the field of metallurgy, foundry, and tanning, and they use in dyes and pigments, wood preservatives, catalysis, and interconnectors for solid oxide fuel cells (Lunk, 2015). The global mine production of the transition metal chromium has been accounted for a gross weight of $41*10^6$ tons in 2022 (URL-2, 2023), and its leading producers have been reported as South Africa, India, Kazakhstan, and Turkey (Coetzee et al., 2020). During enrichment of chromium-related ores, a considerable amount of fine-sized processing tailings is produced. Tailings generated from the processing plant is generally dumped and, therefore, causes space and environmental concerns (Kumar et al., 2021). Because tailings are not recycled or re-used and due to their potential to release Cr^{6+}, they belong to the third, hazardous, group of waste generated by chromite mining (Bolaños-Benítez et al., 2018).

Motivated by these concepts, the main objective of the present study was to determine the optimum operational conditions for leaching of Mg and Fe from chromium ore processing tailings by different leaching solutions. For this purpose, different leaching reactants including HNO_3, H_2SO_4 and H_3PO_4 were used to investigate the effect of acid concentration, reaction time, material dosage, and temperature on the leaching efficiency.

2. MATERIAL AND METHOD

2.1. Materials

All chemicals used in the experiments were of analytical grade and were used without further purification. All solutions were prepared with distilled water. HNO_3 (65%), H_2SO_4 (96%) and H_3PO_4 (65%) solutions were obtained from Merck (Germany). The input material, chromium ore processing tailings, used in experiments was collected from a tailing dam at a chrome mine in Denizli, Türkiye. The main composition of the input material was represented in Table 1. Before use in experiments, the material was powdered using a grinder at 28000 rpm for 1 min and then dried in an oven at 50 °C for 24 h. The obtained material was stored in a desiccator until further use.

Table 1. Chemical composition of the chromium ore processing tailings

Compound	wt.%	Compound	wt.%
MgO	43.15	Al_2O_3	0.4
SiO_2	31.38	Cr_2O_3	1.06
Fe_2O_3	7.43	NiO	0.36
CaO	0.33	Loss of Ignition	15.55

2.2. Leaching procedure

Leaching experiments were performed by adding a known weight of the powdered material into 1 L of acid solutions (HNO_3, H_2SO_4 and H_3PO_4) that were prepared for a desired molar concentration. The prepared suspension was placed on an analogue hotplate stirrer with temperature controller (Wisestir MSH 20D, Daihan Scientific Co., Korea) and was mixed in three-neck round bottom flask under reflux condition at a constant agitation speed of 450 rpm. To determine the optimum operational conditions of the leaching process, a four-stage experimental run was conducted for each of the acid solutions according to the following experimental design (Table 2):

Table 2. Experimental design for the leaching process

Stage	Acid concentration (Molarity)	Reaction time (min.)	Material dosage (g/L)	Temperature (°C)
1	0.5-1.0-2.0-3.0-4.0	30	25	20
2	Optimum molar concentration determined in Stage 1	15-30-45-60-90-120		
3		Optimum reaction time determined in Stage 2	5-15-25-35	
4			Optimum dosage determined in Stage 3	20-50-80

2.3. Sampling and measurements

At the end of the leaching reaction, the mixture was cooled down to room temperature, if required. Then, 25 mL of sample was taken and filtered through filter papers (Millipore AP40). The concentrations of Mg, Fe, Al, Ni, Cr, and Si in the filtrate samples were measured by ICP-OES (Perkin Elmer Optima 2100 DV). According to the obtained data, leaching efficiency (%) for each of the analyte was calculated by the following equation:

$$Leaching\ efficiency\ (\%) = \frac{m_i - m_f}{m_i} * 100 \qquad \text{(Eq. 1)}$$

where; m_i is the initial amount of the analyte corresponding to the amount of the powdered material added into 1 L of acid solution (mg/L), and m_f is the measured concentration of the analyte in the filtrate sample (mg/L). The initial amount of the analytes was calculated based on the related wt.% given in Table 1.

3. RESULTS

3.1. Effect of acid concentration

The effect of acid concentration on the leaching efficiency was investigated by testing different concentration values ranging between 0.5 and 4.0 M under the conditions of 20 °C, 30 min., 25 g material/L, and 450 rpm for each of the acid solutions. The experimental results showed that there was no remarkable change in the leaching efficiency of both Mg and Fe with the increasing acid concentration of HNO_3 and H_3PO_4 (Fig. 1a and b). The leaching efficiencies with HNO_3 were found to be in the range of 23.6 and 25.8% for Mg and 41.4 and 44.6% for Fe under the examined acid concentration conditions while the use of H_3PO_4 resulted in obtaining almost close leaching efficiencies ranging between 25.8 and 28.4% for Mg and 42.8 and 46.0% for Fe. In the case of the leaching with H_2SO_4, relatively higher efficiencies for both Mg and Fe were obtained than those obtained with HNO_3 and H_3PO_4, especially for the acid concentration > 0.5 M. An increase in the acid concentration of H_2SO_4 from 0.5 to 1.0 M increased the leaching efficiency from 26.4 to 30.8% for Mg and 43.0 to 46.9 for Fe while there was no significant increase in the leaching efficiency of both Mg and Fe under the increasing concentration conditions up to 4.0 M.

The leaching efficiency of Al, Ni, and Cr was also investigated as a function of the acid concentration. The experimental results showed that the increasing acid concentration up to 4.0 M did not stimulate the leaching of Al and Ni for each type of acids while the leaching efficiency of Cr increased gradually with the increasing acid concentration for all of the acids used (Table 3). The highest leaching efficiency for Al, Ni, and Cr was found to be 3.8% with 4.0 M H_2SO_4, 58.9% with 3.0 M H_2SO_4 and 2.68% with 4.0 M H_3PO_4, respectively. Even though over half of the total Ni content was leached from the material compared to Al and Cr, it should be noted that the initial wt.% of Al, Ni, and Cr

in the material composition was < 1.0%. These results implied that Al, Ni, and Cr could be determined only with negligible amounts in the supernatant after the leaching reaction compared to Mg and Fe.

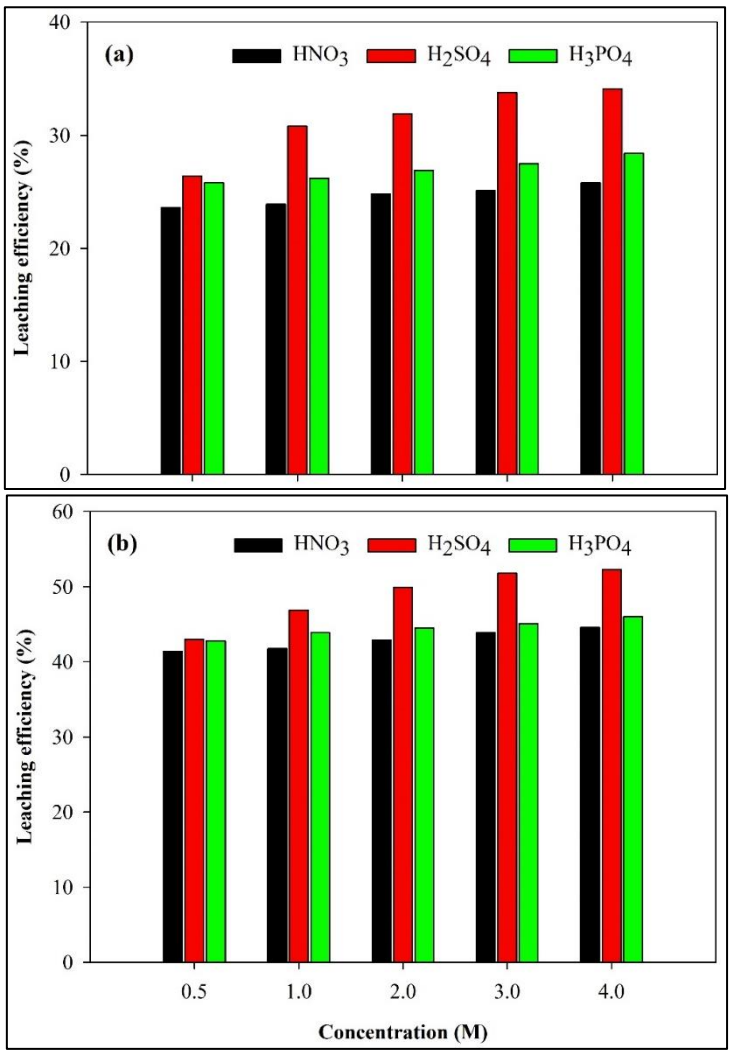

Figure 1. The effect of acid concentration on the leaching efficiency of Mg (a) and Fe (b) (Mixing speed: 450 rpm, reaction time: 30 min., material dosage: 25 g/L, temperature: 20 °C)

Table 3. The effect of acid concentration on the leaching efficiency of Al, Ni, and Cr

Type of acid	Concentration	Leaching efficiency (%)		
		Al	Ni	Cr
HNO_3	0.5	2.1	52.8	0.49
	1.0	2.0	56.0	0.75
	2.0	2.6	51.5	1.72
	3.0	2.7	49.9	1.94
	4.0	3.1	51.4	2.68
H_2SO_4	0.5	2.2	56.5	0.24
	1.0	2.7	56.6	0.32
	2.0	3.1	58.2	0.35
	3.0	3.6	58.9	0.42
	4.0	3.8	55.0	0.43
H_3PO_4	0.5	1.6	53.7	0.12
	1.0	1.4	51.5	0.16
	2.0	1.7	52.3	0.20
	3.0	1.7	53.1	0.23
	4.0	2.0	54.5	0.26

3.1. Effect of reaction time

The effect of reaction time on the leaching efficiency was investigated by testing varying reaction times in the range of 15 and 120 min. under the same experimental conditions applied for the acid concentration. The experimental results showed that the leaching efficiency for both Mg and Fe increased gradually with the increasing reaction time for all acid reagents (Fig. 2a and b, respectively). The leaching efficiencies with HNO_3 were found to be in the range of 17.4 and 32.1% for Mg and 33.5 and 49.1% for Fe while the leaching efficiencies with H_3PO_4 were found to be in the range of 21.0 and 34.2% for Mg and 37.8 and 50.2% for Fe. In the case of the leaching with H_2SO_4, relatively higher efficiencies were obtained for both Mg and Fe than those obtained with HNO_3 and H_3PO_4. The leaching efficiencies with H_2SO_4 varied between 28.9 and 48.3% for Mg and 41.6 and 60.4% for Fe with the increasing reaction time. These results revealed that the highest leaching efficiency for both Mg and Fe followed the order H_2SO_4, H_3PO_4 and HNO_3.

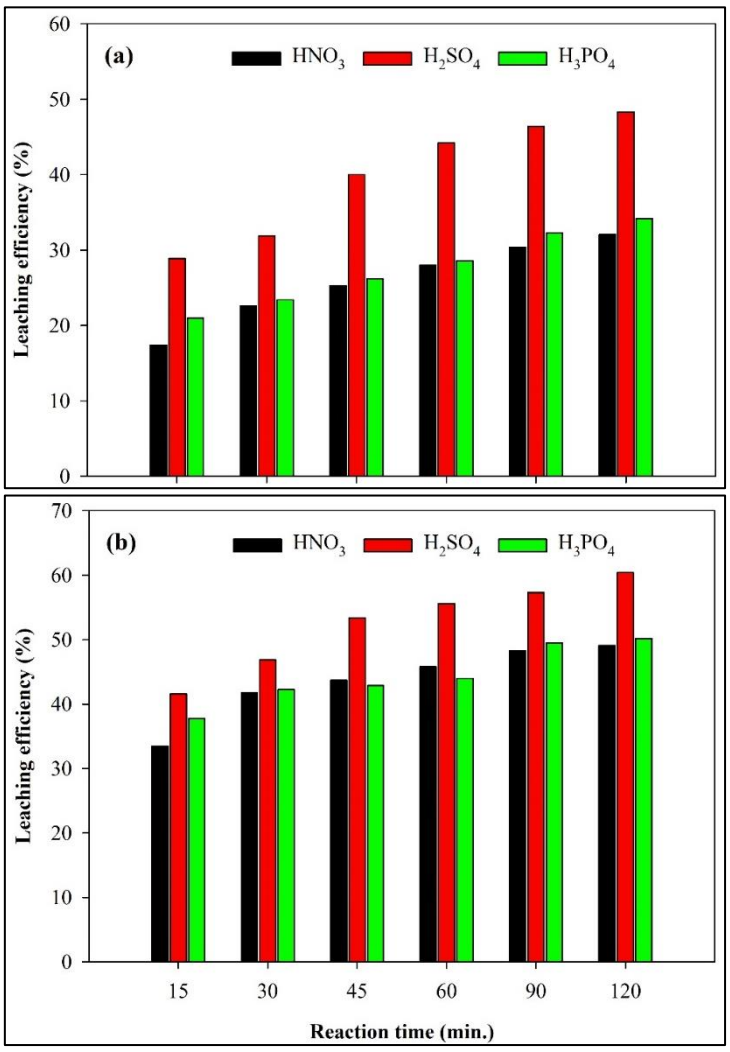

Figure 2. The effect of reaction time on the leaching efficiency of Mg (a) and Fe (b) (Mixing speed: 450 rpm, material dosage: 25 g/L, temperature: 20 °C, acid concentration: 0.5 M HNO_3, 1.0 M H_2SO_4, 0.5 M H_3PO_4)

To quantify the magnitude of change in the efficiency values ($\Delta_{ef.}$, %) as a function of the varying reaction time, a set calculation was done based on the obtained experimental data (Table 4). According to the calculated data, the highest $\Delta_{ef.}$ value was obtained to be 23.0 and 19.9%, respectively, when the reaction time increased from 15 to 30 min. for both Mg and Fe in the case of leaching with HNO_3. On the other hand, in the case of leaching with H_2SO_4, the highest $\Delta_{ef.}$ value was obtained to be 20.3 and 12.2%, respectively, when the reaction time increased from 30 to 45 min. for both Mg and Fe. However, the highest $\Delta_{ef.}$ value was obtained to be 11.5 and 11.1%, respectively, when the reaction time increased from 60 to 90 min. for both Mg and Fe in the case of leaching with H_3PO_4. These results indicated that a relatively longer reaction time was required to achieve a satisfactory leaching efficiency for both Mg and Fe when using H_2SO_4 or H_3PO_4 as leaching reactant compared to HNO_3. This finding was confirmed by the calculated data for the rate of the reaction completion. According to the data, 40.7 and 55.8% of the total leaching reaction was completed for Mg and Fe, respectively, in the first 30 min. with 0.5 M HNO_3 while only 19.6 and 22.1% of the total leaching reaction for

Mg and 31.7 and 39.2% of the total leaching reaction for Fe were completed in the case of the leaching with 1.0 M H_2SO_4 and 0.5 M H_3PO_4, respectively, under the same conditions. Although the leaching with HNO_3 exhibited a relatively faster reaction for Mg and Fe compared to H_2SO_4 and H_3PO_4, over 90% of the total leaching reactions for both Mg and Fe were completed generally in 90 min. for all of the leaching reactants used. Therefore, the optimum reaction time was decided to be 90 min. for each of the reactants to achieve a satisfactory leaching efficiency.

Table 4. $\Delta_{ef.}$ values and rate of the reaction completion values for the leaching of Mg and Fe

Reaction time (min.)	Mg					
	HNO_3		H_2SO_4		H_3PO_4	
	$\Delta_{ef.}$ (%)	Cumulative $\Delta_{ef.}$ (a)	$\Delta_{ef.}$ (%)	Cumulative $\Delta_{ef.}$ (a)	$\Delta_{ef.}$ (%)	Cumulative $\Delta_{ef.}$ (a)
15	-	-	-	-	-	-
30	23.0	23.0 (40.7%)	9.4	9.4 (19.6%)	10.3	10.3 (22.1%)
45	10.7	33.7 (59.6%)	20.3	29.7 (62.1%)	10.7	21.0 (45.1%)
60	9.6	43.3 (76.6%)	9.5	39.2 (82.0%)	8.4	29.4 (63.2%)
90	7.9	51.2 (90.6%)	4.7	43.9 (93.4%)	11.5	40.9 (87.9%)
120	5.3	56.5 (100%)	3.9	47.8 (100%)	5.6	46.5 (100%)
Total $\Delta_{ef.}$ (%) (15 to 120 min.)	56.5	-	47.8	-	46.5	-
Reaction time (min.)	Fe					
	HNO_3		H_2SO_4		H_3PO_4	
	$\Delta_{ef.}$ (%)	Cumulative $\Delta_{ef.}$ (a)	$\Delta_{ef.}$ (%)	Cumulative $\Delta_{ef.}$ (a)	$\Delta_{ef.}$ (%)	Cumulative $\Delta_{ef.}$ (a)
15	-	-	-	-	-	-
30	19.9	19.9 (55.8%)	11.3	11.3 (31.7%)	10.6	10.6 (39.2%)
45	4.3	24.2 (67.9%)	12.2	23.5 (66.0%)	1.4	12.0 (44.4%)
60	4.6	28.8 (80.8%)	4.0	27.5 (77.2%)	2.5	14.5 (53.7%)
90	5.2	34.0 (95.5%)	3.0	30.5 (85.6%)	11.1	25.6 (94.8%)
120	1.6	35.6 (100%)	5.1	35.6 (100%)	1.4	27.0 (100%)
Total $\Delta_{ef.}$ (%) (15 to 120 min.)	35.6	-	35.6	-	27.0	-

(a): The given values in parenthesis represent the value of rate of the reaction completion, which was calculated by dividing the cumulative $\Delta_{ef.}$ value to the total $\Delta_{ef.}$ value.

According to the total $\Delta_{ef.}$ value, which means the total magnitude of the change in the leaching efficiencies at the end of 120 min. of reaction time, the highest total $\Delta_{ef.}$ value followed the order HNO_3, H_2SO_4 and H_3PO_4 for the leaching of Mg, whereas it followed the order HNO_3 = H_2SO_4 and H_3PO_4 for the leaching of Fe. (Table 4) This result showed that the leaching with 0.5 M HNO_3 yielded a relatively higher leaching efficiency for Mg at the end of the 120 min. of reaction time as compared those obtained by 1.0 M H_2SO_4 or 0.5 M H_3PO_4. Combining the results obtained for the leaching efficiencies, the rate of the reaction completion and the total $\Delta_{ef.}$, it could be concluded that leaching with a mixture of 0.5 M HNO_3 and 1.0 M H_2SO_4, which will be prepared in a proper volume combination, might have a positive impact for achieving the same or higher leaching efficiencies for Mg and/or Fe within a shorter reaction time.

The results of the effect of reaction time on the leaching efficiency of Al, Ni, and Cr was shown in Table 5. According to the results, the leaching efficiencies of Al, Ni, and Cr gradually increased with the increasing reaction time for each of the acid reactants. These results showed that the increasing reaction time had an effect similar to that of the effect of the increasing acid concentration on the leaching efficiency of Al, Ni, and Cr. The highest leaching efficiency for Al, Ni, and Cr was found to be 5.6% with H_2SO_4, 62.6% with H_2SO_4 and 0.68% with H_3PO_4, respectively.

Table 5. Effect of reaction time on the leaching efficiency of Al, Ni and Cr

Type of acid	Reaction time (min.)	Leaching efficiency (%)		
		Al	Ni	Cr
HNO_3	15	0.2	42.6	0.07
	30	1.6	53.7	0.12
	45	1.5	54.3	0.20
	60	2.0	56.2	0.25
	90	2.5	59.9	0.30
	120	2.5	57.4	0.32
H_2SO_4	15	2.8	59.4	0.39
	30	2.7	56.6	0.32
	45	4.4	60.7	0.52
	60	4.8	60.1	0.54
	90	4.9	61.1	0.58
	120	5.6	62.6	0.67
H_3PO_4	15	1.2	46.7	0.42
	30	2.1	52.8	0.75
	45	2.0	51.0	0.53
	60	2.5	53.2	0.56
	90	3.2	58.7	0.67
	120	3.4	59.3	0.68

3.3. Effect of material dosage

The effect of material dosage on the leaching efficiency was investigated by testing different material dosages ranging between 5 and 35 g/L. Principally, it was expected that the leaching efficiency should have decreased with the increasing material dosage for a given volume of the acid reactant due to the decreasing volume of acid reactant per the increasing amount of the material. However, interestingly, the experimental results showed that increasing the material dosage did not cause any remarkable change in the leaching efficiency of both Mg and Fe for all of the acid reactants (Fig. 3). The leaching efficiencies with HNO_3 were found to be in the range of 26.7 and 30.4% for Mg and 42.0 and 48.3% for Fe while the use of H_3PO_4 resulted in relatively higher leaching efficiencies ranging between 31.7 and 34.9% for Mg and 45.4 and 51.4% for Fe. In the case of the leaching with H_2SO_4, the efficiencies varied between 44.4 and 46.4% for Mg and 55.3 and 57.4% for Fe.

The results of effect of the material dosage on the leaching efficiency of Al, Ni, and Cr was represented in Table 6. According to the results, the leaching efficiencies of Al, Ni, and Cr exhibited a fluctuating trend with the increasing material dosage for each of the acid reactants. In addition, it was observed that the increasing material dosage did not have any remarkable impact on the leaching efficiency of Al, Ni, and Cr. The highest leaching efficiency for Al, Ni, and Cr was found to be 4.7% with H_2SO_4, 61.1% with H_2SO_4 and 1.06% with H_3PO_4, respectively.

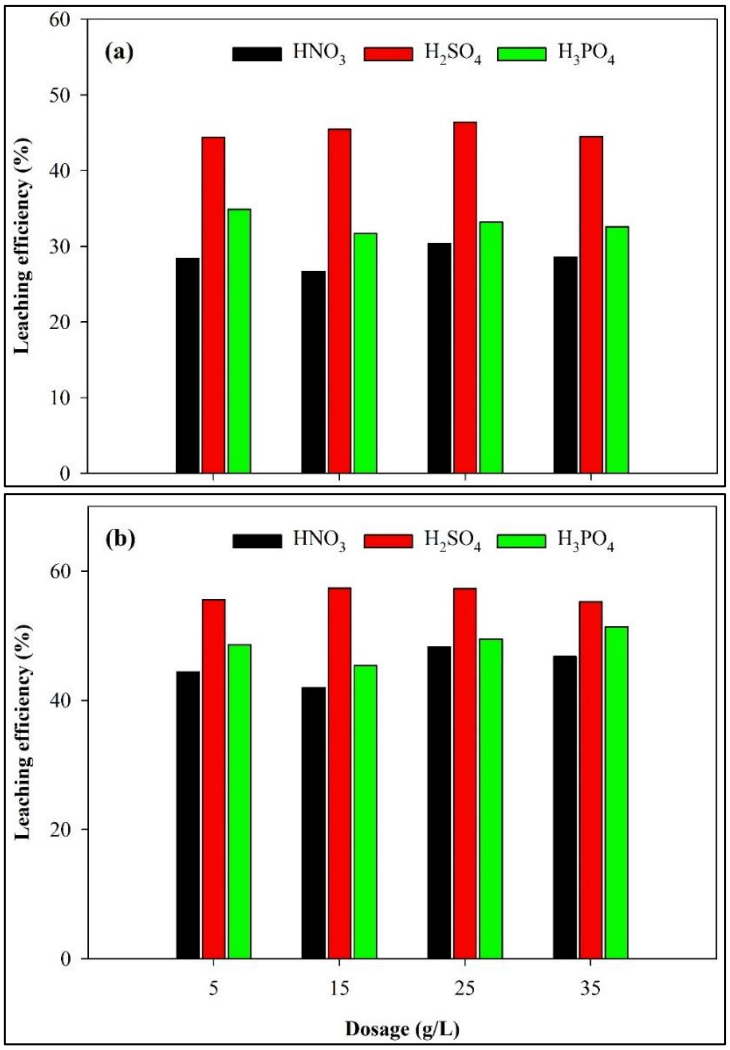

Figure 3. Effect of the material dosage on the leaching efficiency of Mg (a) and Fe (b) (Mixing speed: 450 rpm, reaction time: 90 min, temperature: 20 °C, acid concentration: 0.5 M HNO_3, 1.0 M H_2SO_4, 0.5 M H_3PO_4)

Table 6. Effect of the material dosage on the leaching efficiency of Al, Ni and Cr

Type of acid	Dosage (g/L)	Leaching efficiency (%)		
		Al	Ni	Cr
HNO_3	5		52.5	(*)
	15	0.2	51.4	(*)
	25	2.5	59.9	0.30
	35	1.8	49.9	0.17
H_2SO_4	5	(*)	56.6	(*)
	15	3.1	58.9	0.31
	25	4.9	61.1	0.58
	35	4.7	58.8	0.51
H_3PO_4	5	(*)	52.5	0.56
	15	0.8	51.4	1.06
	25	3.2	59.9	0.67
	35	2.3	49.9	0.91

(*): Not calculated since the measured concentration value was lower than detection limit of 0.05 mg/L.

3.4. Effect of temperature

The effect of temperature on the leaching efficiency was investigated under the conditions of 20, 50 and 80 °C. The experimental results showed that the leaching efficiencies of both Mg and Fe significantly increased with the increasing temperature for each of the acid reactants, especially for H_2SO_4 (Fig. 4). The leaching efficiency with HNO_3 were found

to be 29.6, 45.2 and 52.2% for Mg and 46.4, 56.9 and 64.8% for Fe under the temperature condition of 20, 50 and 80 °C, respectively, while the leaching with H_3PO_4 resulted in quite close leaching efficiencies ranging between 33.4 and 53.0% for Mg and 50.9 and 69.4% for Fe. In the case of the leaching with H_2SO_4, the leaching efficiencies were found to be 45.3, 61.7 and 93.7% for Mg and 55.6, 63.7 and 91.9% for Fe at 20, 50 and 80 °C, respectively. This result showed that over 90% of the total Mg and Fe content of the material could be leached with H_2SO_4 at 80 °C. Furthermore, under this temperature condition, almost 1,5- and 2-fold higher leaching efficiencies were obtained for Fe and Mg, respectively, for each of the acid reactants. Based on the overall results of the study, one can be concluded that temperature had an impact on the leaching efficiency of both Mg and Fe much more than the other examined operational conditions.

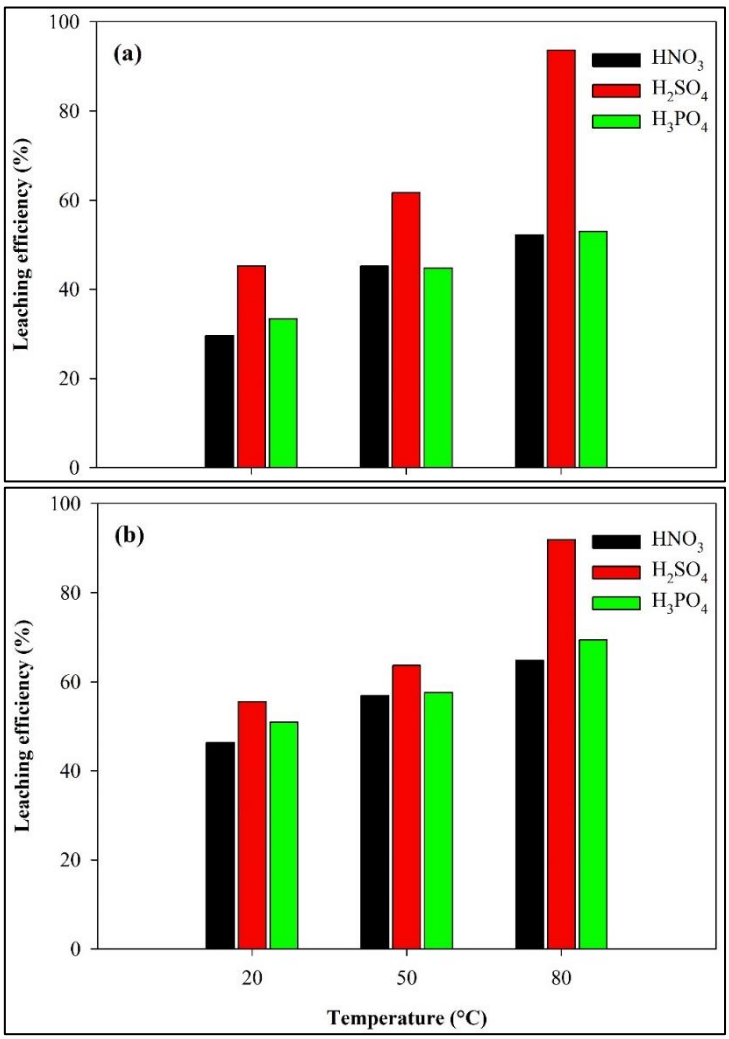

Figure 4. Effect of temperature on the leaching efficiency of Mg (a) and Fe (b) (Mixing speed: 450 rpm, reaction time: 90 min, material dosage: 35 g/L, acid concentration: 0.5 M HNO_3, 1.0 M H_2SO_4, 0.5 M H_3PO_4)

To determine how the examined operational conditions affected the leachability of Si from the material, the residual Si concentration was also measured as well as Al, Ni and Cr in this experimental stage. The obtained results showed that the increasing temperature gradually increased on the leaching efficiency of Al, Ni, Cr, and Si (Table 6). The highest leaching efficiency for Al, Ni, Cr, and Si was found to be 16.5% with H_2SO_4, 88.0% with H_2SO_4, 1.87% with H_3PO_4, and 4.42% with HNO_3, respectively. According to the results, although leaching efficiency of Ni reached a maximum value (88.0%) with H_2SO_4 at 80 °C, only 16.5% of the total Al content could be leached under the same condition. In addition to this, leaching of Cr was maximized at an efficiency of 1.87% in the case of the leaching with H_3PO_4 at 80 °C. On the other hand, the obtained results for the leaching efficiency of Si showed that only a small fraction (< 5.0%) of the total Si content could be leached from the material, meaning that the examined experimental conditions or acid reactants did not have any significant impact on the recovery of Si from the material.

Table 7. Effect of temperature on the leaching efficiency of Al, Ni, Cr and Si

Type of acid	Temperature (°C)	Leaching efficiency (%)			
		Al	Ni	Cr	Si
HNO_3	20	1.66	49.9	0.17	(*)
	50	4.63	55.3	0.39	2.46
	80	6.01	61.4	0.56	4.42
H_2SO_4	20	4.29	58.8	0.51	(*)
	50	8.8	59.5	0.83	1.68
	80	16.5	88.0	1.32	2.46
H_3PO_4	20	2.06	52.8	0.91	(*)
	50	4.1	67.9	1.24	4.13
	80	6.42	68.2	1.87	4.22

(*): Not calculated since the measured concentration value was lower than detection limit of 0.05 mg/L.

This result indicated that the remaining solids fraction was still rich in terms Si content after the leaching process. To take advantage of this Si-rich fraction, an additional process should be considered for the remaining solids fraction after the leaching process.

4. DISCUSSION AND CONCLUSIONS

Using HCl as leaching solution with different concentrations ranging between 1.0 and 9.0 M, Top (2014) investigated the leaching of Mg, Fe, Ni, Cr, and Mn from chromite mining waste, of which the initial chemical composition was quite similar to that of the material used in the present study. The experimental results showed that the leaching efficiency for all analytes, especially for Mg and Fe, significantly increased with the increasing acid concentration up to 7.0 M, but no remarkable change occurred when the concentration increased to 9.0 M. Therefore, an acid concentration of 7.0 M was used as the optimum concentration for the next experimental stages. The difference between the findings obtained by Top (2014) and in the present study might be attributed to the potential differences in characteristics of the leached materials because the material used by Top (2014) was subjected to several pre-treatments (size reduction by wet milling, flocculation, and magnetic separation) prior to the leaching. Although the optimum acid concentration was determined to be 1.0 M for H_2SO_4, which was comparably lower than determined by Top (2014), the leaching efficiency for Mg or Fe in both studies eventually reached a maximum value >90% under the optimized conditions (Table 8). It should also be noteworthy to mention that obtaining relatively high leaching efficiencies using low concentrated acid solutions rather than high concentrated ones ensures a cost-effective process operation. In another study performed by Habbache et al. (2017), the effect of acid concentration on the leaching of Ni from a NiO-bearing catalyst was investigated by using HCl, H_2SO_4 and HNO_3. According to the experimental results, an increase in the acid concentration from 0.5 to 2.0 M resulted in an increase in the leaching efficiency of Ni from 28 to 77% for HNO_3 and 24 to 46% for H_2SO_4 while it increased from 93 to 100% in the case of leaching with HCl. As demonstrated by Habbache et al. (2017) and the present study, one can be concluded that the leaching behaviors of different acid solutions with varying concentrations may exhibit significant or non-significant differences even under the identical experimental conditions applied for a given material.

Top (2014) showed that the leaching efficiency of Mg, Fe, Ni, Cr, and Mn decreased with the increasing solid to liquid ratio. A similar finding was also reported by Yoğurtçuoğlu (2023). However, this was not the case for the present study since the leaching efficiencies for both Mg and Fe remained almost the same although the material dosage increased from 5 to 35 g/L. Moyo et al. (2022) explained that the rate of the reaction is controlled by the reactant's diffusion through the solid material layer and solution boundary layer. Moreover, the increasing temperature results in an increase in the intensity of the collision of reactants, thus, the occurrence of a faster reaction between the Mg-bearing compounds and the leaching solution. Considering the mentioned literature studies were conducted at a temperature condition of 60, 80, and 90 °C, which was quite higher than the applied temperature of 20 °C in the present study, one can be concluded that the complete recovery of Mg or Fe cannot be achieved even for low solid to liquid ratio conditions if the reaction temperature is not sufficiently high. Therefore, the effectiveness of the acid reactants used in the present study did not change with the increasing material dosage at 20 °C.

The effect of the reaction time and temperature on the leachability of Mg, Fe, and Ni from olivine-bearing ore was investigated by Matus et al. (2020). According to the results, it was reported that the efficiencies increased with the increasing reaction time from 30 to 180 min and the increasing temperature 50 to 80 °C. Moyo et al. (2022) also showed that the amount of Mg recovered from ferrochrome slag increased significantly between 30 and 150 min, however, an additional 30 min of reaction time did not cause any significant change on the amount of Mg recovered. In addition, an increase in the temperature from 30 to 80 °C increased the rate of dissolution of Mg. Top and Yıldırım

(2015) reported that the leaching efficiency of Mg and Fe increased with the increasing temperature between 25 and 90 °C and the increasing reaction time between 5 and 60 min. However, the increasing trend for the leaching efficiencies decreased after 20 min of reaction time. These findings were in accordance with the findings of the present study.

Table 8. Comparison of the leaching efficiencies obtained under optimized conditions for several literature studies

Reference	Optimum conditions	Leaching efficiency (%) Amount of the recovered analyte measured in the leachate (mg/L)				
		Mg	Fe	Al	Ni	Cr
Habbache et al. (2017)	• Acid concentration: 2.0 M HCl • Solid to liquid ratio: 2% • Reaction time: 30 min. • Temperature: 80 °C	NA(*) NA	NA NA	NA NA	100% NA	NA NA
Top (2014)	• Acid concentration: 7.0 M HCl • Solid to liquid ratio: 11% • Reaction time: 30 min. • Temperature: 90 °C	92.8% 3372 mg/L	81.5% 735 mg/L	NA NA	87.1% 6.10 mg/L	1.76% 2.06 mg/L
Matus et al. (2020)	• Acid concentration: 1.0 M HCl • Solid to liquid ratio: 10% • Reaction time: 90 min. • Temperature: 80 °C	40-45% NA	40-45% NA	NA NA	30-35% NA	NA NA
Moyo et al. (2022)	• Acid concentration: 5.0 M HCl • Solid to liquid ratio: 10% • Reaction time: 150 min. • Temperature: 70 °C	88.2% 13940 mg/L	NA NA	NA NA	NA NA	NA NA
This study	• Acid concentration: 1.0 M H_2SO_4 • Solid to liquid ratio: 3.5% • Reaction time: 90 min. • Temperature: 80 °C	93.7% 8461 mg/L	91.9% 1672 mg/L	16.5% 14.9 mg/L	88.0% 85.0 mg/L	1.32% 3.16 mg/L

(*): Not available

The overall results of the present study showed that a considerable amount of Mg and Fe could be recovered from the material using HNO_3, H_2SO_4 and H_3PO_4. This means the obtained leachates contained Mg and Fe up to a certain level after leaching of the material, implying that the leachates could be used as Mg and/or Fe source for several applications. For example, the Mg-rich leachate obtained with H_3PO_4 presents itself as a great opportunity for struvite precipitation process, where the external addition of both Mg and PO_4 sources is required to obtain a desired molar ratio for the formation of struvite crystals. Using magnesit ($MgCO_3$) as a low-cost Mg source, Günay et al. (2008) showed that struvite precipitation with $MgCO_3$ significantly lowered the amount of ammonium, phosphate, suspended solid and turbidity from high ammonium contained landfill leachate. On the other hand, the leachates that are rich in terms of both Mg and Fe can also be used to synthesize MgFe layered double hydroxides, which are commonly synthesized by co-precipitation of Mg and Fe salts in an alkaline medium (Kameliya et al., 2023). These potential uses of such leachates may trigger new research studies for cost-effective alternative metal resources.

Acknowledgements
The author appreciates Dr. Barbaros Salih Kumbul's generous help and efforts in the preparation of the material and experimental set-up. The author would also like to express his gratitude to Prof. Dr. Kamil Ekinci for supplying the tailings.

Ethics Committee Approval
N/A

Peer-review
Externally peer-reviewed.

Author Contributions
Hüseyin Yazıcı: Conceptualization, Investigation, Material and Methodology, Supervision, Visualization, Writing-Original Draft, Writing-review & Editing, Other. The author has read and agreed to the published version of manuscript.

Conflict of Interest
The authors have no conflicts of interest to declare.

Funding
The financial support for ICP-OES measurements from Mehmet Arafat Gümüşlü is thankfully acknowledged by the author.

REFERENCES

Álvarez, M.L., Gascó, G., Rodiguez-Pacheco, R., Paz-Ferreiro, J., Méndez, A. (2022). Recovery of metals from mine wastes: The effect of biochar–Fe composites in the immobilization of arsenic. Journal of Sustainable Metallurgy. 8, 419-429. https://doi.org/10.1007/s40831-022-00495-y.

Araujo, F.S.M., Taborda-Llano, I., Nunes, E.B., Santos, R.M. (2022). Recycling and reuse of mine tailings: A review of advancements and their implications. Geosciences. 12, 319. https://doi.org/10.3390/geosciences12090319.

Bellenfant, G., Guezennec, A.G., Bodenan, F., D'Hugues, P., Cassard, D. (2013). Reprocessing of mining waste: combining environmental management and metal recovery?. In: Tibbett, M., Fourie, A.B., Digby, C. (Eds.), Mine Closure 2013: Proceedings of the Eighth International Seminar on Mine Closure, Australian Centre for Geomechanics. Cornwall, U.K., pp. 571-582. https://doi.org/10.36487/ACG_rep/1352_48_Bellenfant.

Bolaños-Benítez, V., van Hullebusch, E.D., Lens, P.N.L., Quantin, C., van de Vossenberg, J., Subramanian, S., Sivry, Y. (2018). (Bio)leaching behavior of chromite tailings. Minerals. 8, 261. https://doi.org/10.3390/min8060261.

BRGM, 2001. Management of mining, quarrying and ore-processing waste in the European Union. https://ec.europa.eu/environment/pdf/waste/studies/mining/0204finalreportbrgm.pdf (accessed 1 August 2023).

Carmo, F.F., Lanchotti, A.O., Kamino, L.H.Y. (2020). Mining waste challenges: Environmental risks of gigatons of mud, dust and sediment in megadiverse regions in Brazil. Sustainability. 12, 8466. https://doi.org/10.3390/su12208466.

Coetzee, J.J. Bansal, N., Chirwa, E.M.N. (2020). Chromium in environment, its toxic effect from chromite-mining and ferrochrome industries, and its possible bioremediation. Exposure and Health. 12, 51-62. https://doi.org/10.1007/s12403-018-0284-z.

Erüst, C., Akcil, A., Gahan, C.S., Tuncuk, A., Deveci, H. (2013). Biohydrometallurgy of secondary metal resources: a potential alternative approach for metal recovery. Journal of Chemical Technology and Biotechnology. 88, 2115-2132. https://doi.org/10.1002/jctb.4164.

Günay, A., Karadağ, D., Tosun, İ., Özturk, M. (2008). Use of magnesit as a magnesium source for ammonium removal from leachate. Journal of Hazardous Materials. 156, 619-623. https://doi.org/10.1016/j.jhazmat.2007.12.067.

Habbache, N., Djerad, S., Tifouti, L. (2017). Optimization of the operation conditions for NiO dissolution with different leachants. Process Engineering Journal. 1, 59-67.

Hitch, M., Ballantyne, S.M., Hindle, S.R. (2010). Revaluing mine waste rock for carbon capture and storage. International Journal of Mining, Reclamation and Environment. 24(1), 64-79. https://doi.org/10.1080/17480930902843102.

Jha, M.K., Shivendra, Kumar, V., Pandey, B.D., Kumar, R., Lee, J. (2010). Leaching studies for the recovery of metals from the waste printed circuit boards (PCBs), in: Vidal, E.E. (Ed.), Proceedings of EPD Congress. John Wiley & Sons, Washington, U.S.A., 945-952.

Kameliya, J., Verma, A., Dutta, P., Arora, C., Vyas, S., Varma, R.S. (2023). Layered double hydroxide materials: A review on their preparation, characterization, and applications. Inorganics. 11, 121. https://doi.org/10.3390/inorganics11030121.

Krishnan, S., Zulkapli, N.S., Kamyab, H., Taib, S.M., Din, M.F.B.M., Majid, Z.A., Chaiprapat, S., Kenzo, I., Ichikawa, Y., Nasrullah, M., Chelliapan, S., Othman, N. (2021). Current technologies for recovery of metals from industrial wastes: An overview. Environmental Technology & Innovation. 22, 101525. https://doi.org/10.1016/j.eti.2021.101525.

Kumar, P., Patra, S.K., Tripathy, S.K., Sahu, N. (2021). Efficient utilization of nickel rich Chromite Ore Processing Tailings by carbothermic smelting. Journal of Cleaner Production. 315, 128046. https://doi.org/10.1016/j.jclepro.2021.128046.

Lèbre, E., Corder, G. (2015). Integrating industrial ecology thinking into the management of mining waste. Resources, 4, 765-786. https://doi.org/10.3390/resources4040765.

Lu, Z., Cai, M. (2012). Disposal methods on solid wastes from mines in transition from open-pit to underground mining. Procedia Environmental Sciences. 16, 715-721. https://doi.org/10.1016/j.proenv.2012.10.098.

Lunk, H.J. (2015). Discovery, properties and applications of chromium and its compounds. ChemTexts. 1, 6. https://doi.org/10.1007/s40828-015-0007-z.

Marra, A., Cesaro, A., Belgiorno, V. (2019). Recovery opportunities of valuable and critical elements from WEEE treatment residues by hydrometallurgical processes. Environmental Science and Pollution Research. 26, 19897-19905. https://doi.org/10.1007/s11356-019-05406-5.

Matus, C., Stopic, S., Etzold, S., Kremer, D., Wotruba, H., Dertmann, C., Telle, R., Friedrich, B., Knops, P. (2020). Mechanism of nickel, magnesium, and iron recovery from olivine bearing ore during leaching with hydrochloric acid including a carbonation pre-treatment. Metals. 10, 811. https://doi.org/10.3390/met10060811.

Moyo, L.B., Simate, G.S., Mamvura, T.A. (2022). Magnesium recovery from ferrochrome slag: Kinetics and possible use in a circular economy. Heliyon. 8, e12176. https://doi.org/10.1016/j.heliyon.2022.e12176.

Ndlovu, S., Simate, G.S., Matinde, E. (2017). Mining and beneficiation waste production and utilization, in: Ndlovu, S., Simate, G.S., Matinde, E. (Eds.), Waste Production and Utilization in the Metal Extraction Industry. CRC Press, London, U.K., pp. 65-112.

Oliveira, P.C., Cabral, M., Taborda, C., Margarido, F., Nogueira, C.A. (2009). Leaching studies for metals recovery from printed circuit boards scrap, in: Proceedings 2nd International Conference Electronics & Battery Recycling '09. Toronto, Canada.

de Palacios, L.T. Rodríguez, J.A.E. (2022). In mining, not everything is a circular economy: Case studies from recent mining projects in Iberia. Resources Policy. 78, 102798. https://doi.org/10.1016/j.resourpol.2022.102798.

Šajn, R., Ristovic, I., Ceplak, B. (2022). Mining and metallurgical waste as potential secondary sources of metals-A case study for the West Balkan Region. Minerals. 12, 547. https://doi.org/10.3390/min12050547.

Tayebi-Khorami, M., Edraki, M., Corder, G., Golev, A. (2019). Re-thinking mining waste through an integrative approach led by circular economy aspirations. Minerals. 9, 286. https://doi.org/10.3390/min9050286.

Top, S. (2014). Preparation of carnallite from Adana/Aladağ chromite ore beneficiation plant tailings. M.Sc. Thesis. (in Turkish). Çukurova University Institute of Natural and Applied Sciences, Department of Mining Engineering. Adana, Turkey. pp. 79.

Top, S., Yıldırım, M. (2015). Magnesium sulphate ($MgSO_4$) synthesis from chromite concentration plant tailings. Madencilik. 54(1), 37-46.

URL-1, 2018. https://ec.europa.eu/research/participants/documents/downloadPublic?documentIds=080166e5ba58c37b&appId=PPGMS (accessed 25 July 2023).

URL-2, (2023). https://www.statista.com/statistics/598320/mine-production-of-chromium-worldwide/ (accessed 27 July 2023).

Weibel, G., Zappatini, A., Wolffers, M., Ringmann, S. (2021). Optimization of metal recovery from MSWI fly ash by acid leaching: Findings from laboratory- and industrial-scale experiments. Processes. 9, 352. https://doi.org/10.3390/pr9020352.

Yoğurtçuoğlu, E. (2023). Multi-metal recovery from flotation tailings with citric acid on the NaCl media. Journal of Scientific Reports-A. 53, 59-73. https://doi.org/10.59313/jsr-a.1243469.

Simulating Input Motion Recordings at Fatih Downhole Array

Yusuf Guzel*[1]

Abstract: Predictions of seismic input motion characteristics at a site is seen as a tool of earthquake hazard mapping and earthquake hazard mitigation. The predictions can be conducted via modelling and simulating the soil layers under equivalent linear or nonlinear analyses in frequency or time domains. In order the predictions to be reliable for the use in building designs, it is necessary to verify the performances of the approaches through the actual input motions recordings at downhole arrays at different depths. When the elastic and nonlinear soil properties are two main driving inputs of the approaches, the modelling depth can be critical in the predictions, too. In this study, it is aimed to test the performance of the equivalent linear approach when the recorded input motions are simulated at different depths in Fatih Downhole Array, Istanbul. For this, the recorded input motions at the bottom (i.e. 136 m from the surface), at 60 m and at 23 m are applied to the models having identical heights. The results demonstrate that the prediction at the surface changes quite dramatically with the changes of soil model height. When the predictions in the East-West direction can be seen as indication of actual spectral accelerations, this is not relatively valid in the North-South direction. The study concludes that the spectral acceleration predictions express great dependency to the soil model length.

Keywords: Fatih Downhole Array, site response analysis, equivalent linear approach, Aegean earthquake, spectral acceleration.

[1]**Address:** Necmettin Erbakan University, Faculty of Engineering, Konya/Türkiye

***Corresponding author**: yusufkurtdereli@hotmail.com

1. INTRODUCTION

A well-known natural hazard that causes, primarily, human losses and huge economic losses is called an earthquake. The risks to urbanized areas associated with such a natural disaster are presented using the maximum ground acceleration (PGA) that reaches to the site of interest (Kramer, 1996). Magnitude of an earthquake event can articulate little about its damages to the surrounding urban areas as earthquake energy is dissipated at rock and soil layers. Therefore, the seismic level of an area or intensity of the earthquake event is represented by the PGA level (Ambraseys et al., 2005; Idriss, 2014).

When the PGA level for a site of interest depends on its distance to the fault lines, the local site condition is also very critical (Yusuf Guzel, 2019). Because the local site can alter the main characteristics of the input motions. Such as, frequency content, peak ground values (e.g., peak ground acceleration (PGA), peak ground velocity (PGV) and peak ground displacement (PGD)), predominant period and important duration of the input motions can be changed. Hence, the site response analysis can be very useful in order to predict such changes in the input motion characteristics (Sextos et al., 2018).

Site response analysis is carried out through with linear or equivalent non-linear methods in the frequency or time domain (Elia, 2015; Y. Guzel et al., 2020). Actual earthquake data recorded from the bottom soil layers is required to test whether the developed method can provide reliable predictions. In this regard, instrumented geotechnical arrays have been deployed in several seismic tectonic regions. For example, Lotung, Treasure Island, Parkfield-Turkey Flat, and La Cienega Geotechnical Arrays are some of the most popular geotechnical arrays installed. The seismic data collected in these arrays have been used in several studies to test equivalent linear and non-linear ground response approaches (Amorosi et al., 2017; Y. Guzel et al., 2020; Hallal and Cox, 2021; Salvati and Pestana, 2006).

This study focuses on the input motion recordings at the Fatih Downhole Array (FTH) and their simulations from different depths. It mainly purposes to reveal the impact of the depth of soil model simulation to the spectral response predictions at the surface. In the following section, site properties of the array are explained. The locations of the considered earthquake event and the downhole array and properties of the actual input motion recordings are presented in the following section. Subsequently, spectral response predictions are illustrated along with the actual ones.

2. FATIH DOWNHOLE ARRAY

Fatih Geotechnical Array (FTH) is positioned on top of stiff soil underlain by rock. It is closer to the historical mosque known as Fatih Mosque. It has been installed by Kandilli Observatory and Earthquake Research Institute of Bogazici University (KOERI) and by German Research Center for Geosciences (GFZ) in 2005 (Kurtuluş, 2011).

Geological formation from the Paleozonic age forms the engineering bedrock at the site named as Trakya Formation. This formation is overlain by the Bakirkoy and Gungoren Formations from the Miocene age. The Trakya formation is observed to be reach of up until the 60 to 80 m depths. Geotechnical surveys conducted at the site demonstrate that the unweathered greywacke is encountered between 136 m and 80 m depths and overlain by weathered greywacke up to the depth of about 40 m. The top 40 m of the soil deposit consists of alternating clay, silty sand and clay soil layers.

The shear wave velocity profile of the array site is depicted from the PS logging tests as represented in Figure 1. The shear wave velocity distribution clearly explain the different soil layering as it changes through the depths (Dikmen et al., 2015). In other words, the Vs alters quite smoothly from soil layers between 300 m/s and 500 m/s up to the depth of 40 m, it increases sharply in the weathered greywacke to almost 600 m/s and in particular in the unweathered greywacke to 1150 m/s. The average Vs profile at the top 30 m equals to 335 m/s and, hence, classified as soil class C according to Eurocode (EC8). The water table is about 4 m depth down from the surface.

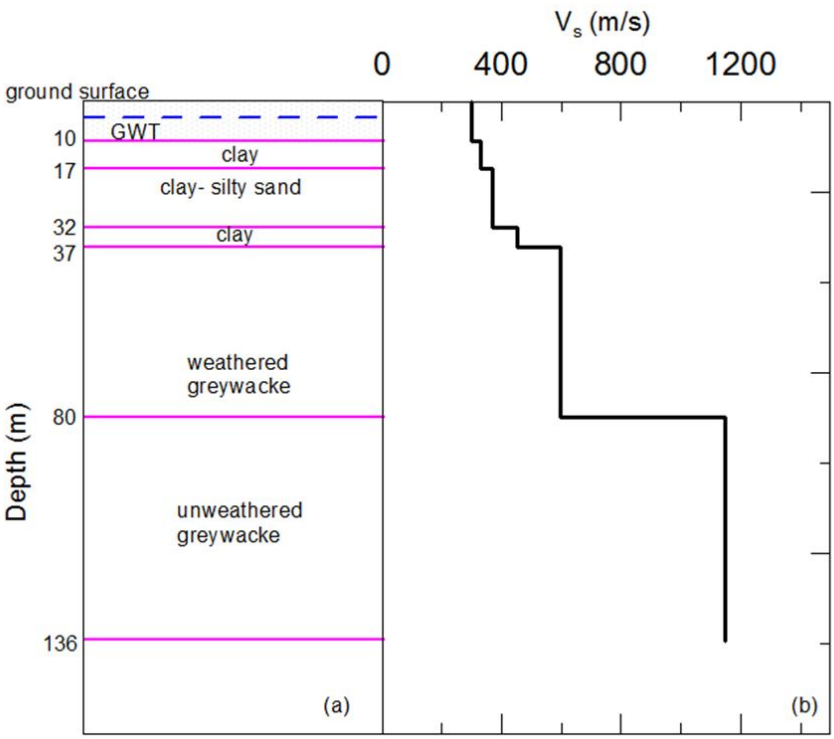

Figure 1. (a) geological features of the site and (b) measured Vs values up to the depth of 136 m

3. INPUT MOTION RECORDINGS

On April 24, 2014, an earthquake event was occurred in Aegean sea with moment magnitude of 6.9. Input motions of the earthquake event (called as Aegean earthquake) were recorded at the FTH downhole array. When the earthquake epicentre located in 40.21080 latitude and 25.30730 longitude, the FTH array located in 41.01972 latitude and 28.949 longitude. The locations are demonstrated in Figure 2. The direct distance between the earthquake epicentre and the array is about 320 km.

The acceleration-time histories in the East-West (EW) and North-South (NS) directions of the input motions in the East-West (EW) and North-South (NS) directions recorded at 136 m, 60 m, 23 m and at the ground surface are shown in Figure 3. The associated PGA values are also given in Table 1. The PGAs at the bottom of the array are 0.452 m/s^2 and 0.0176 m/s^2 in the EW and NS directions, respectively. The PGA reaches to 0.036 m/s^2 in the EW direction when it reaches to 60 m, showing deamplification. In the NS direction, however, it amplifies to the PGA level of 0.05 m/s^2. After 60 m, the

PGA values in the both horizontal directions amplify at the recorded depths. More precisely, they are equal to 0.06 m/s^2 and 0.099 m/s^2 at 23 m and 0.135 m/s^2 and 0.056 m/s^2 at the ground surface in the EW and NS directions respectively.

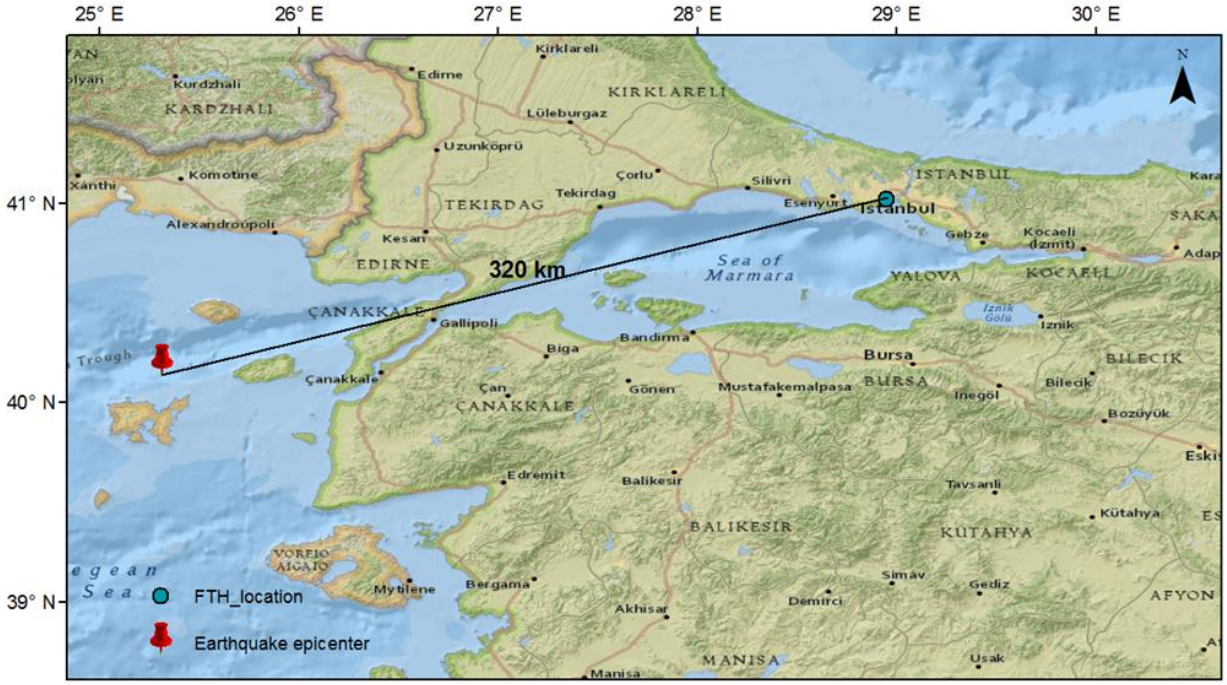

Figure 2. Locations of the Aegean earthquake event and FTH downhole array and distance between them

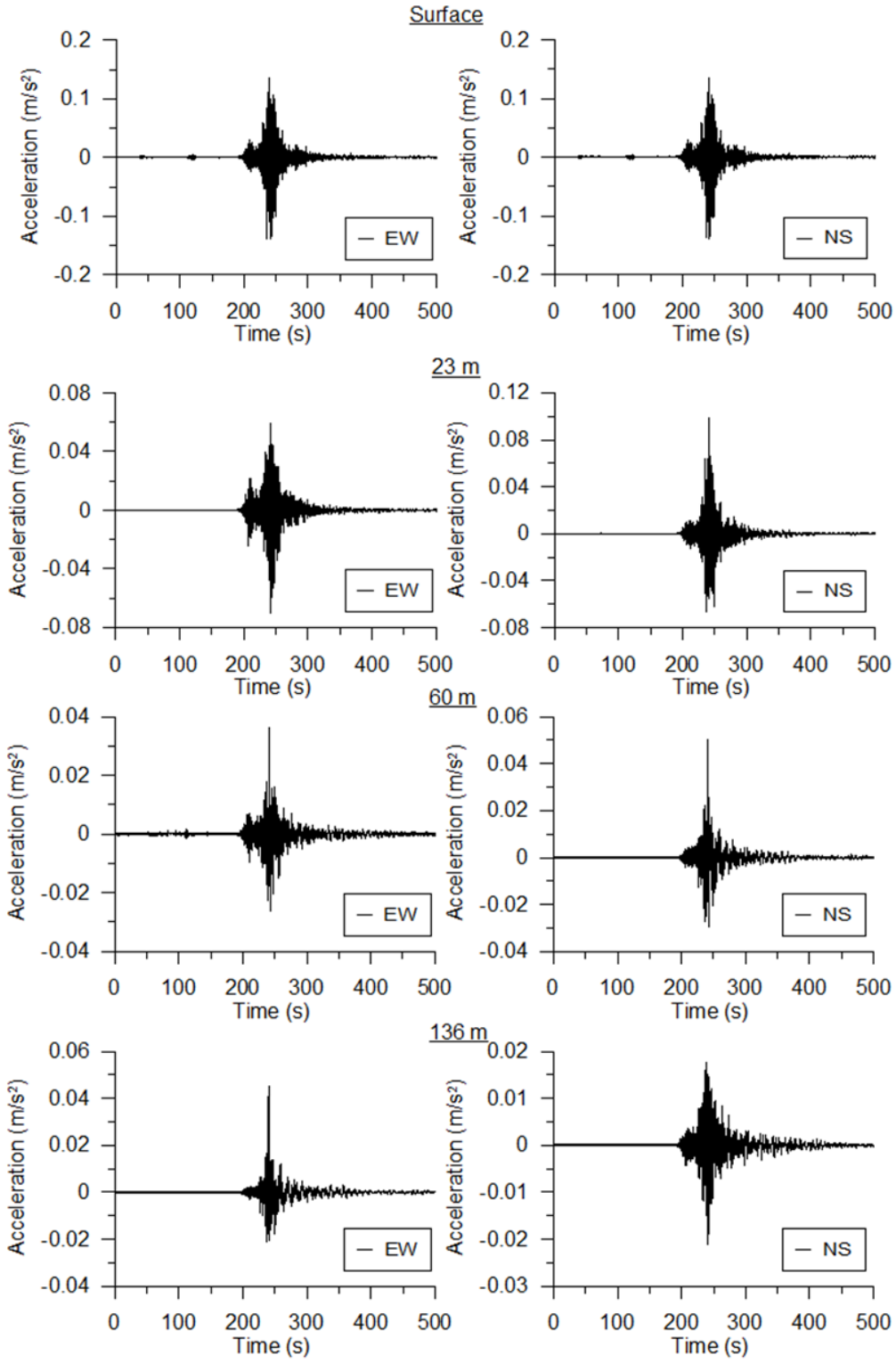

Figure 3. Acceleration-time histories of the input motions from the Aegean earthquake event recorded at the ground surface in the EW and NS directions

Table 1. PGA values of the recorded input motions at different depths

Directions / Depth (m)	PGA (m/s^2)	
	E-W	N-S
Ground surface	0.139	0.066
23	0.145	0.099
60	0.0364	0.05
136	0.045	0.0176

3. RESULTS AND DISCUSSIONS

The PGA and spectral acceleration predictions from the equivalent linear site response analyses (Deepsoil) of the FTH downhole array are illustrated in this section. When the PGA values are regarded as valuable to show the earthquake intensity, the spectral acceleration curves are very crucial for building behaviours, too (Malhotra, 2006).

In Table 2, the predicted PGA values when the FTH downhole array is simulated by the input motions at the 136 m depth are compared with the recorded ones in both horizontal directions. It is clear that the predicted PGA value at 60 m shows amplification from 0.045 m/s^2 to 0.065 m/s^2 while the recorded values deamplify with the value of 0.0364 m/s^2 in the EW direction. At 23 m and at the ground surface both predicted and recorded PGA values intend to amplify to 0.102 m/s^2 and 0.138 m/s^2 and to 0.145 m/s^2 and 0.139 m/s^2, respectively. However, both the predicted and recorded PGA values always in line of amplification at all measured depths. As the predicted and recorded PGA values are always equal to each other (being 0.047 m/s^2 and 0.05 m/s^2, respectively), they differ from each other towards to the ground surface. More precisely, the predicted PGA value increases sharply to the value of 0.1221 m/s^2 and the recorded ones reaches just to the value of 0.066 m/s^2.

Table 2. Predicted PGA values at 60 m, 23 m and at the ground surface when the 136 m of the FTH downhole array is simulated

Directions / Depth (m)	PGA (m/s^2)			
	Recorded/E-W	Predicted/E-W	Recorded/N-S	Predicted/N-S
Ground surface	0.139	0.138	0.066	0.1221
23	0.145	0.102	0.099	0.073
60	0.0364	0.065	0.05	0.047

The PGA values at 23 m and at the ground surface from the simulation of 60 m of the FTH downhole array are given in Table 3. The predicted PGA values reduce significantly and are well lower than the recorded ones in the EW direction, being 0.054 m/s^2 at 23 m and 0.096 m/s^2 at the ground surface. In contrast, the reductions in the NS direction are relatively minimal as the predicted PGA values are 0.079 m/s^2 at 23 m and 0.115 m/s^2 at the ground surface.

Table 3. Predicted PGA values at 23 m and at the ground surface when the 60 m of the FTH downhole array is simulated

Directions / Depth (m)	PGA (m/s^2)			
	Recorded/E-W	Predicted/E-W	Recorded/N-S	Predicted/N-S
Ground surface	0.139	0.096	0.066	0.115
23	0.145	0.054	0.099	0.079

In terms of spectral acceleration values, the predictions show relatively good match with the recorded ones in the EW direction at 23 m and at the ground surface but the period at which the spectral peaks occurred are not captured well (Figure 4). For instance, recorded spectral peak is about 0.75 m/s^2 at 0.5 s, the predicted one equals to 0.77 m/s^2 at 0.72 s at the ground surface. The according values at 23 m are 0.69 m/s^2 at 0.44 s (recorded one) and 0.63 m/s^2 at 0.72 s (predicted

one). However, the equivalent site response analysis cannot able to predict the recorded spectral values well at all considered depths, in particular, at the ground surface and at the 60 m depth.

When the 60 m of the FTH downhole array is simulated, the spectral predictions become better only at 23 m in the NS direction, as seen in Figure 5. Also, the period of spectral peak seems to be well captured at the ground surface in the EW direction.

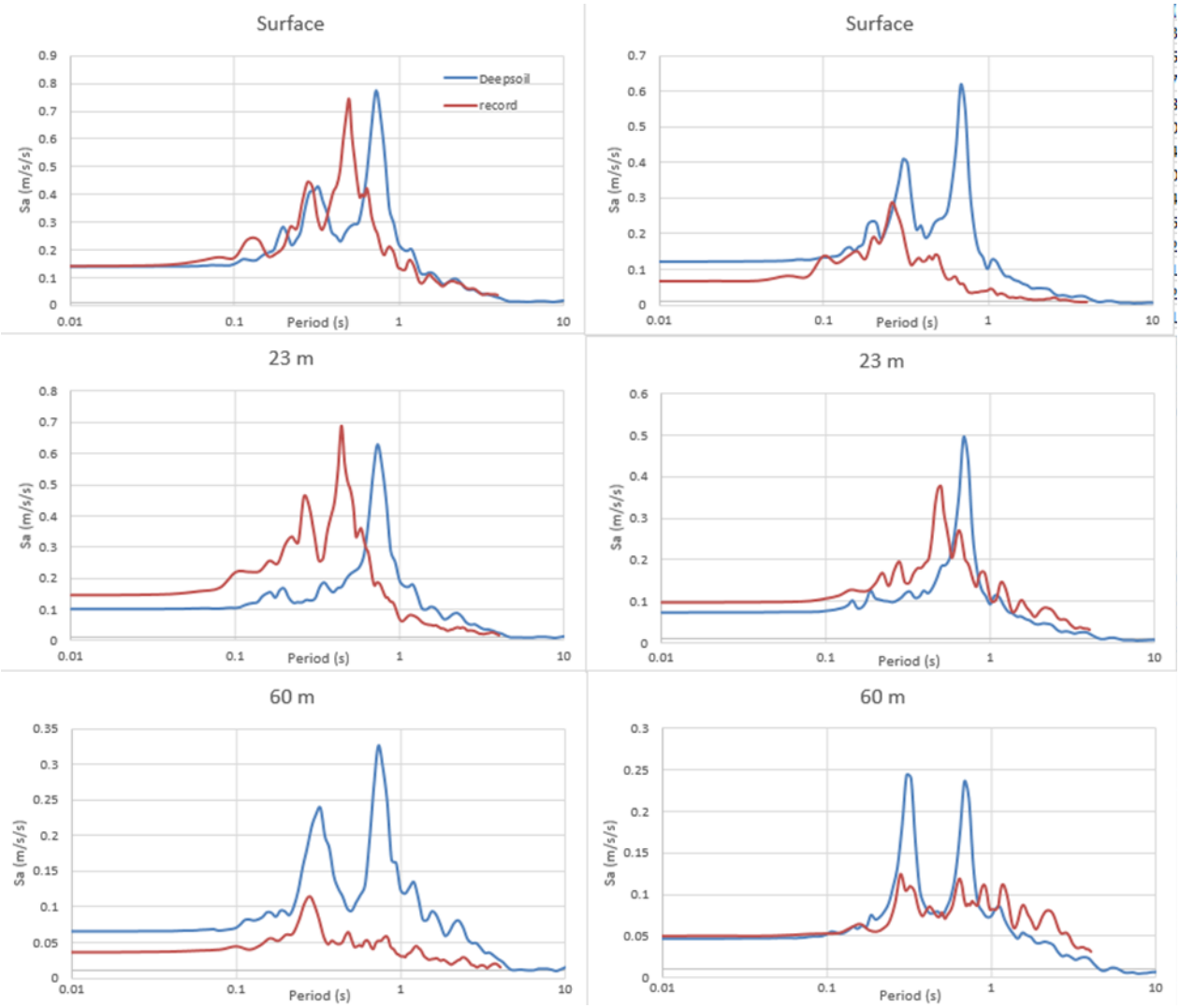

Figure 4. Spectral acceleration curves of the recorded and predicted input motions at 60 m, 23 m and at the ground surface when the recorded input motions at 136 m are simulated

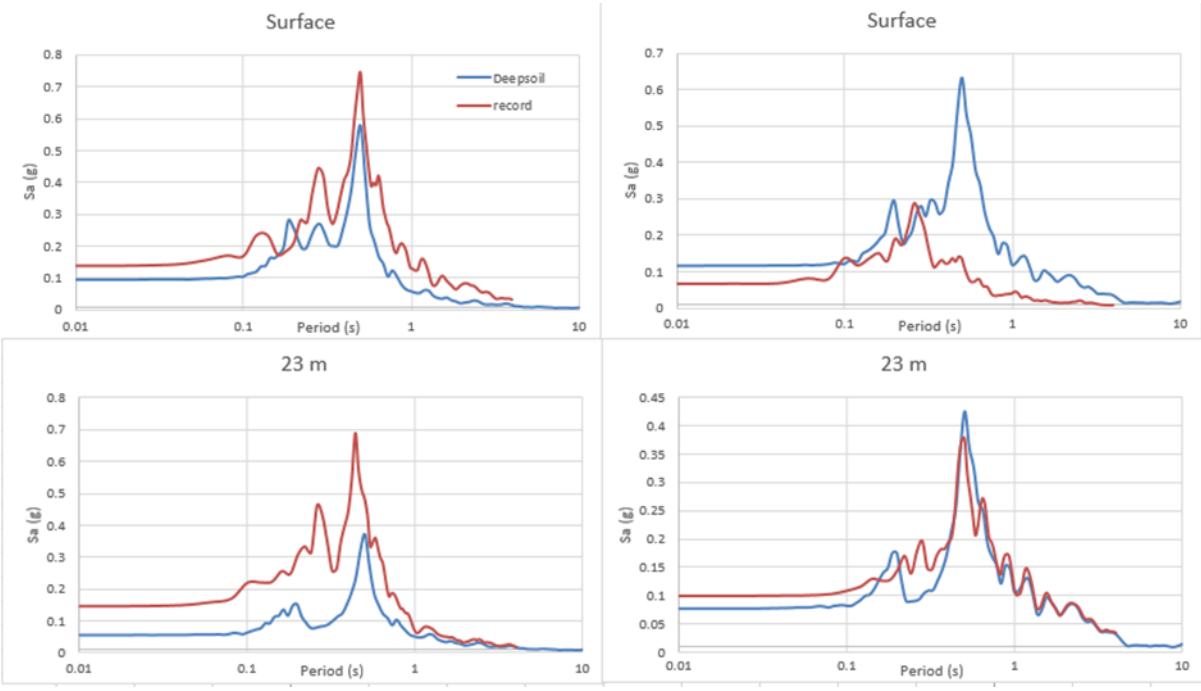

Figure 5. Spectral acceleration curves of the recorded and predicted input motions at 23 m and at the ground surface when the recorded input motions at 60 m are simulated

4. CONCLUSIONS

In this study, the dependency of the PGA and spectral acceleration values on the soil model length is studied at the Fatih Downhole array. The recorded input motions from the Aegean earthquake event occurred on April 24, 2020, are used for simulation and comparison purposes. The equivalent linear site response analyses are conducted.

The results indicate that the PGA predictions in the EW direction demonstrate good indication of the recorded values in the case of applying input motions at 136 m, especially at the ground surface. The predictions in the NS direction are also improved when the 60 m of the array is simulated. These assessments are valid for the spectral acceleration predictions, too. Therefore, the site response predictions express great dependency to the depth at which the input motions applied.

Acknowledgements
The author acknowledges the help of Prof. Erdal Şafak (at Bogazici University) in attaining the recorded data.

Ethics Committee Approval
N/A

Peer-review
Externally peer-reviewed.

Author Contributions
Conceptualization: Y.G.; Investigation: Y.G.; Material and Methodology: Y.G.; Supervision: Y.G.; Visualization: Y.G.; Writing-Original Draft: Y.G.; Writing-review & Editing: Y.G.; Other: All authors have read and agreed to the published version of manuscript.

Conflict of Interest
The authors have no conflicts of interest to declare.

Funding
The authors declared that this study has received no financial support.

REFERENCES

Ambraseys, N. N., Douglas, J., Sarma, S., Smit, P. (2005). Equations for the estimation of strong ground motions from shallow crustal earthquakes using data from Europe and the Middle East: horizontal peak ground acceleration and spectral acceleration. Journal of Bulletin of Earthquake Engineering. 3(1), 1-53.

Amorosi, A., Boldini, D., di Lernia, A. (2017). Dynamic soil-structure interaction: A three-dimensional numerical approach and its application to the Lotung case study. Computers and Geotechnics. 90, 34-54. doi:10.1016/j.compgeo.2017.05.016.

Dikmen, S. U., Edincliler, A., Pinar, A. (2015). Northern Aegean Earthquake (Mw=6.9): Observations at three seismic downhole arrays in Istanbul. Soil Dynamics and Earthquake Engineering. 77, 321-336. doi:10.1016/j.soildyn.2015.06.008.

Elia, G. (2015). Site response for seismic hazard assessment. Journal of Encyclopedia of earthquake engineering.

EC8 (2004). Design of structures for earthquake resistance—Part 1: General rules, seismic actions and rules for building, 2004.

Guzel, Y. (2019). Influence of input motion selection and soil variability on nonlinear ground response analyses. Newcastle University.

ESRI (2019). ArcGIS, ed. Redlands, CA: Environmental Systems Research Institute.

Guzel, Y., Rouainia, M., Elia, G. (2020). Effect of soil variability on nonlinear site response predictions: Application to the Lotung site. Computers and Geotechnics. 121. doi:10.1016/j.compgeo.2020.103444.

Hallal, M. M., Cox, B. R. (2021). An H/V geostatistical approach for building pseudo-3D Vs models to account for spatial variability in ground response analyses Part I: Model development. Earthquake Spectra. 37(3), 2013-2040. doi:10.1177/8755293020981989.

Hashash, Y. M., Musgrove, M., Harmon, J. (2018). Nonlinear and equivalent linear seismic site response of one-dimensional soil columns: User Manual v7. 0, Deepsoil Software. University of Illinois at Urbana-Champaign.

Idriss, I. (2014). An NGA-West2 empirical model for estimating the horizontal spectral values generated by shallow crustal earthquakes. Journal of Earthquake Spectra. 30(3), 1155-1177. doi:10.1193/1.2924362.

Kramer, S. L. (1996). Geotechnical earthquake engineering: Pearson Education India.

Kurtuluş, A. (2011). Istanbul geotechnical downhole arrays. Bulletin of Earthquake Engineering. 9(5), 1443-1461. doi:10.1007/s10518-011-9268-0.

Malhotra, P.K. (2006). Smooth spectra of horizontal and vertical ground motions. Bulletin of the Seismological Society of America. 96(2), pp. 506-518. doi:10.1785/0120050062.

Salvati, L. A., Pestana, J. M. (2006). Small-strain behavior of granular soils. II: Seismic response analyses and model evaluation. Journal of Geotechnical and Geoenvironmental Engineering. 132(8), 1082-1090. doi:10.1061/(ASCE)1090-0241(2006)132:8(1082).

Sextos, A., De Risi, R., Pagliaroli, A., Foti, S., Passeri, F., Ausilio, E., . . . Zimmaro, P. (2018). Local site effects and incremental damage of buildings during the 2016 Central Italy Earthquake sequence. Earthquake Spectra. 34(4), 1639-1669. doi:10.1193/100317EQS194M.

Performance comparison of feature extraction methods in Brain MRI images

Züleyha Yılmaz Acar*[1], Fatih Başçiftçi[1], Kamil Aykutalp Gündüz[2]

Abstract: Neuroimaging is a discipline that aims to unravel the complex anatomy and functioning of the brain. Magnetic Resonance Imaging (MRI) is one of the most commonly used neuroimaging techniques. With the help of high-performance computing tools, neurological abnormalities can be detected and analyzed based on the images obtained through MRI. Research on the diagnosis of diseases using MRI data is still ongoing, with some of the systems working directly with the original data while others require preprocessed data. This study focuses on the diagnosis of an Alzheimer's disease stage using MRI data from patients in the non-demented and very mild demented classes. The diagnosis is performed either by directly using the MRI images or by extracting meaningful features from the data. The discrete wavelet transform, statistical method (mean, standard deviation, and entropy), and deep learning ResNet18 model are employed as feature extractors, both individually and in combination. The performance of these methods is analyzed by a decision tree, support vector machine, k-nearest neighbor traditional machine learning, and ResNet18 deep learning methods. The results are compared with classification criteria calculated using confusion matrices. The results have shown that the highest classification accuracy is achieved by deep features extracted by the ResNet18 model on the original MRI dataset, and classified by support vector machine algorithm.

Keywords: Magnetic resonance imaging, feature extraction, deep learning, machine learning.

[1]**Address:** Selçuk University, Faculty of Technology, Konya/Türkiye
[2]**Address:** Selçuk University, Kadınhanı Faik İçil Vocational School, Konya/Türkiye

***Corresponding author**: zuleyhayilmaz@selcuk.edu.tr

1. INTRODUCTION

Neuroimaging provides detailed information about the structure and functioning of the brain, allowing complex system analysis (Beaulac et al., 2023). Magnetic Resonance Imaging (MRI) technology is a frequently used method for the detection of neurodegeneration in soft tissue. Along with these, analyzing relationships between high-dimensional data and image sets are problems waiting to be solved. Machine Learning (ML) solutions provide models that systematically analyze these complex structures and data. Traditional ML algorithms require a feature extraction step, on the other hand, deep learning can work on raw data without a feature extraction step. The feature extraction process is to reveal meaningful information and connections about the disease by examining the data in depth (Chakraborty et al., 2023).

Various approaches have been proposed for feature extraction methods from MRI images. Kaplan et al. investigate Parkinson's disease MRI images using a pyramid histogram of oriented gradients (HOG) feature extraction method. This approach handles the images segment by segment. Each segment is created as a grid by implementing HOG. After, the segments are aggregated to form a feature vector (Kaplan et al., 2022). Sharma et al. conduct brain tumor detection using HOG features. The analyzes are performed to find the appropriate block size for HOG transformation, and the resulting feature vector is used as a ResNet18 input (Sharma et al., 2023). Kuwil proposes a statistical feature extraction method for different types of medical images. According to this method, data distributions of medical images are examined and skews are analyzed. Thus, hidden features are revealed (Kuwil, 2022). Tasci et. al, in their approach, uses many pre-trained deep learning models as feature extraction method on diffusion MRIs of patients with ischemic acute infarction. The models are tested according to the classification performance metrics in the ML algorithm, and the pre-trained models that give the features that best describe the data are selected as feature extractors. The obtained deep features from the selected models are combined and sent to the feature selection model for feature reduction (Tasci & Tasci, 2022).

In this study, two stages of Alzheimer's disease, non-demented and very mild demented, are classified on brain MRI images. Discrete wavelet transform (DWT), statistical methods, and deep learning methods are used as feature extraction methods from MRI images, both separately and in combination, and the performances of the methods are compared. As the statistical method, the standard deviation, mean, and entropy values of each MRI image are used as features. Another method is the DWT, which is an image compression method and is also used for feature extraction. Haar wavelet mother function, widely preferred in biomedical images, is used in the study. Lastly, ResNet18 deep learning model is used as both a classifier and a feature extractor. Performance comparisons are made through classifiers to measure the success of the methods. As classifiers, tree types of decision tree algorithms (fine, medium, and coarse tree), six types of support vector machine (SVM) (linear, quadratic, cubic, fine gaussian, medium gaussian and coarse gaussian SVM), six types of k-nearest neighbor (KNN) (fine, medium, coarse, cosine, cubic and weighted KNN) and ResNet18 deep learning model are preferred. Based on the confusion matrices, the performance metrics are calculated and the success of feature extraction methods are compared.

The organization of the paper is as follows: The dataset and feature extraction methods are explained in the material and method in the second part. The performance metrics, classification algorithms, and results are in the third section. The comparison of the feature extraction methods according to the metrics and conclusions is given in the fourth section as the discussion and conclusions part.

2. MATERIAL AND METHOD

In this section, the dataset and feature extraction methods are introduced. Figure 1 represents the process of the study.

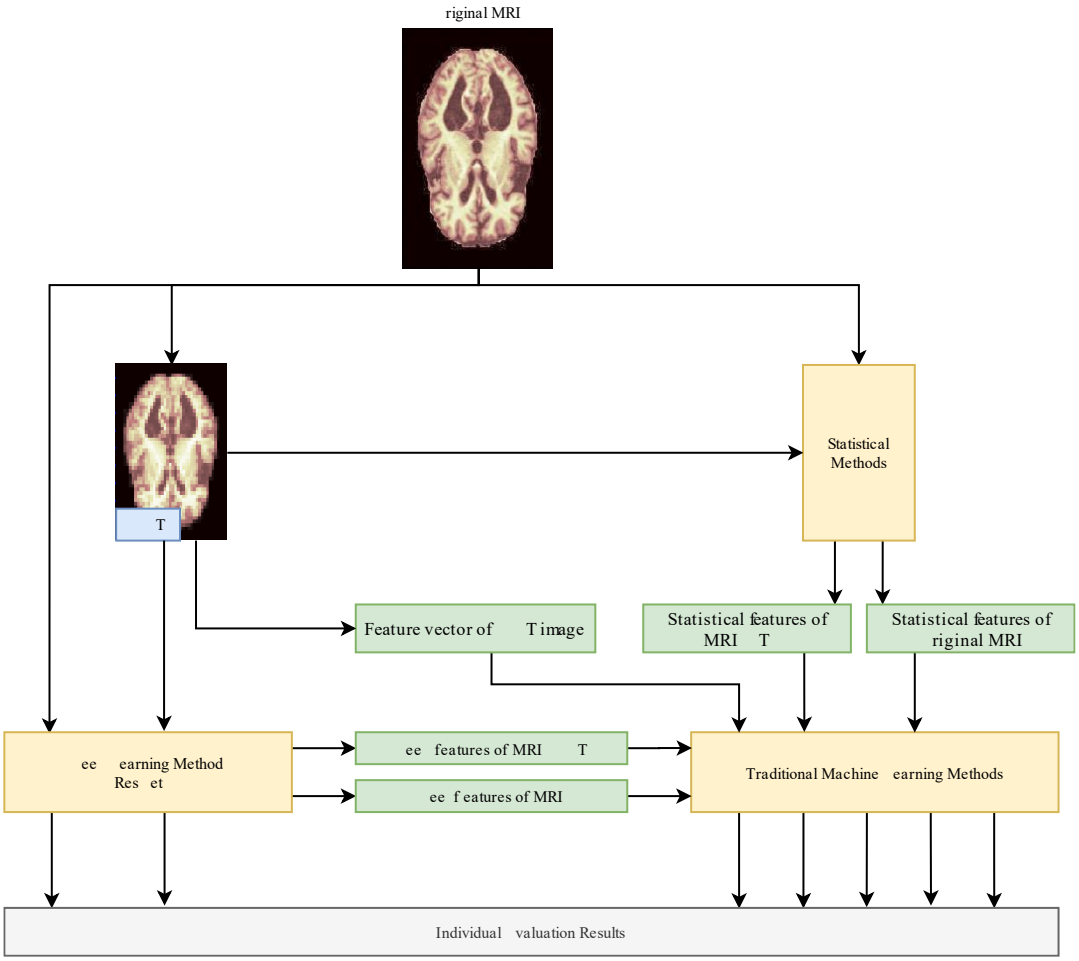

Figure 1. The process of the study

2.1. Dataset

The MRI dataset used in the study is related to Alzheimer's disease. It is available on the open-source Kaggle website (https://www.kaggle.com/tourist55/alzheimers-dataset-4-class-of-images, accessed on 02/08/2023). Since there is an imbalance problem between the classes in the dataset, two classes of similar size are studied. These classes are non-demented and very mild demented. Some images of the dataset are shown in Figure 2.

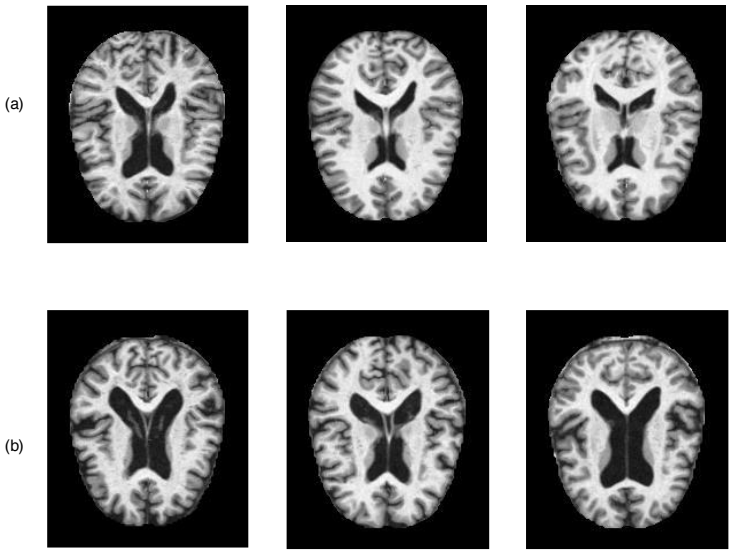

Figure 2. (a) the row with non-demented MRI images, (b) the row with very mild demented MRI images

The dataset contains 3200 images from the non-demented class and 2240 images from the very mild demented class, respectively, with a total of 5440 images in the train and test sets. After the feature extraction step, z-score normalization is applied to the all images. In addition, RGB formats of images are used as deep learning input types.

2.2. Feature Extraction Methods

In this study, feature extraction methods are performed on the raw and the compressed data by applying DWT. One of the aims of this study is to investigate whether there is an advantage in using the DWT of large-sized MRI images as a preprocess and using compressed data as input. On the other hand, the data obtained with the DWT is used directly as a feature vector in the study. Thus, the statistical method, DWT, and deep features are considered both separately and as a combination. Afterward, the dataset is classified. The classifiers and input data types used in the study are listed in Table 1.

Table 1. Input data and feature extraction methods

Classifiers	Inputs
Deep Learning (ResNet18)	MRI
	MRI + DWT
Traditional ML (Decision Tree, SVM, KNN)	MRI + DWT
	MRI + Statistical
	MRI+ DWT + Statistical
	Deep features of MRI
	Deep features of MRI + DWT

The first feature extraction method used is the statistical method. In the study, three features of the data as mean, standard deviation, and Shannon wavelet entropy are used. When extracting the features from the image matrices, two different results are obtained by taking both the original (1) and mean value of the statistical results (2). The applied process is shown in Figure 3.

		2 9
202		9
2	2	

An e am le of image matri

mean		0	9
std	99	20 2	20 9
entro y	e		

Statistical features

mean mean	0 9
mean std	99
mean entro y	e

The mean values of the statistical features 2

Figure 3. The implementation of the mean operation

The other method used as a feature extraction method is the wavelet transform. Discrete wavelet transform (DWT) is utilized in this study. This method is a signal analysis method that performs multiple resolution analysis of signals (Mallat, 9 9; Özmen & Özşen, 20 . Relationships across rows and columns of 2D MRI images are explored. This DWT is used as a feature extraction method. In the study, the "haar" wavelet mother function is a li ed from the second level as the wavelet family. Figure 4 shows the obtained MRI image when DWT with the haar wavelet mother function is applied.

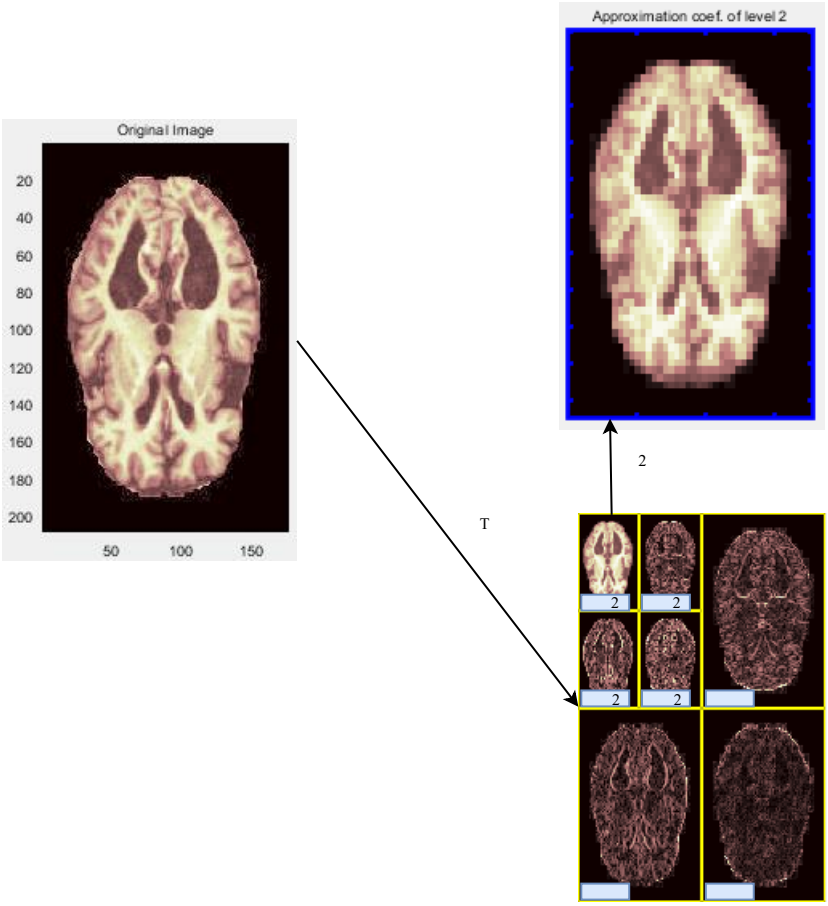

Figure 4. The application of the DWT

The LL2 image in Figure 4 is the detailed image and contains the most meaningful information Yılmaz Acar, Başçiftçi, & Ekmekci, 2022). The LL2 image (expressed as MRI+DWT) and statistical features are extracted from this image. Here, it is aimed to investigate the success of applying DWT to high-dimensional MRI data and creating a smaller image set. The procedures in Figure 3 are also applied for MRI+DWT and are also named (1) and (2). The LL2 image is also converted into vector form as directly a feature vector.

Finally, since deep learning is both an effortless and popular method of recent times, the pre-trained ResNet18 deep learning architecture is utilized in the study. ResNet18 is a convolutional neural network model consisting of 18 layers (He, Zhang, Ren, & Sun, 2016). Input data has been converted to RGB images. The original MRI data and the MRI+DWT are the individual input data of ResNet18. Hereby, it is aimed to compare the success of the MRI+DWT image set and the original image set in the deep learning method. Besides, after applying ResNet18 to both sets, the features obtained

by the model in the last stage are also stored as deep features and given to traditional ML algorithms for classification. The feature extraction performance of the ResNet18 model is examined.

3. RESULTS

The output of the study is the combination of the input data and the feature extraction method that reaches the highest accuracy value. In this section, feature extraction methods are compared based on performance metrics. Extracting the most essential features from the data dramatically affects the results obtained by the classifiers. For this reason, many methods are handled in different ways and the results are examined.

Alzheimer's disease brain MRI datasets are used in the study. The information about the dataset is given in Table 2.

Table 2. The number of images in the dataset

Dataset	Train		Test	
	Class – 1 (Non-demented)	Class – 2 (Very mild demented)	Class – 1 (Non-demented)	Class – 2 (Very mild demented)
Alzheimer's disease MRI images	2560	1792	640	448

Feature extraction methods produce the feature numbers in Table 3.

Table 3. The number of features of the feature extraction methods

Method	Number of features
Statistical features (1)	289
Statistical features (2)	3
Statistical features of MRI+DWT (1)	73
Statistical features of MRI+DWT (2)	3
Vectorial form of MRI+DWT	1252
Deep features of the original MRI	512
Deep features of MRI+DWT	512

Data is classified using traditional ML algorithms using the number of features given in Table 3. The classifiers used in the study are three types of decision tree algorithms (fine, medium and coarse tree), six types of SVM (linear, quadratic, cubic, fine gaussian, medium gaussian and coarse gaussian SVM), six types of KNN (fine, medium, coarse, cosine, cubic and weighted KNN) and ResNet18 model.

The success of the methods is compared by calculating the classification performance metrics over the confusion matrices obtained from each classifier. The confusion matrices and metrics are shown in Figure 5.

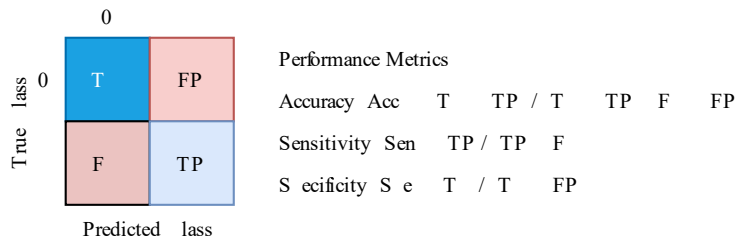

Figure 5. The confusion matrix and performance metrics

In Figure 5, TN is referred to as True Negative, FP is False Positive, FN is False Negative and TP is True Positive. The formulas of the metrics are included in the figure.

The performance results are obtained from all traditional ML algorithms. In addition, the original and MRI+DWT images are classified with the ResNet18 model. The best results among all classifiers are listed in Table 4.

Table 4. The classification results

Inputs	Best Classifier	Performance Metrics		
		Accuracy (Acc) (%)	Sensitivity (Sen) (%)	Specificity (Spe) (%)
Statistical features (1)	KNN (medium)	59.28	3.35	98.44
Statistical features (2)	Decision Tree (coarse)	58.73	31.47	77.81
Statistical features of MRI+DWT (1)	KNN (weighted)	59.65	2.00	100
Statistical features of MRI+DWT (2)	SVM (fine gaussian)	56.71	41.29	67.5
Vectorial form of MRI+DWT	Decision Tree (fine)	63.88	54.02	70.78
Deep features of the original MRI	SVM (medium gaussian)	**76.56**	**74.78**	77.81
Deep features of MRI+DWT	SVM (fine gaussian)	67.65	38.39	88.12
Original MRI dataset	ResNet18	74.82	66.54	82.56
MRI+DWT dataset	ResNet18	66.91	29.46	93.12

According to Table 4, it is presented that the results are below the 60% Acc value for statistical features on both the original MRI and MRI+DWT datasets. Additionally, the Sen values, which are the classification rate of the very mild demented class, are very low. On the hand, the Spe values, which are the classification rate of the non-demented class, are at a sufficient level. A very low Sen value and a very high Spe value indicate that the classifiers failed in the training process and mostly classified the data into non-demented classes. The classification success is to reach balanced and sufficient Sen and Spe values as well as Acc values.

MRI+DWT images are converted to vectorial form and used as a feature vector. This method produces 63.88% Acc, 54.02% Sen, and 70.78% Spe values in the decision tree classifier. It reveals a more meaningful feature vector with a high Acc value and more balanced Sen and Spe values compared to the statistical features.

The ResNet18 model makes classification with two types of input data. The first is the original raw MRI dataset, and the other is the MRI+DWT dataset. According to the results obtained with the original dataset, relatively good results are obtained with 74.82% Acc, 66.54% Sen, and 82.56% Spe values. However, the data belonging to the non-demented class are still classified more accurately, on the other hand, the data of the very mild demented class are not classified accurately enough. There appears to be a tendency towards the non-demented class. Besides, the MRI+DWT dataset demonstrates the result with 66.91% Acc, 29.46% Sen, and 93.12% Spe values which is lower than the original MRI dataset. The results show both a low Acc and an immoderate Sen and Spe values, and not being able to adequately distinguish both class groups. Here, it can be concluded that the DWT process causes a loss of information about the dataset for deep learning.

Looking at the methods and classifiers table, it is seen that the best combination is achieved with the SVM classifier using ResNet18 deep features. The ResNet18 model is trained using the original train MRI dataset, then the activations obtained by the architecture are stored. In addition, the activations of the test MRI dataset are extracted over the trained network. By using the activations as features, the SVM is utilized as the classifier. This method produces the highest Acc value with 76.56% and also obtains stable and balanced results with 74.78% Sen and 77.81% Spe values. The results show that it can distinguish the patient and healthy class. This combination has been the method showing the highest success compared to other methods, especially in the highest true positive rate classification of the patient class. On the other hand, deep features of the MRI+DWT dataset produce a 67.65% Acc value, but a low Sen value of 38.39% and a nonproportional high Spe value of 88.12%.

The confusion matrices obtained by the methods are given in Figure 6. In the figure, the value "0" represents the healthy class (non-demented), and the value "1" represents the patient class (very mild demented).

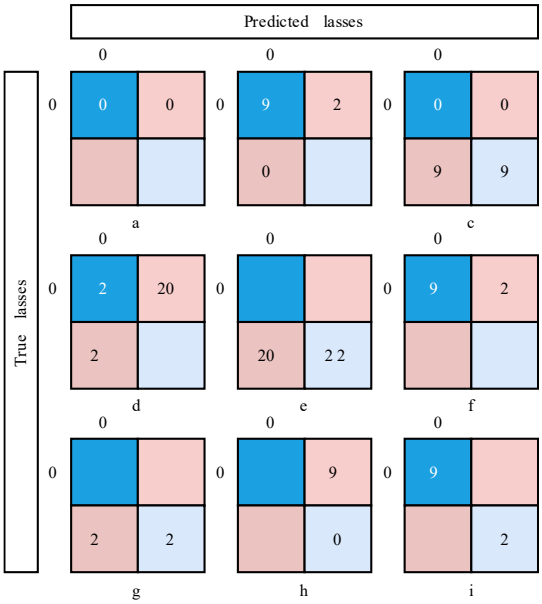

Figure 6. The confusion matrices (a) statistical features (1), (b) statistical features (2), (c) statistical features of MRI+DWT (1), (d) statistical features of MRI+DWT (2), (e) vectorial form of MRI+DWT, (f) deep features of original MRI, (g) deep features of MRI+DWT, (h) original MRI dataset, (i) MRI+DWT dataset

4. DISCUSSION AND CONCLUSIONS

MRI data contains very complex and meaningful information about the brain. The analysis of MRI images is an important role in the diagnosis of the disease. Various analysis and disease detection studies have continued to be carried out with machine learning solutions. In this study, a classification study is carried out using the Alzheimer's disease brain MRI dataset. The results are analyzed and interpreted by applying various feature extraction methods. In the study, seven different feature groups are analyzed separately, including statistical features obtained from the original MRI dataset in the study with two different processes, statistical features obtained from the MRI+DWT dataset with two different processes, directly MRI+DWT vectorial form, and ResNet18 deep features of original MRI and MRI+DWT dataset. The feature groups are classified with sixteen classifiers, including three types of decision trees, six types of SVM, six types of KNN, and the ResNet18 deep learning model.

According to the results, it shows that the statistical features are insufficient in the feature extraction process. In terms of the vectorial form of MRI+DWT, the method is open to improvement, but this combination creates a disadvantage for deep learning. The results of classification performance both in itself and over deep features are unsuccessful since the significant features are lost. On the other hand, the best feature extraction method according to the performance results of all methods is the deep features obtained by the ResNet18 model and the classification of these features with the SVM algorithm. This result demonstrates the success of the deep learning model in making sense of in-depth features in the data. Besides, it shows that the SVM algorithm continues to produce high classification results, especially on biomedical data.

Acknowledgements
e thank Selçuk University and Scientific Research Projects Commission.

Ethics Committee Approval
N/A

Peer-review
Externally peer-reviewed.

Author Contributions
Conceptualization: Z.Y.A., F.B.; Investigation: Z.Y.A., F.B., K.A.G.; Material and Methodology: Z.Y.A., F.B.; Supervision: F.B.; Visualization: Z.Y.A., F.B., K.A.G.; Writing-Original Draft: Z.Y.A.; Writing-review & Editing: Z.Y.A. F.B., K.A.G.; Other: All authors have read and agreed to the published version of manuscript.

Conflict of Interest
The authors have no conflicts of interest to declare.

Funding
This study is supported by Selçuk University Scientific Research Projects Commission with project number 23701136.

REFERENCES

Beaulac, C., Wu, S., Gibson, E., Miranda, M. F., Cao, J., Rocha, L., . . . Nathoo, F. S. (2023). Neuroimaging feature extraction using a neural network classifier for imaging genetics. BMC bioinformatics, 24(1), 271. https://doi.org/10.1186/s12859-023-05394-x

Chakraborty, D., Zhuang, Z., Xue, H., Fiecas, M. B., Shen, X., & Pan, W. (2023). Deep Learning-Based Feature Extraction with MRI Data in Neuroimaging Genetics for Alzheimer's Disease. Genes, 14(3). Retrieved from https://doi.org/10.3390/genes14030626

He, K., Zhang, X., Ren, S., & Sun, J. (2016, 27-30 June 2016). Deep Residual Learning for Image Recognition. Paper presented at the 2016 IEEE Conference on Computer Vision and Pattern Recognition (CVPR).

Kaplan, E., Altunisik, E., Ekmekyapar Firat, Y., Datta Barua, P., Dogan, S., Baygin, M., . . . Rajendra Acharya, U. (2022). Novel nested patch-based feature extraction model for automated Parkinson's Disease symptom classification using MRI images. Computer Methods and Programs in Biomedicine, 224, 107030. https://doi.org/10.1016/j.cmpb.2022.107030

Kuwil, F. H. (2022). A new feature extraction approach of medical image based on data distribution skew. Neuroscience Informatics, 2(3), 100097. https://doi.org/10.1016/j.neuri.2022.100097

Mallat, S. G. (1989). A theory for multiresolution signal decomposition: the wavelet representation. IEEE Transactions on Pattern Analysis and Machine Intelligence, 11(7), 674-693. https://doi.org/10.1109/34.192463

Özmen, G , & Özşen, S 20 A new denoising method for fMRI a sed on weighted three-dimensional wavelet transform. Neural Computing and Applications, 29(8), 263-276. https://doi.org/10.1007/s00521-017-2995-7

Sharma, A. K., Nandal, A., Dhaka, A., Polat, K., Alwadie, R., Alenezi, F., & Alhudhaif, A. (2023). HOG transformation based feature extraction framework in modified Resnet50 model for brain tumor detection. Biomedical Signal Processing and Control, 84, 104737. https://doi.org/10.1016/j.bspc.2023.104737

Tasci, B., & Tasci, I. (2022). Deep feature extraction based brain image classification model using preprocessed images: PDRNet. Biomedical Signal Processing and Control, 78, 103948. https://doi.org/10.1016/j.bspc.2022.103948

Yılmaz Acar, Z , Başçiftçi, F , & kmekci, A 2022 Future activity prediction of multiple sclerosis with 3D MRI using 3D discrete wavelet transform. Biomedical Signal Processing and Control, 78, 103940. https://doi.org/10.1016/j.bspc.2022.103940

Maximum Power Point Transfer of Off-Grid Stored Energy and Battery Management System Design and Implementation

Onur Emre Golen[1], Mehmet Ali Ustuner[1], Mohammed Ruhul Amin Bhuiyan[2], Hayati Mamur[1]*

Abstract: Batteries are used to store energy in areas where there is no grid, and they need various DC-DC converters to use this stored energy. In this study, the current and voltage monitoring system required to operate the maximum power point tracking (MPPT) algorithms from the battery with microcontrollers (MCU) was designed and implemented. Current, voltage, battery output power and duty cycle data of metal oxide semiconductor field effect transistor (MOSFET) were visualized and instantly monitored on the computer screen using STM32F407VGT6 microcontroller (MCU). A voltage divider circuit is used to determine the battery output power used for MPPT. These current and voltage values are digitized for MPPT algorithms. Voltages up to 50 V DC are detected using a voltage divider for the voltage of the load. Ten-bit analog digital converter (ADC) is made by transmitting the voltage information of the voltage divider to the analog inputs of the MCU. Thus, all data were collected on the STM32F407 MCU and both the current, voltage and power data of the battery output were visualized and digitized by recording. As a result, these data have been brought to a state where they can be easily used in the inputs of MPPT algorithms.

Keywords: MPPT, converter, current sensor, voltage sensor, microcontroller.

[1]**Address:** Manisa Celal Bayar University, Faculty of Engineering, Manisa/Türkiye
[2]**Address:** Islamic University, Department of Electrical and Electronic Engineering, Kushtia/Bangladesh

***Corresponding author**: hayati.mamur@cbu.edu.tr

1. INTRODUCTION

Battery management is critical for the efficient operation of electronic devices. Engineers and researchers are working on the best use of power. Various battery management systems (BMS) are being developed to ensure that electronic devices have a longer life and work for longer periods. The more efficient the BMS is designed, the more efficient the operation of electronic devices.

BMS generally works on 24 V DC voltage. Power electronic circuits such as buck converter, boost converter or buck-boost converter are used to regulate this voltage. Voltage to be used with these circuits. It is converted into voltage at which electronic devices can operate. These systems can provide uninterrupted electrical energy to the user, especially in cases where there is no grid, or the grid becomes fault. In addition, they are useful in storing energy and managing the distribution of this energy by using BMSs in thermoelectric generators (TEG) or photovoltaic panel (PV) hybrid systems.

BMS uses DC-DC converters with MPP tracker (MPPT) algorithms for both voltage regulation and MPP. To use these MPPT algorithms, the current and voltage at the output of the DC-DC converter must be known. For this, current and voltage sensors are used. With these sensors, this information is obtained, and the power value is calculated. As a result, MPP monitoring is performed by changing the duty cycle of the metal oxide semiconductor field effect transistor (MOSFET) in the DC-DC converter (Mamur and Çoban, 2020).

In the literature, it is seen that the measurement of battery current and voltage value is done by using various electronic equipment. Dalala *et al.* (Dalala *et al.*, 2018) carried out their studies for MPPT by making current and voltage detections with voltage divider resistors without using any physical connection in their systems. They used the current-voltage general characteristic of TEG as the basis of their system. Twaha *et al.* (Twaha *et al.*, 2017) investigated the performance of DC-DC converter with incremental conductivity (IC) MPPT algorithm. They used both current and voltage sensors in their systems. Chandrarathna and Lee (Chandrarathna and Lee, 2019) made a double stage amplifying converter in the MPPT system they developed. They made their measurements using a current mirror for current and voltage divider resistors for voltage. Gabbar *et al.* (Gabbar *et al.*, 2021) designed a BMS that monitors

battery status using a wi-fi signal. Rodríguez *et al.* (Rodríguez *et al.*, 2022) conducted a study following the open-circuit MPPT algorithm for wireless sensor networks. They have only detected the open circuit voltage, which is a requirement of their algorithm, with the voltage divider. They delivered the current and voltage measurements to the microcontroller (MCU) system with the help of sensors.

In this study, a current mirror has been developed to measure the output voltage and current value of a DC-DC converter. In order for the user to monitor these values, a computer program called Tera Term is used to make the variables in the system appear instantly. In addition, the output current and voltage values of the step-down DC-DC converter used and the value of the duty cycle in which the MOSFET is triggered are visualized on this software, and instant information about the performance of the system is obtained. In this part of the study, after a general introduction, materials and methods are given in the second part. Outputs and comments are given in the third section and the results are presented in the fourth section.

2. MATERIAL AND METHOD

STM32F407 MCU is one of the main materials used in this study. The block diagram of the system is given in Figure 1.

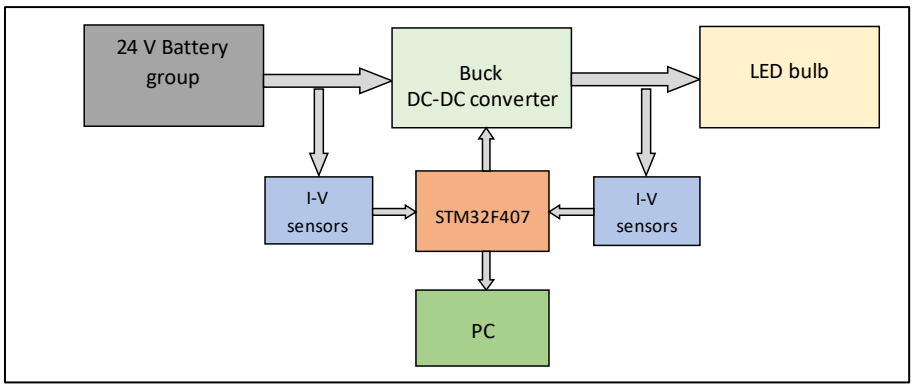

Figure 1. The block diagram of the system.

Tera Term software was used to visualize the data in this system. It was designed and manufactured by performing calculations of a step-down DC-DC converter for making MPPT. A voltage divider circuit capable of measuring up to 50 V is used to detect the current and voltage values at the output of this buck DC-DC converter. These data are sent to the STM32F407 MCU via USART communication. The measurement of the voltage value at the output of the buck DC-DC converter is detected by the voltage divider and transmitted to the analog input of the STM32F407 and converted to a 10-bit digital value. The voltage value passing over 15 kΩ in a voltage divider connected in 100 kΩ and 15 kΩ series connected to the voltage measurement buck converter was determined and delivered to the MCU.

A 24 W buck DC-DC converter designed during the working process is connected to the output of the battery and an LED bulb is connected to the output of this converter. To prevent this designed converter from being affected by sudden voltage fluctuations, two 47 µF 50 V capacitors are connected to its input. The coil value was chosen as 150 µH. 1N5819 schotky diode is used to prevent reverse electromotive force in the coil. The n-channel IRFZ44N MOSFET in the system was triggered at 30 kHz. Since the voltage from this circuit will fluctuate, a capacitor of 47 µF 50 V is used to regulate it. The PWM pin of the STM32F407 MCU is used to trigger this circuit element. This MCU can only output 3.3 V. However, for the circuit to be triggered, the MOSFET must be triggered at a voltage higher than 5 V. For this reason, MOSFET driver integrated circuit (IC) named IR2110 is used for triggering. For this IC to work, a 10 Ω resistor and a flyback diode have been added to the MOSFET output side. When 12 V and 5 V input voltages are applied to this circuit, the output voltage is at least 1.53 V and at most 23 V, while the input current reaches a minimum of 0.06 A and a maximum of 2.0 A.

The visualization and instantaneous monitoring of the variables in this designed system is done through Tera Term software. For the MCU to work with Tera Term software, it provides serial communication with the USART feature, which is standard in STM32F4. Since this method works with the USART communication protocol, there are only transmitter (TX) and receiver (RX) communication ends. In the UART protocol, the serial TX end of the computer is connected to the RX end of the MCU, and the RX end is connected to the TX end of the MCU, since the data in the MCU can receive this data from the receiver end while the data in the MCU is going through the transmitter channel. USART block diagram between STM32F407 MCU and computer is given in Figure 2.

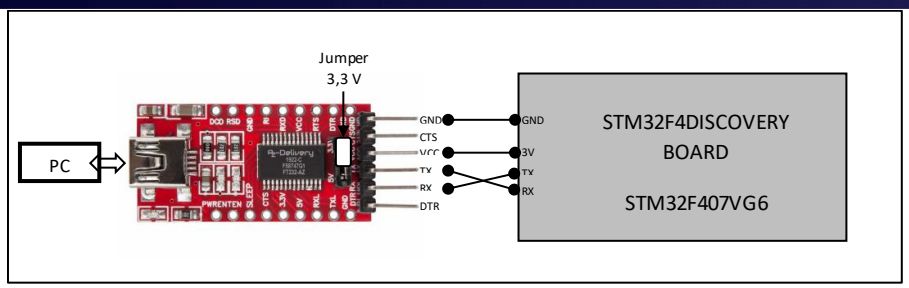

Figure 2. PC- FT232RL USB-TTL converter and MCU connection.

The design of the interface used in the visualization of the system was made over Tera Term software. In this program, by making serial port communication with the USART protocol over the MCU. Thanks to this software, it can transfer the data from the MCU to the user in a simplified way. The current, voltage, power, and duty cycle values of the buck DC-DC converter, which should be at the interface of the designed system, are included in this design. In addition, a chart layout has been used so that these values can appear more regularly. To receive data from this designed interface, it is connected to the USB input of the computer using a FT232RL USB-TTL converter and reflected on the screen with a bandwidth of 115200.

The software of the STM32F407 MCU was written in the compiler called STM32 Cube Integrated Development Environment (STM32 Cube IDE) to be able to switch the DC-DC converter and display the output current, voltage, power and duty cycle values of this converter on Tera Term software, and to run MPPT algorithms. In this program, it can read up to 50 V voltage by using the analog signal output between 0 V and 3.3 V from the voltage divider circuit connected to the output of the battery. Variables are assigned to hold these input analog values and convert the raw value to voltage. Project configuration of STM32F407 MCU via Cube IDE is shown in Figure 3.

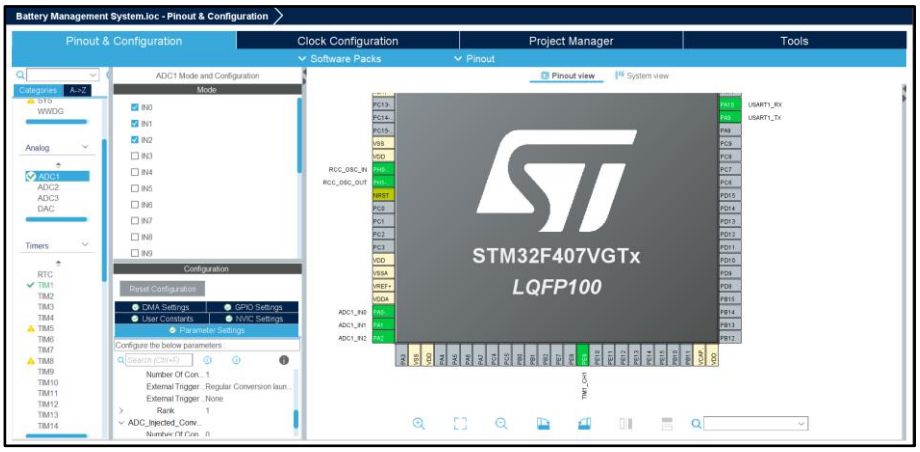

Figure 3. STMCubeMX interface in STMCubeIDE.

Separate variables were used for PWM and duty cycle and MCU configurations were made. It is setup to a 30 kHz PWM signal using the first channel timer for the STM32F407 MCU via the STM Cube IDE compiler. To provide this signal, the clock speed is set to 100 MHz. To read the analog values coming from the voltage divider, the analog values are converted to digital values by assigning the pin on the first (ADC1) channel of the ADC and the voltage reading is made. USART1 channel is used to make serial communication between MCU and computer and USB TTL converter is used to provide the necessary connection. If necessary, MPPT algorithms can be added to this program.

3. RESULTS

The image of the computer screen showing the variables of the implemented system is given in Figure 4. Input current, voltage and power data of the output of the step-down DC-DC converter are reflected via this software.

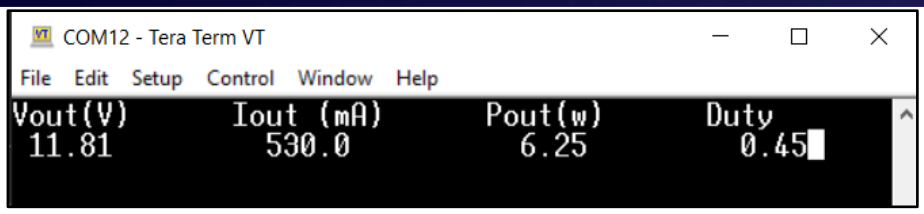

Figure 4. Tera Term interface.

It has been possible to instantly monitor the output data of the buck DC-DC converter on the computer screen. In addition, since this data is digitized, it can be stored in any desired cloud network for later analysis. In addition, since this system will be used in battery MPPT algorithms, it is possible to instantly look at the duty cycle value of the MOSFET. Thus, when the load changes, the change in the output power of the buck DC-DC converter can be monitored. However, the efficiency of this buck DC-DC converter can be calculated. With the visualization of the variables in this developed battery management system, a convenience has been created for MPPT software developers.

4. DISCUSSION AND CONCLUSIONS

In this study, for the control of LED lighting in places where there is no grid, the appropriate voltage regulation of the 24 V battery for the LEDs and the power measurement monitoring system were designed and implemented. The output power variables of the buck converter connected to the battery output are visualized on the computer screen. It is possible to monitor the duty cycle, which is an important criterion in MPPT monitoring and constantly changes depending on the load changes. With this developed system, LED lighting can be controlled by regulating the battery voltage in places where there is no grid.

Acknowledgements
This paper was supported by the Manisa Celal Bayar University Scientific Research Projects Coordination Unit. Project Number: 2023-048.

Ethics Committee Approval
N/A

Peer-review
Externally peer-reviewed.

Author Contributions
Conceptualization: M.R.A.B, and H.M.; Investigation: O.E.G; Material and Methodology: O.E.G., and M.A.U.; Supervision: M.R.A.B, and H.M.; Visualization: O.E.G., and M.A.U.; Writing-Original Draft: O.E.G., and H.M.; Writing-review & Editing: O.E.G, M.R.A.B, and H.M.; Other: All authors have read and agreed to the published version of manuscript.

Conflict of Interest
The authors have no conflicts of interest to declare.

Funding
This paper was supported by the Manisa Celal Bayar University Scientific Research Projects Coordination Unit. Project Number: 2023-048.

REFERENCES

Chandrarathna, S. C., & Lee, J. W. (2019). A dual-stage boost converter using two-dimensional adaptive input-sampling MPPT for thermoelectric energy harvesting. IEEE Transactions on Circuits and Systems I: Regular Papers, 66(12), 4888-4900.

Dalala, Z. M., Saadeh, O., Bdour, M., & Zahid, Z. U. (2018). A new maximum power point tracking (MPPT) algorithm for thermoelectric generators with reduced voltage sensors count control. Energies, 11(7), 1826.

Gabbar, H. A., Othman, A. M., & Abdussami, M. R. (2021). Review of battery management systems (BMS) development and industrial standards. Technologies, 9(2), 28.

Mamur, H., & Çoban, Y. (2020). Termoelektrik jeneratörler için alçaltan-yükselten çeviricili maksimum güç noktası takibi benzetimi. Pamukkale Üniversitesi Mühendislik Bilimleri Dergisi, 26(5), 916-926.

Rodríguez, J., García-Meré, J. R., Lamar, D. G., & Sebastián, J. (2022). A novel version of the ripple-modulation technique for enabling the use of single-phase buck converters in VLC applications. IEEE Journal of Emerging and Selected Topics in Power Electronics.

Twaha, S., Zhu, J., Yan, Y., Li, B., & Huang, K. (2017). Performance analysis of thermoelectric generator using dc-dc converter with incremental conductance based maximum power point tracking. Energy for Sustainable Development, 37, 86-98.

Stacked Autoencoder Feature Selection Based Zero Day Threat Detection

Mahmut Tokmak*[1], Mike Nkongolo[2]

Abstract: Zero-day attacks exploit previously unknown vulnerabilities in software, hardware, or networks. Since these vulnerabilities are not yet patched or protected against, they present a significant risk. Detecting zero-day attacks is crucial due to their exploitation of unknown vulnerabilities, posing significant risks to cybersecurity. Timely detection allows for swift response and deployment of countermeasures, minimizing the window of opportunity for attackers. It protects sensitive data, mitigates financial losses, safeguards reputation, and strengthens cybersecurity practices. Detecting zero-day attacks provides insights into attack vectors, improves security measures, and enhances incident response capabilities. It helps prevent future attacks by understanding adversary techniques and updating defense mechanisms. Overall, zero-day attack detection plays a critical role in mitigating risks, protecting assets, and staying ahead in the evolving threat landscape. This study explores the application of stacked autoencoder (SAE), a type of artificial neural network, for feature selection and zero-day threat classification using a Long Short-Term Memory (LSTM) scheme. The process involves preprocessing the UGRansome dataset and training an unsupervised SAE for feature extraction. Fine-tuning with supervised learning is then performed to enhance the discriminative capabilities of this model. The learned weights and activations of the autoencoder are analyzed to identify the most important features for discriminating between zero-day threats and normal system behavior. These selected features form a reduced feature set that enables accurate classification. The results indicate that the SAE-LSTM performs well across all three attack categories by showcasing high precision, recall, and F1 score values, emphasizing the model's strong predictive capabilities in identifying various types of zero-day attacks. Additionally, the balanced average scores of the SAE-LSTM suggest that the model generalizes effectively and consistently across different attack categories. The SAE-LSTM model excels in detecting signature attacks, while synthetic signature and anomaly attacks pose challenges due to abnormality or absence of patterns. The methodology we put forth utilizes the SAE-LSTM technique, resulting in a remarkable accuracy of 98%, outperforming prior intrusion detection studies. Hence, this research aims to contribute to advanced cyberintelligence to proactively mitigating zero-day threats. Future cyberintelligence can progress by refining the proposed feature selection model, addressing computational efficiency of the UGRansome dataset, and integrating hybrid methodologies for improved intrusion detection capabilities.

Keywords: Stacked Autoencoder, Feature Selection, Zero Day Threats, Machine Learning, Deep Learning, UGRansome, Cyberintelligence

[1]**Address:** Burdur Mehmet Akif Ersoy University, Bucak Zeliha Tolunay School of Applied Technology and Management, Burdur/Türkiye
[2]**Address:** University of Pretoria, Faculty of Engineering, Built Environment and Information Technology, Department of Informatics, Pretoria/South-Africa

***Corresponding author**: mahmuttokmak@mehmetakif.edu.tr

1. INTRODUCTION

In the ever-evolving landscape of cybersecurity, the emergence of advanced and elusive threats poses unprecedented challenges to organizations, governments, and individuals alike. Among these threats, zero-day attacks have garnered substantial attention due to their potential to exploit undiscovered vulnerabilities and wreak havoc on digital infrastructure. A zero-day attack refers to a cyber assault that targets a previously unknown vulnerability in software, hardware, or network systems. These vulnerabilities, referred to as "zero-day vulnerabilities," are named as such because developers have "zero days" to address and patch them before malicious actors exploit them. Zero-day attacks are particularly effective because they can strike unexpectedly and catch defenders off guard. This surprise factor lets them evade regular security measures. Unlike known vulnerabilities, zero-day vulnerabilities have no documented fixes or protections, giving attackers a notable upper hand. Consequently, zero-day attacks present a daunting challenge for defenders, as they often evade signature-based detection systems and intrusion prevention tools (Nkongolo & Tokmak, 2023; Thomas et al., 2021; Tokmak, 2022). In the era of big data, extracting meaningful and representative features from high-dimensional datasets has become a cornerstone of modern data analysis and machine learning. Among the myriad of techniques, stacked autoencoders (SAEs) have emerged as a powerful tool for automated feature learning,

enabling the discovery of intricate data structures and patterns. Rooted in the field of deep learning (DL), SAEs offer a compelling solution to the challenge of high-dimensional data representation, presenting a pathway towards enhanced predictive modeling, efficient dimensionality reduction, and insightful data interpretation (Boussaad & Boucetta, 2021; Kim et al., 2020). Feature selection with SAEs has been explored in several papers. Feature extraction using SAEs has been explored in various domains.

Wang et al. proposed the broad autoencoder features (BAF) which consist of four parallel interconnected SAEs with different activation functions (T. Wang et al., 2021). Kong et al. used a stacked autoencoder with L21-norm regularization for dimensionality reduction and feature extraction from electricity load data (Kong et al., 2020). Wang et al. introduced a stacked supervised auto-encoder (SSAE) to acquire fault-relevant attributes from raw input data and improve fault classification accuracy (Y. Wang et al., 2020). Chatterjee et al. integration of SAE characteristics with wavelet-based and morphological fractal texture attributes for the classification of skin disorders achieved high accuracy (Chatterjee et al., 2019). Kim et al. suggested an enhancement in tool condition diagnosis through the utilization of SAE-based CNC machine tool prognosis, incorporating feature extraction from discrete wavelet transform (Kim et al., 2020). Zero-day threat detection involves identifying and mitigating attacks that exploit unknown vulnerabilities, such as a cybercriminal targeting a newly discovered weakness in a popular software program before the software developer has a chance to release a patch. Nkongolo et al. introduced the UGRansome dataset, which facilitates the identification of anomalies and zero-day attacks that cannot be recognized by known threat signatures (Nkongolo et al., 2021). Kumar and Sinha proposed a resilient and smart cyber-attack detection model that uses the notion of prominent entities and network structure techniques to detect zero-day attacks (Kumar & Sinha, 2021). Sarhan et al. proposed a zero-shot learning approach for assessing the effectiveness of machine learning models in detecting zero-day attacks (Sarhan et al., 2023).

Millar et al. suggested a deep neural network for Android malware detection without prior knowledge of malicious characteristics, achieving high detection rates for zero-day scenarios (Millar et al., 2021). Blaise et al. proposed the utilization of the Split-and-Merge technique to promptly identify emerging botnets and recently exploited vulnerabilities, reducing false positives (Blaise et al., 2020). Long Short-Term Memory (LSTM) networks have displayed significant potential in unknown vulnerabilities and malware detection. Researchers have dedicated significant efforts to studying LSTM hyperparameters for the development of Intrusion Detection Systems (IDS). They have explored diverse LSTM setups and configurations. What they have discovered is that the significance of these hyperparameters in the context of IDS varies from their importance in language model applications. The interplay of hyperparameters significantly influences the assessment of their respective significance. Considering this interaction, the precise order of importance for LSTMs in IDSs includes batch size as the most critical, followed by dropout ratio and padding. Additionally, sensitivity-based LSTM models have been proposed for designing System-call Behavioral Language (SBL) for malware detection. These models achieve impressive Area Under the Curve (AUC) values and specificity on unknown attack datasets.

Another approach involves using LSTM with word embedding and attention mechanisms to effectively represent and classify malware files, achieving high accuracy and F1 scores (Sewak et al., 2021; Q. Xie et al., 2020; W. Xie et al., 2020; Zhang, 2020). A method for zero-day detection using LSTM is proposed in the paper by Fang et al. The model is designed to detect malicious JavaScript code injected into web pages. It extracts features from the semantic level of bytecode and optimizes the method of word vector. The LSTM-based detection model outperformed existing models based on Random Forest and Support Vector Machine (SVM) algorithms (Fang et al., 2018). Another paper by Roberts and Nair introduces a neural architecture for anomaly detection in discrete sequence datasets. Their model combines a modified LSTM autoencoder with an array of One-Class SVMs to find anomalies within sequences. The proposed method shows improved stability and outperforms standard LSTM and sliding window anomaly detection systems (Roberts & Nair, 2018).

This study aims to leverage the synergistic capabilities of SAE and LSTM networks to improve the identification and categorization of zero-day threats using the UGRansome dataset. The primary objective is to integrate feature selection techniques into the SAE architecture to streamline the extraction of pertinent and differentiating features from raw data. By carefully choosing the input data, the subsequent LSTM network can adeptly capture temporal relationships within the feature domain. Ultimately, this research strives to advance proactive and resilient cybersecurity strategies by introducing an innovative approach – a feature-selection-driven SAE-based LSTM model. The subsequent sections of this work delve into the methodology, experimental setup, results, and discussions, all of which culminate in a comprehensive analysis of the proposed SAE-based LSTM model for zero-day threats detection using the UGRansome dataset.

2. MATERIAL AND METHOD

2.1. Experimental Dataset

In 2021, Nkongolo et al. (Nkongolo et al., 2021) introduced the UGRansome dataset, a novel and comprehensive anomaly detection dataset designed to detect unknown network attacks, including zero-day threats (Nkongolo & Tokmak, 2023). Unlike existing datasets in the IDS field, UGRansome includes previously unexplored unknown and ransomware attacks (Nkongolo et al., 2022). The dataset comprises various attack categories, namely Signature (S), Anomaly (A), and Synthetic Signature (SS) (Figure 1), each with labeled instances of zero-day threats such as Locky, CryptoLocker, advanced persistent threats (APT), SamSam, WannaCry, Razy, JigSAW, Globe, TowerWeb, and more (Figure 2). Table 1 provides an overview of the UGRansome features (f1-f18), while Table 2 displays the distribution of the UGRansome subsets. To gain a comprehensive understanding of the dataset statistics, we direct readers to Figure 3, which presents its key characteristics.

Table 1. The data structure of the UGRansome dataset

No	Name	Type	No	Name	Type
f1	SS	Categorical	f2	Cluster	Numeric
f3	S	Categorical	f4	A	Categorical
f5	Spam	Categorical	f6	BTC	Numeric
f7	Blacklist	Categorical	f8	Bytes	Numeric
f9	Nerisbonet	Categorical	f10	USD	Numeric
f11	UDP scan	Categorical	f12	JigSAW	Categorical
f13	SSH	Categorical	f14	Port	Numeric
f15	DoS	Categorical	f16	CryptoLocker	Categorical
f17	Port scanning	Categorical	f18	WannaCry	Categorical

Table 2. The UGRansome subsets

Dataset	A	S	SS
UGRansome19Train	40.323	25.822	9.656
UGRansomeVal	11.869	9.439	1.736
UGRansome18Test	4.701	3.408	6.954
Total	56.893	38.669	18.346
Average (avg)	19.964	12.889	6.115

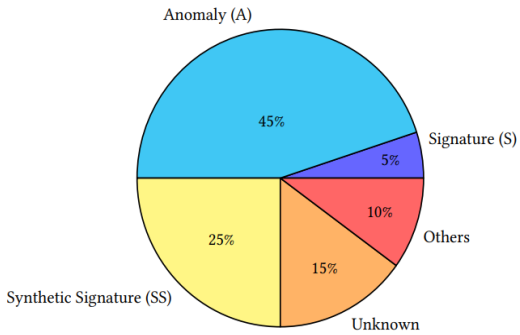

Figure 1. Distribution of zero-day threats categories of the UGRansome dataset

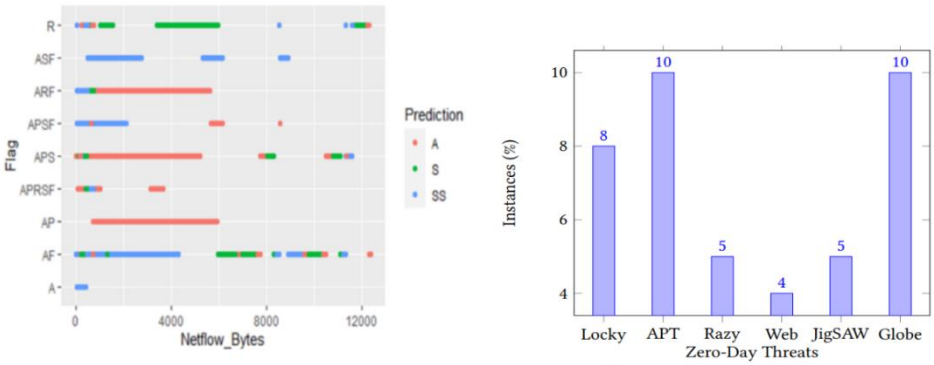

Figure 2. The network flags and distribution of zero-day threats of the UGRansome dataset

Dataset Statistics

Number of Variables	14
Number of Rows	207533
Missing Cells	0
Missing Cells (%)	0.0%
Duplicate Rows	58491
Duplicate Rows (%)	28.2%
Total Size in Memory	106.9 MB
Average Row Size in Memory	540.2 B
Variable Types	Numerical: 4 Categorical: 9 GeoGraphy: 1

Figure 3. The characteristic of the UGRansome dataset

2.2. Stacked Autoencoder

SAEs are a type of neural network (NN) architecture that is used for feature extraction and dimension reduction in various tasks, including biometrics recognition, image recognition, natural language processing, and automatic speech recognition (Tokmak & Küçüksille, 2022). It is called "stacked" because it consists of multiple layers of autoencoders, where each layer is trained to reconstruct the output of the previous layer. The training of SAEs involves two steps: unsupervised pre-training and supervised fine-tuning. In the unsupervised pre-training step, each layer of the network is trained individually using auto-encoders, which learn internal data representations. These representations are then used to initialize the network weights and improve generalization.

In the supervised fine-tuning step, the pre-trained layers are stacked together and trained in a supervised manner using labeled data. This approach has been shown to achieve high accuracy rates in biometrics recognition tasks (Boussaad & Boucetta, 2021). In the context of automatic speech recognition, SAEs have been used to design networks for recognizing speech sounds articulated by children, achieving high accuracy rates (Wei & Zhao, 2019). SAEs can also be enhanced by incorporating data weighting techniques, which improve the robustness and discriminative power of the network (Sun et al., 2021). Additionally, SAEs have been used for automatic voice quality evaluation in call centers, achieving better correlation coefficients compared to traditional methods (L. Wang et al., 2021). In the field of intrusion detection, stacked sparse auto-encoders have been proposed for dimensionality reduction and classifiers, achieving better results compared to existing methods (Manjunatha & Gogoi, 2022). It has also been used effectively in malware detection (Rathore et al., 2018; Samaneh et al., 2022; Zhu et al., 2021). Figure 4 illustrates a SAE architecture.

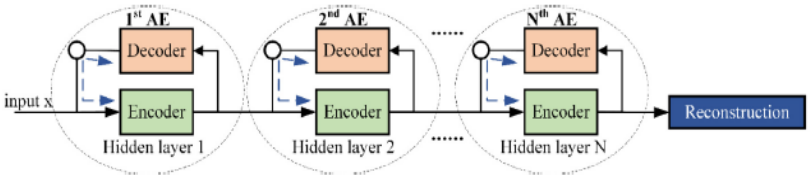

Figure 4. Structure of SAE model (Luo et al., 2022)

2.3. Long Short-Term Memory

Recurrent Neural Network (RNN) is a variation of the feedforward neural network (NN). The architecture of the feedforward NN encompasses several layers, each comprised of neurons, with connections between layers proceeding

unidirectionally, resulting in a sequential arrangement of layers. RNN introduces a recurrent structure within the NN by establishing connections from each node (neuron) to itself. This self-connection mechanism allows the RNN to retain previous inputs, potentially impacting the network's output (Fan et al., 2017; Naik & Mohan, 2019; Yang et al., 2021). In RNN, the inference process is similar to the feedforward NN completed by forward propagation. Training in RNN is done through the mechanism of backpropagation through time, updating the weights using the gradient.

In RNN, the gradient for each output depends not only on the current layer but also on the previous layer. If backpropagation is continuously updated at intervals, the gradient can approach zero, leading to the vanishing gradient problem, followed by the problem of weakening gradients. Similarly, when gradients become too large, the result can grow significantly, leading to the exploding gradient problem (Metin & Karasulu, 2019). The LSTM DL algorithm was developed by Hochreiter and Schmidhuber in 1997 as a variant of the RNN model, aiming to mitigate the drawbacks associated with traditional RNN architecture (Hochreiter & Schmidhuber, 1997). Distinct from classical RNN, LSTM introduces the concept of memory cells for its nodes, enabling the linkage of prior data information to the present nodes. Each LSTM node encompasses three gating mechanisms: an input gate, a forget gate, and an output gate (Figure 5).

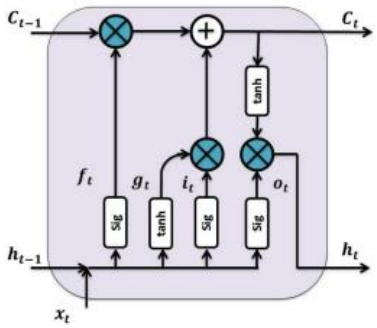

Figure 5. LSTM architecture (Smagulova & James, 2019)

2.4. Performance Evaluation

After the data preprocessing steps, the dataset obtained, consisting of a total of 210.510 examples, was split into 80% training and 20% testing:

```
#The UGRansome colmns names
df.columns = ["Time","Protocol","Flag", "Family", "Clusters", "SeddAddress", "ExpAddress",
            "BTC", "USD","Netflow_Bytes", "IPaddress", "Threats", "Port", "Prediction"]
# Drop the columns to exclude from the analysis
columns_to_drop = ['column_to_drop_1', 'column_to_drop_2']
ugransome_df.drop(columns=columns_to_drop, inplace=True)

# Split the DataFrame into features and labels
X = ugransome_df.drop(columns='target_column')  # Features
y = ugransome_df['target_column']  # Labels

# Split the data into training and testing sets, while preserving specific columns
X_train, X_test, X_preserve_train, X_preserve_test, y_train, y_test = train_test_split(
    X, ugransome_preserve_df, y, test_size=0.2, random_state=42
)
```

The evaluation of the training and testing performance of the established models was conducted by calculating accuracy, precision, recall, and F1scores. The accuracy metric, denoting the proportion of accurately classified instances used to assess the training and testing effectiveness of the formulated model, is mathematically expressed in Equation 1. The precision metric, quantifying the accuracy of positive predictions among the actual positives, is formally defined in Equation 2. The recall metric, indicating the proportion of true positive values correctly identified, is represented as Sensitivity (Recall) in Equation 3. The F1 Score, a composite metric of recall and precision, is mathematically defined as score = 2 * (precision * recall) / (precision + recall).

$$Accuracy = \frac{TP + TN}{TP + FN + TN + FP} \quad (1)$$

$$Precision = \frac{TP}{TP + FP} \tag{2}$$

$$Sensitivity = \frac{TP}{TP + FN} \tag{3}$$

In this study, the training and testing of the proposed data preprocessing, feature extraction, and classification models were conducted with the Python programming language version 3.10.12. The methodology employed for this work is explained in this section. The framework of the study is illustrated in Figure 6 and Algorithm 1.

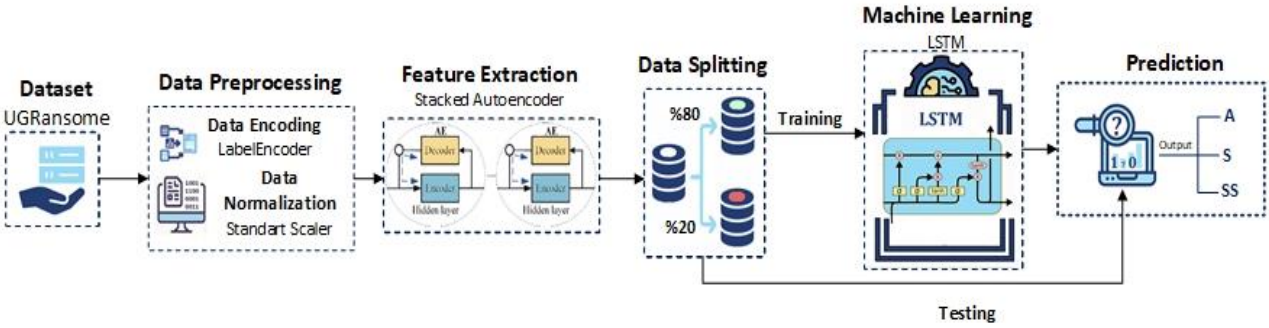

Figure 6. Proposed study model

Algorithm 1 Feature Selection SAE-based LSTM model

```
Require:
  UGRansome dataset
Ensure:
  Prediction results
  function COMBINEDAPPROACH
      LoadDataset
      PreprocessRowsdata
      ApplyNormalizationdata
      ApplyFeatureExtractiondata
      (X_train, y_train), (X_test, y_test) = SplitDatasetdata
      TrainLSTMX_train, y_train

      model = TrainLSTMX_train, y_train
      PerformPredictionmodel, X_test

      predictions = PerformPredictionmodel, X_test
      AnalyzeResultsy_test, predictions
      FeatureSelection
      selected_features = FeatureSelectionX, a, b, c

      return final_results
  function FEATURESELECTION(X, a, b, c)
      Normalize input features X
      Calculate membership degrees μ(x; a, b, c) for each feature x ∈ X
      Initialize feature importance scores I = {0, 0, ..., 0}
      for i = 1 to n do
          for j = 1 to n do
              I[i] ← I[i] + μ(x_j; a, b, c)
      Sort features based on importance scores in descending order
      X_selected ← top-ranked features from X based on I
      return X_selected
```

Algorithm 1. The proposed SAE-LSTM feature selection algorithm, where "a" denotes anomaly class, "b" signature class, and "c" synthetic signature class.

The training and testing processes of the suggested data encoding, normalization, SAE, and LSTM model were conducted using the Google Colaboratory cloud system. This system provides ready access to numerous Python libraries and offers its services for free (*Colab*, 2023). Within the Colab platform, Nvidia CUDA technology was employed to leverage GPU acceleration for faster algorithm execution. Tasks such as file uploading, data preprocessing, setting up the data frame, and more were carried out using Python libraries including numpy, pandas, statistics, sklearn, matplotlib.pyplot, and seaborn. As for the suggested SAE and LSTM architecture, the Python TensorFlow Keras library was utilized. The suggested SAE layers and parameters (params) are given in Table 3. In the established SAE architecture, three encoders with 75, 50, and 13 layers, and three decoders with 50, 75, and 13 layers were employed. The activation function was set to relu, the optimizer parameter to Adam, the loss parameter to mse, and the epoch parameter to 50. The suggested LSTM layers and params are given in Table 4. The constructed LSTM network consists of 3 layers, each containing 168 neurons. The loss parameter was set to sparse_categorical_crossentropy, the optimizer parameter to Adam, and the epoch parameter to 400.

Table 3. SAE layers and params

Layer (type)	Output Shape	Param #
input_1 (InputLayer)	(None, 13)	0
dense (Dense)	(None, 75)	1.050
dense_1 (Dense)	(None, 50)	3.800
dense_2 (Dense)	(None, 13)	663
dense_3 (Dense)	(None, 50)	700
dense_4 (Dense)	(None, 75)	3.825
dense_5 (Dense)	(None, 13)	988
Total params:		11.026

Table 4. LSTM layers and params

Layer (type)	Output Shape	Param #
lstm_3 (LSTM)	(None, 168)	122.304
dense_21 (Dense)	(None, 3)	507
Total params:		122.811

3. RESULTS

After completing the data preprocessing and feature extraction steps, the trained LSTM model was tested, resulting in the following performance metrics: accuracy, precision, recall, and F1score were measured as 0.9849, 0.985, 0.9849, and 0.9849, respectively. These metrics are summarized in Table 5 and Figure 7.

Table 5. Performance metrics

	Precision	Recall	F1 score	Support
A	0.971879	0.986131	0.978953	11320
S	0.991466	0.978024	0.984699	18293
SS	0.987558	0.994367	0.990951	11894
Accuracy			0.984918	41507
Average	0.985004	0.984918	0.984924	41507

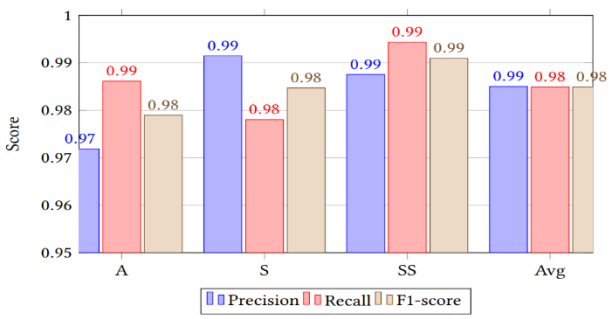

Figure 7. Visualization of the performance metrics

In summary, Table 5 and Figure 7 indicate that the SAE-based LSTM model performs well across all three attack categories—Anomaly (A), Signature (S), and Synthetic Signature (SS). It showcases high precision, recall, and F1-score values, emphasizing the model's strong predictive capabilities in identifying various types of attacks. Additionally, the balanced average scores suggest that the model generalizes effectively and consistently across different attack categories. The confusion matrix is a tool used in machine learning and classification tasks to visualize the performance of a model by presenting the number of true positive (TP), true negative (TN), false positive (FP), and false negative (FN) predictions. It is particularly useful when evaluating the accuracy of a classification algorithm. The confusion matrix showing the test results of the proposed work is shown in Figure 8.

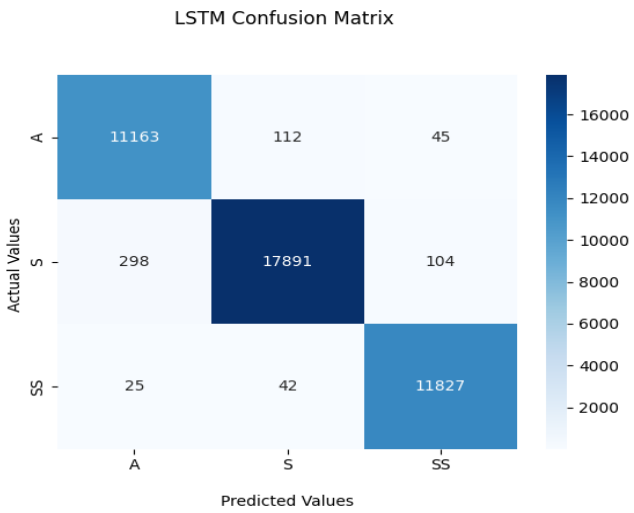

Figure 8. Confusion matrix

The SAE-based LSTM model's superior precision, recall, and F1-score in detecting signature attacks compared to synthetic signature and anomaly attacks signifies its effectiveness in identifying known threat patterns (Figure 7). Signature attacks are recognizable due to established patterns, and the model's adeptness in pinpointing instances aligned with these patterns is pivotal for real-time threat detection. Synthetic signature attacks involve modified or novel attack signatures, and the model's slightly lower performance could suggest difficulty in identifying unconventional or altered signatures, underscoring the challenge of evolving threat detection (Figure 7). Anomaly attacks, representing zero-day or novel threats, pose a greater detection challenge, as their lack of discernible patterns complicates identification (Figure 7). Future work in the IDS landscape can potentially use the UGRansome dataset and improve the proposed model parameters to enhance anomaly detection, adapt the model for modified signatures, implement continuous learning for emerging threats, explore ensemble approaches, and develop interpretable techniques. In essence, the proposed model's strong detection of signature attacks and potential improvements for synthetic signatures and anomalies highlight avenues for advancing IDSs.

4. DISCUSSION

Table 6 presents a comparative assessment of different intrusion detection studies, each employing distinct datasets and models. Our proposed methodology, centered around the UGRansome dataset, leverages the SAE-LSTM technique to achieve an impressive 98% accuracy, surpassing the performance of previous investigations. Additionally, this approach offers distinct advantages, particularly within critical infrastructure contexts. Notably, several discussed studies within the IDS literature share the common limitation of feature selection. Contrasting this, Kim et al. (2020) realized a 97% accuracy utilizing a signal autoencoder model on signal data, promising for signal processing, albeit lacking a tool diagnosis model. Zhang (2020) harnessed LSTM on malware data, achieving 81% accuracy while addressing invasive software, though grappling with dependency issues. Sun et al. (2021) embraced SAE across diverse datasets, achieving a commendable 90% accuracy with data weighting advantages, although computational time remains a concern. Blaise et al. (2020) adopted the Split Merge technique on MAWI and UCSD datasets, yielding 85% accuracy with exceptional attack detection, albeit with false positives.

Lastly, Tokmak (2022) applied deep learning to the UGRansome dataset, securing 97% accuracy with a pronounced focus on zero-day threat detection, also involving feature selection. Pertaining to zero-day attack detection, our approach not only underscores its significance but also highlights its robust accuracy and emphasis, making strides in addressing evolving threats. Considering the importance of zero-day attack detection, our approach not only underscores its significance but also demonstrates robust accuracy and a proactive stance in tackling evolving threats. To further advance cyberintelligence, future efforts could concentrate on refining feature selection techniques, addressing computational efficiency challenges, and exploring ways to integrate various methodologies to enhance overall intrusion detection capabilities.

Table 6. A comparative analysis with existing IDS studies

Author	Year	Dataset	Model	Accuracy	Advantage	Limitation
Nkongolo, M., & Tokmak, M.	2023	UGRansome	Fuzzification	99%	Critical Infrastructure	Feature Selection

Kim J et al.	2020	Signal data	SAE	97%	Signal Processing	Tool diagnosis model
Zhang J.	2020	Malware	LSTM	81%	Invasive Software	Dependency
Sun T et al.	2021	MNIST, CIFAR-10, and UCI	SAE	90%	Data Weighting	Computational time
Blaise et al.	2020	MAWI and UCSD	Split Merge	85%	Attack Detection	False Positive
Tokmak M.	2022	UGRansome	Deep Learning	97%	Zero-Day Threat Detection	Feature Selection

5. CONCLUSIONS

The detection and mitigation of zero-day threats have emerged as critical imperatives in the landscape of cybersecurity. Zero-day threats, by their very nature, exploit vulnerabilities that are yet unknown to software vendors and security teams, posing substantial risks to organizations and individuals. As attackers constantly evolve their techniques, the need for robust and adaptive zero-day threat detection mechanisms becomes increasingly pressing. This research endeavors to harness the potential of deep learning techniques to effectively counter the ever-evolving landscape of zero-day threats. By capitalizing on deep learning's ability to process unstructured data to provide classification and prediction analysis, we present a robust framework for zero-day threat recognition. This framework integrates the LSTM approach with SAE feature extraction. The encouraging results obtained from our detection system underscore its significant effectiveness, thus offering valuable guidance and inspiration for forthcoming research pursuits in the field. In conclusion, the fight against zero-day threats demands a multi-faceted approach that integrates cutting-edge technology, collaborative efforts, and robust risk management practices. While machine learning and deep learning are potent tools, they must be complemented by human expertise to effectively counteract the sophistication of modern cyber threats. As the cybersecurity landscape continues to evolve, the ability to detect and mitigate zero-day threats will be a defining factor in ensuring the security and stability of digital ecosystems.

Ethics Committee Approval
N/A

Peer-review
Externally peer-reviewed.

Author Contributions / Yazar Katkıları
M.T. and M.N. contributed to the design and implementation of the research, to the analysis of the results and to the writing of the manuscript.

Conflict of Interest
The authors have no conflicts of interest to declare.

Funding
The authors declared that this study has received no financial support.

REFERENCES

Blaise, A., Bouet, M., Conan, V., & Secci, S. (2020). Detection of zero-day attacks: An unsupervised port-based approach. *Computer Networks*, *180*, 107391.

Boussaad, L., & Boucetta, A. (2021). Stacked Auto-Encoders Based Biometrics Recognition. *2021 International Conference on Recent Advances in Mathematics and Informatics (ICRAMI)*, 1–6.

Chatterjee, S., Dey, D., & Munshi, S. (2019). Morphological, texture and auto-encoder based feature extraction techniques for skin disease classification. *2019 IEEE 16th India Council International Conference (INDICON)*, 1–4.

Fang, Y., Huang, C., Liu, L., & Xue, M. (2018). Research on Malicious JavaScript Detection Technology Based on LSTM. *IEEE Access*, *6*, 59118–59125. https://doi.org/10.1109/ACCESS.2018.2874098

Google Colaboratory. (2023). Colaboratory. https://colab.research. google.com/

Kim, J., Lee, H., Jeon, J. W., Kim, J. M., Lee, H. U., & Kim, S. (2020). Stacked auto-encoder based CNC tool diagnosis using discrete wavelet transform feature extraction. *Processes*, *8*(4), 456.

Kong, X., Lin, R., & Zou, H. (2020). Feature extraction of load curve based on autoencoder network. *2020 IEEE 20th International Conference on Communication Technology (ICCT)*, 1452–1456.

Kumar, V., & Sinha, D. (2021). A robust intelligent zero-day cyber-attack detection technique. *Complex & Intelligent Systems*, *7*(5), 2211–2234. https://doi.org/10.1007/s40747-021-00396-9

Luo, S., Huang, X., Wang, Y., Luo, R., & Zhou, Q. (2022). Transfer learning based on improved stacked autoencoder for bearing fault diagnosis. *Knowledge-Based Systems*, *256*, 109846.

Manjunatha, B. A., & Gogoi, P. (2022). An Improved Stacked Sparse Auto-Encoder Method for Network Intrusion Detection. *Emerging Research in Computing, Information, Communication and Applications: ERCICA 2020, Volume 1*, 103–118.

Millar, S., McLaughlin, N., del Rincon, J. M., & Miller, P. (2021). Multi-view deep learning for zero-day Android malware detection. *Journal of Information Security and Applications*, *58*, 102718.

Nkongolo, M., & Tokmak, M. (2023). Zero-Day Threats Detection for Critical Infrastructures. In A. Gerber & M. Coetzee (Eds.), *South African Institute of Computer Scientists and Information Technologists* (pp. 32–47). Springer Nature Switzerland. https://doi.org/10.1007/978-3-031-39652-6_3

Nkongolo, M., Van Deventer, J. P., & Kasongo, S. M. (2021). Ugransome1819: A novel dataset for anomaly detection and zero-day threats. *Information*, *12*(10), 405.

Nkongolo, M., van Deventer, J. P., & Kasongo, S. M. (2022). The Application of Cyclostationary Malware Detection Using Boruta and PCA. In *Computer Networks and Inventive Communication Technologies* (pp. 547–562). Springer.

Rathore, H., Agarwal, S., Sahay, S. K., & Sewak, M. (2018). Malware detection using machine learning and deep learning. *Big Data Analytics: 6th International Conference, BDA 2018, Warangal, India, December 18–21, 2018, Proceedings 6*, 402–411.

Roberts, C., & Nair, M. (2018). Arbitrary discrete sequence anomaly detection with zero boundary LSTM. *ArXiv Preprint ArXiv:1803.02395*.

Samaneh, M., Dima, A., & Ghorbani, A. A. (2022). Effective and Efficient Hybrid Android Malware Classification Using Pseudo-Label Stacked Auto-Encoder. *Journal of Network and Systems Management*, *30*(1).

Sarhan, M., Layeghy, S., Gallagher, M., & Portmann, M. (2023). From zero-shot machine learning to zero-day attack detection. *International Journal of Information Security*, *22*(4), 947–959. https://doi.org/10.1007/s10207-023-00676-0

Sewak, M., Sahay, S. K., & Rathore, H. (2021). LSTM Hyper-Parameter Selection for Malware Detection: Interaction Effects and Hierarchical Selection Approach. *2021 International Joint Conference on Neural Networks (IJCNN)*, 1–9. https://doi.org/10.1109/IJCNN52387.2021.9533323

Smagulova, K., & James, A. P. (2019). A survey on LSTM memristive neural network architectures and applications. *The European Physical Journal Special Topics*, *228*(10), 2313–2324.

Sun, T., Ding, S., & Xu, X. (2021). An iterative stacked weighted auto-encoder. *Soft Computing*, *25*(6), 4833–4843. https://doi.org/10.1007/s00500-020-05490-7

Thomas, V. E., Ugwu, C., & Onyejegbu, L. (2021). Comparative Analysis of Dimensionality Reduction Techniques on Datasets for Zero-Day Attack Vulnerability. *Journal of Software Engineering and Simulation*, *7*(8), 48–56.

Tokmak, M. (2022). Deep forest approach for zero-day attacks detection. In S. Tasdemir & A. O. Ozkan (Eds.), *Innovations and Technologies in Engineering* (pp. 44–55). Eğitim Yayınevi.

Tokmak, M., & Küçüksille, E. U. (2022). Comparative Analysis of Dimension Reduction and Classification Using Cardiotocography Data. In M. Karaboyacı & A. Demirçalı (Eds.), *Versatile Multidisciplinary Engineering Research* (pp. 149–164). SRA Academic Publishing.

Wang, L., Wang, Z., Zhao, G., Su, Y., Zhao, J., & Wang, L. (2021). Automatic voice quality evaluation method of IVR service in call center based on Stacked Auto Encoder. *IOP Conference Series: Earth and Environmental Science*, *827*(1), 012021.

Wang, T., Ng, W. W., Li, W., & Kwong, S. (2021). Broad Autoencoder Features Learning for Classification Problem. *International Journal of Cognitive Informatics and Natural Intelligence (IJCINI)*, *15*(4), 1–15.

Wang, Y., Yang, H., Yuan, X., Shardt, Y. A., Yang, C., & Gui, W. (2020). Deep learning for fault-relevant feature extraction and fault classification with stacked supervised auto-encoder. *Journal of Process Control*, *92*, 79–89.

Wei, P., & Zhao, Y. (2019). A novel speech emotion recognition algorithm based on wavelet kernel sparse classifier in stacked deep auto-encoder model. *Personal and Ubiquitous Computing*, *23*(3), 521–529. https://doi.org/10.1007/s00779-019-01246-9

Xie, Q., Wang, Y., & Qin, Z. (2020). Malware Family Classification using LSTM with Attention. *2020 13th International Congress on Image and Signal Processing, BioMedical Engineering and Informatics (CISP-BMEI)*, 966–970. https://doi.org/10.1109/CISP-BMEI51763.2020.9263499

Xie, W., Xu, S., Zou, S., & Xi, J. (2020). A System-call Behavior Language System for Malware Detection Using A Sensitivity-based LSTM Model. *Proceedings of the 2020 3rd International Conference on Computer Science and Software Engineering*, 112–118. https://doi.org/10.1145/3403746.3403914

Zhang, J. (2020). DeepMal: A CNN-LSTM Model for Malware Detection Based on Dynamic Semantic Behaviours. *2020 International Conference on Computer Information and Big Data Applications (CIBDA)*, 313–316. https://doi.org/10.1109/CIBDA50819.2020.00077

Zhu, H.-J., Wang, L.-M., Zhong, S., Li, Y., & Sheng, V. S. (2021). A hybrid deep network framework for android malware detection. *IEEE Transactions on Knowledge and Data Engineering*, *34*(12), 5558–5570.

İlçelerde Bulunan Pazar Yeri Sayılarının Yeterliliklerinin Araştırılması

Durdane Tay*[1], Görkem Gülhan[1]

Özet Üretici ve tüketicinin ticaret amacı ile doğrudan buluştuğu pazaryerleri tarih boyunca ticaretin geliştiği ve kent merkezlerinin hareketlendiği alanlar olmuştur. Her türlü alt sektörlere ait ürünlerin satıldığı pazaryerleri özellikle Türkiye'de kültürel açıdan köklü bir geçmişe sahiptir. Pazar yerleri, ekonomik, sosyal ve kültürel yapıdaki değişiklikler, ulaşım tercihlerinin farklılaşması, AVM ve süpermarket kullanımının zaman içerisinde yaygınlaşması, ilçelerde yer alan pazaryerleri ile ilgili bilgilerin tam olarak belirlenememesi gibi etkenler sebebiyle gün geçtikçe azalmaktadır. Pazar yerlerinin mekân, sayı ve büyüklüklerinin doğru bir şekilde belirlenememesi bu alanların yetersiz kalmasına sebep olmaktadır. Pazar yerlerinin yer seçimi, planlama standartları ve planlama ilkeleri doğrultusunda yapılmaktadır. Devamla, ilçelerde kaç tane pazar yeri kurulacağı ve bu alanların büyüklüklerinin ne olacağı konusunda analitik yöntemler ve niceliksel modeller konusunda literatürde boşluklar bulunmaktadır. Nüfusla doğru orantılı olarak kent merkezine yakın ilçelerde pazar yerleri sayı ve büyüklükleri artmakta ve çeperlerdeki ilçelere doğru azalmaktadır. Pazar yerlerinin sayıları ve alansal büyüklükleri arasında ilişki bulunmaktadır. Pazar yerleri alansal olarak büyükse ilçedeki pazar yeri sayısı az olmakta, eğer ki sayısı çoksa alansal büyüklükleri küçük olmaktadır. Bu çalışmada İzmir ve Denizli illerindeki pazar yeri sayıları ve alansal büyüklükleri arasındaki ilişki çoklu doğrusal regresyon modeli yardımıyla bulunmuştur. Bu doğrultuda İzmir ve Denizli iline ait ilçelerdeki pazar yeri sayıları ve alansal büyüklükleri ölçümlenmiştir. İlçelerdeki nüfus verileri de kullanılarak kişi başına düşen pazar yeri alanı ve pazar yeri başına düşen kişi sayıları hesaplanmıştır. Daha sonra anılan değerler açısından ilçe bazında ortalama altında ve üstünde kalan yerleşmeler tespit edilerek bu bölgelerde pazaryerlerinin geliştirilmesi önerilmiştir. Çalışma kapsamında elde edilen model ile pazaryerleri sayıları büyüklüklerinin ve nüfus büyüklüklerinin gelecekte farklılaşması sonucunda ya da başka şehirlerde önerilen modelden yararlanılarak hangi ilçelerde sayı ve alan büyüklüğü gerektiğinin tespit edilebileceği değerlendirilmektedir.

Anahtar Kelimeler: Pazar yeri, çoklu doğrusal regresyon analizi, İzmir, Denizli

[1]**Adres:** Pamukkale Üniversitesi, Mimarlık ve Tasarım Fakültesi, Denizli/Türkiye
***Sorumlu Yazar**: demiraydurdane@gmail.com

1. GİRİŞ

Pazar yerleri tarihi dönemlerden bu yana üretici ve tüketicilerin buluşma alanları olmuştur. Belediye tarafından haftanın belirli günleri veya her gün satış yapılması için önceden belirlenmiş meyve, sebze, günlük ihtiyaç malzemeleri, giyim ve ev eşyası gibi birçok ihtiyacın satıldığı yerler pazar yeri olarak tanımlanmaktadır (Eroğlu, 1976).Pazar yerleri kırsal bölgelerde genellikle haftada bir kez, günlük gerçekleşirken mevsimlik olarak kurulan pazar yerleri daha uzun süreli, panayır şeklinde gerçekleşmektedir. Kentsel yerleşmelerde ise ihtiyaçların bir kısmı bakkal, manav, market veya alışveriş merkezlerinden karşılanırken, farklı zamanlarda kurulan haftalık semt pazarlarından da karşılanmaktadır (Tunçel, 2003). İnsanların hem sosyal ilişkiler kurmasını sağlayan hem de ihtiyaçların karşılanmasına olanak tanıyan pazarlar, ilk çağ kentlerindeki agoralardan bu yana varlıklarını sürdürmektedir. Kırsal yerleşmelerde pazar kültürü ürün dağıtım ve toplama sisteminin önemli bir elemanıdır (Tunçel, 2006). Pazarlarla ilgili bilim insanları mensubu oldukları araştırma alanları kapsamında çalışmalar yürütmüş ve literatürde çeşitli tanımlamalar yapılmıştır. Kavramsal açıdan pazarların tanımlamasını;

Tax (1953), "Pazar alanları insanlar arası eş zamanlı faaliyetler içermektedir. Pazar yerlerinin özgür ve konforlu bir alan olması ekonomistlerin mükemmel pazarını ifade etmektedir" şeklinde yapmıştır. E.F. Bazman pazarı, satıcıların, ürünleri satın almak veya satmak için ortak bir alanda bir araya gelmesini ifade etmektedir. Coulson ve Cor (1962) ise, pazar yerlerini, hayvansal ve bitkisel ürünlere ulaşmanın kolay olduğu, alım satım işlemlerinin gerçekleştiği alan olarak ifade etmiştir. Hodder ve Bromley'e göre pazarlar ortak konumda belirlenen sürelerde alıcı ve satıcıların bir araya geldiği kamusal organizasyon olarak tanımlanmıştır. Hodder ve Ukwu'ya göre (1969), pazar yerleri, sınırları ve zamanı kabaca belirlenmiş, üretici, alıcı ve satıcıların ticaret yapma amacıyla bir araya geldikleri kurumsal bir faaliyeti ifade etmektedir. Pazarlarla ilgili tanımlamaların bir kısmında ekonomik ve sosyal boyuta dikkat çekilmiştir. Ullman'a göre

pazarlar, insan faaliyetlerinin merkezinde yer aldığı için bir bölgenin yaşamında oldukça önemli bir olgudur. Smailes (1964), ilerleme kaydeden ülkelerin kasabalarında kurulan pazarların yöre halkının sosyal yaşamında mağaza ve alışveriş merkezlerinden daha önemli olduğu sonucu üzerinde durmuştur. Hodder (1965), pazar yerlerinin sosyal ve ekonomik yaşamın en önemli unsurlarından biri olduğunu vurgulamıştır. Afolabi (1972), pazar kurulan alanları ticaret merkezlerinden çok önemli kavşak noktalarında, sosyal, dini tesis ve siyasi ilişkilerin kurulduğu alanlar olarak ifade etmiştir. Webber ve Symanski (1973), pazarların yalnızca alışveriş amaçlı yapılmadığını bununla birlikte sosyal ihtiyaçların karşılanmasında önemli olduğunun altını çizmiştir. Bromley, Symanski ve Good (1975), periyodik pazarların kurulma zamanlarının yalnızca ay, mevsim gibi unsurlarla ilgili olduğu değil aynı zamanda festival, dini tören gibi toplumsal olaylarla da ilişkili olduğu vurgulamıştır (Tunçel, 2018). Türkiye'de haftalık pazarlar üzerine hem teorik hem de uygulamalı olarak birçok çalışma yapılmıştır. Baykara 1994 yılında, Bir Osmanlı Çağı pazarının çöküşünü ele almaktadır. 1999 yılında Doğu Karadeniz yaylalarında pazar yerlerinin tarihsel sürecini inceleyen Bakırcı, özellikle ulaşımın gelişmesiyle yaylaların ekonomik öneminin azaldığını değerlendirmiştir. Pazarlarla ilgili bir diğer çalışma Özgül ve Mitchell tarafından 2000 yılında yapılmıştır. İstanbul'daki periyodik pazarları konu alan çalışma, pazarların alıcı- satıcı ve mal ilişkilerini incelemiştir. Şen ve İlhan ise 2003 yılında İzmir Büyükşehir genelinde geçimini pazarcılık yaparak sağlayan kesimin kentleşme sürecindeki konumlarını ele almışlardır. Elâzığ şehrinde yer alan pazarları değerlendiren Tunçel, 2003 yılında haftalık pazarların tarihçesini, tercih nedenlerini ve dağılış etki alanlarını topolojik olarak değerlendirmiştir. Pazarlarla ilgili bir diğer çalışma Bursa'da kurulan pazarları konu alan Çalışkan tarafından 2005 yılında yapılmıştır. Çalışkan'a göre cadde-sokaklarda kurulan pazarlar sosyo-ekonomik faydaların yanı sıra şehir yaşamı açısından genellikle büyük sorunlara sebep olmaktadır. Dökmeci vd. 2005 yılında İstanbul'da yaptıkları çalışmada gelişmiş ülkelerle kıyaslandığında İstanbul'da geleneksel ve modern ticaret sisteminin birlikteliğine vurgu yapmışlardır. 2006 yılında Özcan, Anadolu Selçuklu Dönemi Pazar ve Panayır Yerleşmelerinin Mekânsal kuruluşunu, ekonomik-demografik büyüklüklerini ve evrim sürecini ele almıştır. Yılmaz 2006 yılında Samsun şehrinde kurulan pazarların genel özellikleri ve sorunları üzerinde durmuştur. Çalışkan 2007 yılında Bursa ve Çanakkale şehrindeki pazarları ele almıştır. 2009 yılında Tunçel Türkiye'de kırsal kesim-kasaba ve şehirlerde kurulan pazarların farklılaşmasını ele almıştır.

Pazar yerlerinin kuruluşuyla ilgili birbirinden farklı iki görüş bulunmaktadır. İlk görüşe göre pazar yerlerinin kurulma sebepleri şehirlerdir. İnsanlar ürettikleri ürünlerini tüketiciye ulaştırmak için ortak bir alana ihtiyaç duymuşlar ve ürettikleri ürünleri satmak için şehirlere getirmişlerdir. Bu şekilde pazar alanları oluşmuştur (Akçi, 2015). İkinci görüşe göre de pazar alanları şehrin kuruluş sebebi olmuştur. Tarihi dönemlerden bu yana insanlar sahip olduğu becerileri sebebiyle ürettikleri gereçleri veya ürünleri birbirleriyle takas etmişlerdir. Takas işlemi için herhangi bir alana gerek duyulmamıştır. Geçmiş dönemlerde pazarlar, yolların kesişim noktasında, cami gibi dini alanlarda ve yakınlarında ve limanlar gibi ortak kullanımı bulunan alanlarda kurulduğu için milletlerin buluşma alanı olmuştur. Roma'da pazar yerleri eğlence vesilesi olarak görülürken Yunan ekonomisinde 5. ve 6. yüzyıllarda çarşı ve pazarların yer aldığı bilinmektedir. Bu dönemde pazarlar bölgesel ihtiyacı karşılarken geniş içerikli ekonomik değişmeyi kapsayan panayırlar da gelişmeye başlamıştır (Eroğlu, 1976). Orta Çağ'a gelindiğinde Antik Yunan ve Roma'da yer alan agora ve forumların benzeri panayır ve fuarlar ortaya çıkmıştır. Osmanlı döneminde halkı bir noktada birleştirmek ve alışverişi o alana taşımak için "ARASTA" adı verilen dükkanlar yapılmıştır (Cezar, 1985). Ülkemizde kentlerde sanayi devrimiyle birlikte şehirler yatay olarak genişlemeye başlamış ve pazar yerleri yetersiz kalmış, bu sebeple kentlerin farklı bölgelerinde insanların ihtiyaçlarına cevap verebilecek pazar alanları oluşmaya başlamıştır. Pazar kurulan yerin coğrafi konumu, iklim özellikleri, hedef kitlenin varlığı, ulaşım ve ulaştırma koşulları ve idari yapı gibi çeşitli unsurlar önem taşımaktadır. Pazarı oluşturan kriterlerin başında finans gelmektedir. Finans, gerekli paranın sağlanması ve yönetimini içermektedir (Berkmen, 1991). Bir diğer kriter fiyat oluşumudur. Pazarlamacı bu konuda tüm etkenleri dikkate almalıdır. Pazarı oluşturan bir diğer kriter depolamadır. Depolama ile ürünlerin uygun koşullarda bekletilmesi ve sonrasında satışa sunulması sağlanmaktadır. Pazarı oluşturan kriterlerden bir diğeri risk taşımadır. Risk zarar etme olasılığı anlamına gelmektedir. Zarar, olasılık gerçekleştiğinde ortaya çıkmaktadır. Risk ortaya çıktığında, malın sahibi zararı karşılamaktadır (Berkmen, 1991). Pazar yerleri kurulma sorumluluğu 1580 sayılı Belediyeler yasasının 15. Maddesinin 42. Fıkrası ile belediyelere verilmiştir. Fen İşleri Müdürlüğü tarafından öncelikle pazar kurulacak alanın arazi mülkiyet durumu incelenmektedir. Müdürlük, pazar yerlerinin seçiminde kriter, yoğunluk, çevresel ilişkiler ve çevre pazarlara olan uzaklığı dikkate almaktadır. Bunlarla birlikte pazar konusunda pazar yerleri esnaf derneği görüşü alınmaktadır (Aksoy, 2009). İktisat İşleri Müdürlüğü pazar yerlerinin yönetiminden sorumludur. Pazar yerlerinin denetiminden ise, İktisat İşleri Müdürlüğü, Veteriner Müdürlüğü, Sağlık Müdürlüğü, Hesap İşleri Müdürlüğü, Zabıta İşleri Müdürlüğü ve Pazar yerleri Esnafı Derneği sorumludur (Aksoy, 2009). Pazar yerlerinin imar planlarında belirlenmesinde, 2012 tarih ve 28351 sayılı resmî gazetede Gümrük ve Ticaret Bakanlığı'nca yayınlanarak yürürlüğe giren Pazar Yerleri Hakkında Yönetmelik'ten faydalanılmaktadır. Yönetmelikte yer alan hükümler belediyeler tarafından dikkate alınmaktadır. Pazar yerlerinin zaman içerisinde gösterdiği değişiklikler belirlenmiş, şehir içindeki konumlarına, sayı ve büyüklüklerine ilişkin İzmir ve Denizli illerinde kurulan pazarların bazı özellikleri ortaya konmuştur. Pazar yerlerinin sayı ve büyüklüklerinin belirlenmesi için model önerisi geliştirilmiştir. İzmir ve Denizli illerinde kurulan pazarların mekân üzerindeki dağılımları, sayı ve büyüklükleri tespit edilmiştir. İzmir ve Denizli illeri

pazar yerleri sayı ve büyüklüklerinin belirlenmesinde regresyon analizinden yararlanılmıştır. Bunun sonucunda İzmir ve Denizli illerinin pazar alanları karşılaştırılmıştır.

2.MATERYAL VE METOT

Pazar yeri sayı ve alansal büyüklükleri ihtiyaçlarının belirlenmesi için çalışmada üç aşamalı bir yöntem geliştirilerek İzmir ve Denizli ilçeleri kapsamında uygulanmıştır. Geliştirilen yöntemde kullanılan veriler sanal veri depoları, yerinde araştırma- gözlem, konu ile ilgili yayınlanmış rapor ve çalışmalar derlenerek, idari kurumlardan ilgili konu kapsamında sorular sorularak elde edilmiştir. Harita ölçümleme metodu ile pazar alanlarının büyüklükleri ölçülmüştür. Şekil 1'de, anılan yöntemin akış şeması verilmiştir.

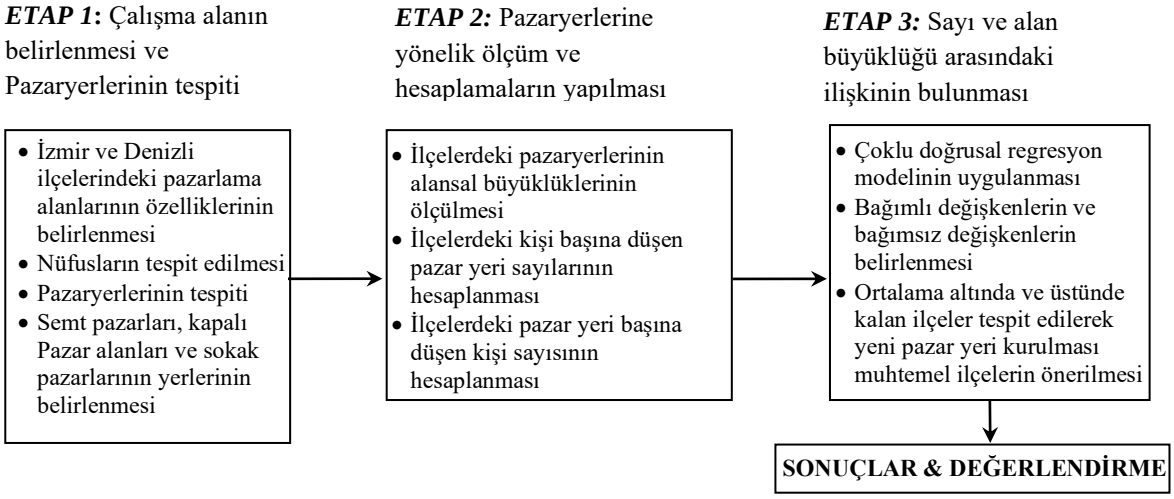

Şekil 1: Akış şeması

Etap1'de; Çalışma alanı ve özellikleri belirlenmiştir. Çalışma alanı olarak seçilen İzmir ve Denizli illeri kapsamında demografik veriler ve pazaryerlerinin konumları belirlenerek haritalara işlenmiş ve tablo haline getirilmiştir. Pazaryerlerinin özellikleri ve gruplama işlemleri yapılarak ölçüme hazır hale getirilmiştir. Etap 2'de; İzmir ve Denizli ili ilçelerindeki pazaryerleri tespit edilerek sayıları tablolara işlenmiştir. Her bir pazar yerinin alansal olarak büyüklüğü haritalar üzerinden yaklaşık olarak ölçümlenerek tablo haline getirilmiştir. Daha sonra ilçelerdeki kişi başına düşen pazar yeri sayıları ve pazar yeri başına düşen kişi sayıları hesaplanarak ortalamaları bulunmuştur. Etap 3'te; bağımlı ve bağımsız değişkenler tanımlanarak çoklu doğrusal regresyon analizi yapılmıştır. Yapılan analiz sonucunda modelin anlamlılık düzeyleri ve bağımsız değişkenleri, anlamlılık düzeyleri sorgulanarak yorumlanmıştır. Daha sonra ortalama altında ve üstünde kalan ilçeler tespit edilerek ulaşım ve erişilebilirlik ilişkileri de dikkate alınarak yeni pazar yeri kurulması ya da alansal olarak büyütülmesi muhtemel ilçeler önerilmiştir. Bununla birlikte İzmir ve Denizli Pazaryerleri modeli sonuçları kapsamında benzer ve farklılıkları ortaya koymak, ilçelerde kişi başına düşen pazar alanı ve pazar başına düşen kişi sayılarının karşılaştırmasını yaparak bu kapsamda çıkan sonuçları ortaya koymak ve değerlendirmeye sunmak amacıyla karşılaştırma yöntemi de kullanılmıştır. Çalışma kapsamında uygulanan çoklu doğrusal regresyon analizi detaylı olarak anlatılmıştır.

2.1. Çoklu Doğrusal Regresyon Analizi

Regresyon, bir değişken ile farklı bir veya birden fazla değişkenler arasında ilişki kurma şeklidir. Bağımsız değişkenlerin farklı değerlerine karşılık bağımlı değişkenin alacağı değerin tahmin edilmesi Regresyon denklemi kapsamında yapılmaktadır. Regresyon analizinin farklı alt başlıkları bulunmaktadır. Çalışma kapsamında kullanılan metot da regresyon analizinin bir çeşidi olan çoklu doğrusal regresyon analizidir. Regresyon analizinde birden fazla bağımsız değişken bulunuyorsa bu modellere "Çoklu Doğrusal Regresyon Analizi" denmektedir. Çoklu doğrusal regresyon denkleminde yer alan bağımsız değişkenlerin (X), gelecekte alacakları değerler farklı projeksiyon yöntemleri ile hesaplanarak, denklemde bu değerlerin yerine konulması ile gelecek için sonuçlar ortaya konmaktadır.
Çoklu Doğrusal Regresyon eşitliği (Kılınçarslan, 2012);

Y= a0 + b1x1 + b2x2 + b3x3 + …… + bixi

Bu formülde;

Y: Bağımlı değişken

a0, b1, b2, b3, ….. bi: katsayılar

x1, x2, ……. xi: bağımsız değişkenler (nüfus, araç sahipliliği vb.)

Regresyon analizinde; bağımsız değişkenlerin detaylı olarak birbirleriyle ve bağımlı değişkenle incelendiği hesaplamaların sonuçları korelasyon katsayısı (R) ile kontrol edilmelidir. Yüksek korelasyon değeri veren bağımsız değişken formülde kalmalıdır.

2.2. Çalışma Alanı

Tez çalışması kapsamında çalışma alanı olarak İzmir ve Denizli illeri seçilmiştir. İzmir ve Denizli illeri detaylı olarak analiz edilmiştir. İzmir ili, Türkiye'nin batı kısmında Ege Bölgesi'nde yer almaktadır. 26 15 ile 28 20 doğu boylamları ve 37 45 ile 39 15 kuzey enlemleri arasında bulunan il, 12.012 km^2 yüz ölçümüne sahiptir. İzmir, kuzeyde Mandra dağları, güneyde Kuşadası körfezi batıda Çeşme Yarımadası'nın Tekne Burnu, doğuda ise Aydın ve Manisa il sınırları ile çevrilidir. Batıda ise İzmir körfezine bağlanmaktadır. Şekil 2'de ilin coğrafi konumu gösterilmiştir.

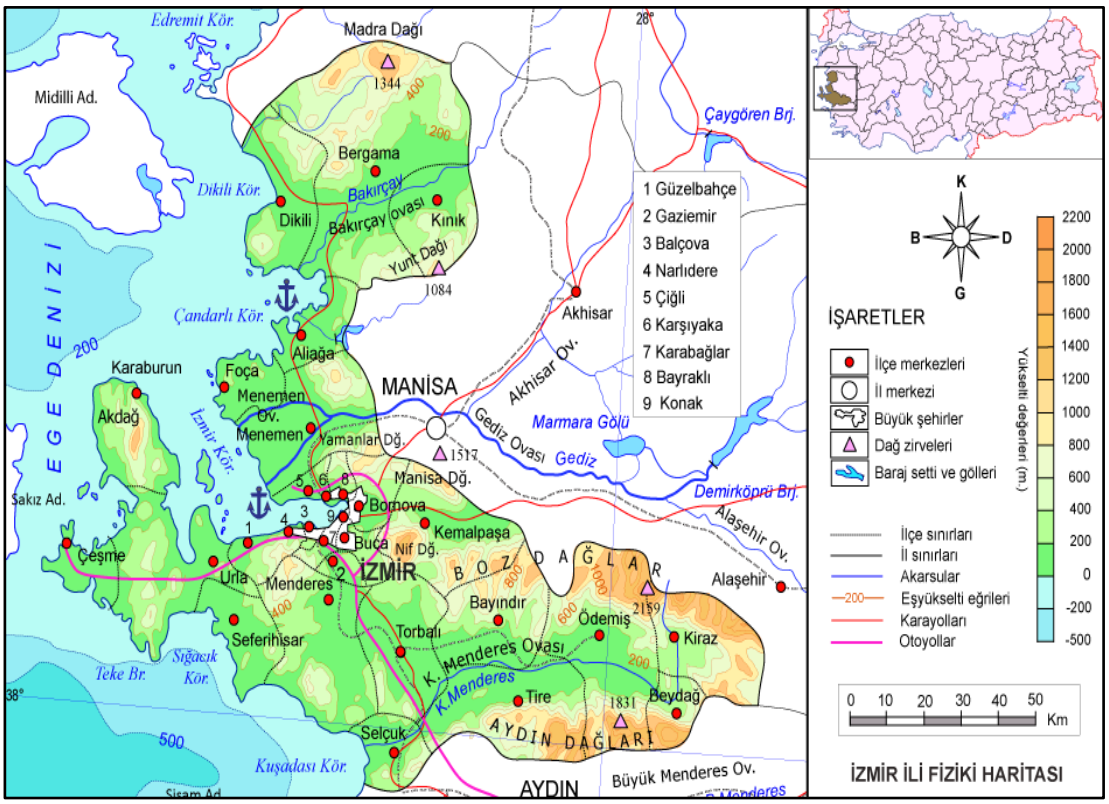

Şekil 2: Ege bölgesi fiziki haritası

İzmir ilinin Adrese Dayalı Nüfus Kayıt Sistemi sonuçlarına göre 2022 yılı nüfusu 4.462.056 kişi olarak tespit edilmiştir. Bu nüfusun %49,66'lık orana sahip 2.215.716'sı erkek, %50,34'lük orana sahip 2.246.340'ı kadınlardan oluşmaktadır. İlde kilometrekareye 372 kişi düşmektedir. İlin nüfus yoğunluğu 372 (kişi/km2)'dir. İzmir ilinin 30 ilçesi bulunmaktadır. Bu ilçeler; Aliağa, Balçova, Bayındır, Bayraklı, Bergama, Beydağ, Bornova, Buca, Çeşme, Çiğli, Dikili, Foça, Gaziemir, Güzelbahçe, Karabağlar, Karaburun, Karşıyaka, Kemalpaşa, Kınık, Kiraz, Konak, Menderes, Menemen, Narlıdere, Ödemiş, Seferihisar, Selçuk, Tire, Torbalı ve Urla'dır. Çalışma kapsamında analiz edilen bir diğer il ise Denizli'dir. Anadolu Yarımadası'nın güneybatısında, Ege bölgesinin de güneydoğusunda yer alan Denizli, Ege ve Akdeniz bölgeleri arasında yer alıp Ege bölgesine bağlı bir ildir. İl, 28 30-29 30 doğu meridyenleri ile 37 12-38 12

kuzey paralelleri arasında yer almaktadır (T.C. Denizli Valiliği, 2022). Denizli'nin batısında Aydın ve Manisa, güneyinde Muğla, kuzeyinde Uşak illeri bulunmaktadır (Şekil 3).

Şekil 3: Denizli ili konumu

Denizli ilinin Adrese Dayalı Nüfus Kayıt Sistemi sonuçlarına göre 2022 yılı nüfusu 1.056.332 kişi olarak tespit edilmiştir. Bu nüfusun %49,73'lük orana sahip 525.359'u erkek, %50,27'lik orana sahip 530.973'ü kadınlardan oluşmaktadır. İlde kilometrekareye 89 kişi düşmektedir. İlin nüfus yoğunluğu 89 (kişi/km2)'dur. Denizli'de merkeze bağlı 19 ilçe bulunmaktadır. Bu ilçeler; Acıpayam, Babadağ, Baklan, Bekilli, Beyağaç, Bozkurt, Buldan, Çal, Çameli, Çardak, Çivril, Güney, Honaz, Kale, Merkezefendi, Pamukkale, Sarayköy, Serinhisar ve Tavas'tır.

3. BULGULAR

3.1. İzmir Pazar Yerleri Verilerinin Toplanması ve Ölçümlenmesi

İzmir ilçe Belediyeleri sınırlarına göre mevcut "Pazar Yerleri" ve konumlarına ilişkin olarak bir dağılım bilgisi çalışmaya veri olarak aktarılmamıştır. Bu nedenle mevcut durum haritalarından ve resmi kurum internet siteleri taranarak bir veri ortamı yaratılmaya çalışılmıştır. Söz konusu veriler üzerinden, erişilebilen bilgilere dayalı olarak değerlendirmeler yapılmıştır. Ticari araç yük dinamizmi, lojistik faaliyetlerin kümelenmesi ve sosyo-ekonomik özellikler dikkate alınarak İzmir, çalışma kapsamında üç ana çekirdek bölgeye ayrılmıştır. İzmir ili ilçelerinde yer alan pazar yerleri bilgileri Tablo 1'de verilmiştir. Tablo'da 2. ve 3. çekirdekte yer alan standart geleneksel halk pazarı alanları, organik ve doğal ürün pazar alanları bilgileri görülmektedir. Veriler Büyükşehir Belediyesi yayınları ve harita tabanlı ölçümlemeler sonucu elde edilmiştir. 1. çekirdekte yer alan ilçeler ise toplam olarak verilmiştir.

Tablo 1. İzmir ili pazar alanları bilgileri

İlçeler	Nüfus	Pazar Alanları (m^2)	Pazar Yeri Sayısı	Organik Pazar (m^2)	Kişi Başına Pazar Alanı	Pazar Başına Düşen Kişi Sayısı
Aliağa	95.392	20.232	4	0	0,21	23,85
Bayındır	40.584	3.965	4	0	0,10	10,15
Bergama	103.185	27.992	1	2541	0,27	103,19
Beydağ	12.507	500	1	0	0,00	0,00
Çeşme	43.489	585	7	109	0,01	6,21
Dikili	44.172	5.359	4	0	0,12	11,04
Foça	33.131	4.636	5	0	0,14	6,63
Karaburun	10.603	415	1	104	0,04	10,60
Kemalpaşa	106.298	13.025	10	0	0,12	10,63
Kınık	29.803	600	1	0	0,00	0,00
Kiraz	43.989	350	1	0	0,01	43,99
Menderes	93.796	10.297	4	0	0,11	23,45
Menemen	174.564	39.827	10	0	0,23	17,46
Ödemiş	132.511	7.592	13	0	0,06	10,19
Seferihisar	43.546	15.606	3	294	0,36	14,52
Selçuk	36.360	6.479	8	0	0,18	4,55
Tire	84.457	440	2	0	0,01	42,23
Torbalı	178.772	4.257	19	0	0,02	9,41
Urla	66.360	6.974	4	107	0,11	16,59
1. Çekirdek	2.947.000	120.321	55	1504	0,04	53,58
2. ve 3. Çekirdek Ortalaması					0,11	19,19

İzmir İli genelinde ortalama 19 bin kişi için bir pazar kurulmaktadır. Bu değer kentsel alan olarak tanımlanan 1. Çekirdekte yaklaşık 54.000 olarak hesaplanmıştır. İl genelinde Beydağ ve Kınık ilçelerinde büyük şehir belediyesi envanterinde yer alan pazar yeri bulunmamakta olup bölgede faaliyet gösteren pazar yerleri tespit edilmiştir. Son yıllarda yaygınlaşan organik pazarlar ise il genelinde denetimli olarak Balçova ve Bostanlı olmak üzere iki ilçede kurulmaktadır. Diğerleri ise pazarlar içerisinde kurulan doğal ürün satış noktalarıdır. Pazar alanlarının konumları ve il sınırları içindeki dağılım biçimi verilmiştir (Şekil 4-Şekil 5).

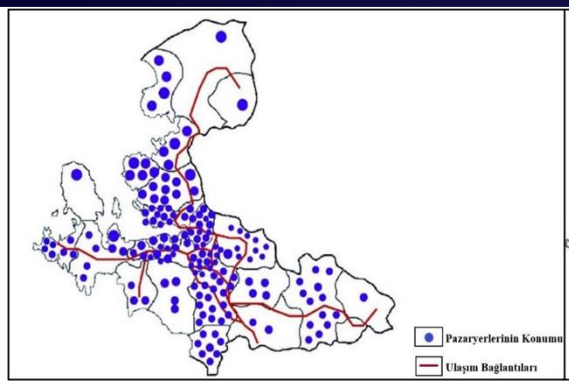

Şekil 4. Pazar yerlerinin konumları

Şekil 5. Organik pazarların konumları

İzmir ili pazar yerleri bilgileri topladıktan sonra elde edilen veriler yardımı ile kişi başına düşen pazar alanı büyüklüğü ve pazar başına düşen kişi sayıları hesaplanmış ve çoklu doğrusal regresyon analizi yapılmıştır. Kişi başına düşen pazar alanı büyüklüğü incelendiğinde 2. ve 3. Çekirdekte yer alan pazarlar baz alındığında kişi başına ortalama 0,11 m^2 pazar alanı düşerken kentsel alanda bu rakam 0,04 m^2'ye düşmektedir (Şekil 6-Şekil 7).

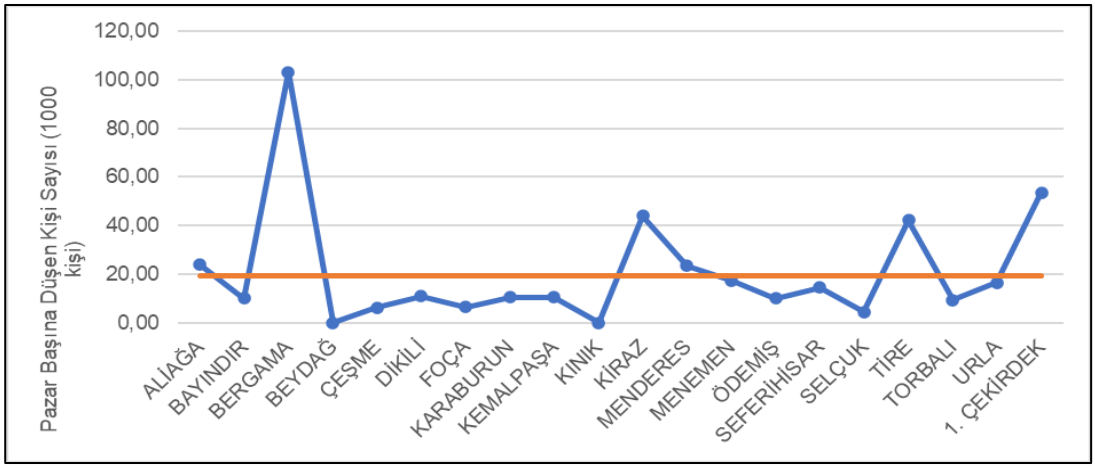

Şekil 6. Pazarlara göre kişi sayılarının dağılımı (Kişi Sayısı/Pazar)

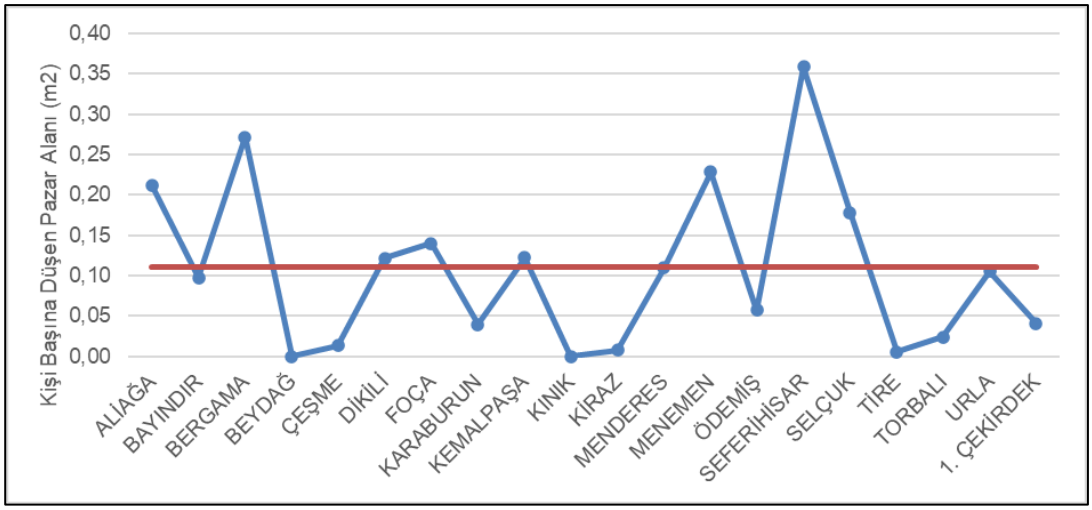

Şekil 7. Pazar alanı/Kişi dağılımı

Kırsal ilçelerde bulunan pazar alanları sayılarının nüfus ve alansal büyüklüklerle olan ilişkisi çoklu doğrusal regresyon analizi ile araştırılmıştır. Bu amaçla üretici ve semt pazarları bilgilerinin de yararlı olacağı düşünülebilir (Tablo 2).

Tablo 2. Üretici ve semt /halk pazarları özet tablosu

İlçeler	Pazar Yeri Sayısı	Nüfus	Pazar Alanları (m^2)	Kişi Başına Pazar Alanı	Pazar Başına Düşen Kişi Sayısı
Aliağa	**4**	95.392	20.232	0.21	23.848
Bayındır	**4**	40.584	39.65	0.10	10.146
Bergama	**2**	103.185	30.533	0.30	51.593
Beydağ	**1**	12.507	500	0.04	12.507
Çeşme	**8**	43.489	694	0.02	5.436
Dikili	**4**	44.172	5.359	0.12	11.043
Foça	**5**	33.131	4.636	0.14	6.626
Karaburun	**2**	10.603	519	0.05	5.302
Kemalpaşa	**10**	106.298	13.025	0.12	10.630
Kınık	**1**	29.803	600	**0.02**	**29.803**
Kiraz	**1**	43.989	350	**0.01**	**43.989**
Menderes	**4**	93.796	1.0297	**0.11**	**23.449**
Menemen	**10**	174.564	39.827	0.23	17.456
Ödemiş	**13**	132.511	7.592	0.06	10.193
Seferihisar	**4**	43.546	15.900	0.37	10.887
Selçuk	**8**	36.360	6.479	0.18	4.545
Tire	**2**	84.457	440	**0.01**	**42.229**
Torbalı	**19**	178.772	4.257	0.02	9.409
Urla	**5**	66.360	7.081	0.11	13.272
Ortalama	**0,12**	**18.019**			

Yukarıdaki tabloda üretici ve semt pazar alanları birleştirilerek kişi başına pazar alanları ve pazar yerleri başına düşen kişi sayıları bulunarak ortalamaları verilmiştir. Yani bir anlamda anılan regresyon modelinin istatistik sonuçları verilmiştir (Tablo 3).

Tablo 3. Pazar yerleri modeli regresyon istatistikleri tablosu

Bağımlı Değişken Pazar Yeri Sayısı			
R Kare	**0.85476525**		
Bağımsız Değişkenler	Katsayı	Standart Hata	**t stat**
Nüfus	9.8E-05	1.25471E-05	**7.810069**
Pazar Alanı	-0.00018	7.84358E-05	**-2.32461**

Model sonucuna göre ilçelerdeki "Pazar Alanı" sayıları, nüfus ve pazar alanı ile ilişkilidir. Kişi başına düşen pazar alanı ortalaması altında ve pazar başına düşen kişi üzerinde kalan ilçeler belirlenmiştir. Model sonuçlarına göre ikinci çekirdekte Menderes ve üçüncü çekirdekte Kınık, Kiraz ve Tire ilçelerindeki pazar alanlarının sayılarının ve erişilebilirliklerinin olanaklarının araştırılarak arttırılması önerilmektedir.

3.2. Denizli Pazar Yerleri Verilerinin Toplanması ve Ölçümlenmesi

Denizli il genelinde ortalama 7.414 kişi için bir pazar kurulmaktadır. Kişi başına düşen pazar alanı büyüklüğü ortalama 0.36 m^2 pazar alanı düşmektedir. Denizli ilinde toplam124 adet pazar yeri bulunmaktadır. Toplam pazar yerleri alanı yaklaşık olarak 234.435 m^2 olarak hesaplanmıştır. Şekil 8'den de görüldüğü üzere pazar başına düşen kişi sayısı en fazla Sarayköy ilçesinde 15.384 kişi, en az Babadağ ilçesinde 1.631 kişi düşmektedir.

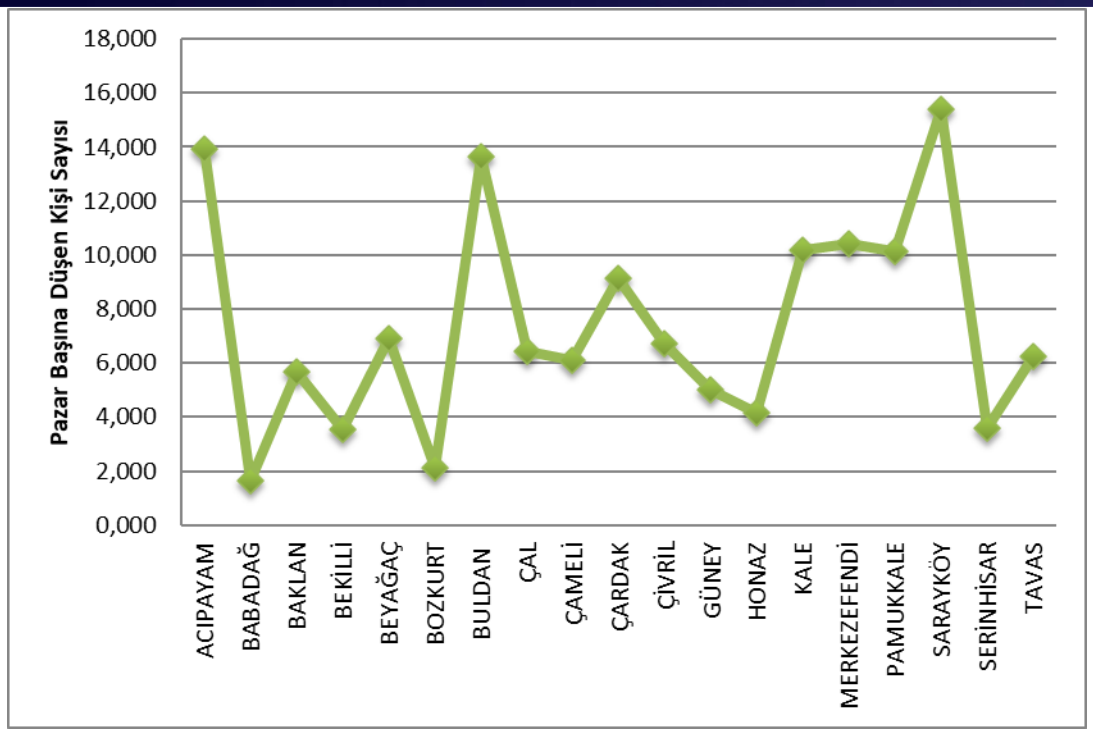

Şekil 8. Pazar başına düşen kişi sayısı

Şekil 9'dan da anlaşılacağı üzere kişi başına düşen pazar alanı miktarının 0.79 m^2 ile en fazla Serinhisar ilçesinde iken 0.20 m^2 ile en az Beyağaç ilçesinde olduğu tespit edilmiştir.

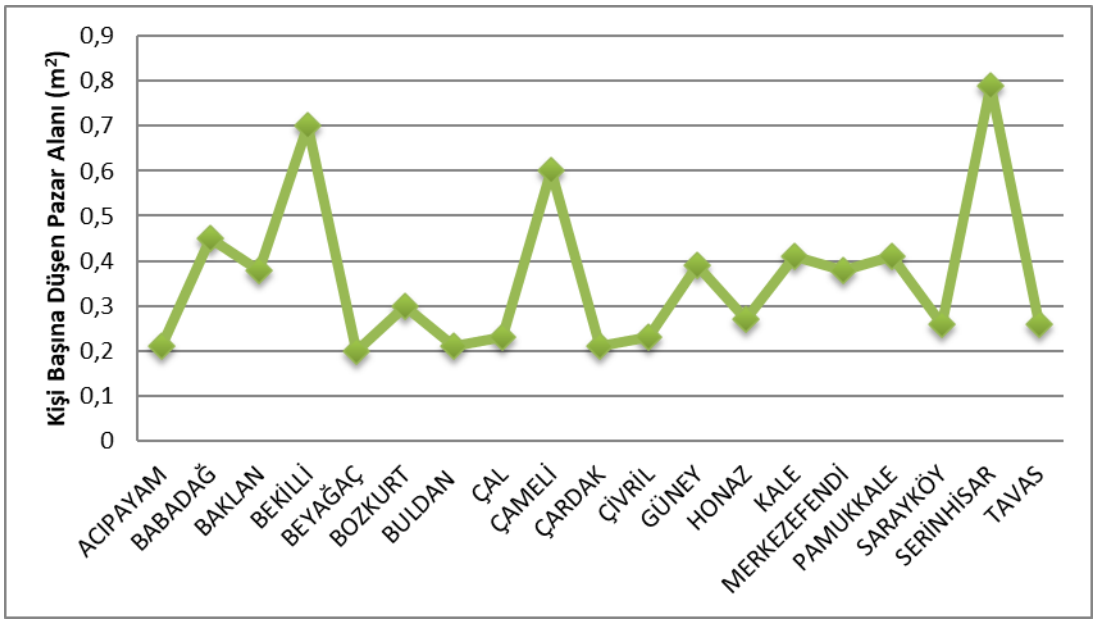

Şekil 9. Kişi başına düşen pazar alanı (m^2)

Modelde bağımlı değişken olarak pazar yeri sayıları *(Y_1)*, bağımsız değişkenler nüfus *(X_1)*, pazar alanı *(X_2)*, kişi başına düşen pazar alanı *(X_3)*, pazar başına düşen kişi sayısı *(X_4)* olarak belirlenmiştir. Model sınamasından önce merkezi ilçe olarak tanımlanan Merkezefendi ve Pamukkale İlçeleri kategoriden çıkartılmıştır. Yapılan çoklu doğrusal regresyon modelinin sonuçları verilmiştir (Tablo 4).

Tablo 4. Çoklu doğrusal regresyon modeli istatistik sonuçları

R^2	0.9197		
Bağımsız Değişkenler	Katsayı	Standart Hata	***T*değeri**
Nüfus(X_1)	0.0002	0.0001	**4.0513**
Pazar alanı(X_2)	-0.0003	0.0002	**-1.3134**
Kişi başına düşen pazar alanı(X_3)	7.1766	2.3241	**3.0879**
Pazar başına düşen kişi sayısı(X_4)	-0.0003	0.0001	**-3.8221**

Kişi başına düşen pazar alanı ortalamasının altında kalan ve aynı zamanda pazar başına düşen kişi sayısı ortalamasının üstünde kalan ilçelerde pazar olanaklarının araştırılarak geliştirilmesi değerlendirilmektedir. Anılan değerlerin tespit edilmesi için ortalamalar alınarak iki koşulu da aynı anda sağlayan ilçeler Tablo 5'te işaretlenmiştir.

Tablo 5. Ortalama eşikleri aynı anda geçen ilçeler

İlçeler	Kişi Başına Pazar Alanı	Pazar Başına Düşen Kişi Sayısı
Acıpayam	**0.216**	**13.912**
Babadağ	0.460	1.631
Baklan	0.389	5.654
Bekilli	0.702	3.533
Beyağaç	0.203	6.903
Bozkurt	0.305	2.131
Buldan	**0.213**	**13.621**
Çal	0.231	6.420
Çameli	0.603	6.085
Çardak	**0.212**	**9.144**
Çivril	0.232	6.714
Güney	0.391	4.988
Honaz	0.271	4.148
Kale	0.417	10.197
Sarayköy	**0.270**	**15.384**
Serinhisar	0.797	3.608
Tavas	0.266	6.264
ORTALAMA	**0.363**	**7.078**

Tablo 5'teki ortalama değerler incelendiğinde aynı anda iki ortalama eşik değeri sınırlarını geçen ilçeler Acıpayam, Buldan, Çardak ve Sarayköy olarak belirlenmiştir. Dolayısı ile bu ilçelerde bulunan pazaryeri sayılarının veya alanlarının geliştirilmesinin araştırılması ve arttırılmasının öncelikli olarak araştırılması önerilmektedir.

3.3. İzmir ve Denizli Pazar Yerleri Modelin Karşılaştırması

İzmir İli genelinde ortalama 19 bin kişi için bir pazar kurulmaktadır. Bu değer kentsel alan olarak tanımlanan 1. Çekirdekte yaklaşık 54.000 olarak hesaplanmıştır. Denizli İlinde merkeze bağlı toplam 19 adet ilçe bulunmaktadır. Her ilçede açık veya kapalı pazar yeri bulunmaktadır. İl genelinde ortalama 7.414 kişi için bir pazar kurulmaktadır. İzmir'de kişi başına düşen pazar alanı büyüklüğü incelendiğinde 2. ve 3. Çekirdekte yer alan pazarlar baz alındığında kişi başına ortalama 0,11 m^2 pazar alanı düşerken kentsel alanda bu rakam 0,04 m^2'ye düşmektedir. Denizli ilinde ise kişi başına düşen pazar alanı büyüklüğü ortalama 0.36 m^2 pazar alanı düşmektedir. İzmir ili model sonuçlarına göre Pazar başına düşen kişi sayısının en fazla Bergama'da, kişi başına düşen pazar alanı büyüklüğünün ise en fazla Bergama ve Seferihisar'da olduğu gözlemlenmiştir. Bununla birlikte model sonuçlarına göre ikinci çekirdekte Menderes ve üçüncü çekirdekte Kınık, Kiraz ve Tire ilçelerindeki semt ve üretici pazar alanlarının sayılarının ve erişilebilirliklerinin olanaklarının araştırılarak arttırılması önerilmektedir. Denizli ilinde ise pazar başına düşen kişi sayısının en fazla Sarayköy ilçesinde, en az Babadağ ilçesinde olduğu tespit edilmiştir. Kişi başına düşen pazar alanı miktarının ise en fazla Serinhisar ilçesinde en az Beyağaç ilçesinde olduğu tespit edilmiştir. Elde edilen veriler doğrultusunda Denizli ili ilçeleri için regresyon analizi yapılmış, aynı anda iki ortalama eşik değeri sınırlarını geçen ilçeler Acıpayam, Buldan, Çardak ve Sarayköy olarak belirlenmiştir. Dolayısı ile bu ilçelerde bulunan pazaryeri sayılarının veya alanlarının geliştirilmesinin araştırılması ve arttırılmasının öncelikli olarak araştırılması önerilmektedir.

3.4. Pazar Yerleri Sayılarının Demografik ve Sosyo-Ekonomik Açılardan Analizi

İzmir ve Denizli ili ilçeleri için kişi başına düşen pazar alanı büyüklüğü ve pazar başına düşen kişi sayıları hesaplanarak yapılan çoklu regresyon analizi, sosyo-ekonomik ve demografik değişkenler kapsamında yeniden değerlendirilmiştir. Pazar yeri sayılarının belirlenen bağımsız değişkenlerden hangileri ile ilişkili olduğu belirlenmiştir. Tablo 6'da İzmir ili pazar yeri sayıları, pazarı alanları, ortalama hanehalkı büyüklüğü, tarım alanı ve nüfus yoğunluğu bilgileri görülmektedir.

Tablo 6. İzmir ili pazar alanı, sosyo-ekonomik ve demografik veriler

İlçeler	Pazar Yeri Sayısı	Nüfus	Pazar Alanları (m^2)	Kişi Başına Pazar Alanı	Pazar Başına Düşen Kişi Sayısı	Ortalama Hanehalkı Büyüklüğü	Tarım Alanı (Dekar)	Nüfus Yoğunluğu
Aliağa	**4**	95,392	20,232	0,21	23,848	3,01	112.574	252
Bayındır	**4**	40,584	39,65	0,1	10,146	2,80	304.671	74
Bergama	**2**	103,185	30,533	0,3	51,593	2,71	384.582	67
Beydağ	**1**	12,507	500	0,04	12,507	2,61	49.192	73
Çeşme	**8**	43,489	694	0,02	5,436	2,61	16.869	153
Dikili	**4**	44,172	5,359	0,12	11,043	2,33	115.169	83
Foça	**5**	33,131	4,636	0,14	6,626	2,42	44.602	132
Karaburun	**2**	10,603	519	0,05	5,302	2,23	37.661	25
Kemalpaşa	**10**	106,298	13,025	0,12	10,63	3,20	219.431	156
Kınık	**1**	29,803	600	**0,02**	**29,803**	3,23	84.109	62
Kiraz	**1**	43,989	350	**0,01**	**43,989**	2,99	171.051	77
Menderes	**4**	93,796	1,0297	**0,11**	**23,449**	2,98	227.270	121
Menemen	**10**	174,564	39,827	0,23	17,456	3,17	204.543	305
Ödemiş	**13**	132,511	7,592	0,06	10,193	2,76	330.719	130
Seferihisar	**4**	43,546	15,9	0,37	10,887	2,55	86.177	116
Selçuk	**8**	36,36	6,479	0,18	4,545	2,80	147.574	115
Tire	**2**	84,457	440	**0,01**	**42,229**	2,70	266.109	118
Torbalı	**19**	178,772	4,257	0,02	9,409	3,27	292.552	310
Urla	**5**	66,36	7,081	0,11	13,272	2,65	70.392	91

Pazar yeri sayısı ile belirlenen bağımsız değişkenler arasındaki ilişkinin regresyon modelinin istatistik sonuçları verilmiştir (Tablo 7).

Tablo 7. İzmir ili regresyon istatistikleri tablosu

Bağımlı Değişken Pazar Yeri Sayısı			
R^2	**0,825199084**		
Bağımsız Değişkenler	Katsayı	Standart Hata	**t stat**
Ortalama Hanehalkı Büyüklüğü	-0,520950845	0,71875912	-0,724791979
Tarım Alanı	9,71189E-06	7,43332E-06	1,306534413
Nüfus Yoğunluğu	0,042046044	0,010906718	**3,85505904**

Modelde bağımlı değişken olarak pazar yeri sayıları ***(Y_1)***, bağımsız değişkenler ortalama hanehalkı büyüklüğü ***(X_1)***, tarım alanı ***(X_2)***, nüfus yoğunluğu ***(X_3)*** olarak belirlenmiştir. Model sonucuna göre ilçelerdeki "Pazar Alanı" sayıları, nüfus yoğunluğu ile ilişkilidir. İzmir ili regresyon değerlendirmesi sonrasında Denizli ili için de pazar yeri sayılarının sosyo-ekonomik ve demografik değişkenler ile arasındaki ilişki analiz edilmiştir (Tablo 8).

Tablo 8. Denizli ili pazar alanı, sosyo-ekonomik ve demografik veriler

İlçeler	Pazar Yeri Sayısı	Nüfus	Pazar Alanları (m^2)	Kişi Başına Pazar Alanı	Pazar Başına Düşen Kişi Sayısı	Ortalama Hanehalkı Büyüklüğü	Tarım Alanı (Dekar)	Nüfus Yoğunluğu
Acıpayam	4	55.648	12.016	0,21	13.912	2,72	441.075	34
Babadağ	4	6.522	3.000	0,45	1.631	2,97	29.751	48
Baklan	1	5.654	2.200	0,38	5.654	2,57	121.838	15
Bekilli	2	7.065	4.960	0,7	3.533	2,24	117.347	22
Beyağaç	1	6.903	1.400	0,2	6.903	2,73	31.900	16
Bozkurt	6	12.788	3.898	0,3	2.131	2,63	139.504	36
Buldan	2	27.241	5.800	0,21	13.621	2,69	145.175	54
Çal	3	19.259	4.450	0,23	6.420	2,39	384.527	22
Çameli	3	18.256	11.000	0,6	6.085	2,5	122.322	25
Çardak	1	9.144	1.935	0,21	9.144	2,7	96.695	38
Çivril	9	60.429	14.000	0,23	6.714	2,99	510.780	41
Güney	2	9.975	3.900	0,39	4.988	2,49	159.185	19
Honaz	8	33.184	9.000	0,27	4.148	3,18	130.460	66
Kale	2	20.393	8.500	0,41	10.197	2,86	135.513	38
Merkezefendi	29	302.213	116779	0,38	10.421	3,08	39.551	104
Pamukkale	34	344.065	143.989	0,41	10.120	2,86	285.533	421
Sarayköy	2	30.768	8.300	0,26	15.384	2,92	152.092	65
Serinhisar	4	14.430	11.501	0,79	3.608	2,99	59.357	53
Tavas	7	43.845	11.652	0,26	6.264	2,67	471.956	26

Pazar yeri sayısı ile belirlenen bağımsız değişkenler arasındaki ilişkinin regresyon modelinin istatistik sonuçları verilmiştir (Tablo 9).

Tablo 9. Denizli ili regresyon istatistikleri tablosu

Bağımlı Değişken Pazar Yeri Sayısı			
R^2	**0,801142141**		
Bağımsız Değişkenler	Katsayı	Standart Hata	**t stat**
Ortalama Hanehalkı Büyüklüğü	0,544285952	0,762308407	0,713997047
Tarım Alanı	9,91654E-07	8,15614E-06	0,121583656
Nüfus Yoğunluğu	0,082698154	0,01428974	**5,787240035**

Model sonucuna göre nüfus yoğunluğu arttıkça pazar yeri sayısının arttığı, nüfus yoğunluğu azaldıkça pazar yeri sayısının azaldığı tespit edilmiştir.

4. TARTIŞMA VE SONUÇLAR

İzmir ve Denizli illeri sanayi ve ticaretin en yoğun olduğu kentlerdir. İzmir ili ticari araç yük dinamizmi, lojistik faaliyetlerin kümelenmesi ve sosyo-ekonomik özellikler dikkate alınarak üç ana çekirdek bölgeye ayrılmıştır. İzmir ilinde ortalama 19.000 kişi için bir pazar kurulurken Denizli ilinde haftanın yedi günü ortalama 7.414 kişi için bir pazar kurulmaktadır. İzmir ilinde 2. ve 3. Çekirdekte kişi başına ortalama 0.11 m^2 pazar alanı düşerken kentsel alanda kişi başına ortalama 0.04 m^2 pazar alanı düşmektedir. Denizli ilinde kişi başına ortalama 0.36 m^2 pazar alanı düşmektedir. İzmir ilinde pazar başına düşen kişi sayısı en fazla Bergama ilçesinde Denizli ilinde pazar başına düşen kişi sayısı en fazla Sarayköy ilçesinde en az Babadağ ilçesindedir. İzmir ilinde kişi başına düşen pazar alanı en fazla Bergama ve Seferihisar ilçelerinde Denizli ilinde ise en fazla Serinhisar en az Beyağaç ilçelerindedir. İzmir ilinde 2. çekirdekte Menderes 3. çekirdekte Kınık, Kiraz ve Tire ilçelerinde semt ve üretici pazarlarının sayısının arttırılması önerilmektedir. Denizli ilinde ise Acıpayam, Buldan, Çardak ve Sarayköy ilçelerinde pazar yeri sayılarının ve alanlarının arttırılması önerilmektedir. İlçelerde kaç tane pazar yeri olması gerektiği ilçelere ait birçok konu ile ilgilidir. Bu kapsamda İzmir ve Denizli ili ilçeleri için kişi başına düşen pazar alanı büyüklüğü ve pazar başına düşen kişi sayıları hesaplanarak yapılan çoklu regresyon analizi, sosyo-ekonomik ve demografik değişkenler kapsamında yeniden değerlendirilmiştir. Modelde her iki il ve ilçeleri için de bağımlı değişken olarak pazar yeri sayıları ***(Y_1)***, bağımsız değişkenler ortalama hanehalkı

büyüklüğü ***(X_1)***, tarım alanı ***(X_2)***, nüfus yoğunluğu ***(X_3)*** olarak belirlenmiştir. Model sonucuna göre her iki ilin ilçelerindeki "Pazar Alanı" sayıları, nüfus yoğunluğu ile ilişkilidir.

KAYNAKLAR

Akçi, Y. (2015). Alternatif Alışveriş Mekanı Olan Geleneksel Semt Pazarlarının Yapısı, İşleyişi ve Sorunlarının İncelenmesi (Adıyaman Örneği). Akademik Sosyal Araştırmalar Dergisi. 229-247.

Aksoy, Y. (2009). Pazar Yerlerinin Şehir Planlaması Standart ve İlkeleri Yönünden İncelenmesi: İstanbul İli Bakırköy İlçesi Örneği. Çukurova Üniversitesi Sosyal Bilimler Enstitüsü Dergisi.

Berkmen, H. (1991). İstanbul'da Semt Pazarları Üzerine Bir Araştırma (Beşiktaş, Kadıköy, Fatih Pazarları). Yüksek Lisans Tezi. İTÜ Fen Bilimleri Enstitüsü.

Cezar, M. (1985). Tipik Yapılarıyla Osmanlı Şehirciliğinde Çarşı ve Klasik Dönem İmar Sistemi. İstanbul: Milli Eğitim Yayın Evi.

Eroğlu, G. (1976). Kurtuluş Semt Pazarı Araştırması. Bitirme Tezi. İTÜ Mimarlık Fakültesi.

Kılınçarslan, T. (2012). Kentsel Ulaşım (Ulaşım Sistemi-Toplu Taşım-Planlama-Politikalar). Ninova Yayıncılık.
T.C. Denizli Valiliği (2022). Coğrafi Konum. Erişim Adresi: http://www.denizli.gov.tr/cografi-konu.

Tunçel, H. (2003). Anadolu Şehirlerinde Semt Pazarları: Elazığ Örneği. Journal of Social Science. 49.

Tunçel, H. (2006). Türkiye'nin Kırsal Pazar Bölgeleri. Ankara: Ankara Üniversitesi IV. Ulusal Coğrafya (Avrupa Birliği Sürecindeki Türkiye'de Bölgesel Farklılıklar) Sempozyumu (25-26 Mayıs 2006) Ankara.

Tunçel, H. (2018). Türkiye'deki Periyodik Pazarların Sınıflandırılması. TÜCAUM 30. Yıl Uluslararası Coğrafya Sempozyumu. Bilecik Şeyh Edebali Üniversitesi. Fen Edebiyat Fakültesi. Coğrafya Bölümü.

Development of Gas-Cooled Modular Reactor Based Helium Gas Turbine with Bottoming Transcritical CO_2 Rankine Cycle and Hydrogen Production

Gamze Soyturk[1], Onder Kizilkan*[1], Shoaib Khanmohammadi[2]

Abstract: The development of a gas-cooled modular reactor (GCMR) based on a helium gas turbine with a bottoming transcritical CO_2 Rankine cycle and hydrogen production represents a significant advancement in the field of nuclear energy. The system designed in this study combines multiple technologies to increase energy conversion efficiency and produce clean hydrogen, a versatile energy carrier. The use of helium as a coolant in the GCMR offers several advantages, including its excellent heat transfer properties, chemical inertness, and ability to operate at high temperatures. These characteristics enable efficient heat extraction from the reactor core, minimize the likelihood of corrosion, and increase thermal efficiencies and power output. The integration of a bottoming transcritical CO_2 Rankine cycle with the helium gas turbine is a key feature of this design. By utilizing waste heat from the gas turbine, the system generates additional power through the CO_2 Rankine cycle, thereby maximizing energy conversion efficiency and resource utilization. Furthermore, the system incorporates a hydrogen production module, allowing to produce clean hydrogen as a byproduct of the nuclear energy production process. Hydrogen is a versatile energy carrier that can be used for various applications, contributing to the sustainability of the system and offering opportunities for transportation, industry, and energy storage. According to the results of the analysis, the highest exergy destruction is in the reactor core with 91282 kW. HE PEM has the lowest exergy destruction among system components, with 3.56 kW. In addition, this study includes parametric studies to investigate the effect of helium exit temperature and pressure ratio on system performance.

Keywords: Gas-Cooled Modular Reactor Based Helium Gas, transcritical CO_2 Rankine Cycle, hydrogen Production, energy, exergy

[1]**Address:** Isparta University of Applied Sciences, Technology Faculty, Department of Mechanical Engineering, Isparta/Türkiye
[2]**Address:** [2]Department of Mechanical Engineering, Kermanshah University of Technology, Kermanshah, Iran

***Corresponding author**: onderkizilkan@isparta.edu.tr

1. INTRODUCTION

The development of advanced nuclear power technologies holds great potential for addressing global energy challenges while minimizing environmental impact. One promising avenue of research is the integration of Gas-Cooled Modular Reactors (GCMRs) with innovative power conversion systems, such as helium gas turbines and transcritical carbon dioxide (CO_2) Rankine cycles, along with concurrent hydrogen production. This integrated approach aims to enhance overall system efficiency, increase power generation capabilities, and enable the production of clean hydrogen as a versatile energy carrier (Wang et al., 2022). GCMRs utilize helium as the coolant, providing advantages over traditional water-cooled reactors, including higher thermal efficiency, improved safety features, and reduced water consumption. The utilization of helium allows for efficient heat extraction from the nuclear reactor core, enabling the transfer of heat to the power conversion systems (Wang and Dai, 2016). The integration of a helium gas turbine with a bottoming transcritical CO_2 Rankine cycle within the GCMR system is a significant development in advanced nuclear power technology. The helium gas turbine serves as the primary power conversion system, harnessing the energy from the hot helium to drive turbine blades and generate electricity. The utilization of helium, with its exceptional heat transfer properties, enables higher operating temperatures, thereby enhancing the overall thermodynamic efficiency of the system. To further optimize energy extraction, a bottoming transcritical CO_2 Rankine cycle is integrated into the system. This secondary power conversion cycle captures waste heat from the helium gas turbine and utilizes CO_2 as the working fluid. The transcritical CO_2 Rankine cycle operates at high pressures and temperatures, facilitating efficient power generation by effectively utilizing the available heat energy. In addition to improved energy efficiency, this integrated system enables concurrent hydrogen production. Excess heat from the GCMR can be utilized in a thermochemical water-splitting process to produce hydrogen. Hydrogen is a clean energy carrier with various applications, including fuel cells, transportation, and industrial processes. The development of a Gas-Cooled Modular Reactor Based Helium Gas Turbine with a bottoming

transcritical CO_2 Rankine cycle and hydrogen production represents a significant advancement in nuclear power technology. This integrated system offers the potential for higher thermal efficiencies, reduced greenhouse gas emissions, and the production of a clean, versatile fuel source (Labar et al., 2004). Dardoura et al. (2007) presented the successive stages that led to the development of physical and mathematical models enabling the calculation of desalination costs of the gas turbine-modular helium-cooled reactor and the pebble bed modular reactor providing free thermal energy. El-Genk and Tournier (2008) investigated the attributes and limitations of noble gases and binary mixtures as potential working fluids for gas-cooled nuclear power plants with closed Brayton cycles. They compared the heat transfer coefficient and pressure losses of helium and other noble gases and binary mixtures at typical operating conditions in commercial power plants (7.0 MPa and 400–1200 K) for the same molecular flow rate and geometry. Tournier and El-Genk (2008) conducted a review of the properties of the noble gases helium, neon, argon, krypton, and xenon and their binary mixtures at pressures from 0.1 to 20 MPa and temperatures up to 1400 K. An extensive database of experimental measurements is compiled and used to develop semi-empirical properties correlations. Zhao and Peterson (2008) predicted the performance of the helium Brayton cycles with multiple reheat and intercooling states for SFRs with reactor outlet temperatures in the range of 510–650 °C. The resulting thermal efficiencies range from 39% to 47%, which is comparable with that of supercritical recompression CO_2 cycles. The study indicates that the multiple reheat helium cycle is the preferred choice over the sCO_2 cycle for sodium-cooled fast reactors. In this study, it is aimed to investigate the performance of the gas-cooled modular reactor-based system that integrates a helium gas turbine with a bottoming transcritical CO_2 Rankine cycle while concurrently facilitating hydrogen production. At the same time, parametric studies were carried out to investigate the effects of helium temperature and pressure ratio at the reactor outlet on the cycle performance.

2. SYSTEM DESCRIPTION

Figure 1 shows the schematic representation of the integrated system consisting of a gas-cooled modular reactor, a helium gas turbine, a transcritical CO_2 Rankine cycle, and a hydrogen generation system. The GCMR serves as the core component of the system. It utilizes helium as the coolant, providing advantages such as higher thermal efficiency, improved safety features, and reduced water consumption. The GCMR produces high-temperature helium gas because of nuclear fission, which is used as a heat source for subsequent power conversion processes. The helium gas turbine is the primary power conversion system in the integrated setup. It utilizes the high-temperature helium gas from the GCMR to drive the turbine blades and generate electricity. The gas turbine operates based on the principles of thermodynamics, extracting energy from the hot helium, and converting it into mechanical energy, which is then transformed into electrical energy through a generator.

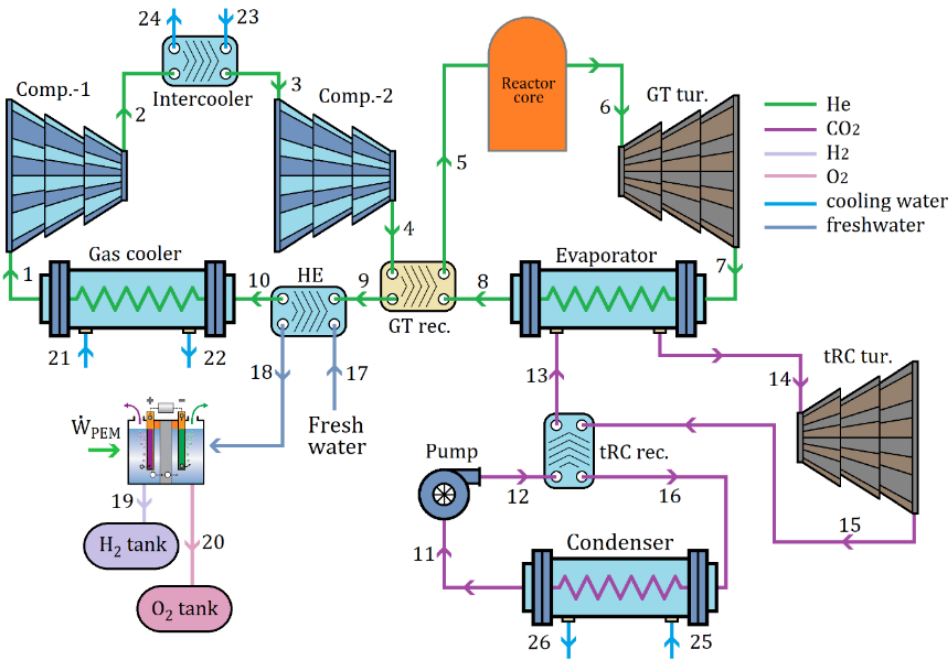

Figure 1. Schematic diagram of a gas-cooled modular reactor combined with the TRC cycle and hydrogen production.

To further optimize the system's energy extraction, a bottoming transcritical CO_2 Rankine cycle is incorporated. This secondary power conversion cycle captures waste heat from the helium gas turbine. The transcritical CO_2 Rankine cycle

operates at high pressures and temperatures, making efficient use of the waste heat by utilizing CO_2 as the working fluid. The CO_2 expands through a turbine, driving a generator to produce additional electricity. Concurrent with power generation, the system facilitates hydrogen production. Excess heat from the GCMR, which is not utilized by the gas turbine or the bottoming transcritical CO_2 Rankine cycle, is diverted to a thermochemical water-splitting process. This process utilizes the excess heat to separate water molecules into hydrogen and oxygen, generating clean hydrogen as a valuable byproduct. The hydrogen can be captured, stored, and utilized for various applications, such as fuel cells, transportation, and industrial processes. Overall, the integrated system operates in a closed-loop manner, with heat being extracted from the GCMR using helium as the coolant. The high-temperature helium is used to drive the gas turbine, generating electricity. Waste heat from the gas turbine is further harnessed through the bottoming transcritical CO_2 Rankine cycle, maximizing the energy extraction from the system. Concurrently, excess heat is utilized in a thermochemical process for hydrogen production, enhancing the overall efficiency and sustainability of the system.

3. METHODOLOGY

In this subchapter, a detailed definition of the thermodynamic methodology utilized in this paper is introduced. Energy and exergy analyses are performed using the Engineering Equation Software (EES) (Klein, 2022) program for the performance evaluation of the system. In this paper, the thermodynamic analysis is made under the following assumptions:

- The steady-state and steady-flow conditions are chosen for all system elements.
- The energetic change for kinetic and potential energies is neglected.
- The heat losses from pumps and turbine are neglected.
- The pressure drops through the pipelines and heat exchangers are neglected.
- The reference state properties are 20°C and 101.325 kPa.

The mass balance equation for steady-state and steady-flow processes can be written as (Cengel and Boles, 2006):

$$\sum \dot{m}_{in} = \sum \dot{m}_{out} \tag{1}$$

Here, $\dot{m}$ is the mass flow rate, and the subscript in denotes inlet and out denotes outlet. The energy balance is expressed as:

$$\dot{Q} + \sum \dot{m}_{in} h_{in} = \dot{W} + \sum \dot{m}_{out} h_{out} \tag{2}$$

where $\dot{Q}$ is the heat transfer rate, $\dot{W}$ is the work, and h is the specific enthalpy. For the exergy analysis, the balance equation is defined as (Dincer and Rosen, 2007):

$$\dot{E}x_Q - \dot{E}x_W = \sum \dot{E}x_{in} - \sum \dot{E}x_{out} + T_0 \dot{S}_{gen} \tag{3}$$

where the first and the second terms are exergy of heat and work, respectively, $\dot{E}x$ is the rate of flow exergy, T_0 is the reference state temperature, and the last term is entropy generation. In the above equation, each term is defined as follows:

$$\dot{E}x_{dest} = T_0 \dot{S}_{gen} \tag{4}$$

$$\dot{E}x_Q = \dot{Q}\left(\frac{T - T_0}{T}\right) \tag{5}$$

$$\dot{E}x_W = \dot{W} \tag{6}$$

$$\dot{E}x_W = \dot{m}\, ex \tag{7}$$

In Equation (7), ex is the specific flow exergy and can be calculated using the equation below:

$$ex = (h - h_0) - T_0(s - s_0) \tag{8}$$

3. RESULTS

In this study, it is purposed to examine the performance of the gas-cooled modular reactor-based system that integrates a helium gas turbine with a bottoming transcritical CO_2 Rankine cycle while concurrently facilitating hydrogen production. At the same time, parametric studies were carried out to examine the effects of helium temperature and pressure ratio at the reactor outlet on the cycle performance. Using the balance equations and under the assumptions given above, the analyses are performed by EES software. The assumed operational parameters of the proposed system are tabulated in Table 1.

Table 1. The assumed operational parameters

Parameter	Value
Reference temperature	25 °C
Reference pressure	100 kPa
Thermal power from the reactor	600 MW (Gauthier et al., 2006)
Gas cycle turbine inlet temperature	750 °C (Wang et al., 2002)
Gas cycle turbine inlet pressure	8000 kPa (Wang et al., 2002)
Gas cycle compressor inlet temperature	30 °C (Genk and Tournier, 2008)
Gas cycle compressor inlet pressure	2500 kPa
Gas cycle recuperator efficiency	0.9
tRC pump inlet temperature	23.5 °C
tRC pressure ratio	1.45
tRC turbine isentropic efficiency	0.90
tRC pump isentropic efficiency	0.85
tRC recuperator efficiency	0.85
PEM temperature	80 °C

Figure 2 shows the exergy destruction rate of the components that make up the system. The green color on the right side of the graph shows the exergy destruction rate in the reactor core, and the blue color on the left shows the exergy destruction rate on the other components of the system. As seen in the figure, the highest exergy destruction is in the reactor core with 91282 kW. The reactor core is followed by the evaporator, gas cooler, gas turbine intercooler, and gas turbine, respectively. The lowest exergy destruction among the system components is in the HE PEM, with 3.56 kW.

Parametric studies have been carried out to examine the effects of helium temperature at the reactor exit on the system performance. Figure 3 shows the effect of helium temperature at the reactor outlet on total power generation and energy efficiency. As seen in the figure, when the helium temperature at the reactor outlet is increased from 700 °C to 900 °C, the total power generation and overall energy efficiency increase.

The effect of helium temperature at the reactor outlet on total exergy destruction and overall energy efficiency is shown in Figure 4. It is quite clear that as the helium temperature at the reactor exit increases, the exergy destruction rate decreases; on the contrary, the exergy efficiency increases.

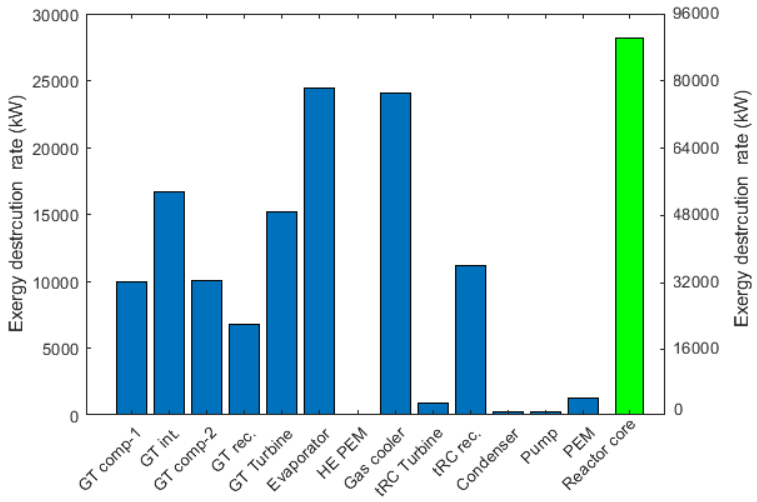

Figure 2. Total exergy destruction rates of system components

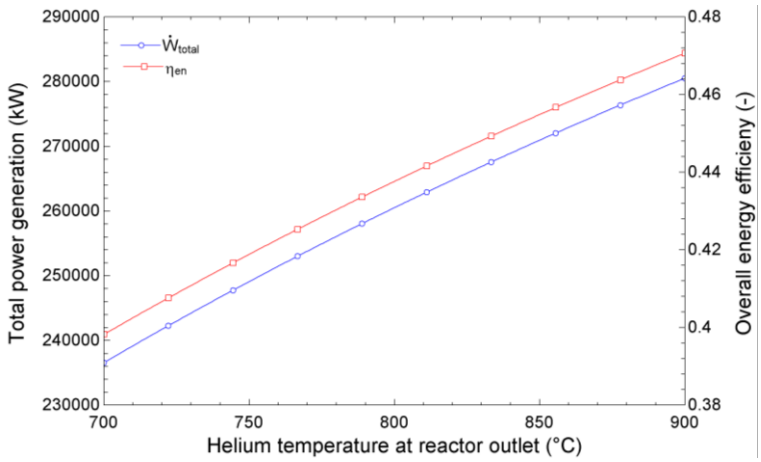

Figure 3. Effect of helium temperature at the reactor outlet on total power generation and overall energy efficiency

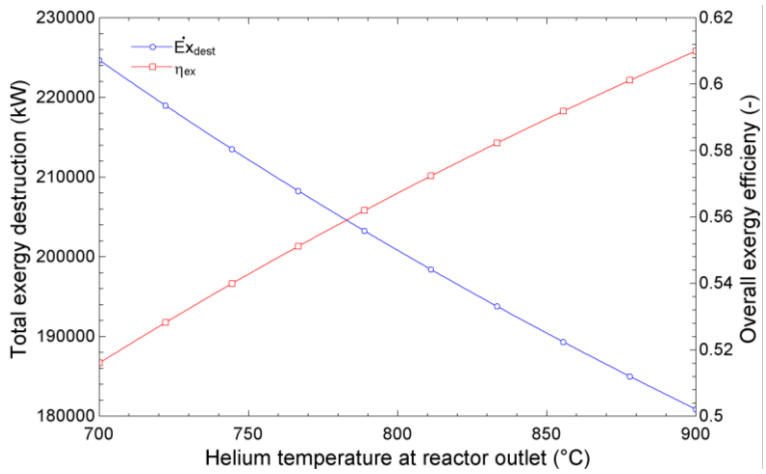

Figure 4. Effect of helium temperature at the reactor outlet on total exergy destruction and overall exergy efficiency

The effect of helium temperature at the reactor outlet on hydrogen production and tRC net power generation is shown in Figure 5. As seen in the figure, as the helium temperature at the reactor outlet increases, hydrogen production and the net power output of the tRC decrease. As expected, hydrogen production decreases as the power generation of the transcritical Rankine cycle decreases.

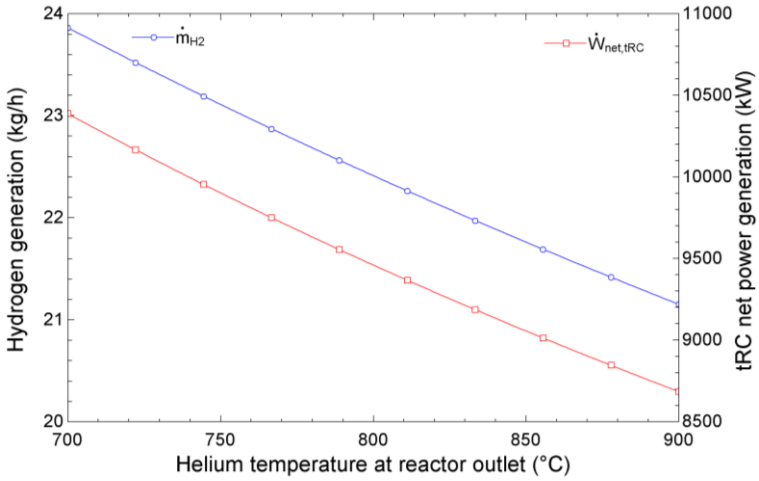

Figure 5. Effect of helium temperature at the reactor outlet on hydrogen generation and tRC net power generation

The effect of the pressure ratio on overall power generation and overall energy efficiency is shown in Figure 6. Total power generation and efficiency increase with turbine inlet temperature and show a maximum value relative to the pressure ratio at any temperature. This maximum value shifts to higher pressure ratios when higher turbine inlet temperatures are used. Increasing temperature increases the average temperature of heat reception of the cycle, which increases the corresponding Carnot and, as a result, our cycle efficiency. Increasing temperature also increases the enthalpy difference across the turbine, allowing more power to be produced and consequently achieving higher efficiencies for all the cycles. Moreover, increasing temperature results in a higher turbine inlet temperature and pressure in the tRC, leading to produce more power in the tRC turbine.

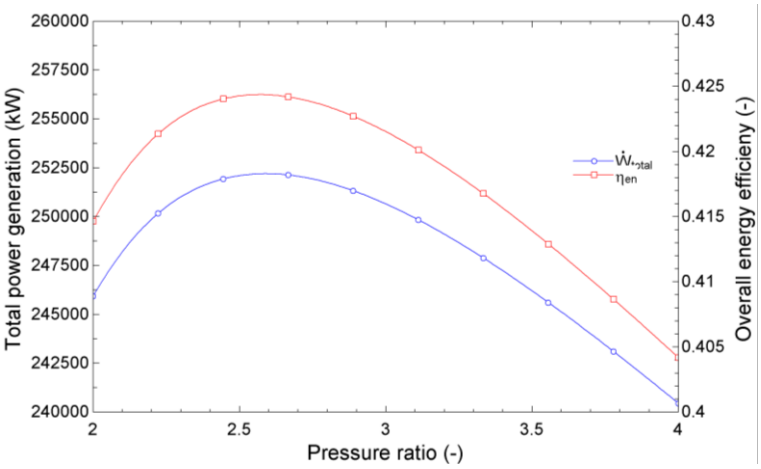

Figure 6. Effect of pressure ratio on total power generation and overall energy efficiency

Figure 7 shows the effect of the pressure ratio on total exergy destruction and overall exergy efficiency. It is seen that the energy efficiency seen in Figure 6 and the increasing-decreasing trend of the exergy efficiency seen here are the same. Also, the effect of the pressure ratio on hydrogen production and tRC net power generation is shown in Figure 8. The hydrogen production and tRC net power generation decrease with the pressure ratio.

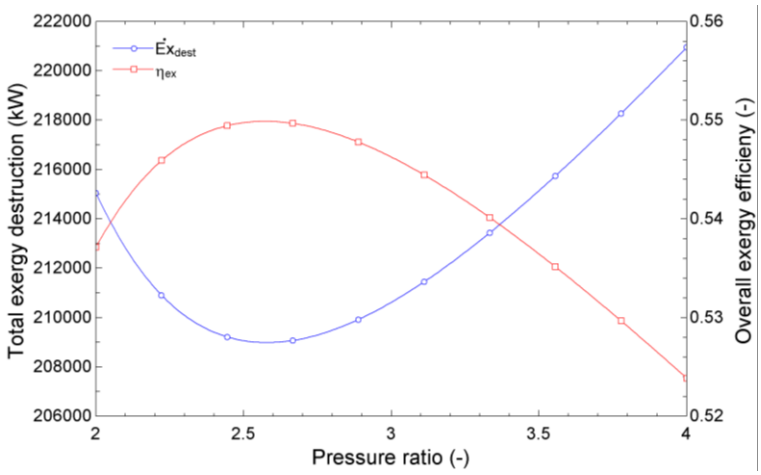

Figure 7. Effect of helium temperature at the reactor outlet on hydrogen generation and tRC net power generation

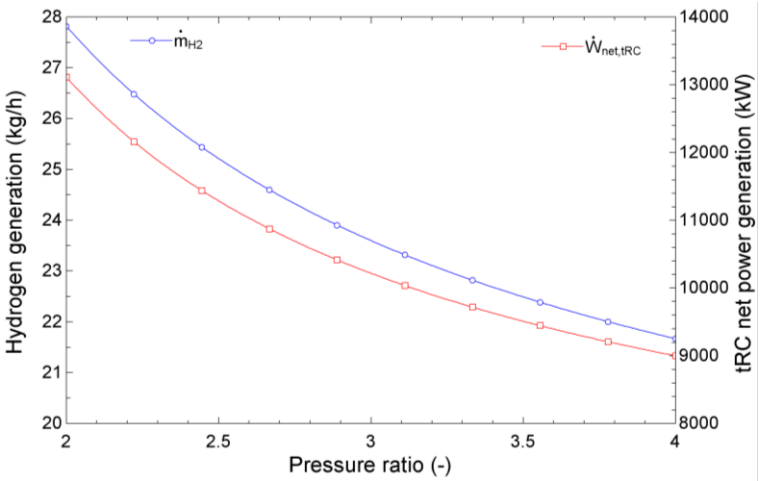

Figure 8. Effect of helium temperature at the reactor outlet on hydrogen generation and tRC net power generation

4. CONCLUSIONS

In this study, the performance of a gas-cooled modular reactor-based system that facilitates hydrogen production while integrating a helium gas turbine with the bottoming out transcritical CO_2 Rankine cycle is investigated. At the same time, parametric studies were carried out to investigate the effects of helium temperature and pressure ratio at the reactor outlet on the cycle performance. According to the results of the analysis, a net power of 241679 kW was obtained from the gas turbine and 9902 kW from the tRC cycle. In addition, the amount of hydrogen produced was 23.11 kg/h, and the amount of O_2 was calculated as 183.4 kg/h. The total exergy destruction rate in the system is 212199 kW, the overall energy efficiency of the system is 41.8%, and the overall exergy efficiency is 54%. At the same time, in this study, parametric studies were carried out to investigate the effects of helium temperature and pressure ratio at the reactor outlet on the cycle performance.

In conclusion, the development of a GCMR based on a helium gas turbine with a bottoming transcritical CO_2 Rankine cycle and hydrogen production holds significant promise for advancing the field of nuclear energy. This innovative approach combines multiple technologies to enhance the overall efficiency of the system while enabling the production of hydrogen, a clean and - versatile energy carrier. The use of helium as a coolant in the GCMR offers several advantages. Helium has excellent heat transfer properties, allowing for efficient heat extraction from the reactor core. It is also chemically inert, reducing the likelihood of corrosion or chemical reactions within the system. Furthermore, helium operates at high temperatures, enabling higher thermal efficiencies and increased power output. The integration of a bottoming transcritical CO_2 Rankine cycle in conjunction with the helium gas turbine is a key feature of this design. By utilizing the waste heat from the gas turbine, the system can generate additional power through the CO_2 Rankine cycle, thereby maximizing the overall energy conversion efficiency. This approach enhances the sustainability of the system by optimizing resource utilization and minimizing waste. Another significant benefit of this integrated system is the

production of hydrogen. Hydrogen is a clean and versatile energy carrier that can be used for various applications, including transportation, industry, and energy storage. By incorporating a hydrogen production module within the GCMR system, it becomes possible to generate hydrogen as a byproduct of the nuclear energy production process, further enhancing the system's economic viability and environmental sustainability. The development of a gas-cooled modular reactor based on a helium gas turbine with a bottoming transcritical CO_2 Rankine cycle and hydrogen production represents a crucial step towards the realization of advanced nuclear energy systems. This integrated approach offers a range of advantages, including high thermal efficiency, reliable and safe operation, reduced environmental impact, and the production of clean hydrogen. However, further research, development, and demonstration efforts are required to optimize and validate the technical and economic feasibility of this concept at a larger scale. With continued advancements in nuclear technology and a focus on sustainable energy solutions, the gas-cooled modular reactor with a bottoming transcritical CO_2 Rankine cycle and hydrogen production holds immense potential for transforming the energy landscape and driving us toward a greener and more sustainable future.

REFERENCES

Cengel, Y.A., Boles, M.A. (2006). Thermodynamics: an engineering approach. McGraw-Hill, New York.

Dincer, I., Rosen, M.A. (2007). Exergy: Energy, Environment and Sustainable Development. Elsevier Science.

Dardoura, S., Nisan, S., Charbit, F. (2007). Utilization of Waste Heat from GT-MHR and PBMR Reactors for Nuclear Desalination. Desalination. 205, 254–268.

El-Genk, M.S., Tournier, J.M. (2008). On the Use of Noble Gases and Binary Mixtures as Reactor Coolants and CBC Working Fluids. Energy Conversion and Management. 49, 1882–1891.

Gauthier, J.C., Brinkmann G., Copsey B., Lecomte, M. (2006). ANTARES: The HTR/VHTR project at Framatome ANP. Nuclear Engineering and Design. 236, 526–533

Klein, S.A. (2022) Engineering Equation Solver (EES) V11, F-Chart Software, Madison, USA. http://www.fchart.com

Labar, M., Shenoy, A.S., Simon, W.A., Campbell, E.M. (2004). The Gas-Turbine Modular Helium Reactor. Nuclear Energy. 43(3), 165-175.

Tournier, J.M., El-Genk, M.S. (2008). Properties of Noble Gases and Binary Mixtures for Closed Brayton Cycle Applications. Energy Conversion and Management. 49, 469–492.

Zhao, H., Peterson, P.F. (2008). Multiple Reheat Helium Brayton Cycles for Sodium Cooled Fast Reactors. Nuclear Engineering and Design. 238, 1535–1546.

Wang, Q., Liu, C., Luo, R., Li, D., Juan, R.M. (2022). Thermodynamic Analysis and Optimization of the Combined Supercritical Carbon Dioxide Brayton Cycle and Organic Rankine Cycle-Based Nuclear Hydrogen Production System. International Journal of Energy Research. 46, 832-859.

Wang C, Ballinger RG, Stahle PW, Demetri E, Koronowski M, (2002). Design of a power conversion system for an indirect cycle, helium cooled pebble bed reactor system. In: Proceedings of first international topical meeting on HTR technology (HTR2002), international atomic energy agency, 22–24 April 2002, Vienna, Austria, Petten, Netherlands; 2002.

Wang, X., Dai, Y. (2016). An Exergoeconomic Assessment of Waste Heat Recovery from a Gas Turbine-Modular Helium Reactor Using Two Transcritical CO_2 Cycles. Energy Conversion and Management. 126, 561-572.

Dynamic Modeling of a Photovoltaic/Thermal (PV/T) Collector for Isparta

Gamze Soyturk[1], Onder Kizilkan[*1]

Abstract: Although the performance of photovoltaic/thermal (PV/T) panels has been studied both computationally and experimentally for some time, the thermal models created in previous research were mostly steady-state models to predict annual efficiencies. In this study, solar thermal collector and photovoltaic (PV) cells are combined to form a PV/T collector, and water-ethylene glycol is used as a coolant to lower the temperature of the PV panels. The aim of this study is to analyze a water-ethylene glycol-based PV/T collector in Isparta conditions numerically. Time-dependent dynamic analyzes were performed using the MATLAB software program. Research has also been conducted on how the generated electrical energy and fluid output and the temperature of the PV/T surface change over time.

Keywords: Photovoltaic/Thermal collector, solar energy, thermal efficiency, electrical efficiency, ethylene glycol

[1]**Address:** Isparta University of Applied Sciences, Technology Faculty, Department of Mechanical Engineering, Isparta/Türkiye

***Corresponding author**: onderkizilkan@isparta.edu.tr

1. INTRODUCTION

The growing demand for renewable energy sources has led to extensive research and development in the field of photovoltaic/thermal (PV/T) collectors. These innovative devices combine the benefits of both solar photovoltaic and solar thermal technologies, enabling simultaneous electricity generation and heat production. The dynamic modeling of PV/T collectors plays a crucial role in optimizing their performance and assessing their feasibility for specific locations. The hybrid photovoltaic/thermal (PV/T) solar collector integrates a PV module with a solar thermal collector, simultaneously producing electric and thermal energy. In this way, a reduction of the PV cell temperature, which is beneficial for the electric conversion efficiency, and a simultaneous increase of coolant (air or water) temperature are achieved. Although the electrical and the thermal performance of PV/T collectors are lower than the ones of separate PV and conventional thermal collectors, the converted energy per unit surface area is usually than the one produced by one PV panel and one thermal collector next to each other and, therefore, the PV/T technology results strongly attractive for applications where the surface area availability is a constraint (Zondag and Vries, 1999). The development of both thermal and electric models and their coupling are necessary to predict the performance of PV/T solar collectors accurately. Different approaches are found in the scientific literature leading to various models, from simple to complex. Zondag et al. (2002) developed and validated a 3D dynamical model and three steady-state (3D, 2D, and 1D) models of a double-glazed PV/T collector. The electric modeling was based on the adoption of the power coefficient to correct the power production at different temperatures. Numerical data agreed with experimental ones within 5%. Chow (2003) developed a dynamic model for a single-glazed flat plate PV/T collector based on the control-volume approach. The influence of cell temperature on collector power production was accounted for using the typical power coefficient correction. The model was later updated and validated by Bhattarai et al. (2012) through a comparison with experimental data, finding that the maximum difference between the measured and predicted values was 1.17 K for water temperature at the collector outlet, 2% for collector thermal efficiency and 0.2% for collector electrical efficiency. Amrizal et al. (2013) developed a dynamic model of a flat plate PV/T collector based on the equation reported in the report coupled with the single-diode photovoltaic model. The model required four parameters to simulate the dynamic operation of the PV/T collector calibrated against experimental data. Once calibrated, the model accuracy was satisfactory. Touafek et al. (2014) developed a dynamic model of a sheet-and-tube PV/T collector, assuming an average value of the temperature for each layer and using the power coefficient relation between cell temperature and conversion efficiency to account for its influence on power production. Khelifa et al. (2014) developed and validated a dynamic model of a sheet-and-tube PV/T collector using a 2D control-volume approach. The influence of cell temperature on cell power production was accounted using the power coefficient relation. The model was validated using in-house experimental results, finding that the root mean square of percentage deviations is equal to 2.66% for water outlet temperature and 16.17% for useful thermal energy. Haurant et al. (2015) developed and validated a 3D dynamic model for a sheet-and-tube PV/T collector. The Shockley single-diode approximation to describe the PV cell was implemented. The model was validated under steady-

state and transient conditions, showing a tendency to overestimate the collector power production with a maximum difference equal to 1.7 W in steady-state conditions and larger values in transient ones. Moreover, the fluid temperature at the collector outlet was predicted within 0.2 K and 2 K during steady and transient conditions, respectively. Aste et al. (2015) developed a dynamic model of an innovative roll bond PV/T collector, assuming a uniform temperature in each layer and using the power coefficient to correct the PV cell conversion efficiency. The model was validated against in-house experimental results finding a root mean square percentage deviation of around 15% for the power production and around 4–5% for the water temperatures. Later this model was improved to simulate a commercial roll-bond PV/T collector (2016). After a calibration of the model parameter using a best-fitting procedure, an agreement between the measured and model collector daily electrical energy and the water temperatures within 2.52% and within 0.27 K was found, respectively. This paper focuses on the dynamic modeling of a PV/T collector specifically designed for the city of Isparta. Isparta, located in southwestern Turkey, experiences a Mediterranean climate characterized by abundant sunshine throughout the year. Such favorable weather conditions make Isparta an ideal location for harnessing solar energy and evaluating the efficiency of PV/T collectors. Dynamic modeling involves the simulation and analysis of various factors that influence the performance of PV/T collectors over time. These factors include solar radiation, ambient temperature, wind speed, and system design parameters. By employing mathematical models and computer simulations, researchers can accurately predict the electrical and thermal outputs of PV/T collectors under varying weather conditions. The outcomes of this dynamic modeling study provide valuable insights into the energy generation potential and efficiency of PV/T collectors in Isparta. By accurately predicting the system's performance, researchers and engineers can optimize the design and operation of PV/T collectors, leading to improved energy utilization and cost-effectiveness.

2. MATHEMATICAL MODELING

In photovoltaic thermal systems, some solar irradiation is transformed into electrical energy, while a large part of it creates a thermal load on the material. This thermal load can reduce the collector's efficiency and damage the material's structure. PV/T systems have been designed to minimize this thermal load created by solar irradiation that cannot be converted into electrical energy in the collector. These hybrid systems can simultaneously provide hot air or domestic water and electrical power. The most widely used PV/T type is the system where hot water is provided. While these systems generate electrical energy with the modules on their upper surfaces, they store the domestic water with the copper plates on the back of the collector. Thanks to the working fluid in the collector, the temperature of the cell is diminished, and the electrical energy efficiency is raised. The schematic representation of the PV/T panel is shown in Figure 1. As seen from the figure, the PV/T collector comprises a set of PV panels, a glass cover, pipes, an absorber surface, and insulation. In Figure 1, the thermal resistance network of the PV/T panel is shown.

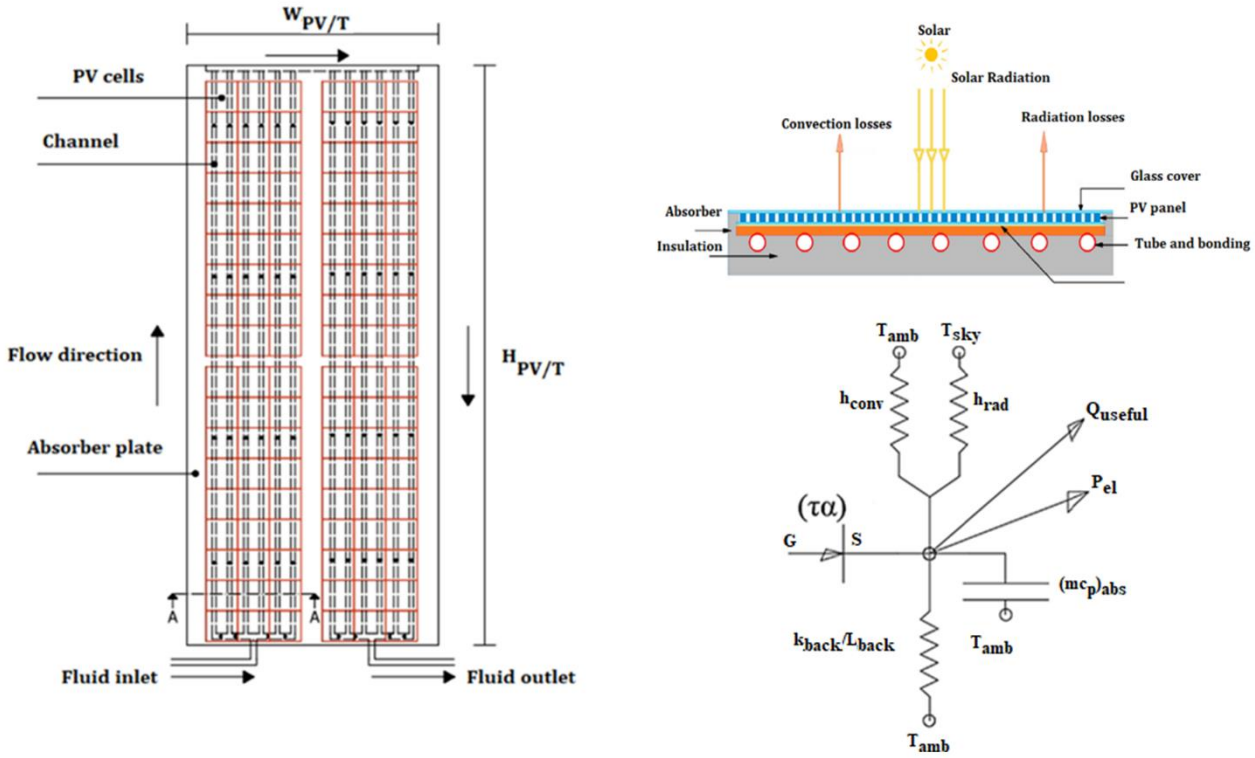

Figure 1. PV/T collector schematic and thermal resistance network

The following assumptions were considered in the PV/T mathematical modeling (Sakellariou and Axaopoulos, 2018):

1) PV/T panels are connected in series.
2) Air gaps between the glass cover and the PV cells are neglected.
3) PV/T is considered as a single layer, and heat transfer between layers is neglected.
4) PV/T mass and specific heat capacity are neglected.
5) Heat transfer by natural convection is neglected, and heat losses by wind are only considered for the upper surface of the collector.
6) The heat losses from the edge surfaces of the PV/T panel are neglected.
7) The thermal capacities of the PV/T components are neglected. Only the thermal capacities of the heat transfer fluid are considered.

The properties of the PV/T panel used in the mathematical modeling are given in Table 1.

Table 1. Properties of PV/T panel working with ethylene glycol –water mixture (Sakellariou and Axaopoulos, 2018):

Basic data		Value
PV/T length	L(m)	1.649
PV/T width	W (m)	0.992
PV/T total area	$A_{PV/T}$ (m^2)	1.635
PV/T cell area	A_{cell} (m^2)	1.417
PV/T mass	$m_{PV/T}$ (kg)	3.75
PV/T specific heat	$Cp_{PV/T}$ (J/kgK)	8081
PV/T conductivity	$k_{PV/T}$ (W/mK)	187.1
PV/T thickness	$\lambda_{PV/T}$ (m)	0.0065
Absorptivity coefficient	α	0.85
Emissivity coefficient	ε	0.88
Transmissivity coefficient	τ	0.9
Packing factor	PF	0.9
Electrical data		
Cell type		p-Si
Reference electrical efficiency	η_{ref} (%)	0.143
Temperature power coefficient	β (1/K)	0.0046
Thermal data		
Mass flow rate	$\dot{m}_{HTF}$ (kg/s)	0.02
Number of tubes	n_{tube}	10
External tube diameter	D (m)	0.008
Internal tube diameter	D_i (m)	0.006
Distance between tubes	w (m)	0.099
Insulation thickness	λ_{back} (m)	0.03
Insulation conductivity	k_{back} (W/mK)	0.04
Boundary conductivity	k_{bond} (W/mK)	250
Boundary width	b_{bond} (m)	0.01
Boundary thickness	λ_{bond} (m)	0.05
Boundary heat transfer coefficient	h_{ca} (W/m^2K)	30.3214

In this work, heat that had accumulated in various parts of the hybrid solar system was removed using ethylene glycol-water as a heat transfer fluid. 50% by weight ethylene glycol-water mixture has been shown to have a higher energy and exergy efficiency than pure ethylene glycol and a lower freezing point than pure ethylene glycol when used as the working fluid for PV/T. As a result, ethylene glycol-water mixture (50 percent by weight) was utilized as a working fluid that was appropriate for cold climates. Temperature-dependent thermophysical properties for ethylene glycol (50%) were formulated using curve-fit curves from the Engineering Equation Solver (EES) database. Required property values in the following equation:

$$y = a + bT + cT^2 + dT^3 + eT^4 + fT^5 + gT^6 \quad (1)$$

In the above equation, y is the thermophysical property (Cp, k, ρ, μ, Pr), and the coefficients a, b, c, d, e, f, and g are obtained for the temperature of T = 25°C and pressure of P = 101.325 kPa. Various thermophysical property coefficients can be defined for different temperature and pressure values. These coefficients are obtained from the real table value

with the help of curve-fitting methods. In determining the size of the linear regression error in curve fittings, the correlation coefficient 'R^2' is determined. An R^2 value close to 1 means that the fitted curve best expresses the data. Table 2 shows the equation coefficients of the thermophysical properties of the water-ethylene glycol mixture (50% by weight).

Table 2. Coefficients of the thermophysical properties in Equation (1)

	Cp (kj/kgK)	k (W/m^{2}K)	ρ (m^3/kg)	μ (kg/ms)	Pr
a	3202.88	0.37	1074.62	0	67.19
b	5.64	0.0006	-0.43	-0.0002	-2.48
c	-0.008	3.17×10^{-7}	-0.002	0.000009	0.081
d	-0.0003	-50	0.000006	-42	-0.0029
e	0	0	0	7.3×10^{-9}	0.00006
f	0	0	0	-80.3	-64.7
g	0	0	0	2.39×10^{-13}	1.98×10^{-9}

The heat transfer coefficient of the working fluid in the pipe by convection is calculated as follows:

$$h_f = \frac{Nuk}{D_i} \tag{2}$$

Here, h_f (W/m^{2}K) is the heat transfer coefficient of the fluid, and k (W/mK) is the thermal conductivity of the fluid. To calculate the h_f value of the working fluid, the Reynolds (Re) number must first be determined.

$$Re = \frac{\rho V D_i}{\mu} \tag{3}$$

where ρ (kg/m^3) is the density of the fluid, V (m/s) is the velocity of the fluid, D_i (m) is the inner diameter of the pipe, and μ (kg/ms) is the absolute viscosity. If Re<2500, laminar flow occurs, if Re≥2500, turbulent flow occurs in the pipe (Çengel and Ghajar, 2014).

L (m), the hydrodynamic inlet length, is expressed as the length from the pipe inlet where the shear stress (and, therefore, the friction factor) approaches the fully developed value by 2% pipe (Çengel and Ghajar, 2014). The hydrodynamic inlet lengths in laminar and turbulent flow are calculated as follows:

$$L_{laminar} = 0.05ReD \tag{4}$$

$$L_{turbulent} = 10D \tag{5}$$

$$x^* = \frac{L}{RePrD} \tag{6}$$

Here, Pr is the Prandtl number, and D (m) is the hydraulic diameter.

The Nusselt number for thermally developing laminar flow is determined by Equation (7) and Equation (8):

$$Nu = 1.953(x^*)^{-\frac{1}{3}} \qquad x^* \leq 0.03 \tag{7}$$

$$Nu = 4.364 + \frac{0.0722}{(x^*)^{-\frac{1}{3}}} \qquad x^* > 0.03 \tag{8}$$

In the case of turbulent flow, the Nusselt number can be determined by Equation (9) as pipe (Çengel and Ghajar, 2014):

$$Nu = \frac{\frac{f}{8}(Re-1000)Pr}{1+12.7\left(\frac{f}{8}\right)^{\frac{1}{2}}\left(Pr^{\frac{2}{3}}-1\right)} \tag{9}$$

Here f is the friction factor, and it is determined by Equation (10) (Kalagirou, 2015):

$$f = \frac{1}{(0.79\,ln(Re)-1.64)^2} \tag{10}$$

The total heat loss coefficient U_L (W/m^{2}K) in the collectors is calculated by Equation (11). Here, U_e (W/m^{2}K) heat losses from the side surfaces are disregarded, while the total heat loss from the collector is calculated with the sum of the heat losses from the upper and lower surfaces pipe (Kalagirou, 2015):

$$U_L = U_t + U_b \tag{11}$$

where U_t (W/m^{2}K) denotes the heat loss coefficient from the collector top surface, and U_b (W/m^{2}K) represents the loss coefficient from the collector back surface (Kalagirou, 2015):

$$U_t = h_{conv} + h_{rad} \tag{12}$$

Here, h_{conv} (W/m^{2}K) denotes the heat transfer coefficient with forced convection, and h_{rad} (W/m^{2}K) denotes the heat transfer coefficient with radiation (Kalagirou, 2015):

$$h_{conv} = 2.2V_{wind} + 8.3 \tag{13}$$

$$h_{rad} = \varepsilon\sigma\left(T_{PV/T}^2 + T_{sky}^2\right)\left(T_{PV/T} + T_{sky}\right) \tag{14}$$

$$T_{sky} = 0.0552T_{amb}^{1.5} \tag{15}$$

Here, V_{wind} (m/s) represents the average wind speed, $T_{PV/T}$ (K) means the average PV /T surface temperature, T_{sky} (K) represents the sky temperature, and T_{amb} (K) the ambient temperature (Kalagirou, 2015):

$$U_b = \frac{k_{back}}{\lambda_{back}} \tag{16}$$

Here, k_{back} (W/mK) represents the thermal conductivity of the back surface insulation material, and λ_{back} (m) refers to the thickness of the back surface insulation material.

A one-dimensional steady-state model was developed to study the thermal and electrical efficiency of PV/T systems, and Hottel-Whillier equations were employed in these calculations. The overall energy balance of the PV/T collector is calculated by Equation (17) (Sakellariou and Axaopoulos, 2018):

$$\dot{Q}_u = F_R\left(I(\alpha\tau)\left(A_{PV/T} - A_{cell}\eta_{el}\right)\right) - \left(A_{PV/T}U_L(T_{in} - T_{out})\right) \tag{17}$$

Here, $\dot{Q}_u$ (W) represents the useful heat supplied from the collector, I (W/m^2) solar radiation, $(\alpha\tau)$ absorbance-permeability coefficient, η_{el} collector electrical efficiency, $A_{PV/T}$ (m^2) collector surface area, A_{cell} (m^2) PV/T cell area, T_{in} (K) fluid inlet temperature.

The collector heat gains factor (F_R) is calculated by Equation (18) as follows (Kalagirou, 2015):

$$F_R = \frac{\dot{m}_{HTF}c_p}{A_{PV/T}U_L}\left(1 - exp\left(\frac{-A_{PV/T}U_LF'}{\dot{m}_{HTF}c_p}\right)\right) \tag{18}$$

Here, $\dot{m}_{HTF}$ (kg/s) is the mass flow rate of the fluid, c_p (J/kgK) is the specific heat capacity of the fluid, and F' is the collector efficiency factor.

$$F' = \frac{\frac{1}{U_L}}{w\left(\frac{1}{U_L(D+(W-D)F)} + \frac{1}{h_{ca}} + \frac{1}{\Pi D_i h_f}\right)} \tag{19}$$

Here, w (m) is the space between the pipes through which the PV/T fluid passes, D (m) is the outer diameter of the tube, h_{ca} (W/m^{2}K) is the boundary heat transfer coefficient, D_i (m) is the inner diameter of the tube, h_f (W/ m^{2}K) represents the heat transfer coefficient of the fluid.

$$F = \frac{tanh\left(\frac{m(w-D)}{2}\right)}{\frac{m(w-D)}{2}} \tag{20}$$

The value of m here is calculated by Equation (21) (Kalagirou, 2015):

$$m = \sqrt{\frac{U_L}{(k\lambda)_{PV/T}}} \tag{21}$$

P_{el}, which is the electrical power gained from PV/T, is calculated by Equation (22) (Sakellariou and Axaopoulos, 2018):

$$P_{el} = \eta_{el} I A_{cell} (\alpha\tau) \tag{22}$$

Average PV/T temperature $T_{PV/T}$ is calculated by Equation (23) (Sakellariou and Axaopoulos, 2018):

$$T_{PV/T} = T_{in} + \left(\frac{\dot{Q}_u}{A_{PV/T} F_R U_L}\right)(1 - F_R) \tag{23}$$

Also, the fluid mean outlet temperature T_{HTF} (K) can be found by Equation (24):

$$T_{HTF} = \dot{Q}_u + \frac{\dot{m}_{HTF} c_p (T_{in} - T_{out}) dt}{m_{HTF} c_p} + T_{out} \tag{24}$$

Electrical and thermal efficiencies of PV/T could be calculated using Equation (25) and Equation (26) (Yazdanifard et al., 2016):

$$\eta_{el} = \eta_{ref}\left(1 - \beta\left(T_{PV/T} - T_{amb}\right)\right) \tag{25}$$

Here, η_{ref} denotes the electrical efficiency at the reference point, and β denotes the temperature power coefficient.

$$\eta_{th} = \frac{\dot{m}_{HTF} c_p (T_{HTF} - T_{in})}{I(\alpha\tau) A_{PV/T}} \tag{26}$$

The total efficiency of the PV/T system is determined by Equation (27):

$$\eta_{PV/T} = \eta_{el} + \eta_{th} \tag{27}$$

3. RESULTS

Using the equaitons given in the previous section, analyzes were carried out for a water-ethylene glycol-based PV/T collector for Isparta conditions. For the time-dependent dynamic investigation, meteorological information such as annual solar radiation, wind velocity, and environment temperature of Isparta is obtained and shown in Figure 2.

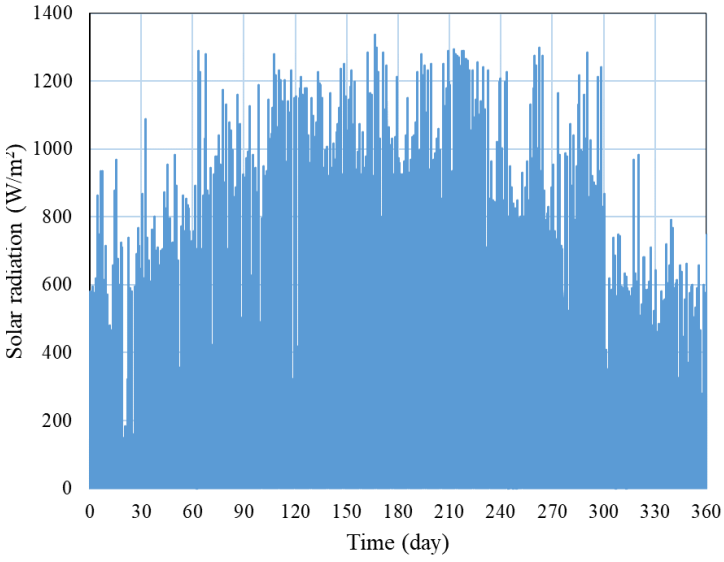

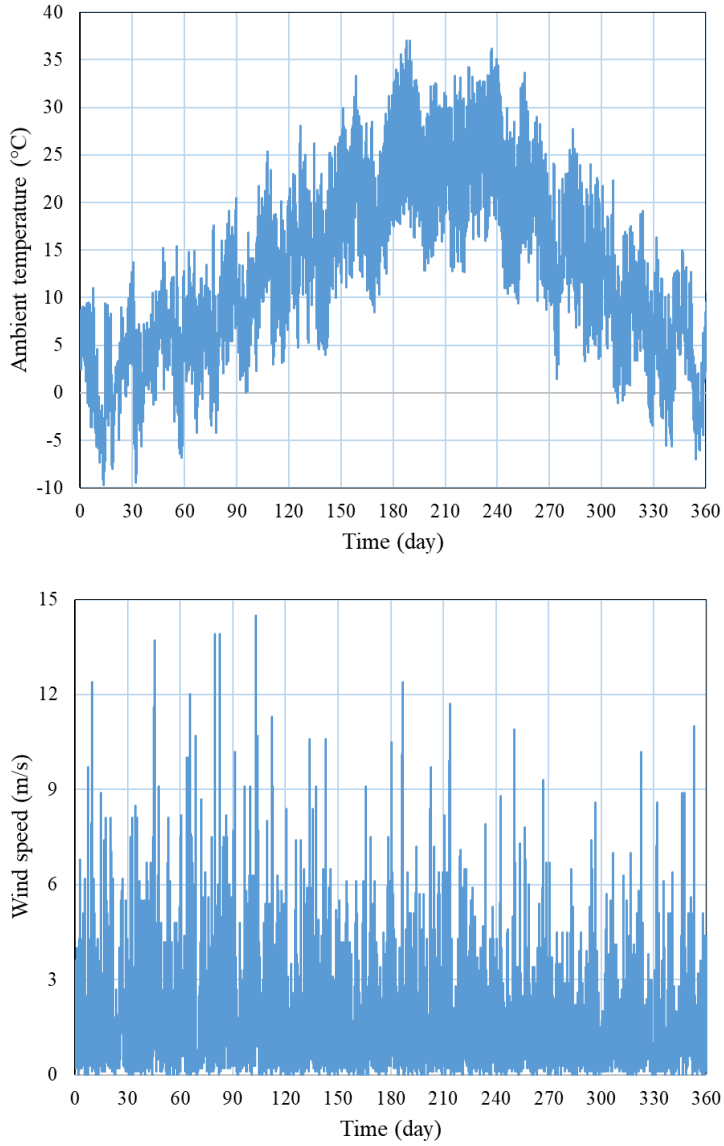

Figure 2. Meteorological data for Isparta

In the second part of the study, the validation of the modeling was carried out. In Figure 3, the graph of variation of the collector flow factor (F") and the dimensionless number $(\dot{m}c_p) / (AU_LF')$ in the reference study by Duffie and Beckman (2013) was shown to validate the current mathematical model. As can be seen from the figure, the trend in the PV/T mathematical modeling and the trend in the reference study are compatible with each other.

Figure 4 shows the thermal efficiency based on the $(T_{in} - T_{amb}) / I_{solar}$ ratio, which is an indicator for evaluating the performance of PV/T. As can be observed in the figure, for flow rates of 0.03, 0.1, 0.2, 0.3, and 0.36 kg/s, there was a tendency for thermal efficiency to decrease as the $(T_{in} - T_{amb}) / I_{solar}$ increased due to the rise in heat losses due to the temperature difference between the working fluid and the ambient air. In addition, verification studies were carried out considering the reference study of Kim and Kim (2012), and the average efficiency at a flow rate of 0.36 kg/s reached the highest value of 40% when the difference between the inlet temperature and the ambient temperature was zero. As seen in the figure, in the current study, thermal efficiency reaches 40% from 26% by raising the mass flow rate from 0.03 kg/s to 0.36 kg/s under 800 W/m^2 radiation conditions.

The variation in the electrical efficiency of PV/T according to the temperature difference is shown in Figure 5. As in thermal efficiency verification studies, electrical efficiency variation was observed for flow rates of 0.03, 0.1, 0.2, 0.3, and 0.36 kg/s depending on the $(T_{in} - T_{amb}) / I_{solar}$ ratio. As can be seen in the figure, verification studies were carried out with the reference study of Kim and Kim (2012), and it was observed that the $\Delta T/I_{solar}$ ratio and the electrical efficiency tended to decrease.

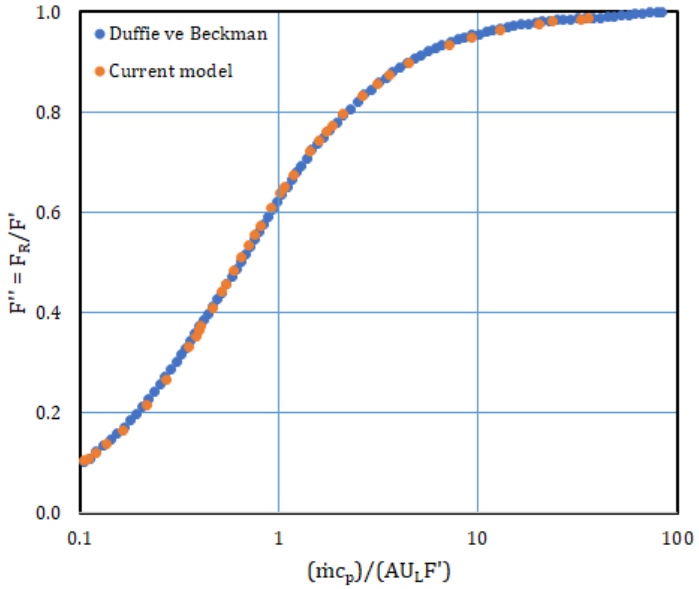

Figure 3. PV/T collector flow factor F'' as a function of $(\dot{m}_{HTF}\ C_p)/(A_{PV/T}\ U_L\ F')$

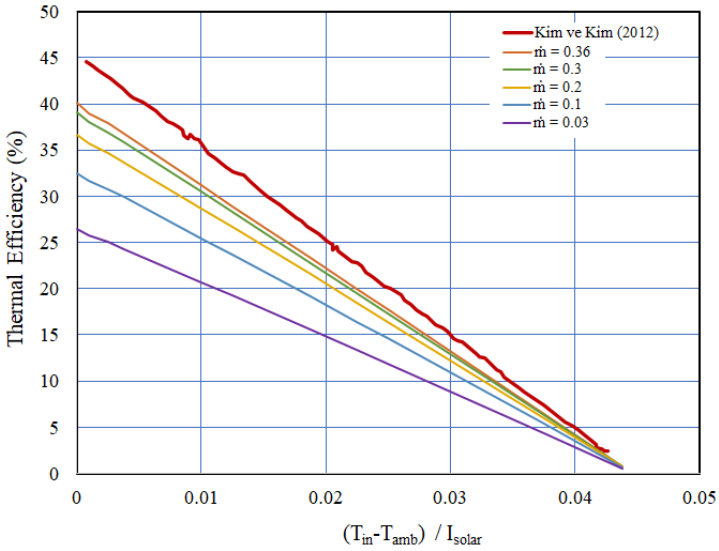

Figure 4. PV/T thermal efficiency curve according to $\Delta T/I_{solar}$

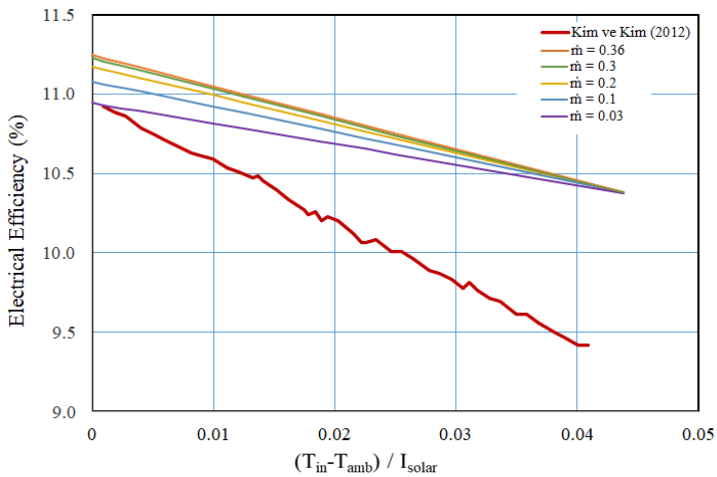

Figure 5. PV/T electrical efficiency curve according to $\Delta T/I_{solar}$

Figure 6 depicts the PV/T surface temperature's fluctuation over the first five days of January. The PV/T surface temperature rises as solar irradiation rises, as shown in the figure. The three-day analysis produced a maximum panel temperature estimate of about 37°C. Figure 7 shows the change in the heat transfer fluid's output temperature over time. The output temperature of the heat transfer fluid rises with an increase in solar radiation, as seen in the image. The maximum exit temperature of the heat transfer fluid was determined to be almost 12.5°C as a result of the five-day analysis.

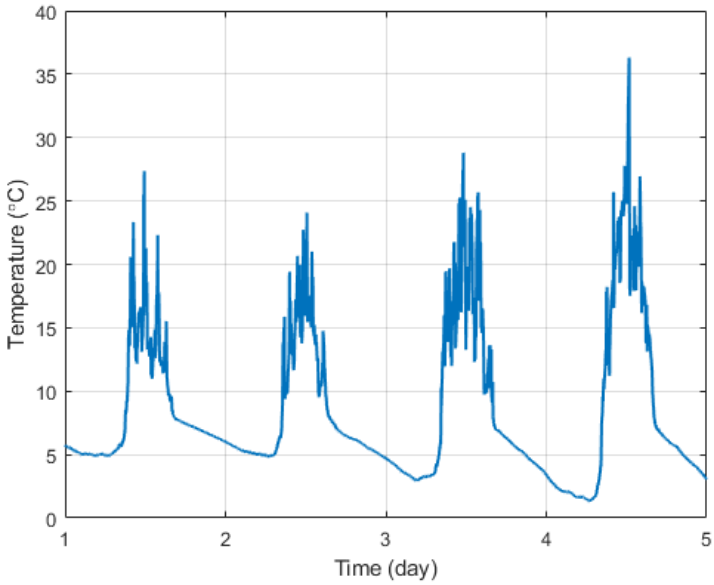

Figure 6. Variation of the PV/T surface temperature

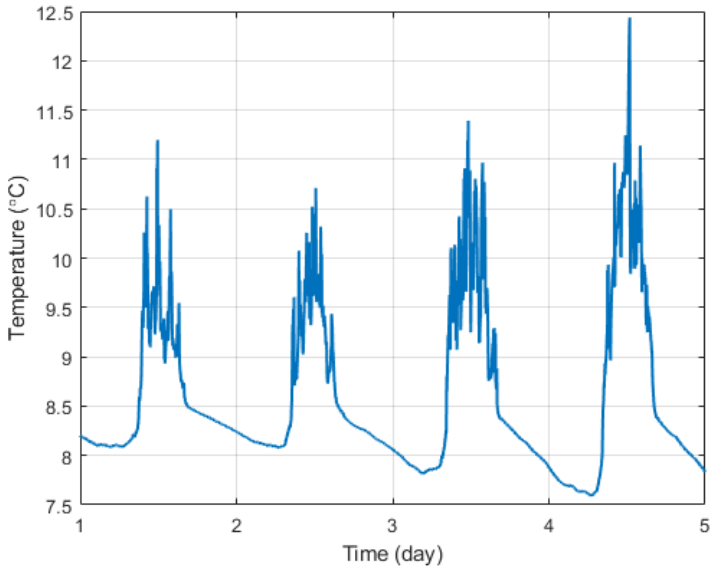

Figure 7. Variation of the outlet temperature of the HTF

Figure 8 depicts the fluctuation in the working fluid outlet temperature and PV/T surface temperature for the chosen three days. The change of the PV/T surface temperature and the working fluid outlet temperature follow the same trend, as shown in the figure. In rare circumstances, the working fluid's output temperature climbs above the PV/T surface temperature. This is since just the mass and specific heat of the working fluid are considered in the PV/T mathematical modeling, but the PV/T has no resistance and heats up and cools down quickly.

The electrical power's change over time is depicted in Figure 9. Throughout the analysis time, the solar radiation value changed simultaneously with the electrical power produced by the PV collector and the PV/T panel, and the highest electrical efficiency was attained at noon when the radiation was at its highest.

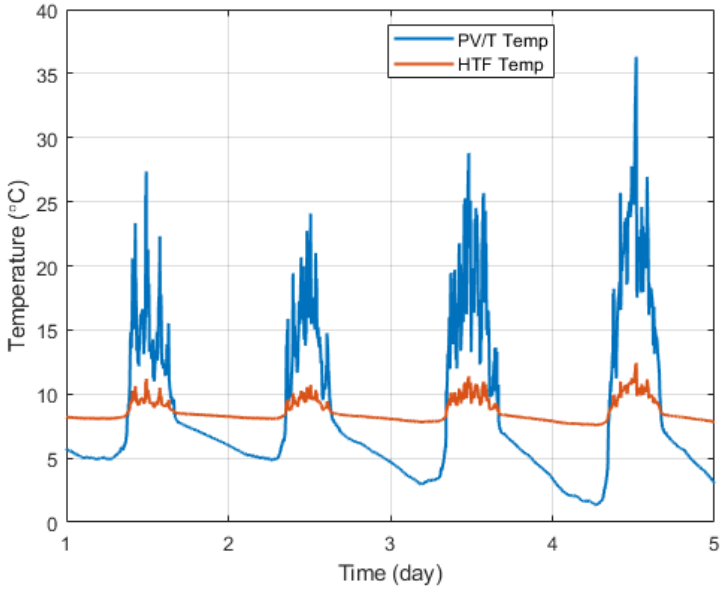

Figure 8. Variation of the outlet temperature of the heat transfer fluid and PV/T surface temperature with time

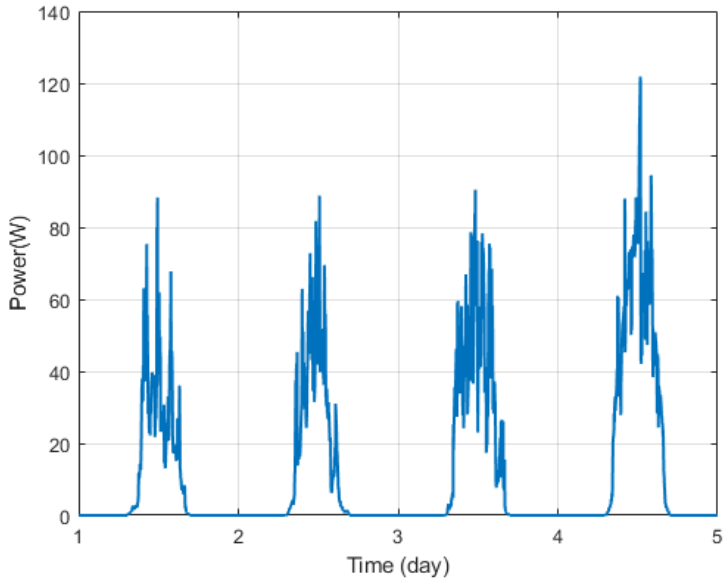

Figure 9. Variation of the electrical power

4. CONCLUSIONS

In this study, a mathematical model was conducted with the purpose of validating the water-ethylene glycol-based PV/T panel. Based on the energy balance of the PV/T panel, which is made up of several parts, including PV cells, insulation, transparent cover, pipes, plate absorber, and fluid inside the pipe, a model has been created to predict the dynamic behavior of the PV/T panel. Comparing the data found in the literature allowed us to confirm that the obtained theoretical results were in good agreement. During the analyses, the mass flow rate was taken as 0.02 kg/s, and the change of PV/T surface temperature, fluid outlet temperature, and electrical power over time was calculated for three days selected in Isparta conditions. As a result of the analysis, the maximum surface temperature of PV/T panels is 37°C. Also, the maximum power of PV/T is calculated as 122 W. In summary, the dynamic modeling of a PV/T collector for Isparta offers a detailed understanding of the system's performance and its potential contributions to sustainable energy generation. By combining photovoltaic and thermal technologies, this approach represents a significant step towards achieving cleaner and more efficient energy utilization in the region and beyond.

REFERENCES

Amrizal, N., Chemisana, D., Rosell, J.I. (2013). Hybrid Photovoltaic-Thermal Solar Collectors Dynamic Modeling. Applied Energy. 101797–807.

Aste, N., Del Pero, C., Leonforte, F., Manfren, M. (2016). Performance Monitoring and Modeling of an Uncovered Photovoltaic-Thermal PVT Water Collector. Solar Energy. 135, 551–568.

Aste, N., Leonforte, F., Del Pero, C. (2015). Design, Modeling and Performance Monitoring of a Photovoltaic-Thermal PVT Water Collector. Solar Energy. 112, 85–99.

Bhattarai, S., Oh, J.H., Euh, S.H., Kafle, G.K., Kim, D.H. (2012). Simulation and Model Validation of Sheet and Tube Type Photovoltaic Thermal Solar System and Conventional Solar Collecting System in Transient States. Solar Energy Mater. Sol. Cells. 103, 184–193.

Chow, T.T. Performance Analysis of Photovoltaic-Thermal Collector by Explicit Dynamic Model. (2003). Solar Energy 75, 143–152.

Çengel, YA., Ghajar, A. (2014). Heat and Mass Transfer, McGraw Hill Education.

Duffie JA, Beckman WA. (2013). Solar Engineering of Thermal Processes (4th ed.). New York: Wiley.

Haurant, P., Ménézo, C., Gaillard, L., Dupeyrat, P. (2015). Dynamic Numerical Model of a High Efficiency PV-T Collector Integrated into a Domestic Hot Water System. Solar Energy. 111, 68–81.

Kalogirou, SA. (2015). Solar Energy Engineering Processes and System, Elsevier.

Khelifa, A., Touafek, K., Moussa, H.B. (2014). Approach For the Modelling of Hybrid Photovoltaic-Thermal Solar Collector. IET Renewable Power Generation. 207–217.

Kim, JH., Kim, JT. (2012). Comparison of Electrical and Thermal Performances of Glazed and Unglazed PVT Collectors. International Journal of Photoenergy.

Sakellariou, E., Axaopoulos, P. (2018). An Experimentally Validated, Transient Model for Sheet and Tube PVT Collector. Solar Energy, 174, 709-718.

Touafek, K., Khelifa, A., Adouane, M. (2014). Theoretical and Experimental Study of Sheet and Tubes Hybrid PVT Collector, Energy Conversion and Management. 80, 71–77.

Yazdanifard, F., Ebrahimnia-Bajestan, E., Ameri, Mehran. (2016). Investigating the Performance of a Water-Based Photovoltaic/Thermal (PV/T) Collector in Laminar and Turbulent Flow Regime. Renewable Energy. 99, 295-306.

Zondag, H., Vries, D., Van Steenhoven, A.A., Van Helden, W.G.J. (1999). Van Zolingen, R.J.C. The Thermal and Electrical Yield of a Combi-Panel, in: Proceedings of ISES World Congress. Jerusalem. vol. 3, pp. 96–101.

Zondag, H.A., De Vries, D.W., Van Helden, W.G.J., Van Zolingen, R.J.C., Van Steenhoven, A.A. (2002). The Thermal and Electrical Yield of a PV-Thermal Collector. Solar Energy. 72, 113–128.

The Effect of Grape Seed on Phenolic Properties in Different Fermentation Applications and Production Process in Wine Produced from Öküzgözü Grape

Alev Akpınar Borazan, *[1], Berrin Bozan [2]

Abstract: The effect of grape seed on phenolic compounds and antioxidant activity of the wine production process from Öküzgözü grape was investigated. Öküzgözü wine was produced by using 3 different fermentation methods; classical, enzyme addition, and thermovinification. The change in phenolic properties during the production process in each fermentation method was monitored in terms of total phenolic content, total flavanol, and total anthocyanin contents and determined in five production stages: I- maceration/marc fermentation, II- alcoholic fermentation, III- final fermentation/resettle, IV- stabilization and clarification, V- bottling and aging. In addition, to observe the effect of seed on processes and phenolic properties, marc fermentation (5 days, 25 ^{o}C) was made in two different applications both skin and skin & seed. Spectrophotometric methods were used to determination of phenolic compounds and anthocyanins. Antioxidant activity was evaluated by DPPH free radical scavenging activity. In all fermentations and stages, the total phenolic contents varied from 2.72 to 1.41 g GAE L^{-1} by skin & seed extracts; from 1.70 to 0.8 g GAE L^{-1} by skin extracts; the total flavan-3-ol contents varied from 6.00 to 1.11 g catechin L^{-1} by skin & seed extracts; from 5.31 to 0.44 g catechin L^{-1} by skin extracts; the total anthocyanin contents varied from 0.1552 to 0.0170 g Mvd-3-O-glu L-1 by skin & seed extracts; from 0.1835 to 0.0201g Mvd-3-O-glu L^{-1} by skin extracts. As a result, the highest phenolic contents were determined in all fermentation applications and stages in marc fermentation, where seeds and skins were used together, and the lowest values were determined at the end of alcohol fermentation and 3rd month maturation. On the other hand, the total anthocyanin value was not as high as expected in all fermentations in which marc fermentation was applied without using seeds. The highest total amount of phenolic compounds and antioxidant activity were observed in the wines obtained by the thermovinification process, which was pre-processed at 65 ^{o}C for 8 hours. The amounts of phenolic compounds and antioxidant activity were affected by each step of the wine process.

Keywords: Öküzgözü, Fermentation, Seed, Phenolics, Antioxidant activity.
[1]**Address:** Bilecik Seyh Edebali University, Faculty of Chemical, Bilecik/Turkiye
[2]**Address:** Eskişehir Technıcal University, Faculty of Chemical, Eskişehir/Turkiye

***Corresponding author**: alev.akpinar@bilecik.edu.tr

1. INTRODUCTION / GİRİŞ (Times New Roman 10pt)

Experimental studies in the literature have confirmed that foods rich in antioxidants show significant positive effects in the prevention of many diseases (Roussis et.al. 2008). Some beverages such as tea, red wine and cocoa, which are frequently consumed in many different cultures, are also rich in phenolic phytochemicals, which are known for their high antioxidant activities (Tabart, et.al. 2009; Lee, et.al. 2003). The phenolic composition of wine depends on many factors: viticulture practices, quality of grapes used in wine production, maturity level, grape variety, winemaking conditions and techniques etc. (Garciafalcon et.al., 2007; Gutiérrez-Escobar et.al., 2021; Merkytė et.al., 2020; Coletta et.al., 2013). According to those factors, red wine contains many important antioxidant phenolics at different level.

Phenolic compounds are extracted from the skin, pulp and seeds of grapes during the wine production process, and their levels may change with the factors applied during the production process (Feliciano et.al., 2009; Gutiérrez-Escobar et.al., 2021).

The aim of the present study was the assessment of the influence of the fermentation process, changing of the phenolics from maceration to bottling stages during winemaking, and differentiation of extraction with skin /seed&skin on the phenolic fraction öküzgözü wines produced in Turkey

2. MATERIAL AND METHOD / MATERYAL VE METOT

The optimum mature Öküzgözü grapes were harvested manually in the Kırklareli area. They were kept into cold storage until begins to production. The procedures in Öküzgözü red winemaking, respectively, are given figure 1.

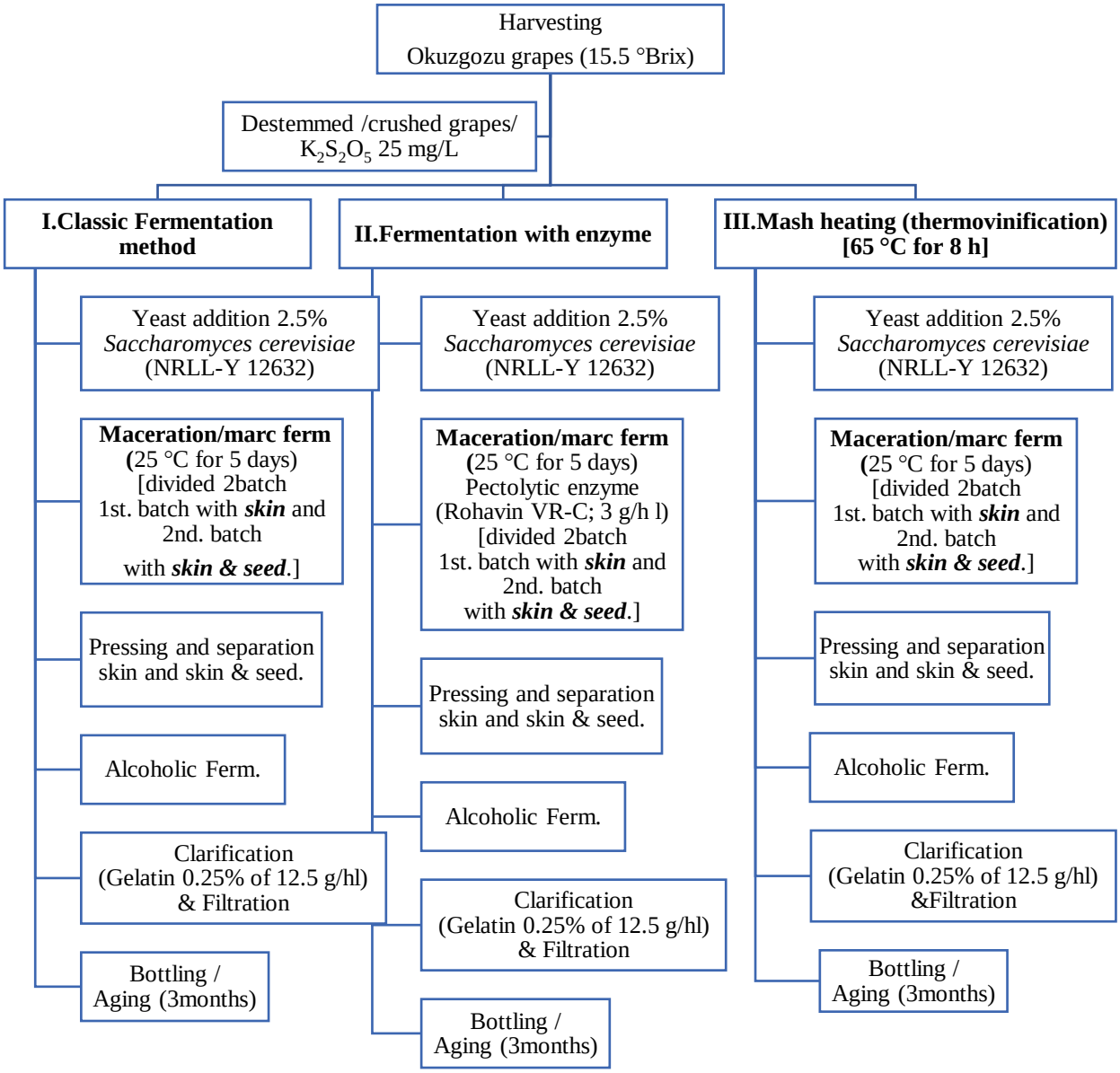

Figure 1 Scheme of generating Öküzgözü grape-to-wine with different fermentation techniques

2.1. Determination of total phenolic, total flavanol, total anthocyanin content and antiradical activity

The total phenolic (TP) content in the samples was determined by the Folin–Ciocalteu colorimetric method (Prior et al., 1998).

The total phenolic content was expressed as gallic acid (g GAE/L) equivalents. The total flavan-3-ol (TF) content was estimated by the vanillin–HCl method (Price, Van Scoyoc, & Butler, 1978). The total flavan-3-ol content was expressed as (+)-catechin (g catechin/L) equivalents. The total anthocyanins (TA) were estimated by a pH differential method (Lee, Durst, & Wrolstad, 2005), using a spectrophotometer (SP-3000, Optima). The results were calculated as mg malvinidin-3-O-glucoside equivalents per L

The antiradical activity of phenolic extracts was measured using DPPH method (Sanchez-Moreno, Larrauri, & Saura-Calixto, 1998), and expressed as EC_{50} (µg/mL), the concentration necessary for 50% reduction of DPPH.

2.2. Statistical analysis

Phenolic analyses were performed in either two or three replicates, and the determined results are presented as mean ± standard deviation. Analysis results were subjected to ANOVA test. Multiple comparisons of means were performed with the least significant difference (LSD) test at the a = 0.05 level.

3. RESULTS / BULGULAR

The phenolic properties during the production process with different fermentation methods were determined in five production stages. Analyzes were made on the samples taken at the stages when the relevant processes were completed. The effect of seed on processes and phenolic properties are given in Table 1-3.

Table 1. Effect of grape seed on phenolic properties during Öküzgözü wine making processes by classical fermentation

a) Process (maceration with skin&seed)	Total Phenolic (g GAE/L)	Total Flavanol (g catechin/L)	Total Anthocyanin (g Mvd-3-o-glu/L)	DPPH (EC_{50}, µg/mL)
Maceration/marc ferm.	2.61±0.15^{b}	2.47±0.24^{c}	0.1552±3.1E-3^{d}	57.79±2.74^{b}
Alcoholic ferm.	1.70±0.11^{a}	1.11±0.77^{a}	0.0362±7.0E-3^{ab}	45.69±0.98^{a}
Finish ferm./resettle	1.97±0.18^{a}	1.48±0.18^{ab}	0.0529±5.5E-3^{c}	58.16±5.93^{b}
Stabilize and Clarify	1.68±0.05^{a}	1.91±0.34^{abc}	0.0435±0.4E-3^{bc}	53.72±1.03^{b}
Bottling /aging (3mnths)	2.51±0.26^{b}	1.98±0.24^{bc}	0.0266±24.4E-3^{a}	54.48±1.58^{b}

b) Process (maceration with skin)	Total Phenolic (g GAE/L)	Total Flavanol (g catechin/L)	Total Anthocyanin (g Mvd-3-o-glu/L)	DPPH (EC_{50}, µg/mL)
Maceration/marc ferm.	1.70±0.09^{b}	1.20±0.09^{bc}	0.1835±20.6E-3^{c}	87.35±7.78^{b}
Alcoholic ferm.	1.05±0.05^{a}	1.22±0.10^{c}	0.0872±0.3-3^{b}	94.67±7.03^{b}
Finish ferm./resettle	1.12±0.14^{a}	1.04±0.29^{bc}	0.0367±4.4E-3^{a}	123.82±0.48^{c}
Stabilize and Clarify	1.02±0.06^{a}	0.77±0.08^{ab}	0.0429±4.7E-3^{a}	93.24±5.13^{b}
Bottling /aging (3mnths)	1.71±0.17^{b}	0.44±0.41^{a}	0.0386±37.E-3^{a}	76.06±6.94^{a}

* Mean values marked with the same letters in the same column ($p < 0.05$) there is no difference

Table 2. Effect of grape seed on phenolic properties during Öküzgözü wine making processes by addition of the Pectolitic Enzyme

a) Process (maceration with skin&seed)	Total Phenolic (g GAE/L)	Total Flavanol (g catechin/L)	Total Anthocyanin (g Mvd-3-o-glu/L)	DPPH (EC_{50}, µg/mL)
Maceration/marc ferm.	1.96±0.13^{b}	1.33±0.07^{a}	0.0902±5.8E^{-3c}	52.46±2.24^{b}
Alcoholic ferm.	1.41±0.08^{a}	1.88±0.15^{b}	0.0209±1.9E^{-3a}	45.37±0.45^{a}
Finish ferm./resettle	1.45±0.06^{a}	1.87±0.02^{b}	0.0179±0.2E^{-3a}	45.66±5.45^{a}
Stabilize and Clarify	1.41±0.20^{a}	1.74±0.22^{b}	0.0485±0.9E^{-3b}	52.13±3.12^{b}
Bottling /aging (3mnths)	1.47±0.10^{a}	1.91±0.16^{b}	0.0496±50.8E^{-3b}	54.20±2.36^{b}

b) Process (maceration with skin)	Total Phenolic (g GAE/L)	Total Flavanol (g catechin/L)	Total Anthocyanin (g Mvd-3-o-glu/L)	DPPH (EC_{50}, µg/mL)
Maceration/marc ferm.	1.41±0.13^{c}	1.22±0.13^{a}	0.0763±4.0E-3^{d}	92.84±7.32^{b}
Alcoholic ferm.	1.03±0.05^{b}	1.37±0.10^{a}	0.0761±1.5E-3^{d}	73.46±5.92^{a}
Finish ferm./resettle	1.00±0.12^{b}	1.82±0.29^{b}	0.0295±2.8E-3^{b}	73.79±2.67^{a}
Stabilize and Clarify	0.80±0.14^{a}	1.36±0.14^{a}	0.0409±1.1E-3^{c}	113.58±13.26^{c}
Bottling /aging (3mnths)	0.77±0.01^{a}	1.88±0.19^{b}	0.0176±16.2E-3^{a}	87.34±0.09^{ab}

* Mean values marked with the same letters in the same column ($p < 0.05$) there is no difference

Table 3. Effect of grape seed on phenolic properties during Öküzgözü wine making processes by thermovinification

a) Process (maceration with skin&seed)	Total Phenolic (g GAE/L)	Total Flavanol (g catechin/L)	Total Anthocyanin (g Mvd-3-o-glu/L)	DPPH (EC_{50}, µg/mL)
Maceration/marc ferm.	2.72±0.12[c]	6.00±0.51[c]	0.0626±5.3E-3[b]	51.86±3.69[b]
Alcoholic ferm.	1.79±0.02[a]	5.53±0.18[bc]	0.0939±0.5E-3[c]	28.56±0.09[a]
Finish ferm./resettle	1.81±0.12[a]	4.54±0.30[a]	0.0845±0.2E-3[c]	56.44±1.34[c]
Stabilize and Clarify	2.25±0.10[b]	4.98±0.29[ab]	0.0570±4.6E-3[b]	40.09±2.32[ab]
Bottling /aging (3mnths)	2.22±0.15[b]	4.40±0.32[a]	0.0433±49.6E-3[a]	46.14±2.83[ab]

b) Process (maceration with skin)	Total Phenolic (g GAE/L)	Total Flavanol (g catechin/L)	Total Anthocyanin (g Mvd-3-o-glu/L)	DPPH (EC_{50}, µg/mL)
Maceration/marc ferm.	1.53±0.07[c]	3.69±0.11[a]	0.0201±7.0E-3[a]	81.50±6.14[b]
Alcoholic ferm.	1.08±0.01[a]	3.07±0.26[a]	0.0564±0.8E-3[b]	62.34±2.23[a]
Finish ferm./resettle	1.17±0.04[a]	3.13±0.32[a]	0.0547±6.8E-3[b]	118.50±8.65[c]
Stabilize and Clarify	1.34±0.04[b]	3.57±0.46[a]	0.0474±3.6E-3[b]	72.10±6.79[ab]
Bottling /aging (3mnths)	1.15±0.10[a]	5.31±0.38[b]	0.0254±24.8E-3[a]	72.16±6.58[ab]

* Mean values marked with the same letters in the same column ($p < 0.05$) there is no difference

4. DISCUSSION AND CONCLUSIONS / TARTIŞMA VE SONUÇLAR

Total phenolic content has changed in different processes in wine production with different methods (classical, enzyme added and hot maceration). The differences in the values were found to be statistically significant ($p>0.05$). The total amount of phenolic compounds showed their maximum values in applications where seeds and grape skin were used together. Total phenolic component values, respectively; It decreased gradually in hot maceration, classical fermentation, and enzyme added fermentation applications. There was a significant decrease in all methods with the clarification process. The clarifying agent used here is thought to be effective. While no significant difference could be determined in the amount of total phenolic compounds between alcoholic fermentation, resting and clarification processes, the highest value was generally reached in maceration/marc fermentation stages.

It was determined that the total flavanol value showed statistically significant differences in different fermentation applications and process stages. The total flavanol value had the highest value within the mash heating method, with and without seeds, among the fermentation and processing stages applied. In the literature, it has been stated that high-temperature applications increase the tannin and the prolongation of the contact time of the seeds with the must also increases the flavanols. Complex formation between anthocyanins and tannins and reactions between polyphenols and acetaldehyde during the aging process of the wine affected the total amount of flavanols.

Total anthocyanin was determined to be higher in each process with applied only skin maceration as expected. It was observed that the wines obtained from the fermentation processes in which only the skin was used were rich in phenolic acid and monomeric anthocyanin compounds, and the products obtained from the fermentation processes in which the grape skin and seed were used were rich in catechin derivatives (catechin, epicatechin).

In the study was determined, the antioxidant activity values are largely in correlation with the total phenolic component content. The highest antioxidant activity value in wines was obtained by the mash heating/maceration method in all processes. Wine producers minimize the phenol content due to turbidity and adverse taste, but when the health-protective effect is considered, these problems can be eliminated to provide more phenolic substances and the thermovinification method can be preferred in wine production.

In applications made with grape skin maceration, all values are lower than in fermentation applications and stages where grape skin and seed are macerated together.

Author Contributions

Conceptualization: B.B.; Investigation: A.A.B; Material and Methodology: A.A.B., B.B.; Supervision: B.B.; Writing-Original Draft: A.A.B., B.B.; Writing-review & Editing: A.A.B., B.B..: All authors have read and agreed to the published version of manuscript.

Conflict of Interest
The authors have no conflicts of interest to declare.

Funding
The authors declared that this study has received no financial support.

REFERENCES

Coletta, A., Trani, A., Faccia, M., Punzi, R., Dipalmo, T., Crupi, P., Antonacci, D., & Gambacorta, G. (2013). Influence of viticultural practices and winemaking technologies on phenolic composition and sensory characteristics of Negroamaro red wines. International Journal of Food Science & Technology, 48(11), 2215-2227. doi.org/10.1111/ijfs.12207

Feliciano, R.P., Bravo, M.N., Pires, M.M. et al. Phenolic Content and Antioxidant Activity of Moscatel Dessert Wines from the Setúbal Region in Portugal. Food Anal. Methods 2, 149–161 (2009). https://doi.org/10.1007/s12161-008-9059-

Garciafalcon, M., Perezlamela, C., Martinezcarballo, E., & Simalgandara, J. (2007). Determination of phenolic compounds in wines: Influence of bottle storage of young red wines on their evolution. Food Chemistry, 105(1), 248–259. doi:10.1016/j.foodchem.2006.11.006

Gutiérrez-Escobar R, Aliaño-González MJ, Cantos-Villar E. (2021) Wine Polyphenol Content and Its Influence on Wine Quality and Properties: A Review. Molecules. 30;26(3):718. doi: 10.3390/molecules26030718.

Lee, J., Durst, R. W., & Wrolstad, R. E. (2005). Determination of Total Monomeric Anthocyanin Pigment Content of Fruit Juices, Beverages, Natural Colorants, and Wines by the pH Differential Method: Collaborative Study. Journal of AOAC International., 88(5), 1269–1278. https://doi.org/10.1093/jaoac/88.5.1269

Lee, K. W., Kim, Y. J., Lee, H. J., & Lee, C. Y. (2003). Cocoa Has More Phenolic Phytochemicals and a Higher Antioxidant Capacity than Teas and Red Wine. Journal of Agricultural and Food Chemistry, 51(25), 7292–7295. doi:10.1021/jf0344385

Merkytė V, Longo E, Windisch G, Boselli E. (2020) Phenolic Compounds as Markers of Wine Quality and Authenticity. Foods. 9(12):1785. doi.org/10.3390/foods9121785

Price, M. L., Van Scoyoc, S., & Butler, L. G. (1978). A critical evaluation of the vanillin reaction as an assay for tannin in sorghum grain. Journal of Agricultural and Food Chemistry, 26, 1214–1218. https://doi.org/10.1021/jf60219a031

Prior, R., Cao, G., Martin, A., Sofic, E., McEwen, J., O'Brien, C., Lischner, N., Ehlenfeldt, M., Kalt, W., Krewer, G., & Mainland, C. (1998). Antioxidant capacity as influenced by total phenolic and anthocyanin content, maturity, and variety of Vaccinium species. Journal of agricultural and food chemistry, 46, 2686-2693. https://doi.org/10.1021/jf980145d

Roussis, I. G., Lambropoulos, I., Tzimas, P., Gkoulioti, A., Marinos, V., Tsoupeis, D., & Boutaris, I. (2008). Antioxidant activities of some Greek wines and wine phenolic extracts. Journal of Food Composition and Analysis, 21(8), 614–621.doi:10.1016/j.jfca.2008.02.011

Sanchez-Moreno, C., Larrauri, J. A., & Saura-Calixto, F. A. (1998) Procedure to measure the antiradical efficiency of polyphenols. Journal of the Science of Food and Agriculture, 76, 270–276. Doi: 10.1002/(SICI)1097-0010(199802)76:2<270::AID-JSFA945>3.0.CO;2-9

Tabart, J., Kevers, C., Pincemail, J., Defraigne, J.-O., & Dommes, J. (2009). Comparative antioxidant capacities of phenolic compounds measured by various tests. Food Chemistry, 113(4), 1226–1233. doi:10.1016/j.foodchem.2008.08.013

A Barrier-Free City Proposal for Disabled Individuals Gostivar/North Macedonia Example

Ayse ARICI*[1]

Abstract: In this study, while an ergonomic, convenient, comfortable urban planning design is designed so that the people of the city can live their lives in a healthy, equal life, safe, free, happy, and peaceful way, it will improve the welfare of the people of the city at minimum cost with the proposals of building materials suitable for the current situation in the most economical way. Is to develop a solution proposal that will increase. For this purpose, it has been investigated whether urban outdoor spaces and urban equipment are compatible with the living conditions of disabled individuals. In the study, It is important that all the spaces in the city appeal to all segments of society and should be designed in this way, and what features should be added for the region that is the study universe? The answer to the question has been sought. In this context, in the example of the city of Gostivar, North Macedonia, especially in the streets and streets in the city center, the city center, parks, playgrounds, the entrances of religious places of worship and accessibility, the floor elements in public areas (ramps, stairs, pedestrian paths, parking areas), urban equipment (living and rest areas, lighting elements, garbage cans), access opportunities to public buildings, and access opportunities at the entrances to the buildings have been taken into account. As a result of the findings, it has been revealed how easily disabled users can use the problems they experience outdoors and what their expectations are from the city. As solution proposals, suggestions were made regarding the suitability for the new conditions, how to make changes in the current situation, the existence of the transformation, and the spatial use and organizational structure for the change, planting, and ecology in order to provide solutions for the transformation and change needs.

Keywords: Disability, Urban Accessibility, Building Materials, Sustainability.

[1]**Address:** VizyonUniversity, Faculty Of Architecture Engineering, Gostivar/Nort Makedonia

***Corresponding author**: aysearici.iut@gmail.com

1. INTRODUCTION

Today, the principles of equality and inclusiveness for all segments of society are becoming more important by combining them with the goals of sustainability and livability. Disability, urban accessibility, building materials, and sustainability are key concepts that come together to transform the construction industry and build a more inclusive future.

Disability refers to the difficulties an individual faces in different areas of life due to limitations in their physical, mental, or sensory abilities. Disability not only affects the daily lives of individuals but also affects all layers and infrastructures of society. One of the problems with disability is the lack of accessibility in urban areas. Many cities are littered with obstacles such as narrow roads, stairs, or buildings full of obstacles, making it difficult for people with disabilities to enjoy basic rights such as independence, employment, and social inclusion.

Disability is understood as the inequalities of opportunity and limitations that arise between individuals based on the principle of equality in society. This definition emphasizes the difficulties that prevent disabled people from taking part in society on an equal basis with other individuals and their full participation in activities in various fields. Disability is associated with deficiencies in existence and active participation in areas such as information, communication, and education. These deficiencies are considered factors that prevent people with disabilities from integrating with society and interacting fully. (Çınar et al., 2015).

Urban accessibility aims at minimizing or eliminating physical barriers so that individuals with disabilities and other disadvantaged groups can perform their daily living activities. These include planning and arranging various infrastructure and services in a city, such as roads, sidewalks, buildings, public transport systems, parks, and utilities, to suit accessibility needs. Urban accessibility encourages the full and equal participation of people with disabilities in society while enabling everyone to live in a more comfortable and usable environment. Measures such as disabled

ramps, elevators, low-floor buses, non-slip floors, and information systems for the hearing and visually impaired can be given as examples of urban accessibility. Urban accessibility aims to increase the access of people with disabilities to basic rights, independence, freedom, and quality of life. It also enables disadvantaged groups such as the elderly, pregnant women, children, and other individuals with temporary disability or injuries to access activities and services in the city easily.

The "barrier-free or accessible city" approach has been put forward as a solution proposal for the accessibility problem of people with disabilities in urban areas. Today, cities are accepted as focal points of social, cultural, economic, and political interaction of society. The fact that people with disabilities can move freely in the urban space and have access to all kinds of resources, services, and physical environment forms the basis of the idea of a barrier-free city. With this approach, it is aimed that disabled people to participate effectively in all areas of life and live independently. (Erten and Aktel, 2020).

According to the concept of universal design, the needs and expectations of individuals belonging to different groups are taken into account. Solutions are offered to facilitate the use of everyone, such as the elderly, children, pregnant women, or people with temporary disability, as well as disabled individuals. In this way, barriers to social participation are removed, and it is ensured that everyone can be found in spaces of independence, safety, and comfort (Pouya, 2021).

The squares that play a central role in urban life and the urban furniture in these squares should be designed to meet the needs of everyone. Unfortunately, applications made by ignoring the needs of elderly and disabled individuals are quite common in our country (Aykıl et al., 2018).

The diversity and intensity of disability problems necessitate a large number of services to be provided to people with disabilities in terms of quantity and variety. Although disability is handled from the perspective of human rights, individuals with disabilities face problems such as not being able to access health services, education, and employment opportunities equally, not getting the disability services they need, and not being able to participate in daily life activities (Arab et al., 2021).

The ability of a person to develop within the social structure and to benefit equally from the opportunities offered by social life is closely related to the access and use of the space. However, the ability of disabled individuals to live in the same conditions as all other individuals depends on the accessibility of the built environment for them. In order to ensure the full participation of disabled people in social life, the design and arrangement of the spaces should be carried out in accordance with accessibility standards. In this way, disabled people's access to the spaces becomes easier, their use becomes unhindered, and it is ensured that they can take a full place in society (Çivici and Gönen, 2015).

In this context, this article aims to research the building entrances of public institutions in the Municipality of Gostivar in North Macedonia and the roads to be accessed to this building, suitable for the disabled, elderly, and raising children, and to offer solutions to the deficiencies in this area. This study was carried out with the aim of making better use of the accessibility difficulties for the disabled, elderly, and children in the surrounding area and disseminating applicable solutions to reveal these problems. In addition, developments in building materials and accessibility offer a promising way to address these challenges. The construction industry is developing new concepts and technologies to design and build more barrier-free and accessible structures based on sustainability and usability accessibility. The sustainability of building materials is also of great importance in terms of reducing environmental impacts, increasing energy efficiency and creating long-lasting structures. This article will highlight the relationship between urban accessibility, building materials and sustainability in the fight against disability by evaluating the accessibility status of public institutions in the Municipality of Gostivar and offering solutions. This work is an important step towards raising awareness about disability and contributing to the building of a more inclusive society in the future.

2. MATERIAL AND METHOD

The main material of the study is the streets and sidewalks that provide access to the public institutions in the city center of Gostivar Municipality in North Macedonia and to these institutions. In addition, the Vardar River, which flows through the city of Gostivar, has great importance for the city's people and is an important natural resource in the context of sustainability as a global value. For this reason, the city park and walking paths around the river were also examined, and the content of the study was further enriched. The river offers the residents of Gostivar the opportunity to spend time with nature, relax and engage in physical activities. At the same time, the contribution of the river to the city's ecosystem and environmental balance is remarkable. The city park and walking paths allow people to discover natural beauty and continue their recreational activities. However, they must be designed in an environmentally friendly way. In addition, it has been examined whether this urban park is suitable for the comfort of disabled, elderly, or sick

individuals. The fact that it has an important location that can be used for walking by patients providing transportation to the hospital, which is close to this city park, and patients in the hospital increases the importance of this park.In this way, the city of Gostivar plays a leading role in the conservation of natural resources and the sustainable use of natural beauties by offering sustainable living space to its local people and local and foreign visitors. For this purpose, in this study, the necessary measures will be researched so that the city of Gostivar can appeal to all segments of the city, and it will contribute to the acquisition of a comfortable urban identity in accordance with the standards for the disabled, the elderly and the sick. The method of the study includes the determination of the purpose and scope first, and a literature review of similar studies on the subject has been made. Current and valid resources in areas such as the arrangement of roads for the disabled, urban planning, accessibility, design standards, and the needs of people with disabilities have been researched. Useful information on academic resources, research articles, regulations, and national and international standards were reviewed.

During the data collection phase, data on the arrangement of roads for people with disabilities were collected, field studies were carried out, and interviews were conducted with disabled individuals. Measurements were made in the sample areas in the study universe and were processed into observation forms and visual materials. The measurement results were evaluated in terms of compliance with the standards determined for people with disabilities, and suggestions were developed based on the results. Within the scope of the study, the suitability of urban outdoor elements for disabled individuals was investigated in the example of the Municipality of Gostivar. While the research includes examining the standards for people with disabilities in national and international standards, areas such as floor elements, open parking areas, reinforcement elements, and public building entrances are emphasized. The study, organized in this way, aims to contribute to the city of Gostivar to gain a sustainable urban identity suitable for disabled individuals.

3. RESULTS

Gostivar Municipality Building, Municipal Support Building, Provincial Directorates Building, Court of First Instance Building, İşkur Building and Social Security and Health Institution Building, Gostivar Post Office Building, Gostivar Culture House Entrance, and Transportation When the accessibility arrangements made for Gostivar, Vardar River Walkways and City Park are examined. It was observed that some important shortcomings were identified. Accessibility improvements need to be made in these buildings. Deficiencies were identified and visual materials and measurements supported possible arrangements. In this direction, if we make an academic analysis, the following points include suggestions for accessibility regulations:

GOSTIVAR MUNICIPAL BUILDING AND MUNICIPAL SERVICE BUILDING		
		
A- Municipal Service Building Entrance	**B-** Municipal Service Building Entrance Stair Tread Height: 15 cm Step Width: 30 cm Stair Width: 280 cm There is no stair railing.	**C-** Municipal Service Building Entrance ramp width: 140cm
		
D- The width of the pavement in front of the Municipal Service Building, the Municipality Building and the Provincial Directorates: 278 cm	**E-** Municipal Service Building - Entrance to the area where the Municipality Building and Provincial Directorates are located	**F-** City Hall Main Entrance - Stair Tread Height: 15cm Step Width: 30 cm Stair Width: 480cm There is no ramp.

Figure 1. Gostivar City Hall and Municipal Support Building Entrances and Access (ARICI A,2023)

An important factor limiting the mobility of persons with disabilities is difficulties in transportation. Participants in the research emphasize that difficulties in accessing transportation vehicles and the lack of audio signaling for the visually impaired and colored/light signaling for the deaf and hard of hearing are prominent problems (Doğruel, 2022).

According to the deficiencies identified in the entrances and transportation of the Gostivar Municipality Building and the Municipality Support Building, the following arrangements can be made suitable for the disabled, the sick, and the elderly: Stairs: They should be arranged in a way that is suitable for the access of disabled people. The stair step height must be lower than the existing 15 cm. Preferably, a 10 cm high step should be added, and a platform or border should be created that will enable visually impaired individuals to perceive with their walking sticks. Also, stair railings should be added. Ramp: Municipal Service Building Entrance ramp width should be wider than the current 140 cm. Braille signs are not used. There are no non-slip floor coverings. There are no discretionary sidewalks. There are no colored road signs. There are no reactive road signs. These arrangements will facilitate the access of the disabled, the sick, and the elderly to the town hall and support the building and ensure their safety. When making arrangements, it is important to comply with local regulations and disability accessibility standards. In addition, suitable building materials should be used, and all arrangements should be designed in a way that disabled people can easily perceive and use.

The diversity and intensity of disability problems necessitate many services to be provided to the disabled in terms of quantity and variety. Although disability is handled from the perspective of human rights, individuals with disabilities face problems such as not being able to access health services, education, and employment opportunities equally, not getting the disability services they need, and not being able to participate in daily life activities (Arab et al., 2021).

GOSTİVAR PROVINCIAL DIRECTORATES BUILDING ENTRANCE AND TRANSPORTATION		
		
A- Gostivar, Provincial Directorates Building Entrance Stair Tread Height: 16 cm Step Width: 30 cm Stair Width: 320 cm No handrail is on the stairs.	**B-** Gostivar, Provincial Directorates Building Entrance Stair Tread Height: 16 cm Step Width: 30 cm Stair Width: 320 cm No Ramp	**C-** There are no suitable passages for wheelchairs when crossing the street, no directions for walking for the visually impaired, and no voice warning system.

Figure 2. Gostivar Municipality Provincial Directorates Building Entrance and Transportation (ARICI. A ,2023)

According to the deficiencies detected in the entrances and transportation of the Gostivar Provincial Directorates building, the following arrangements can be made: Stairs: The stair step height should be lower than the existing 16 cm so that people with disabilities can use it easily. Generally, an acceptable height of up to 10-12 cm is preferred. The stair step width is specified as 30 cm; this size can be considered appropriate. Railings should be added. Handrails allow disabled people to use stairs safely. Railings should be designed with an average height of 80-90 cm and a suitable holding surface. Braille signs are not used. There are no non-slip floor coverings. There are no discretionary pavements. There are no colored road signs. There are no responsive road signs. Ramp: Ramps should be constructed to provide convenient passages for wheelchair users. The slope and width of the ramp should be such that disabled people can easily pass. Generally, the slope rate is accepted as 6%. The ramp surface should be equipped with non-slip floor coverings. Non-slip floor coverings will ensure the safety of people with disabilities and reduce the risk of slipping. A 10 cm high platform or border should be provided for visually impaired individuals to perceive with the help of a walking stick.

GOSTİVAR, COURT BUİLDİNG ENTRANCE		
		
A- Gostivar, Court Building Entrance	**B-** Ramp Width: 130 cm	**C-** Stair Step Height: 15 cm Step Width: 30 cm Stair Width: 330 cm There is no railing on the stairs.

Figure 3. Gostivar Court of First Instance Entrance and Transportation ARICI.A,2023)

The following arrangements can be made for the Gostivar Court of First Instance building in order to solve the identified deficiencies and make it suitable for all types of disability: Stairs: The stair step height must be lower than the existing 15 cm. Preferably, a 10 cm high step should be added, and a platform or border should be created that will enable visually impaired individuals to perceive with their walking sticks. Railings should be added on the stairs. Handrails are important to provide grip and stability when using stairs. Ramp: The width of the ramp must be wider than the current 130 cm. A ramp should be provided where disabled people can easily pass using a wheelchair or walking aid. The ramp slope should be determined according to appropriate standards. Generally, 6% slope is preferred. The ramp surface must be non-slip and properly designed to ensure a safe passage. Braille Signs: Signs written in the Braille alphabet should be used to enable visually impaired individuals to access information. Non-slip floor coverings should be used. Discreet pavements should be used for the road safety of visually impaired individuals. Colored road signs should be used for road safety and guidance for visually impaired individuals. Signs in different colors can be used to identify a particular route or landmarks within the building. Reactive Road Signs: Responsive road signs should be used to improve road safety for people with disabilities. Building materials that can be used to achieve these regulations are: Rubber coatings or antistatic materials may be preferred for durable and non-slip floor coverings. Stainless steel or aluminum materials can be used for ramp and stair railings. Aluminum or plexi materials can be preferred for Braille signs. For discretionary pavements, polymeric or epoxy coatings can be used. Durable paint or colored stones can be preferred for colored road signs. Electronic systems and audible warning devices can be used for responsive road signs. These building materials provide advantages for facilitating the access of people with disabilities, ensuring their safety, and complying with current standards. Having durable, cleanable, and long-lasting features, they can offer an effective solution for solving the deficiencies in the building. In addition, with the use of materials, it is aimed to increase the independence and participation of disabled people, ensure social accessibility, and ensure that everyone can use the building comfortably.

GOSTİVAR İŞKUR BUILDING ENTRANCE- GARDEN- TRANSPORTATION		
		
A- Gostivar, İşkur Building Entrance Stair Tread Height: 16 cm Step Width: 30 cm Stair Width: 320 cm There is no handrail on the stairs.	B-Stair Step Height: 22 cm Step Width: 30cm Stair Width: 325 cm There is no railing on the stairs.	**C-** While crossing the street, there are no suitable passages for wheelchairs, there are no directions for walking for the visually impaired, and there is no voice warning system.

Figure 4. Gostivar İşkur Building Entrance and Access (Arıcı, 2023)

The following arrangements can be made for the Gostivar İşkur building in order to solve the identified deficiencies and make it suitable for all types of disability: Stairs: The stair step height should be lower than the existing 16 cm. Preferably, a 10 cm high step should be added, and a platform or border should be created that will enable visually impaired individuals to perceive with their walking sticks. Railings should be added on the stairs. Handrails are important to provide grip and stability when using stairs. Disabled Crossings: Appropriate transitions for wheelchairs should be provided when crossing the street. For this, ramps or smooth ground transitions of appropriate width and slope should be created. Directions and audio warning systems should be added for walking for the visually impaired.

Direction signs should be equipped with signs in embossed or Braille. Non-slip floor coverings should be used. Non-slip surfaces should be preferred to prevent slipping, especially on wet floors. Non-slip floor coverings should be applied at the ramp and stair entrances. Non-slip floor coverings should be durable and easy to clean. Discreet pavements should be used for the road safety of visually impaired individuals. Colored road signs should be used for road safety and guidance for visually impaired individuals. Responsive road signs should be used to increase road safety for people with disabilities. With these arrangements, the Gostivar İşkur building can be made suitable for all types of disability, and accessibility can be provided. Appropriately sized ramps, wide passages, and Braille signs will make it easier for people with disabilities to use the building comfortably and access information. Non-slip floor coverings, discreet pavements, and colorful and responsive road signs will increase their safety and make their journey safer.

GOSTİVAR SOCIAL SECURITY AND HEALTH INSTITUTION BUILDING ENTRANCE AND TRANSPORTATION		
		
A- Gostivar, Social Security and health institution Building Entrance	**B-** Stair Step Height: 17 cm Step Width: 30 cm Stair Width: 170 cm There is no railing on the stairs.	**C-** When crossing the street, there are no wheelchair-friendly passages, no walking directions for the visually impaired, and no voice warning system.

Figure 5. Gostivar Social Security and Health Institution Building Entrance and Transportation (Arıcı,2023)

Gostivar Social Security and Health Institution accessibility arrangements for construction must be made. Information on correcting the detected deficiencies and the suitable dimensions: Stair tread tension must be lower than the current 17 cm. A 10 cm long step should be added to create a platform or border that will enable visually impaired people to perceive a walking stick. Railings should be added on the stairs.Handrails are important to provide grip and stability when using stairs. Disabled Crossings: Appropriate transitions for wheelchairs should be provided when crossing the street. For this, ramps or smooth ground transitions of appropriate width and slope should be created. Directions and audio warning systems should be added for walking for the visually impaired. Direction signs should be equipped with signs in embossed or Braille. Signs written in the Braille alphabet should be used to enable visually impaired individuals to access information. Braille signs must be placed. Braille signs should be made of durable materials and be long-lasting.

Non-slip floor coverings should be used. Non-slip surfaces should be preferred to prevent slipping, especially on wet floors. Non-slip floor coverings should be applied at the ramp and stair entrances. Discreet pavements should be used for the road safety of visually impaired individuals. There are no Colored Road Signs. Responsive road signs should be used to increase safety. With these arrangements, the Gostivar Social Security and Health Institution building can be made suitable for all types of disability, and accessibility can be provided. Appropriately sized stairs, ramps, transitions, and Braille signs make it easier for people with disabilities to use the building comfortably and access information. Non-slip floor coverings, discreet pavements, and colorful and responsive road signs should increase their safety and make their journey safer.

GOSTIVAR POSTHOUSE ENTRANCE- TRANSPORTATION		
		
A- Post Office Building Entrance	**B-** Stair Step Height: 15 cm Step Width: 32 cm Stair Width: 300 cm There is no railing on the stairs.	**C-** There are no directions for walking on the pavement for the visually impaired and no audio warning system. In addition, there are no discretionary pavements for the visually impaired on the pavement.

Figure 6. Gostivar Post Office Building Entrance and Access (Arıcı,2023)

Accessibility arrangements need to be made for the Gostivar Post Office building. Below is information on how the detected deficiencies can be eliminated and which dimensions are appropriate: Stairs: Stair step height must be lower than the existing 15 cm. Preferably, a 10 cm high step should be added, and a platform or border should be created that will enable visually impaired individuals to perceive with their walking sticks. Railings should be added on the stairs. Handrails are important to provide grip and stability when using stairs. Disabled Crossings: Directions and audio warning systems should be added for walking for the visually impaired. Visually impaired individuals should be able to perceive directions by using embossed or Braille signs on the pavement. Discreet pavements should be used. Discretionary pavements make a crackling sound on the wheeled surface of the cane, allowing disabled people to cross the pedestrian path and realize the dangers. Ramp: A suitable ramp should be added to the entrance. The ramp allows wheelchair users to enter the building easily. The ramp width must be at least 90 cm. The slope should not be more than 6%. Doors: Entrance doors should be suitable for the passage of disabled individuals. It is preferred that the doors are sufficiently wide and equipped with automatic opening features.

GOSTIVAR CULTURAL ENTRY- TRANSPORTATION		
		
A- Culture House Building Entrance	**B-** Stair Step Height: 13cm Step Width: 40 cm 1. Ladder Width:630 cm 2. Ladder Width:230 cm There is no railing on the stairs. There is no ramp.	**C-** When crossing the street, there are no wheelchair-friendly passages, and there are no walking directions for the visually impaired, and there is no voice warning system.

Figure 7. Gostivar Culture House Entrance and Transportation (Arıcı,2023)

Accessibility arrangements need to be made for the Gostivar Post Office cultural house building. Below is information on how the detected deficiencies can be eliminated and which dimensions are appropriate: Stairs: The stair step height must be lower than the existing 13 cm. Preferably, a 10 cm high step should be added, and a platform or border should be created that will enable visually impaired individuals to perceive with their walking sticks. Railings should be added on the stairs. Handrails are important to provide grip and stability when using stairs. Disabled Crossings: Directions and audio warning systems should be added for walking for the visually impaired. Visually impaired individuals should be able to perceive directions by using embossed or Braille signs on the pavement. Discreet pavements should be used. Discretionary pavements make a crackling sound on the wheeled surface of the cane, allowing disabled people to cross the pedestrian path and realize the dangers. Ramp: A suitable ramp should be added to the entrance. A ramp should be built. Moreover, the ramp allows wheelchair users to enter the building with ease. The ramp width must be at least 90 cm. The slope should not be more than 6%. Doors: Entrance doors should be suitable for the passage of disabled individuals. It may be preferable that the doors are sufficiently wide and equipped with an automatic opening feature.

GOSTIVAR VARDAR RIVER WALKING PATH AND CITY PARK		
		
A- Gostivar, The Pedestrian Pavement on the Bridge Over the Vardar River, is 200 cm wide.	**A-** Gostivar, Vardar River is divided into two parts by a bridge. On the left side of the bridge, there is no area for bicycles, and there is no special walking area for disabled people.	**C-** Gostivar, the walking area along the Vardar River The area reserved for walking is 240 cm wide.
		
D- In Gostivar, there is no walking area along the Vardar River and no access to a walking area for people with disabilities.	**E-** General view of the walking area along the Vardar River in Gostivar	**F-** Gostivar, walking area along the Vardar River; The width of the bicycle path indicated in red is 160cm 80cm between the bicycle path and the middle reflux
		
G- Gostivar, walking area along the Vardar River, walkway width 240 cm	**L-** Gostivar, Stairs used for access to the walking area along the Vardar River; step height: heights vary in steps. It has 12 cm-16 cm and 17cm heights. The step width is 30 cm, stair width is 320 cm.	**F-** Gostivar, the city park walking area next to the Vardar River, has a wide area. However, the walking paths in the park do not have the opportunity to walk around with a wheelchair, and there are no other measures for people with disabilities.

Figure 8. Gostivar, Vardar River Walkways and City Park (Arıcı, 2023)

One of the biggest reasons why people with disabilities cannot benefit from important social policies such as education, health, and employment is the limited and limited accessibility of living spaces. Therefore, central and local governments should organize the physical environment in accordance with universal design principles. Urban furniture should not be placed randomly, and factors such as pavement width (minimum 150 cm) and slope (maximum 2%) should be planned in accordance with the use of disabled individuals. Opinions and suggestions of disabled individuals should be included in the decisions to be taken on these issues (Bektaş et al., 2020).

We can evaluate the compliance of parks and walking paths in Gostivar with disability standards. The precautions to be taken and the materials to be used in order to provide comfortable and safe transportation for people with disabilities are as follows:

The width of the walkways should be a minimum of 200 cm. Special walking areas should be reserved for people with disabilities along the walking path. These areas should be a minimum of 240 cm wide and should be arranged in a way that allows easy passage with wheelchairs. The road surface should be non-slip and smooth. It is important to use a non-slip floor covering. For visually impaired individuals, there should be a 10 cm high platform or border on the road to enable them to perceive with the help of a walking stick. Directions such as braille signs, directional signs, and colored road signs should be used. There should be low-response sidewalks along the way. The step heights of the stairs should be close to each other. Step heights should be between 10 cm and 12 cm. Also, steps of different heights should be

avoided. A non-slip surface coating should be used. This ensures that the stairs are safe even when wet or slippery.

The walking paths in the park should be suitable for walking around with a wheelchair. Paths must be smooth, non-slip, and unobstructed. Braille signs and directions should be used for visually impaired individuals. For example, signposts at the entrance of the park may contain directional and informational signs. Benches, picnic tables, and other seating areas should be suitable for use by people with disabilities. For example, it should be of suitable height and accessibility for wheelchair users. Toilets are required in the park. It is important to have suitable toilets for people with disabilities. These toilets should be wide enough and equipped for wheelchairs to enter easily.

Construction Materials, Rubber, or similar materials specially designed for non-slip floor coverings can be used. Durable and non-slip materials should be preferred for stair steps. It may be necessary to add a non-slip coating to wooden or metal steps. Durable and tactile materials should be used for braille signs and directions. For example, embossed lettering and steel plates may be preferred.

4. DISCUSSION AND CONCLUSIONS

In order to solve the accessibility problems of stairs that are not suitable for people with disabilities, there is information with solutions and measures below:
Ramp Construction: Ramp slope: The optimal slope ratio for disabled ramps is 1:12. This means a 2.5 cm rise for every 30 cm horizontally. Ramp width: The minimum ramp width is at least 90 cm for wheelchair users. Ramp surface: A non-slip surface coating should be used on the ramp to ensure safety.

Platform Lift: Platform dimensions: Platform width should be at least 90 cm, and depth should be at least 140 cm for wheelchair users to sit comfortably. Platform height: The platform should go up and down by the height of the stairs.

Stairlift: Stairlift dimensions: A platform with a minimum width of 80 cm and a depth of 110 cm is usually required to provide adequate space for wheelchair users.
Building an Alternative Road: Road width: A road wide enough for disabled people to pass side by side should be created. The minimum width can be considered as 150 cm. Road surface: A non-slip and flat surface should be preferred to provide a safe walking surface. In case there is no ramp suitable for people with disabilities, it is necessary to produce a cost-effective solution, and the recommendations should be implemented as follows. Alternative Crossing Point: An alternative crossing point can be provided to the building for persons with disabilities. For example, consider adding a ramp or elevator by arranging a nearby entrance.

Temporary Ramps: Portable or foldable ramps can provide temporary access to the building for people with disabilities. These ramps can be used when needed, offering a lower-cost solution.

Project Support: You can request support for accessibility projects from public institutions or local administrations. It is possible to benefit from the funds provided to improve the access of persons with disabilities.

Solution suggestions were presented to create resting areas for the disabled and the elderly on the walking paths;

Seating Units: Seating height: The seating units should be between 45-50 cm for disabled individuals to sit comfortably. Seating area width: A minimum width of 90 cm is recommended to provide a suitable seating area for wheelchair users. Backrest angle: Backrests should be positioned at an ergonomically appropriate angle.

Shades and Umbrellas: Canopy height: The canopies' height should be at least 210 cm for disabled people to pass easily. Width and depth: Generally, shades should be at least 120 cm wide and 120 cm deep.

Dimensions and features of handicapped tables: At least 70 cm of space should be left under the table to provide unhindered access. Seat height and width must be suitable for wheelchair users. Generally, a height of 45-50 cm and a width of 90-120 cm are recommended. The surface of the desk should have a non-slip coating and should have a smooth surface for users to access it comfortably.

Dimensions and features of fountains designed for people with disabilities: Height: The height of the fountains should generally be between 75-85 cm for easy access by wheelchair users. Handles: There should be handles in fountains so that disabled people can get support. Pressurized water: Providing pressurized water in fountains can be beneficial in terms of ease of use.

The standards and dimensions of the toilets suitable for people with disabilities are as follows: Door height: The door height must be at least 90 cm for wheelchair users to enter the session. Indoor maneuvering area: Covering a maneuvering area of at least 150 cm x 150 cm for wheelchair users. Handles: In toilets, the handles should be at a suitable height and above to provide support. Stepping on the sink: There should be approximately 70 cm from the sink for wheelchair users to watch.

Features of signs and information boards: High contrast: High contrast of signs and texts makes it easier for visually impaired individuals to perceive. Braille signs: Information marked with the Braille alphabet enables visually impaired individuals to access information. Sufficient size: Enough size of the text improves readability. Correct placement: Signs must be placed correctly so users can easily notice and read them.

Disabled-friendly roads should be designed according to the following dimensions and standards: Road width: At least 150 cm width should be provided so that disabled people can pass side by side comfortably. Discretionary sidewalks: There should be discretionary ramps on sidewalks for wheelchair users.

Colored road signs: Colored markings can be used to separate different sections of roads. Responsive road signs: To attract the attention of people with disabilities, road signs can provide audio or tactile feedback.

The absence of a 10 cm high platform or border for the perception of people with disabilities may cause accessibility problems. To remedy this situation: Adding a platform or border: A 10 cm high platform or border can be added to facilitate the perception of visually impaired individuals. High-contrast markings: High-contrast markings can be used to attract the attention of visually impaired individuals. Smooth surface: Providing a smooth and non-slip floor on walkways increases safety.

The types, names, and properties of building materials that can solve the identified deficiencies should be as follows;

Non-Slip Ceramic or Tile Coatings: Non-slip ceramic or tile coatings are specially designed to prevent slipping on their surfaces. Thanks to its high coefficient of friction, it reduces slippage and provides safe walking. It provides grip even on wet or slippery surfaces. Advantages: It provides a safe and non-slip floor; it must be durable and easy to clean.

Stainless Steel or Aluminum Railings: Railings made of stainless steel or aluminum provide a secure hold on stairs and ramps. It is durable, corrosion-resistant, and long-lasting.
It is preferably ergonomically designed to facilitate the use of people with disabilities. Advantages: Provides a secure hold, is durable, and is long-lasting.

Braille Sign Materials: Braille sign materials contain braille writings especially suitable for the Braille alphabet.
Stainless steel or plastic materials can be used. It is touchable, durable, and weather resistant.
Advantages: Provides visually impaired individuals access to information, is durable and long-lasting.

Non-Slip Floor Coverings: Non-slip floor coverings are specially designed to reduce the risk of slipping. Different materials can be used, for example, non-slip rubber or non-slip epoxy coatings. It prevents slipping even on wet or slippery floors. Advantages: Provides safe walking, reduces the risk of slipperiness, is durable, and is easy to clean.

These building materials are the preferred options for facilitating the access and safety of people with disabilities. Factors such as durability, safety, cleanability, and longevity should be considered in material selection. It is also important to comply with local legislation and standards.

These building materials are the preferred options for facilitating the access and safety of people with disabilities. Factors such as durability, safety, cleanability, and longevity should be considered in material selection. It is also important to comply with local legislation and standards.

REFERENCES

Arap, S. K., Yücebaş, E., & Arap, İ. (2021). Local Governments' Goal Of Life Without Barriers: The Case Of The Izmir Metropolitan Municipality. Anemon Muş Alparslan University Journal of Social Sciences, 9(1), 139-156.

Aykıl, F. D., Erbaş, M., & Meltem. (2018). The Suitable Design of Urban Furniture for Elderly and Disabled: The Suitability Analysis on Elazig Town Squares. Inonu University Journal of Art and Design, ISSN: 1309-9876, E-ISSN: 1309-9884.

Bektaş, B., & Develi, A. (2020). Engelli Bireylerin Erişilebilirlik Sorunu: Destekler, Eksiklikler. Uluslararası Anadolu Sosyal Bilimler Dergisi, 4(3).

Çınar, H., Arslan, A. R., Öztürk, A. M., & Bülbül, R. (2015). Public Buildings: Life Analysis for the Disabled and Furniture Use Reinforcement. Suleyman Demirel University Journal of Engineering Sciences and Design, 3(3), 329-337. SI: Ergonomi2015. ISSN: 1308-6693. Special Issue of 21. National Congress of Ergonomics, Turkey.

Çivici, T., & Gönen, D. (2015). Evaluating Accessibility to Social Areas for Physical Disabled Students in Balıkesir University Çağıs Campus. Süleyman Demirel Üniversitesi Mühendislik Bilimleri ve Tasarım Dergisi, 3(3), 639-646. ÖS: Ergonomi2015. ISSN: 1308-6693. Special Issue of 21. National Congress of Ergonomics, Turkey.

Doğruel, F. (2022). Accessibility Experiences of People with Disabilities at the Intersection of Body, Individual, and Society. Journal of Sociological Research, 25(2), ISSN 2148-9947.

Enginöz, E., B. (2015). Herkes için Tasarım, Mimarlık, 381.

Erten, Ş., & Aktel, M. (2020). Right of Accessibility of People with Disabilities: An Assessment in the Framework of Barrier-Free City Approach. Süleyman Demirel University Visionary Journal, 11(28), 898-912. ISSN: 1308-9552.

Mutluer, S. Y. (1997). Tekerlekli Sandalye Kullanan Bedensel Özürlüler İçin Uygun Konut Tasarımı ve Çevre Düzenlemesi. Yüksek Lisans Tezi. Selçuk Üniversitesi, Konya.

Pouya, S. (2021). The importance of universal equipment designs for people with disabilities and some design suggestions in the related landscape areas. Sosyal Çalışma Dergisi, 5(2), 209-229.